# Petrological and geochemical study of Platreef chromitites, northern Bushveld, South Africa

Rhian Eleri Jones

2013

Thesis submitted for the degree of

*Doctorate of Philosophy*

‘This alluvial platinum must come from somewhere in the surrounding basic rocks, and if only we can find it in payable quantities in the main source, the mother reef, then we would have discovered something far bigger and far more important than the Russian and American deposits’

Hans Merensky, 1924.

## Declaration

This work has not been submitted in substance for any other degree or award at this or any other university or place of learning, nor is it being submitted concurrently in candidature for any degree or other award.

Signed: Rhian Eleri Jones

Date:

This thesis is being submitted in partial fulfilment of the requirements for the degree of PhD.

Signed: Rhian Eleri Jones

Date:

This thesis is the result of my own independent work/investigation, except where otherwise stated. Other sources are acknowledged by explicit references. The views expressed are my own.

Signed: Rhian Eleri Jones

Date:

I hereby give consent for my thesis, if accepted, to be available for photocopying and for inter-library loan, and for the title and summary to be made available to outside organisations.

Signed: Rhian Eleri Jones

Date:

## Abstract

The Platreef, located in the northern limb of the Bushveld Complex in South Africa, is a world-class Ni-Cu-PGE deposit. The complexity of the deposit has meant that despite the numerous studies, developing an accepted genetic model to account for the variations observed has been difficult. While some authors have suggested that it is part of the Upper Critical Zone, correlating it to the Merensky Reef, others have suggested that the Platreef is unrelated to mineralisation found elsewhere in the Bushveld Complex. The model tested is the multiple staging chamber model developed by McDonald and Holwell, that proposes that the parental magma was upgraded in PGE (plus Ni and Cu) prior to emplacement.

Key to testing this model has been the analysis of immiscible sulphide inclusions trapped within chromite grains, believed to represent the early parental magma. Analysis has shown that they contain high PGE tenors, significant semi-metal (Bi, Te and As) content and the low S/Se ratios of the inclusions suggest a mantle source. Interaction of the sulphide liquid with multiple batches of magma in the staging chamber is proposed to have enabled enrichment to occur prior to emplacement through a process known as multi-stage dissolution upgrading.

The analysis of chromite grains from the three study farms has shown that the variation in chromite composition is dependent on host lithology and the location of the sample along strike of the Platreef. Some correlation can be made with chromites from the UG2 but Platreef chromites cannot be directly correlated to those from the Merensky Reef.

Investigation of PGE concentrations within the BMS from Zwartfontein has shown a strong association between PGE and BMS and that the distribution of PGE is consistent with fractional crystallisation of a sulphide liquid.

The PGM study has shown that variation along strike and down dip of the Platreef is not strictly controlled by footwall lithologies as previously proposed. Variation is suggested to be the result of differing temperatures and $fO_2$ conditions due to the proximity around proposed feeder zones.

In order to further test the staging chamber model, S isotope analysis should be carried out on the sulphide inclusions to ascertain if a magmatic signature is present. In addition, further support to the model may be achieved by examining other Lower Zone bodies for chalcophile element depletion.

## Acknowledgements

It has been a great privilege not only to complete my PhD studies, but to spend my whole university career at the School of Earth and Ocean Sciences at Cardiff University and the experience has left me with great memories.

I would like to start with a big thank you to my main supervisor Dr Iain McDonald for all his insight, advice and encouragement over the course of this PhD project, which he devised in conjunction with Dr Dave Holwell from Leicester University. Thank you to Iain for his help in accompanying me to South Africa on my multiple trips to collect samples and attend conferences. Additional thanks must also go to Dr Hazel Prichard for all her help with the PGM associations and Dr Ian Butler for his assistance in homogenising the samples at Edinburgh University.

I would also like to thank the technical staff for all their assistance in various experiments and sample preparation. Pete Fisher was of invaluable help during my many months on the SEM, as was Lawrence Badham for producing hundreds of polished blocks. Tony Oldroyd and Ley Woolley were also a huge help in the geochemistry laboratory.

I thank James Winch, Trust Muzondo and Llewelyn Whitecross of Anglo Platinum for their efforts in helping me obtain samples for this project and for negotiating the red tape involved in accessing such a big mining operation. Thanks must also go to everyone who gave me advice and guidance during my multiple trips to South Africa including Judith Kinnaird, Paul Nex, Marina Yudovskaya and Tony Naldrett, to name but a few. Huge thanks must also go to Gordon Chunnett for acquiring the funding from Anglo Platinum that made this project possible. Additional funding was also provided by the Sir Charles Wright Scholarship at Cardiff University.

Many thanks to all the PhD students at Cardiff University (past and present) who I shared offices with, for their support and friendship over the last few years. Thanks must especially go to Pauline and Hannah for keeping me sane and encouraging me to the end, to Jake for interesting discussions in the office and for Joe's friendship since we met in our tutor's office during the first week as undergraduates. This thesis was written on two different continents so thanks must also go to my friends from all over the world who were my source of laughter and support during the last couple of months writing. And lastly, a huge thanks to my parents, sister Sara and extended family for their love, support and belief in me.

# Table of Contents

**Declaration**.....ii

**Abstract**.....iii

**Acknowledgments**.....iv

**Chapter 1: Introduction**

1.1 The platinum-group elements.....1

1.2 Historical review of the PGE.....2

1.3 Uses of PGE.....4

1.4 Economic occurrences of PGE.....6

1.5 Outline of study.....6

**Chapter 2: Regional Geology**

2.1 The Bushveld Complex.....8

2.1.1 Structural history.....9

2.1.2 Stratigraphy.....11

2.1.3. Emplacement and magma source.....14

2.2 The Northern Limb.....21

2.2.1 Structural setting of the northern limb.....21

2.2.2 Age of northern limb.....22

2.2.3 Stratigraphical correlation of the northern limb.....23

**Chapter 3: Local Geology**

3.1 The Platreef.....27

3.1.1 Definition of the Platreef.....27

3.2 Lithologies.....30

3.2.1 Platreef lithologies.....30

3.2.2 Main Zone lithologies.....31

3.2.3 Footwall lithologies.....31

3.2.4 Lower Zone lithologies.....32

3.3 Stratigraphic relationships.....32

3.3.1 Relationship between the Platreef and the Main Zone.....32

3.3.2 Relationship between the Platreef and the footwall rocks.....33

3.3.3 Relationship between the Platreef and the Lower Zone.....33

3.4 Platreef sectors.....34

3.4.1 Central Sector.....34

3.5 Mineralogy.....38

3.5.1 Silicate mineralogy.....38

3.5.2 Sulphide mineralogy.....40
3.5.3 Chromite mineralogy.....42
3.5.4 Platinum-group mineralogy.....45
3.6 Geochemistry.....46
3.6.1 Major and trace elements.....46
3.6.2 PGE & Au.....48
3.6.3 Isotopes.....50
3.7 Comparison of the Platreef to the Merensky Reef.....52
**Chapter 4: Mineral Deposit Formation**
4.1 Magmatic sulphide deposits.....53
4.2 Formation of magmatic sulphide deposits.....56
4.3 Classification of PGE deposits.....64
4.4 Platreef formation.....65
4.4.1 Staging chamber model.....68
**Chapter 5: Geochemistry**
5.1 Introduction and methods.....73
5.2 Classification of rocks based on geochemistry.....79
5.3 Major elements.....79
5.4 Trace elements.....84
5.4.1 Rare earth element plots.....84
5.4.2 Multi-element variation diagrams.....89
5.5 PGE.....93
5.6 Variation spatially across study area.....98
5.7 Summary.....104
**Chapter 6: Mineralogical Study Of The Platreef Chromites**
6.1 Introduction.....106
6.1.1 Major trends in chromite compositional space.....107
6.1.2 Chromite in the Bushveld Complex.....109
6.1.3 Aims of the study.....110
6.2 Materials and methods.....110
6.3 Chromite distribution and morphology.....110
6.4 Chromite mineral chemistry.....112
6.4.1 Cr# vs. Mg#.....114
6.4.2 Cr# vs. $Fe^{2+}$#.....115

6.4.3 $Fe^{3+}$# vs. $Fe^{2+}$#.....116
6.4.4 $Fe^{3+}$# vs. $TiO_2$.....117
6.5 Variation within different lithologies.....118
6.6 Variations along strike of the Platreef.....121
6.6.1 Cr# vs. Mg#.....121
6.6.2 Cr# vs. $Fe^{2+}$#.....126
6.6.3 $Fe^{3+}$# vs. $Fe^{2+}$#.....130
6.6.4 $Fe^{3+}$# vs. $TiO_2$.....135
6.6.5 Examination of Platreef data.....139
6.7 Comparison to other Platreef data.....141
6.7.1 Cr# vs. Mg#.....142
6.7.2 Cr# vs. $Fe^{2+}$#.....143
6.7.3 $Fe^{3+}$# vs. $Fe^{2+}$#.....144
6.7.4 $Fe^{3+}$# vs. $TiO_2$.....145
6.8 Comparison of Platreef data to other Bushveld data.....146
6.8.1 Cr# vs. Mg#.....148
6.8.2 Cr# vs. $Fe^{2+}$#.....149
6.8.3 $Fe^{3+}$# vs. $Fe^{2+}$#.....150
6.8.4 $Fe^{3+}$# vs. $TiO_2$.....151
6.9 Conclusion.....152
**Chapter 7: Study of PGM In The Chromitites Of The Platreef**
7.1 Introduction.....153
7.2 Material and methods.....154
7.3 PGM mineralogy.....155
7.3.1 PGE sulphides.....161
7.3.2 PGE arsenides.....163
7.3.3 PGE tellurides.....164
7.3.4 PGE bismuthides.....165
7.3.5 PGE antimonides.....166
7.3.6 PGE sulpharsenides.....166
7.3.7 PGE alloys.....167
7.3.8 Au-Ag bearing minerals.....169
7.4 Variation in hosts for the PGM.....169
7.5 Variation in PGM distribution across the study area.....176

7.5.1 North-south variation.....179
7.5.2 West-east variation.....180
7.6 Discussion.....183
7.6.1 Previous Platreef PGM studies.....183
7.6.2 Relationship between PGM and host minerals.....184
7.6.3 Model for spatial distribution of PGM observed in the study area.....189
7.7 Conclusion.....196
**Chapter 8: PGE Concentration Of The BMS On Zwartfontein**
8.1 Introduction.....196
8.2 Methods.....200
8.3 Results.....200
8.4 Comparison to other Bushveld Complex data.....211
8.5 Discussion.....217
8.6 Conclusion.....221
**Chapter 9: Magmatic Sulphide Melt Inclusions Within Chromites**
9.1 Introduction.....223
9.1.1 Use of S isotopes.....223
9.1.2 S/Se ratios.....223
9.1.3 Importance of sulphide inclusions.....225
9.2 Methods.....226
9.2.1 Homogenisation of samples.....227
9.2.2 Analysis.....229
9.3 Results.....230
9.4 Discussion.....235
9.4.1 Variation in tenors across the study area.....237
9.4.2 S/Se ratio.....240
9.5 Conclusion.....249
**Chapter 10: Conclusions**.....250
**References**.....255
**Appendix 1A: Bulk rock geochemistry**.....281
**Appendix 1B: Bulk rock PGE**.....288
**Appendix 1C: Chromite chemistry**.....290

# List of Figures

**Chapter 1: Introduction**

Figure 1.1: Demand by application of Pt, Pd and Rh for 2011.....5

**Chapter 2: Regional Geology**

Figure 2.1: Simplified geological map of Bushveld Complex.....8

Figure 2.2: Schematic showing tectomagmatic evolution of Kaapvaal Craton.....11

Figure 2.3: Gravity map of the Bushveld Complex.....19

Figure 2.4: Schematic showing differences in the crust north and south of the TML.....20

Figure 2.5: Traditional correlation of stratigraphy of the eastern and western limbs of the Bushveld Complex and the northern limb.....25

**Chapter 3: Local Geology**

Figure 3.1: Map of northern limb showing the locations of the farms.....29

Figure 3.2: Stratigraphy of Transvaal Supergroup floor rocks beneath the Platreef.....32

Figure 3.3: 3D block model for Platreef development at Sandsloot.....36

Figure 3.4: Mantle normalised spidergram averages for Central Sector.....47

**Chapter 4 – Mineral Deposit Formation**

Figure 4.1: Distribution of PGE and Ni-Cu deposits worldwide.....53

Figure 4.2: Stages in the formation of a magmatic sulphide deposit.....56

Figure 4.3: pMELT modelling of variation of Ni, Cu and (Pt+Pd) contents of partial melts developed through mantle melting of spinel lherzolites at 20 kbar.....57

Figure 4.4: Fractional crystallisation of magma produced by 18 % partial melting.....61

Figure 4.5: Effects of variation in silicate magma-sulphide liquid mass ratio on the concentrations of Cu and Pd of sulphides.....63

Figure 4.6: Staging chamber model developed by McDonald and Holwell.....69

**Chapter 5: Geochemistry**

Figure 5.1: Map of study area showing drillholes sampled.....75

Figure 5.2: Major element plots with end-member minerals.....81

Figure 5.3: Bivariate graphs for (a) Ni vs. MgO; (b) Zr vs. MgO and (c) V vs. Cr.....82

Figure 5.4: Bivariate graphs for (a) Zn vs. Cr and (b) Ga vs. Cr.....83

Figure 5.5: REE plots for the various lithologies and comparable plot for the central Platreef pyroxenites and chromitites.....86

Figure 5.6: Histograms showing Eu anomaly for (a) chromitiferous gabbronorites; (b) chromitiferous norites; (c) chromitiferous pyroxenites and (d) chromitites.....87

Figure 5.7: Histograms showing Eu anomaly for (a) gabbronorites; (b) norites; (c) pyroxenites and (d) combined for all lithologies.....88

Figure 5.8: Mantle normalised multi-element variation diagrams for (a) chromitiferous gabbronorite; (b) chromitiferous norite and (c) chromitiferous pyroxenite.....90
Figure 5.9: Mantle normalised multi-element variation diagrams for (a) chromitite; (b) gabbronorite and (c) norite.....91
Figure 5.10: Mantle normalised multi-element variation diagrams for pyroxenite.....92
Figure 5.11: Condensed spidergram showing range from this study vs. average Merensky Reef and B1 magma.....92
Figure 5.12: Cr vs. PGE plots.....96
Figure 5.13: Chondrite normalised PGE profiles for various lithologies compared to rest of Bushveld Complex.....97
Figure 5.14: Map showing N-S lines.....99
Figure 5.15: N-S line 1.....100
Figure 5.16: N-S line 2.....100
Figure 5.17: Map showing W-E lines.....101
Figure 5.18: W-E line 1.....102
Figure 5.19: W-E line 2.....102
Figure 5.20: W-E line 3.....103
Figure 5.21: W-E line 4.....103
Figure 5.22: W-E line 5.....104

**Chapter 6: Mineralogical Study Of The Platreef Chromites**

Figure 6.1: Trivalent ion plot for spinel data set from Barnes and Roeder.....107
Figure 6.2: World production of chromite ore and reserves.....110
Figure 6.3: Typical textures of chromitites.....111
Figure 6.4: Trivalent ion plot including study data.....112
Figure 6.5: Trivalent ion plot for continental mafic intrusions.....113
Figure 6.6: Mg# vs. Cr# for entire data set.....115
Figure 6.7: Corroded chromite with phlogopite inclusions.....115
Figure 6.8: Cr# vs. $Fe^{2+}$# for entire data set.....116
Figure 6.9: $Fe^{2+}$# vs. $Fe^{3+}$# for entire data set.....116
Figure 6.10: $TiO_2$ vs. $Fe^{3+}$# for entire data set.....117
Figure 6.11: (a) MgO vs. $Cr_2O_3$ and (b) $TiO_2$ vs. $Cr_2O_3$ for different lithologies.....119
Figure 6.12: (a) $TiO_2$ vs. $Al_2O_3$ and (b) $TiO_2$ vs. FeO for different lithologies.....120
Figure 6.13: Mg# vs. Cr# for different lithologies across the 3 farms.....122

Figure 6.14: Mg# vs. Cr# for (a) chromitiferous gabbronorites; (b) chromitiferous norite and (c) chromitiferous pyroxenites.....124
Figure 6.15: Mg# vs. Cr# for (a) chromitites; (b) norite and (c) pyroxenite.....125
Figure 6.16: Cr# vs. $Fe^{2+}$# for different lithologies across the 3 farms.....127
Figure 6.17: Cr# vs. $Fe^{2+}$# for (a) chromitiferous gabbronorites; (b) chromitiferous norite and (c) chromitiferous pyroxenites.....128
Figure 6.18: Cr# vs. $Fe^{2+}$# for (a) chromitites; (b) norite and (c) pyroxenite.....129
Figure 6.19: $Fe^{3+}$# vs. $Fe^{2+}$# for chromitiferous norites from Sandsloot.....130
Figure 6.20: $Fe^{3+}$# vs. $Fe^{2+}$# for different lithologies across the 3 farms.....131
Figure 6.21: $Fe^{3+}$# vs. $Fe^{2+}$# for (a) chromitiferous gabbronorites; (b) chromitiferous norite and (c) chromitiferous pyroxenites.....132
Figure 6.22: $Fe^{3+}$# vs. $Fe^{2+}$# for (a) chromitites; (b) norite and (c) pyroxenite.....133
Figure 6.23: $TiO_2$# vs. $Fe^{3+}$# for different lithologies across the 3 farms.....136
Figure 6.24: $TiO_2$# vs. $Fe^{3+}$# for (a) chromitiferous gabbronorites; (b) chromitiferous norite and (c) chromitiferous pyroxenites.....137
Figure 6.25: $TiO_2$# vs. $Fe^{3+}$# for (a) chromitites; (b) norite and (c) pyroxenite.....138
Figure 6.26: $Fe^{3+}$ vs. Al cations for chromitiferous pyroxenites and pyroxenites.....139
Figure 6.27: Trivalent ion plots comparing Platreef data.....142
Figure 6.28: Mg# vs. Cr# comparing Platreef data.....142
Figure 6.29: Chromite crystal composition from Overysel from Holwell and McDonald.....143
Figure 6.30: Cr# vs. $Fe^{2+}$# comparing Platreef data.....144
Figure 6.31: $Fe^{3+}$# vs. $Fe^{2+}$# comparing Platreef data.....144
Figure 6.32: $TiO_2$# vs. $Fe^{3+}$# comparing Platreef data.....145
Figure 6.33: Trivalent ion plots comparing Bushveld data.....147
Figure 6.34: Mg# vs. Cr# comparing Bushveld data.....148
Figure 6.35: Cr# vs. $Fe^{2+}$# comparing Bushveld data.....149
Figure 6.36: $Fe^{3+}$# vs. $Fe^{2+}$# comparing Bushveld data.....150
Figure 6.37: $TiO_2$# vs. $Fe^{3+}$# comparing Bushveld data.....151
**Chapter 7: Study Of PGM In The Chromitites Of The Platreef**
Figure 7.1: Pie charts showing area proportion of each type of PGM.....156
Figure 7.2: Cooperite and palladoarsenide inclusion within chromite grain.....161
Figure 7.3: Cooperite grains showing differing morphology.....162
Figure 7.4: Laurite grains showing differing morphology.....163
Figure 7.5: Sperrylite grains showing differing morphology.....164

Figure 7.6: Moncheite grains showing differing morphology.....165
Figure 7.7: Isoferroplatinum grains showing differing morphology.....168
Figure 7.8: Pie chart showing PGM association for whole study area.....169
Figure 7.9: Pie chart showing PGM associations across the three farms.....171
Figure 7.10: Pie chart showing the simplified distribution of PGM associations.....172
Figure 7.11: Breakdown of PGM that occur as chromite inclusions or carbonate grains....173
Figure 7.12: Breakdown of PGM that occur within silicates, within sulphides or on the boundary between silicate and sulphide grains.....174
Figure 7.13: Breakdown of PGM that occur on rim of chromites in silicates, rim of chromites in sulphides or rim of chromites on boundary between silicate and sulphide grains.....175
Figure 7.14: PGE alloy association by group.....176
Figure 7.15: Map showing N-S lines.....177
Figure 7.16: Map showing W-E lines.....178
Figure 7.17: Graph showing distribution of PGM for N-S line 1.....179
Figure 7.18: Graph showing distribution of PGM for N-S line 2.....179
Figure 7.19: Graph showing distribution of PGM for N-S line 3.....180
Figure 7.20: W-E graphs showing distribution of PGM in lines 1 & 2.....181
Figure 7.21: W-E graphs showing distribution of PGM in lines 3-6.....182
Figure 7.22: Proportion of Pt-, Pd- and other PGE-phase PGM.....184
Figure 7.23: Mineral equilibrium curves.....185
Figure 7.24: Distribution of cooperite and braggite within chromitites.....187
Figure 7.25: Distribution of Pt-Fe alloys.....188
Figure 7.26: Kinloch feeder zone model.....190
Figure 7.27: Map showing location of 18 drill holes sampled.....191
Figure 7.28: Map showing location of 18 drill holes samples with overlying geology.....192
Figure 7.29: 3D block model along X-Y cross section.....192
Figure 7.30: Bar chart showing relationship between PGE antimonides and PGE alloys.....193
Figure 7.31: Distribution of Pd- and Pt-alloys across the three farms.....195
Figure 7.32: Pd-alloy PGM identified from Sandsloot.....196

**Chapter 8: PGE Concentration Of BMS On Zwartfontein**

Figure 8.1: Schematic representation of fractionating sulphide droplet.....198
Figure 8.2: Proportion by area of Pt-, Pd- and other PGE-dominated PGM.....199
Figure 8.3: Sample map showing location of drillholes on Zwartfontein.....201

Figure 8.4: Total PGE contents in BMS from Zwartfontein in (a) pentlandite; (b) pyrrhotite; and (c) chalcopyrite.....203
Figure 8.5: Binary variation diagrams of (a) Pd vs. Co and (b) Co vs. Ni.....204
Figure 8.6: (a) Ir vs. Os; (b) Ir vs. Ru; (c) Ir vs. Rh; (d) Ir vs. Pd; (e) Pd vs. Rh and (f) Ir vs. Ni for pentlandite and pyrrhotite.....205
Figure 8.7: TRA spectra of sulphides containing pentlandite and chalcopyrite.....207
Figure 8.8: TRA spectra of sulphides containing pyrrhotite with zoned Ir and Ru.....208
Figure 8.9: TRA spectra of sulphides containing pentlandite, chalcopyrite and PGM inclusion.....209
Figure 8.10: TRA spectra of sulphides containing pentlandite and pyrrhotite zoning.....210
Figure 8.11: Comparison of BMS from Zwartfontein and study by Holwell and McDonald.215
Figure 8.12: Histograms showing variation in Pd concentration across Bushveld.....216
Figure 8.13: Concentration of Pd in pentlandite vs. pyrrhotite and pentlandite vs. chalcopyrite.....219
Figure 8.14: Average Pd contents in pentlandite compared to average whole rock Cu.....220
**Chapter 9: Magmatic Sulphide Melt Inclusions Within Chromites**
Figure 9.1: Unhomogenised sulphide inclusions in chromite.....227
Figure 9.2: Schematic diagram showing fractionation and polishing problems.....227
Figure 9.3: Schematic diagram of quench furnace.....228
Figure 9.4: Exsolution texture observed in homogenised inclusions.....229
Figure 9.5: TRA spectra of homogenised inclusions in samples 101 and 88.....233
Figure 9.6: TRA spectra of homogenised inclusions in samples 99 and 56.....234
Figure 9.7: S/Se ratios vs. (a) Pd tenors; (b) Pt tenors and (c) combined Pt and Pd tenors..236
Figure 9.8: Map of study area showing average tenors of inclusions.....238
Figure 9.9: Variation in strike across study area from N-S.....239
Figure 9.10: Variation up-dip across study area W-E.....239
Figure 9.11: S/Se vs. Pd for samples analysed by Ihlenfeld and Keays.....241
Figure 9.12: Batch equilibrium model with no sulphide destruction.....243
Figure 9.13: Multistage staging chamber model.....245
Figure 9.14: Sulphide destruction models.....246

# List of Tables

**Chapter 1: Introduction**

Table 1.1: Selected physical properties of the PGE.....1

Table 1.2: Prices of traded PGE.....4

Table 1.3: Relative abundances of PGE in Earth's crust.....6

**Chapter 2: Regional Geology**

Table 2.1: Ages of the different Bushveld rocks using U/Pb dating.....9

Table 2.2: Northern limb ages.....22

**Chapter 3: Local Geology**

Table 3.1: Mineral data for the Platreef and other Bushveld rocks.....39

Table 3.2: Chemical composition of chromite in northern limb.....43

Table 3.3: Metal ratios for the northern Bushveld vs. Merensky Reef and UG2.....49

Table 3.4: Sulphur isotope data for Transvaal Supergroup sediments and basement rocks in the northern limb.....50

**Chapter 4: Mineral Deposit Formation**

Table 4.1: Selection of Ni-Cu-PGE deposits showing their resources and value.....54

Table 4.2: Comparison of contact-type sulphide deposits.....67

**Chapter 5: Geochemistry**

Table 5.1: Summary of samples analysed.....76

Table 5.2: Lithologies of the samples based on IUGS classification.....79

Table 5.3: Fractionation ratios for LREE and HREE for various lithologies.....89

Tabel 5.4: Various PGE ratios for each lithology.....93

**Chapter 7: Study Of PGM In The Chromitites Of The Platreef**

Table 7.1: Abundance of PGM in samples from 3 farms in Central Sector.....157

Table 7.2: Host association for the different PGM sulphides.....162

Table 7.3: PGE-Fe alloys identified across three farms.....167

Table 7.4: Total PGM area for each association.....170

**Chapter 8: PGE Concentration Of BMS On Zwartfontein**

Table 8.1: Composition of BMS from Zwartfontein.....202

Table 8.2: Coefficient of determination of PGE for various BMS.....202

Table 8.3: Mean composition of BMS from Holwell and McDonald.....212

Table 8.4: Comparison of mean composition of BMS for Platreef.....214

**Chapter 9: Magmatic Sulphide Melt Inclusions Within Chromites**

Table 9.1: S/Se ratios from Upper Critical Zone and chill margins.....224

Table 9.2: Absolute concentrations of homogenised sulphide inclusions.....231

Table 9.3: Average concentrations of homogenised sulphide inclusions.....232
Table 9.4: Results from analysis of inclusions by Holwell et al (2011).....235
Table 9.5: Average tenor values and ratios for analysed inclusions.....237

# Chapter 1: Introduction

## 1.1 The platinum-group elements

The platinum-group elements (PGE) are often grouped with gold and silver and are termed 'precious' metals. They include the transition elements, ruthenium, rhodium, palladium, osmium, iridium and platinum, which occupy the second and third rows of Group VIII of the periodic table. All of the PGE are metals in pure form. In compounds they show variable oxidation states and display coloured ions and compounds in one, if not all, of these oxidation states (Cotton et al. 1999).

Table 1.1 Selected physical properties of the platinum-group elements (Westland 1981).

| Property | Ru | Rh | Pd | Os | Ir | Pt |
|---|---|---|---|---|---|---|
| Atomic number | 44 | 45 | 46 | 76 | 77 | 78 |
| Atomic weight | 101.07 | 102.94 | 108.42 | 190.23 | 192.22 | 195.08 |
| Density at 20°C *kgm$^{-3}$*10$^{-3}$ | 12.2 | 12.4 | 12.0 | 22.5 | 22.4 | 21.5 |
| Melting point (°C) | 2334 | 1967 | 1555 | 3040 | 2454 | 1768 |
| Boiling point (°C) | 3900 | 3727 | 3140 | 5027 | 4130 | 3827 |
| Hardness (annealed, VHN) | 200-350 | 100-102 | 40-42 | 300-670 | 200-240 | 40-42 |
| Atomic radius (cm$^{-8}$) | 1.336 | 1.342 | 1.373 | 1.350 | 1.355 | 1.385 |
| Oxidation state (common) | +3 | +3 | +2 | +4 | +3 | +2 |
| (highest) | +8 | +6 | +4 | +8 | +6 | +6 |

Various schemes for grouping the PGE have been suggested, principally to account for some of their grouped occurrences in nature. Barnes et al. (1985) saw the metals Os, Ir and Ru as Ir associated (IPGE) and Rh, Pt and Pd as Pt associated (PPGE) without defining any physical property which caused such a discrimination. Authors such as Cabri (1972) grouped the PGE on the basis of their atomic weight or density. They can also be divided into a light triad, (Ru, Rh and Pd) and a heavy triad (Os, Ir and Pt). The light triad elements have densities roughly half that of the heavy triad.

As they are metallic elements, they display all of the physical properties normally expected of metals, namely the formation of alloys, a degree of malleability and ductility and the ability to conduct heat and electricity. Platinum and palladium are relatively soft and ductile. In contrast, ruthenium and osmium are hard and brittle and are therefore of limited industrial use.

Chemically, the PGE show highly siderophile tendencies in the presence of metallic iron and are also mutually soluble in one another. The PGE are relatively unreactive in dilute acids and alkalis, but can be dissolved slowly in concentrated acid, and Pt and Pd, in particular, are more reactive in this sense than the other PGE and are readily dissolved in aqua regia. At elevated temperatures the PGE all react with oxygen to yield volatile oxides and with the

halogens to produce PGE halide compounds such as hexafluorides and chlorides. In addition, and perhaps most importantly in the formation of natural platinum-group minerals (PGM), the PGE will dissolve in molten bases of the P block of the periodic table and form a wide range of sulphides, tellurides, arsenides, bismuthides, antimonides, and selenides.

## 1.2 Historical review of the PGE

Of all the chemical elements, platinum has attracted the active interest of more distinguished scientists than any other since it was first brought to their attention in 1750. Its high melting point and the great difficulties encountered in rendering its invaluable properties available for practical use frustrated people for many years (McDonald and Hunt 1982).

It is very doubtful whether platinum was recognised as a separate body in the early civilisations. Occasional traces of it have been found among artefacts from ancient Egypt, the best known example being the small strip of native platinum set on the surface of a box among many hieroglyphic inscriptions, made of gold on one side and of silver on the other. This originally came from Thebes and is dated to the 7$^{th}$ century BC (McDonald and Hunt 1982).

The pre-Columbian South American natives exploited the natural occurrence of platinum in alluvial sands of various rivers and developed a technique for sintering it with gold on charcoal, to produce artefacts. A pre-Columbian platinum ingot has been found which contains 85 % pure platinum. Although the metal was used by pre-Columbian natives, the first European reference to platinum appears in 1557 in the writings of the Italian humanist Julius Caesar Scaliger as a description of an unknown noble metal first discovered in the Choco district of Columbia ‘which no fire nor any Spanish artifice has yet been able to liquefy’(Weeks 2010).

In 1735 the French and Spanish governments sent a scientific expedition to Peru and Ecuador to measure a degree of meridian at Quito, close to the equator. One of the two naval officers appointed was Don Antonio de Ulloa. When a log of his famous voyage was published in 1748, it contained a description of the metal platinum, which he had seen in Peru, and described it as being neither separable nor calcinable (Weeks 2010). The Spaniards called this white metal ‘platina’, a derogatory diminutive of plata, their word for silver. It was also known as ‘oro blanco’, white gold or ‘juan blanco’. It was considered by the Spanish as a worthless impurity and during the 16$^{th}$ and 17$^{th}$ centuries it was used in

counterfeiting operations, filling the centres of hollowed out gold bars. It was long thought by some that it was a kind of unripe gold that had not been long enough in the ground to mature and to turn yellow (McDonald and Hunt 1982).

Charles Wood, an Assay Master of Jamaica brought the first known sample of platinum to Europe in 1741 and passed a sample by way of William Brownrigg FRS to Sir William Watson FRS who described it to the Royal Society in 1750. Brownrigg presented these specimens to the Royal Society of London. The exhibit included the natural ore, the purified metal, the fused metal and a sword with a pommel made partly of platinum (McDonald and Hunt 1982). A fairly definitive account of platinum was published in 1755 and 1757 by William Lewis FRS (Hartley 1991).

For nearly a century after its discovery, platinum had few uses because of the difficulty of working it. It was not until the experiments of W.H. Wollaston FRS that the working of platinum became easy. He found the spongy platinum becomes malleable when strongly compressed and that it can be annealed and hammered. This process made possible the wide-spread use of the metal for laboratory apparatus (Weeks 2010). Palladium was discovered by Wollaston while he was investigating the refining of platinum. He named it after the recently discovered asteroid Pallas. Rhodium was also discovered in 1803 by Wollaston, who named it rhodium from the Greek *rhodes* (rose) as a consequence of the rose red colour of solutions of its salts. Osmium and iridium were discovered together by Smithson Tennant in 1804 who was working on the material from platina that was insoluble in aqua regia. Iridium was so called from the Greek i*ris* (rainbow) in recognition of the striking variety of the colours of its salts. Osmium is less romantically named after the Greek *osme* (a smell) as a consequence of the characteristic odour of its tetroxide (Hartley 1991).

The last member of the platinum-group metals to be discovered was ruthenium. Although first reported in 1826 by G.W. Osann, it was definitively isolated by K.K. Klaus in 1844. Originally Osann believed he had found three new metals, which he named pluranium, ruthenium and polinium (Weeks 2010). In 1844 however, Klaus showed that Osann's ruthenium oxide was very impure, but it did contain a small amount of a new metal. Klaus took the insoluble residues from the aqua regia treatment of platinum concentrated from a sample from the Urals and ignited them with a potassium nitrate-potash mixture in a silver crucible. After dissolving the melt in water and distilling with aqua regia to remove osmium as its tetroxide, the residue was heated with ammonium chloride to yield ammonium hexachlororuthenate(IV). When this was heated in an inert atmosphere, ruthenium was

isolated. It is named after Ruthenia, the Latin name for Russia, where it was discovered (Hartley 1991).

## 1.3 Uses of PGE

The prices at the time of writing of the PGE are shown in table 1.2.

Table 1.2. Prices of the traded PGE as of the 14th August 2013 (data from Johnson Matthey website).

| | US$ per troy oz |
|---|---|
| **Platinum** | 1492 |
| **Palladium** | 736 |
| **Rhodium** | 1010 |
| **Ruthenium** | 80 |
| **Iridium** | 825 |

The current principal uses for the most industrially important PGE (Pt, Pd and Rh) as stated by Butler (2012) are shown in figure 1.1. The largest use of PGE is for catalytic converters (autocatalysts). Platinum, palladium and rhodium are coated onto a substrate housed in the exhaust system and act as catalysts to reduce levels of carbon monoxide, hydrocarbons and oxides of nitrogen to legalised levels. The second largest area of PGE demand is the jewellery sector. 85 % of platinum jewellery is made and consumed in China, Japan and the USA. Manufacturers have also recently started producing palladium jewellery, making it a significant demand sector. Ruthenium and iridium are also used as constituents in jewellery alloys, and rhodium is used for decorative electroplating. Platinum is a tangible asset which has many attributes of other precious metal investments. The platinum price reached a three-year high in August 2011, but suffered a severe downwards correction in September as investors turned away from risk assets. Since the 2008 global credit crisis there has also been an increase in the amount of palladium purchased for speculative investment as prices recovered. However, in recent months, uncertainty has returned to the market with increasing fears over the national deficit of major nations. Platinum prices hit their highest levels in 5 months in September 2012 as a result of labour-related supply disruptions in South Africa.

The platinum-group elements are also used in a number of industries. In the chemical and petroleum industries, platinum-based catalysts and compounds are used in the manufacture of nitric acid and silicones. Platinum catalysts are used to upgrade low octane petroleum naphtha and to make petrochemical feedstocks for the manufacture of plastics, synthetic rubber and polyester fibres. Palladium is used in hydrocracking while iridium is used with platinum in niche reforming applications. In electronics, palladium-containing components are used as multi-layer ceramic (chip) capacitors, conductive tracks in hybrid

integrated circuits and for plating connectors and lead frames. Platinum is also used to improve the data storage capacity of hard disks. In health and medicine platinum, palladium and small amounts of ruthenium and/or iridium are used to produce alloys for dental restorations and crowns when mixed with gold, silver, copper and zinc. In certain chemical forms, platinum inhibits the division of living cells resulting in the development of platinum-based drugs to treat cancer. Pacemakers and internal defibrillators used for cardiac conditions also contain Pt and Ir electrodes.

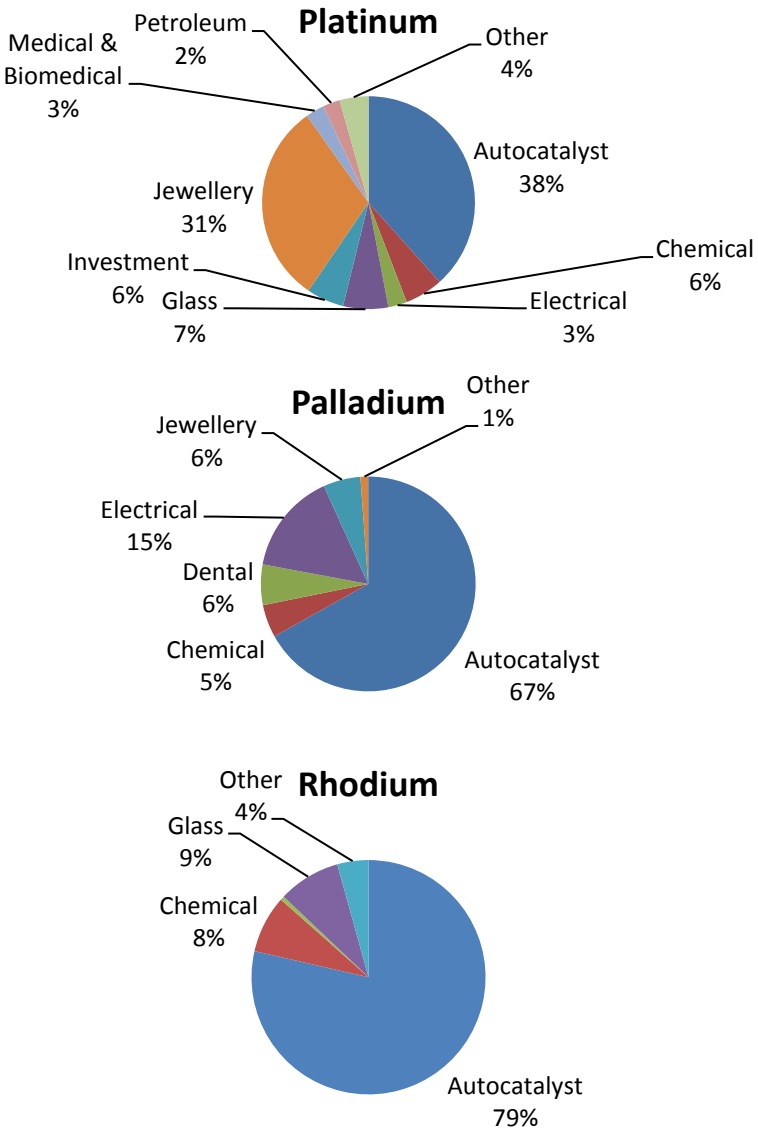


Figure 1.1. Demand by application of Pt, Pd and Rh for 2011 (data from Butler 2012). N.B. Not included in this chart is the negative demand for palladium in the investment industry that resulted from deep sell-off due to elevated prices in 2011.

## 1.4 Economic occurrences of PGE

The platinum-group metals are amongst the 90 or so elements that comprise less than 2 % by weight of the Earth's crust. The relative abundances of the PGE in the Earth's crust are shown in table 1.3.

Table 1.3 Relative abundances of PGE in the Earth's crust according to Rudnick and Gao (2003) with C1 chondrite abundances from Lodders (2003).

| PGE | Crustal abundance (ppb) | C1 Chondrite abundance (ppm) |
|---|---|---|
| **Ru** | 0.34 | 0.692 |
| **Rh** | 0.03 | 0.141 |
| **Pd** | 0.52 | 0.588 |
| **Os** | 0.03 | 0.486 |
| **Ir** | 0.02 | 0.470 |
| **Pt** | 0.50 | 1.004 |

The PGE are thought to be concentrated in the mantle at chondritic proportions, reflecting the Earth's early evolution by accretion from chondritic meteorites. Concentration from these mantle proportions is thought to occur through partial melting, whereby PGE are preferentially removed to the melt, before further concentration via a 'carrier phase' in the crystallising magma chamber (e.g. Mungall and Naldrett 2008).

Deposits associated with magmatic sulphides, whereby platinum-group elements are collected by immiscible sulphide liquids following the separation of a sulphide melt from a silicate magma, make up some of the largest and most economically important resources of platinum-group elements (PGE) worldwide (Naldrett 2004). The largest deposits in terms of PGE content are the Bushveld Complex in South Africa, the Great Dyke in Zimbabwe and the Stillwater Complex in Montana, USA which account for more than 90 % of the world's resources of PGE. The PGE, and in particular Pd, are also significant by-products in large magmatic Ni-Cu sulphide deposits, the most significant of which are the Noril'sk deposit in Siberia, Russia and the Sudbury Igneous Complex in Canada. Further details about different massive sulphide deposits will be discussed in chapter 4.

## 1.5 Outline of study

This thesis can be split into 3 sections. The first four chapters are produced to summarise the existing knowledge of the study area, covering the regional and local geology as well as reviewing the published models for Ni-Cu-PGE deposits and the Platreef. Chapter 2 contains a review of the regional geology of the Bushveld Complex while chapter 3 contains a more detailed review of the northern limb and the Platreef. Chapter 4 summarises the processes involved in the formation of magmatic sulphide deposits.

The next 5 chapters comprise 5 different studies involving the chromitite samples. Chapter 5 describes the geochemistry of the Platreef chromitite samples and compares the data to other Bushveld lithologies. Chapter 6 contains the SEM mineral study conducted on chromites throughout the study area, in particular the differences in the chromite mineralogy depending on the host rock. Chapter 7 examines the PGM occurrences throughout the chromitite samples and how they differ spatially across the study area. Chapter 8 investigates the PGE concentration of the base metal sulphides and how they account for overall concentration of PGE in the Platreef. Chapter 9 examines the magmatic sulphide inclusions within the chromites and the use of S/Se ratios to deduce the source of sulphur in the Platreef.

The final section comprises of chapter 10 and is final summary which draws on the conclusions of the previous chapters in addition to combining the data to produce a genetic model for the formation of the Platreef. In addition, this chapter contains recommendations for future research.

# Chapter 2: Regional Geology

## 2.1 The Bushveld Complex

The Bushveld Complex is the world's largest layered igneous intrusion, located in the north-eastern part of South Africa (fig. 2.1). It is comprised of a succession of 7-8 km thick mafic and ultramafic cumulates that extend 450 km east-west and 250 km north-south, covering an area of approximately 65,000 km$^2$ (Eales and Cawthorn 1996). Despite its age, it is extremely well preserved, having undergone minimal structural disturbance or metamorphism after its solidification (Cawthorn et al. 2002b).

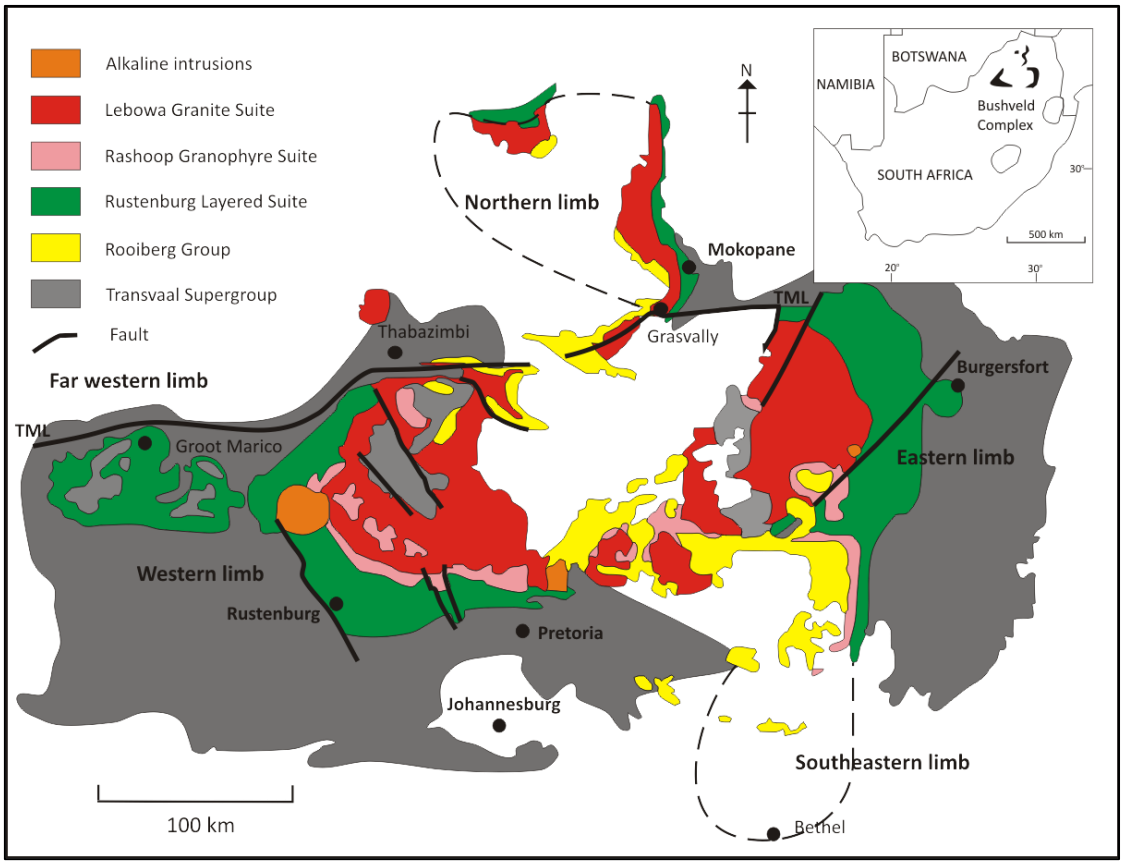


Figure 2.1. Simplified geological map of the Bushveld Complex (modified from Kinnaird et al. 2005)

The Bushveld Complex contains 75 % of the world's resources of Pt, 52 % of Pd, 82 % of Rh and 16 % of Ni (Naldrett 2004). These metals are concentrated in three principal stratigraphic units, the UG-2 chromitite, the Merensky Reef and the Platreef. The Bushveld Complex is not only the largest and most extensively studied of the known layered intrusions, it is also the richest in terms of mineral deposits. In addition to the deposits of platinum-group minerals, Ni-Cu sulphide, titanifeous and vanadiferous magnetite associated with the mafic and ultramafic layered rocks, and endogenetic and exogenetic deposits of tin and fluorite associated with the granitic rocks are all found in the Bushveld Complex. South

Africa is also the world's leading producer of chromium. This is mined from chromitite layers that are characteristic of the Critical Zone of the Bushveld Complex as well as from massive chromitite bodies in the Lower Zone at Grasvally in the northern Bushveld (Misra 2000).

### 2.1.1 Structural history

The Bushveld Complex is located within the Kaapvaal Craton and was intruded around 2.05 Ga. Table 2.1 shows the ages of different Bushveld Complex rocks. Olsson et al. (2010) presented a 2057.7 Ma U-Pb baddeleyite age for a noritic intrusion of the Marginal Zone of the Rustenburg Layered Suite (RLS). The Marginal Zone only occurs along the base of the intrusion, onlapped by a subsequently deposited cumulate stratigraphy (Cawthorn et al. 2006). The upper intercept age of 2057.7 Ma is the first published U-Pb baddeleyite age for the Bushveld. According to the compilation of geochronological data by Scoates and Friedman (2008), the duration of the Bushveld-related magmatism occurred over a period of 5 Myr, whereas Cawthorn and Walraven (1998) suggested that the entire RLS was emplaced in only 75,000 years or less. Their calculation is based on thermal modelling of emplacement of a series of successive injections of magma closely spaced in time so that the previous magma had not cooled and differentiated significantly before the next was emplaced. The U-Pb result of the 2057.7 Ma Marginal Zone does not solve the problem of the duration of magma emplacement, but constrains the timing of initial emplacement of the RLS.

Table 2.1. Ages of the different Bushveld rocks using U/Pb dating. References: (1) (Scoates and Friedman 2008); (2) (Olsson et al. 2010); (3) (Harmer and Armstrong 2000); (4) (Scoates et al. 2012); (5) (Robb et al. 2000); (6) (Dorland et al. 2006).

| Unit | Age (Ma) | Error (Ma) | Reference |
|---|---|---|---|
| **RLS (Critical Zone)** | 2054.4 | 1.3 | (1) |
| **RLS (Marginal Zone)** | 2057.7 | 1.6 | (2) |
| **Raashop Granophyre** | 2055.7 | 1.0 | (4) |
| **Steelport Granite** | 2057.5 | 4.2 | (3) |
| **Nebo Granite** | 2054.2 | 0.8 | (4) |
| **Makhutso Granite** | 2053.4 | 3.9 | (3) |
| **Lebowa Granite** | 1957.0 | 15 | (5) |
| **Nylstroom Subgroup (Waterberg)** | 2054.0 | 4.0 | (6) |

The Waterberg Group comprises a series of virtually undeformed and unmetamorphosed red bed successions that rest unconformably on a wide range of Archaean and early Proterozoic rocks of the Kaapvaal craton, including the Bushveld Complex. SHRIMP $^{207}Pb/^{206}Pb$ zircon ages of 2054 Ma were obtained for the porphyritic lavas near the base of the Nylstroom Subgroup (Dorland et al. 2006). This suggests that the deposition of the Waterberg Group started very soon after the emplacement of the Bushveld Complex.

The Kaapvaal Craton comprises of a jigsaw of crustal blocks that amalgamated between 3.7 and 2.6 Ga , which have been subdivided into two periods by de Wit et al. (1992). The first period from 3.7 Ga to 3.1 Ga records the initial separation of continental lithosphere of the craton from the mantle, termed the Kaapvaal Shield formation. This occurs through interoceanic obduction and amalgamation followed by within-shield melting, granite formation and chemical differentiation of the upper lithosphere to create the Kaapvaal Shield (fig. 2.2). The second period, from 3.1 to 2.6 Ga, known as the Kaapvaal Craton formation, has been defined by Silver et al. (2004) using mantle fabrics revealed by seismic anistropy. This period involves 500 million years of inter- and intra- continental tectonics starting with an unknown orogen imparting a mantle fabric on the Zimbabwe Craton pre-2.9 Ga (fig. 2.2 a). Around 2.9 Ga, the Pietersburg and Kimberley blocks collided with the Kaapvaal Shield (Schmitz et al. 2004), which imparted an arc-like mantle fabric, and formed the Thabazimbi-Murchison Lineament (TML; fig. 2.2 b). During the Limpopo orogen at 2.6-2.7 Ga, the Limpopo Belt formed between the Kaapvaal and Zimbabwe cratons. During this time, the Great Dyke and Ventersdorp Supergroup were intruded (fig. 2.2 c). At around 2.0 Ga, during the Magondi orogen (fig. 2.2 d), shear zones in the Limpopo Belt were reactivated and the Bushveld Complex was emplaced along the axis of the TML. Finally, the 1.8-1.9 Ga Kheis orogen produced the Soutpansberg trough (fig. 2.2 e).

The Thabazimbi-Murchison Lineament (TML) defines the northern margin of the western Bushveld Complex and separates the eastern and northern lobes (fig. 2.1). This structure has been subjected to repeated reactivation, with the earliest record of deformation at about 2.7 Ga (Good and De Wit 1997). The TML is a 500 km long, 25 km wide, ENE-WSW trending deformation belt, reactivated as a fault (McCourt and Vearncombe 1987). The structure remains active to the present day and is associated with active hot springs and relatively recent hydrothermal Pt mineralisation (Armitage et al. 2007). According to Good and De Wit (1997) and Silver et al. (2004) the TML represents a fundamental crustal, and probably deep, lithospheric-mantle break within the Kaapvaal Craton as it delineates a major cratonic subterranean boundary. It is important to emphasise that the crust and associated subcontinental lithospheric mantle on either side of the TML had already formed and shared no common history prior to juxtaposition (Silver et al. 2004). According to McDonald and Holwell (2011) it is therefore very possible that the Bushveld thermal event involved melting of different types of mantle and crust, north and south of the TML. The degree to which these magmas were homogenised or remained separated is poorly understood.

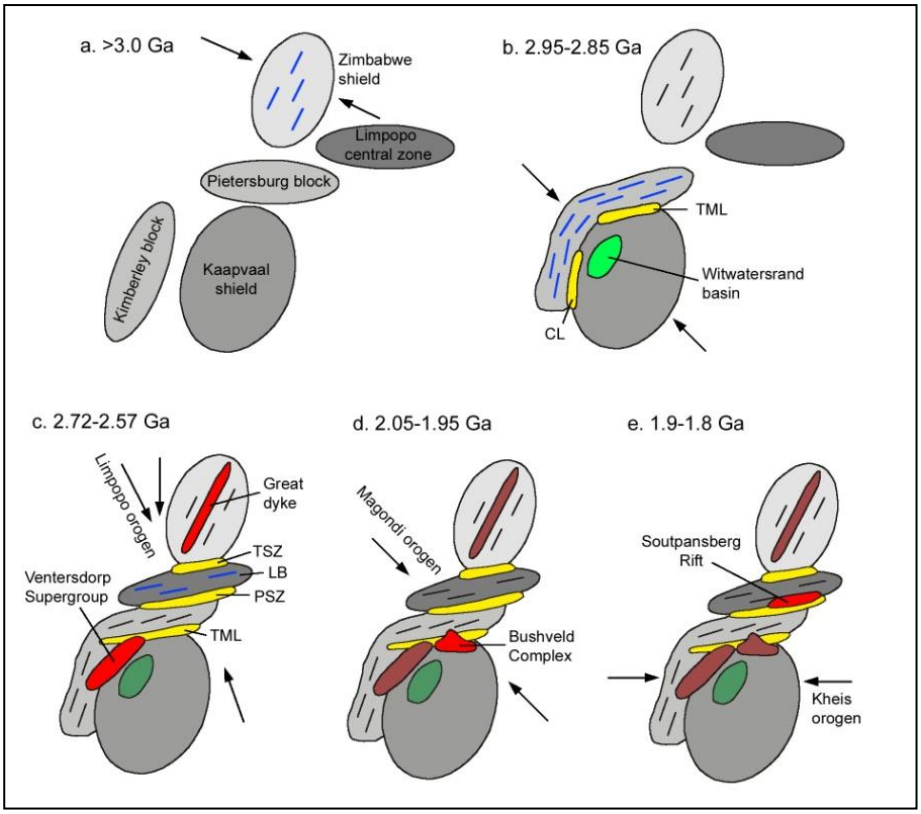


Figure 2.2. Schematic showing tectomagmatic evolution of the Kaapvaal Craton. Key: TML – Thabazimbi-Murchison Lineament, CL – Colesberg Lineament, PSZ – Palala Shear Zone, TSZ – Triangle Shear Zone, LB – Limpopo Belt. Redrawn from Holwell (2006) from Silver et al. (2004) .

### 2.1.2 Stratigraphy

According to South African stratigraphic literature the Bushveld Complex comprises of three stratigraphic units (SACS 1980):

1. The ultramafic to mafic layered rocks known as the Rustenburg Layered Suite (RLS);

2. The granophyres and granites (Lebowa Granite Suite) overlying the RLS; and

3. A suite of ultramafic to mafic sills which underlie the RLS and intrude into the country rock sediments.

RLS lithologies range between the extremes of dunite and pyroxenite to anorthosite and pure oxide layers, with almost all conceivable intermediate varieties. Layering is present at all vertical scales from millimetres to hundreds of metres and is very continuous laterally (Eales and Cawthorn 1996).

The emplacement of the Bushveld Complex in the south was close to the unconformity between the sedimentary country rocks and the Rooiberg Group volcanics (Cheney and Twist 1991). The country rocks in most parts of the Complex consist mainly of quartzites, argillites and dolomites of the Transvaal Supergroup, in particular the 2.1-2.3 Ga Pretoria

Group, although parts of the Complex lie directly on Archaean granitoids and greenstones. Emplacement was concordant to the sedimentary layers in the western limb and discordant in the eastern and northern limbs (White 1994), such that in the north the intrusion transgresses the Transvaal Supergroup rocks northwards from the TML and rests on a footwall of Archaean granites and gneisses. Until recently, the Rooiberg Group was considered to be the uppermost constituent of the Transvaal Supergroup, however age dating has shown it to be similar in age to the RLS, 2057.3 ± 3.8 Ma (Harmer and Armstrong 2000). As a result it is considered to represent the initial volcanic phase of the Bushveld Complex rather than the terminal stages of the Transvaal Supergroup (Hatton and Schweitzer 1995).The Rooiberg Group forms part of the roof of the Bushveld Complex where the majority of RLS is intruded, however there are parts of the Rooiberg succession (Dullstroom lavas) that lie beneath the RLS in the eastern Bushveld (Schweitzer et al. 1995).

Spatially the Bushveld Complex is divided into five limbs; roughly symmetrical eastern and western limbs, a southern (Bethel) limb that is covered by younger sediments which has been sampled by drilling, a largely eroded far western limb, and a northern limb. The RLS crops out in four of these limbs. It is in the RLS that the giant deposits of PGE, chromium and vanadium are hosted. The world class PGE deposits of the UG2 chromitite and Merensky Reef are located in the eastern and western limb with the Platreef being located in the northern limb.

The RLS is typically composed of ~ 8 km thickness of magmatic rocks (Cawthorn et al. 2006). Traditionally, the RLS in the western and eastern limbs is divided into five zones, as originally defined by Hall (1932):

- Lower Zone (LZ) - composed mainly of orthopyroxenites, harzburgites and minor dunites;
- Critical Zone (CZ) - comprised of cyclical units of chromitite-orthopyroxenites in the lower CZ and chromitite-orthopyroxenite-norite-anorthosite in the upper CZ;
- Main Zone (MZ) - composed of more massive norites, gabbronorites and anorthosites;
- Upper Zone (UZ) - composed of differentiated Fe-rich gabbros, anorthosites and magnetites; and
- Marginal Zone - composed of fine-grained rocks between the country rock and the more coarse grained layered rocks of the rest of the RLS in addition to contact rocks and sills that penetrate into the country rock. The contact zone is thickest (up to

400 m) at the base of the Lower Zone and thinnest at the contact with the Main Zone (10 m) (Barnes et al. 2010).

Early studies by Sharpe (1981), Harmer and Sharpe (1985) and Sharpe and Hulbert (1985) divided the marginal rocks into three groups based in part on their stratigraphic position and in part on their composition. Norites with quenched textures in contact with the Lower Zone and Lower Critical Zone are referred to as the B1 (Bushveld) magma. Ultramafic sills that are present in the country rock to the Lower Zone are referred to as B1 UM. These orthocumulate rocks consist of a mixture of B1 liquid and cumulate olivine and chromite and have been interpreted to result from crystal slurries being injected into the country rock from the Lower Zone during synmagmatic tectonism (Davies and Tredoux 1985; Sharpe and Hulbert 1985). Gabbronorites that are in contact with the Upper Critical Zone are referred to as the Bushveld 2 (B2) magma and those in that are in contact with the Main Zone have been termed Bushveld 3 (B3) magma.

Hall (1932) noted similarities between the eastern and western limbs, which include the correlation of marker horizons such as the Merensky Reef chromitites. This led him to propose that these two limbs were originally connected. The form of the intrusion remains controversial. Whereas some authors have suggested that the various limbs represent disconnected, deep and narrow bodies (Sharpe 1981; Hatton and Schweitzer 1995) or steeply dipping conical intrusions (Meyer and De Beer 1987), other workers have described the Bushveld Complex as a giant lopolith (e.g. Hall 1932; Cawthorn and Walraven 1998; Webb et al. 2004). Mayer and De Beer (1987) questioned Hall's (1932) model and stated that the absence of a positive gravity anomaly between the two limbs suggested that the two limbs were in fact two discrete, inwardly-dipping sheets. Cawthorn and Webb (2001) however, showed that a mass of magma such as that in the Bushveld Complex would have caused isostatic subsidence, cancelling out the expected gravity anomaly. This led the authors to favour the original interpretation of Hall (1932), that the eastern and western limbs of the complex formed as a single lopolithic intrusion, that has been subsequently downwarped and is connected at depth. This latter viewpoint is supported by Kruger (2005a), who likened the intrusion to a flat-bottomed soup-dish, successively filled by influxes of distinct magmas. A lopolithic form is consistent with the striking lateral coherency of portions of the igneous stratigraphy e.g. the UG1 unit and its footwall stringers, which are reproduced in outcrops of the RLS that are separated by hundreds of kilometres.

### 2.1.3 Emplacement and magma source

Despite all the data that is available for the Bushveld Complex, there has been no agreement on several of the key aspects relating to the nature, volume and source of the different magma types and the overall tectonic setting for magmatism.

One of the earliest theories was described by Mills Davies (1925), who suggested the Bushveld Complex was formed by "an active molten rock magma of common or normal composition deep down in the Central Transvaal area and its gradual advance upwards through thousands of feet of strata until it emerged through devious ways through quartzites and shales of the Pretoria Group and... spread out like a colossal cake". Wagner (1929) referred to its lopolithic or great basin-shaped sheet nature stating it was probable that the intrusion was intruded into horizontal strata that later subsided due to the load of the overlying igneous rocks. He did not suggest a mechanism for the intrusion. However, Cousins (1959) suggested that the Bushveld Complex was a series of disconnected lopoliths.

Structural data has shown that floor contacts become shallower with depth in the eastern and western lobes of the Bushveld Complex i.e. steepest floor dips are noted at the surface and become shallower towards the centre of the Complex (e.g. Kruger 2005a). This implies that the Bushveld is a lopolith, continuous at depth. However, numerous workers (e.g. Cousins 1959) have interpreted the varying floor rock structural data to be indicative of separate intrusions each characterised by their own lopolithic geometries. Clarke et al. (2009) stated that although this may be true in some cases, such as adjacent to updomed floor sections, it is not applicable for the RLS as a whole.

Some of the earliest proposals for the mechanism of formation of the Bushveld include the rapid decompression melting at the leading edge of a mantle plume, triggered by the impact of a large (20 km) iron bolide (e.g. Rhodes 1975). Evidence presented for an initial catastrophe comes from the interpretation that high-energy, high-temperature debris flows are present at the base of the Rooiberg Group and from intense deformation occurring at the end of the Transvaal sedimentation. Buchanan and Reimold (1998) have strongly questioned this evidence.

In a detailed study of the geochemistry of the Rooiberg Group, Buchanan et al. (2002) noted that none of the Rooiberg Group rocks represent true crustal melts and that the upward stratigraphic trend in the Rooiberg Group is towards more silicic compositions. Hatton (1995) interpreted these features as being indicative of a mantle plume generation. The enormous volumes of magma involved in the formation of the Bushveld large igneous

province suggest that optimum conditions for such an event involved the interaction between a mantle plume with lithosphere that had been thinned to between 100 and 50 km (Gibson and Stevens 1998). Hatton (1995) envisaged a hot Lower Zone magma derived from a mantle diapir which halted in the lower crust, flattened, melted the lower crust and formed the lower Critical Zone magma. Hatton (1995) considered the Bushveld Complex to be the intrusive equivalent of a continental flood basalt province, with the magma sourced from a mantle plume that impinged through the base of the crust. Calculations using MgO and $SiO_2$ contents suggest that melting took place between 18 and 40 km. Hatton (1995) therefore suggested that the only way to achieve melting at such depths in an intracratonic setting would be for a sufficiently buoyant mantle plume to penetrate the bottom of the crust. Cawthorn et al. (2002b) however stated that this was unlikely, and that using MgO and $SiO_2$ contents could not be used to infer depth of melting due to the possible effects of contamination and fractionation. In addition, they noted that mantle xenoliths in kimberlites that penetrate the Bushveld Complex are 3 Ga (i.e. older than the Complex) and suggested that it would have been impossible for these to be preserved if a mantle plume had penetrated the sub-continental lithospheric mantle (SCLM). Cawthorn et al. (2002b) therefore concluded that melting took place at a much greater depth in the asthenosphere and it was magma, rather than a plume, that invaded the lithospheric upper mantle.

In southern Africa, most peridotite xenoliths extracted from on-craton kimberlites give Archaean Re-depletion model ages, and show no clear trend in age versus depth of origin (at least to depths of 180–200 km; Carlson et al. 1999). Therefore most of the upper 180–200 km of the Kaapvaal Craton mantle root formed in the Archaean and has been attached to the overlying crust since that time. This is also true of the mantle beneath the Limpopo belt, as indicated by Archaean ages for xenoliths from the Venetia kimberlite, but not for the area beneath the 2.05 Ga Bushveld Complex (Eales and Cawthorn 1996). Many of the mantle xenoliths from the Premier kimberlite, which penetrate the Bushveld Complex, give ca. 2 Ga ages suggesting substantial modification of the mantle during the same time period as the intrusion of the Bushveld Complex took place (Carlson et al. 1999).

In addition, evidence of later Proterozoic to Cretaceous diamondiferous kimberlites, which contain a 3.1 Ga diamond population (Richardson et al. 1984; Shirley et al. 2003) indicates that a lithospheric root in excess of 140 km must have existed beneath the Craton in the Archaean and that it survived the Bushveld event (Gibson and Stevens 1998). They envisage a model for the Bushveld magmatothermal event in which a hot juvenile plume reached the

base of the Kaapvaal lithosphere at ca. 2.06 Ga, leading to partial melting within the plume head and in the asthenosphere beneath thinned regions of the lithosphere. Once these mantle melts formed, they rose to levels immediately below, or within, the crust where partial fractional crystallisation occurred. The heat released from these magmas resulted in an elevated crustal geotherm to values approaching 40-50 $^{o}C\ km^{-1}$, and regional metamorphism of the adjacent crust. Crustal anatectic magmas rose to form the felsic volcanic succession of the Rooiberg Group and shallow level intrusions of the Rashoop Granophyre and Lebowa granite suite. At the same time, partially fractioned and contaminated mafic magmas were remobilised and rose to intrude shallow crustal levels as the RLS and its extensions of the Molopo Farms complex to the west, the Uitkomst Complex to the east and potentially other satellite intrusions. Clarke et al. (2010) highlighted that the mantle plume evidence seemingly spans from the time of the Pretoria Group formation to post-Pretoria extensional tectonics to the geochemistry of the Rooiberg and Bushveld magmas, thus covering an enormous geological time span. However, Bryan and Ernst (2008) stated that on average, mantle plume events last up to 60 Myr and so counteract this statement.

Before the syn-Bushveld collisional ages from the Limpopo belt (Holzer et al. 1998) were known, Harmer and Von Gruenewaldt (1991) suggested that the persistent subduction zone signature in the magmatic rocks of the Transvaal Supergroup and the Bushveld Complex was due to earlier processes that acted on the Kaapvaal Craton lithosphere. Hatton and Sharpe (1989) interpreted the low Ti/Zr ratio of the marginal Bushveld rocks (most likely to be closest in composition to the parental magma), as well as the boninite-like LILE enrichment, to have been the result of the contamination of the Bushveld magmas by a significant upper crustal source, and ruled out crustal assimilation during magma ascent as the origin. They considered that the upper crustal component was added to the SCLM through the subduction of sediment. In support of this model, Willmore et al. (2002) noted that anomalous enrichment of the Bushveld Complex in chlorine, coupled with the boninitic affinity of the Bushveld magmas, is suggestive of formation in a subduction-related setting. Buchanan et al. (2002) noted that the upward trend in the Rooiberg Group towards more silicic composition could be consistent with generation in a subduction zone rather than being interpreted to be plume related. This interpretation supports the work of Harmer and von Gruenewaldt (1991), who examined volcanic rocks associated with the Transvaal basin (including the Rooiberg Group), as well as the intrusive rocks of the RLS. They noted that the calc–alkaline, andesitic nature of volcanic horizons within the Pretoria Group and the mafic

base of the Rooiberg Group are in contrast with most other continental volcanic provinces, which tend to be basaltic. Furthermore, they noted that the boninitic affinity of the marginal rocks of the Bushveld Complex and trace element patterns in the volcanic rocks are consistent with a subduction origin. Kruger (2002) also suggested a back-arc, subduction-related setting for magmatism.

Emplacement of the Bushveld Complex may have been controlled by the TML and other fault zones, such as the Crocodile River fault. Maier and Eales (1997) suggested that these fault systems were already active during Bushveld emplacement. This is indicated by thinning of cumulate zones in the Brits graben. Other evidence to support this theory is possible Bushveld -aged upgrading of iron mineralisation along the northern extension of the Crocodile River fault at Thabazimbi (Maier and Groves 2011).

Gibson and Stevens (1998) suggested that during the Bushveld event, the Kaapvaal Craton experienced extensional and strike-slip reactivation of Archaean structures, consistent with a NE-SW directed extension. They stated that the lack of significant pre-Bushveld deformation of the Transvaal Supergroup, together with their preservation over large parts of the Kaapvaal Craton, indicates a lack of significant erosional exhumation which is a normal consequence of crustal thickening. The occurrence of A-type granites, which are generally associated with crustal extension, is consistent with this hypothesis. The preservation of the volcanic and shallow-level intrusive rocks of the Bushveld Complex indicates that a significant magmatic thickening related to the Bushveld event must have been compensated for by associated crustal thinning. However, work carried out by Alexandre et al. (2006) has shown that the central parts of the Kaapvaal Craton experienced a regional low-grade metamorphism synchronous with brittle-ductile deformation at 2.04 Ga that predates the intrusion of Bushveld Igneous Complex.

The whole of the RLS is enriched in Si, K and Rb relative to many mafic magmas and $^{87}Sr/^{86}Sr$ and Re-Os isotopes are too radiogenic for a purely mantle-derivation of the magmas. This suggests that the source magma was highly enriched or there was contamination of the magmas by large amounts of middle to lower crustal material in a staging chamber beneath the Bushveld Complex (e.g. McCandless et al. 1999; Barnes and Maier 2002b; Ashwal et al. 2005; Harris et al. 2005). McCandless et al. (1999) suggested assimilation of 5 % granulitic lower crust to account for the Re-Os radiogenic values although Nd isotope data (Maier et al. 2000) suggested that there may be a significant component of upper crustal source,

especially for the Main Zone with little evidence that the lower crust contributed to the Bushveld magmas.

Numerous authors (e.g. Harmer and Sharpe 1985; Curl 2001) have shown that the parental magma to the Bushveld Complex had a pronounced and homogenous crustal component. This has led to two contrasting models. The first model suggests that significant (up to 30 %) contamination of asthenospheric mantle melts took place during ascent through the crust, in staging chambers to the intrusion proper (e.g. Maier et al. 2000). This model is consistent with the strong crustal oxygen isotope signature of the Bushveld cumulates that cannot be explained by any known mantle source (Harris et al. 2005). The contrasting model suggests magma generation in metasomatised and therefore relatively fusible portions of the SCLM (Harmer and Sharpe 1985; Lambert and Simmons 1987). This model is usually only applied to small degree mantle melts such as kimberlites (Smith 1983) but it has been argued that larger degree partial melts may form when a mantle plume heats the base of the SCLM, and/or from melting more pervasively metasomatised SCLM sections. Begg et al. (2009) interpreted seismic tomography data to show that the Kalahari Craton (which hosts both the Bushveld Complex and the Great Dyke) is amongst the most metasomatised major cratons in Africa. Maier and Barnes (2004) attempted to use PGE data to constrain the mantle source of the basalts. They suggested that relatively high Pt/Pd ratios (>1) observed in many alkali basalts and in the Bushveld magmas reflect a signature of SCLM derived melts. The available database on PGE contents in Kaapvaal mantle xenoliths suggests that the Kaapvaal SCLM has high Pt/Pd, similar to the Bushveld magmas, but it is relatively poor in both elements (av. 4 ppb Pt and 2 ppb Pd; Maier et al. 2012). It may seem contradictory that one of the world's most PGE enriched systems formed from a mantle source that was significantly depleted in Pt and Pd relative to the primitive upper mantle (PUM), but 25 % melting of a source with 4 ppb Pt and 2 ppb Pd produces a magma with 16 ppb Pt and 8 ppb Pd, not too dissimilar to the PGE content of the inferred Bushveld parental magmas provided that the Pt and Pd are in a form that can be easily melted (Maier and Barnes 2009).

The most accepted idea is that the Bushveld Complex was emplaced as a sill-like intrusion. Palaeomagnetic investigations have demonstrated that the layering in the Complex was essentially horizontal when the sequence cooled through the Curie Point (Hattingh 1995). This indicates that any dip variations must be attributed to post-emplacement processes, such as subsidence.

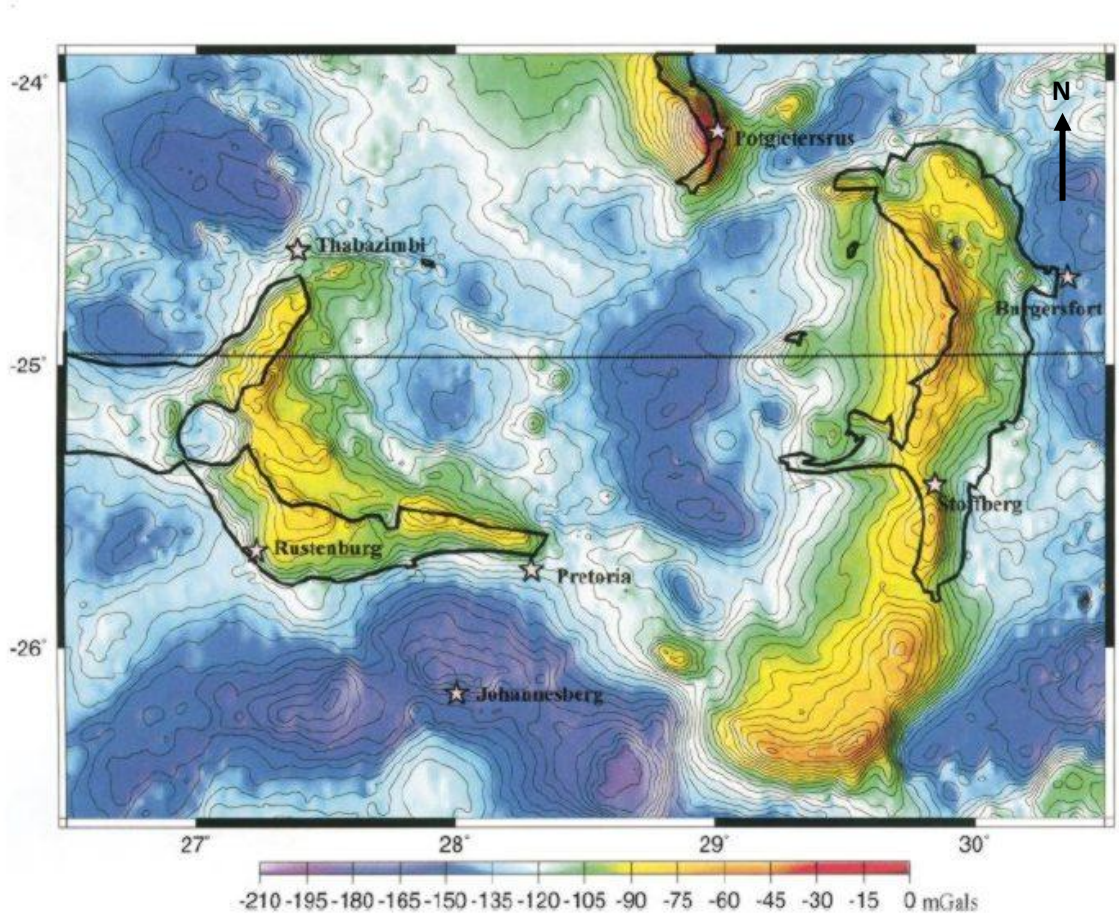


Figure 2.3. Gravity map of the Bushveld Complex. The outline of the outcropping mafic rocks is shown (modified after Cawthorn and Webb 2001).

No feeder systems have been positively identified in the Bushveld Complex but several have been inferred on the basis of positive gravity anomalies (Kinloch 1982). However, du Plessis and Kleywegt (1987) have noted that in the eastern and western Bushveld, the anomalies coincide with the upper contact of the Upper Zone where the thickness of the mafic rocks is greatest, and so a positive anomaly would be expected. As a result these anomalies are unlikely to represent feeders. The strongest gravity anomaly in the Complex is located on the northern limb, just to the west of Mokopane, and does not correspond with an area of thickest mafic sequence. Van der Merwe (1976) interpreted this as a feeder vent, and also found no evidence of any physical link between the northern and eastern limbs of the Complex on the basis of gravity data. The Mokopane anomaly is shown on a gravity map (fig. 2.3) published by Cawthorn and Webb (2001), but only less convincing anomalies in the eastern and western limbs are discussed in the paper.

Cawthorn et al. (2002b) proposed that the emplacement of the Complex were due to linear feeder zones and considered the Steelpoort Fault to be a likely feeder zone. Either side of this lineament, differences in stratigraphic thickness of individual units of the Lower and

Critical Zone have been identified. Cawthorn et al. (2002b) have explained this difference by proposing that magma flowing to the north and south of the feeder would have produced different depths of magma leading to the difference in stratigraphic thickness observed. It has also been stated by these authors that they believe that the Steelpoort Fault was unlikely to be the only feeder and that many of the large faults that separate compartments of the Complex may have acted as feeders. An alternative view was presented by Kruger (2005a) who considered the TML to be a likely feeder zone, with magmas ascending along the deep-seated shear zones until a critical point was reached in the crust where the magmatic pressure equalled lithostatic pressure and triggered the sill-like intrusion of the Complex.

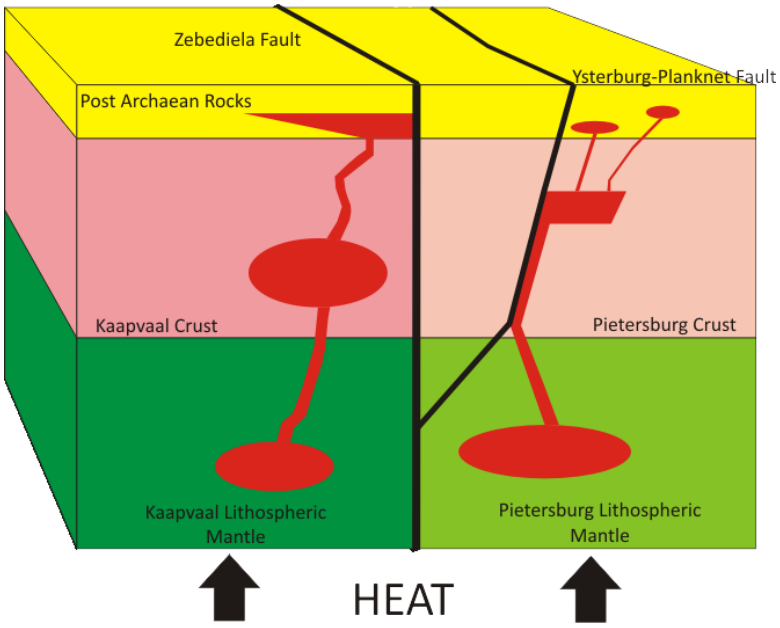


Figure 2.4. Schematic figure showing the difference in the crust north and south of the TML as proposed by McDonald et al. (2005; 2009)

Due to the presence of the TML, crust to the south of it belongs to the Kaapvaal Shield, whereas crust to the north belongs to the Pietersburg block (fig. 2.4). As a result, the crusts, and crucially for magma genesis, the sub continental lithospheric mantle on either side of the TML are fundamentally different (Silver et al. 2004). As the Bushveld Complex straddles the TML, magmas in the northern limb may have been generated from compositionally distinct mantle from that of the rest of the Complex. The compositional differences in Bushveld and Archaean basement rocks across the TML has been highlighted by McDonald et al. (2005; 2009).

## 2.2 The Northern Limb

Based on gravity surveys by van der Merwe (1976), the northern limb is inferred to be triangular in shape. It crops out as a slightly sinuous N-S striking, WSW-dipping body around 100 km in length and up to 15 km wide, which makes up the eastern edge of this triangle (fig. 2.1). To the north, the northern limb is covered by younger Waterberg sediment whereas to the south the Karoo sediments are juxtaposed against the layered mafic rocks and the Zebediela and Ysterberg-Planknek faults, which are part of the TML. These separate the northern limb of the Bushveld Complex from the rest of the Bushveld Complex.

### 2.2.1 Structural setting of the northern limb

The entire sequence of the northern limb is disturbed by a number of faults which strike roughly northwest and have a vertical or near-vertical dip. The trend of these faults is consistent with a NE–SW trend which was formed during pre-Bushveld deformation (Friese 2004; Nex 2005). In the south, the northern limb is cut by the Zebediela and Ysterberg-Plankneck faults (Good and De Wit 1997). It is these structural features in the underlying rocks that have influenced the sinuous outcrop of the northern limb (van der Merwe 1976).

A detailed structural investigation of the northern limb was carried out by Friese (2004) who interpreted the following set of structures that are listed from oldest to youngest:

(i) Shallow, NW dipping, SE verging thrusts and associated ENE trending, sub-horizontal, low-amplitude regional folds within the Archaean basement.

(ii) NW to WNW trending, moderate to steeply dipping extensional faults within the Transvaal Supergroup. These were formed by reactivation of the structures that are similarly orientated formed in the Archaean basement during the Murchison Orogeny that formed the TML.

(iii) ENE to NNE trending, steep to subvertical, mainly SE dipping, dextral strike slip shear zones with associated NE verging, layer-parallel thrusts. This system developed in the Transvaal Supergroup by reactivation of the upper section of a Neoarchaean sinistral strike slip system.

(iv) N-S striking, moderately west dipping extensional faults with imbricate, normal dip slip and sinistral strike slip duplexes in their immediate hangingwall.

(v) NW dipping, SE verging thrusts and associated ENE trending, sub-horizontal, low amplitude regional folds of pre- to syn-RLS age. These were formed by mild SE directed

stress within the northern Kaapvaal Craton at an early stage of the Magondi Orogeny at ~2.1 Ga.

(vi) WNW to WSW trending extensional fractures and joints with minor displacement that cut all other structural features.

In addition to the regional structural studies, local studies have been carried out (e.g. Armitage 2011) which focus on the relationship of the footwall rocks with the Platreef and will be discussed further in the next chapter.

### 2.2.2 Age of northern limb

Until recently very little has been done to determine the age of the northern limb, partly due to the assumption that it formed at the same time as the rest of the Bushveld Complex, where most of the dating work has been done. Table 2.2 shows some ages that have been determined in the northern limb.

Table 2.2. Northern limb ages. References: (1) (Kinnaird et al. 2010); (2) (Hutchinson et al. 2004); (3) (Scoates and Friedman 2008); (4) (Ruiz et al. 2004); (5) (Reisberg et al. 2006); (6) (Pronost et al. 2008)

| | Age | Error | Method | Reference |
|---|---|---|---|---|
| **Platreef zircons** | **2056.7** | 4.4 | SHRIMP | (1) |
| **Platreef granite dyke** | **2053.7** | 3.2 | SHRIMP | (2) |
| **Merensky Reef** | **2054.4** | 4.2 | U-Pb | (3) |
| **Merensky Reef** | **2055.0** | 3.9 | U-Pb | (3) |
| **Lower Platreef zircon** | **2042.1** | 4.2 | SHRIMP | (1) |
| **Lower Platreef zircon** | **2038.0** | 4.7 | SHRIMP | (1) |
| **Platreef Turfspruit** | **2011.0** | 50.0 | Os-Re | (4) |
| **Platreef Sandsloot** | **2011.0** | 90.0 | Os-Re | (5) |
| **Platreef Overysel** | **2170.0** | 200.0 | Sm-Nd | (6) |

Kinnaird et al. (2010) dated two zircon crystals from chromitite in the upper part of the Platreef from Vaalkop. These yielded a concordant SHRIMP age of 2056.7 ± 4.4 Ma which is indistinguishable within error of a SHRIMP zircon age of 2053.7 ± 3.2 Ma reported by Hutchinson et al. (2004) who dated a zircon in a granitic dyke cross-cutting the Platreef. These ages are in agreement with a U-Pb crystallisation age of 2054.4 ± 4.2 Ma determined from single-crystal chemical abrasion ID-TIMS U-Pb dating of zircon, and multigrain fractions of rutile yielding a U-Pb cooling age of 2055.0 ± 3.9 Ma (Scoates and Friedman 2008). However, zircons from a Lower Platreef chromitite on Sandsloot yield concordant ages of 2042.1 ± 4.2 and 2038 ± 4.7 Ma respectively (Kinnaird et al. 2010). Using Os and Re variations in pyrrhotite from Platreef pyroxenite from Turfspruit, Ruiz et al. (2004) presented data which defined an isochron of 2011±50 Ma. This age agrees with that obtained from a Sandsloot locality (Reisberg et al. 2006) where analyses define an isochron of 2011 ± 90 Ma. Pronost et al. (2008) obtained a Sm-Nd age of 2170 ± 0.2 Ga from

pyroxenites at Overysel. This is around the age range determined for the rest of the Bushveld Complex, especially the most recent Merensky Reef data for which Scoates et al. (2012) presented the two ages 2055.30 ± 0.61 Ma and 2056.13 ± 0.7 Ma. Until the error margin is reduced further for northern limb data, it is not possible to determine if the northern limb intrusion is separate from the rest of the Bushveld Complex. However, even if they are separate, it is likely that both intrusions were emplaced within a relatively short time of each other. Hattingh (1995) presented paleomagnetic data indicating that in the main part of the Complex, the Critical Zone's remnant magnetisation was fixed before that of the Main and subsequent Upper Zone. After this, magnetisation of the Main Zone in the northern limb occurred and the youngest magnetisation recorded is that of the Upper Zone in the northern limb.

### 2.2.3. Stratigraphical correlations of the northern limb

In the eastern and western limbs of the Bushveld Complex, the RLS stratigraphy has traditionally been split into the major divisions of Marginal Zone, Lower Zone, Critical Zone, Main Zone and Upper Zone. However, north of the TML it has been demonstrated (e.g. van der Merwe 1976; Ashwal et al. 2005; McDonald et al. 2005) that the stratigraphy of the northern limb cannot be correlated easily with the rest of the Bushveld Complex as key horizons are either missing in the northern limb or entirely different units occur instead. The traditional view of its relationship to the rest of the Complex is shown in figure 2.5.

There appears to be a major change in Bushveld stratigraphy across the Ysterberg-Plankneck fault which forms part of the TML system and trends NE-SW through Mokopane (part of the TML). Structural, stratigraphic and petrological observations by authors such as Hulbert and von Gruenewaldt (1982) have suggested that successions on the farms of Rooiport, Grasvally and War Springs to the south of the fault can be correlated directly with those of the eastern and western limbs. South of Mokopane, the Grasvally Norite-Pyroxenite-Anorthosite (GNPA) member, as defined by Hulbert (1983), is a 350 m thick sequence of layered pyroxenites, norite, anorthosites, and a chromitite. This member had been referred to as the Critical Zone in the literature until 2005.

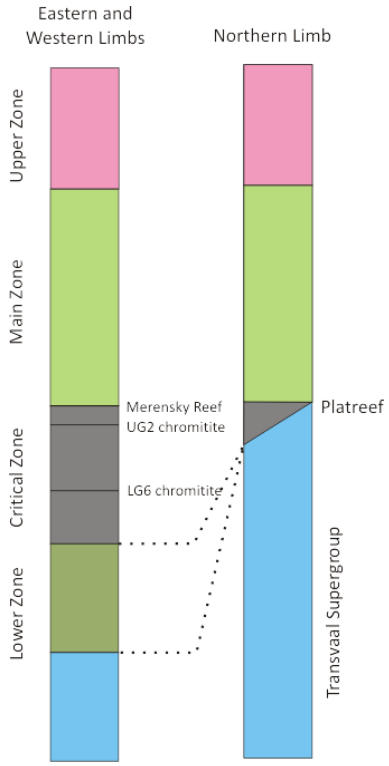


Figure 2.5. Traditional correlation of stratigraphy of the eastern and western limbs of the Bushveld Complex, and the northern limb, with an inferred correlation between the Platreef with the Merensky Reef (after White 1994) .

Lower Zone cumulates are most extensively developed to the south of Mokopane, whereas to the north they only occur as isolated satellite bodies intruded into the floor rocks. The sequence to the south of Mokopane of Lower Zone cumulates comprise of at least 1600 m of 37 cyclic units of pyroxenite and harzburgites with chromitites (Hulbert and von Gruenewaldt 1982; Hulbert 1983). This sequence differs from the Lower Zone elsewhere in that it contains orthopyroxene with higher enstatite content and olivine with higher forsterite content (van der Merwe 1976), chromitite layers with highest $Cr_2O_3$ content and Cr# in the whole Bushveld Complex (Hulbert 1983), and a PGE-rich sulphide horizon, which is not found in any of the Lower Zone cumulates in the rest of the Complex (Hulbert and von Gruenewaldt 1982). Several bodies of Lower Zone rocks, known as ‘satellite bodies’, occur in an area to the north of Mokopane. They are intruded into the floor rocks beneath the main Bushveld intrusion, that are generally made up of orthopyroxene and orthopyroxene-olivine cumulates with occasional chromitite layers as noted by van der Merwe (1978). It has been proposed by van der Merwe (1978; 2008) that a major hiatus occurred between the emplacement of the Lower Zone and the rest of the sequence. This is based on the intrusion and metamorphism of the Lower Zone by the Platreef which transgresses the Lower Zone in the north. The angular uniformity between the Lower Zone pyroxenite and the Platreef has also been presented as evidence of this theory.

To the north of the Ysterberg-Plankneck fault, the succession differs from those found in the eastern and western limbs both in terms of the thickness and the individual ultramafic to mafic units within the succession. For example, the Lower Zone ultramafic lithologies may form as sills between the Platreef and the footwall lithologies or as isolated bodies in footwall metasediments or gneiss. The Marginal Zone norites may occur within the succession or at the base in the northern limb north of the Ysterberg-Plankneck fault (Kinnaird 2005).

The correlation of the Critical Zone found in the eastern and western limbs with the Platreef package north of the Ysterberg-Plankneck fault is debatable (McDonald et al. 2005). Traditionally they have been correlated according to the stratigraphic position between the Main Zone and the Lower Zone as well as by similarities in the silicate geochemistry. The correlation is based on observations by Hulbert (1983) and van der Merwe (1978) of marked layering, the presence of cumulus chromite, and a chromitite layer with apparent similarities to the UG-2 chromitite of the Critical Zone in the eastern and western limbs. However, it has been shown that the Platreef does not show the typical layered cyclic sequences. Instead there are impersistent chromitite layers and the PGE grade may be moderate throughout the whole package or the grade may be top- or bottom-loaded (Kinnaird et al. 2005). Mills Davies (1925) stated that “the Potgietersrus occurrences may prove to be a separate type of deposit” whereas Wagner (1929) considered the feldspathic pyroxenite “platiniferous horizon” north of Mokopane was analogous to the Merensky Reef.

The Main and Upper Zones are present in the northern limb although it has been highlighted by Ashwal et al. (2005) that they exhibit a slightly different stratigraphy compared to the same zones in the eastern and western limbs. The Main Zone, which occurs above the Platreef, is 2,200 m thick (van der Merwe 1976). It is dominated by fairly homogenous gabbronorites and norites with a prominent layer of troctolite and interlayered anorthosite. The four pyroxenite layers in the lower part of the succession and the 110 m thick trocolite layer 1,100 m above the Platreef are the only reliable marker horizons, all of which are unique to the northern limb. Elsewhere in the Bushveld Complex the Main Zone gabbronorite may reach almost 4,000 m in thickness with several markers including the Giant Mottled Anorthosite at the base and the Pyroxenite Marker towards the top (Mitchell 1990). It appears that the correlation between the sequence in the northern limb and the rest of the Complex has not been rigorously tested and major differences have yet to be explained using a common genetiv model. van der Merwe (1976) correlated a

pyroxenite layer near the top of the Main Zone in the northern limb with the Pyroxenite Marker in the eastern and western limbs. Ashwal et al. (2005) however, argue that the two horizons cannot be correlated on the basis of mineralogy and they referred to the unit as the Pyroxenite Horizon to avoid confusion. The Upper Zone of the northern limb is around 1500 m thick in the Bellvue core (Ashwal et al. 2005). Cyclic units are characteristic with magnetite layers at the base, followed by magnetite gabbro, gabbro, olivine diorite and anorthosite. The Upper Zone of the northern limb more closely matches that of the eastern and western limbs. However, only one of the magnetite layers can be reliably correlated with the Main Magnetite layer of the rest of the Complex, on the terms of thickness and $V_2O_5$ content (van der Merwe 1976). To the west, overlying the mafic rocks are the roof rocks, which comprise a variety of Bushveld granites and metasedimentary rocks.

# Chapter 3: Local Geology

## 3.1 The Platreef

The Platreef is a world-class PGE orebody located in the northern limb of the Bushveld Complex that contains significant reserves of Ni and Cu (according to Naldrett 2010c, it amounts to around 30 % of in-situ value at 2010 prices). The Platreef is estimated to contain reserves in excess of 16.3 million oz Pt+Pd (Cawthorn 1999) and as the orebody is up to 400 m thick, it is amenable to open pit mining. Anglo Platinum currently operates 4 open pits on the Sandsloot, Zwartfontein and Overysel farms (fig. 3.1) with current exploration programmes identifying further targets. Mogalakwena Platinum Mines (MPM) is a division of Anglo Platinum formerly known as Potgietersrust Platinum Limited (PPL) and this project has been carried out in conjunction with them. The MPM complex comprises 6 farms situated ~30 km north of Mokopane. Other companies that own farms overlying the Platreef include Lonmin, Ivanplats Platreef Resources, Anooraq Resources, Blackthorn Resources, Platinum Group Metals Ltd, Sylvania Resources and Caledonia Mining.

### 3.1.1 Definition of the Platreef

From its discovery in the 1920s to the mid 1970s the unit was termed the Merensky Platinum Horizon (Wagner 1929). Van der Merwe (1976; 1978) first proposed the term Platreef to refer to a porphyritic pyroxenite which graded down into a feldspathic pegamatitic pyroxenite and he considered these pyroxenites to form the base of the Main Zone. Since then, there has been significant debate over what exactly constitutes Platreef, its lateral extent, and whether the Platreef should define a lithological unit with stratigraphic significance, or simply a zone of exploitable mineralisation. The most widely accepted lithological definition of igneous Platreef summarised by Kinnaird and McDonald (2005) is '***mafic units enriched in Ni-Cu-PGE that occur between the Archaean granite-gneiss basement or the Transvaal Supergroup and the gabbronorites of the Main Zone, north of the Planknek Fault***'. This definition currently excludes any Ni-Cu-PGE mineralisation south of Mokopane, known to occur within the Grasvally norite-pyroxenite-anorthosite (GNPA) association on the farms of Vaalkop, Volspruit, Zoetveld, Rooiport and Oorlongsfontein. Mineralisation on these farms is hosted by lithologies with similarities to the Lower Zone (Hulbert and von Gruenewaldt 1982; Hulbert 1983; von Gruenewaldt et al. 1989; De Klerk 2005; McDonald et al. 2005) and overlying Critical Zone (Maier et al. 2008). This definition also excludes the Aurora Project which contains Cu-rich mineralisation developed in Main Zone norites and gabbronorites immediately above the Platreef in the far north, on the farms of Altona, La Pucella, Kransplaats and Nonnenwerth (fig. 3.1).

Kinnaird (2004) has referred to this mineralisation as 'Platreef style'. The Kinnaird and McDonald definition effectively regards the Platreef as a magmatic mineralisation event with stratigraphic significance and therefore any PGE mineralisation occurring in evidently younger or older rocks in the northern limb cannot be classified as Platreef (McDonald and Holwell 2011). The Platreef, as defined above, crops out on the farms (from north to south) Witrivier, Drenthe, Overysel, Zwartfontein, Sandsloot, Vaalkop, Tweefontein, Turfspruit, Macalacaskop and Townlands.

In mining industry terms, the Platreef is regarded as a stratabound, but not necessarily stratiform, body within a dominantly pyroxenite lithology. The definition by Kinnaird and McDonald (2005) does not define a position within the body that can be used for the cut-off grade, as grade regularly extends down into the footwall. This occurs either where sulphides have seeped down fractures into underlying lithologies, as has been shown by Holwell and McDonald (2006) in the granite or granofels. Grade may also be present in the footwall where a reaction has occurred between the Platreef sills and the Malmani dolomites (Holwell et al. 2006) and the Platreef mineralisation locally takes on the characteristics of a skarn (Armitage et al. 2002).

The Platreef is characterised as being more widespread and richer in sulphide mineralisation compared with relatively restricted, sulphide-poor mineralisation of the Merensky and UG2 Reefs. Syn- and post-magmatic fluid alteration also occurred on a much greater scale (Buchanan et al. 1981; Hutchinson and Kinnaird 2005; Holwell and McDonald 2006).

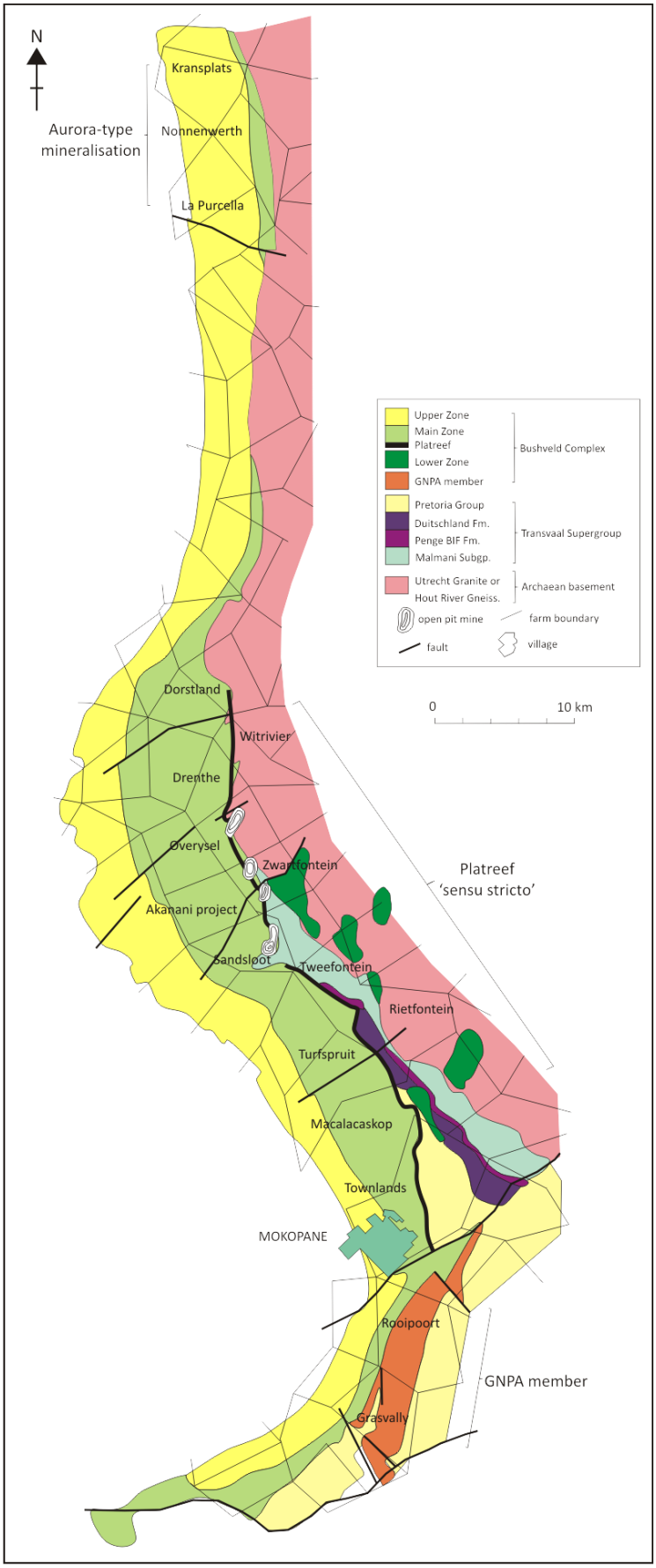


Figure 3.1. Map of the northern limb showing the locations of the farms discussed in the text (based on van der Merwe 1976).

## 3.2 Lithologies

Mining company geologists are known to use the informal local Bushveld nomenclature developed from the publications of Wager et al. (1960) and Hunter (1996). This results in rocks being logged based on the cumulus and intercumulus mineral contents rather than the IUGS recommendations based on modal percentages, cumulate phases and intercumulus assemblages (Streckeisen 1976). Nex et al. (2006) published a manual detailing the rock types that have been found in Platreef drillholes, specifically those at Anglo Platinum's lease areas, in order to promote the consistency of rock names, using internationally agreed terminology.

Detailed descriptions of the various Platreef lithologies have been given in papers such as Nex et al. (2006), Kinnaird et al. (2005), Armitage et al. (2002) and Holwell and McDonald (2006) and are therefore only summarised below:

### 3.2.1 Platreef lithologies

All Platreef rocks comprise orthopyroxene, clinopyroxene, olivine and plagioclase in varying proportions from less than 10 % to more than 90 %, resulting in rock types ranging from dunite to pyroxenite to norite.

The Platreef pyroxenites are an ultramafic rock containing more than 90 % pyroxene and are the major rock type of the Platreef. Grain size varies from fine to coarse although the most common is medium-to-coarse grained and pegmatoidal (Nex et al. 2006). The pyroxenites are often subdivided further into orthopyroxenites and clinopyroxenites. They may contain up to 10 % plagioclase before they are termed norites or gabbronorites according to IUGS classification (Streckeisen 1976). The major variation in pyroxenites found in the Platreef are the grain size of the orthopyroxene and the amount of interstitial plagioclase (Nex et al. 2006). In the Bushveld, there is the informal use of the term feldspathic pyroxenite, which is used for rocks containing cumulus orthopyroxene and intercumulus plagioclase.

Also occurring within the Platreef package are olivine-bearing lithologies, with harzburgites occurring the most frequently. The majority of harzburgites in the Platreef are serpentinised. The degree of serpentinisation reflects the differences in the modal mineralogy and alteration within the harzburgites.

A typical norite in the Bushveld Complex contains more plagioclase feldspar than orthopyroxene. Norite occurs both within the Platreef package and as a chilled micronorite

sill at the base of the Platreef package where it is in contact with the floor rocks. They are also found between the Platreef and the Lower Zone.

### 3.2.2 Main Zone lithologies

The hangingwall to the Platreef pyroxenites is made up of medium-grained norites and gabbronorites containing cumulus plagioclase, cumulus and intercumulus orthopyroxenes and generally oikocrystic clinopyroxene. The Main Zone rocks above the Platreef have been noted to resemble those of the Main Zone elsewhere in the Bushveld Complex (Nex et al. 2006). The base of the hangingwall is characterised by a thin fine-grained poikolitic leuconorite up to 30 cm thick, containing up to 90 % cumulus plagioclase and oikocrystic pyroxenes (Holwell et al. 2005). With increasing stratigraphic height above the Platreef, medium- to coarse-grained gabbronorites dominate (Weise 2010). Occasional xenoliths of calc-silicate derived from metamorphosed dolomite, similar to those identified by Kinnaird and Nex (2003) in the footwall, are also present in the hangingwall.

### 3.2.3 Footwall lithologies

There are a wide range of granitic rocks forming the footwall to the Platreef, showing variable texture (fine grained to pegmatoidal) and colour (white to red, depending on which type of feldspar is dominant). The Archaean basement (Hout River gneisses and Utrecht granite) consists of tonalitic gneiss intruded by heterogeneous potassic granites, which have been compared to other Archaean exposures on the Kaapvaal Craton (Cawthorn et al. 1985). Where the footwall of the Platreef is Archaean granite, the term granofels is used for rocks which have developed at the contact zone. This rock contains pyroxenitic fragments within a granitic matrix (Nex et al. 2006).

The other group of footwall lithologies consists of the sediments of the Transvaal Supergroup that have been subsequently metamorphosed. They were deposited on the Archaean basement during the period 2670-2100 Ma (Eriksson et al. 2001). The Supergroup is comprised of a thin basal clastic unit (Black Reef Fm.) followed by a sequence of dolomites, ironstones and minor shales with diamictite (Malmani Subgroup, Penge Fm., Duitschland Fm.). These are overlain disconformably by the Pretoria Group (Timeball Hill Fm.), which is dominantly clastic with minor volcanic rocks (fig. 3.2). According to Eriksson et al. (2001) the Transvaal Supergroup reaches a maximum thickness of 12 km within the Transvaal Basin.

In areas where the Platreef pyroxenites are in contact with the calc-silicates, the term parapyroxenite (originally introduced by Wagner 1929) is used to name the hybrid rocks that exhibit metamorphic rather than igneous textures.

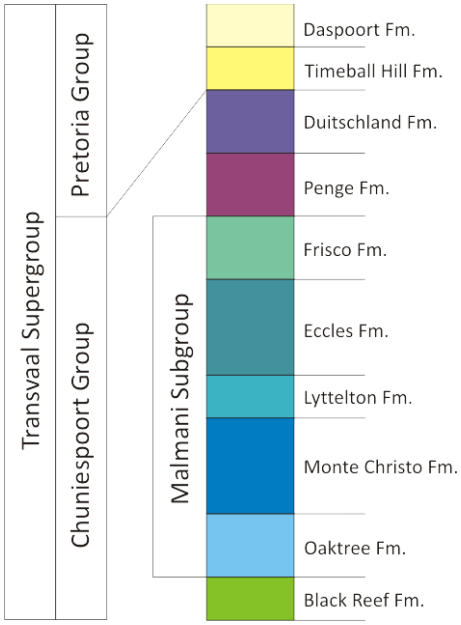


Figure 3.2. Stratigraphy of Transvaal Supergroup floor rocks beneath the Platreef.

### 3.2.4 Lower Zone lithologies

The Lower Zone dunites are characterised by anhedral cumulus olivines with minor orthopyroxene, and may also contain net-textured sulphide blebs and chromite. The orthopyroxenes, noted to be unaltered, have high Mg# compared to those of the Platreef package (Kinnaird et al. 2005). Data from drill core has shown that the Lower Zone pyroxenites, harzburgites and dunites are thicker and more widespread than originally thought (Kinnaird et al. 2005).

## 3.3 Stratigraphic relationships

### 3.3.1 Relationship between the Platreef and the Main Zone

Prior to 2005, the gabbronorites of the Main Zone had generally been assumed to be younger than, but co-magmatic, with the Platreef (e.g. Wagner 1929; van der Merwe 1976; White 1994; Kruger 2005b). Since then, relationships between the Platreef and the Main Zone have been clearly established. Observations on the nature of the contact between the Platreef and its hangingwall have revealed that the hangingwall gabbronorites were intruded after the Platreef, with a significant time-break separating the two intrusive events (Holwell et al. 2005; Holwell and Jordaan 2006). These observations have major implications on some of the models that have been presented as a genetic model for the Platreef.

### 3.3.2 Relationship between the Platreef and the footwall rocks

As the Platreef strikes north from Mokopane, it rests upon a series of progressively older Paleoproterozoic sedimentary Transvaal Supergroup units until it rests directly on the Archaean basement, in an onlapping relationship, described by Wagner (1929) as 'igneous transgression'. This transgressive relationship is the result of a divergence in strike between the Platreef and the footwall rocks resulting from the steepening dips of the sediment package towards the north (van der Merwe 1978; Kinnaird et al. 2005).

It is now widely accepted that the whole mineralised Platreef package is composed of several different pyroxenite sills of variable thickness (Kinnaird et al. 2005; Manyeruke et al. 2005; Maier et al. 2008). These sills are sometimes separated by thick layers of metasediments that may be compositionally different from the immediate footwall.

Pre- and syn-Platreef faulting which determined the morphology of the footwall contact is likely to have controlled the thickness of the Platreef. Thickened Platreef seems to occur within fault-bounded 'grabens' that, according to Yudovskaya and Kinnaird (2010), may have been deepening during magma emplacement, emphasising the syn-magmatic timing of this tectonism. Previous studies suggested that the dip of the Platreef should decrease down dip from 45° to 15–20°, as suggested by drillhole core logs by Yudovskaya and Kinnaird (2010). The abundance of incorporated sedimentary material decreases down dip, although metamorphosed dolomite and anhydrite lenses may still occur as xenoliths close to the footwall.

### 3.3.3 Relationship between the Platreef and the Lower Zone

At no point along its strike is the Platreef directly in contact with the Lower Zone on the surface, however, it has been shown that there is an angular discordance between the dip of layering in the Platreef (30-45°) and more shallow layering (15-30°) in nearby Lower Zone satellites (van der Merwe 1978; Kinnaird et al. 2005). Intrusions such as Uitloop, Zwartfontein and Bultongfontein are present as sills up to 800 m thick between the Platreef and footwall lithologies, or as entirely separate sills and fingers into the footwall metasediments or gneiss that appear isolated at the surface, but may be interconnected at depth (Kinnaird et al. 2010).

A number of pyroxenite 'satellite bodies' occur in the immediate footwall of the Platreef in the proximity to the Mogalakwena Platinum Mines and are emplaced along the strike faults (White 1994). These bodies consist of very finely crystalline orthopyroxenites which have been intruded into the footwall rocks and according to van der Merwe (1976) are the

remnants of the Lower Zones of the Bushveld Complex. Several small discontinuous lenses of chromite have been found in these satellite bodies (Colloty 2008).

## 3.4 Platreef sectors

Different localities within the northern limb are discussed by reference to the farm from which the samples were collected. Kinnaird (2005) devised the sector concept in which farms are grouped into zones where the Platreef has similar characteristics. The Central sector consists of farms from Tweefontein to Overysel, where the highest PGE grades are found and where current mining operations are located. The corresponding Northern (Drenthe-Witrivier) and Southern (Townlands-Turfspruit) sectors occur to the north and south along strike of this Central sector.

The samples for this study are collected from the farms Overysel, Zwartfontein and Sandsloot and therefore the remainder of this chapter will concentrate on characteristics of these farms in the Central sector. McDonald and Holwell (2011) have summarised work carried out on the Northern and Southern sectors as well as the remaining farms in the Central sector. The general geology, including footwall lithology, Platreef lithologies, xenolith types, together with a summary of the base metal sulphide (BMS) and platinum-group mineral (PGM) mineralogy of the Platreef with a comprehensive reference list for each farm along strike has been summarised by Holwell (2006).

### 3.4.1 Central Sector

Underground mining took place in the Central Sector between 1925-1929. Mining recommenced in 1992 at the Sandsloot open pit and since then open pits have been developed northwards at Mogalakwena North (formerly Overysel) at Mogalakwena Central and South (formerly Zwartfontein) and Zwartfontein South pit (fig. 3.3). Further operations are also planned to the south. Proven resources are 317 million tonnes at 3.28 g/t (Anglo Platinum 2009). The Sandsloot pit produced 20,000,000 t in 2007 at a rate of 55,000 t per day. The pit is 1700 m long, 600 m wide and has 15 m bench heights. The pit is currently closed with a final depth of 270 m but there are plans to extend it to more than 300 m. The Zwartfontein South pit will be mined at surface until 2014 and production was 36,000,000 t in 2007 at a rate of 98,000 t per day. The current pit is 1300 m long, 430 m wide and 120 m deep with 10 m bench heights. The final depth will be 245 m. Mining started on Overysel in 2006 and the pit has expanded considerably since then. Surface mining is anticipated to extend to 2048. Production was 34,000,000 t in 2007 at a rate of 93,000 t per day. The pit will reach maximum dimensions of 5,800 m long, 1,100 m wide, 300 m deep with 15 m

bench heights. Underground mining in the Mogalakwena lease area is expected to add another 200 years of operations to the area.

#### *3.4.1.1 Sandsloot*

Until 2008, the Malmani dolomite was regarded as the footwall to the Platreef on this farm. The dolomite 'tongue' is a prominent structural feature of the northern limb and is attached to the floor rocks on the Central Sector farms of Sandsloot, Vaalkop and Tweefontein. Original work carried out by van der Merwe (1978) interpreted the dolomite lobe as an early dome created by the interference of two fold phases. Clarke et al. (2009) interpret the dolomite lobe as an interfinger deformation zone formed as Lower Zone magma fingers were injected either side of it. Work carried out by Friese (2004) on the south wall of Sandsloot pit showed that the dolomite is a tongue-shaped feature where the surrounding landscape shows little topography, supporting van der Merwe's dome theory. Annotated images from locations in the Sandsloot pit are presented by Friese (2004) showing features interpreted as thrust-generated structures in the footwall immediately below the reef. Structural observations in the Sandsloot pit by Armitage (2011) have only found significantly sheared and duplexed footwall rocks at one locality. Also noted were the lack of thrust-related fabrics in the footwall that would support the theory that the reef intruded along a thrust zone. Armitage (2011) suggests that although the development of a thrust zone within the Transvaal Supergroup, pre-Main zone time, cannot be totally dismissed, it is unlikely due to the fact that the dolomite tongue stayed intact and still attached to the sedimentary floor, as seen in the south of the pit.

Van der Merwe (1978) recorded antiform and onlap relationships between the tongue and the Main Zone layering, suggesting that the dolomite tongue structure predated the Platreef intrusion. Armitage (2011) agrees with this theory and suggests that although it appears to be largely a pre-Platreef structure, it may have continued to form at a very late stage of Platreef emplacement or even after emplacement. It is likely that the tongue formed by N-S and ENE-SSW compressional fold interference prior to the intrusion of the Bushveld Complex, with at least one of these folding events remaining active during the Platreef emplacement.

The Platreef has been shown to follow the shape of the dolomite tongue, at least where it connects to the main body of the country rocks, suggesting that the Platreef magma filled the synformal zones of the pre-existing folds (Kinnaird et al. 2005; Armitage 2011). Armitage (2011) produced a 3-D block model for the Platreef development at Sandsloot (fig. 3.3).

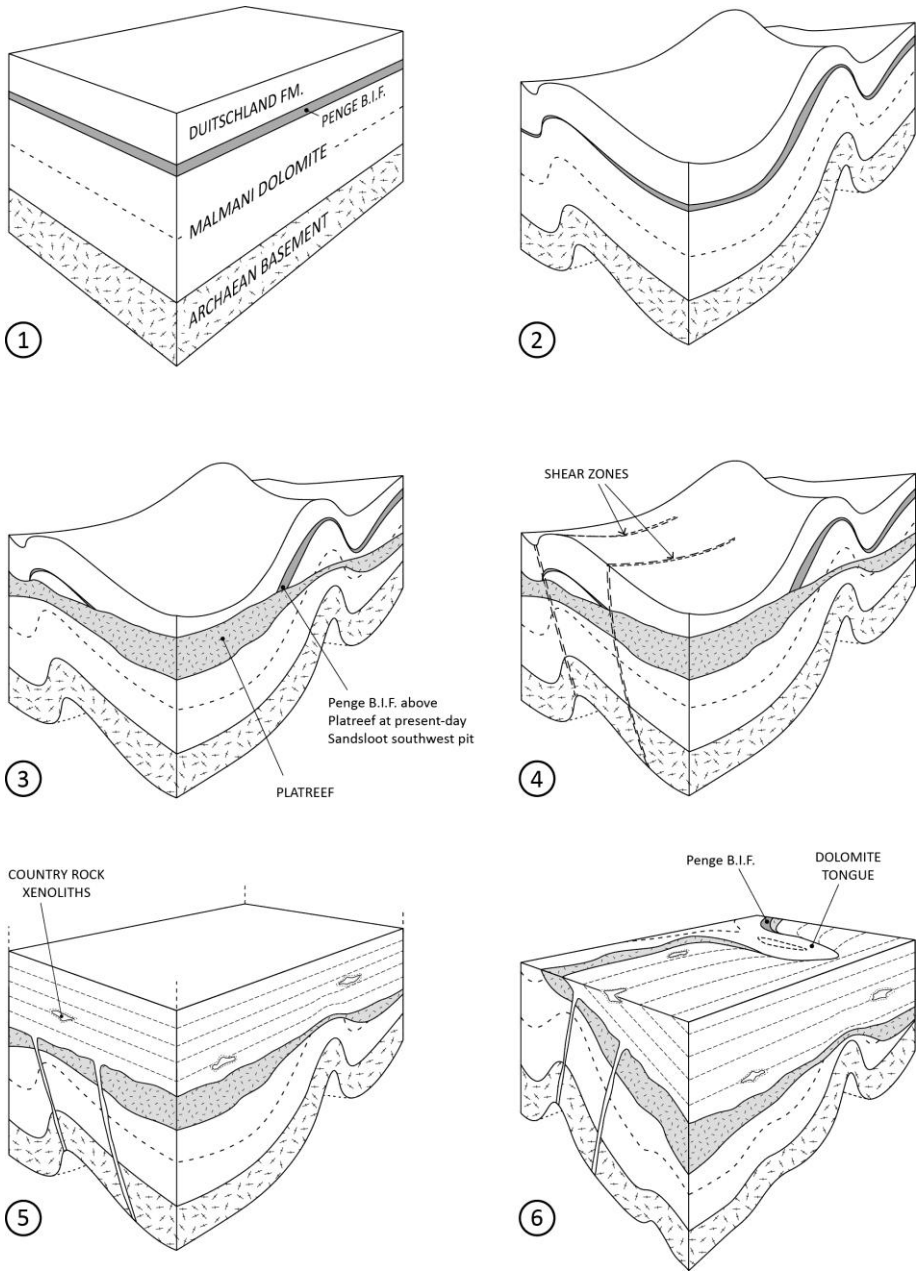


Figure 3.3. Three dimensional block model viewed to the southeast for Platreef development at Sandsloot. (1) Deposition of the Transvaal Supergroup sediments; (2) Two-phase compressive deformation of sediments, during or culminating with Magondi Orogeny; (3) Intrusion of Platreef sill with thickness controlled locally by pre-existing structures; (4) Deformation of cooling Platreef and Transvaal Supergroup sediments, possibly at late stage of Magondi Orogeny; (5) Emplacement of Main Zone, eroding uppermost section of Platreef; (6) Subsidence of northern limb down to the west and erosion to present-day surface (Armitage 2011)

In 2008, following a deep drilling program by Anglo Platinum, it was found that a section of what has been considered coherent dolomite 'footwall' was in fact a 'xenolith' or 'interlayer' when a thick mineralised pyroxenite package was discovered >200 m beneath it (Winch 2011). This package is interpreted by Kinnaird et al. (2010) as Lower Platreef.

Where the Platreef is in direct contact with the Malmani dolomite, a complex zone of highly altered metasomatic rocks occurs, termed parapyroxenites by the mine geologists. Although not an internationally defined rock term, it was first used by Wagner (1929) for calc-silicate rocks in which the dominant mineral is diopside. In the Platreef, the term is frequently used for a rock that exhibits more of a metamorphic rather than igneous texture (Nex et al. 2006). It is also used for rocks that appear to be a hybrid between the calc-silicates and the Platreef pyroxenites. Also within this zone are calc-silicate hornfelses that are often serpentinised and may be variably mineralised (Armitage et al. 2002; Holwell et al. 2006).

At Sandsloot, the Platreef varies in thickness from 30 m to a maximum of almost 600 m (true thickness of 400 m; Yudovskaya and Kinnaird 2010). An upper medium-coarse grained pyroxenite package is separated from a lower pyroxenite unit by interlayered parapyroxenite and calc-silicate.

The overlying Main Zone gabbronorites often have a mottled anorthosite at the base and the nature of this contact is described in detail by Holwell et al. (2005) suggesting that it may represent a magmatic unconformity.

#### *3.4.1.2 Zwartfontein*

The 'footwall' rocks on the southern portion of the farm are similar to the adjacent farm of Sandsloot with Malmani dolomite displaying bedding that is emphasised by lenses and bands of serpentinite. On the northern part of the farm, the footwall changes to Archaean Utrecht granite and Hout River gneiss, although xenoliths of calc-silicate are still found in the Platreef package.

The reef package on Zwartfontein is much thicker on average than on Sandsloot (up to 400 m). Parapyroxenites are common at the base of the Platreef and there is a greater proportion of xenoliths of serpentinised lithologies occurring throughout the Platreef package. This has been interpreted to be related to the alteration of large rafts of calc-silicates within the Platreef (Holwell and Jordaan 2006).

The Platreef extends down-dip to the west of the surface outcrop and is known as the Akanani prospect on the farms Zwartfontein and Moordkoppie. Following deep drilling by Lonmin, it was discovered that the intersected Platreef contains calc-silicate xenoliths and a white-grey granofels footwall above Hout River Gneiss. Above the granofels, Lower Zone pyroxenite and harzburgite have been intersected. The Platreef package is variable in thickness from ~80 m to ~300 m. It is thinner on Moordkoopie than on Zwartfontein (Spies 2005). According to Kinnaird et al. (2010) average PGE grades and metal tenors in 100 % sulphide are higher at Akanani than in the Platreef up-dip on Anglo Platinum's property.

#### *3.4.1.3 Overysel*

On the farm of Overysel the footwall to the Platreef consists of the Archaean Utrecht granite and Hout River gneisses. The series of banded tonalitic gneisses are commonly referred to as granofels, particularly when brecciated by granitic veins. Holwell and McDonald (2006) interpreted the gneisses as being a pre-existing lithology and not hybrid melts of the granite and the Platreef. Beneath the gneisses, the domal body of the Utrecht granite is encountered.

Cawthorn et al. (1985) describe the Platreef package of coarse-grained pyroxenites varying from 25 m to > 100 m in thickness with considerable thickening. Holwell and McDonald (2006) noted a 'hybrid' norite below the Platreef equating with the 'chilled' norite of Kinnaird et al. (2005). It is dominantly fine-grained and composed of ~55 % plagioclase, 30 % orthopyroxene often altered to amphiboles, 10 % clinopyroxene and 5 % quartz. Coarse-grained patches contain more quartz and abundant blebs of BMS. Trial mining during the 1980s also encountered some thick, but discontinuous bands of chromitite (White 1994; Holwell and McDonald 2006).

## 3.5 Mineralogy

### 3.5.1 Silicate mineralogy

As mentioned above, the Platreef lithologies are mostly composed of varying percentages of orthopyroxene, clinopyroxene, plagioclase and olivine. Mineral compositions for orthopyroxene, plagioclase and olivine from different farms were summarised by McDonald and Holwell (2011) and are compared with available data for the base of the Main Zone of the northern limb, the various parts of the GNPA member south of Mokopane and the Upper Critical and Main Zones from south of the TML (table 3.1).

The values in the table represent the most 'primary' mineral composition at each location and have excluded any contaminated data as the presence of ironstone or dolomite

contamination cause anomalously Fe-rich or Mg-rich compositions respectively (e.g. Buchanan and Rouse 1984; Harris and Chaumba 2001; McDonald et al. 2005).

Table 3.1. Mineral data for the Platreef and other Bushveld rocks compiled by McDonald and Holwell (2011).

| | Orthopyroxene | Plagioclase | Olivine |
|---|---|---|---|
| **Main Zone – Northern Limb** | | | |
| Drenthe | $En_{60}$ | $An_{70-73}$ | |
| Overysel | $Mg\#_{60-63}$ | $An_{71-82}$ | |
| | | | |
| **Platreef** | | | |
| Drenthe | $En_{71-74}$ | $An_{73}$ | |
| Overysel | $Mg\#_{74-80}$ | $An_{73-81}$ | |
| Akanani | $Mg\#_{83-84}$ | | $Fo_{82-83}$ |
| Zwartfontein | $Mg\#_{73-77}$ | $An_{70-82}$ | |
| Sandsloot | $Mg\#_{76-80}$ | $An_{73-85}$ | $Fo_{76-77}$ |
| Tweefontein | $Mg\#_{74-81}$ | $An_{71-80}$ | $Fo_{75-76}$ |
| Turfspruit | $Mg\#_{72-76}$ | | |
| Townlands | $Mg\#_{68-82}$ | $An_{55-85}$ | $Fo_{78-83}$ |
| | | | |
| **GNPA Member** | | | |
| Grasvally-Rooipoort (MANO) | $Mg\#_{72-78}$ | $An_{65-75}$ | |
| Grasvally-Rooipoort (LGN) | $Mg\#_{60-63}$ | $An_{71-82}$ | |
| Grasvally-Rooipoort (LMF) | $Mg\#_{71-78}$ | $An_{65-77}$ | |
| | | | |
| **Eastern & Western Bushveld** | | | |
| Upper Critical Zone | $Mg\#_{78-84}$ | $An_{68-85}$ | $Fo_{77-82}$ |
| Merensky Reef | $Mg\#_{78-83}$ | $An_{70-80}$ | $Fo_{79-80}$ |
| Lower Main Zone | $Mg\#_{62-75}$ | $An_{65-75}$ | |

As can be seen from table 3.1, mineral compositions in the Main Zone above the Platreef are similar to those found in the LGN unit south of Mokopane, supporting the suggestion by De Klerk (2005) that this latter unit represents a chilled sheet of Main Zone magma intruded into the GNPA member. The range of mineral compositions in the Platreef overlaps with the range seen in the Upper Critical Zone in the eastern and western Bushveld. The pyroxene and feldspar compositions of the MANO and LMF units of the GNPA member also overlap with the Platreef compositions but are slightly lower than those of the Upper Critical Zone.

#### *3.5.1.1 Pyroxene*

Some of the earliest mineralogical work on the composition of Platreef pyroxenes by Buchanan (1981) showed that they were comparable to those of the Merensky Reef. McDonald and Holwell (2011) highlight the occurrence of a sharp compositional break for orthopyroxene (and clinopyroxene) at the junction between the Platreef and the overlying Main Zone, with the Main Zone pyroxenes having lower Mg# as shown in table 3.1. This supports the break in time of the formation of the two units, as discussed earlier.

#### *3.5.1.2 Feldspar*

Feldspar seen in the Platreef occurs as post-cumulus and cumulus plagioclase and forms anhedral interstitial grains between the cumulus orthopyroxene. In thin section, both cumulus and intercumulus plagioclase may occur. In the Main Zone, plagioclase is always a cumulus phase in the norites and gabbronorites (Nex et al. 2006). Plagioclase compositions do not show such a sharp break as the pyroxenes and the range of compositions generally overlap between the Platreef and the Main Zone.

#### *3.5.1.3 Olivine*

The olivines are frequently so extensively serpentinised that there are few available data sets for olivines. They are also much less abundant than pyroxene, for example, no olivine occurs in the Lower Platreef. Magmatic olivines can be distinguished from their metamorphic counterparts by the occurrence of high Cr and Ni values, however, equilibration of olivine with sulphides can cause considerable within-sample variation in Ni content.

McDonald and Holwell (2007) discovered that the nickel concentrations in olivine from Lower Zone satellite bodies such as Grasvally in the northern limb appear significantly lower than the expected range for mafic intrusions. Kinnaird et al. (2010) and Yudovskaya et al. (2012) have found similar Ni depletion in olivine from the Lower Zone at Turfspruit. McDonald and Holwell (2011) state that this kind of metal depletion generally indicates interaction between magma and sulphides in a deeper magma chamber and highlight the fact that to date no evidence has been found for Ni depletion in Lower Zone olivine from south of the TML, suggesting this may have genetic implications for the formation of the Platreef. Yudovskaya et al. (2012) also analysed olivine from the Lower Zone at Sandsloot. Some of the olivines analysed contained the highest Ni content for the Bushveld Complex, with the mean Ni content for Sandsloot around twice that of those analysed from Turfspruit. This range of Ni content may reflect the gradual mixing of fresh magma with more evolved resident liquid (Teigler and Eales 1993).

### 3.5.2 Sulphide mineralogy

Sulphides are more abundant in the Platreef compared to the Merensky Reef and the UG2, with ranges from <1 % to 30 %. In the Platreef, pyrrhotite is the dominant sulphide. Chalcopyrite, pentlandite (often Ag-, Co or Pd-bearing) and pyrite occur in lesser amounts, except where pyrite has replaced pyrrhotite. Chalcopyrite usually occurs around the rims of pyrrhotite, frequently with associated pentlandite. Pentlandite also occurs as veins up to 2 mm thick, and as exsolution lamellae within the pyrrhotite. More rarely the massive

sulphides may be dominated by chalcopyrite, with cross-cutting pyrrhotite veins. Also occurring in the Platreef, in order of abundance, are sphalerite, galena, bornite, chalcocite, covellite, vallerite, millerite, mackinawite (Ni-bearing), cubanite, gersdoffite, tetrahedrite, marcasite, stibnite and molybdenite (Nex et al. 2006). The overall grade of Cu is between 0.1-0.25 % and 0.15-0.35 % for Ni (Lee 1996; Kinnaird et al. 2005).

Hutchinson and Kinnaird (2005) recognised four principal sulphide associations for the Platreef:

- *Early magmatic sulphides* – simple in composition and represented by millimetre- to centimetre-sized fractionated blebs, micron- to millimetre-sized disseminated interstitial grains, sub-massive ores, and net-textured and vein-type ores composed almost exclusively of pyrrhotite and minor pentlandite. In pyrrhotite-rich grains, chalcopyrite and pentlandite typically occur either at their margins or as inclusions within them. Flame exsolution of pentlandite in pyrrhotite is common on all scales and textures;
- *Late magmatic sulphides associated with interstitial felsic assemblages* – they are more complex and occur between altered and often embayed cumulus silicates, in an intergranular felsic assemblage of plagioclase, quartz and quartz-feldspar symplectites. Chalcopyrite and pentlandite are common with pyrrhotite and trace sulphides that include galena and sphalerite. Sulphides within the felsic assemblages are mineralogically more complex than the magmatic sulphides associated with the pyroxenites and norites;
- *Late magmatic sulphides associated with granitic dykes (QF veins)* – these sulphides occur in many of the concordant-to-discordant granitic dykes, known locally as QF (quartzofeldspathic) veins and include pyrrhotite, chalcopyrite, pyrite, sphalerite and galena; and
- *Low temperature sulphides within secondary alteration assemblages* – these sulphides are common in altered assemblages. Many sulphides appear relatively fresh, even in rocks that have undergone extreme alteration. With increasing alteration, sulphides occur as progressively smaller monomineralic grains of pentlandite, chalcopyrite, pyrrhotite and pyrite that are interstitial to talc, tremolite and serpentine. Other sulphides associated with alteration include pyrite in some serpentinised peridotites, bornite, chalcocite, covellite, vallerite, godlevskite and

millerite, mackinawite (Ni-bearing), gersdoffite, terahedrite, marcasite, stibnite and molybdenite.

### 3.5.3 Chromite mineralogy

Chromite-bearing layers are not as thick, massive or continuous as those found in the eastern and western limbs of the Bushveld Complex. Hulbert (1983) and Hulbert and von Gruenewaldt (1985) produced detailed petrological analysis of chromitites of the Lower and 'Critical' Zones in the northern limb for the Grasvally area south of Mokopane. Other chromitite layers in the northern limb that are found in the Platreef north of Mokopane have not been described previously in detail (von Gruenewaldt et al. 1989; White 1994). Scoon and Teigler (1994) reported that the general upward decrease in the Cr/Fe ratio of chromite observed through the Critical Zone in the eastern and western limbs of the Bushveld Complex is consistent with a trend of magmatic differentiation of the whole complex. However, various theories that try to account for the origin of monomineralic chromitite layers recognise their formation as a result of a sharp disturbance of routine process of crystallisation, possibly related to: (1) a pressure change (Cameron 1977; Cawthorn 2005); (2) an influx of new primitive magma and chromite saturation during mixing (Irvine 1977; Eales et al. 1990; Scoon and Teigler 1994; Kinnaird et al. 2002); (3) an injection of magma carrying a chromite suspension (Eales 2000; Mondal and Mathez 2007; Maier and Barnes 2008b); or (4) contamination of a new influx by acid material from a roof (Irvine 1975; Kinnaird et al. 2002; Spandler et al. 2005). While disseminated chromite is likely to be a product of in situ crystallisation and is supposed to equilibrate with other cumulate minerals, massive chromite could be in disequilibrium with either hanging wall or footwall silicates or both (Yudovskaya and Kinnaird 2010). However, it has been shown that interaction with intercumulus liquid can result in significant changes in the chemistry of disseminated chromite compared to those in a massive layer (Cameron 1975; Hulbert and von Gruenewaldt 1985).

#### *3.5.3.1 Platreef chromitite distribution and morphology*

According to Yudovskaya and Kinnaird (2010) the chromitite layers and seams of the Platreef form two main chromite-bearing horizons that are traceable along strike: the Upper Chromitite (UCR) on Sandsloot, Vaalkop and Zwartfontein and the Lower Chromitite (LCR) on Overysel, Zwartfontein, Sandsloot, Tweefontein, Vaalkop and Macalacaskop. The UCR occurs as two to three discontinuous disseminated and massive seams in feldspathic pyroxenite approximately 20 m below the Platreef top contact. Where the UCR is closer to, or at the top contact in the north the upper part of the original Platreef may have been

removed by the Main Zone magma. The LCR is composed of multiple seams in feldspathic harzburgite, pyroxenite and norite close to the bottom contact of the Platreef with the footwall. The occurrence of chromitite locally at different distances from the contact between the upper Platreef sills and the overlying Main Zone magma has been suggested by Yudovskaya and Kinnaird (2010) to be the result of erosion of the upper Platreef by the Main Zone as it was emplaced.

Table 3.2. Chemical composition of chromite in the northern limb according to host rock. Data from Yudovskaya and Kinnaird (2010) and Holwell and McDonald (2006).

| | $Cr_2O_3$ wt% | MgO wt% |
|---|---|---|
| **Chromitite** | 41.74 | 1.37 |
| **Feldspathic pyroxenite** | 40.0-49.4 | 1.02-10.0 |
| **Norite** | 42.0-49.6 | 6.0-8.0 |
| **Lower Zone** | 55.0 | 4.0 |
| **Harzburgite** | 30.0-42.0 | 4.0-10.0 |

The chemical composition of chromite varies according to host rock as shown in table 3.2. The wide range of chromite composition has been explained by Yudovskaya and Kinnaird (2010) as being due to late magmatic processes including post-cumulus growth and re-equilibration, interaction with fluid- and sulphide-saturated magmatic liquid and contact-metamorphism. Although each process has a distinct geochemical signature, generally they lead to decrease in Mg and Al and an increase in both di- and tri-valent Fe in the chromite composition.

The PGE profiles for chromitiferous rocks and massive chromitites differ from PGE-rich reef pyroxenites, with positive Rh and a negative Pt anomaly caused by a relative enrichment in Rh and Ru rather than actual Pt depletion as noted by Holwell and McDonald (2006). The M-shaped pattern is also emphasised by a notable Au depletion in chromitiferous units.

#### *3.5.3.2 Origin of chromitite*

The various theories concerning the origin of chromitites have been well reviewed in several recent papers (Eales 2000; Kinnaird et al. 2002; Cawthorn 2005; Mondal and Mathez 2007; Maier and Barnes 2008b). Below are some key points that can be added from the study of Yudovskaya and Kinnaird (2010) on the Platreef.

The transgressive relationship with the overlying MZ norite–gabbronorite indicates that the top-loaded PGE reef did not form through magmatic settling of silicates and sulphides from the MZ (McDonald and Holwell 2007). It is also widely accepted that MZ gabbronorite differs drastically in terms of geochemistry and cumulate mineralogy from the Platreef pyroxenite (Hulbert 1983; Kinnaird et al. 2005). The former crystallised from a Cr-poor

tholeitic magma that cannot be the source for significant chromite. The composite structure of the Platreef indicates that chromitite is not a result of cumulative settling from the overlying column of melt, but they crystallised within relatively thin sills of insufficient thickness to provide the required chromium balance. In addition, chromites hosted in different rock types have distinct chemical compositions so the separate sills contain their own primary chromites that could not be derived from an overlying heterogeneous sequence and, therefore, provide evidence for a pre-concentration of chromite during fractionation in an intermediate chamber. A portion of the chromite could be supplied as suspended chromite crystals or a semi-consolidated crystal mush analogous to the model proposed by Mondal and Mathez (2007), but a significant amount of chromium must have been in the magma in order to form post-cumulus interstitial chromite and Cr-bearing silicates. In addition, the Platreef chromitites were deposited in a marginal position where intrusive processes were more dynamic and turbulent in comparison to the tranquil magmatic settling typical for the deeper eastern and western parts of the Bushveld Complex, according to Yudovskaya and Kinnaird (2010). Bushveld chromites of different composition form across a wide range of oxygen fugacity, so a shift in oxygen fugacity is unlikely to be a cause of their precipitation but rather a cause of their post-cumulus growth since increasing oxygen fugacity decreases the Cr contents of the melts at chromite saturation (Murck and Campbell 1986) and allows chromite crystallisation from a Cr-poor melt fraction. Yudovskyaya and Kinnaird (2010) favour a model for chromitite formation similar to that initially proposed by Irvine (1975, 1977). It suggested that chromite deposition was a response to a new ultramafic magma influx carrying a chromite slurry and its interaction with residual magma or another contaminant. Some Platreef chromitites, which formed as thin bands along calc-silicate xenolith boundaries, are evidence that chromite deposition may have been triggered by country rock assimilation. This model is also consistent with the composite structure of the Platreef and is supported by radiogenic isotope data for the Bushveld Complex (Kinnaird et al. 2002; Kruger 2005a). A mixing model is also appropriate as a mechanism of coeval sulphide and PGE saturation in chromite-bearing reefs (Naldrett et al. 2009b).

The presence of xenoliths (possible rip-up clasts), together with the discontinuity of layers, suggest a highly turbulent and most likely a multi-phase emplacement environment. It has been proposed by Kruger (2005b) that the Platreef is the product of Main Zone magma which has ripped up and assimilated previously solidified Lower Zone rocks and as such, the chromites within the Platreef could be Lower Zone chromitite xenoliths. The difference

between the compositions of the chromites within the layers and xenoliths in the Platreef and those in the Lower Zone pyroxenite in the Platreef footwall in core from Overysel and in the Lower Zone rocks of the northern limb reported by van der Merwe (1976) and Hulbert and von Gruenwaldt (1982; 1986) does not support the idea that the xenoliths are rip-up clasts of Lower Zone material, unless they have equilibrated by invading melt.

The chromitites studied by Holwell and McDonald (2006) contain some of the highest level of Ir, Ru and Rh in the Platreef rocks. The association of the IPGE and Rh with chromitites is well known and the discovery that laurite is stable at chromite-based liquidus temperatures, together with its common inclusion within chromite grains, indicates this can be treated as a primary magmatic texture (Brenan and Andrews 2001). The lack of laurite in the samples studied by Holwell and McDonald (2006) is indicative of base metal sulphide saturation. The fact that Pt/Pd ratios within the chromitites are comparable to the pyroxenites would also imply that during chromitite formation, the PGE-rich magma was also sulphur-saturated. If chromite precipitated significantly before sulphur-saturation, it would be expected to fractionate Pt over Pd, leading to higher Pt/Pd ratios within the chromitites (e.g. Barnes and Maier 2002b), which is not observed in the Platreef chromitites. Holwell and McDonald (2006) state that it is likely that chromite precipitation occurred at a similar time or slightly after sulphur saturation, with some IPGE and Rh fractionating with the chromite.

If the chromitite lenses and blocks represent rip-up clasts, they must have formed prior to emplacement of the Platreef, possibly in an external staging chamber or conduit and this would support the theory of Barton Jr et al. (1986) and Lee (1996) that the PGE-rich sulphides in the Platreef formed before emplacement. Conversely, if the chromitites formed virtually in situ in the Platreef magma, they must have been affected by further turbulent pulses of magma that disturbed them and entrained them as xenoliths.

### 3.5.4 Platinum-group mineralogy

Kinloch (1982) produced the first detailed mineralogical study of the platinum-group minerals (PGM) in the Platreef. He identified 8 major categories of PGM and noted lateral variations in PGM assemblages, which he attributed to different footwall rocks. A number of other studies have been carried out since, focussing on smaller areas such as sectors or individual farms (e.g. Armitage et al. 2002; Hutchinson and Kinnaird 2005; Kinnaird et al. 2005; Holwell et al. 2006; Hutchinson and McDonald 2008; Yudovskaya et al. 2011; van der Merwe et al. 2012).

The most common PGM in the Platreef are Pt and Pd phases. In the pyroxenites, Pt and Pd tellurides and bismuthides are the most common. PGM include moncheite, kotulskite, sobolevskite, michenerite and sperrylite. It has been suggested that this assemblage may represent the initial mineralisation style, with any variation in assemblage due to hydrothermal redistribution and the effects of local contamination (McDonald and Holwell 2011). Studies by Holwell et al. (2006) on Sandsloot showed that Pt-Fe alloys were rare in normal pyroxenite reef, although they were more common where olivine replaced reef was found. Pt-Fe alloys were found in chromitites by Yudovskaya et al. (2011) and have been attributed to desulphurisation of primary PGE sulphides.

Where the footwall rock is granite or gneiss, PGE sulphides (e.g. cooperite and braggite) have been found, representing the strongest association between PGE and BMS in the Platreef. In addition to the PGE sulphides, PGE bismuthides and tellurides are also found. Alternatively, where the Platreef intrudes volatile country rocks, PGM mineralogy is altered due to the effects of fluid activity and/or contamination. Here, there is a dominance of PGE arsenides, antimonides and stannides. At Overysel, where no obvious hydrothermal activity has occurred, the PGE telluride – base metal sulphide association is regarded as a 'primary' association (McDonald and Holwell 2011)

Laser ablation ICP-MS studies on the base metal sulphides (BMS) has shown that PGE distribution between the BMS and PGM are consistent with fractional crystallisation of a sulphide liquid (Holwell and McDonald 2007; Hutchinson and McDonald 2008). Os, Ir, Rh and Ru (+/- Pd) are present within solid solution in the cooling products of mono sulphide solution (mss), pentlandite and pyrrhotite, whereas Pt and Pd are present as PGM around the margins of the BMS. PGM containing Os, Ir, Ru and Rh are also present as rare inclusions within chromites or in chromite-rich pyroxenites (McDonald and Holwell 2011).

## 3.6 Geochemistry

### 3.6.1 Major and trace elements

Whole rock geochemical data has been presented for Townlands (Manyeruke et al. 2005; Maier et al. 2008), for Turfspruit (Kinnaird 2005), Tweefontein (Nyama et al. 2005), Sandsloot (Harris and Chaumba 2001; McDonald et al. 2005) and Overysel (Holwell and McDonald 2007).

Rare earth plots are useful as they show the incompatible elements that do not enter olivine, orthopyroxene or the spinels and therefore can be taken to represent the

intercumulus trapped liquid. The Central Sector rocks show depletions in Nb and Ta and strong enrichment in the large ion lithophile elements, a trait that has been shown to be common to all RLS magmas (Barnes and Maier 2002a) and also the Merensky Reef as shown in figure 3.4.

McDonald and Holwell (2011) plotted selected data for different sectors of the Platreef, the GNPA member, the Upper Critical Zone and Main Zone. Using major and trace element ratios, such as Cr/MgO, it was observed that at most localities in the Platreef the ratios were within the Main Zone and Critical Zone ratio ranges, but outside the range for the Merensky Reef. Ce/Sm ratios for the Platreef were within the range of those recorded for the Main Zone but also fell within the range of the Merensky Reef.

It has been suggested that it may be possible to correlate individual sills along strike based on the recognition of separate sills. Even though the Platreef package has been subdivided into different units in other sectors, no correlation has so far been made due to textural and geochemical variations in various sills, magma-xenolith interaction, effects of floor-rock composition, percolation of a late-stage felsic melt, development of subsolidus mineral assemblages and mobilisation of PGM during fluid-rock interaction. In addition, it has been recognised that different sills might have intruded in different sectors.

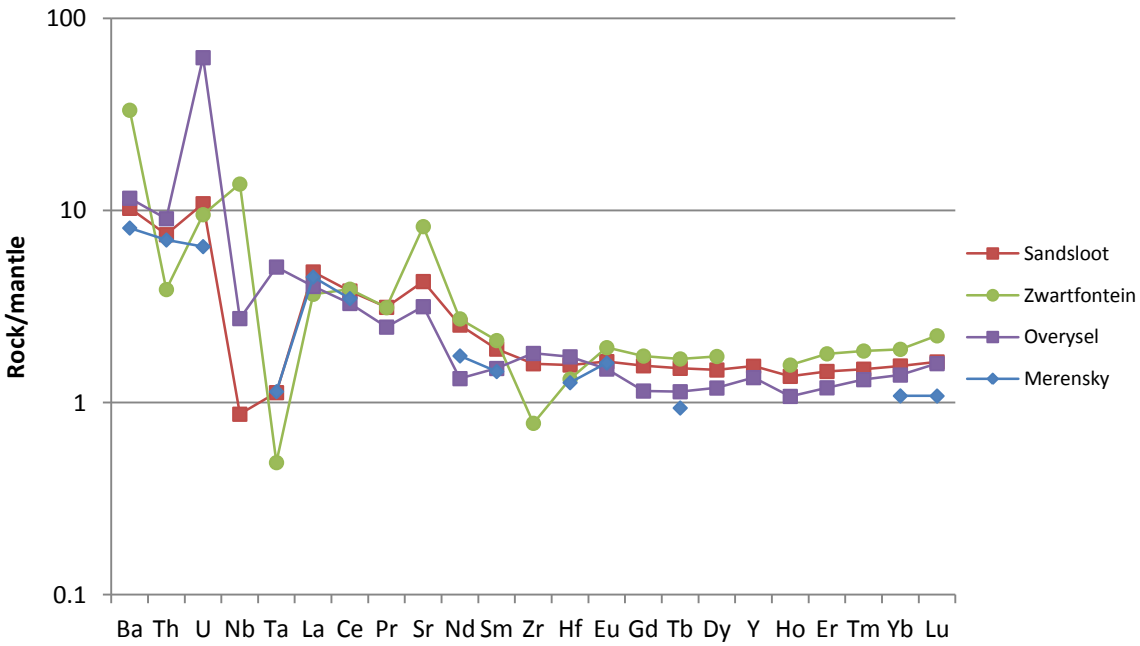


Figure 3.4. Mantle normalised multi-element variation diagram averages for the Central Sector farms of Sandsloot, Zwartfontein and Overysel (McDonald et al. 2005; Holwell 2006; Holwell and McDonald 2006) compared with the average Merensky Reef (Barnes and Maier 2002b). Mantle normalised data from McDonough and Sun (1995).

### 3.6.2 PGE & Au

A number of papers have been published demonstrating the enrichment of noble metals within the Platreef (e.g. Gain and Mostert 1982; Armitage et al. 2002; Naldrett 2004; Kinnaird 2005; Kinnaird et al. 2005; Manyeruke et al. 2005; Holwell and McDonald 2006). Typically, the grade for the Platreef is 3-4 g/t (Pt+Pd+Rh+Au) but may vary from <2.5 to 15 ppm and occasionally up to 25 ppm (Lee 1996) although the PGE grade is highest in association with chromite horizons where it commonly exceeds 8 g/t and values up to 260 g/t have been recorded (White 1994). Highest grades occur in the Central Sector where the footwall comprises of dolomite (see table 3. 3). Grades of > 4 g/t have been reported over tens of metres compared with grades for the mined interval of the Merensky Reef of 5-7 g/t uniform over 100 km of strike length. Naldrett et al. (2008b) showed that when the PGE abundances are expressed as tenors (where the Pt and Pd are recalculated to content in 100 % sulphide) there is a marked difference both through the Platreef package and along strike.

Several authors have recognised that often there is an association between visible sulphides and enhanced PGE grade in the Platreef (Lee 1996; Viljoen and Schurmann 1998; Manyeruke et al. 2005) although Kinnaird et al. (2005) showed that while there is a correlation between PGE and S at low abundances, high concentrations of Cu+Ni may not be matched by high PGE, and conversely increased PGE grade may not be linked to high Cu+Ni.

Wagner (1929) first recognised that the Platreef is notably Pd-rich (Pt/Pd ≤ 1) compared with PGE deposits in the rest of the Bushveld Complex, particularly the Merensky Reef where the ratio is 2-2.5 (table 3.3). Lee (1996) suggested that there is a systematic variation in the Pt:Pd ratio from north to south. On a local scale, variations in Pt/Pd from <0.1 to >10 do occur, especially in thick Platreef where different sills may carry different PGE budgets (e.g. Kinnaird 2005; Hutchinson and McDonald 2008; Naldrett et al. 2008b). Maier et al. (2008) have suggested that Pt/Pd variation correlates with varying amounts of sulphide and consider that the Platreef is an extension of the UG2-Merensky sequence. They suggest that the low Pt/Pd ratios are a consequence of the greater mobility of Pd in the margins of the intrusion due to the devolatisation of the floor rocks. To support this theory they would expect to see high Pt/Pd ratio cumulates away from the margins of the intrusion, to the west/south and down-dip of the Platreef. Data from Akanani, which is located in the proposed area, so far does not support this suggestion. McDonald et al. (2009) have suggested that the different metal ratios either side of TML could be a feature of magmas

arising from different types of sub-continental lithospheric mantle on either side of the lineament as discussed in the previous chapter.

Table 3.3. Metal ratios for the northern Bushveld (Aurora Project, Platreef and GNPA member) compared with the Merensky Reef and UG2 deposits from the eastern and Western Bushveld. Compiled by McDonald and Holwell (2011).

| | Grade (2PGE+Au) | Ni/Cu | Pt/Pd | (Pt+Pd)/Au |
|---|---|---|---|---|
| **Aurora Project** | | | | |
| Kransplaats | 1.17 | 0.73 | 0.73 | 6.62 |
| Nonenwerth | 1.36 | 0.64 | 0.60 | 5.98 |
| La Pucella-Altona | 1.37 | 0.81 | 0.60 | 5.97 |
| | | | | |
| **Platreef** | | | | |
| Drenthe | 1.05 | 1.50 | 0.83 | 12.1 |
| Akanani P2 Unit | 3.88 | 1.77 | 0.88 | 15.2 |
| Akanani P1 Unit | 2.51 | 1.88 | 0.73 | 17.8 |
| Zwartfontein South | 3.30 | 2.06 | 0.94 | 15.4 |
| Sandsloot | 3.19 | 1.33 | 0.97 | 14.1 |
| Tweefontein North | 6.90 | 1.75 | 1.05 | 12.9 |
| Tweefontein Hill | 5.00 | 1.21 | 0.62 | 7.21 |
| Townlands | 0.55 | 1.72 | 0.67 | - |
| | | | | |
| **GNPA Member** | | | | |
| War Springs (C Reef) | 1.24 | 1.33 | 0.21 | 16.7 |
| War Springs (B Reef) | 0.88 | 1.28 | 0.45 | 9.63 |
| Rooipoort M2 (MANO) | 1.34 | 1.70 | 0.51 | 13.1 |
| Rooipoort L3 (LMF) | 1.15 | 1.54 | 1.16 | 22.5 |
| | | | | |
| **NE Bushveld** | | | | |
| Lebowa Plats Merensky | 4.22 | - | 2.17 | 13.5 |
| Lesago Merensky | 5.89 | 1.54 | 1.73 | 12.8 |
| Lebowa Plats UG2 | 6.68 | - | 0.84 | 49.3 |
| GaPasha UG2 | 6.53 | - | 0.88 | 53.5 |
| Lesago UG2 | 6.27 | 2.00 | 1.15 | 44.5 |
| | | | | |
| **SE Bushveld** | | | | |
| Booysendal Merensky | 4.28 | 2.36 | 1.86 | 11.2 |
| Booysendal UG2 | 4.24 | 9.00 | 1.68 | 112 |
| | | | | |
| **Western Bushveld** | | | | |
| Frischgewaagd Merensky | 5.70 | 3.28 | 2.38 | 23.7 |
| Amandebult Merensky | 8.10 | - | 1.87 | 21.5 |
| RPM Merensky | 7.33 | 2.25 | 2.76 | 18.6 |
| Frischgewaagd UG2 | 4.51 | - | 2.43 | 100 |
| Amandebult UG2 | 5.21 | 11.00 | 2.23 | 125 |
| RPM UG2 | 5.36 | 9.00 | 1.60 | 128 |

### 3.6.3 Isotopes

The review paper of McDonald and Holwell (2011) summarises isotope work carried out in the northern limb. Some of the key findings are highlighted below:

#### *3.6.3.1 Sulphur isotopes*

Using sulphur isotope studies allows for the source of sulphur within a magmatic system to be determined as well as the timing of sulphur addition. The addition of external country rock S in the system can be quantitatively shown by the degree of deviance from the mean values for primary mantle values, providing the isotopic composition of S in the country rocks is sufficiently different from the mantle-derived S. Tsai (1979) showed that the range of $\delta^{34}S$ values for magmatic sulphides in the lithospheric mantle beneath the Kaapvaal Craton have $\delta^{34}S$ values of +0.2 to +2.1 ‰ in eclogites and associated kimberlites. Westerlund et al. (2004) analysed sulphide inclusions within diamonds from the Klipspringer kimberlites, close to the TML, producing $\delta^{34}S$ values in the range of -1.8 to +2.4 ‰.

Table 3.4. Sulphur isotope data for the Transvaal Supergroup sediments and basement rock in the northern limb.

| Formation | $\delta^{34}S$ Range | Reference |
|---|---|---|
| **Duitschland – pyrite** | +8.2 ‰ | (Sharman-Harris et al. 2005) |
| **Duitschland – hornfels** | +9.7 ‰ | (Sharman-Harris et al. 2005) |
| **Duitschland – anhydrite** | +20 ‰ | (Sharman-Harris et al. 2005) |
| **Duitschland – calc-silicates** | +16 ‰ to +29 ‰ | (Sharman-Harris et al. 2005) |
| **Timeball Hill + Silverton** | up to +17 ‰ | (Manyeruke et al. 2005) |
| **Malmani - calc-silicates** | +6 to +10 ‰ | (Buchanan and Rouse 1984) |
| **Malmani - anhydrite** | up to +20 ‰ | (Buchanan and Rouse 1984) |
| **Basement gneiss and granite** | -1.5 to +0.5 ‰ | (Holwell et al. 2007) |

Recent data for the footwall Transvaal Supergroup metasedimentary rocks frequently shows $\delta^{34}S$ values outside the mantle range (table 3.4). As a result, contamination of the Platreef sills by crustal sulphur can be assessed. In contrast basement granites and gneisses typically record S isotope ratios that are indistinguishable from mantle sulphur.

In the Central sector, $\delta^{34}S$ values of sulphides from 'primary' igneous pyroxenites have been shown to cluster around magmatic values (Holwell et al. 2007). Sulphur-bearing minerals from late veins are generally characterised by heavy sulphur isotope values that are similar to those of lithologies within the Malmani sub-group (Sharman-Harris et al. 2005; Holwell et al. 2007). Holwell et al. (2007) suggest that the addition of external S into the system was an ore-modifying process rather than an ore forming process.

### *3.6.3.2 Multiple sulphur isotopes*

Multiple sulphur isotope data has been generated for the Platreef to test whether sulphur saturation and the subsequent sulphide formation were triggered by the addition of sulphur from the underlying footwall.

Work by Penniston-Dorland et al. (2008) has shown that rocks from the Platreef and uncontaminated Main Zone rocks have mass independent S values that are much lower (average $\Delta^{33}S$ = 0.15 ‰) than the surrounding Transvaal Supergroup sediments ($\Delta^{33}S$ to 5.04 ‰), supporting the work of Holwell et al. (2007) that the source of the S is not due to contamination. Sharman et al. (2013) suggested that crustal sulphur in the Platreef originated from a restricted stratigraphic horizon (specifically the Duitschland Formation) and the widespread signature along strike suggests that it is not the result of sulphur inputs from the local footwall.

### *3.6.3.3 Samarium-neodymium isotopes*

Limited Sm-Nd isotope analysis has been carried out in the Platreef, mainly due to the low concentrations of Nd in most mineral phases. Sm-Nd isotope work carried out by Pronost et al. (2008) at Overysel and Maier et al. (2008) at Drenthe showed elevated εNd values with a range of -6.2 to -9.6. These values overlap with the Main Zone values obtained from western limb of -6.9 to -7.7 (Stevens 2004) and are at the upper range of the values for the Merensky Reef. They are however distinct from the values for the Critical and Lower Zone.

### *3.6.3.4 Osmium isotopes*

Reisberg et al. (2011) obtained a $^{187/186}Os$ isotopic range of 0.1820 to 0.1848 from the Sandsloot mine. This range is higher than contemporary mantle (~0.115) and higher than most Bushveld samples. They state that the values obtained in their study support a genetic link between the Platreef and the Merensky Reef (0.170-0.182; Schoenberg et al. 1999). They propose that their data are consistent with a parental magma for the Platreef that resembled either the magma that gave rise to the Critical Zone or that which gave rise to the Main Zone, and state that they cannot distinguish between these possibilities. The higher ratio for the Platreef may be due to more extensive assimilation in a crustal magma chamber or alternatively be due to the addition of a minor local contamination signature superimposed on a deep crustal signature (Harris and Chaumba 2001).

## 3.7 Comparison of the Platreef to the Merensky Reef

The Platreef has been equated to the Merensky Reef by many authors (e.g. Wagner 1929; van der Merwe 1978; Buchanan et al. 1981) but there are several significant differences between the Platreef and the Merensky Reef that have also been noted:

- ***The Platreef is much thicker than the Merensky Reef*** – The Platreef has been shown to exceed 400 m on parts of Turfspruit (Kinnaird et al. 2005) and Sandsloot (Holwell et al. 2006) but the Merensky Reef is typically only 1 m thick and rarely exceeds 10 m in thickness (Viljoen and Schurmann 1998).
- ***The Platreef is in direct contact with the basement floor or pre-Bushveld lithologies*** – The Platreef ore body lies either on the Transvaal Supergroup sediments or the Archaean basement (unless it is separated from these by the Lower Zone), whereas the Merensky Reef occurs within a layered sequence 2-3 km above the base (Cawthorn et al. 2006).
- ***PGE grades are more consistent in the Merensky Reef*** – Typically the grade for the Platreef is 3-4 g/t (Pt+Pd+Rh+Au) but may vary from <2.5 to 15 ppm, with higher grade zones of more than 17 g/t on the Akanani project (Kinnaird et al. 2010). This is in comparison to the mined interval of the Merensky Reef where grades of 5-7 g/t are uniform over 100 km of strike length (Cawthorn et al. 2006).
- ***Different PGM assemblages*** – PGMs in the Merensky Reef are dominated by sulphides and/or Pt-Fe or Pd alloys (Cawthorn et al. 2002b), whereas in the Platreef, data collected to date has shown that PGE- and semi metals (Te, Sb, Se, Bi and Ge-) bearing platinum-group minerals are common (Armitage et al. 2002; Hutchinson and Kinnaird 2005; Holwell et al. 2006).

Regardless of the differences between the Platreef and the Merensky Reef, the relationship between the Platreef and the rest of the Bushveld Complex stratigraphy remains uncertain. The Platreef may represent the northern limb equivalent of the Critical Zone, equate with the Merensky Reef or may have formed from magma that is entirely different from that which formed the rest of the Bushveld Complex. The various models are discussed further in the next chapter.

# Chapter 4: Mineral Deposit Formation

## 4.1 Magmatic sulphide deposits

Magmatic sulphide deposits form as the result of the segregation and concentration of droplets of liquid sulphide from mafic or ultramafic magma, and the partitioning of chalcophile elements into these from the silicate magma (Naldrett 2010c). These deposits contain a wide range of base, precious and semi-metals, with the most important products by value being Ni and Pd. The size of the deposits, their grades and ratio of economic metals are very variable and a selection is summarised in table 4.1 and their distribution worldwide is shown in figure 4.1.

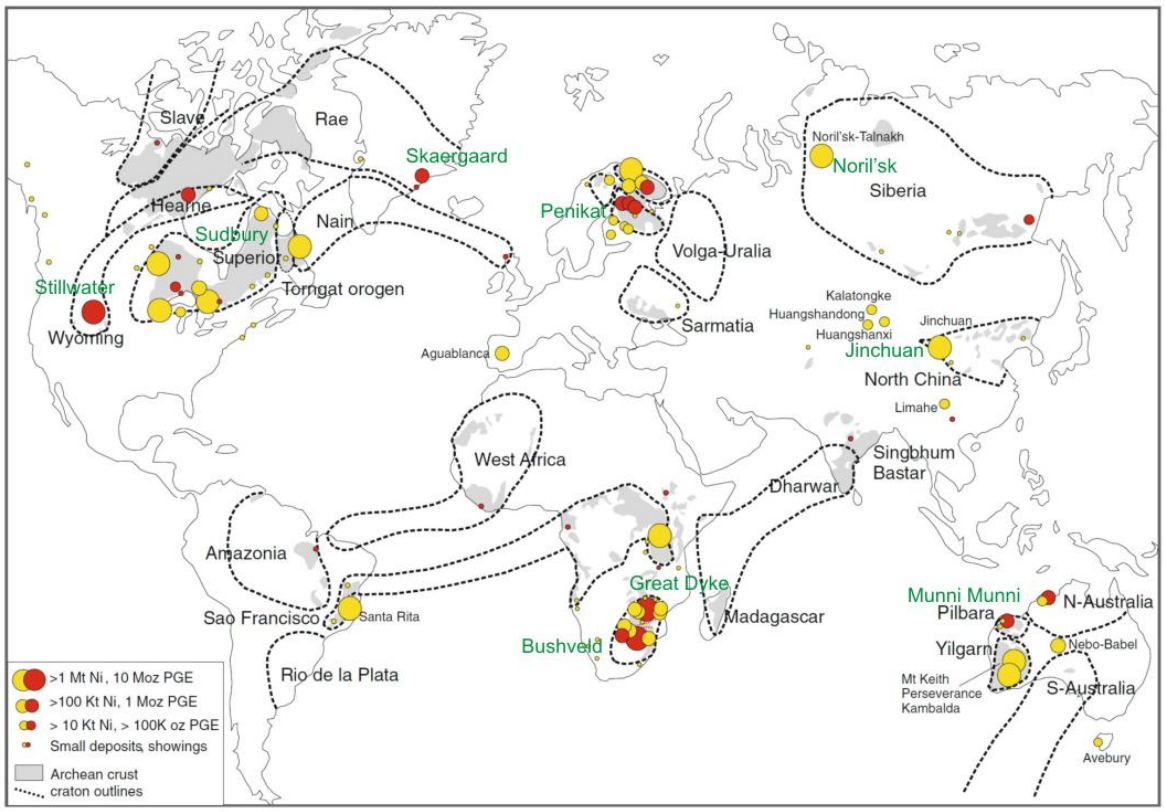


Figure 4.1. Distribution of PGE (in red) and Ni–Cu (in yellow) deposits worldwide. Some major deposits are labelled in green. Shaded pattern shows the distribution of Archaean crust and dotted lines show outlines of cratons and composite cratons amalgamated during the Proterozoic (modified from Maier and Groves 2011).

Table 4.1. Selection of Ni-Cu-PGE deposits worldwide showing their resources and value (compilation of data from Naldrett 2004; Naldrett 2010c and references therein). Prices used for August 2013: Ni = 14,730 US$/t; Cu = 7,821 US$/t; Pt = 1,492 US$/tr oz; Pd = 736 US$/tr oz; Rh = 1,010 US$/tr oz; Ru = 80 US$/tr oz; Ir = 825 US$/tr oz; Os = 360 US$/tr oz.

| Deposit/Camp | Ore resource ($10^6$ t) | Ni (wt%) | Cu (wt%) | Pt (g/t) | Pd (g/t) | Rh (g/t) | Ru (g/t) | Ir (g/t) | Os (g/t) | Total PGE (g/t) |
|---|---|---|---|---|---|---|---|---|---|---|
| **Raglan** | 32.8 | 2.87 | 0.81 | 0.825 | 2.266 | 0.150 | 0.374 | 0.065 | 0.080 | 3.759 |
| **Noril'sk** | 1,257.0 | 1.84 | 3.75 | 1.900 | 7.700 | 0.228 | 0.124 | 0.032 | 0.047 | 10.030 |
| **Duluth** | 4,000.0 | 0.20 | 0.60 | 0.146 | 0.490 | 0.007 | 0.007 | 0.003 | 0.003 | 0.655 |
| **Jinchuan** | 515.0 | 1.06 | 0.75 | 0.127 | 0.098 | 0.005 | 0.010 | 0.010 | 0.011 | 0.262 |
| **Voisey's Bay** | 136.7 | 1.59 | 0.85 | 0.075 | 0.097 | 0.005 | 0.007 | 0.002 | 0.002 | 0.188 |
| **Sudbury** | 1,648.0 | 1.20 | 1.09 | 0.463 | 0.583 | 0.056 | 0.044 | 0.019 | 0.008 | 1.173 |
| **Great Dyke** | 2,574.0 | 0.21 | 0.14 | 2.700 | 2.130 | 0.130 | 0.289 | 0.052 | 0.047 | 5.418 |
| **Merensky** | 4,210.0 | 0.15 | 0.06 | 3.566 | 1.850 | 0.216 | 0.449 | 0.082 | 0.051 | 6.214 |
| **UG-2** | 5,742.6 | 0.04 | 0.02 | 2.661 | 1.708 | 0.428 | 0.710 | 0.131 | 0.062 | 5.700 |
| **Platreef** | 1,597.3 | 0.41 | 0.20 | 1.765 | 2.006 | 0.114 | 0.165 | 0.038 | 0.033 | 4.121 |
| ***Total Bushveld*** | *11,549.9* | *0.13* | *0.06* | *2.870* | *1.800* | *0.307* | *0.539* | *0.100* | *0.054* | *5.670* |
| **Stillwater** | 323.2 | 0.04 | 0.02 | 4.340 | 15.850 | 0.270 | 0.100 | 0.096 | 0.043 | 20.699 |

| Deposit/Camp | Ni ($10^3$t) | Cu ($10^3$t) | Pt (t) | Pd (t) | Rh (t) | Ru (t) | Ir (t) | Os (t) | PGE (t) |
|---|---|---|---|---|---|---|---|---|---|
| **Raglan** | 942.3 | 265.5 | 27.1 | 74.32 | 4.92 | 12.26 | 2.13 | 2.62 | 123.30 |
| **Noril'sk** | 23,128.8 | 47,137.5 | 2,388.3 | 9,678.90 | 286.00 | 155.77 | 39.66 | 58.75 | 1,2607.38 |
| **Duluth** | 8,000.0 | 24,000.0 | 585.0 | 1,959.00 | 27.26 | 27.04 | 10.64 | 11.75 | 2,620.72 |
| **Jinchuan** | 5,459.0 | 3,888.0 | 65.5 | 50.57 | 2.53 | 5.14 | 5.26 | 5,76 | 134.75 |
| **Voisey's Bay** | 2,173.5 | 1,162.0 | 10.2 | 13.21 | 0.64 | 1.01 | 0.22 | 0.32 | 25.65 |
| **Sudbury** | 19,766.0 | 17,798.4 | 762.7 | 961.19 | 91.78 | 72.54 | 31.36 | 13.13 | 1,932.70 |
| **Great Dyke** | 5,405.4 | 3,603.6 | 7,130.0 | 5,482.62 | 335.32 | 743.76 | 134.88 | 119.76 | 13,946.32 |
| **Merensky** | 6,315.0 | 2,652.3 | 15,012.0 | 7,790.0 | 909.00 | 1,891.00 | 345.0 | 214.00 | 26,161.00 |
| **UG-2** | 2,411.9 | 1,033.7 | 15,279.0 | 9,809.00 | 2,457.00 | 4,077.00 | 752.00 | 356.00 | 32,730.00 |
| **Platreef** | 6,549.1 | 3,194.7 | 2,820.0 | 3,204.00 | 182.00 | 263.00 | 60.00 | 53.00 | 6,582.00 |
| ***Total Bushveld*** | *15,014.9* | *6,929.9* | *33,148.2* | *20,789.82* | *3,545.82* | *6,225.40* | *1,154.99* | *623.69* | *65,487.93* |
| **Stillwater** | 129.3 | 64.6 | 1,402.7 | 5,122.72 | 87.26 | 32.32 | 31.03 | 13.90 | 6,689.92 |

| Deposit/Camp | Ni ($10^6$US$) | Cu | Pt | Pd | Rh | Ru | Ir | Os | Total ($10^6$US$) | US$/t of ore | Value of PGE ($10^6$US$) | % as PGE |
|---|---|---|---|---|---|---|---|---|---|---|---|---|
| **Raglan** | 13,880 | 1,933 | 1,300 | 1,759 | 160 | 32 | 56 | 30 | 19,150 | 584 | 3,337 | 17 |
| **Noril'sk** | 340,687 | 343,185 | 114,564 | 229,031 | 9,287 | 401 | 1,052 | 680 | 1,038,886 | 826 | 355,015 | 34 |
| **Duluth** | 117.840 | 174,732 | 28,062 | 46,356 | 885 | 70 | 282 | 136 | 369,362 | 92 | 75,790 | 21 |
| **Jinchuan** | 80,411 | 28,307 | 3,142 | 1,197 | 82 | 13 | 140 | 67 | 113,358 | 220 | 4,640 | 4 |
| **Voisey's Bay** | 32,016 | 8,460 | 489 | 313 | 21 | 3 | 6 | 4 | 41,310 | 302 | 835 | 2 |
| **Sudbury** | 291,153 | 129,581 | 36,586 | 22,745 | 2,980 | 187 | 832 | 152 | 484,215 | 294 | 63,481 | 13 |
| **Great Dyke** | 79.622 | 26,236 | 342,018 | 129,735 | 10,889 | 1,913 | 3,578 | 1,386 | 595,375 | 231 | 489,518 | 82 |
| **Merensky** | 93,020 | 19,310 | 720,108 | 184,334 | 29,517 | 4,864 | 9,151 | 2,477 | 1,062,781 | 252 | 950,451 | 89 |
| **UG-2** | 35,527 | 7,526 | 732,916 | 232,110 | 79,784 | 10,486 | 19,946 | 4,120 | 1,122,416 | 195 | 1,079,363 | 96 |
| **Platreef** | 96,468 | 23,259 | 135,272 | 75,816 | 5,910 | 676 | 1,591 | 613 | 339,607 | 213 | 219,879 | 65 |
| ***Total Bushveld*** | 221,169 | 50,453 | 1,590,081 | 491,948 | 115,141 | 16,012 | 30,635 | 7,219 | 2,522,658 | 218 | 2,251,035 | 89 |
| **Stillwater** | 1,905 | 470 | 67,286 | 121,218 | 2,834 | 83 | 823 | 161 | 194,780 | 603 | 192,405 | 99 |

Magmatic sulphide deposits can be divided into two economic groups, those that are exploited for their Ni and Cu content and those whose economic value lies primarily with the PGE content. Deposits that are Ni and Cu rich tend to be rich in sulphide with the ore containing between 20 and 90 % sulphide, whereas those that are PGE rich tend to be sulphide poor with ore containing 0.5 to 5 % sulphide (Naldrett 2010c).

Although major Ni-Cu and PGE deposits occur worldwide, figure 4.1 shows that all of the major PGE deposits are located within stabilised cratons and many occur within the central segments of the cratons. Groves et al. (2005) suggest this attribute may simply be a preservation effect, although it could also be due to the melting of the SCLM, to be discussed later in this chapter. Large Ni-Cu deposits, however, are preferentially located

near craton margins. This has been suggested to be as a result of the deposits crystallising from magmas that are predominantly derived from convecting mantle (Maier and Groves 2011).

Well mineralised cratons include the Kaapvaal (mainly PGE deposits), Zimbabwe (PGE and Ni-Cu), Superior (PGE and Ni-Cu), Karelia and Kola cratons (PGE and Ni-Cu), and the Yilgarn (Ni-Cu only). The cratons of West Africa, Volga-Uralia, Congo and Rio de la Planta appear to be unmineralised with respect to Ni-Cu and PGE according to figure 4.1, but these tend to be the least explored cratons as exploration companies are drawn to the cratons which have historic record of discoveries.

In terms of the distribution of PGE deposits through time, all of the largest PGE deposits are older than ca. 1.8 Ga (e.g. Bushveld, Great Dyke, Stillwater, Stella etc). An exception to this is the Skaergaard intrusion which is only 0.06 Ga.

More than 75 % of world's known PGE resource occurs in two complexes, the Bushveld and the Great Dyke (Mungall and Naldrett 2008). Spatially, these deposits are less than 600 km apart, which might suggest that the mantle in this region was particularly PGE enriched during the late Neoarchaean and Paleoproterozoic. This observation was first made by Wagner (1929) who extended a potential 'ore canal' from South Africa through Zimbabwe to the East African Rift Valley. As shown in the previous chapters, the Bushveld Complex was intruded into the Kaapvaal Craton, whereas the 2.58 Ga Great Dyke intruded the Zimbabwe Craton. The Zimbabwe Craton combined with the Kaapvaal Craton to form the Kalahari Craton – initial collision occurred at 2.61 Ga with final welding around 2.0 Ga (Griffin et al. 2003; Griffin et al. 2004). Variable seismic velocities below the Kalahari Craton have been interpreted by Begg et al. (2009) and Griffin et al. (2009) to be a result of refertilisation of depleted mantle by subsequent intrusion of magma and introduction of fluids. Below the Zimbabwe Craton and the southern part of the Kaapvaal Craton there are roots of highly depleted dunite and harzburgite that reach depths of 300 km or more. However, the northern Kaapvaal Craton, in between these two cratons, only has a root that reaches a depth of up to 175 km as suggested by lower seismic velocities (Begg et al. 2009). They interpret this to be as a result of refertilisation of this portion of the roots of the Kaapvaal Craton and suggest that this is related to the Bushveld event. However, to the north of the Bushveld Complex, the Great Dyke cuts through what is considered classic depleted Archaean lithosphere. Therefore, it has been pointed out by Naldrett (2010c) that if there is a PGE-rich zone within the mantle in southern Africa, it is unlikely to be in the

roots of what is now the Kalahari Craton but must be a feature of the deep (>300 km) asthenosphere that survived for the 500 million year intervening between emplacement of the two bodies, or of a very long-lived PGE-rich deep mantle plume that cut through both asthenosphere and lithosphere. However, had these PGE deposits formed as a result of mantle plumes, then their distribution could be expected to have been more widespread.

## 4.2 Formation of magmatic sulphide deposits

Magmatic sulphide deposits form from relatively magnesian, primitive, mantle-derived magmas or their products. The magma needs to become saturated in a sulphide liquid during cooling, the chalcophile elements need to partition effectively into the sulphide liquid, and the sulphide liquid needs to be concentrated during crystallisation of the magma, either on top of a cumulate pile or in flow dynamic traps within magma feeder conduits (Maier and Groves 2011). Above all, the sulphides need to have reacted with enough magma to concentrate the chalcophile metals to economic levels. The formation of magmatic sulphide deposits is considered by Naldrett (2010c) as a series of stages. These are illustrated in figure 4.8 and the stages are discussed below.

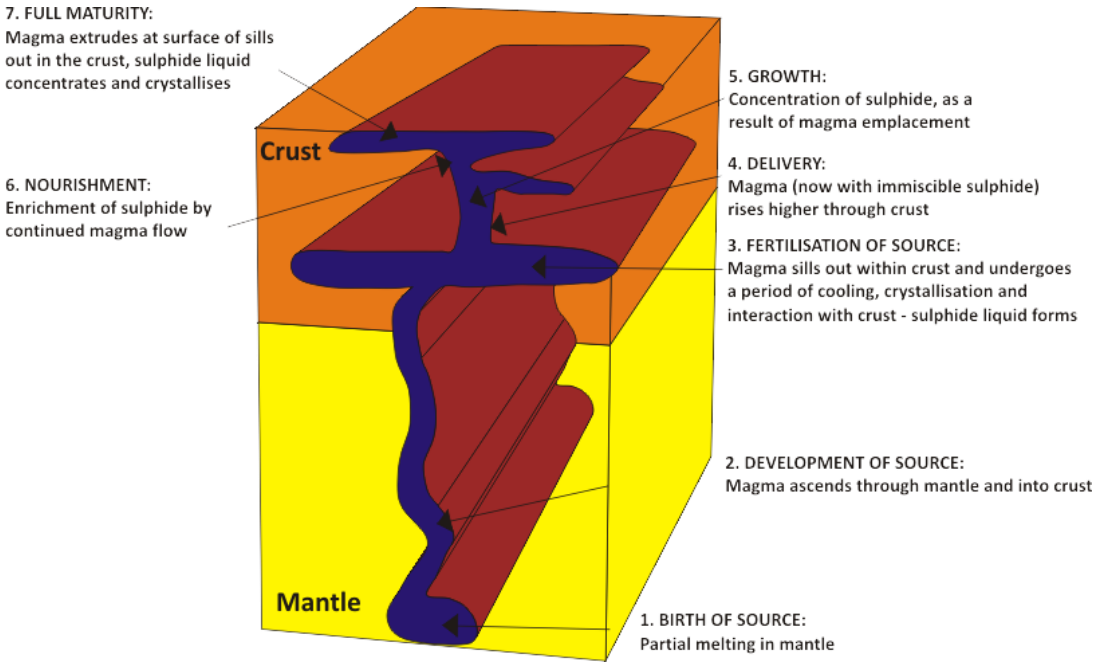


Figure 4.2. Stages in the formation of a magmatic sulphide deposit, starting with the partial melting in the mantle and then the rise of the magma into the crust, and the processes that it undergoes there (modified from Naldrett 2010c)

***(1) BIRTH OF SOURCE:*** Generation of mafic-ultramafic magma as a result of mantle melting;

The parental magmas for PGE deposits are derived from the mantle, where most mafic/ultramafic magmas originate, as crustal rocks tend to be poor in PGE (e.g. 1 ppb Pd in the crust vs. 7 ppb in primitive mantle; Becker et al. 2006).

## Degree of partial melting

In order to get fertile magmas, in terms of chalcophile metals, large degrees of melting are required. Phases present in the mantle are silicates (98 %), spinel (2 %), sulphides (0.07 %) and possibly metal alloys (<0.05 %; Barnes and Maier 1999). PGEs and Cu in the mantle are hosted by sulphides (Alard et al. 2000), whereas the Ni in the mantle is predominantly hosted by olivine. Since the initial study of mantle nodules by Mitchell and Keays (1981), sulphides have been regarded as the main host for the highly siderophile elements (PGE, Au & Re) in the mantle. Laser ablation studies of mantle sulphides by Alard et al. (2000) have shown that the PGEs, with the common exception of Pt, are hosted by sulphide phases. It was also shown that Os, Ir & Ru are hosted both by the sulphides and the alloys associated with them. Under conditions of decreasing oxygen fugacity Pt is more stable as an alloy than in solid solution in a base metal sulphide. The Ni content of the magmas increases proportionally with the olivine content of the molten source (Maier and Groves 2011). For the magma to be both PGE- and Cu- rich, the mantle sulphides need to be dissolved in the mantle melt.

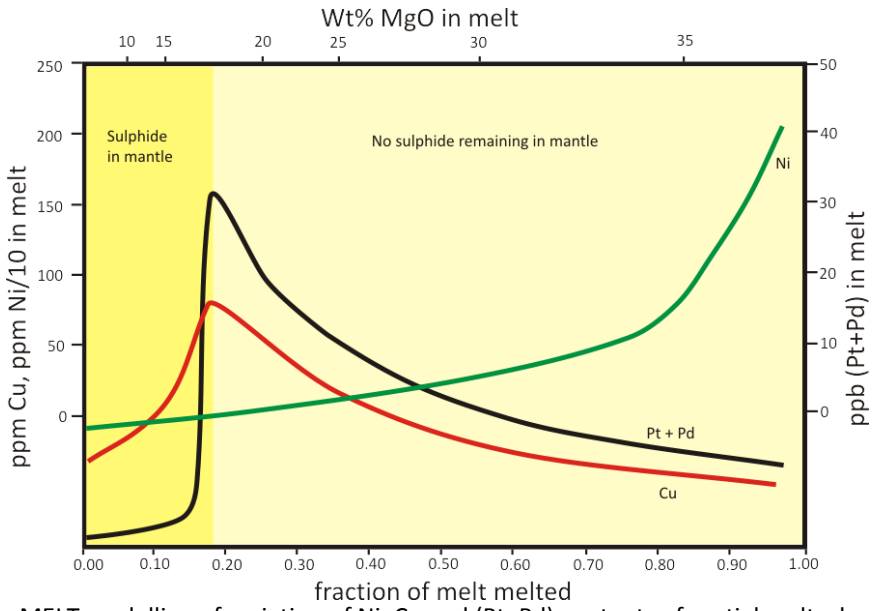


Figure 4.3. pMELT modelling of variation of Ni, Cu and (Pt+Pd) contents of partial melts developed though mantle melting of spinel lherzolites at 20 kbar (redrawn from Naldrett 2010c)

Naldrett (2010c) used the pMELTS program (Ghiorso et al. 2002) to calculate the variation in the Ni, Cu, and Pt+Pd contents of partial melts derived through melting spinel lherzolites mantle at 20 kbars (≈ 60 km depth), which is shown in figure 4.3. As the degree of melting increases, and subsequently the amount of sulphide dissolved in the melt increases, the concentration of Cu and PGE increases. Due to the relatively low S solubilities of most basaltic-komatiite magmas a significant amount of melting is required. The model shows that by 18 % melting, the sulphide present in source is entirely dissolved. Once all the sulphide in the magma is dissolved, the Cu and PGE concentrations reach their maximum concentration. The concentrations of Cu and some PGE (Pt, Pt and Rh) subsequently decrease due to their dilution as the degree of melting increases. The PGE are much more chalcophile than Cu and as a result the effect is more noticeable. Conversely, Ni concentration only increases slowly during partial melting, which can be attributed to the release of Ni from olivine structure as it melts.

With very few chilled margins or fine grained feeder dykes to PGE mineralised intrusions that are uncontaminated by country rocks or percolating sulphides from the overlying cumulates, Maier and Barnes (2009) stated that it is unclear how much PGE the magma should have in order that an ore deposit can form. Fine grained sills in the floor rocks of the Bushveld Complex that are generally interpreted to represent the parental magmas have ca. 12 ppb Pd and 18 ppb Pt (Davies and Tredoux 1985; Barnes and Maier 2002a), comparable to most continental and oceanic mafic-ultramafic magmas (Maier and Barnes 2004). The North Atlantic flood basalt province hosting the Skaergaard intrusion tends to have relatively elevated PGE contents (up to 15 ppb Pt and 25 ppb Pd).

The timing in which the magma is released from its source is very important. If a magma is released from its source after only a small amount of partial melting has taken place, then it will have a very low concentration of PGE. Magmas that are released once all the sulphide has been dissolved in the magma are the richest in PGE and Cu (fig. 4.3).

### Composition of mantle source

Most PGE and Ni deposits tend to be associated with rocks that crystallised from primitive relatively magnesian (>8 to 10 % MgO) mantle-derived magmas and the most primitive magmas are interpreted to be derived from the adiabatic melting of mantle plumes in a convecting mantle (Maier and Groves 2011). In contrast, very few magmas are generally believed to be SCLM derived, with the exception of some kimberlites and lamproites (Lambert et al. 1995; Gurney et al. 2005).

Richardson and Shirey (2008) suggested that the parental magmas to PGE deposits are derived from both convecting mantle and the SCLM and attribute their Archaean-Proterozoic ages and locations within Archaean cratons to a combination of factors including the composition of the SCLM, the relatively stable tectonic environment and the resulting enhanced preservation potential of the deposits. Maier and Groves (2011) also suggested that the location of most PGE deposits within cratons and the recurrent nature of PGE-Ni-Cu mineralisation events on some cratons such as Karelia suggest that a SCLM control on magma generation is a possibility. Hamlyn and Keays (1986) first proposed a SCLM derivation of parental magmas to PGE deposits. They assumed that a mantle source that had undergone a previous small-degree melting event would be PGE-rich due to residual enrichment in PGE. Subsequent second-stage melting of such mantle would liberate the PGE, resulting in a PGE-rich magma. However, work by authors such as Pearson et al. (2004) has shown that the SCLM is relatively PGE-depleted, probably as a result of Archaean and early Proterozoic melting events. An exception to this is work carried out by McInnes et al. (1999) who showed a PGE-enriched source to ore metals in an island arc setting. Other than the Bushveld magmas, very few other terrestrial magmas have been identified that are abnormally PGE-enriched (Barnes et al. 2010) and therefore lend little support to the SCLM derivation of the parental magmas.

However, a SCLM component in the magmas is consistent with the relative Pt enrichment of many SCLM samples that match the Pt enrichment of the Bushveld Complex (Maier and Barnes 2004; Pearson et al. 2004). A possible model to combine the contrasting observations has been proposed by Barnes et al. (2010) who suggested that the SCLM is infiltrated by magmas derived from the sub-lithospheric mantle, preferentially extracting Pt from relatively PGE-poor lithologies, essentially representing a type of zone melting. Maier and Groves (2011) suggested that metasomatism would be the key process because it may cause refractory Pt alloys to become fusible in some portions of the SCLM.

The main alternative model to a SCLM origin of the parental magmas to PGE deposits is the convecting mantle, via adiabatic melting of mantle plumes (Maier and Groves 2011). In this model, significant contamination with the upper crust is modelled to achieve the high crustal component (Maier et al. 2000). This model implies that the PGE contents of the magmas would have been much higher than those recorded. Work by Maier et al. (2009) showed that by 2.9 Ga the lower mantle had largely equilibrated with the late veneer and the PGE content was broadly similar to that of modern primitive upper mantle, yet the

19 ppb Pt in the Bushveld magmas already constitute the upper limit of the terrestrial data field of basaltic-komatiitic magmas (e.g. Maier et al. 2009).

Another alternative proposed is to suggest an anomalous Pt-enriched mantle source. Examples include the addition of Pt-rich late veneer or addition of core material (Maier and Groves 2011). While these ideas are essentially speculative, ultimately there needs to be some explanation as to why more than 50 % of the world's PGE resources are hosted in a single intrusion.

***(2) DEVELOPMENT OF SOURCE:*** Ascent of the magma through the mantle and into the crust;

Magmas need a pathway from the mantle to ascend into the crust. These can be created through the extension of the crust and the lithosphere, with the extension driven by mantle convection. Extension may be on a regional (e.g. rifts) or local scale. Naldrett (2010c) stated that with primitive magmas, the ascent pathways need to be trans-lithospheric as the dense magmas cannot ascend through the relatively light upper crust. The ascent also needs to be rapid in order to prevent differentiation and loss of metals to segregating olivine and sulphide.

The pathways for magma ascent may be crustal-scale lineaments within cratons, which represent long-lived suture zones between proto-cratons e.g. the TML for the Bushveld Complex. Reactivation of such suture zones causes localised extension and may rarely lead to rifting and even cratonic-continental break-up, causing the development of flood basalts. In most cases, however, the brief extension and minor rifting is then aborted. These produce ideal conditions for the emplacement of large sill-like layered intrusions.

Begg et al. (2010) demonstrated that crustal-scale lineaments are particularly common along craton margins because deformational strain is focused in these environments. Kerrich et al. (2000) suggested that mantle plumes may be channelled to irregularities along lithospheric boundaries below cratonic margins.

The magma needs to ascent to the upper crust without losing the PGE component en route. As the magma ascents from the source, the decreasing pressure increases the ability of a magma to dissolve sulphur. Work by Mavrogenes and O'Neill (1999) has shown that sulphur content at sulphide saturation (SCSS) in basaltic magma increases with falling pressure. Their work showed that a basaltic magma can dissolve a maximum of ~1000 ppm sulphur at upper mantle pressures. If this effect outweighs the decrease in SCSS resulting from cooling

of the magma, primary mantle-derived basic-ultramafic magmas should be initially sulphide undersaturated during emplacement in the crust. As a result, a magma that was saturated in sulphur when it left the source area is no longer saturated as it reaches the surface.

***(3) FERTILISATION OF SOURCE:*** Interaction of the magma with the crust. This is usually required for the early development of the immiscible sulphide liquid.

Unlike in the formation of Ni-Cu deposits, interaction of the magma with the crust does not necessarily result in sulphide immiscibility being induced during the formation of PGE-rich deposits, although it may have occurred during magma emplacement (Barnes and Maier 2002b). It is possible that sulphide immiscibility is achieved as a result of only a portion of the magma reacting with the crustal rocks resulting in a high ratio of sulphide formed to magma affected (Naldrett 2010c). This situation is also characterised by low R factor (ratio of magma to sulphide involved in the interaction; Campbell and Naldrett 1979). As a result, the Ni, Cu, and PGE contents of a small amount of magma are contained within a relatively large amount of sulphide. The low tenors of these metals in the sulphide means that the ore is often uneconomic (Naldrett 2010c).

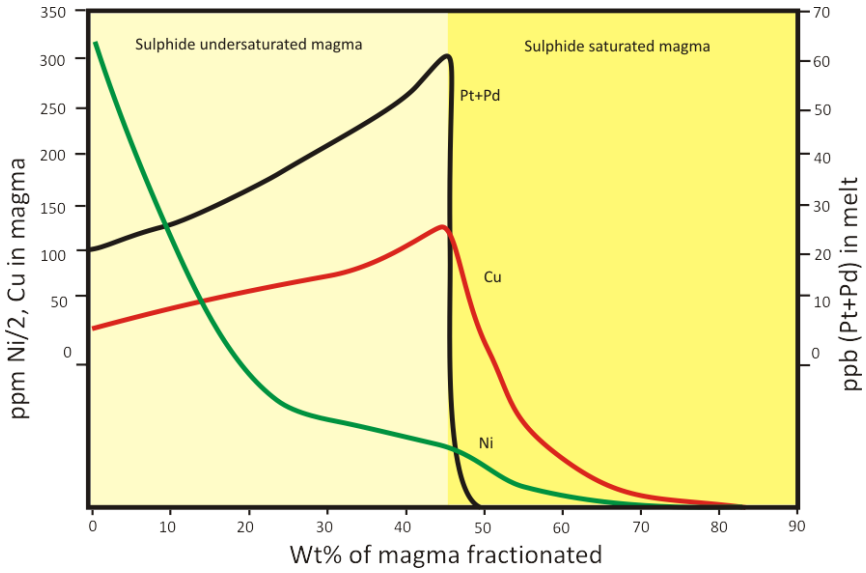


Figure 4.4. Fractional crystallisation of the magma produced by 18 % partial melting produced from figure 4.3 produced by Naldrett (2010c) using the pMELTS program (Ghiorso et al. 2002). In the 18 % melt chosen for this example all of the sulphide in the mantle had just been dissolved at the stage that the partial melt left its source so that Cu and Pt+Pd are at their maxima (redrawn from Naldrett 2010c)

Once a magma starts to crystallise, its dissolved sulphide content is held in a progressively smaller amount of liquid so that concentration increases to reach the sulphide solubility limit of the liquid. Once an immiscible sulphide liquid develops in a silicate magma, it concentrates chalcophile metals in proportion to their effective partition coefficients (e.g.

Peach et al. 1990; Fleet et al. 1993; Crocket et al. 1997). Certain elements, notably the Group VIII transition metals Fe, Co, Ni, Pd, Pt, Rh, Ru, Ir and Os together with Cu and Au, partition strongly into the sulphide-oxide liquid, becoming concentrated within it (Naldrett 2004).

On cooling, the magma will crystallise silicates and the sulphur content will build up in the remaining magma, eventually reaching saturation level. Figure 4.4 shows the variation in Ni, Cu and PGE resulting from fractional crystallisation. Sulphide immiscibility is not reached until 45-50 % of the magma has crystallised, by which stage most of the Ni has been removed in early-formed silicates. PGE concentrations rapidly decrease once sulphide saturation is reached and the sulphides are removed from the magma.

***(4) DELIVERY:*** Further ascent of the magma plus immiscible sulphide droplets to higher levels in the crust;

During further ascent of the magma, the addition of new magma displaces early-depleted magma, adding additional chalcophile elements to the sulphides, and dissolving some of the sulphide liquid (as it is sulphide undersaturated) which leaves the remaining sulphide liquid enriched in its more chalcophile portions.

***(5) GROWTH:*** Concentration of the sulphides as a result of magma emplacement;

The sulphide liquid needs to be concentrated during crystallisation of magma in order for an economic deposit to form, with concentration occurring either on top of a cumulate pile or in flow dynamic traps within magma feeder conduits.

The density of sulphide liquid varies depending on its composition, as shown by Mungall and Su (2005), with densities from around 4.0 g/cm$^3$ for pure FeS liquid to in excess of 5 g/cm$^3$ for both NiS and $Cu_2S$ liquids. This affects the rate at which the sulphide droplets settle and settling can also be affected by the presence of phenocrysts in the silicate magma (Naldrett 2010a). The surface tension within the magma has an influence on concentrating the sulphide liquid. The effects have been investigated experimentally by a number of studies (e.g. Lesher and Groves 1986; De Bremond d'Ars et al. 2001; Mungall and Su 2005; Chung and Mungall 2009). If there is a density difference between the sulphide liquid and the silicate liquid, the sulphides may be transported vertically in the liquid if its upward velocity is greater than the settling rate but any decrease in velocity may cause sulphides to settle and pond (Naldrett 2010a).

***(6) NOURISHMENT:*** Enrichment of the sulphides due to reaction with further flowing magma.

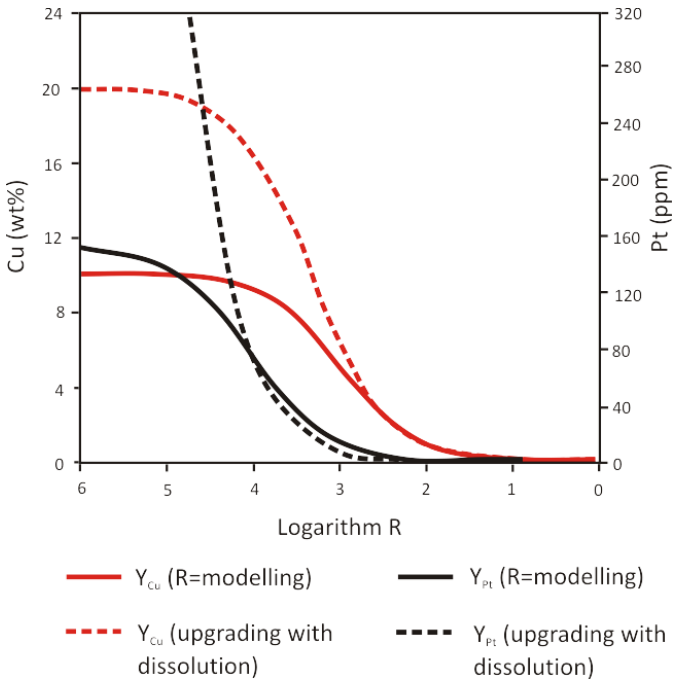


Figure 4.5. The effect of variations in silicate magma-sulphide liquid mass ratio on the concentrations of Cu and Pt of sulphides in equilibrium with basaltic magma containing typical concentrations of these elements (100 ppm Cu, 15 ppb Pt; DCu = 1,000, DPt = 10,000). One set of curves illustrates simple variations in R factor. The other set illustrates the variation in metals if a series of pulses (or a continuous stream) of magma interact with the sulphides, exchanging chalcophile metals and dissolving away some of the FeS component of the sulphide liquid. In the example shown, it is assumed that each successive pulse of magma has 100 times the mass of the remaining sulphide, and that the magma dissolves an amount of sulphide equal to 0.05 percent of its own mass. R in this case is the sum of all pulses of magma that have passed through the system (based on Kerr and Leitch 2005; redrawn from Naldrett 2010c).

Naldrett (2010b) stated that it is possible that this step is not always involved, but has been documented to have occurred in several deposits. Examination of magmas at Noril'sk and Voisey's Bay has shown that the first sulphides to form had low chalcophile metal tenors (Naldrett 2010a), at sub-economic levels. However, it has been suggested that the sulphides in both deposits were enriched to economic levels through interaction with later magma batches passing through the same magma conduits (e.g. Naldrett et al. 1995; Li and Naldrett 1999). The effect of a fresh pulse of magma interacting with the early sulphide is shown in figure 4.5 based on modelling by Kerr and Leitch (2005). The dashed lines represent the variation in metals if a series of pulses of magma interact with the sulphides, exchanging chalcophile metals and dissolving some of the FeS component of the sulphide liquid, in a process known as multi-stage dissolution upgrading. This type of enrichment is not

necessarily constrained to this stage, Naldrett (2010c) stated that it may occur during ascent (stage 4) or once the sulphides have reached their final resting place (stage 5).

It is proposed that long-lived conduit systems, which are exploited by many generations of magma pulses, provided a setting for the initial deposition of the sulphide liquid and any subsequent enrichment. This is an important factor in the development of many magmatic Ni-Cu deposits. The development of such a model for the Platreef is discussed later in this chapter.

***(7) FULL MATURITY:*** Cooling and crystallisation of the host magma and related sulphide liquids.

Sulphide liquids cool over a temperature interval, with different minerals appearing on the liquidus at different temperatures (Naldrett 2004). Once the sulphide liquid cools it begins to fractionate, with the early-forming monosulphide solid solution (mss) concentrating Rh, Ir and Os, with the remaining sulphide liquid concentrating Cu, Pt, Pd and Au. The base metal sulphides are important carriers of PGE in addition to other chalcophile elements and the general process of BMS fractionation is discussed in greater depth in chapter 8.

## 4.3 Classification of PGE deposits

PGE mineralisation in layered intrusions occurs in a range of rock types and at various stratigraphic levels in intrusions of any age, size and magmatic lineage. However, the most important deposits occur as relatively narrow, broadly stratiform PGE-rich layers, known as reefs, in the lower to central parts of ultramafic to mafic, large layered intrusions of late Archaean to early Proterozoic age (Maier and Barnes 2009).

PGE mineralisation is generally associated with sulphides (pyrrhotite, pentlandite and chalcopyrite). Exceptions to this occur in some chromitite reefs where the PGE are mainly hosted by the platinum-group minerals (Cawthorn et al. 2005). Typically, the sulphide content is low (<1–3 %), but the sulphides have high metal tenors (hundreds of parts per million PGE). There is a whole spectrum of mafic-ultramafic host rocks (dunite, harzburgite, pyroxenite, norite–gabbronorite–gabbro, troctolite, anorthosite, chromitite and magnetite), but the most common types of reef are chromitite- and orthopyroxenite-hosted reefs (Maier and Groves 2011). In a review of PGE deposits worldwide, Maier and Groves (2011) found that some reefs (Merensky Reef, J-M Reef) may be characterised by pegmatoidal textures, and some contain thin chromitite stringers associated with the silicate rocks (Merensky Reef, SJ Reef of the Penikat intrusion). They found that the richest and most

continuous reefs tend to occur in the largest intrusions. For example, the PGE reefs of the giant Bushveld Complex can be laterally correlated over tens of kilometres. Less continuous and more irregular reefs are characteristic of smaller intrusions (e.g. Penikat, Finland; Munni Munni and Panton, Australia). They also found that reef thickness varies significantly. The thinnest reefs have the highest grades, and tend to be located within larger intrusions.

PGE deposits can be classified based on their stratigraphic position within layered intrusions. Maier and Barnes (2009) divided them into 5 groups:

(1) PGE mineralisation intervals at the contact with the country rocks, often hosted by varied-textured gabbronoritic rocks (e.g. Platreef, Bushveld Complex);

(2) PGE reefs within ultramafic silicate cumulates in the lower portion of the intrusions (e.g. Kapalagula, Main Sulphide Zone of Great Dyke);

(3) PGE enriched chromitites (e.g. UG2 of Bushveld Complex);

(4) PGE reefs associated with strongly layered mafic-ultramafic cumulates in the central portions of intrusions (e.g. Merensky Reef of Bushveld Complex, J-M reef of Stillwater Complex);

(5) PGE mineralisation zone in the upper, gabbroic-dioritic, often magnetite-rich, portion of intrusions (e.g. Skaergaard, Rinco del Tigre), occasionally forming mineralised massive magnetite layers (e.g. Stella).

Maier and Barnes (2009) stated that the different types of reefs can be distinguished in terms of their composition and width. For example, reefs located at stratigraphically low positions tend to relatively enriched in IPGE (Os, Ir, Ru) compared to the PPGE (Rh, Pt, Pd). Contact-style reefs and reefs in the ultramafic and upper portions of the intrusions tend to be relatively thick (on the order of 10s of metres), whereas chromitite- and silicate-hosted reefs in the central, layered portions of intrusions tend to be thinner (centimetre to metres).

## 4.4 Platreef formation

The Platreef provides a challenge to those trying to unravel its genesis. Its heterogenetic stratigraphy and localised variability, discussed in the previous chapter, make it very hard to correlate with the relatively straightforward stratigraphy of the eastern and western limbs. As a result, its economic mineralisation and its relationship with the rest of the Bushveld

remains poorly understood. As yet there is no general agreement as to whether the Platreef is related to the Bushveld intrusions of the eastern and western limbs.

Over the past decade, various models have been proposed in order to explain the formation of the Platreef. It is still being debated whether the Platreef formed as a product of a single continuous magmatic event or from multiple intrusive pulses. Authors such as Kinnaird et al. (2005) and Kruger (2005a) generally believed that the Platreef is a result of at least three magmatic pulses.

According to McDonald and Holwell (2011) any comprehensive genetic model for the Platreef must account for, or explain, the following:

- The marginal setting;
- Why sulphide mineralisation is present along the entire strike length of the Platreef, regardless of type of country rock with which the reef is in contact;
- Why primary sulphides in the high grade Central Sector are dominated by mantle-type sulphur (with a component of mass independent sulphur);
- The source (or sources) of the Ni, Cu, and PGE and a mechanism to concentrate them in the Platreef;
- The Sr, Nd and Os isotope signatures found in the Platreef;
- The mineral chemistry and trace element geochemistry of the Platreef;
- The apparently Pd-rich chemistry of PGE deposits in the northern limb compared to the rest of the Bushveld;
- The cause(s) of variations in mineralogy and geochemistry – particularly bulk PGE grades and PGE tenors in sulphides – observed along strike, down dip, and vertically within the Platreef;
- The sill-like form of the Platreef and intrusion of the Main Zone significantly after it formed;
- Evidence for chalcophile element depletion and interaction with sulphide in some Lower Zone intrusions.

Table 4.2 Comparison of a few contact-type sulphide deposits found worldwide.

| Deposit | Intrusion | Age (Ma) | Resource (Mt) | 4E Grade (Pt+Pd+Rh+Au) | Reference |
|---|---|---|---|---|---|
| **Mogalakwena (Platreef)** | Bushveld | 2054 | 2170.5 | 2.03 g/t | (Anglo Platinum 2010) |
| **Sheba's Ridge (E Limb)** | Bushveld | 2054 | 241 | 0.9 g/t | (Anglo Platinum 2010) |
| **Birch Lake** | Duluth | 1099 | 131.2 | 0.9 g/t | (Duluth Metals Ltd) |
| **Ahmavaara** | Portimo | 2440 | 187.7 | 1 g/t | (Zientek 2012) |
| **Dana** | River Valley | 2440 | 16.5 | 1.36 g/t | (Anglo Platinum 2010) |

At first glance, the Platreef can be likened to a standard contact-type sulphide deposit similar to those found in the Duluth Complex (table 4.2; Ripley 1990). However PGE grades in the Central Sector (e.g. Holwell and McDonald 2006) are often an order of magnitude greater than in other contact-type settings and are comparable to those found in the Merensky Reef (e.g. Godel et al. 2007).

To achieve such high grades, the PGE in the Platreef must have been concentrated from a very large volume of magma. Cawthorn et al. (2002b) calculated that assuming the complete removal of PGE from an overlying magma with an average PGE concentration of 0.02 ppm, requires a magma column ~10,000 metres high in order to produce a model Platreef that is 100 metres thick with an average grade of 2 ppm PGE. In reality, the Platreef has been shown (e.g. Hutchinson and Kinnaird 2005; Kinnaird 2005; Holwell and McDonald 2006) to only carry the high grades (1-10 ppm PGE) in tens of metre intervals with lower grade zones in between. This would suggest that Cawthorn et al.'s (2002b) calculation was probably an overestimation but it shows the problems associated with trying to develop a genetic model for the Platreef. One criticism of this model is that it considers the PGE in the Platreef being derived from an overlying magma represented by the Main Zone gabbronorites, however the relationship between the Platreef and the Main Zone rocks indicates this cannot be the case as has been discussed in the previous chapter.

McDonald and Holwell (2011) divided current and past Platreef models into two classes. Class 1 models involve the generation of sulphide and the collection of PGE through in situ contamination, whilst the Class 2 models involve the introduction of sulphides that have been collected and transported from an external source.

They disregarded the Class 1 models involving in-situ contamination alone due to the lack of country rock sulphur in the primary magmatic sulphides of the high grade Sandsloot-Overysel Platreef, the high PGE tenors and the limited volume of magma available if the Main Zone intruded after the Platreef.

Of the various Class 2 models that have been presented to explain the formation of the Platreef, three remain under test.

The Naldrett et al. (2008a) 'pudding bowl' model suggested that the Platreef formed from a mixture of Critical and Main Zone-type magma that moved outwards and upwards during chamber expansion associated with the formation of the Upper Critical Zone and the Merensky Reef. The Maier et al. (2008) model interpreted the Platreef as a lateral extent of a complete UG2-Merensky sequence west of the Grasvally Fault.

McDonald and Holwell (2011) reviewed these models and have highlighted the pros and cons of each model. The Maier and Naldrett models are based on the assumption that the Platreef represents a marginal facies of the Upper Critical Zone, or specifically the Merensky Reef, and that genetic processes between the different deposits are linked. One of the strongest factors that have led many authors to link the Platreef with the Merensky Reef has been geochemical evidence in the form of overlapping $^{187}Os/^{188}Os$ initial ratios and εNd values (Reisberg et al. 2006; Pronost et al. 2008). However, it has been highlighted by McDonald and Holwell (2011) that although the Merensky Reef and the Platreef share a range of lithophile element geochemical signatures that are intermediate between a tholeiitic (Main Zone) component and a more ultramafic (potentially Critical Zone) component, in both cases a combination of Ce/Sm, $^{187}Os/^{188}Os$ initial ratios and εNd values exclude a purely Upper Critical Zone type magma. They state that models involving this component alone (e.g. the low Pt/Pd eastern Bushveld UG2-type magma suggested by Cawthorn et al. 2002b) cannot reproduce the observed isotope signatures.

McDonald and Holwell (2007) presented the third model, the staging chamber model, that is under test for the Platreef in which magmatic processes are specific to the northern limb and are not linked to events in the other limbs.

### 4.4.1 Staging chamber model

It has been mentioned in chapter 3 that contamination and/or addition of S from the country rock (with non-mantle S isotope signature) is not the primary trigger for mineralisation in the Platreef (Holwell et al. 2007). Any contamination that occurred, although shown to be locally important (e.g. Manyeruke et al. 2005; Sharman-Harris et al. 2005), only modifies the existing magmatic sulphide liquid and post-dates formation of the early cumulus minerals (Barton Jr et al. 1986). Based on these observations, it has been proposed that the Platreef magma was held in a staging chamber, in a model originally advocated by Lee (1996), prior to emplacement. Maier et al. (2001) noted the importance of

staging chambers for forming massive sulphide deposits such as Voisey's Bay and Uitkomst and stated that while the Platreef contains significantly more sulphide than Uitkomst (although more dispersed), they did not consider such a setting for the Platreef.

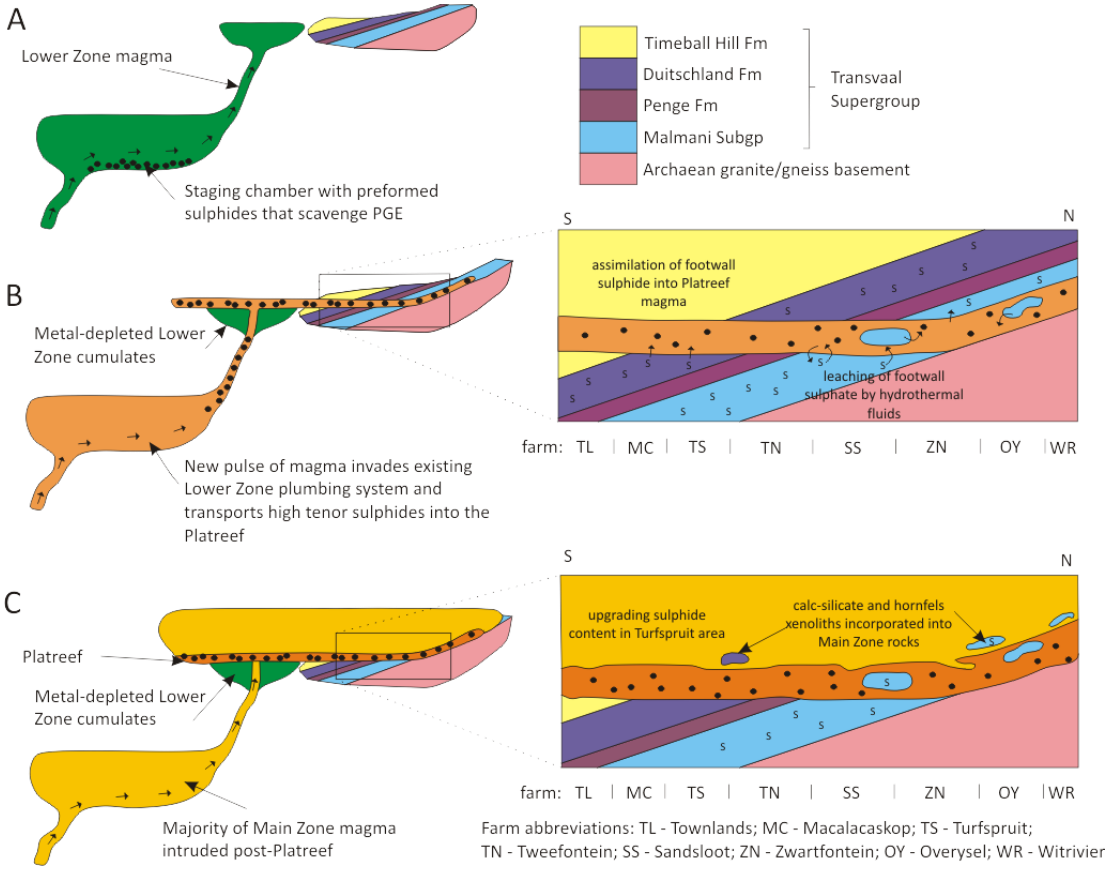


Figure 4.6. Staging chamber model developed by McDonald and Holwell (e.g. Holwell and McDonald 2007; McDonald and Holwell 2007; McDonald et al. 2009). Platreef is formed by the expulsion of pre-existing sulphides from a staging chamber; (a) S saturation is achieved in the intermediate chamber and the immiscible sulphide liquid collects at the bottom of the chamber. The Lower Zone magma passes over the sulphides, increasing their metal tenors, as it is expelled out of the chamber and intruded as metal-depleted cumulates; (b) an early Main Zone magma pulse exploits the pre-formed plumbing system and mixes with the remaining Lower Zone liquid, silicate cumulates and enriched sulphides, emplaces the mixture from a feeder in the Central sector to form a series of sills that becomes the Platreef. In addition, assimilation of local S is achieved through melting and hydrothermal leaching of the dolomite and shale; (c) Injection of the Main Zone magma occurs after the solidification and shearing of the Platreef, forming a magmatic unconformity. The Main Zone magma chills against, partially erodes and intrudes into the Platreef. Redrawn from McDonald and Holwell (2011).

The deep staging chamber model developed by McDonald and Holwell (2007) and Holwell et al. (2007) and McDonald et al. (2009) is represented in figure 4.6. The model proposes that sulphides were introduced into the Platreef from a pre-existing magmatic plumbing system that supplied the pre-Platreef Lower Zone. During the formation of the Lower Zone (fig. 4.6 a), the sulphide immiscible liquid remained in the staging chamber and was able to

achieve high PGE tenors through interaction with fresh Lower Zone magma flowing through the system at relatively low R factors (c.f. Kerr and Leitch 2005). As a result, the Lower Zone cumulates are chalcophile element depleted, as observed in the satellite intrusions of Zwartfontein and Grasvally (McDonald et al. 2009).

Subsequent to the formation of the Lower Zone, a proto-Main Zone pulse of magma exploited the pre-formed conduit system and remobilised the enriched sulphide liquid in addition to any remaining Lower Zone silicate cumulates in the staging chamber and the mixture was emplaced as a series of sills to form the Platreef (fig. 4.6 b). Injection of the main mass of the Main Zone occurred after the Platreef solidified to form a magmatic unconformity (fig. 4.6 c) as it chilled against, partially eroded and intruded into the Platreef (Holwell et al. 2005).

The attraction of this model is that it explains the mass-balance problem of how such an apparently small volume of magma such as the Platreef could have attained such a high concentration of PGE in the absence of an overlying magma column from which to extract these metals (c.f. Cawthorn et al. 1985; Cawthorn et al. 2002b; Holwell et al. 2005; Holwell and Jordaan 2006).

Examination of the Lower Zone satellite intrusions may provide support for the staging chamber model. A study carried out by McDonald and Holwell (2007) demonstrated that the northern limb olivines are systematically depleted in Ni compared to those from the eastern and western Bushveld (De Waal et al. 2001). Pyroxenites and harzburgites of the Lower Zone within the northern limb were also shown to be very depleted in Cu and have a higher Ni/Cu ratio than corresponding sulphide-poor cumulates in the western limb (McDonald and Holwell 2007).

Where the local country rocks contain significant amounts of sulphur (e.g. Duitschland Formation at Turfspruit, fig. 4.6 b), assimilation leads to contamination of the Platreef sulphides resulting in elevated $\delta^{34}S$ values (Sharman-Harris et al. 2005). In addition, where the Platreef assimilated the Malmani dolomite in the Sandsloot area, fluid fluxing occurred that led to extensive redistribution of PGE into the footwall rocks (Holwell et al. 2006). Where the Platreef is in direct contact with the Archaean basement (north of Zwartfontein), silicic contamination does not significantly affect mineralisation although Holwell and McDonald (2006) observed that PGE-bearing sulphide liquid locally penetrated the country rock as a result of partial melting.

In summary, McDonald and Holwell (2007), Holwell et al. (2007) and McDonald et al. (2009) proposed that the mechanisms for concentrating Ni, Cu, and PGE into an early sulphide liquid and emplacing the metal-rich sulphides into the Platreef are essentially magmatic. Intrusion of the magma and entrained sulphides was followed by assimilation of country rocks that led to local upgrading of the S content (and dilution of the metal tenors) and modification of the S isotope ratios. These assimilation and contamination processes are superimposed on the primary magmatic mineralisation and are not the cause of the metal enrichment in the Platreef.

#### *4.4.1.1 Testing the staging chamber model*

In order for the staging chamber model to be developed further, a number of predictions arising from the model have been identified by McDonald and Holwell (2007) that should be tested by further research:

i) Ni-depleted olivine should occur in other Lower Zone intrusions in addition to Grasvally;

ii) Droplets of highly PGE-rich sulphide may be preserved as inclusions in early formed Platreef minerals;

iii) Where the Platreef has not assimilated high Re/Os sedimentary rocks, then Platreef $^{187}Os/^{188}Os$ initial ratios should be dominated by Lower Zone Os and be similar to the initial ratio of the northern Bushveld Lower Zone. This initial ratio has not yet been determined.

While other authors focus on some of the tests, this study will concentrate on the second prediction involving the sulphide inclusions. Key predictions from the new model that will be tested include: (a) any evidence for early metal-rich sulphides; (b) whether any observed early sulphides are chemically different from later modified sulphides; and (c) in order to generate the metal-rich sulphide droplets the model infers the presence of early (pre-Platreef) magma chambers where silicate magma and sulphide droplets were mixed together and Ni, Cu and the PGE were extracted from the magma and concentrated in the sulphides.

One of the key means of addressing points (a) and (b) above comes with the recent discovery that some crystals of Platreef chromite contain inclusions of sulphides with negative crystal shapes imposed by the chromite host. This is strong evidence that they were trapped as a liquid droplet as the chromite crystallised during earliest Platreef development. The inclusions are 20-50 µm in diameter and made up of 2-4 different sulphide phases along with platinum-group minerals in some cases. Preliminary laser

ablation studies by Holwell et al. (2010) showed that the sulphide inclusions within chromite from Overysel carry extremely high PGE tenors (Pt up to 900 ppm, Pd up to 680 ppm). Chapter 9 discusses the significance of these sulphide inclusions further.

# Chapter 5: Geochemistry

## 5.1 Introduction and methods

Samples of pyroxenite, norite and gabbronorite, with or without chromitite, associated with the Lower Chromitite Zone (LCZ; Yudovskaya and Kinnaird 2010) were collected from 20 drill holes on the farms Overysel, Sandsloot and Zwartfontein (fig. 5.1) and analysed by ICP-MS and ICP-OES for bulk rock geochemistry and bulk rock PGE content. Samples were primarily selected to provide material for sulphide inclusion analysis (chapter 9) but in addition to add new data on the chemistry of the LCZ down dip and along strike.

The chromite-rich sections were cut out of each sample in order to make polished blocks and the remainder was crushed and powdered for geochemical analysis. It should be noted that as the samples have been collected to study the chromite mineralogy and PGE mineralisation, the geochemistry of the samples discussed below corresponds to the bulk lithology around the chromitites. Where the chromitite sections were large enough, a separate analysis was carried out of the chromitite as well as the surrounding silicates. The lithology of the samples are stated in table 5.1. Four samples were too small for bulk geochemistry to be run on them once a polished block was produced and are shown in the table without a geochemical sample number.

The quarter-core samples were crushed into chips using a steel jaw crusher. The crushed material was then powdered in an agate planetary ball mill. Approximately 2 g of this resultant powder was ignited in a furnace at 900$^{o}$C for two hours to drive off volatile substances and determine loss on ignition values (LOI). The LOI of a sample can be calculated using the following equation:

$$\text{LOI (wt\%)} = \frac{\text{Mass of 'wet' powder} - \text{Mass of ignited powder}}{\text{Mass of wet powder}} \times 100$$

The ignited powders were then fused with Li metaborate on a Claisse Fluxy automated fusion system to produce a melt that could be dissolved in 2 % $HNO_3$ for analysis. To prepare the samples, 0.1 ± 0.001 g of each ignited sample was mixed with 0.6 ± 0.006 g of lithium metaborate flux in a platinum crucible. To each crucible, a couple of drops of lithium iodide wetting agent were added and the mixtures fused using the automated fusion system. Each mixture was then dissolved in a 50 ml solution of 20 ml of 10 % $HNO_3$ and 30 ml of 18.2 Ω deionised water. After the mixture had dissolved fully, 1 ml of 100 ppm Rh spike was added to the solution, which was then made up to 100 ml with 18.2 Ω deionised water.

Bulk analyses for major and trace element concentrations were determined at Cardiff University using a JY Horiba Ultima 2 inductively coupled plasma-optical emission spectrometer (ICP-OES) and a Thermo X7 series inductively coupled plasma-mass spectrometer (ICP-MS) using procedures outlined in McDonald and Viljoen (2006).

Concentration of PGE and Au were determined by Ni sulphide fire assay with Te co-precipitation followed by ICP-MS procedure, following the methodology described by Hoffman and Dunn (2002). 15 g of soda ash ($NaCO_3$), 30 g of di-lithium tetraborate ($B_4Li_2O_7$), 0.9 g of sulphur, 1.08 g of carbonyl-purified Ni, 10 g of silica and 5 g of sodium hydroxide (NaOH) were required for fusion of a 5 g sample. Carbonyl-purified Ni is used in order to produce a low blank as the carbonyl process ensures that when the Ni is re-precipitated, the PGE are left behind. For blank production, the amount of silica was increased to 15 g to accommodate for the lack of sample. The flux and sample were fired for 90 minutes in a fire-clay crucible at a temperature of 1100 $^{o}$C to produce sulphide buttons. The nickel and sulphur combined to form nickel sulphide droplets, which scavenged the PGE and Au from the molten flux and settled to the bottom of the fire-clay crucible. The sulphide buttons were then dissolved in concentrated HCl, and the noble metals that had entered the solution were co-precipitated with Te, using $SnCl_2$ as a reductant. Finally, soluble PGE chloro-complex solutions were spiked with Tl as an internal standard to monitor for instrument drift, and the noble metal concentrations were determined by external calibration on the ICP-MS.

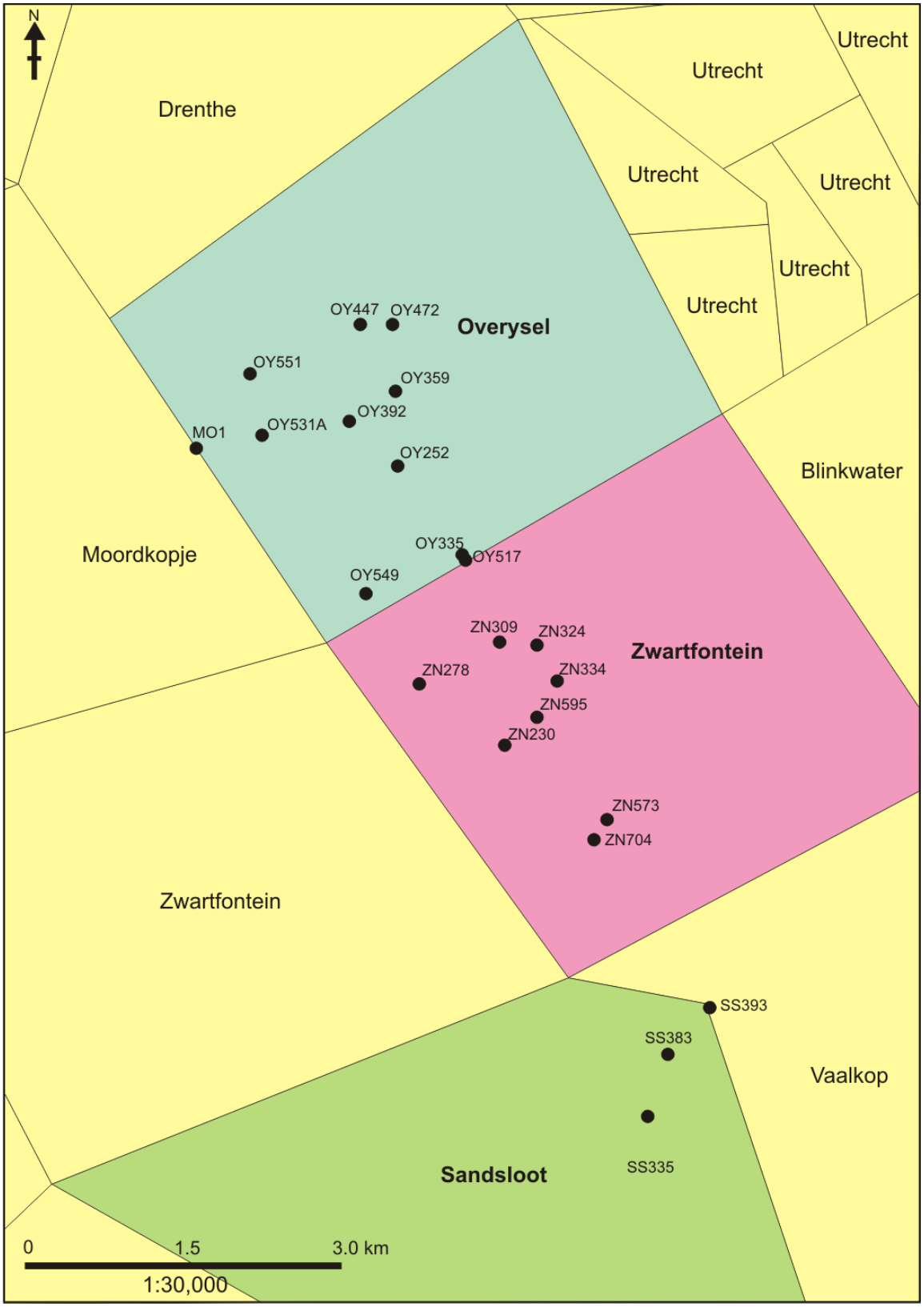

Figure 5.1. Map of study area showing drillholes sampled.

Table 5.1. Summary of samples analysed. Key: OY- Overysel; SS-Sandsloot; ZN-Zwartfontein; pyrox – pyroxene, chr - chromite, serp – serpentinised, fld - feldspar

| Drill hole | | Depth min | Depth max | Lithology | Grainsize |
|---|---|---|---|---|---|
| **REJ1** | OY447-1 | 313.90 | 314.00 | Norite | Fine to medium |
| **REJ2** | OY447-2 | 325.60 | 325.73 | Chromitiferous norite | Fine to medium |
| **REJ3** | MO1D-1 | 1392.33 | 1392.56 | Gabbronorite | Fine to medium |
| **REJ4** | MO1D-2 | 1411.08 | 1411.30 | Norite | Fine to medium |
| **REJ5** | ZN230-1 | 721.87 | 722.12 | Pyroxenite | Medium to coarse |
| **REJ6** | ZN230-2 | 722.44 | 722.46 | Pyroxenite | Medium to coarse |
| **REJ7** | ZN230-3 | 733.33 | 733.61 | Pyroxenite | Medium to coarse |
| **REJ8** | ZN230-4 | 734.14 | 734.24 | Chromitiferous norite | Medium |
| **REJ9** | ZN230-5 | 735.47 | 735.60 | Chromitiferous pyroxenite | Medium |
| **REJ10** | ZN595-1 | 489.27 | 489.47 | Pyroxenite | Pegmatitic |
| **REJ11** | ZN595-2 | 509.00 | 509.10 | Chromitiferous norite | Fine |
| **REJ12** | ZN595-3 | 511.10 | 511.27 | Pyroxenite | Fine |
| **REJ13** | SS335-1 | 765.25 | 765.48 | Pyroxenite | Fine to medium |
| **REJ14** | SS335-2 | 823.40 | 823.60 | Pyroxenite | Medium to coarse |
| **REJ15** | SS335-3 | 847.20 | 847.27 | Chromitiferous norite | Fine to medium |
| **REJ16** | SS335-4 | 847.54 | 847.69 | Chromitiferous gabbronorite | Fine |
| **REJ17** | SS393-1 | 355.14 | 355.25 | Chromitiferous norite | Fine to medium |
| **REJ18** | SS393-2 | 364.14 | 364.34 | Chromitiferous norite | Fine to medium |
| **REJ19** | SS393-3 | 371.25 | 371.40 | Chromitiferous pyroxenite | Fine to medium |
| **REJ20** | SS393-4 | 383.20 | 383.50 | Chromitiferous gabbronorite | Fine to medium |
| **REJ21** | SS393-5 | 391.39 | 391.66 | Chromitiferous norite | Fine to medium |
| **REJ22** | OY551-1 | 926.00 | 926.09 | Chromitiferous norite | Medium |
| **REJ23** | OY551-2 | 928.00 | 928.15 | Chromitiferous norite | Pegmatitic |
| **REJ24** | OY551-3 | 928.30 | 928.41 | Chromitiferous norite | Medium |
| **REJ25** | OY551-4 | 932.14 | 932.26 | Pyroxenite | Medium |
| **REJ26** | ZN334-1 | 54.40 | 54.63 | Chromitiferous norite | Fine |
| **REJ27** | ZN334-2 | 63.21 | 63.41 | Chromitite | Fine |
| **REJ28** | ZN334-3 | 72.32 | 72.59 | Chromitiferous norite | Medium to coarse |
| **REJ29** | OY472-1 | 144.17 | 144.36 | Gabbronorite | Medium |
| **REJ30** | OY472-2 | 144.72 | 144.91 | Norite | Fine |
| **REJ31** | OY472-3 | 151.48 | 151.66 | Chromitiferous pyroxenite | Fine to medium |

Table 5.1. cont.

| | | | | | |
|---|---|---|---|---|---|
| **REJ32** | OY472-4 | 152.53 | 152.71 | Chromitiferous gabbronorite | Fine to medium |
| **REJ33** | ZN573-1 | 223.06 | 223.19 | Chromitite | Fine |
| **REJ34** | ZN573-2 | 223.34 | 223.48 | Chromitiferous norite | Fine |
| **REJ35** | ZN573-3 | 224.32 | 224.58 | Chromitite | Fine |
| **-** | ZN573-4 | 225.03 | 225.09 | - | Fine |
| **-** | ZN573-5 | 225.67 | 225.78 | - | Fine |
| **REJ36** | ZN704-1 | 424.66 | 424.79 | Pyroxenite | Medium to coarse |
| **-** | ZN704-2 | 426.40 | 426.52 | - | Medium |
| **REJ37** | ZN704-3 | 428.74 | 428.90 | Chromitite | Medium |
| **REJ38** | ZN704-4 | 442.71 | 442.88 | Chromitite | Medium |
| **-** | ZN704-5 | 444.15 | 444.24 | - | Medium |
| **REJ39** | ZN704-6 | 453.00 | 454.25 | Chromitiferous norite | Medium to coarse |
| **-** | SS383-1 | 593.57 | 593.69 | - | Pegmatitic |
| **REJ40** | SS383-2 | 597.36 | 597.69 | Pyroxenite | Pegmatitic |
| **REJ41** | SS383-3 | 613.08 | 613.18 | Chromitite | Fine to medium |
| **REJ42** | SS383-4 | 613.36 | 613.55 | Chromitiferous norite | Fine to medium |
| **REJ43** | SS383-5 | 613.63 | 613.81 | Chromitiferous norite | Medium to coarse |
| **REJ44** | SS383-6 | 614.33 | 614.47 | Chromitiferous pyroxenite | Fine to medium |
| **REJ45** | SS383-7 | 618.69 | 618.90 | Chromitiferous norite | Fine to medium |
| **REJ46** | OY531A-1 | 904.43 | 904.70 | Chromitiferous norite | Fine |
| **REJ47** | OY531A-2 | 938.78 | 939.03 | Chromitiferous pyroxenite | Medium to coarse |
| **REJ48** | OY392-1 | 457.55 | 457.73 | Chromitite | Fine |
| **REJ49** | OY392-2 | 459.03 | 459.31 | Chromitiferous norite | Fine |
| **REJ50** | OY359-1 | 86.52 | 86.79 | Chromitite | Fine |
| **REJ51** | OY252-1 | 194.38 | 194.64 | Chromitite | Medium |
| **REJ52** | OY549-1 | 871.36 | 871.50 | Norite | Pegmatitic |
| **REJ53** | OY549-2A | 946.73 | 947.16 | Norite | Fine to medium |
| **REJ54** | OY549-2B | 946.73 | 947.16 | Chromitite | Fine |
| **REJ55** | ZN278-1 | 696.23 | 696.32 | Chromitiferous pyroxenite | Medium |
| **REJ56** | ZN278-2A | 721.19 | 721.48 | Pyroxenite | Medium |
| **REJ57** | ZN278-2B | 721.19 | 721.48 | Chromitiferous norite | Fine |
| **REJ58** | ZN278-3 | 739.33 | 739.48 | Chromitiferous pyroxenite | Pegmatitic |

Table 5.1. cont.

| | | | | | |
|---|---|---|---|---|---|
| **REJ59** | ZN309-1 | 298.43 | 298.70 | Pyroxenite | Fine to medium |
| **REJ60** | ZN309-2 | 300.45 | 300.70 | Chromitite | Fine to medium |
| **REJ61** | ZN324-1 | 86.43 | 86.60 | Chromitite | Fine to medium |
| **REJ62** | ZN324-2A | 89.25 | 89.57 | Pyroxenite | Medium |
| **REJ63** | ZN324-2B | 89.25 | 89.57 | Chromitite | Fine |

## 5.2 Classification of rocks based on geochemistry

Each sample was initially logged in the field by Anglo Platinum geologists and classified according to the field lithologies defined by Nex et al. (2006). The Nex classification is based on the modal mineralogy of each sample (table 5.1). However each hole was logged by a different geologist, therefore in order to standardise the data set, the samples were relogged for this study as per IUGS classification (table 5.2). Where a sample contained disseminated chromite, it is classified a chromitiferous- pyroxenite, -gabbronorite or –norite, depending on the remaining mineralogy. Samples that contained concentrated chromite were classified as chromitite.

Table 5.2. Lithologies of the samples based on IUGS classification

| Lithology | Mineralogy |
|---|---|
| **Pyroxenite** | Less than 10 wt% plagioclase |
| **Norite** | More than 10 wt% plagioclase + orthopyroxene + <15 wt% clinopyroxene |
| **Gabbronorite** | More than 10 wt% plagioclase + orthopyroxene + >15 wt% clinopyroxene |

## 5.3 Major elements

The major element chemistry of the samples can be modelled as a function of the proportions of plagioclase, orthopyroxene, clinopyroxene and chromite that the rock contains. The plots (figs. 5.2 a & b) which include the average composition of Platreef silicates are produced based on work by McDonald and Holwell (2011), Harris and Chaumba (2001), Manyeruke et al. (2005) and Maier et al. (2008). The chromite composition represents the average values obtained in the study from chapter 6. It is likely that the composition of the sample is influenced by the composition of the local country rock (and xenoliths) due to the deviation from the mixing lines between orthopyroxene and plagioclase.

Little correlation is seen in the plot of Ni vs. MgO (fig. 5.3 a), suggesting that a significant portion of the Ni is being held within the sulphides rather than in the silicates. Two chromitiferous norite samples and a norite sample have the highest Ni content (more than 2000 ppm more than the rest of the samples) due to significant amounts of sulphide.

In the bivariate plots of Zr vs. MgO (fig. 5.3 b), a few samples (the gabbronorite samples and a chromitiferous norite sample) contain much higher Zr concentrations than the remainder of the samples. This may represent a more evolved magma, or the samples could contain a greater proportion of trapped melt, enriching the samples in more incompatible elements.

Finally, the bivariate plot of V vs. Cr (fig. 5.3 c) shows a strong correlation between the elements. This indicates that V is in solid solution in chromite given the proportion of

chromite in each of the samples. Similar strong correlation is also seen when Cr is plotted against Zn and Ga (fig. 5.4 b). The chromitite samples plot away from the main trend at higher Zn values on the Zn vs. Cr plot (fig. 5.4 a) and a correlation is observed when Zn is plotted against Zr (fig. 5.4 c) for the chromitites. This correlation is also observed when Zn is plotted against other lithophile elements (e.g. Ti and Rb) for the chromitite population and may be the result of equilibration between some of the chromites and an evolved melt.

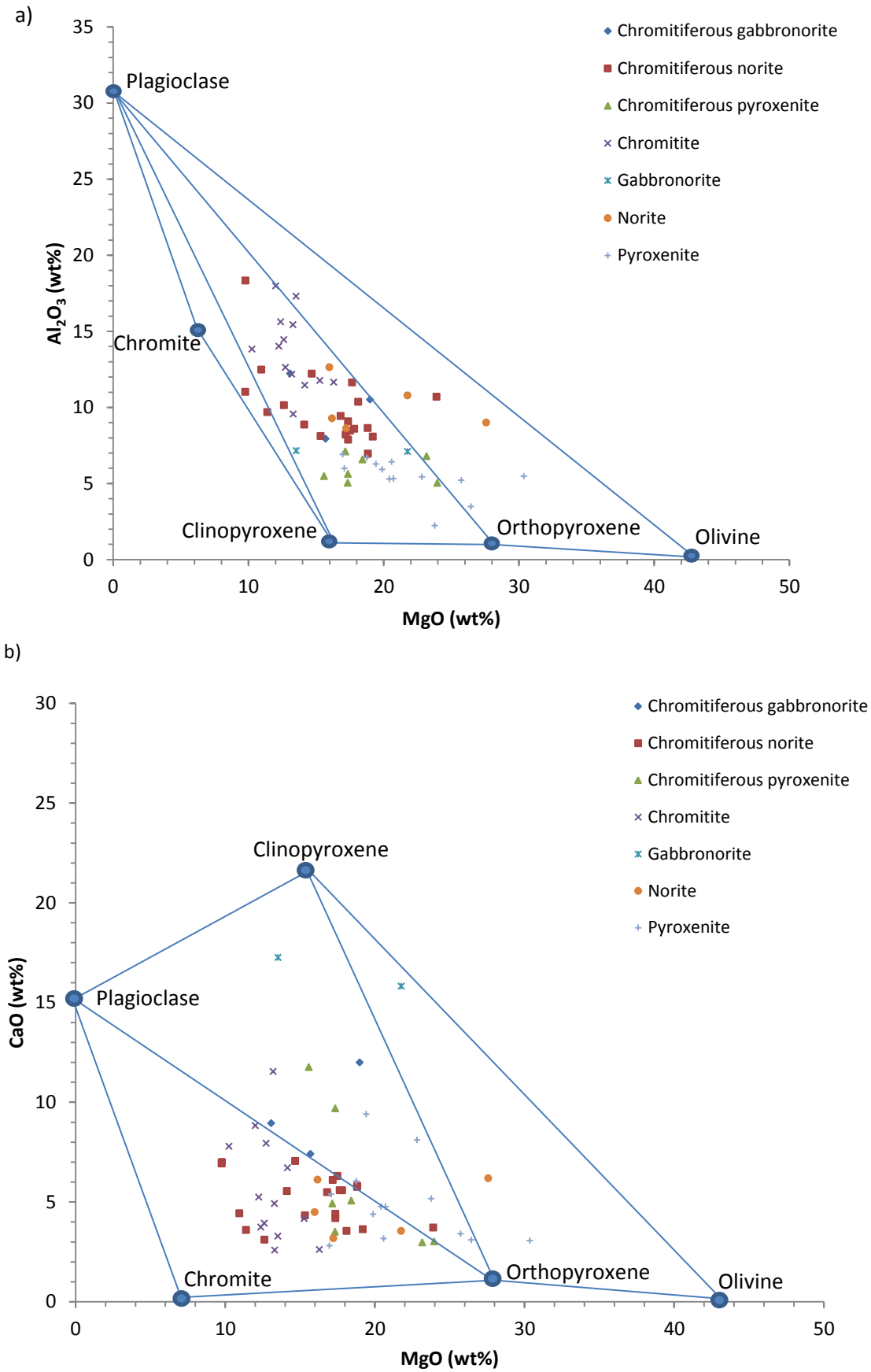


Figure 5.2. Major element plots with end-member minerals for the Platreef (a) $Al_2O_3$ vs. MgO and (b) CaO vs. MgO. Adapted from McDonald and Holwell (2011).

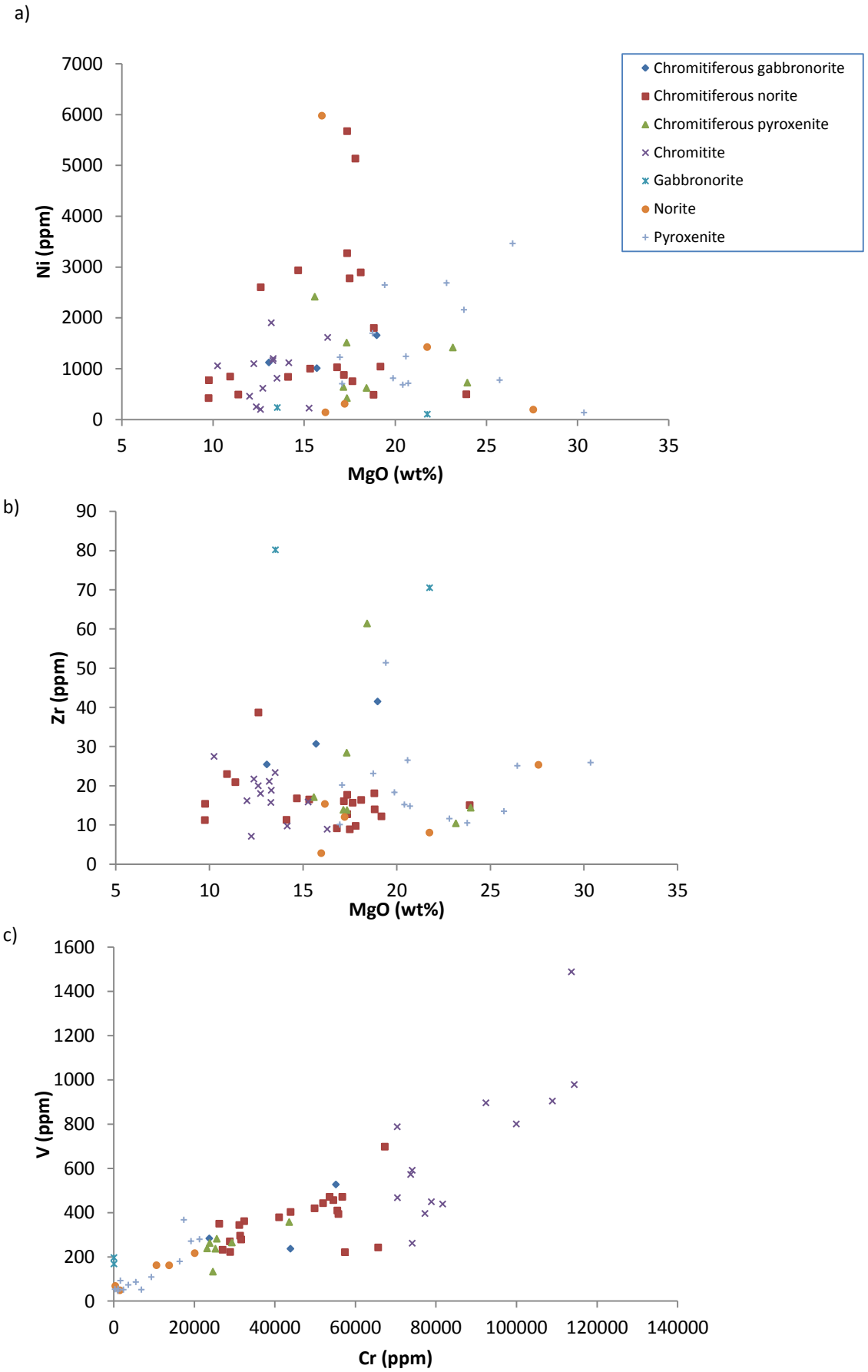


Figure 5.3. Bivariate graphs for major elements subdivided into lithology for (a) Ni vs. MgO; (b) Zr vs. MgO; and (c) V vs. Cr.

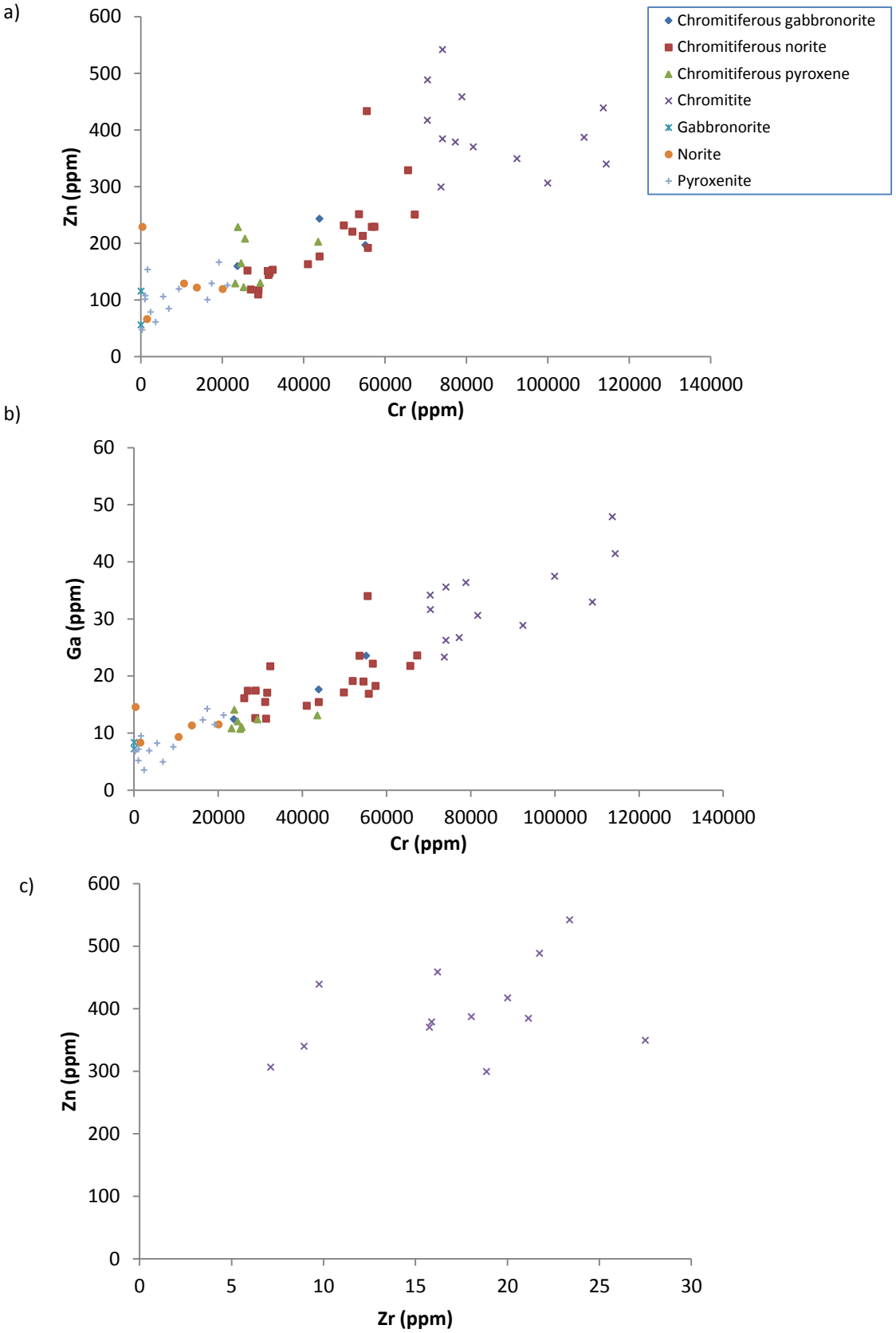


Figure 5.4. Bivariate graphs for the major elements subdivided into lithology for (a) Zn vs. Cr; (b) Ga vs. Cr and (c) Zn vs. Cr for the chromitite lithology.

## 5.4 Trace elements

### 5.4.1 Rare earth element plots

Chondrite-normalised rare earth element (REE) patterns for the individual lithologies are shown in figure 5.5. The chondrite normalised field for all lithologies are relatively fractionated, with enrichment in the light rare earth elements (LREE). Most profiles are trough-shaped with a slight positive gradient in the heavy rare earth elements (HREE) from Ho to Lu. This feature has been observed in previous studies of Platreef pyroxenite data by McDonald et al. (2005) and Holwell and McDonald (2006). An anomalous profile is seen in one of the pyroxenite unit, where there is limited fractionation, with similar concentrations of both LREE and HREE and a negative Eu anomaly, although there is nothing anomalous in the logs or core photos to account for this anomaly.

The REE patterns can be explained by the relative proportions of the minerals that the rocks contain. The gabbronorite samples which contain the highest amounts of clinopyroxene have the flattest profiles because clinopyroxene is typically more accommodating of the REE 3+ cations than orthopyroxene or plagioclase (Rollinson 1993). Orthopyroxene does not typically accept LREE and plagioclase rarely has detectable amounts of middle or HREE (Rollinson 1993). $Eu^{2+}$ is compatible in plagioclase and, therefore, samples that contain high amounts of plagioclase generally have positive Eu anomalies. Overall, highly fractionated magmas tend to have strong negative Eu anomalies (Rollinson 1993).

As can be seen from the REE profiles, there are both positive and negative Eu anomalies present in the data. Eu anomalies are primarily controlled by feldspar, as Eu (present in the divalent state) is compatible in plagioclase and potassium feldspar, whereas the trivalent REE are incompatible in those minerals. Therefore, a negative Eu anomaly would be the result of feldspar removal from a felsic melt by crystal fractionation or by the partial melting of a rock in which feldspar is retained in the source. Conversely, hornblende, sphene, clinopyroxene, orthopyroxene and garnet may contribute to a positive Eu anomaly, although to a lesser extent than the plagioclase anomaly (Rollinson 1993).

The extent of the Eu anomaly can be quantified by comparing the measured Eu with the expected concentration obtained by interpolating between the normalised values of Sm and Gd (Eu*). The ratio of Eu/Eu* is a measure of the europium anomaly and is displayed for the various lithologies in a series of histograms (figs. 5.6 and 5.7). Where Eu/Eu* anomaly is more than 1, it represents a positive anomaly, while values under 1 represent a negative anomaly.

All of the units except for the gabbronorite and pyroxenite show overall positive Eu anomalies. The average Eu/Eu* is 1.04 (fig. 5.7 d). The norite, chromitiferous norite and chromitiferous pyroxenite all contain samples that have strong positive Eu anomalies (>+2) which can be attributed to the occurrence of significant cumulus plagioclase within these units.

The extent of the true Eu anomaly within a lithology is likely to be masked by the effects of contamination. Parapyroxenites at Sandsloot and Zwartfontein were found to have negative Eu anomalies as a result of contamination by the Malmani dolomite and this feature is observed in a number of lithologies, even those containing a significant proportion of plagioclase (McDonald et al. 2005). It is therefore possible, especially in the norite or gabbronorite samples, that any positive Eu anomaly caused by plagioclase abundance could be swamped by the negative Eu anomaly due to significant contamination.

REE plots for the central Platreef pyroxenites (fig. 5.5) show similar profiles to the samples analysed in this study with comparable LREE fractionation and various Eu anomalies.

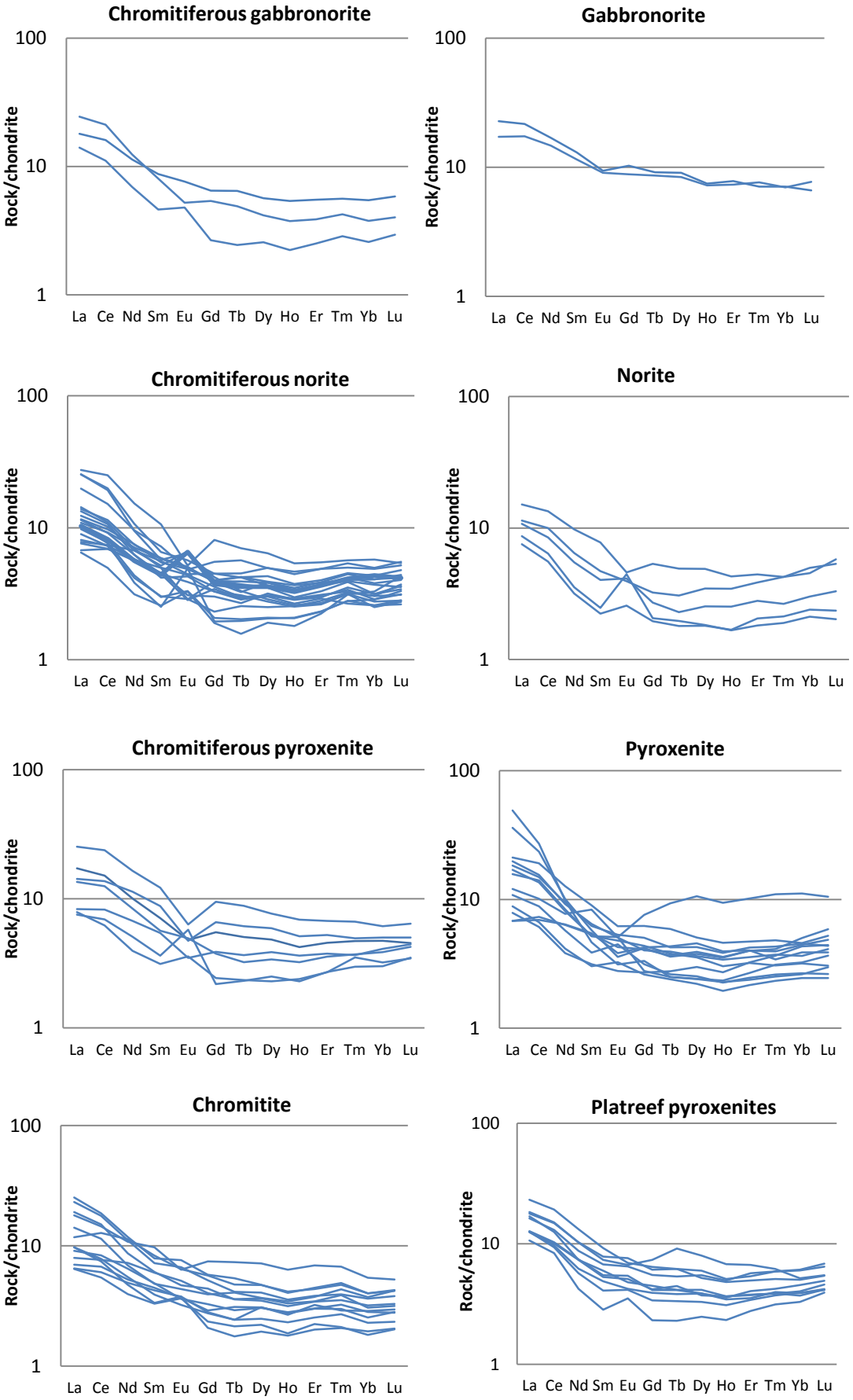


Figure 5.5. REE plots for the various lithologies and comparable plot for the central Platreef pyroxenites from Holwell and McDonald (2006), McDonald et al. (2005) and Ihlenfeld and Keays (2011).

a)

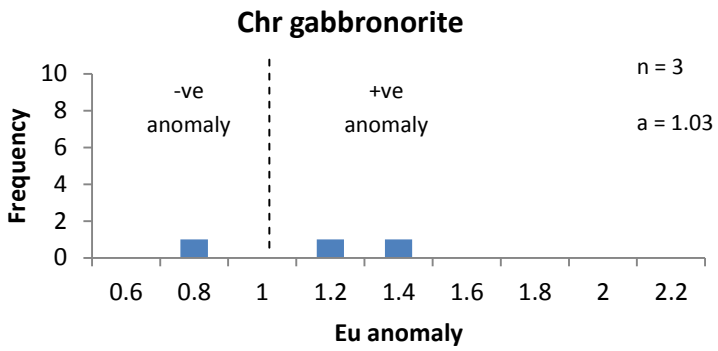


b)

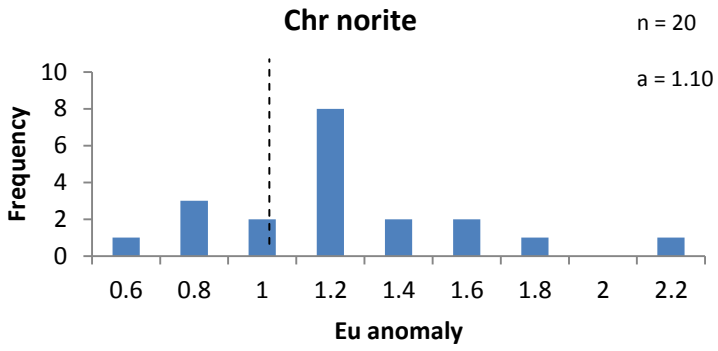


c)

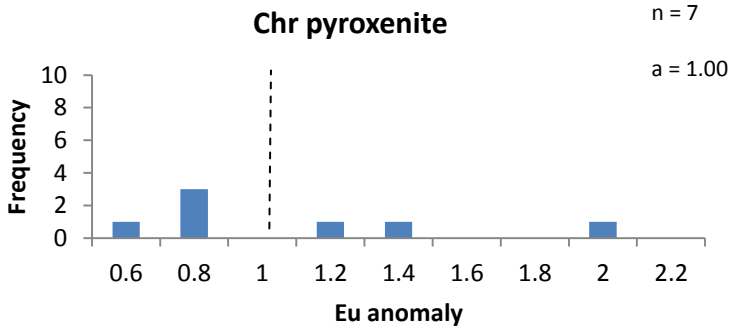


d)

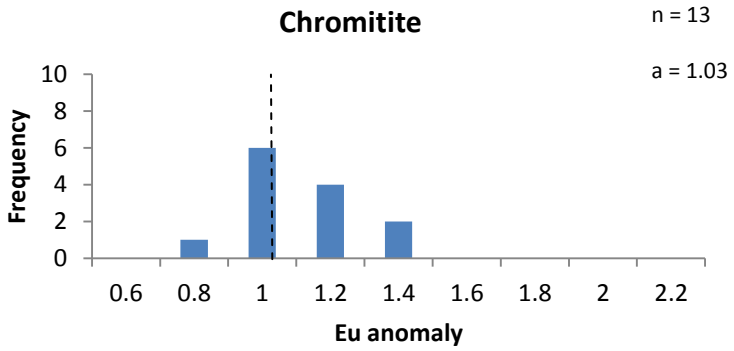


Figure 5.6. Histograms showing the Eu anomaly for (a) chromitiferous gabbronorite, (b) chromitiferous norite; (c) chromitiferous pyroxenite and (d) chromitite.

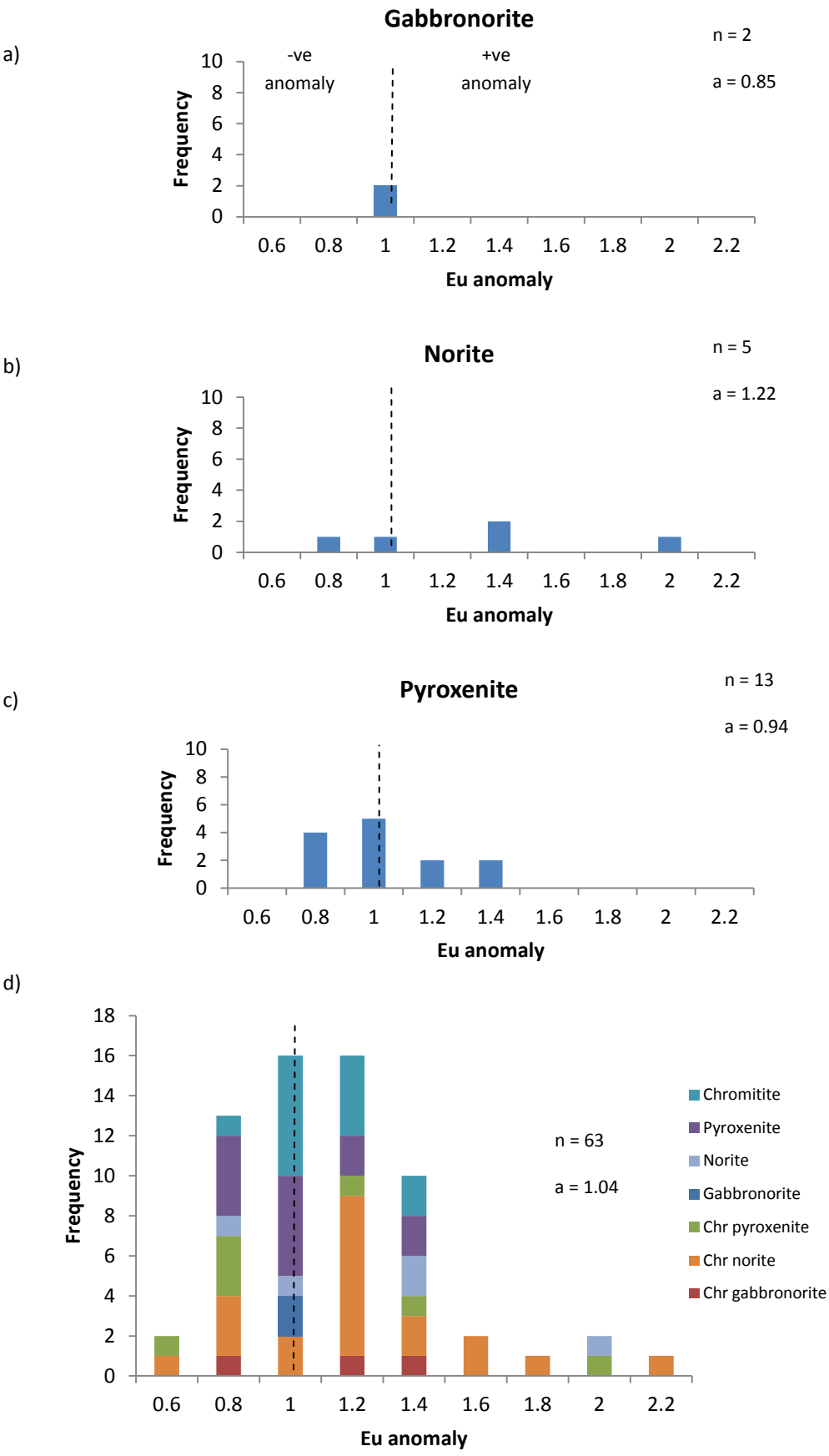


Figure 5.7. Histograms showing the Eu/Eu* for (a) gabbronorite; (b) norite; (c) pyroxenite and (d) combined histogram for all lithologies.

Table 5.3. Fractionation ratios for LREE and HREE for various lithologies

| | La/Sm | Dy/Yb |
|---|---|---|
| **Chromitiferous gabbronorite** | 2.71 | 1.05 |
| **Chromitiferous norite** | 2.69 | 0.96 |
| **Chromitiferous pyroxenite** | 2.09 | 0.97 |
| **Chromitite** | 2.26 | 1.13 |
| **Gabbronorite** | 1.62 | 1.24 |
| **Norite** | 2.78 | 0.84 |
| **Pyroxenite** | 3.36 | 0.93 |

The amount of fractionation within the LREE and the HREE is shown in table 5.3. It is evident that there is relatively more fractionation within the LREE, with the pyroxenite units showing the greatest amount and the gabbronorites showing the least amount of fractionation. The HREE are relatively unfractionated with most lithological units having values close to unity. The greatest amount of fractionation within the HREE is seen in the gabbronorite unit, which combined with the low ratio for the LREE, exhibits the flattest patterns in the REE profile (fig. 5.4). The chromitite, gabbronorite and chromitiferous gabbronorite units show slight HREE enrichment while the other lithologies show a negative HREE profile.

### 5.4.2 Multi-element variation diagrams

Mantle normalised multi-element variation diagrams for the Platreef samples are shown in figures 5.8 to 5.10 for the various lithologies. All of the samples display a negative Nb-Ta anomaly and enrichment in U relative to Th. As shown in the chondrite normalised REE plots above, all lithologies are strongly enriched in LREE, while there is limited enrichment in the HREE, shown by flat or minor negative or positive shaped profiles.

Fractionation of LREE relative to HREE may be caused by the presence of olivine, orthopyroxene and clinopyroxene. In addition, profiles that are enriched in LREE and have negative Nb and Ti anomalies may be caused by crustal contamination (Rollinson 1993).

The chromitite unit shows a strong Ti enrichment relative to the other rocks and this can be attributed to the Ti content of the spinels. In addition, the chromite bearing units are not Zr-Hf enriched, as is seen in most of the other samples from other lithologies.

Across the different lithologies, both negative and positive Sr anomalies are displayed, although the anomalies do not correlate with other elements.

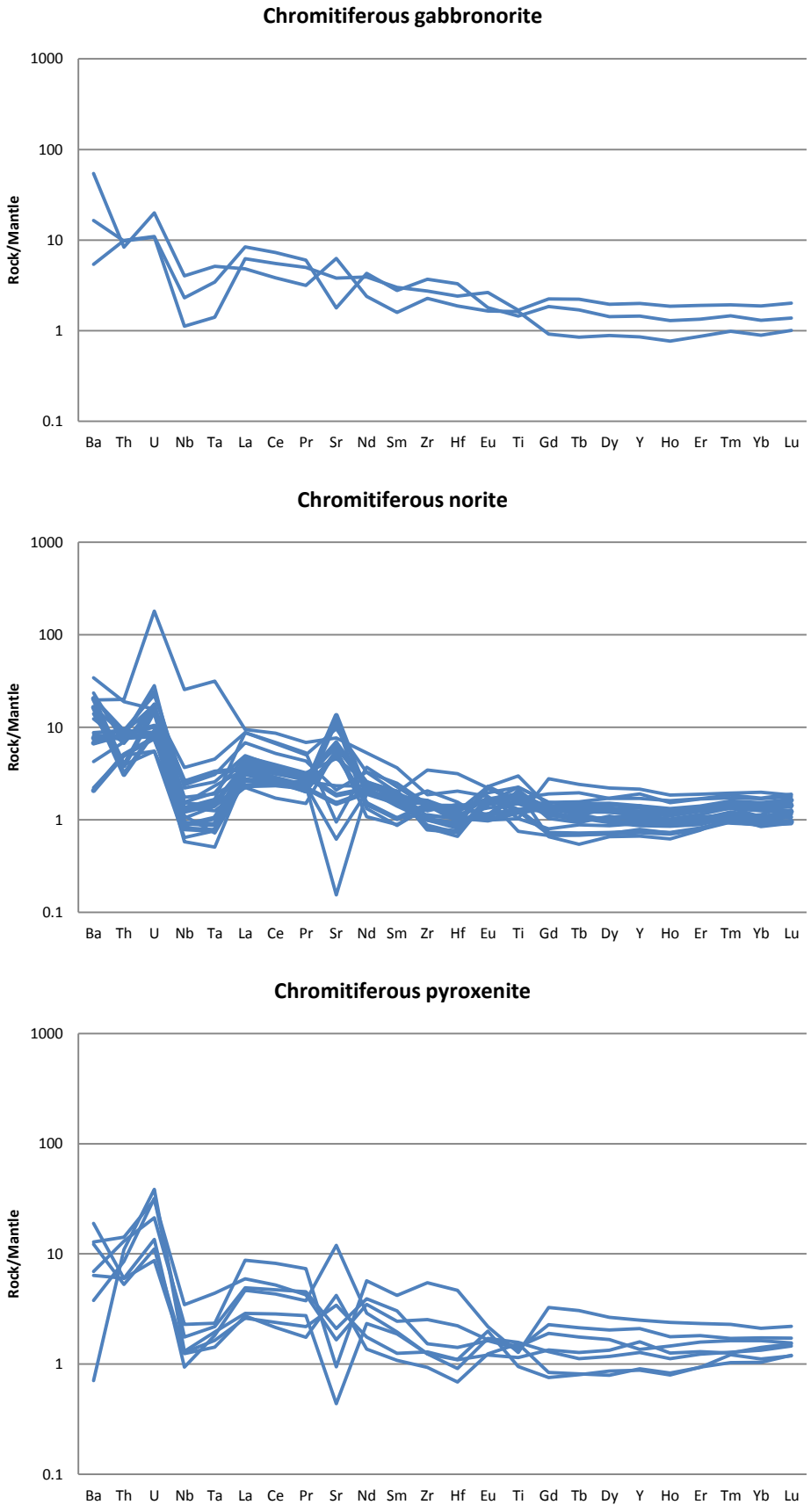


Figure 5.8. Mantle normalised multi-element variation diagrams for (a) chromitiferous gabbronorite; (b) chromitiferous norite and (c) chromitiferous pyroxenite.

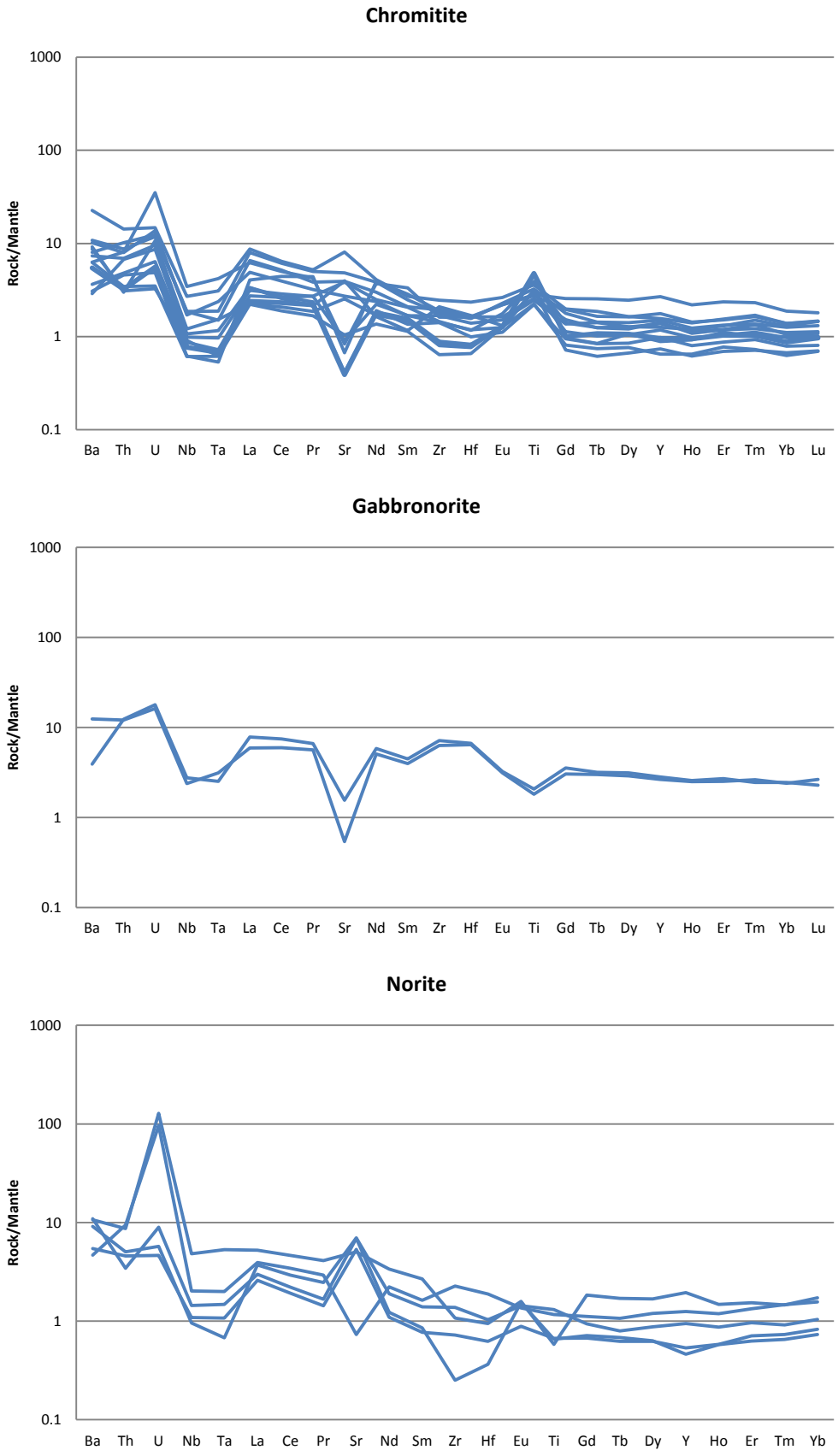


Figure 5.9. Mantle normalised multi-element variation diagrams for (a) chromitite; (b) gabbronorite and (c) norite.

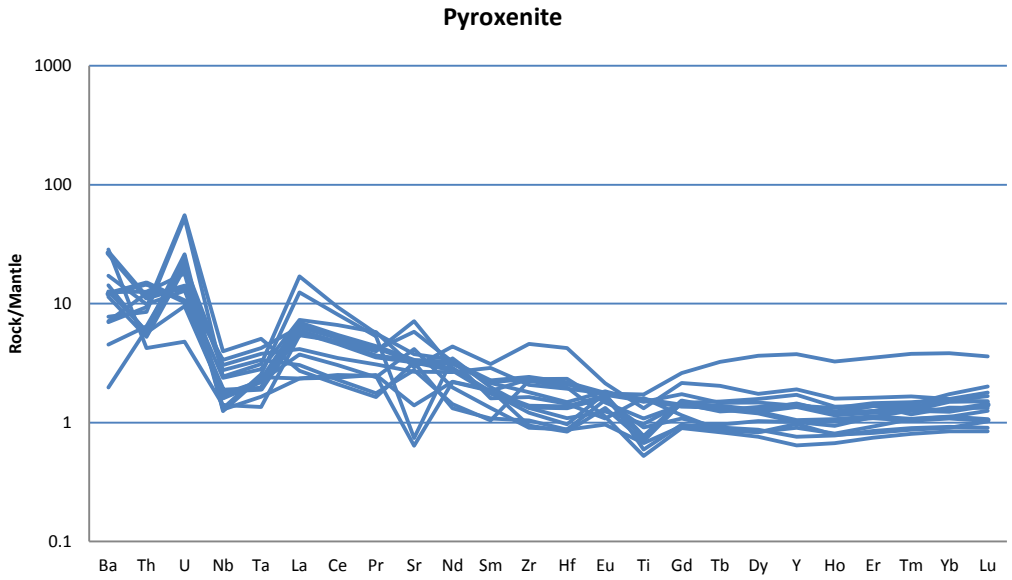


Figure 5.10. Mantle normalised multi-element variation diagram for pyroxenite.

Comparison of the trace element data from this study to those of the Merensky Reef (fig. 5.11) shows that there are similar characteristics in both data sets, e.g., the negative Ta and Sr anomalies. The profile for the average composition of the Merensky Reef does not display a strong Eu anomaly as is seen in the Platreef data. The data are also compared to the B1 magma profile, which lies at the upper limit of the range observed in this study.

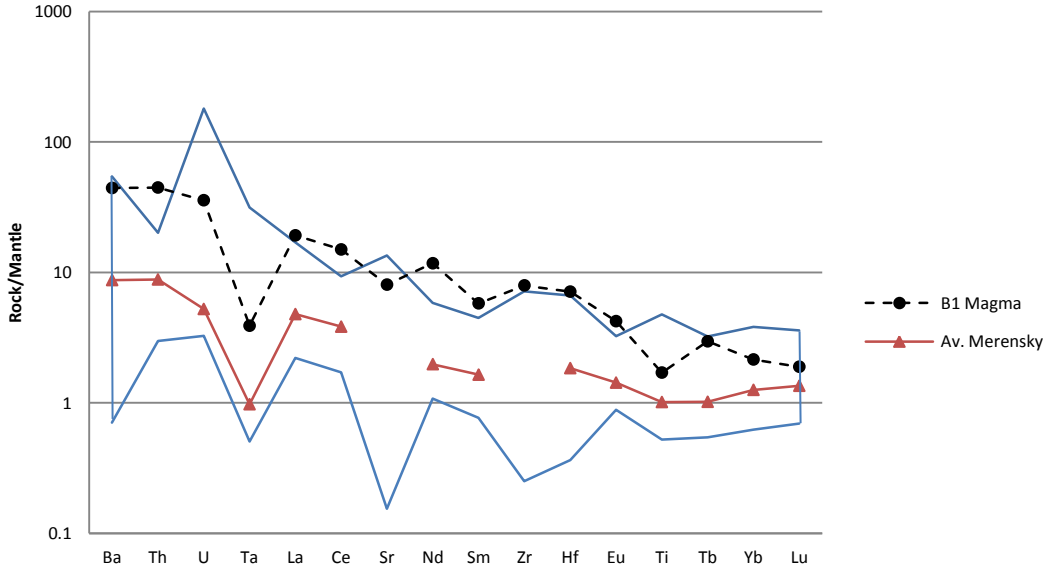


Figure 5.11. Condensed multi-element variation diagram depicting the range of values observed from the samples in this study compared to the average Merensky Reef and B1 magma (Barnes and Maier 2002a; Barnes and Maier 2002b).

## 5.5 PGE

PGE can be divided into two groups based on their associations. The IPGE group comprise of Ir, Os and Ru, while the PPGE group comprise of Pt, Pd and Rh. Gold is often associated with PPGE (Barnes et al. 1985).

The 4E combined grade (Pt+Pd+Rh+Au) for the samples in this study ranges from 0.03 to 37.92 g/t, with an average grade of 2.82 g/t (table 5.4), and is close to the average grade of 3-4 g/t in the Platreef as was shown in chapter 3. Within each sample, the most chromitiferous part was removed in order to study chromite composition (chapter 6), PGM association (chapter 7), PGE content in BMS (chapter 8) and sulphide inclusion composition (chapter 9). As a result, the actual grade may be slightly higher due to the association of PGE with chromite. PGE grades for individual samples are displayed in Appendix 1B.

Table 5.4. Various PGE ratios showing the average, minimum and maximum values for each lithology.

| Lithology | 4E (g/t) | Pt/Pd | Pt/Ir | Ru/Ir |
|---|---|---|---|---|
| Chr gabbronorite av. (n=3) | 2.37 | 1.14 | 25.40 | 4.60 |
| Chr gabbronorite min. | 0.70 | 0.64 | 14.24 | 3.41 |
| Chr gabbronorite max. | 5.11 | 1.81 | 44.63 | 6.08 |
| Chr norite av. (n=20) | 2.76 | 0.83 | 21.12 | 4.98 |
| Chr norite min. | 0.04 | 0.35 | 0.37 | 0.99 |
| Chr norite max. | 12.29 | 1.89 | 68.11 | 6.49 |
| Chr pyroxenite av. (n=7) | 2.49 | 0.85 | 16.08 | 4.97 |
| Chr pyroxenite min. | 0.39 | 0.30 | 12.54 | 3.59 |
| Chr pyroxenite max. | 12.00 | 1.81 | 21.17 | 6.20 |
| Chromitite av. (n=19) | 2.41 | 1.07 | 17.36 | 5.63 |
| Chromitite min. | 0.86 | 0.43 | 9.12 | 1.81 |
| Chromitite max. | 7.93 | 1.54 | 67.05 | 7.78 |
| Gabbronorite av. (n=2) | 0.55 | 0.60 | 58.09 | 5.57 |
| Gabbronorite min. | 0.09 | 0.51 | 16.64 | 5.10 |
| Gabbronorite max. | 1.01 | 0.69 | 99.54 | 6.04 |
| Norite av. (n=5) | 8.57 | 0.94 | 36.41 | 3.75 |
| Norite min. | 0.07 | 0.57 | 21.42 | 2.23 |
| Norite max. | 37.92 | 1.48 | 74.64 | 4.76 |
| Pyroxenite av. (n=13) | 1.90 | 0.65 | 55.20 | 4.60 |
| Pyroxenite min. | 0.03 | 0.28 | 15.60 | 3.43 |
| Pyroxenite max. | 4.88 | 1.49 | 108.09 | 5.94 |
| Average (n=64) | 2.82 | 0.88 | 28.36 | 5.00 |

The grade differs considerably between the different lithologies as well as within each lithology, as shown by the minimum and maximum values (table 5.4). The highest PGE content of almost 38 g/t is found in a 10 cm norite sample from Overysel. Overall the highest grades are found in the chromitiferous samples rather than the chromite poor samples (fig. 5.12 a).

The average Pt/Pd ratio for the samples is 0.88, with a range from 0.28 to 1.89, compared to the average of 1:1 for the Central Platreef. The Pt/Pd ratio varies considerably depending on the lithology. The chromitiferous gabbronorite samples contain the highest average Pt/Pd (1.14), while the lowest average Pt/Pd ratio (0.60) is found in the gabbronorite samples.

The ratio of Pt to Ir gives an indication of the amount of fractionation between PPGE and IPGE. As can be seen, the amount of fractionation is greatest in the chromite-poor lithologies, implying that the IPGE are closely associated with chromite.

The ratio of Ru to Ir illustrates the degree of fractionation within the IPGE, specifically due to the formation of laurite ($RuS_2$) or irarsite ($IrS_2$). The average value of 5.0 indicates that there is considerably more Ru than Ir in the samples, presumably as PGM of laurite. This will be examined further in chapter 7 when the PGM within the samples are investigated.

There is limited correlation between the 4E and Cr values (fig. 5.12 a), whereas a strong positive correlation is observed between the IPGE and Cr (as displayed in Cr vs. Ru; fig. 5.12 b). There does not appear to be a strong correlation between the PPGE and Cr. Figure 5.12 c shows potentially two trend lines for Pt vs. Cr, with a steep trend line of increasing Cr with relatively little Pt. and a second shallower trend line with a wide variation of Pt values for relatively low Cr values.

Chondrite normalised PGE plots for the various lithologies are shown in figure 5.13. The PGE and Au concentrations are plotted in order of decreasing melting points (Naldrett et al. 1979). All of the profiles show fractionation within the PGE, with increased amounts of PPGE compared to IPGE. The M-shaped profiles highlight the negative Pt anomaly in some profiles or a slight positive anomaly for Rh in others, or a combination of both anomalies. A sample from the chromitiferous norite unit has an anomalous profile where a positive Rh and negative Ru, Pt and Pd anomalies are recorded.

The chondrite normalised profiles for these samples are very similar to those from previous Platreef studies from the Central sector and the Merensky Reef and UG2 profiles (fig. 5.13). The Merensky Reef chromitite samples are more heavily enriched in PGE than the other

samples and exhibit a strong Pt enrichment, which is not seen in the Platreef chromites. All of the samples show PGE enrichment (higher grade) of a factor of around 100 when compared to the Main Zone samples. The Merensky Reef also shows less of an PPGE:IPGE fractionation compared to the Platreef samples.

a)

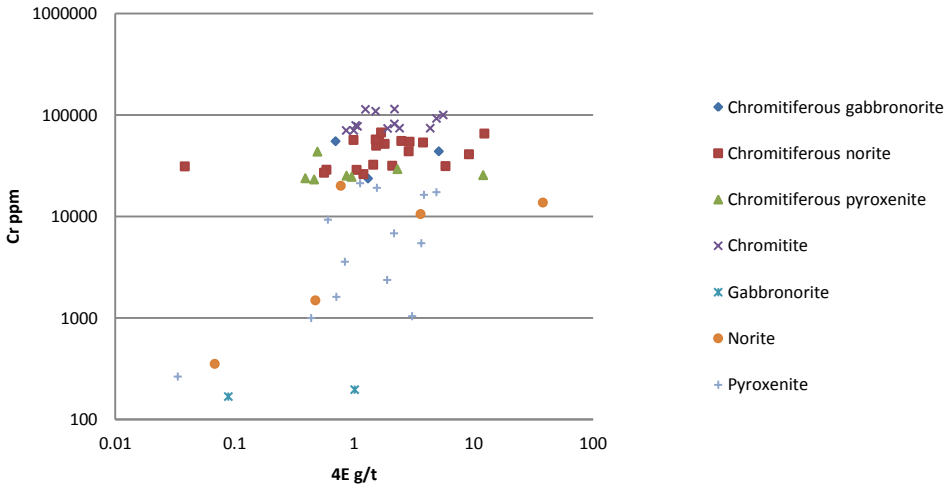


b)

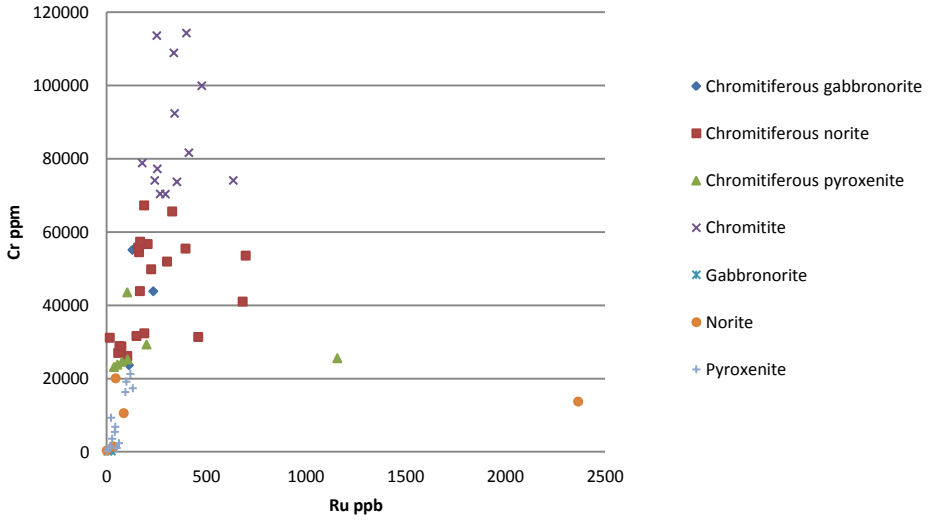


c)

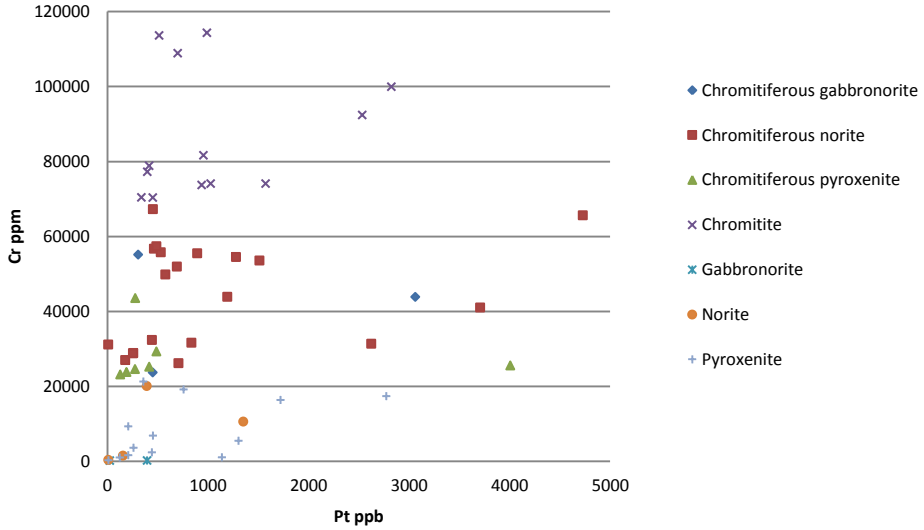


Figure 5.12. Cr vs. PGE plots (a) Cr vs. 4E, (b) Cr vs Ru, (c) Cr vs. Pt

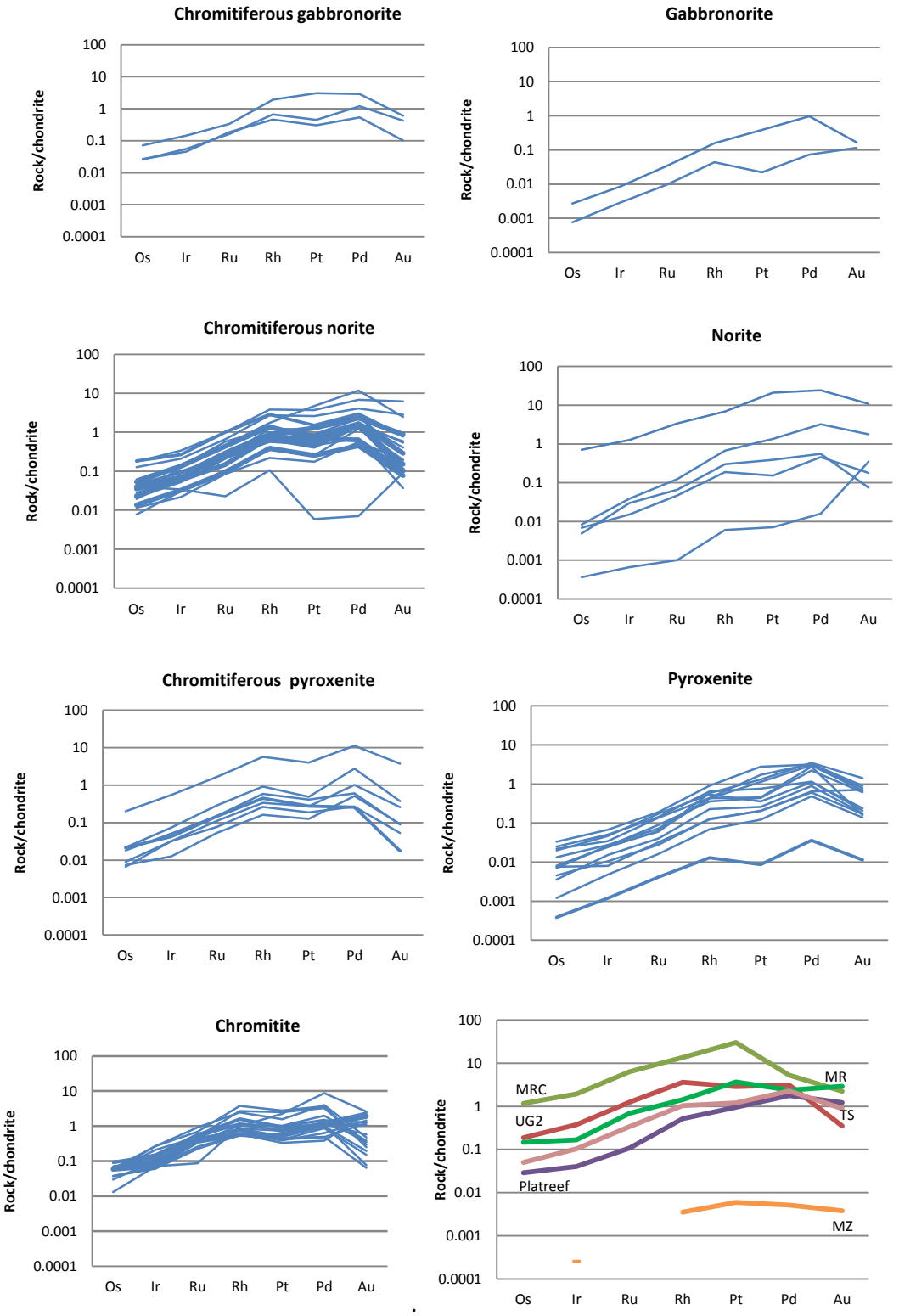


Figure 5.13. Chondrite normalised PGE profiles for various lithologies and comparison to the rest of the Bushveld Complex. Key: MRC – Merensky Reef chromitite (Barnes and Maier 2002b), MR – Merensky Reef (Barnes and Maier 2002b), MZ – Main Zone (Maier and Barnes 1999), TS – this study, UG2 (Barnes and Maier 2002a and references therein), Central Platreef (McDonald et al. 2005; Holwell and McDonald 2006) .

## 5.6 Variation spatially across study area

As samples have been collected from the three farms of Overysel, Zwartfontein and Sandsloot. Lateral variation can be studied as a function of the country rock. The drill holes can be grouped in a series of N-S strike lines (fig. 5.14) and W-E dip lines (fig. 5.17). As the Platreef is intruded as a series of sills, the average composition of each drillhole is plotted. As the magma flowed in, any assimilation of the country rock is likely to have affected the overall geochemistry rather than the samples closest to the base of the Platreef.

On the most northerly farm of Overysel, the country rock consist of granite and granofels, with minor calc-silicate identified in some of the drillholes. On the middle farm of Zwartfontein, the Platreef is in contact with granofels, but in the south the country rocks are Malmani dolomite. The Platreef on Sandsloot is in contact with the calc-silicate tongue and minor ironstone.

The N-S traverses may potentially show the influence of country rock across the study area. Using the lines on figure 5.14, two spider grams have been produced (figs. 5.15 and 5.16). There is relatively little variation shown along strike and down-dip, with no obvious change in the geochemistry as the traverse moves from the granite/gneiss country rock to one dominated by the dolomite tongue. Those localities that have a granofels footwall (Overysel and northern Zwartfontein) have mostly positive Eu anomalies, while those that are in contact with the calc-silicate have mostly negative Eu anomalies.

Little variation is shown in the dip sections (W-E; figs. 5.18 to 5.22) with the only difference being differences in Sr and Ti anomalies (some samples show positive anomalies while others show negative anomalies). Sr anomalies are likely to be a consequence of contamination, while variation in Ti reflects the amount of chromite in the sample (cf. the positive Ti anomalies in the chromitites vs. mostly negative Ti anomalies in pyroxenites shown in figs. 5.9 and 5.10).

.

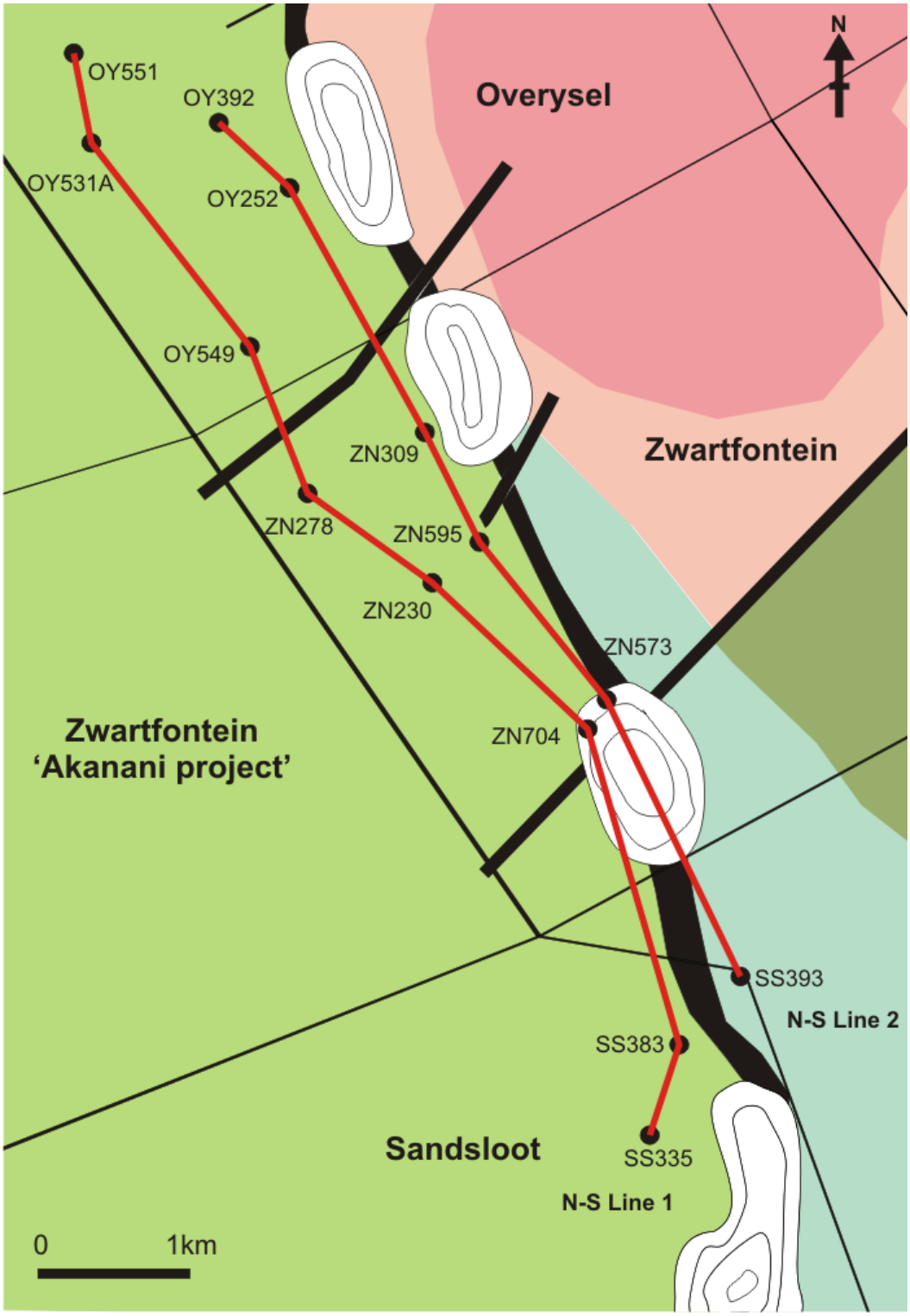

Figure 5.14. Map showing N-S lines (for key see fig. 3.1).

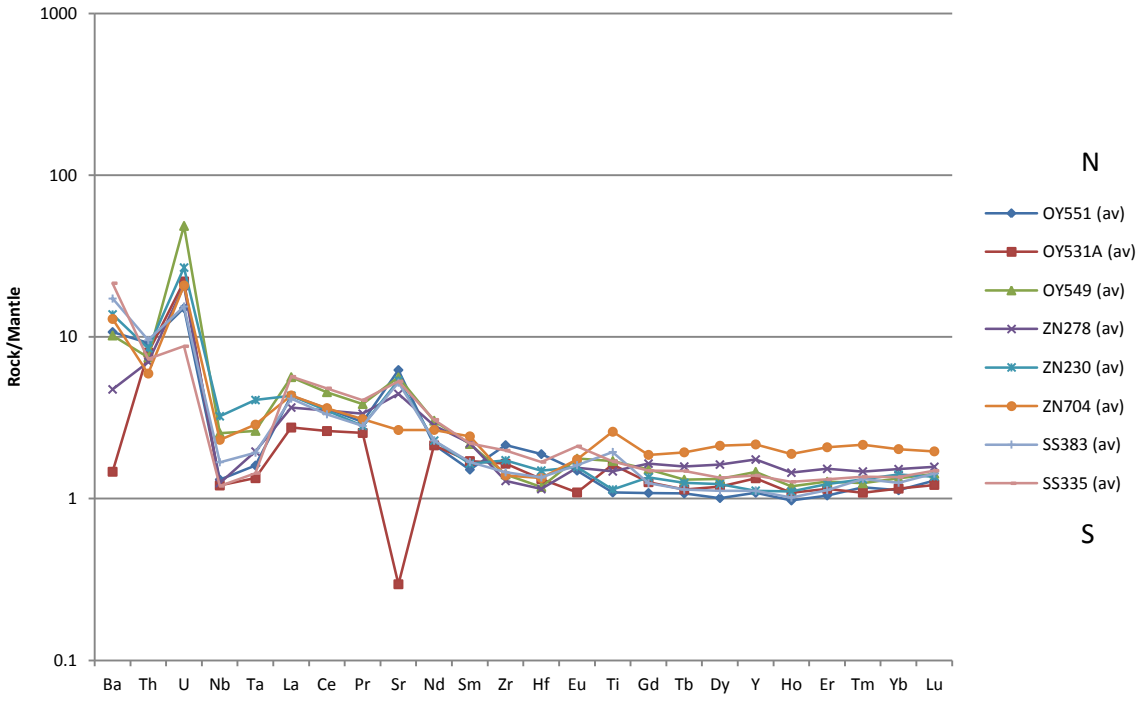


Figure 5.15. N-S line 1

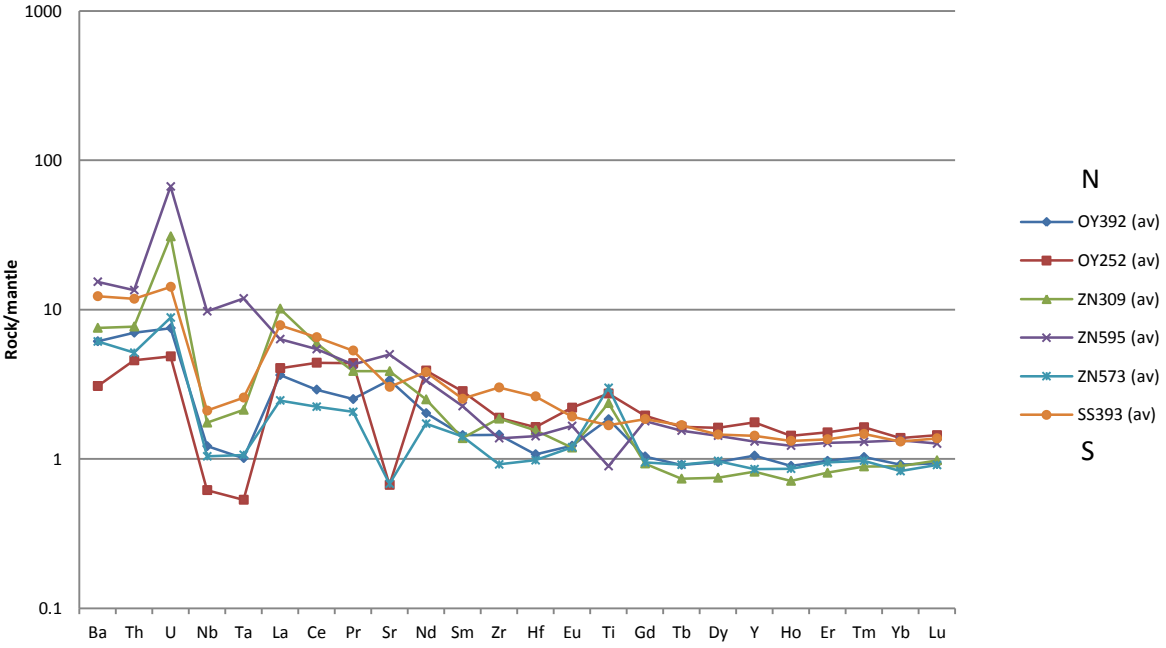


Figure 5.16. N-S line 2

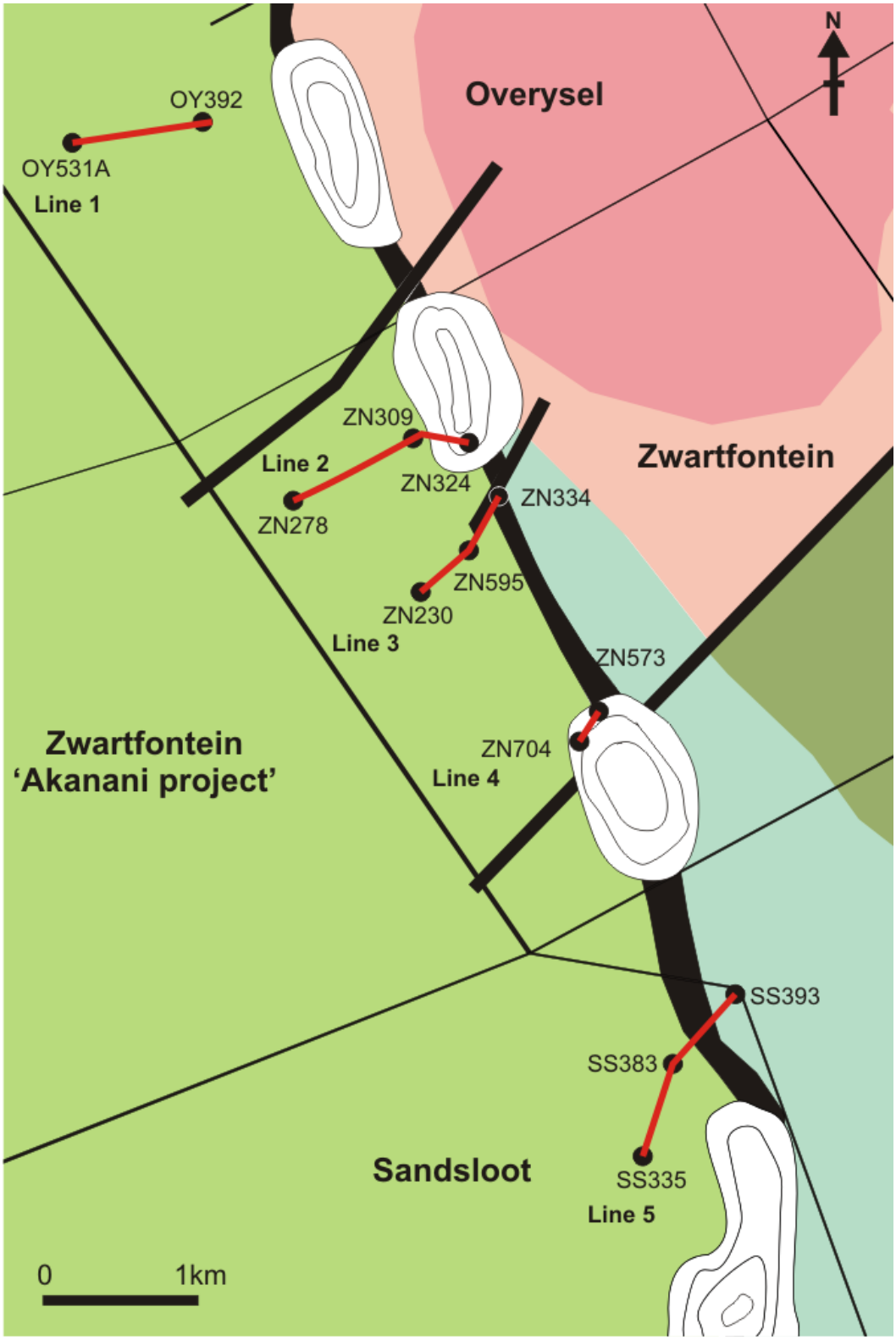


Figure 5.17. Map showing W-E lines (for key see fig. 3.1).

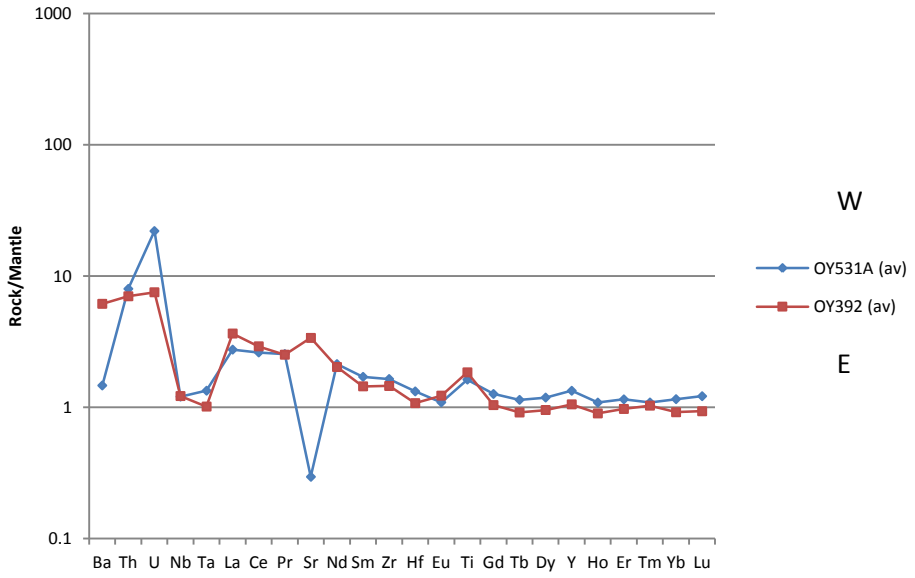


Figure 5.18. W-E line 1

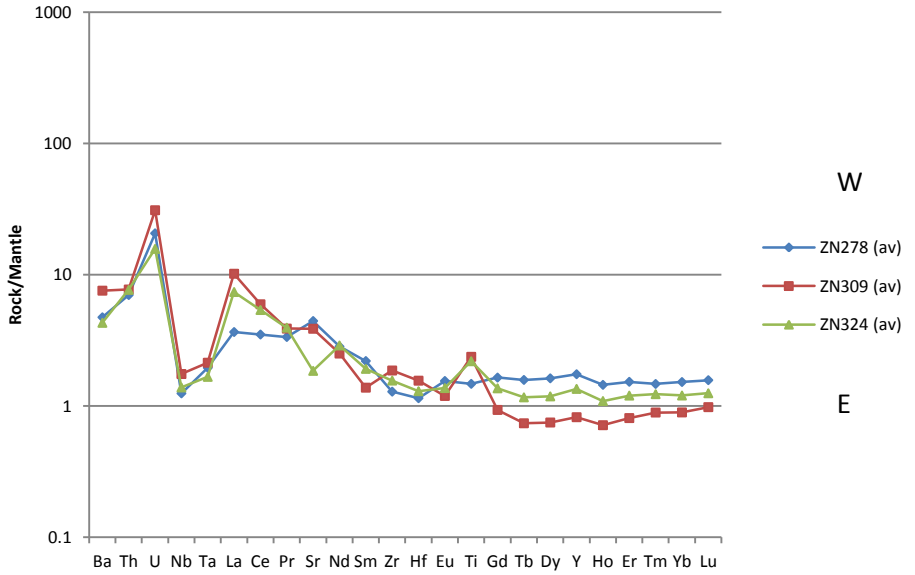


Figure 5.19. W-E line 2

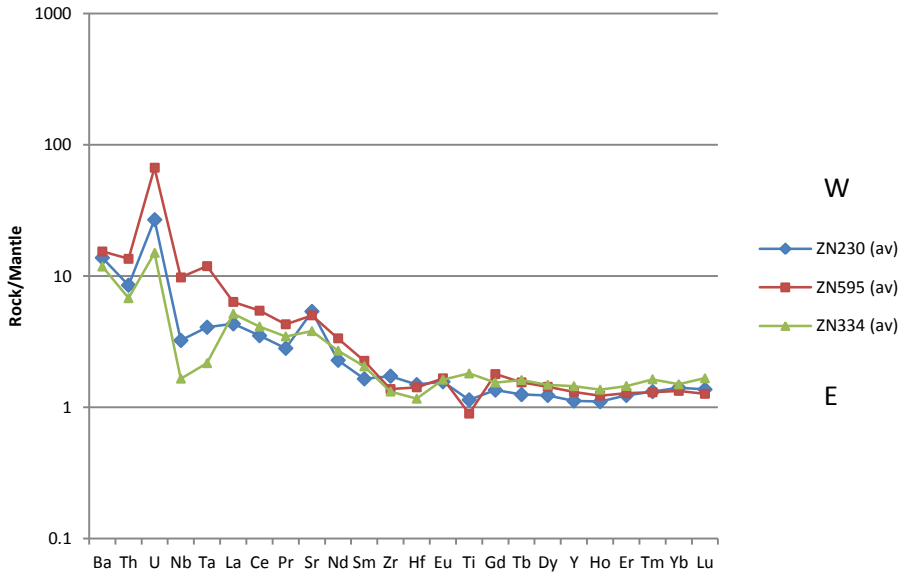


Figure 5.20. W-E line 3

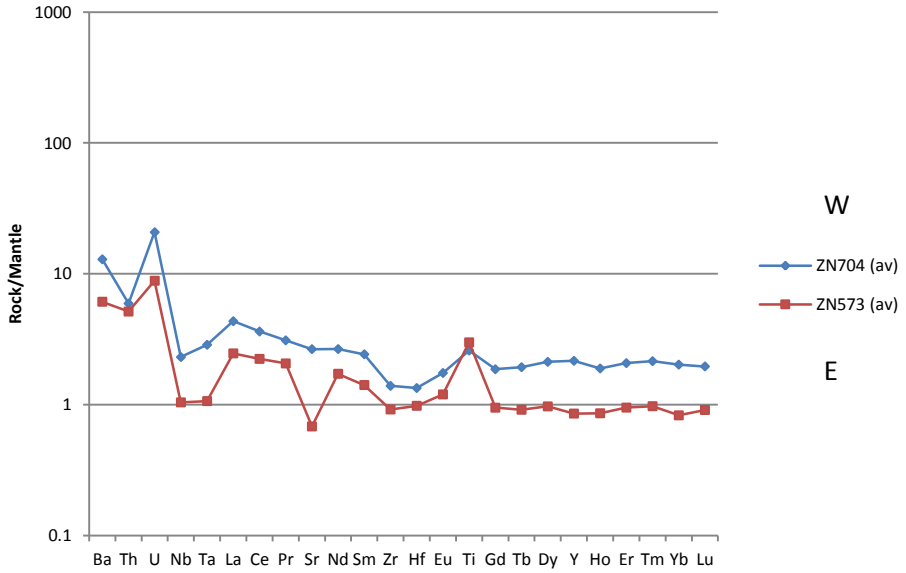


Figure 5.21 W-E line 4.

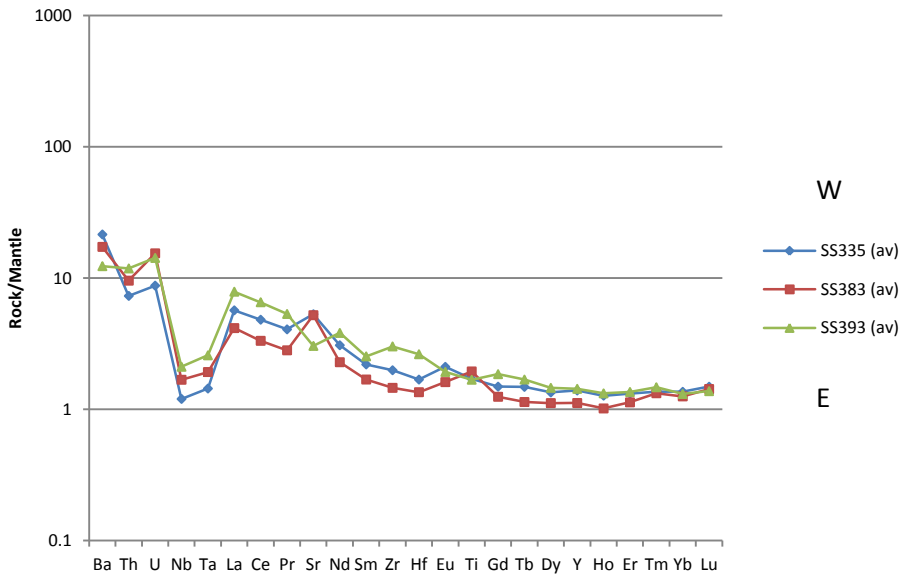


Figure 5.22. W-E line 5.

## 5.7 Summary

The samples analysed were reclassified from the logged Anglo Platinum lithologies to CIPW lithologies in order to standardise the data set. Little variation has been shown from other Platreef studies based on their major and trace element chemistry, in addition to the PGE profiles. Major element chemistry has shown deviation from mixing lines between minerals and is a likely consequence of contamination.

Chondrite normalised REE patterns mostly show fractionated profiles, with enrichment in the LREE. Some profiles show a slight positive gradient in the HREE from Ho to Lu. This feature has also been observed in other Platreef studies. The shape of the profiles is directly related to the relative proportions of the minerals that the samples contain. The Eu anomaly was quantified based on lithology, with the majority of the units showing overall positive Eu anomalies, suggesting possible oxidation of the magma. Overall, the REE plots show similar profiles to central Platreef pyroxenites and chromitites from previous studies.

Mantle normalised multi-element variation diagrams were produced for each sample. All of the samples display a negative Nb-Ta anomaly and enrichment in U relative to Th. Both negative and positive Sr anomalies are shown, with no correlation with other elements. Chromitite units show a strong Ti enrichment relative to the other lithological units and can be attributed to the Ti content of spinel. ] The B1 magma profile is situated at the top of the range displayed by the Platreef samples while the Merensky Reef profile lies within the range and is undistinguishable from Platreef profiles.

The average 4E PGE grade of the samples is 2.82 g/t which is consistent with the average grade of the Platreef at 3-4 g/t. The grade differs considerably between the different lithologies. The chromitiferous units are more PGE rich than the chromite poor rocks. However the highest PGE grade (38 g/t) is found in a noritic sample, thus increasing the average for this unit. The overall Pt/Pd ratio for the samples is 0.88, which is also similar to the average of 1:1 for the Central Platreef. PGE fractionation is shown to be highest in chromite-poor units, implying a strong association of the IPGE with chromite. Overall, the PGE profiles show a M-shape highlighting the negative Pt anomaly and positive Rh anomaly. When comparing the Platreef profiles to other Bushveld profiles, it is seen that the Merensky Reef profiles are more strongly enriched in PGE and exhibit a strong Pt enrichment. The Platreef, UG2 and Merensky Reef are enriched by a factor of around 100 compared to the Main Zone.

Examination of samples that are in contact with different country rocks has shown that there is little variation across the study area (both along strike and down dip) and that any contamination signatures observed are likely a result of primary contamination that occurred prior to emplacement.

# Chapter 6: Mineralogical Study Of The Platreef Chromites

## 6.1 Introduction

Chromite is an oxide mineral forming part of the spinel group. The general spinel formula is $XY_2O_4$ where X = $Fe^{2+}$, Ni, Mg, Mn, Co, Zn and Y = $Cr^{3+}$, $Fe^{3+}$, Al. Typically, Mg and $Fe^{2+}$ fill the X cation sites, with Cr, Al and $Fe^{3+}$ filling the Y cation site. Chromite has a high relative density (3.8 – 4.9) and a Mohr hardness of ~ 5.5 (Barnes and Roeder 2001).

Most of the large concentrations of chromite found in igneous rocks are thought to result from crystallisation and concentration of chromite from melts of basaltic or ultrabasic composition. Although chromite is one of the first phases to crystallise, the amount of chromite that a melt can crystallise is small, because of the low solubility of Cr in the melt (Roeder and Reynolds 1991). Various mechanisms have been presented to account for the origin of monomineralic chromitite layers, as discussed in chapter 3.

It has long been recognised (Irvine 1965, 1967) that the composition of spinels is highly sensitive to the environment in which they form, particularly the composition of their parent magma. Spinels are therefore valuable petrogenetic indicators. In general, the $Fe^{2+}/Fe^{3+}$ ratio of chromite is proportional to, but lower than the $Fe^{2+}/Fe^{3+}$ of the co-existing melt (Roeder and Campbell 1985) and its Al/Cr ratio tends to be proportional to that of the coexisting melt but does not necessarily reflect that of the whole rock (Roeder and Reynolds 1991). Spinels are useful petrogenetic indicators because they crystallise over a wide range of conditions from basic and ultrabasic magmas and, in the case of chromites, are often among the first phases to crystallise. They also exhibit a wide range of solid solutions, the thermodynamics of which have been studied extensively (O'Neill and Wall 1987; Sack and Ghiorso 1991). The substitution between Cr-Al in the trivalent site is quantified by the chrome number (Cr#=Cr/(Cr+Al)). Cr# of chromite increases during melting and so is used as an indicator for partial melting (Barnes and Roeder 2001). The substitution of Mg-$Fe^{2+}$ in the divalent site is quantified by the magnesium number (Mg#=Mg/(Mg+$Fe^{2+}$)). During partial melting and crystallisation there is a strong coupled behaviour between the divalent and trivalent ions. This coupled behaviour, however, is strongly affected by Mg and $Fe^{2+}$ exchange between spinels and silicates, such as olivine, during subsolidus re-equilibration. The Mg# may also become decoupled from the Cr# by alteration of chromite to ferrochromit.

Spinels are relatively refractory and resistant to alteration, particularly compared with other high-temperature igneous minerals such as olivine. They occur in a high proportion of

terrestrial mafic and ultramafic rocks and a very large volume of microprobe data are available on their compositions (Barnes and Roeder 2001).

### 6.1.1 Major trends in chromite compositional space

In a review of various datasets worldwide, Barnes and Roeder (2001) identified a number of distinct features that appear regularly (fig. 6.1), such as the spinel gap, the Cr-Al trend, the Fe-Ti trend and the Rum trend. In addition to these trends, Naldrett et al. (2009a) defined a further 2 trends, trend A and trend B. All of these features are discussed further below.

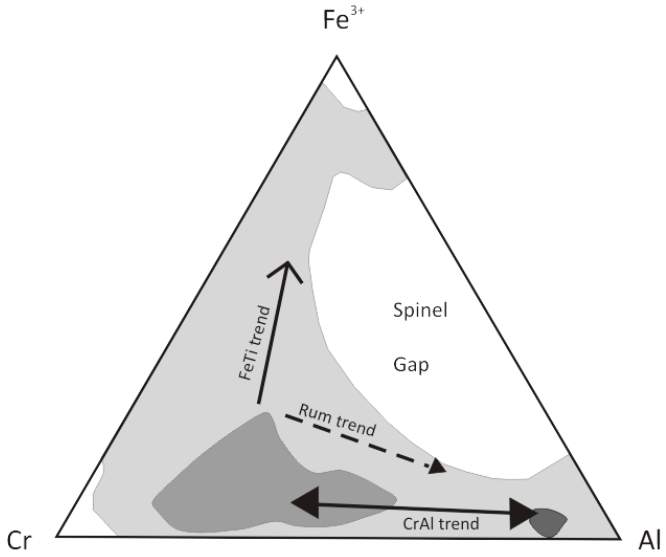


Figure 6.1.Trivalent ion plot of the entire terrestrial spinel data set of Barnes and Roeder (2001). The spinel gap and generalised trends discussed below are labelled. Contours enclose the most densely packed 50 % (dark shading) and 90 % (light shading) of the data points.

#### *The spinel gap*

The spinel gap describes an observed data density minimum between chrome-rich spinels (usually chromites) and $Fe^{3+}$ rich spinels (approaching magnetite composition). Barnes and Roeder (2001) state that there are two main causes for this. Firstly, there is an extensive solvus in the spinel solid solution (Mattioli and Wood 1988; Sack and Ghiorso 1991). Secondly, the reaction relationship in igneous rocks between chromite and Cr-bearing clinopyroxenes causes the crystallisation of chromite to cease. This causes a hiatus before the onset of crystallisation of magnetite. This crystallisation gap is not universally present in all geological settings but is typical in basaltic suites and layered mafic-ultramafic intrusions such as the Bushveld Complex (Roeder 1994).

#### *The Cr-Al trend*

The Cr-Al trend is particularly evident in various mantle and lower-crustal samples. It is defined by widely variable Cr# at generally low $Fe^{2+}$# ($Fe^{2+}/(Mg+Fe^{2+})$), and at low

concentrations of $Fe^{3+}$ and $TiO_2$. There is a slight trend of increasing Cr# with an increasing $Fe^{2+}$#. The general trend displays an increase in Cr# with decreasing Mg#. This sloping trend was first described by Irvine (1967) in the Muskox layered intrusion in the Northwest Territories of Canada, and the author suggested that it is caused by the equilibration of chromite with olivine of constant composition at constant temperature. The slope of the trend is a consequence of non-ideality within the spinel solid solution, and the temperature dependence on this line is the basis of the olivine geothermometer (Sack and Ghiorso 1991).

### *The Fe-Ti trend*

The Fe-Ti trend identifies a positive trend with $Fe^{3+}$# ($Fe^{3+}$/($Fe^{3+}$+Cr+Al)) and $Fe^{2+}$# increasing and is typically accompanied by increasing $TiO_2$ wt%. A negative trend is observed between Cr# and Mg#. According to Barnes and Roeder (2001), this trend is attributed to the evolution of spinel compositions during fractional crystallisation of olivine or pyroxene (with or without plagioclase) from the parental magma. This causes the Fe/Mg ratio and the Ti content of the melt to increase. This trend is identified in chromites from basalt and differentiated mafic-ultramafic igneous bodies. Strong Fe-Ti trends are seen in chromites of orthocumulate rocks that interact with trapped evolving intercumulus melt (e.g. Henderson 1975; Henderson and Wood 1982; Roeder and Campbell 1985; Scowen et al. 1991). The variation in $Fe^{2+}$# is attributed to two sources; evolving melt compositions during crystallisation as well as the exchange of $Fe^{2+}$ and Mg between spinels and coexisting silicates (usually olivine) which favours increasing $Fe^{2+}$# in spinel with decreasing temperatures (Irvine 1965). According to Barnes and Roeder (2001), the effect is more pronounced in slowly cooled rocks.

### *The Rum trend*

The Rum trend resembles a steeper Cr-Al trend. It was initially observed by Henderson (1975) in the Rum layered intrusion. According to Barnes and Roeder (2001), this trend is restricted to mafic layered intrusions where chromite occurs within gabbroic orthocumulate rocks. This trend shows an increase in Al at the expense of Cr, with some decrease in $Fe^{3+}$ (which is not seen in the Cr-Al trend). In addition there is a decrease in $Fe^{2+}$#. It has been attributed to a reaction between cumulus chromite, trapped intercumulus liquid, plagioclase and olivine. It arises from the effect of the Cr/Al ratio changing in the spinel, where it causes the Fe-Mg exchange coefficient ($K_d$) between the surrounding silicates and chromite to compensate. If the Cr/Al ratio of chromite decreases, its corresponding Fe/Mg ratio is constrained to fall due to the effect of $K_d$ values falling with temperature, and that the silicate Fe/Mg ratio remain relatively constant. Both the Rum and the Fe-Ti trend may

be seen in the same samples depending on the micro-environment of the chromite crystals (Barnes and Roeder 2001).

#### *Trend A*

Trend A defined by Naldrett et al. (2009a) is similar to the Rum trend of Barnes and Roeder (2001) with the exception that there is little change in $Fe^{3+}$ with changing Cr#. This trend has been related to changing melt composition, due to rapid, sequential pulses of fresh magma, as the chromite crystallises from it. The disturbance prevents fractional crystallisation from being recorded in the chromite mineralogy. This trend is observed in chromites from layered intrusions, especially in chromitites where there are minimal interstitial silicates.

#### *Trend B*

Trend B there is a positive correlation between Cr# and Mg#, as opposed to the negative correlation shown in trend A. This has been interpreted by Naldrett et al. (2009a) to correspond with periods of fractional crystallisation within the magma chamber. This increases the $Al_2O_3$ content of the magma, resulting from silicates (olivine and orthopyroxene +/- plagioclase) crystallising simultaneously with the chromite. The crystallising chromites have subsequently lower Cr# and Mg#. This trend is not seen as often as trend A in chromites from layered intrusions.

### 6.1.2 Chromite in the Bushveld Complex

South Africa is the world's leading producer of chromite according to the US Geological Survey's Mineral Commodity Summary (2012 ; fig. 6.2). The Bushveld Complex contains 14 major chromitite horizons, with three seams mined principally for chromite (the LG-6, MG-1 and MG4; Naldrett et al. 2009a). The majority of chromitite layers occur in the Critical Zone of the RLS, but in addition, massive chromitite bodies occur in the Lower Zone of the northern limb (e.g. Grasvally).

Numerous studies on the chromites from the Bushveld Complex have been carried out (e.g. Cousins and Feringa 1964; Cameron 1975; Cameron 1977; Hiemstra 1979; Cameron 1980; McLaren and De Villiers 1982; Hulbert and von Gruenewaldt 1985, 1986; Hatton and von Gruenewaldt 1987; Teigler and Eales 1993; Penberthy and Merkle 1999; Eales 2000; Kinnaird et al. 2002; Mondal and Mathez 2007; Maier and Barnes 2008a; Naldrett et al. 2009a; Yudovskaya and Kinnaird 2010; Naldrett et al. 2012).

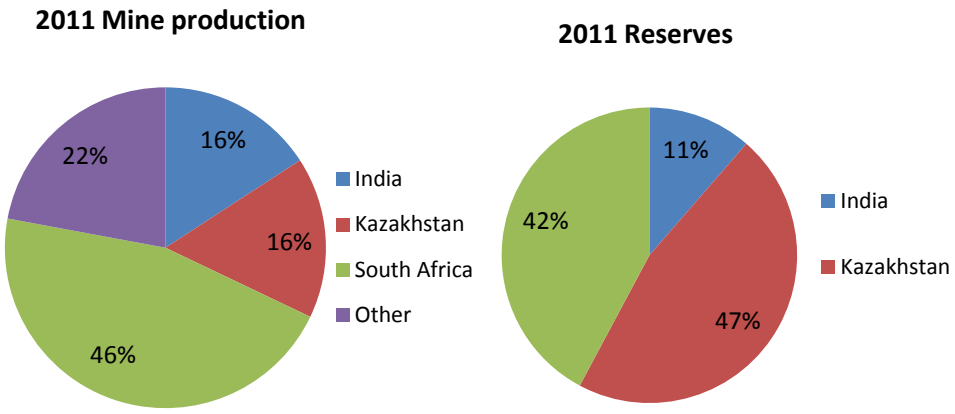


Figure 6.2. World production of chromite ore and reserves according to data complied by the USGS Mineral Commodity Summary (2012)

### 6.1.3 Aims of the study

The aim of this study is to investigate the mineral chemistry of the Platreef chromites in order to establish what variation is present in chromitites along strike and down dip within the ore body. In addition, the mineral chemistry of chromites in different host lithologies will be compared. The data can then be compared to other data sets for the Platreef as well as to the Upper Critical Zone in the rest of the Bushveld Complex.

## 6.2 Materials and methods

62 polished blocks were analysed in back-scattered electron mode of a Cambridge Instruments S360 scanning electron microscope (SEM). Quantitative analysis of the chromite crystals was made using an Oxford Instruments INCA energy-dispersive (EDX) analyser attached to the SEM. Operative conditions for the quantitative analyses were: 20 kV, with a specimen calibration current of ~ 1 nA and a working distance of 25 mm. A cobalt reference standard was regularly analysed in order to check for any drift in the analytical conditions. A comprehensive set of standards was obtained from Micro Analysis Consultants Ltd (St Ives, Cambridgeshire) and used to calibrate the EDX analyser. ZAF corrections were performed using the INCA software program. Instrument variability at time of analysis was assessed by Brough (2011). Each chromitite sample was analysed to maximise areal coverage, with ~ 10 chromite crystals per sample analysed (Appendix 1). Area analysis of each chromite grain was carried out rather than spot analysis to obtain the average result for each grain. Cations were calculated using the Barnes and Roeder (2001) spreadsheet.

## 6.3 Chromite distribution and morphology

The chromitite samples contain up to 80 vol. % of chromite and the chromitite layers are up to 30 cm thick in the samples studied. Most of the chromites are found as discrete crystals

with euhedral to subhedral, equant habit. The chromite crystals are not uniform in size. Crystals have an average diameter of 80 microns with a maximum diameter of around 300 microns.

The majority of chromite crystals are enclosed within silicates (fig. 6.3 a). Orthopyroxene is a dominant host phase along with chromite. It is commonly associated with minor clinopyroxene. Orthopyroxene is generally of cumulus habit, with associated post-cumulus overgrowth. Plagioclase is an intercumulus phase and therefore the morphology of the crystals is controlled by the shape of the space left by the other phases. Olivine is rarely seen in the samples and is often serpentinised.

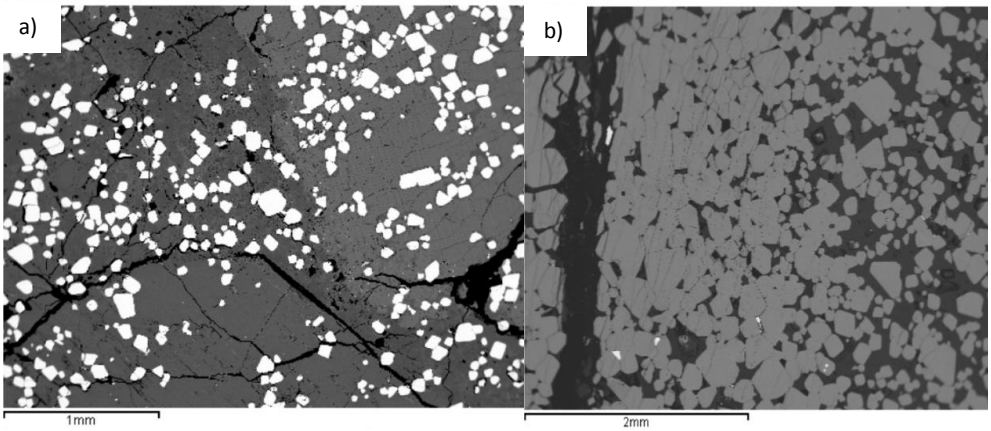

Figure 6.3. (a) Typical texture of chromitite with euhedral chromite crystals enclosed within orthopyroxene; (b) Chromite with annealed texture.

Occasionally, some samples exhibit annealed chromite (fig. 6.3 b). This is believed to be a result of sintering of small but originally separate crystals (Hulbert and von Gruenewaldt 1985) and has been suggested to represent the location of pockets of late intercumulus melt (Roeder and Campbell 1985). Due to the very low solubility of chromium in silicate melts (Roeder and Reynolds 1991), there has been little significant change in the volume proportion of chromite in the chromitite during postcumulus processes. As a result, the number of chromite crystals would have decreased but the size of the crystals would have increased, due to the sintering process. In addition, chromite growth would have been restricted after enclosure by other early phases such as olivine and orthopyroxene.

Examination of chromite morphology (e.g. fig. 6.3) and stratigraphic position within the drillholes selected for study are consistent with descriptions by Yudovskaya and Kinnaird (2010) of the Lower Chromitite zone (LCR) in the Platreef. The LCR occurs as multiple seams in the Southern and Central sectors close to the basal contact of the Platreef. The basal package that hosts the LCR is extremely heterogeneous and includes pyroxenite, norite,

harzburgite in addition to parapyroxenite and calc-silicates that are variably altered and often completely serpentinised. Chromites in the LCR are up to 0.2 m thick (Yudovskaya and Kinnaird 2010). The fact that all the samples in this study are consistent with the LCR is coincidental as originally the samples were selected for the sulphide melt inclusion study (chapter 9) from the database at Anglo Platinum. The areas chosen to sample were holes that contained the most entries of chromitite as well as ones that had the largest thicknesses of logged chromitite.

## 6.4 Chromite mineral chemistry

The geochemistry for all the major and trace elements for the Platreef samples has been described in chapter 5.

A total of 593 chromite crystals were analysed from 62 polished blocks, representing the three farms of Overysel, Sandsloot and Zwartfontein. The average composition of chromite in this study is Cr# = 0.64, $Fe^{2+}$# = 0.66 and Mg# = 0.34. The Cr# varies from 0.42 to 0.87, with an associated $Fe^{2+}$# of 0.32 to 0.96. The Mg# ranges from 0.04 to 0.68. $Cr_2O_3$ content range from 27.3 to 53.9 wt%. $TiO_2$ content range from 0.31 to 4.45 wt%. All the data points plot within the trivalent ion plots for terrestrial spinel as defined by Barnes and Roeder (2001; fig. 6.4).

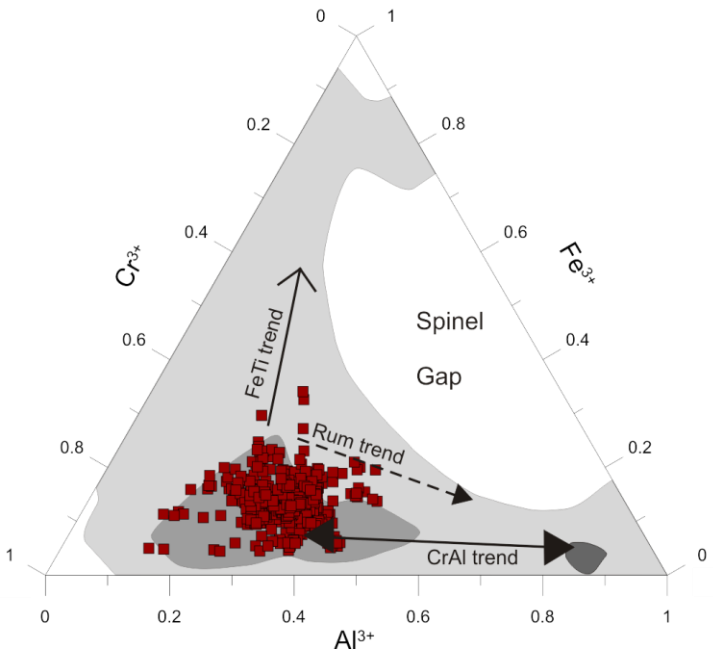


Figure 6.4. Trivalent ion plot of the terrestrial spinel data set of Barnes and Roeder (2001) with the data from this study superimposed. Contours enclose the most densely packed 50 % (dark shading) and 90 % (light shading) of the data points.

a)

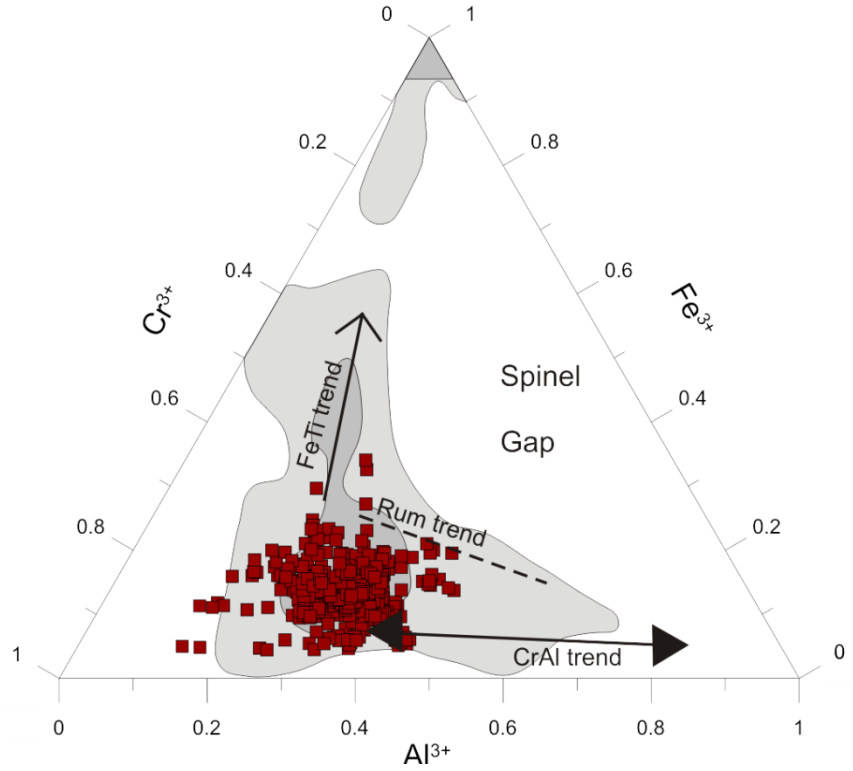


b)

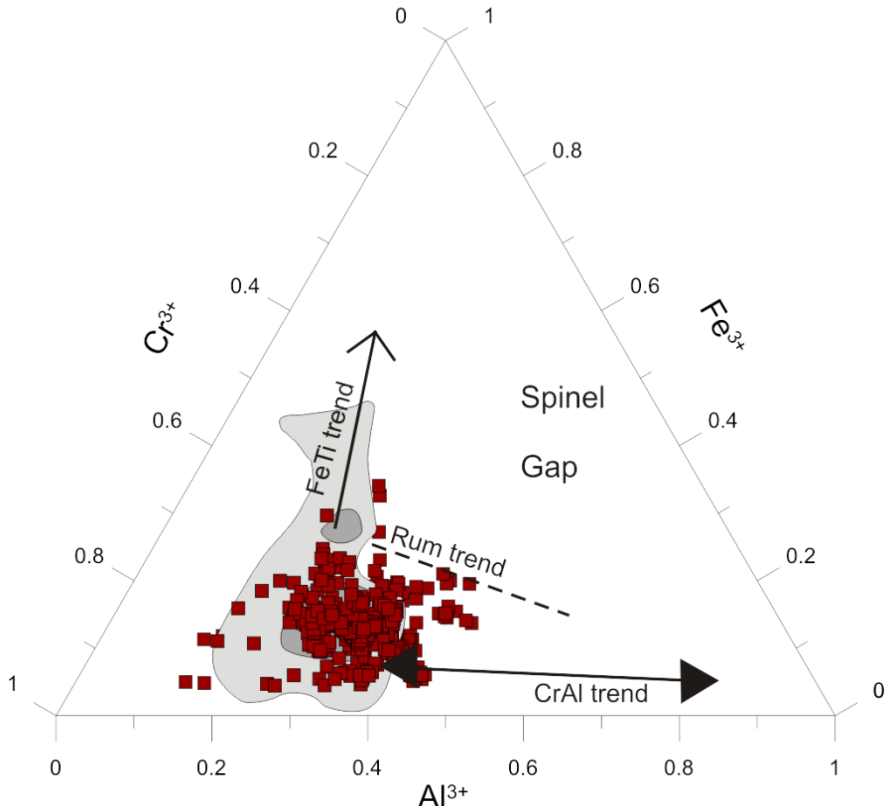


Figure 6.5. Data from this study superimposed on Barnes and Roeder fields for (a) layered intrusions; and (b) chromitites within layered intrusions. Contours enclose the most densely packed 50 % (dark shading) and 90 % (light shading) of the data points that were analysed by Barnes and Roeder (2001).

The major element geochemistry for the analysed chromites lie within the layered intrusion fields as defined by Barnes and Roeder (2001). The data density contour plots for layered mafic-ultramafic intrusions are very different depending on whether chromitites are included in the dataset. Figure 6.5 a & b show that the majority of the data plot within the layered intrusions chromitites-only field, while all but 4 data points plot within the existing layered intrusion fields. This is unlikely to be significant as the outer lighter field drawn on the plot represent 90 % confidence limits of the expected range of compositions as defined by Barnes and Roeder (2001). The chromites from this study are strongly clustered at relatively low $Fe^{3+}$ contents, with a less developed Fe-Ti trend. This lack of Fe-Ti trend is due to a buffering effect. Chromite is less susceptible to the trapped liquid reaction effects discussed above when the proportion of chromite to trapped liquid is high. It is likely then that the compositional field of chromitites closely matches the composition of primary liquidus chromites (Barnes and Roeder 2001).

### 6.4.1 Cr# vs. Mg#

Figure 6.6 shows two broad trend lines of increasing Cr# with decreasing Mg#. Chromites with moderately high Cr# and Mg# can be considered primary chromites. Chromites with higher Cr# but low Mg# may have had their chemistry altered by one of two processes. Either re-equilibration has occurred with the surrounding Mg-rich pyroxenes or phlogopite replacement has occurred. Re-equilibration results in a decrease in Mg and Al, and increase in Ti, Fe and Cr. The remobilisation in Mg and Al from the chromite into the pyroxenes causes the Mg# of chromite to decrease and Cr# to increase. In samples containing sulphide mineralisation, iron exchange between the chromite and the sulphides also causes the Mg# of chromite to decrease. In some samples phlogopite replacement was evident where chromite grains were embayed (fig. 6.7). Where this occurs there is an increase in Cr and Ti due to Al and Mg removal to the mica, resulting in a higher Cr# and lower Mg#.

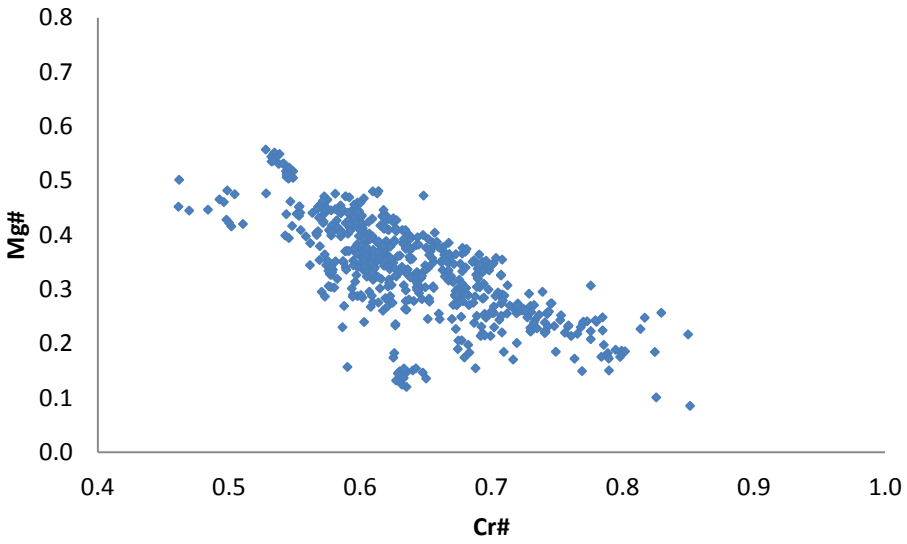


Figure 6.6. Compositional variations for chromites from the farms of Overysel, Sandsloot and Zwartfontein.

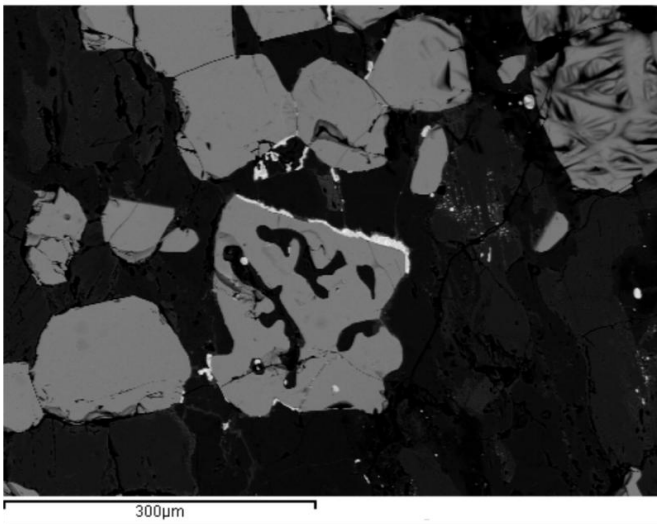


Figure 6. Altered chromite in phlogopite with phlogopite embayments.

### 6.4.2 Cr# vs. $Fe^{2+}$#

Plotting Cr# vs. $Fe^{2+}$# illustrates whether the Cr-Al trend is present in the data set. As can be seen from figure 6.8, a strong trend is present in the data, again highlighting the re-equilibration between the chromite and host pyroxenes. The increase of Cr# with $Fe^{2+}$# represents the Cr-Al trend. Where the trend line is less steep, representing a greater increase in $Fe^{2+}$# than Cr#, it is more representative of the Rum trend. This is produced due to the reaction between the cumulus chromite, trapped intercumulus liquid and plagioclase.

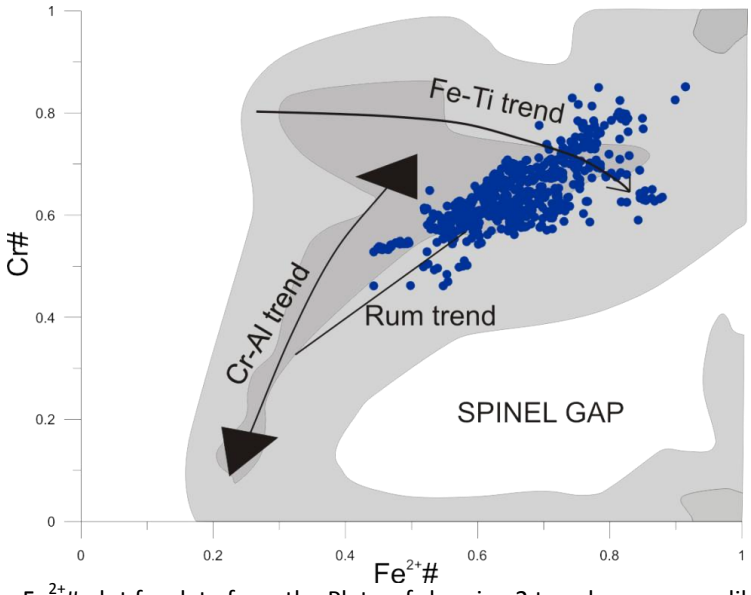


Figure 6.8. Cr# vs. $Fe^{2+}$# plot for data from the Platreef showing 2 trends, one more like the Rum trend than Cr-Al trend.

### 6.4.3 $Fe^{3+}$# vs. $Fe^{2+}$#

The purpose of plotting $Fe^{3+}$# against $Fe^{2+}$# is to illustrate whether a Fe-Ti trend exists within the dataset. Figure 6.9 shows a moderate Fe-Ti trend in the data. Variation of $Fe^{2+}$# may have a number of causes. Firstly, it may represent the evolution of the melt during fractional crystallisation, or it may represent the exchange of $Fe^{2+}$ and Mg between the spinel and the coexisting silicates or sulphides. This exchange favours the increase of $Fe^{2+}$# in the chromite with falling temperatures.

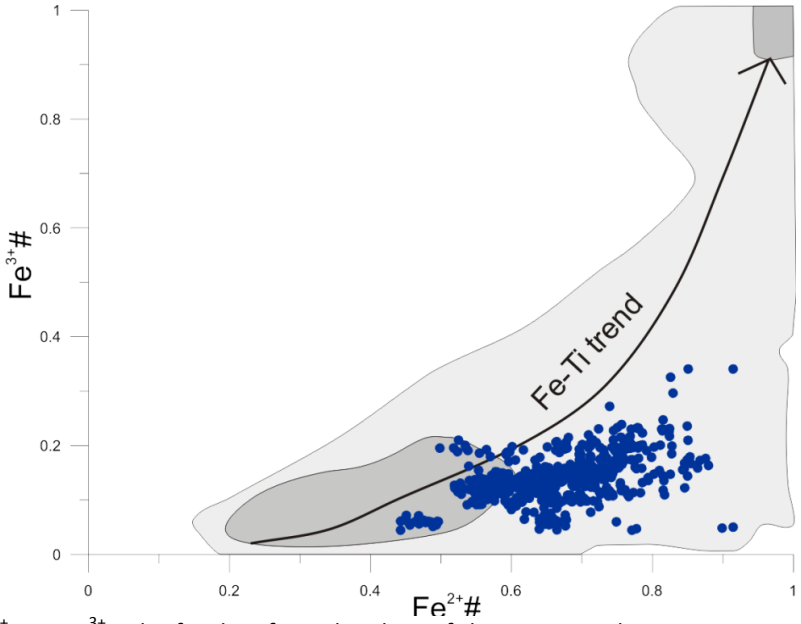


Figure 6.9. $Fe^{2+}$# vs. $Fe^{3+}$# plot for data from the Platreef showing a moderate Fe-Ti trend for the data.

### 6.4.4 $Fe^{3+}$# vs. $TiO_2$

This plot is another way of evaluating the extent of the Fe-Ti trend and figure 6.10 shows a moderate trend for the data set. The increase of $TiO_2$ suggests that the chromites equilibrated with a relatively evolved Ti rich melt. An increasing $Fe^{3+}$# may also represent fractionation (fig. 6.9). Typically, chromites with Lower Zone signatures have very low $TiO_2$ contents (Hulbert and von Gruenewaldt 1985). Provided the chromite crystals are not included in silicates and thus could react with the interstitial melt and fluid, equilibration could have resulted in relatively low $TiO_2$ and high Fe, accounting for the trend.

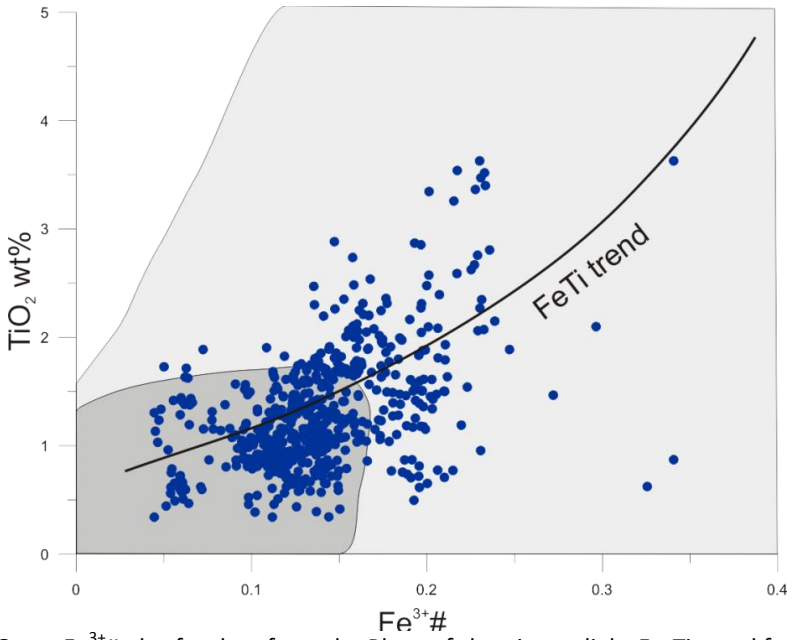


Figure 6.10. $TiO_2$ vs. $Fe^{3+}$# plot for data from the Platreef showing a slight Fe-Ti trend for the data.

## 6.5 Variations within different lithologies

For the remainder of this chapter the samples have been divided according to the geochemical lithologies that were defined in chapter 5. They are also further separated into individual farms in order to determine if there is any spatial correlation with the mineral chemistry of the chromites. As can be seen from figures 6.11 and 6.12, there is a difference in the composition of chromites hosted by different lithologies, although the compositional fields overlap. This suggests that the variation in mineral chemistry is not controlled strictly by lithology.

The variation in $Cr_2O_3$ contents shows that all of the lithologies have ranges that overlap and therefore cannot be used to distinguish lithology. MgO values (fig. 6.11 a) show a similar profile. However, chromites analysed from the chromitiferous pyroxenite units group together at the top end of the MgO value range (8-11 wt%). There is also a group of analyses from the chromitite units (as defined by the geochemistry analyses of chapter 5) that have very high MgO values (11-12.5 wt%). Analysis of the $TiO_2$ content (fig. 6.11 b) shows a similar picture to $Cr_2O_3$, with all the lithologies spanning the range of values, apart from chromites analysed from the norite units, which plot at the high end of the $TiO_2$ values (1.6-2.6 wt%) and the chromitiferous pyroxenite values grouping at the low end of the values (0.5-1.25 wt%). The distribution of the various lithological groups when analysing FeO, is similar to $TiO_2$ (fig. 6.12 b), with chromite crystals from the chromitiferous pyroxenite grouping at low FeO values (30-37 wt%) and those from the norite units grouping together at the high end of the range (35-45 wt%).

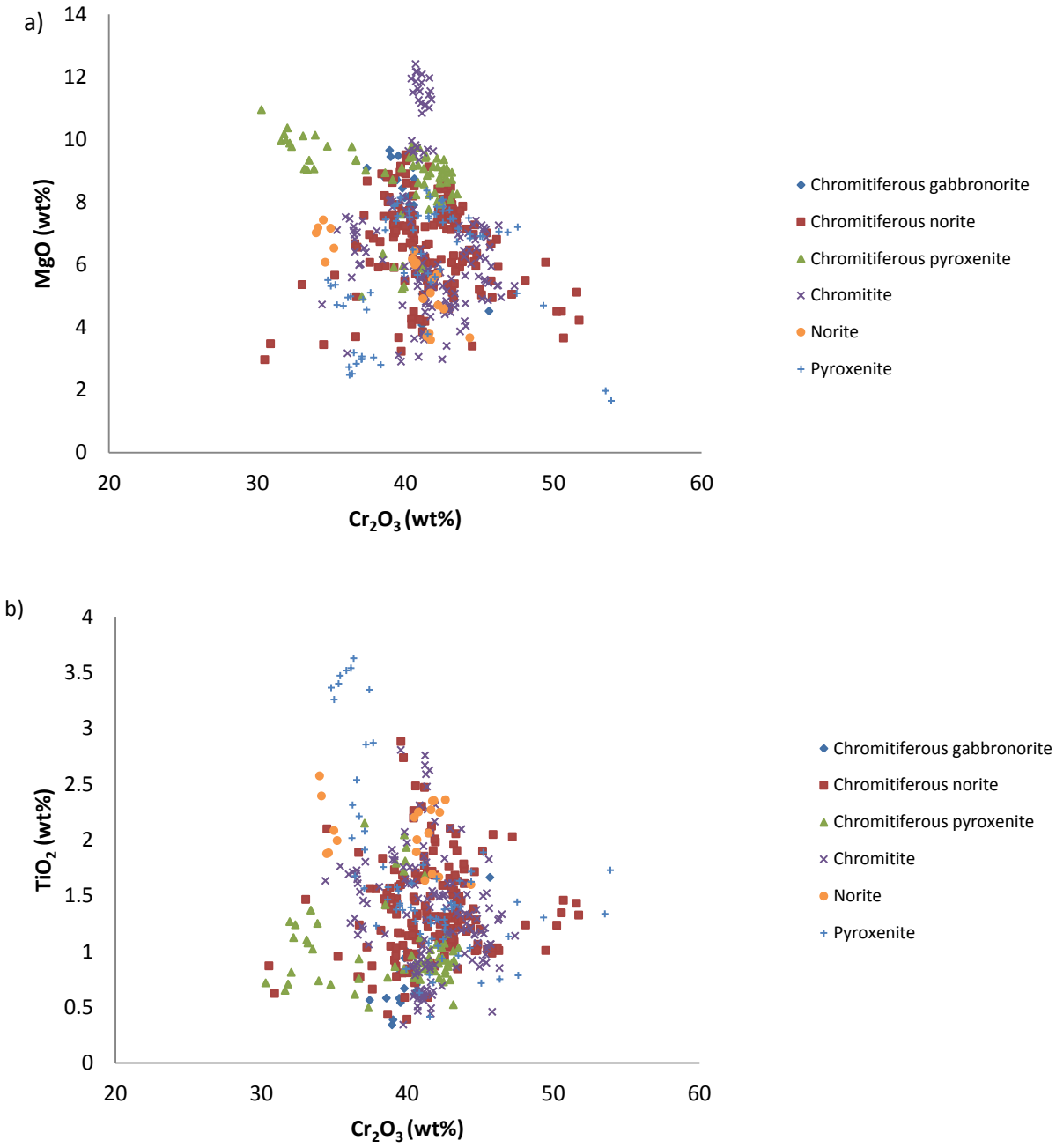


Figure 6.11. Geochemical plots of chromite composition from different lithologies across 3 different Platreef farms; (a) MgO vs. $Cr_2O_3$ and (b) $TiO_2$ vs. $Cr_2O_3$;

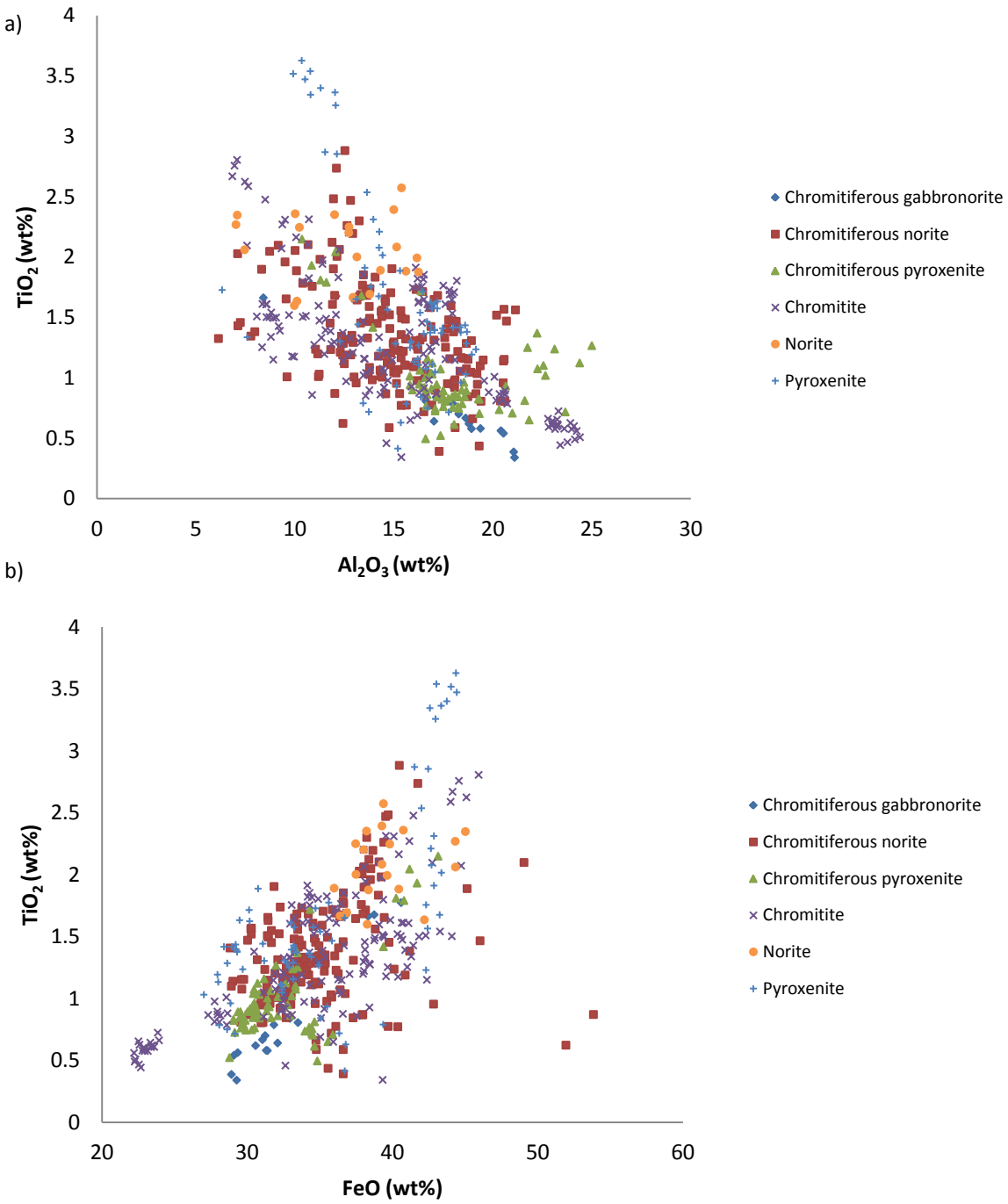


Figure 6.12. Geochemical plots of chromite composition from different lithologies across 3 different Platreef farms; (a) $TiO_2$ vs. $Al_2O_3$ and (b) $TiO_2$ vs. FeO.

## 6.6 Variations along strike of the Platreef

As has been shown above, it appears that host lithology exercises limited influence on chromite chemistry. In order to investigate this further, the samples will be divided depending on their geographical location to see whether there is any variation in chromite chemistry along strike. The location of the three farms of Overysel (the most northerly of this study), Zwartfontein and Sandsloot (the most southerly of this study) can be seen in figure 3.1.

### 6.6.1 Cr# vs. Mg#

Chromite analyses from Overysel displays a strong overall negative relationship between Mg# and Cr#. Chromite crystals within chromitites have the highest Mg# but lowest Cr#, whereas chromite crystals from dominantly pyroxenite units display the lowest Mg# but highest Cr#. Chromites from the other lithologies all group together along this range, with the two end members (chromitite and pyroxenite lithology data) having the widest range of Cr# values, overlapping with the other fields (fig. 6.13 a).

Overall, the chromites from Zwartfontein display a wider Mg# range over a smaller Cr# range compared to the data from Overysel resulting in a steeper primary trend line (fig. 6.13 b). There is also a secondary (steep negatively sloping) trend suggested by low Mg#, and low Cr# values for some chromite crystals mostly within the chromitite lithology. Unlike the data from Overysel, the data from each lithology have a wide range and overlap with data from other lithologies. Chromite crystals from the pyroxenite units typically have the highest Cr# values whereas, like at Overysel, chromites from the chromitite units have the lowest Cr# and highest Mg# values.

Data from Sandsloot chromites plot on a trend line with the flattest gradient of the three farms; the data shows a limited Mg# range but a wide Cr# range (fig. 6.13 c). Chromites from the chromitiferous norite units display the widest range of values. Data from the chromitiferous pyroxenite units appear to form a steeper trend line (with lower Mg# values) compared to chromites analysed from the pyroxenite units (which also have higher Cr# values in addition to the higher Mg# values).

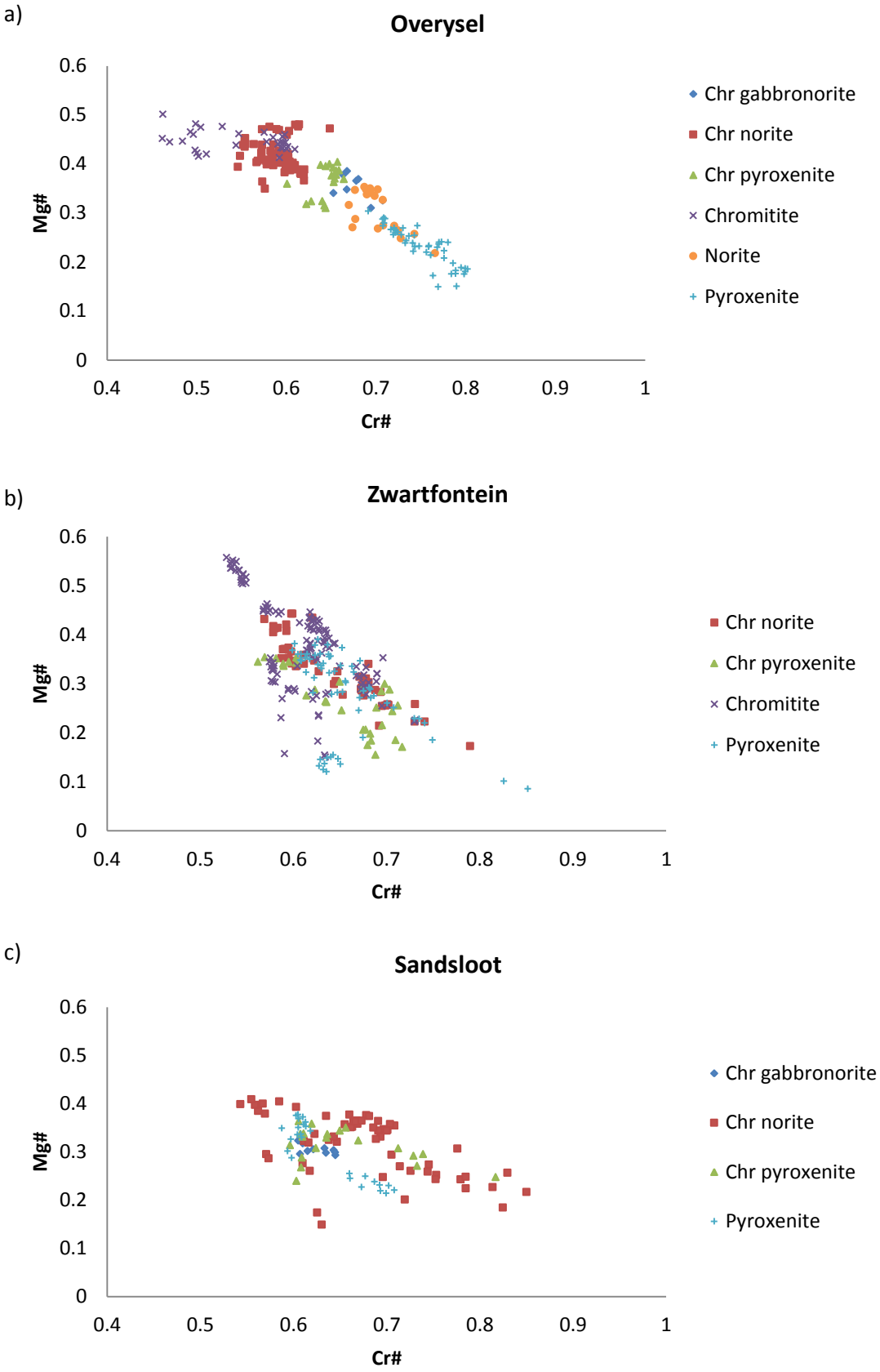


Figure 6.13. Geochemical plots showing Mg# vs. Cr# for chromite composition from different lithologies across 3 different Platreef farms from N-S (a) Overysel; (b) Zwartfontein; and (c) Sandsloot.

In figure 6.14, the data were regrouped according to host lithologies, to investigate any changes in chromitite composition along strike.

For chromite crystals analysed from the chromitiferous gabbronorite units (fig. 6.14 a), samples from Overysel display high Cr# and high Mg# values whereas those from Sandsloot have lower Cr# and Mg# values.

Chromite crystals from the chromitiferous norite units have the highest Mg# with low Cr# at Overysel. The samples from Sandsloot and Zwartfontein have a much wider range of Cr# and Mg#, with some of the Sandsloot data plotting on a steeper secondary trend line, showing low Cr# and Mg# (fig. 6.14 b).

Within the chromitiferous pyroxenite units, data from Overysel plot in the middle of the range displayed (low Cr# and high Mg#). Data from Sandsloot and Zwartfontein show a wide range of Cr#. Chromite crystals from Zwartfontein also have a wide range of Mg# values (fig. 6.14 c).

Crystals analysed from the chromitite units plot on two trend lines. Those from Overysel have high Mg# and low Cr#, whereas the Zwartfontein crystals have a wide range in both Mg# and Cr#. Some of the Zwartfontein crystals have both low Mg# and low Cr# (fig. 6.15 a).

Chromite crystals within norite units have only been recorded on Overysel and show moderate Mg# and Cr# when compared with chromite crystals from other lithologies (fig. 6.15 b).

Chromites from Overysel have the highest Cr# and lowest Mg# of the pyroxenites. The crystals analysed from Zwartfontein have the widest range of Cr# and Mg# values. A separate cluster can be seen on figure 6.14 c at lower Mg# values (and corresponding low Cr#) than the rest of the values. Chromite crystals from Sandsloot also plot as two separate groups, one with high Mg# and low Cr#, the other with moderate Cr# and moderate Mg# (fig. 6.15 c).

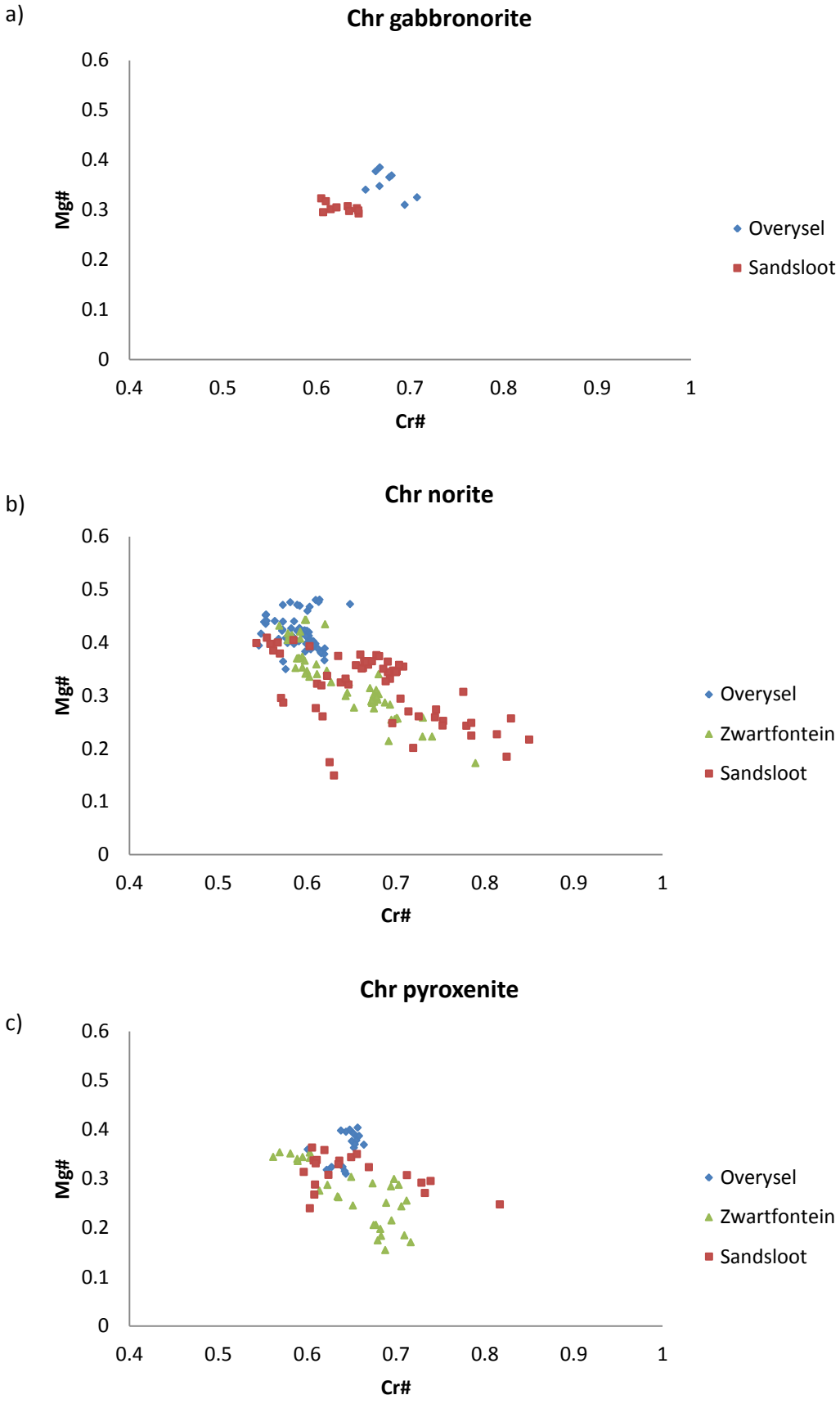


Figure 6.14. Geochemical plots showing the variation in Mg# vs. Cr# for (a) chromitiferous gabbronorite; (b) chromitiferous norite; and (c) chromitiferous pyroxenite for the three farms N-S.

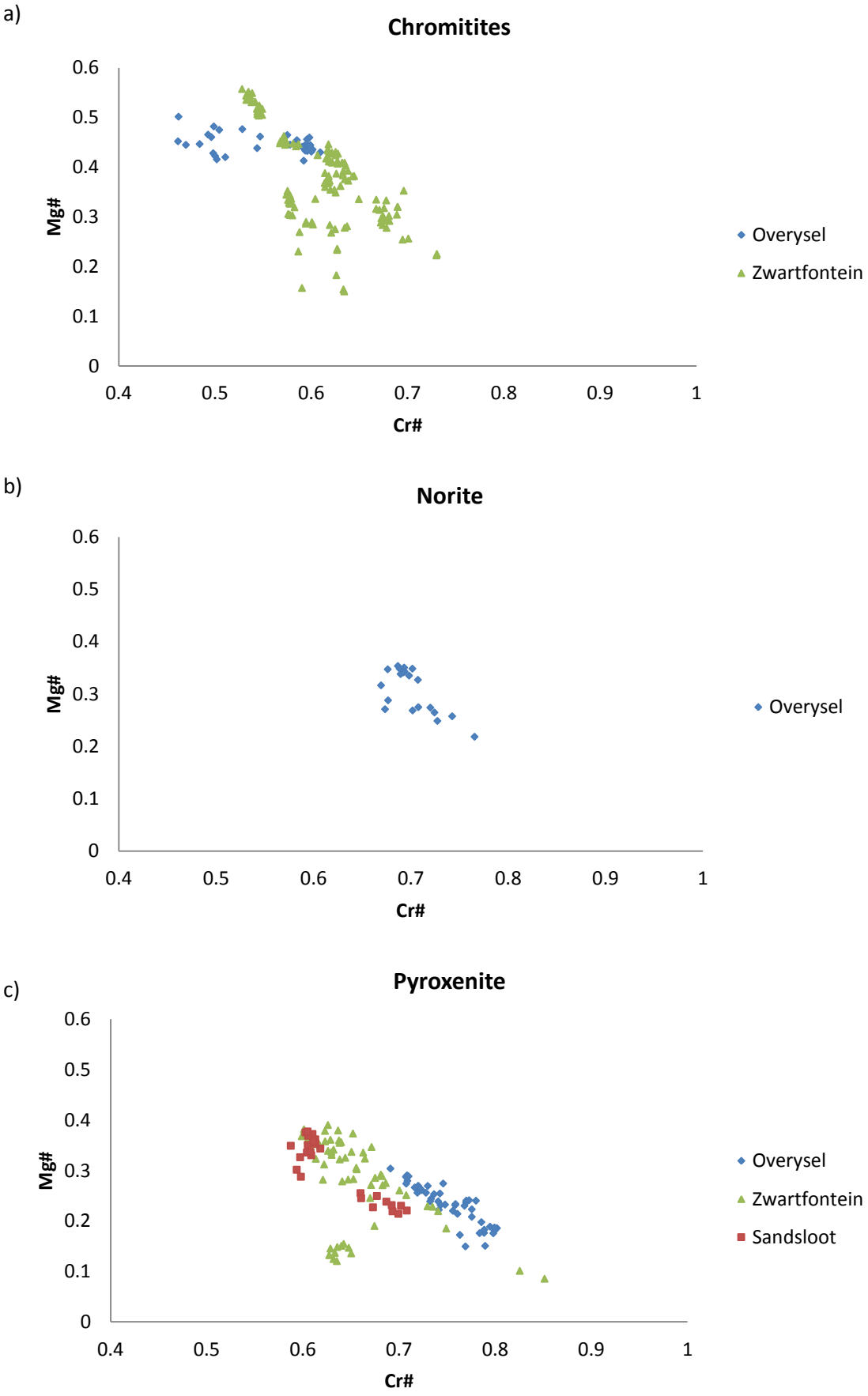


Figure 6.15. Geochemical plots showing the variation in Mg# vs. Cr# for (a) chromitites; (b) norite; and (c) pyroxenite for the three farms N-S.

### 6.6.2 Cr# vs. $Fe^{2+}$#

A strong positive correlation is shown in the Overysel data between Cr# and $Fe^{2+}$# (fig. 6.16 a). Chromites analysed from the chromitite lithology have the lowest $Fe^{2+}$#and Cr#, with the chromites analysed from the pyroxenite units having the highest values. Chromites from each lithology plot within a fairly restricted area along the trend line, apart from data from the two end members lithologies (chromitites and pyroxenites) which overlap with some of the other lithologies.

The data for Zwartfontein form a less well defined trend line (fig. 6.16 b) but the positive correlation is still evident. Overall, chromites from the chromitite units have lower $Fe^{2+}$# values than those measured on Overysel. The trend line for Zwartfontein has a shallower gradient than that produced from the Overysel data. Chromites analysed from all the lithologies on Zwartfontein plot along a wide range of $Fe^{2+}$# values and do not group as well as the Overysel chromites.

Sandsloot chromites plot within a narrower range of $Fe^{2+}$# than the chromites from the other two farms (fig. 6.16 c), although no massive chromitites are represented in this data set, which in the other two farms account for the low Cr# and low $Fe^{2+}$# values. As with the Zwartfontein data, all chromites analysed from the different lithologies plot across a range of $Fe^{2+}$# values rather than in distinct fields defined by lithology, as was seen in the Overysel data.

When the data are rearranged according to lithology, variations within the farms can be identified (figs. 6.17 & 6.18). Within the chromitiferous gabbronorite units, samples from Overysel have lower $Fe^{2+}$# and higher Cr# than the samples analysed from Sandsloot (fig. 6.17 a). The same is evident in the chromitiferous norite units, with a wider compositional range observed in the Sandsloot and Zwartfontein samples compared to Overysel data (fig. 6.17 b). Within the chromitiferous pyroxenite units, the Overysel samples plot at the lowest $Fe^{2+}$# and Cr# values whilst those from Sandsloot and Zwartfontein show increasing $Fe^{2+}$# values with varying Cr# values (fig. 6.17 c). Chromite samples within the chromitite units from Overysel have low Cr# and $Fe^{2+}$#, whereas those from Zwartfontein display a wide range of $Fe^{2+}$# values (fig. 6.18 a). Within the pyroxenite units, samples from Overysel have high $Fe^{2+}$# and Cr# values. Samples from Zwartfontein have a wide range of $Fe^{2+}$#, representing the highest and lowest values within this unit from all 3 farms. The samples from Sandsloot define two groups, with a low $Fe^{2+}$# and Cr# group and a moderate $Fe^{2+}$# and Cr# value group (fig. 6.18 c).

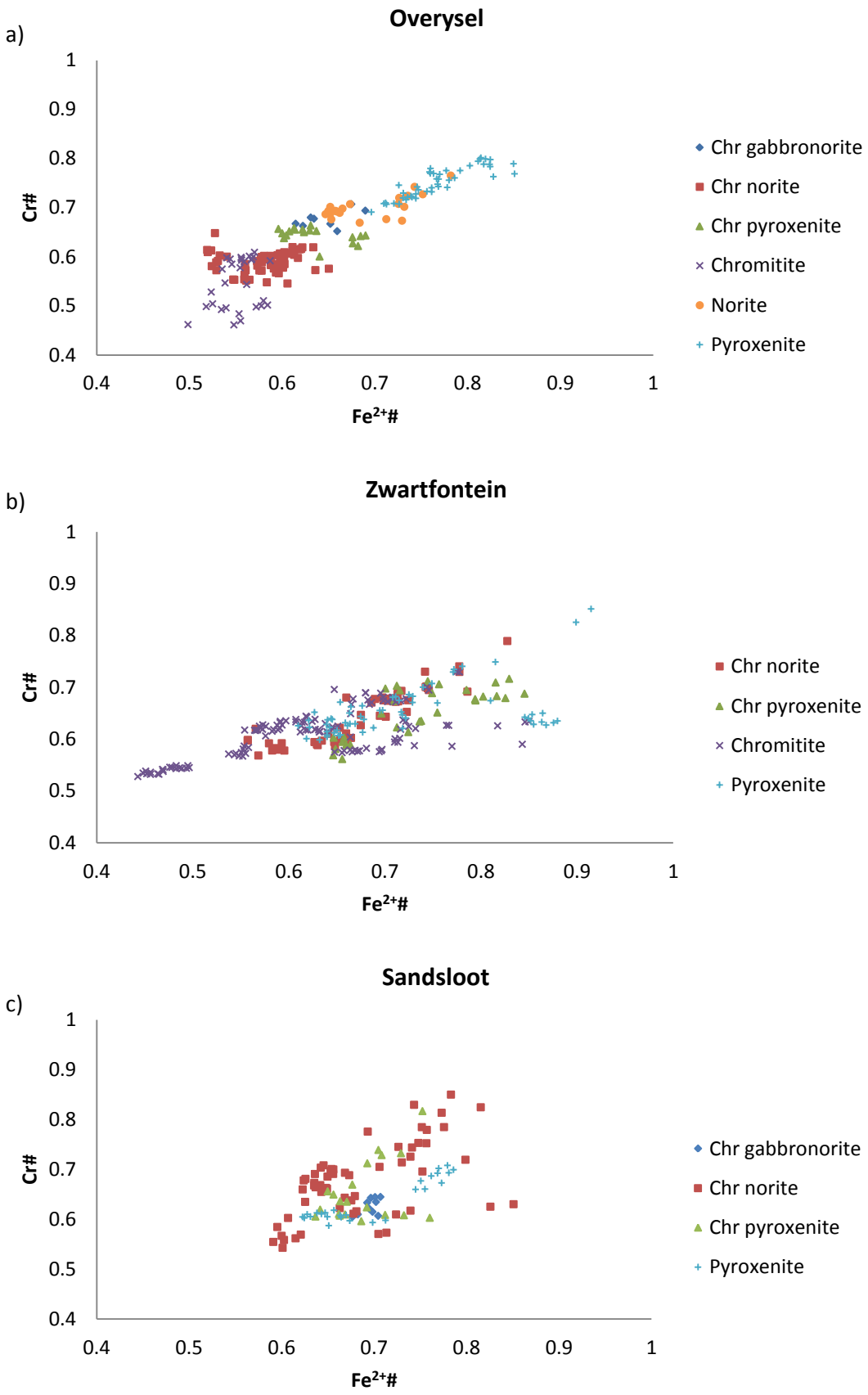


Figure 6.16. Geochemical plots of chromite composition from different lithologies across 3 different Platreef farms; (a) Overysel, (b) Zwartfontein, and (c) Sandsloot.

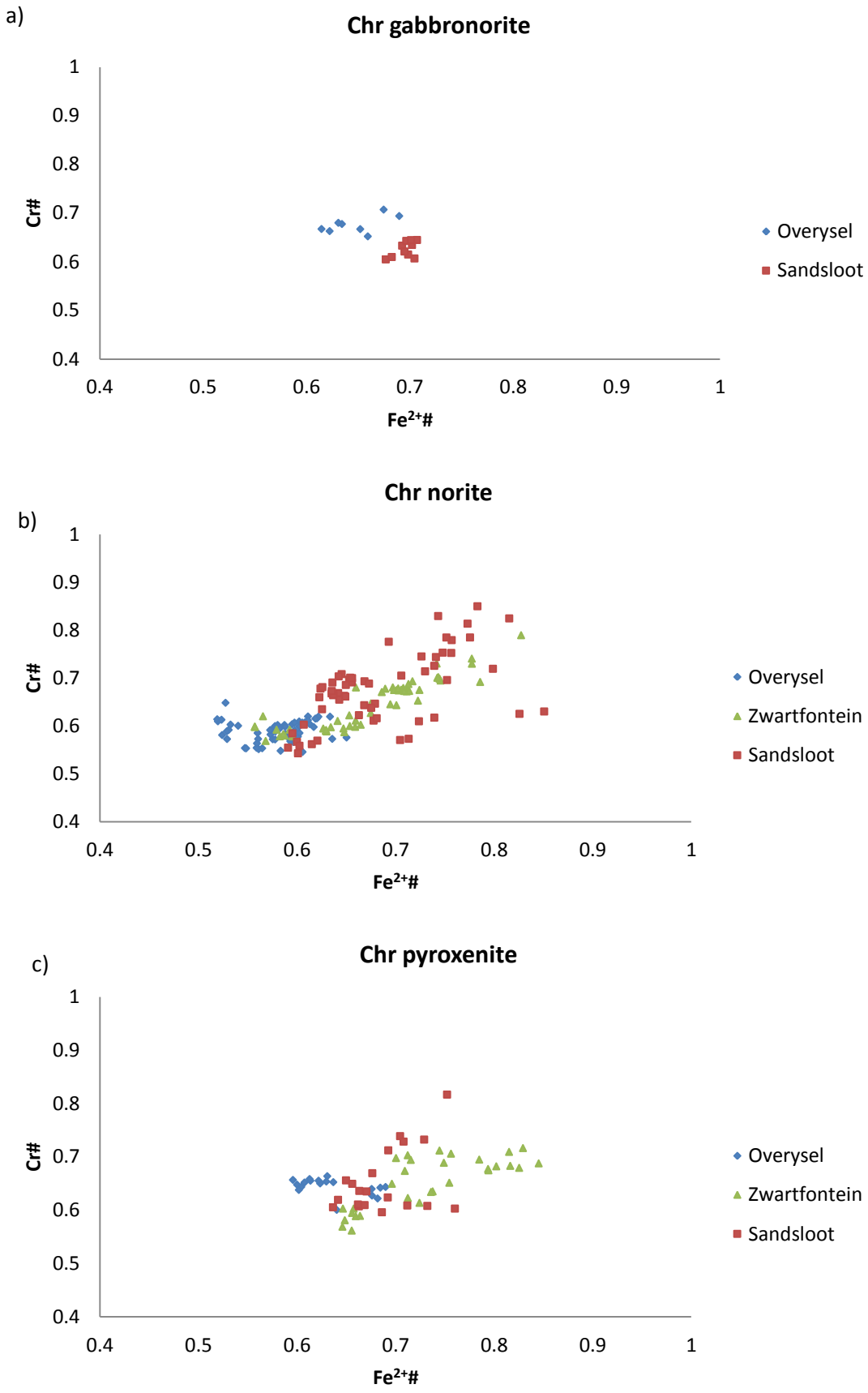


Figure 6.17. Geochemical plots showing the variation in Cr# vs. $Fe^{2+}$# for (a) chromitiferous gabbronorite; (b) chromitiferous norite; and (c) chromitiferous pyroxenite for the three farms N-S.

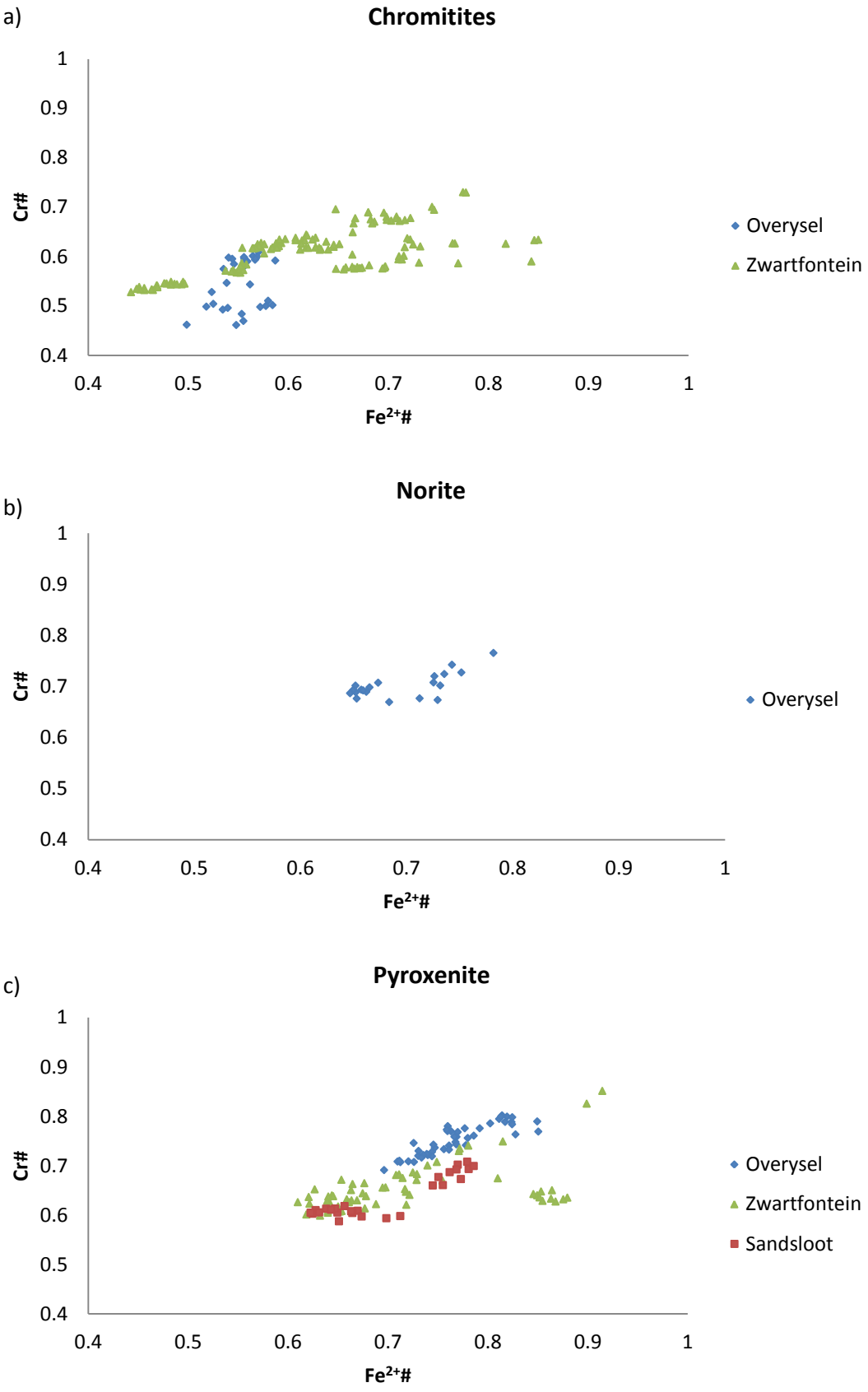


Figure 6.18. Geochemical plots showing the variation in Cr# vs. $Fe^{2+}$# for (a) chromitites; (b) norite; and (c) pyroxenite for the three farms N-S.

### 6.6.3 $Fe^{3+}$# vs. $Fe^{2+}$#

Chromites analysed from Overysel show a moderate positive correlation (fig. 6.20 a) between $Fe^{3+}$# and $Fe^{2+}$#. Samples from the chromitite and chromitiferous norite lithologies have the lowest $Fe^{2+}$# values, with those from the chromitite units having slightly higher $Fe^{3+}$# values.

Data for Zwartfontein (fig. 6.20 b) form a less well defined positive correlation compared to the data for Overysel. Chromites analysed from the chromitite units have very low $Fe^{2+}$# and $Fe^{3+}$# values but also exhibit a wide range of values. Some chromites analysed from the pyroxenite and chromitiferous norite units have low $Fe^{3+}$# values. Chromite crystals analysed from the chromitiferous pyroxenite units display high $Fe^{3+}$# and $Fe^{2+}$# values.

Chromite crystals from Sandsloot produce the steepest trend line when plotting $Fe^{2+}$# against $Fe^{3+}$# (fig. 6.20 c). Samples from the chromitiferous norite units show the widest range of values and show two trend lines, with one trend line being very flat (fig. 6.21 b). There does not appear to be any difference in the morphology of the chromite crystals that sit on the different trend lines, as shown by the textural pictures in Appendix 2, but as can be seen from figure 6.19, chromite crystals analysed from different samples plot on different trend lines. The two drillholes are located within 200 m of each other and have similar sulphide content and have both been altered significantly due to the proximity of the dolomite tongue. Samples from SS383 plot mostly on the steeper trend line (apart from sample 4A which plot midway between the two trend lines), whereas those from SS393 plot on the shallower trend line. Chromite crystals analysed from the chromitiferous pyroxenite and chromitiferous gabbronorite units have moderate $Fe^{2+}$# and $Fe^{3+}$# values.

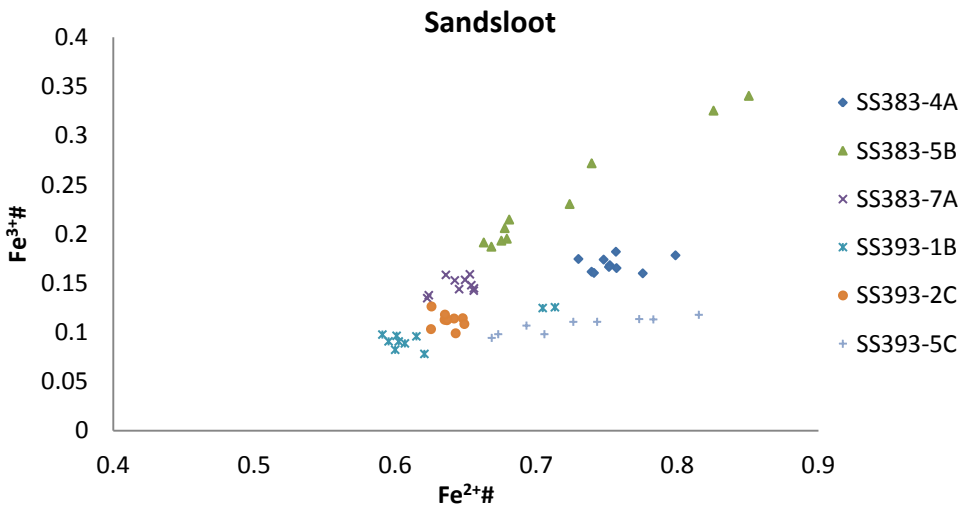


Figure 6.19. Analysis of chromite crystals from the chromitiferous norite units of Sandsloot samples showing the variation in $Fe^{3+}$# vs. $Fe^{2+}$# for depending on the sample number.

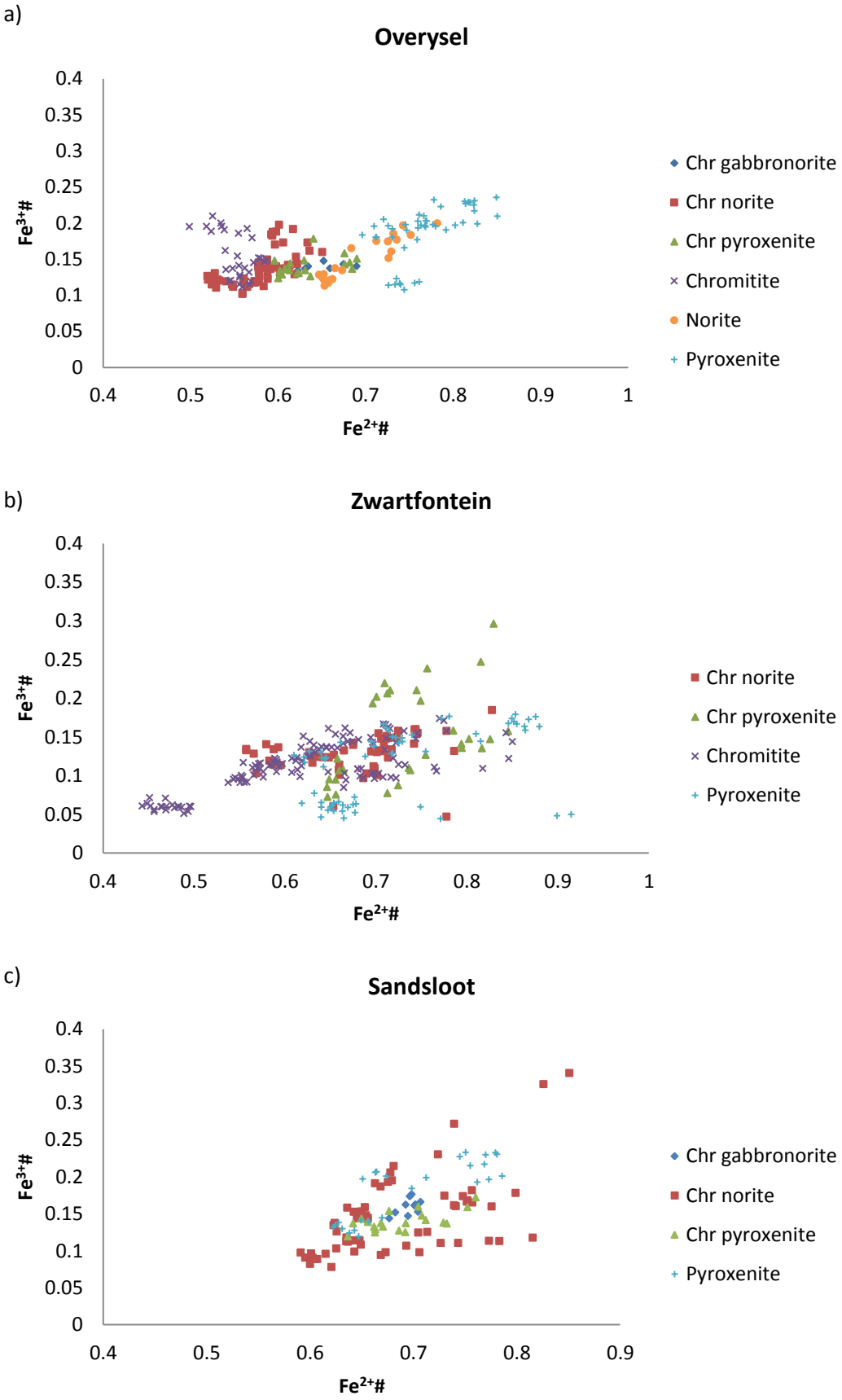


Figure 6.20. Geochemical plots of chromite composition for $Fe^{3+}$# vs. $Fe^{2+}$# from different lithologies across 3 different Platreef farms; (a) Overysel, (b) Zwartfontein and (c) Sandsloot.

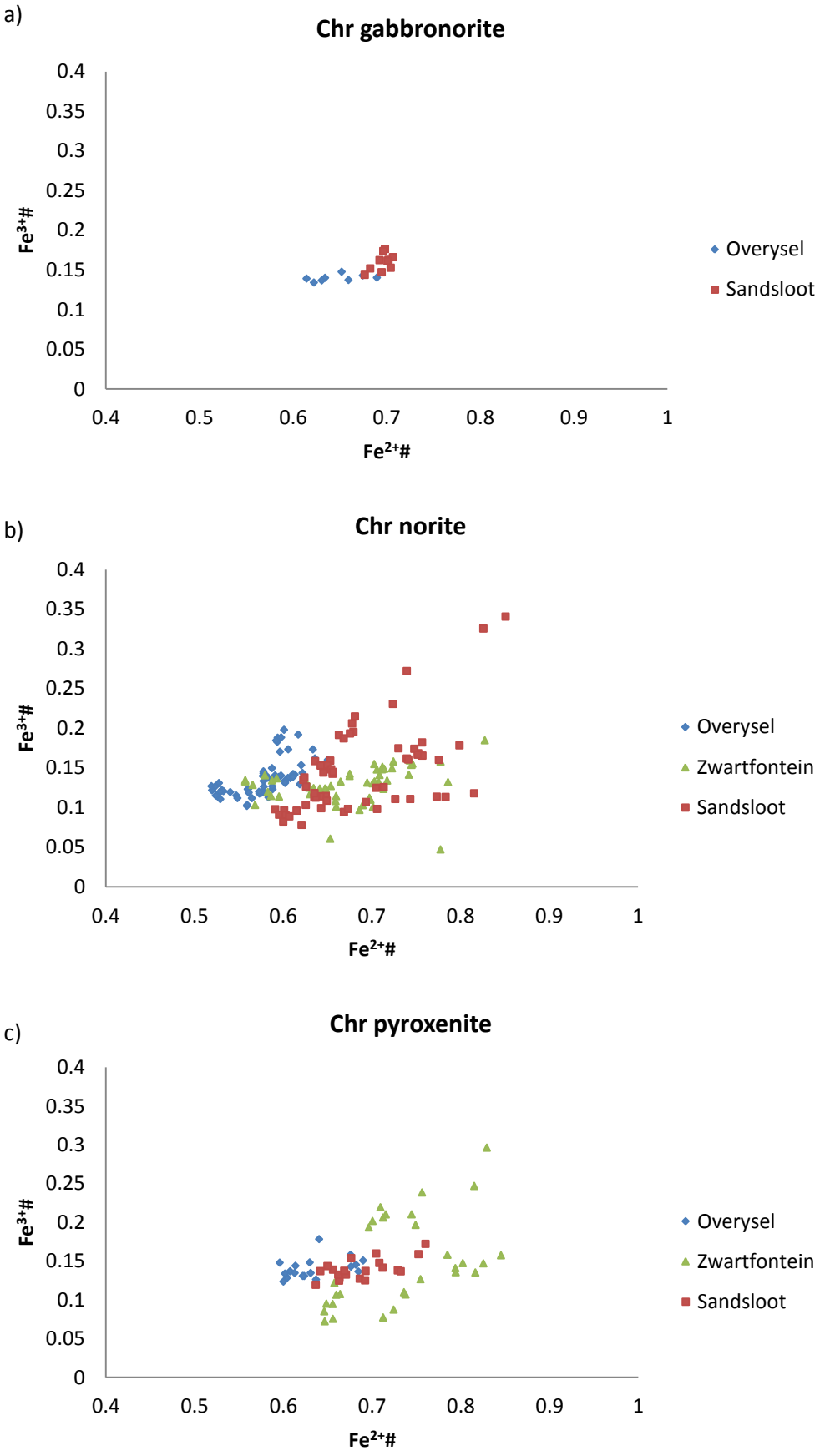


Figure 6.21. Geochemical plots showing the variation in $Fe^{3+}$# vs. $Fe^{2+}$# for (a) chromitiferous gabbronorite; (b) chromitiferous norite; and (c) chromitiferous pyroxenite for the three farms N-S.

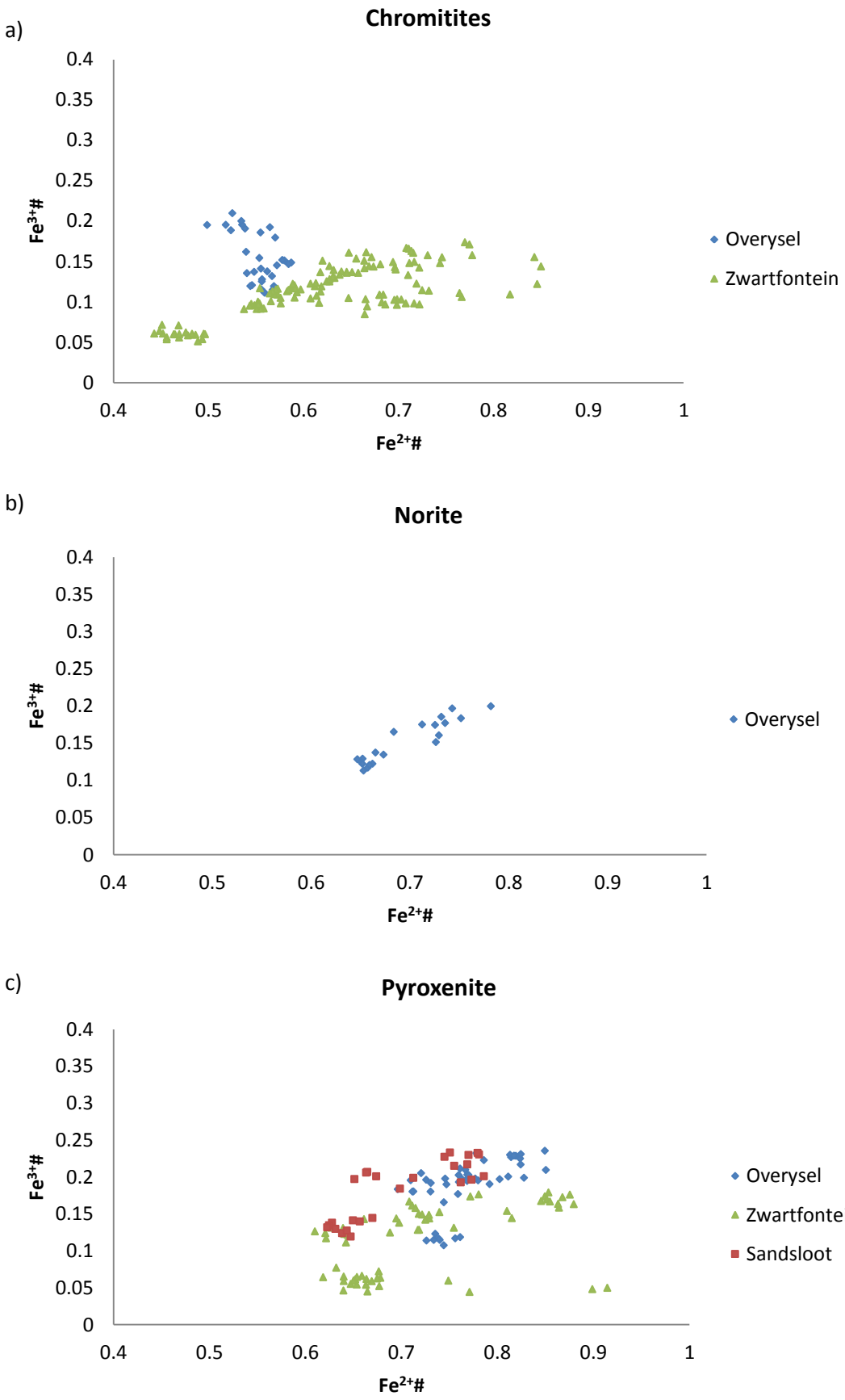


Figure 6.22. Geochemical plots showing the variation in $Fe^{3+}$# vs. $Fe^{2+}$# for (a) chromitites; (b) norite; and (c) pyroxenite for the three farms N-S.

Within the chromitiferous gabbronorite units, samples from Overysel have lower $Fe^{2+}$# and $Fe^{3+}$# compared to those from Sandsloot (fig. 6.21 a). Chromite crystals analysed from the chromitiferous norite units also exhibit a similar relationship, with those from Overysel having the lowest values. Samples from Sandsloot plot potentially on two trend lines as mentioned above. Data from Zwartfontein and Overysel plot on the flatter trend line which has a limited $Fe^{3+}$# range but a large $Fe^{2+}$# range (fig. 6.21 b). Within the chromitiferous pyroxenite units, samples from Overysel and Sandsloot have a limited $Fe^{3+}$# range, whereas the samples from Zwartfontein display a large range in both $Fe^{3+}$# and $Fe^{2+}$#. This produces 3 different trend lines. The data from Overysel and Sandsloot form one trend line, whereas some of the Zwartfontein data produce two steeper trend lines, one at higher $Fe^{2+}$# values than the other (fig. 6.21 c). Chromite crystals from the chromitite units on Overysel plot in a group at low $Fe^{2+}$# whereas those from Zwartfontein plot across a wider range of $Fe^{2+}$# values. Within the samples from Zwartfontein, a number of chromites plot as a group at very low $Fe^{2+}$# and $Fe^{3+}$# values. Overall, the Zwartfontein samples have a limited range of values for $Fe^{3+}$# resulting in a flat low gradient trend line (fig. 6.22 a). The chromites from the norite units plot at moderate $Fe^{2+}$#, $Fe^{3+}$# values in comparison to the other lithologies (fig.6.22 b). Chromite crystals from the pyroxenite units show no clear correlation. Samples from Zwartfontein have the largest range of values, with some sample plotting at low $Fe^{3+}$# values but at varying $Fe^{2+}$# values (fig. 6.22 c).

### 6.6.4 $Fe^{3+}$# vs. $TiO_2$

As with the other sections above, chromites analysed from Overysel show a moderate positive correlation (fig. 6.23 a) between $Fe^{3+}$# and $TiO_2$. Data obtained from the chromitiferous norite lithology plot as the lowest $Fe^{3+}$# and $TiO_2$, with data obtained from the pyroxenite units plotting as the highest values (figs. 6.23 & 6.24). Data from the chromitiferous pyroxenite are grouped together at low-moderate $TiO_2$ and $Fe^{3+}$# values. Data from all other lithologies span the range of values for both $TiO_2$ and $Fe^{3+}$#.

A slightly less well defined positive correlation is produced by the data from Zwartfontein (fig. 6.23 b). None of the lithologies contain well constrained data points. Some data points from the chromitite units have very low $TiO_2$ values (around 0.5 wt%). In addition, data points from the chromitiferous pyroxenite plot with high $Fe^{3+}$# values, away from the remainder of the data points.

Chromite crystals from Sandsloot produce two trend lines when plotting $TiO_2$ (wt%) against $Fe^{3+}$# (fig. 6.23 c). The first line contains data from the pyroxenitic units and the second contains data from the chromitiferous norite units. The first trend line has a similar gradient to those observed for Overysel and Zwartfontein, while the second trend line is very flat, with a wide range of $Fe^{3+}$# values for a limited range of $TiO_2$ values. Data obtained from the chromitiferous pyroxenite and chromitiferous gabbronorite plot at low $TiO_2$ and $Fe^{3+}$# values.

Within the chromitiferous gabbronorite units, samples from Overysel have lower $Fe^{3+}$# and $TiO_2$ values compared to those from Sandsloot (fig. 6.24 a). Chromite crystals analysed from the chromitiferous norite show that those from Overysel have lower $TiO_2$ values compared to other farms at the same $Fe^{3+}$# values (fig. 6.24 b). Some chromites from Sandsloot show much higher $Fe^{3+}$# values than the other farms. Chromites analysed in the chromitiferous pyroxenite units from Zwartfontein have a wide range of $Fe^{3+}$# values compared to those from Overysel and Sandsloot, although those from Sandsloot have a wider $TiO_2$ range than Overysel (fig. 6.24 c). Within the chromitite units, chromites from Overysel have lower $Fe^{3+}$# and $TiO_2$ than those from Overysel. Data from chromites from Zwartfontein plot along a steeper trend line than those from Overysel which show a range of $Fe^{3+}$# values for a constricted $TiO_2$ range (fig. 6.25 a). Within the pyroxenite units, data from Zwartfontein has the lowest $TiO_2$ and $Fe^{3+}$# values, with those from Overysel and Sandsloot having higher values (fig. 6.25 c). There is a group of Sandsloot and Overysel data that sits at lower $Fe^{3+}$# values than the rest of the data set.

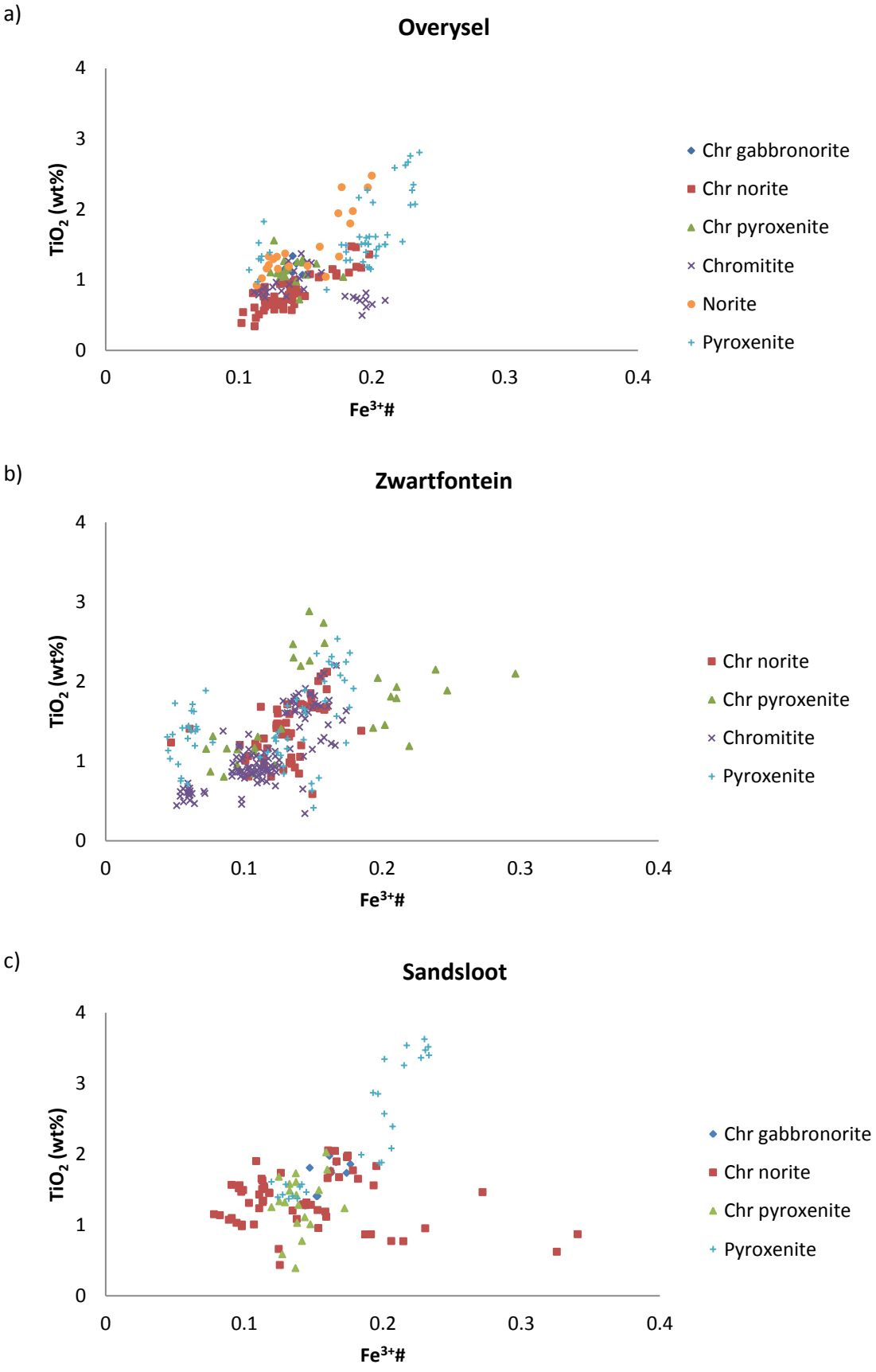


Figure 6.23. Geochemical plots of chromite composition from different lithologies across 3 different Platreef farms; (a) Overysel, (b) Zwartfontein and (c) Sandsloot.

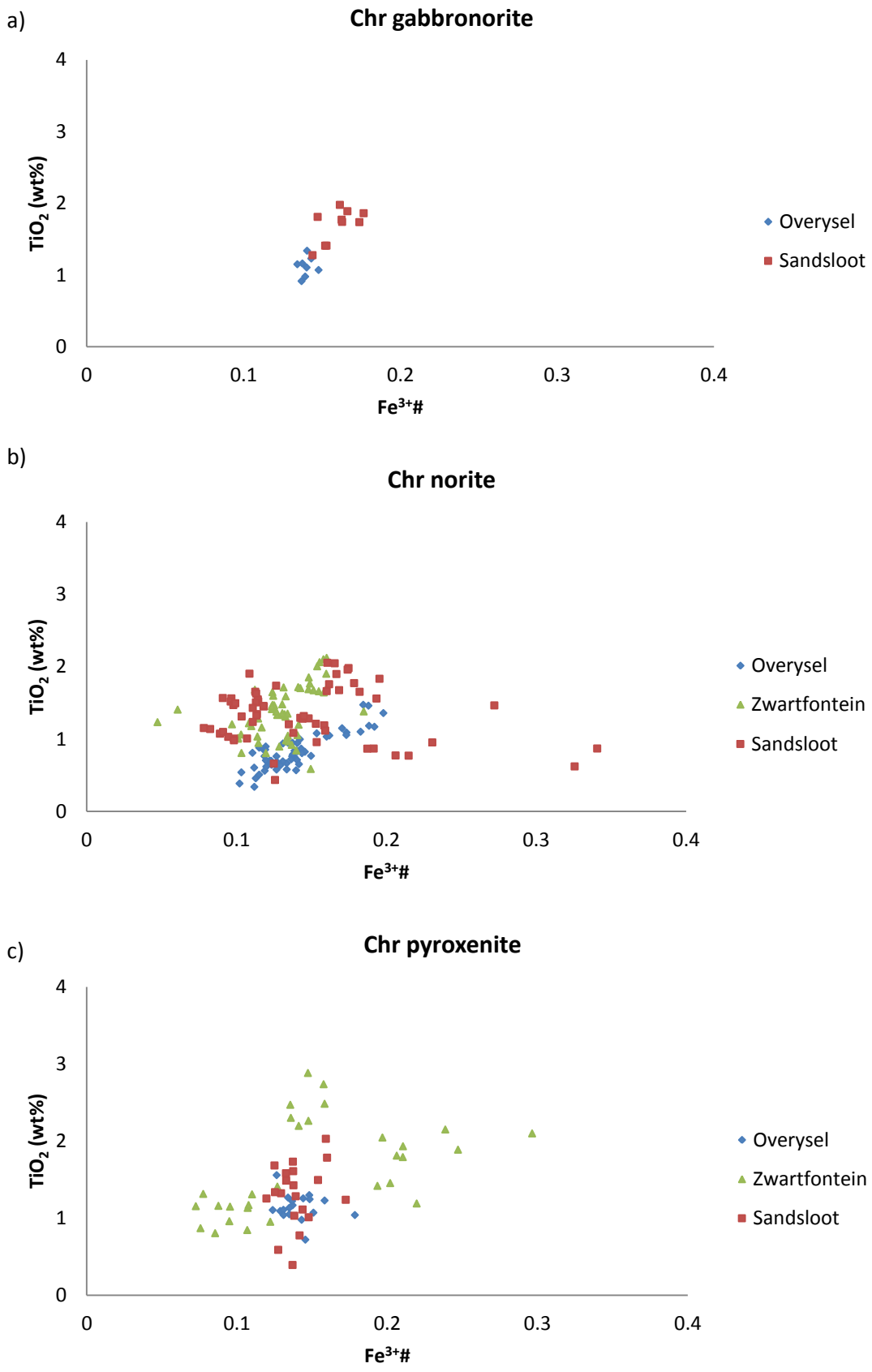


Figure 6.24. Geochemical plots showing the variation in $TiO_2$ vs. $Fe^{3+}$# for (a) chromitiferous gabbronorite; (b) chromitiferous norite; and (c) chromitiferous pyroxenite for the three farms N-S.

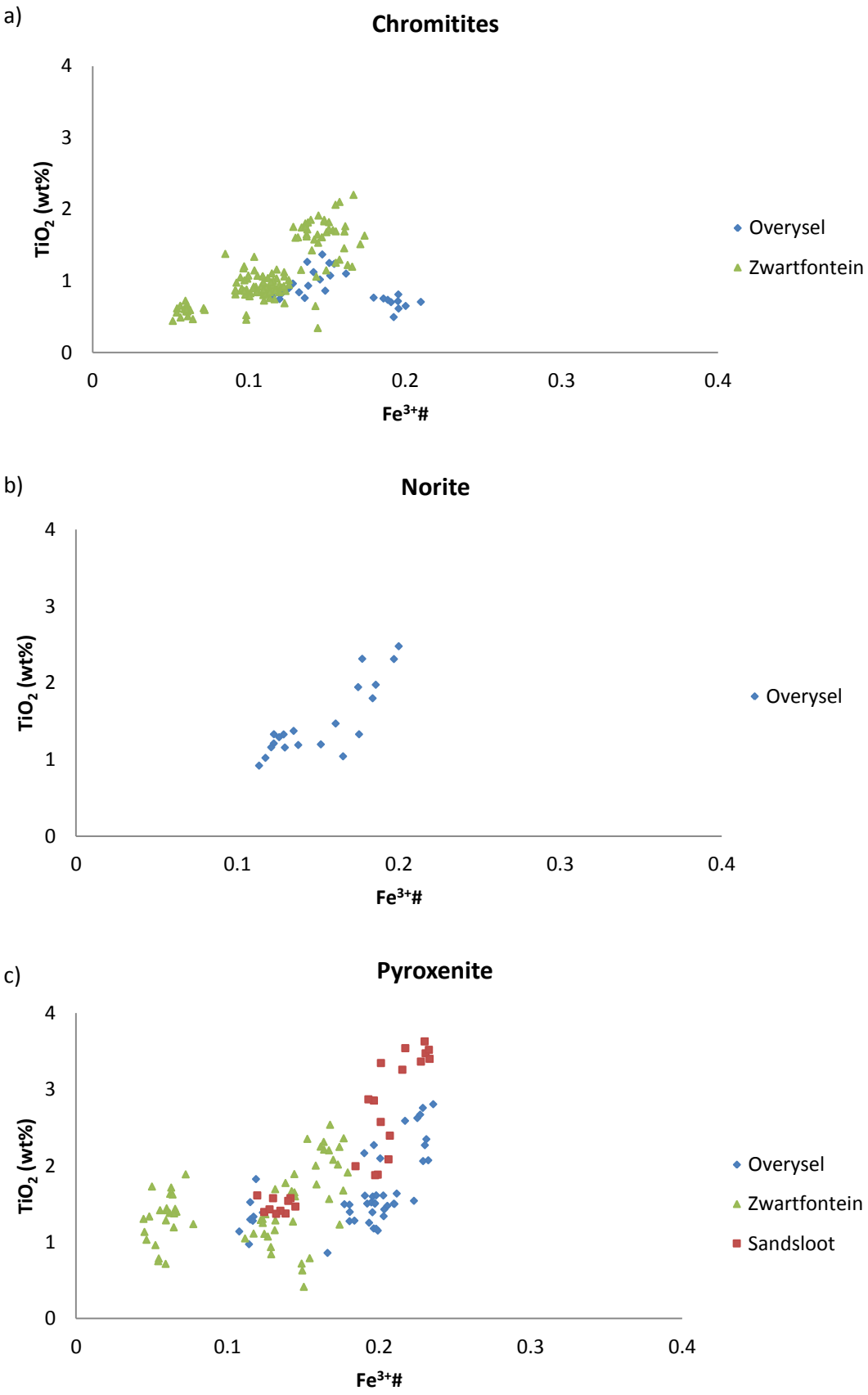


Figure 6.25. Geochemical plots showing the variation in $TiO_2$ vs. $Fe^{3+}$# for (a) chromitites; (b) norite; and (c) pyroxenite for the three farms N-S.

### 6.6.5 Examination of Platreef data

Examining chromite composition grouped by lithology and by farm has shown that variation in composition can be attributed to both the host lithology and to the known or likely country rock lithology on the different farms.

It has been shown above, specifically using the $Fe^{3+}$# vs. $Fe^{2+}$# plots (fig. 6.21) for the chromitiferous norite and chromitiferous pyroxenite units, that multiple trend lines can be produced by the data set. A steeper trend line on a $Fe^{3+}$# vs. $Fe^{2+}$# plot suggests that the chromite crystals are more oxidised than those on the flatter trend line.

It is not clear when examining the chromite composition data on the $Fe^{3+}$# vs. $Fe^{2+}$# plots which of the trend lines is primary. If the primary signature is the oxidised steeper one, then local reduction must be occurring to produce the data that sit on the more reduced trend line. In order to form the reduction signature, $Fe_2O_3$ was converted to FeO by reaction with $H_2$ or CO. Reaction with the dolomite as the Platreef intruded caused the release of $CO_2$ from the carbonate and the formation of diopside and olivine in the more siliceous portions of the dolomite. Later fluids extensively serpentinised many of the carbonate xenoliths as seen in the core, especially in those samples that are most affected. The release of $H_2$ from the reaction that altered the carbonate minerals into serpentine is likely to also have caused reduction locally.

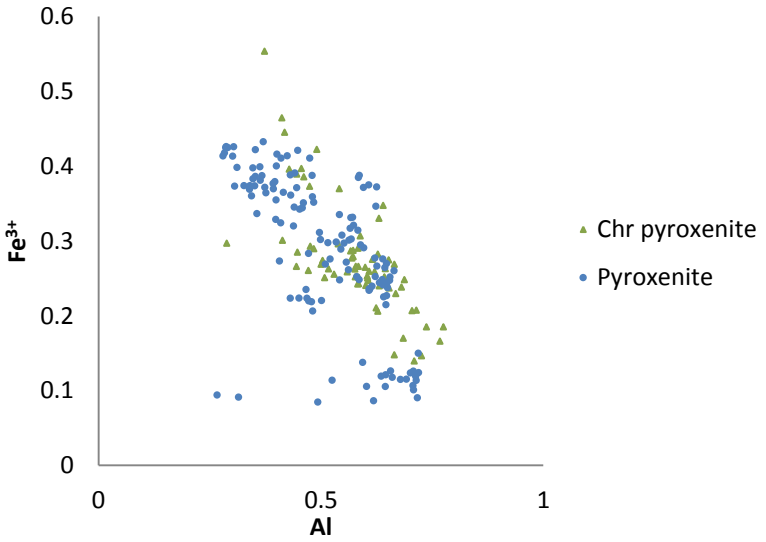


Figure 6.26. $Fe^{3+}$ vs. Al cations for the chromitiferous pyroxenite and pyroxenite units.

Alternatively, the original signature within the chromite crystals could be the reduced (less steep) trend line with some of the samples having been oxidised. The direct correlation between $Fe^{3+}$ and Al in the pyroxenite samples (fig. 6.26) indicates that Al can substitute for

$Fe^{3+}$ in the Y site in the chromite structure. In the chromitiferous norite units, there is the potential for increased $Fe^{3+}$ within the crystal where Al has been removed by interaction with plagioclase feldspar surrounding it. However, in the pyroxenitic units there is limited plagioclase, which results in a shallower trend line i.e. the original trend line is the more reduced line.

The relationship between the chromite and the surrounding silicates was documented by Irvine (1977), who proposed that in addition to Al transfer from chromite to plagioclase, there is Cr transfer between chromite and pyroxene during crystallisation. In order to investigate fully the variation in chromite composition across the study area, it is beneficial to study the chromitite units, which would show limited post-crystallisation re-equilibration due to the minor occurrence of silicates. As previously mentioned, the chromites with the highest Cr and Mg content probably represent the least altered and closest to the primary composition. Those from Overysel fit in this category, with the samples from Zwartfontein showing decreasing Cr and Mg contents suggesting that their compositions have been increasingly altered. However, with the absence of any chromitite unit samples from Sandsloot, the idea that this might reflect a progressive alteration southwards cannot be fully tested. The effect of post-cumulus re-equilibration on chromite composition has been studied elsewhere in the Bushveld Complex where it was found to have a negligible effect on chromite composition in massive chromites (Cameron 1975; Cameron 1977; Eales and Reynolds 1986; Hatton and von Gruenewaldt 1987). However, the samples labelled chromitites in this study were grouped as such if the chromite content exceeded 15 wt% compared to the chromitites of the rest of the Bushveld which exceed 50 wt%. As such, many of the chromitite samples in this study will have significantly more silicates than true chromitites found elsewhere in the Bushveld.

As discussed previously, the Platreef is considered to represent a series of sills, with the input of magma proposed to have been fed by a series of feeder zones to the west of the study area. This study has shown that the feeder zone was unlikely to be in the south of the study area as the effect of the country rock has clearly had an influence on the chromite composition when in contact with the sediments of the Malmani formation. Instead, it is suggested that the source for the feeder is to the west of Zwartfontein or Overysel, leading to the more primary signatures observed for the chromites on Overysel.

## 6.7 Comparison to other Platreef data

A number of studies have described the nature of chromite in the Platreef, but only a few have carried out studies on the mineral chemistry (e.g. Holwell and McDonald 2006; Wela 2008; Yudovskaya and Kinnaird 2010). This section compares the major element data set of the Platreef chromite chemistry to that produced above.

The Platreef data of Yudovskaya and Kinnaird (2010) were collected from 18 drillholes that have been drilled along 20 km of strike from Overysel to Macalacaskop (fig. 3.1). According to Yudovskaya and Kinnaird (2010), the chromites can be grouped into an Upper Chromitite Zone (UCR) and a Lower Chromitite Zone (LCZ). These zones have been defined depending on the relative location relative to the top and bottom contacts of the Platreef. The zones can be distinguished by host rock petrography and chromite morphology, with the LCR chromites being smaller and more euhedral. Yudovskaya and Kinnaird (2010) found no difference in chromite composition between the LCR and UCR along strike. Any differences found were between chromites hosted by different lithologies containing different mixtures of silicate minerals.

The data of Holwell and McDonald (2006) were obtained from two drillholes on Overysel (OY335 and OY387). Holwell and McDonald (2006) observed the chromitites as small angular xenoliths within the feldspathic pyroxenites but not as layers or stringers. They analysed chromite crystals from the chromitite zones and xenoliths and disseminated crystals within the feldspathic pyroxenite units. Some samples were also analysed from the Lower Zone pyroxenite units in the footwall of one of the drillholes, although these have not been included in order to allow a direct comparison to the data generated in this study.

The trivalent ion plots (fig.6.27) show the variation in chromite chemistry between the data from the Yudovskaya and Kinnaird (2010) study, the Holwell and McDonald (2006) study and data produced in this study. The chromites from this study have a slightly wider range of values of Al and Cr compared to the other two studies. The Holwell and McDonald data set does have low Al values but at lower Cr values than the data produced in this study.

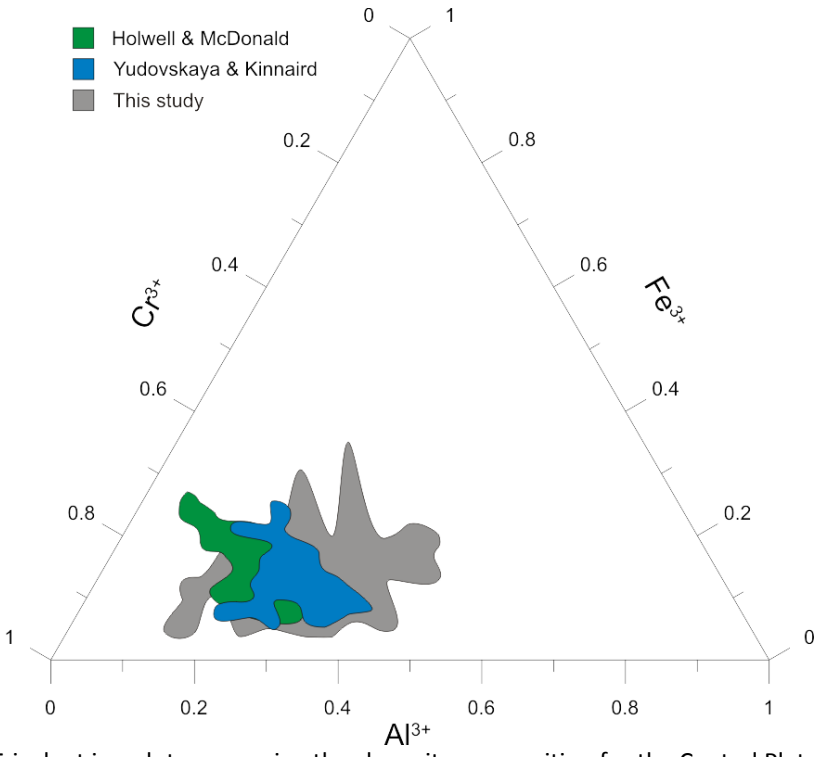


Figure 6.27. Trivalent ion plots comparing the chromite composition for the Central Platreef from the Yudovskaya and Kinnaird study (2010), Holwell and McDonald (2006) study and the data from this study.

### 6.7.1 Cr# vs. Mg#

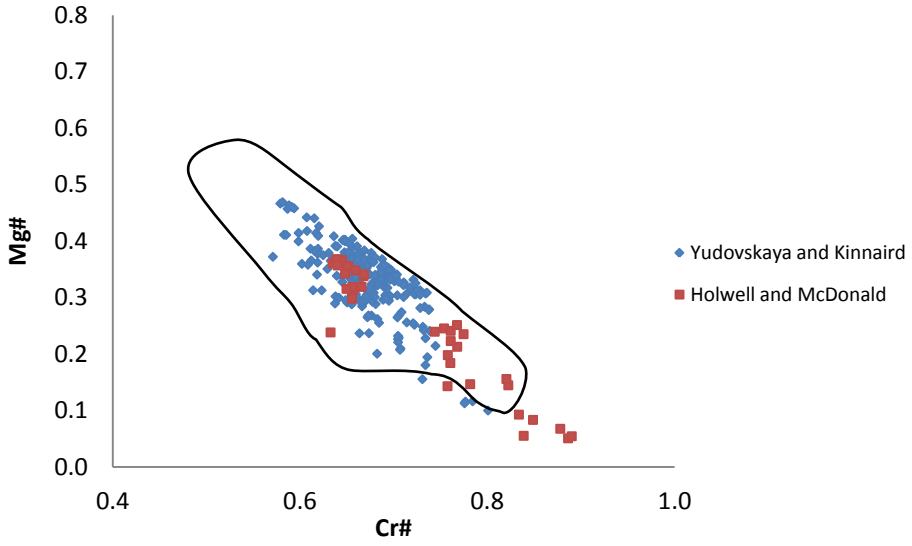


Figure 6.28. Geochemical plots of chromite composition for Mg# vs. Cr# for the Yudovskaya and Kinnaird (2010) data set and the Holwell and McDonald (2006) data set with the black outline showing data from this study.

The Platreef data of Yudovskaya and Kinnaird (2010) mostly plot within the range obtained for this study (fig. 6.28). Some of the data from this study plot at higher Mg# and lower Cr# than those obtained by Yudovskaya and Kinnaird (2010). The data from Holwell and McDonald (2006) also mostly plot within the range obtained for this study. There are

however a number of analyses, at the higher range of Cr# around 0.8-0.9, plot at very low Mg# (less than 0.1). There are two groups in the Holwell and McDonald data, those at moderate Mg# and Cr# which correspond to the chromites analysed from the chromitite xenoliths. The other group that have lower Mg# and higher Cr# correspond to the disseminated chromites within the feldspathic pyroxenite units (fig. 6.29), although both groups lie on the same trend line. The lower Mg# in the chromites in the feldspathic pyroxenite has been attributed to the exchange reactions with the surrounding silicates (Holwell and McDonald 2006).

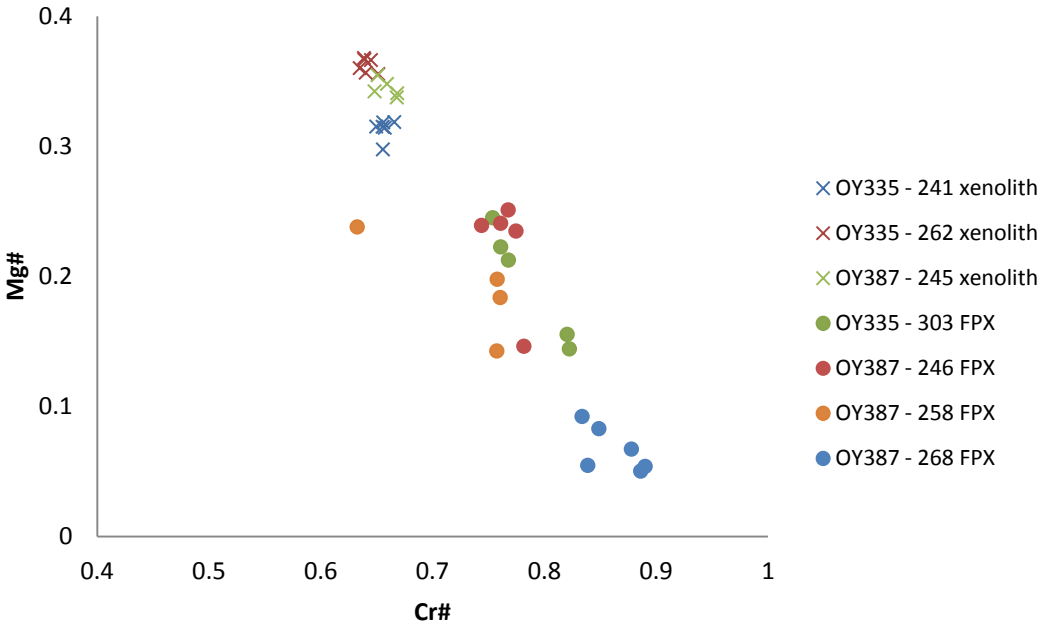


Figure 6.29. Chromite crystal composition from Overysel (Holwell and McDonald 2006) showing the two groups of data, one for the chromite xenoliths, the other for feldspathic pyroxenite (FPX) units.

### 6.7.2 Cr# vs. $Fe^{2+}$#

All but one of the analyses from the Yudovskaya and Kinnaird (2010) study plot within the range of the data obtained in this study (fig. 6.30). The data from Holwell and McDonald (2006) also mostly plot within the range obtained in this study but some of the chromites analysed from the feldspathic pyroxenite units plot at a higher Cr# and $Fe^{2+}$# than the remainder of the data.

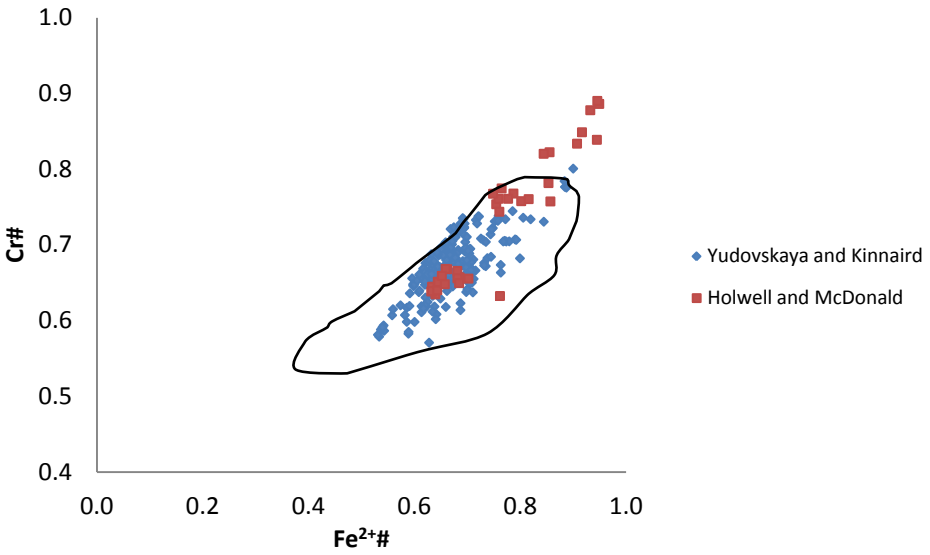


Figure 6.30. Geochemical plots of chromite composition for the Yudovskaya and Kinnaird (2010) and Holwell and McDonald (2006) for Cr# vs. $Fe^{2+}$# from Platreef, with the black outline representing the data from this study.

### 6.7.3 $Fe^{3+}$# vs. $Fe^{2+}$#

Both Platreef data sets show similar trend lines with increasing $Fe^{3+}$# at increasing $Fe^{2+}$# and mostly plot within the range obtained by the samples in this study (as shown by the outline in fig. 6.31). Some analyses from Yudovskaya and Kinnaird (2010) plot at higher $Fe^{2+}$# values than those obtained in this study. Similarly, a number of analyses from the Holwell and McDonald (2006) plot at higher $Fe^{2+}$# values but also at higher $Fe^{3+}$# values than those from the Yudovskaya and Kinnaird data set.

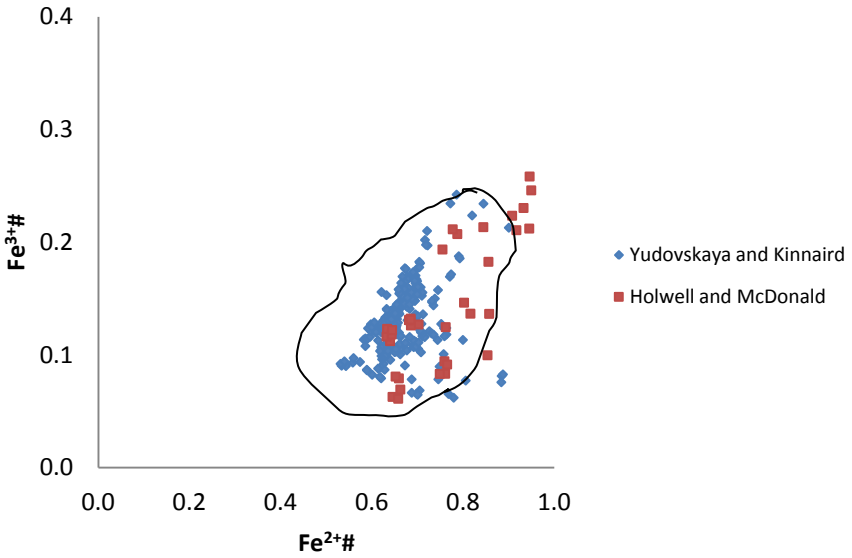


Figure 6.31. Geochemical plots of chromite composition for $Fe^{3+}$# vs. $Fe^{2+}$# from Platreef (Holwell and McDonald 2006; Yudovskaya and Kinnaird 2010) with the black outline representing the data from this study.

### 6.7.4 $Fe^{3+}$# vs. $TiO_2$

All Platreef data sets plot at a similar position on a $TiO_2$ vs. $Fe^{3+}$# graph (fig. 6.32). A few data points from this study have higher $Fe^{3+}$# than the data set from Holwell and McDonald (2006), but overall both data sets plot within the same region. Plotting $Fe^{3+}$# against $TiO_2$ has shown that a significant number of the chromite crystals analysed by Yudovskaya and Kinnaird (2010) plot at higher $TiO_2$ values than those obtained in this study. The bulk of the data also plot at a lower $Fe^{3+}$#, producing a steeper trend line than the one produced using the data from this study. The data from Holwell and McDonald (2006) plot mostly within the range obtained by the data from this study but their data plot on a shallower trend line, produced from a more constricted range of $TiO_2$ for corresponding $Fe^{3+}$# range.

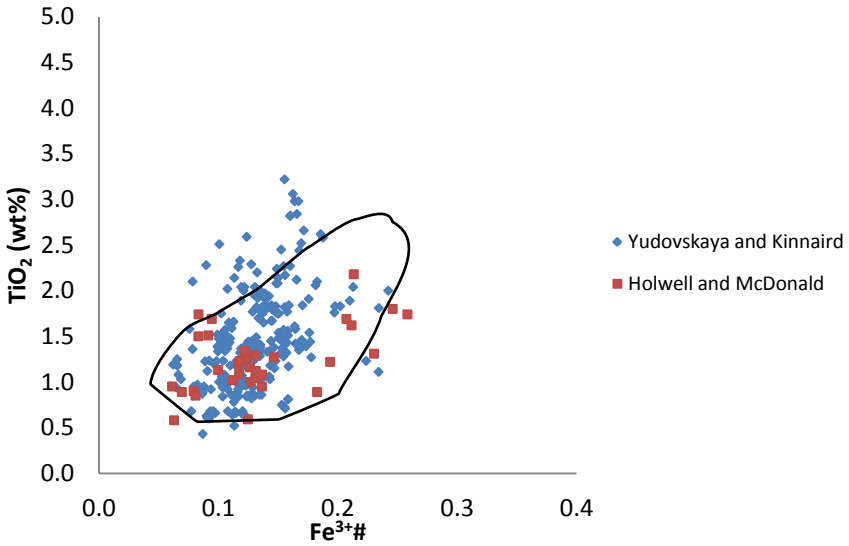


Figure 6.32. Geochemical plots of chromite composition for $TiO_2$ vs. $Fe^{3+}$# from the Platreef (Holwell and McDonald 2006; Yudovskaya and Kinnaird 2010) with black outline representing the data from this study.

The relatively high $TiO_2$ contents in the Yudovskaya and Kinnaird data set has been attributed to contact metamorphism (Yudovskaya and Kinnaird 2010), although no source for the Ti was given. The footwall lithology in their study area was mostly dolomite. Since the $TiO_2$ content of serpentinite xenoliths contained in the Platreef is around 0.01 % $TiO_2$ (McDonald et al. 2005) it is therefore difficult to see how this could have provided the Ti. As a result, an alternative explanation for the elevated $TiO_2$ that characterises much of the chromite in the Platreef must be presented.

## 6.8 Comparison of Platreef data to other Bushveld data

Whilst the data set obtained in this study has been compared to other chromite data from the Platreef, it is important to also compare the data to the wider Bushveld, to answer the question, 'Are Platreef chromites directly comparable to the chromites of the Upper Critical Zone?'

In order for this to be achieved, the Platreef data are compared to data sets for the Merensky Reef (Li et al. 2005) and the UG2 (Mathez and Mey 2005), both part of the Upper Critical Zone, in addition to the chromites analysed by Eales and Reynolds (1986) from an UCZ section. The Platreef data are also compared to the Lower Zone and 'Critical Zone' of the northern limb (Hulbert 1983).

The Merensky chromite samples analysed by Li et al. (2005) are from the farm Vlakfontein of the Impala Platinum mine in the western limb of the Bushveld Complex. The basal chromitite seam sampled is around 3 cm in thickness (the upper seam is absent on Vlakfontein) and contains ~70 % chromite, ~15 % plagioclase and 10 % orthopyroxene.

The UG2 chromite dataset is based on samples from the Middelpunt mine in the northeast of the Bushveld Complex. The sampled UG2 chromitite is a massive, 70 cm thick layer composed of 75 to 90 % chromite with plagioclase as the dominant interstitial mineral (Mathez and Mey 2005).

The UCZ data are from a 80 m section from the Union mine in the western limb of the Bushveld Complex containing (from the top downwards) the Bastard unit, Merensky unit, Merensky footwall unit (including the Pseudoreef marker), Pseudoreef unit, UG-2 unit and UG-1 units (Eales and Reynolds 1986). Due to the wide range of units covered, a black dotted outline of the UCZ data will be used in subsequent graphs in order to compare with more specific data from other authors.

The Lower Zone chromite data are from drillholes drilled on the farm Grasvally where Lower Zone rocks of the northern limb that include two chromitite seams are exposed along the western margin of the Grasvally Fault (De Klerk 2005; van der Merwe 2008).

In addition to the Lower Zone chromite data of Hulbert (1983), a number of analyses on the 'Critical Zone' from the same area in the northern limb were added to the data set for comparison. The 'Critical Zone' chromitite units come from the Grasvally Norite-Pyroxenite-Anorthosite (GNPA) member as defined by Hulbert (1983), which is a 350 m thick sequence of layered pyroxenites, norites, and anorthosites that overlies the Lower Zone in this area.

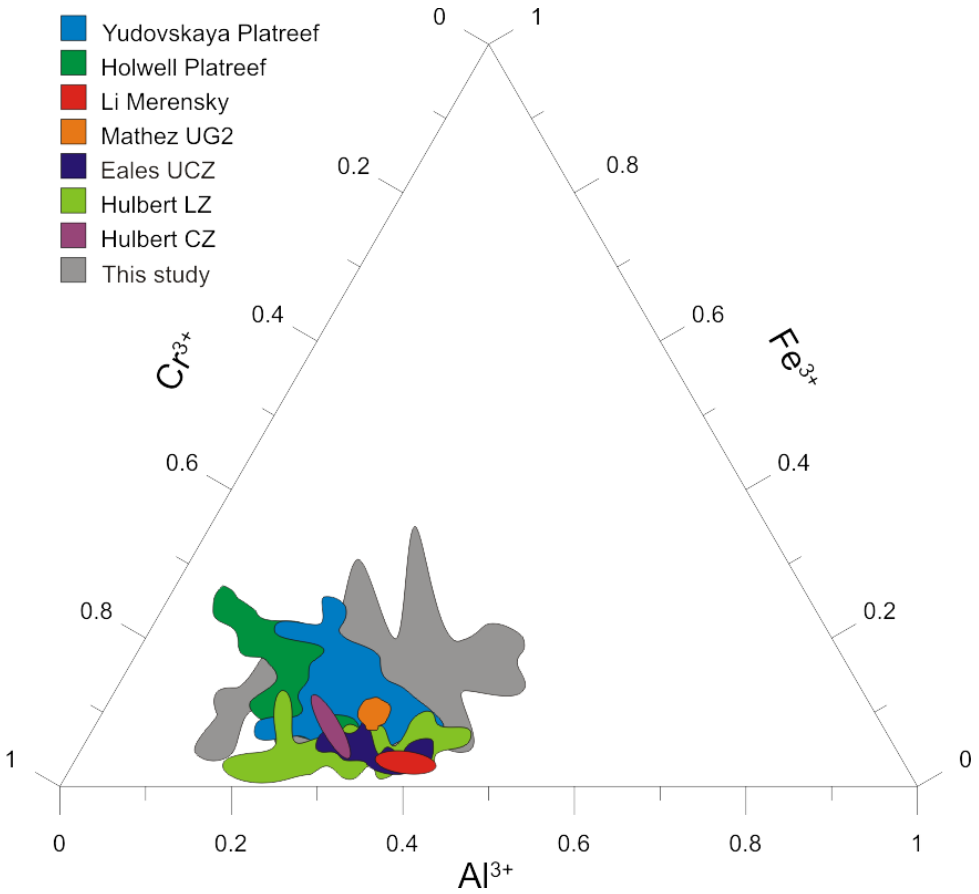


Figure 6.33. Trivalent ion plots for chromites from this study, Platreef (Holwell and McDonald 2006; Yudovskaya and Kinnaird 2010); Merensky Reef (Li et al. 2005), UG2 (Mathez and Mey 2005), UCZ (Eales and Reynolds 1986), northern limb Lower Zone (Hulbert 1983) and northern limb 'Critical Zone' (Hulbert 1983).

The trivalent ion plots (fig. 6.33) show the variation in chromite chemistry between the seven data sets compared, as well as this study. The chromites from this study have slightly wider range of values of Al and Cr compared to the Platreef studies of Yudovskaya and Kinnaird (2010) and Holwell and McDonald (2006). Non-Platreef data have lower $Fe^{3+}$ values than Platreef chromites. The UG2 data from Mathez and Mey (2005) have slightly higher $Fe^{3+}$ values than those for the UCZ section from Eales and Reynolds (1986), while chromites from the Merensky Reef have the lowest $Fe^{3+}$ values. Chromites from the Lower Zone have a similar Cr range to the Platreef data but have lower $Fe^{3+}$ and Al values. Values from GNPA member of the northern limb (the northern limb 'Critical Zone' inferred by Hulbert (1983)) plot within the range observed in this study and also overlap with data obtained from the other Platreef studies, albeit at lower $Fe^{3+}$, and the range produced by the UCZ data.

As the Platreef data of Yudovskaya and Kinnaird (2010) and Holwell and McDonald (2006) studies have already been discussed above, they will not be discussed further in this section and are included in the following charts for reference only.

### 6.8.1 Cr# vs. Mg#

The chromite compositions for the six different areas of the Bushveld Complex are shown in figure 6.34, with outlines for the data obtained in this study and for the UCZ (Eales and Reynolds 1986). The Merensky data plot in a very constrained field at the lower Cr# and higher Mg# range of the Platreef data. The UG2 data also plot within a very constrained field and have higher Mg# for a given Cr# compared to the Platreef data but mostly plot within the area produced from data for this study. The Lower Zone data plot at a similar Cr# to the Platreef data but at a much higher Mg#. The general trend line is perpendicular to that of the Platreef data, with a large Mg# range for a corresponding small Cr# range. The data of the GNPA member also plot within the range for this study, although at the high end of the Cr# scale and the low end of Mg# scale. The general trend line for the data from the GNPA member is parallel to that of the Lower Zone data.

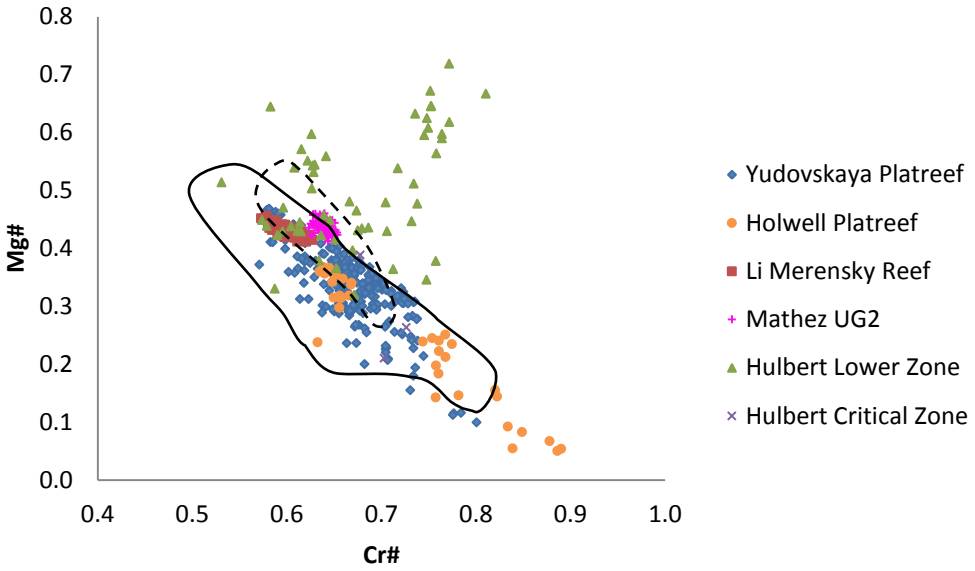


Figure 6.34. Geochemical plots of chromite composition for Mg# vs. Cr# from Platreef (Holwell and McDonald 2006; Yudovskaya and Kinnaird 2010); Merensky Reef (Li et al. 2005), northern limb Lower Zone (Hulbert 1983), northern limb 'Critical Zone' (Hulbert 1983) and UG2 (Mathez and Mey 2005); black outline is data from this study, dotted outline represent UCZ data (Eales and Reynolds 1986).

### 6.8.2 Cr# vs. $Fe^{2+}$#

The Merensky Reef data plot at the lowest end of the range for the Cr# and $Fe^{2+}$# (fig. 6.35). The UG2 data plot within the range obtained for the Platreef data but with a slightly shallower trend line. Both Merensky Reef and UG2 data sets plot within the field produced by the UCZ. The Lower Zone data have a very strong Fe-Ti trend when compared to the other data. Overall the Lower Zone data have a lower $Fe^{2+}$# than the rest of the data. This is likely to be the consequence of $Fe^{2+}$ and Mg exchange between the chromite and olivines. The GNPA member data plot at the high end of the $Fe^{2+}$# range of the data at corresponding high Cr# values.

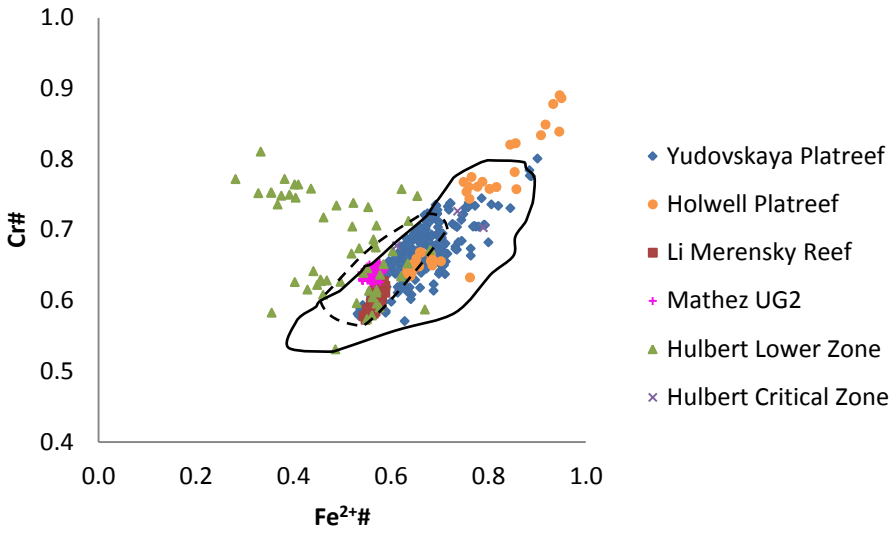


Figure 6.35. Geochemical plots of chromite composition for Cr# vs. $Fe^{2+}$# from Platreef (Holwell and McDonald 2006; Yudovskaya and Kinnaird 2010); Merensky Reef (Li et al. 2005), UG2 (Mathez and Mey 2005), northern limb Lower Zone (Hulbert 1983) and northern limb 'Critical Zone' (Hulbert 1983); black outline is data from this study, dotted outline represent UCZ data (Eales and Reynolds 1986).

### 6.8.3 $Fe^{3+}$# vs. $Fe^{2+}$#

The strong enrichment in $Fe^{3+}$# evident in the Platreef data sets is not repeated in the chromites analysed from the Merensky Reef (fig. 6.36). The samples analysed from the UG2, however, have moderate $Fe^{3+}$# values. The chromites analysed from the UG2 in the eastern limb appear enriched in $Fe^{3+}$# compared to those analysed from the western limb as shown by the UCZ data set. The chromites from the GNPA member plot along a flatter trend line that shows an increase in $Fe^{2+}$# but limited change in $Fe^{3+}$# values (fig. 6.36). Some of the samples analysed in the Lower Zone data set from Grasvally have the lowest values of both $Fe^{3+}$# and $Fe^{2+}$#, although this data set has a wide range of $Fe^{2+}$# values. Overall the data from the Platreef have higher $Fe^{2+}$ and $Fe^{3+}$ compared to data from elsewhere.

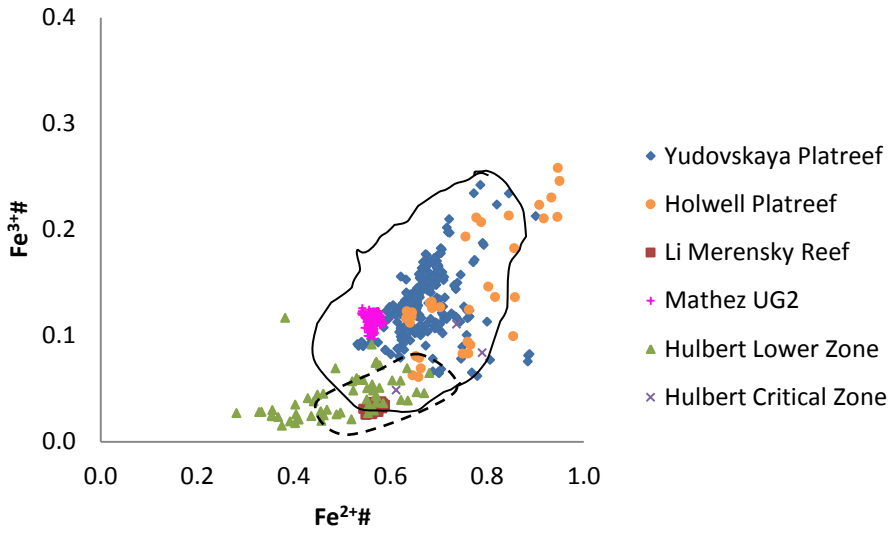


Figure 6.36. Geochemical plots of chromite composition for $Fe^{3+}$# vs. $Fe^{2+}$# from Platreef (Holwell and McDonald 2006; Yudovskaya and Kinnaird 2010); Merensky Reef (Li et al. 2005), northern limb Lower Zone (Hulbert 1983), northern limb 'Critical Zone' (Hulbert 1983) and UG2 (Mathez and Mey 2005); black outline is data from this study, dotted outline represent UCZ data (Eales and Reynolds 1986).

### 6.8.4 $Fe^{3+}$# vs. $TiO_2$

The Lower Zone samples have the lowest $TiO_2$ contents as can be seen from figure 6.37. The Merensky Reef data also plot within the Lower Zone data field and display the low $TiO_2$ values typical of the Critical Zone. The UG2 data plot at slighter higher $Fe^{3+}$# values than the Merensky Reef but at similarly low $TiO_2$ values. The data for the GNPA member plot at relatively low $Fe^{3+}$# values but have some of the highest $TiO_2$ values for all the data sets. The difference between the Critical Zone data (UG2 and Merensky) and the GNPA member data indicates that the latter formed from more evolved and possibly more oxidised magma than the former.

Hulbert and von Gruenewaldt (1985) suggested that the $TiO_2$ content in chromite should reflect the degree of differentiation. As a result, the Platreef parental magma should be more evolved than melts of the Critical Zone as is indicated by the majority of the Platreef data plotting at higher $TiO_2$ values than those from the Critical Zone.

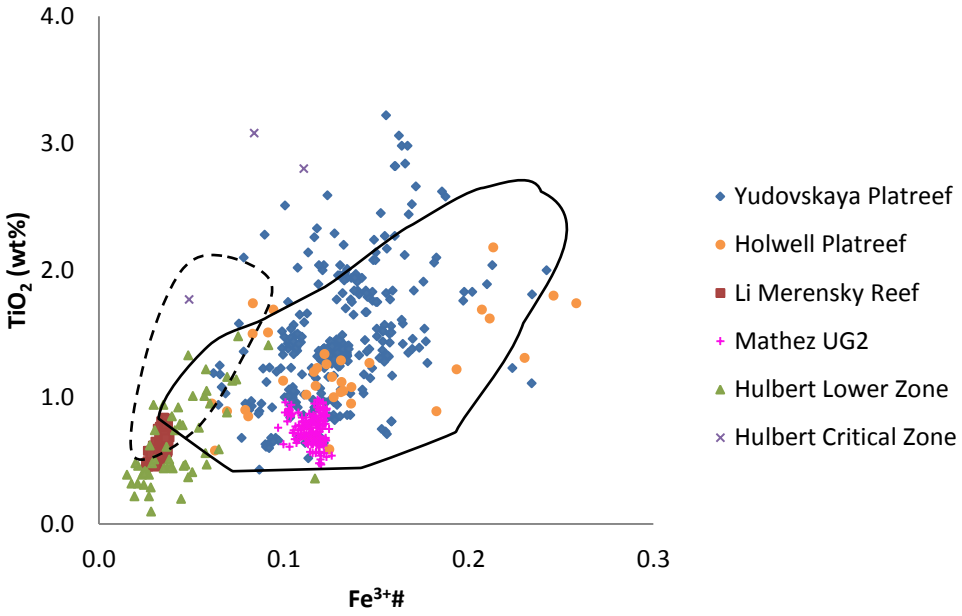


Figure 6.37. Geochemical plots of chromite composition for $TiO_2$ vs. $Fe^{3+}$# from Platreef (Holwell and McDonald 2006; Yudovskaya and Kinnaird 2010); Merensky Reef (Li et al. 2005), northern limb Lower Zone (Hulbert 1983), northern limb 'Critical Zone' (Hulbert 1983) and UG2 (Mathez and Mey 2005); black outline is data from this study, dotted outline represent UCZ data (Eales and Reynolds 1986).

## 6.9 Conclusion

This study has shown that there are differences in chromite composition depending on the host lithology and the location of the sample along strike of the Platreef. Chromite samples from Overysel display the most uniform patterns and this is consistent with earlier suggestions by Holwell and McDonald (2007) and Yudovskaya and Kinnaird (2010) that they represent the most primary Platreef, least affected by interaction with the reactive country rocks. Samples from Sandsloot and Zwartfontein are harder to interpret given the reactive footwall and xenolitic dolomite in these areas. In addition, chromites analysed from chromitite lithologies have been shown to be primary in composition, while chromites from the pyroxenite lithologies have been altered the most by reaction with the intercumulus silicates through post-crystallisation re-equilibration.

Comparison of this data set with other chromite analyses in the Bushveld Complex has shown that the Platreef chromite data sets cannot be directly correlated with the chromitites from the Merensky Reef, nor those from the southern portion of the northern limb (south of the TML), with the main difference being the elevated $Fe^{3+}$ and $TiO_2$ contents for Platreef chromite. These features are attributed to interaction with a more evolved (and possibly more oxidised) magma which led to chromite crystallisation during formation of the Platreef. Introducing this additional Ti via local assimilation of country rocks seems to be unlikely given the generally low $TiO_2$ concentration in both the Malmani dolomite and the basement gneiss (McDonald et al. 2005; Holwell and McDonald 2006). An alternative may be a Main Zone-type magma which would be expected to have a higher $TiO_2$ content than the B1 magma which formed much of the Lower and Critical Zones in the eastern and western Bushveld.

However, there is some correlation with the UG2 chromites, with the fields produced from Mathez and Mey (2005) consistently plotting within the data field produced by this study in addition to other Platreef data (Holwell and McDonald 2006; Yudovskaya and Kinnaird 2010) at least for some parameters. It has also been shown that the UG2 chromite composition appears to differ by location, as in the Platreef. Those grains sampled from the eastern limb have higher $Fe^{3+}$# that are comparable to the Platreef, whereas those sampled from the western limb have values closer to those seen in the Merensky Reef (e.g. Eales and Reynolds 1986; Li et al. 2005). Therefore, based on the chromite composition solely, it cannot be ruled out that there might be some relationship between the Platreef with the Upper Critical Zone of the Bushveld Complex.

# Chapter 7: Study Of PGM In The Chromitites Of The Platreef

## 7.1 Introduction

As has been shown in chapter 4, magmatic sulphide deposits that contain economic concentrations of PGE are rare. Numerous studies have shown that PGEs are hosted in the primitive mantle within a monosulphide solid solution (mss) and intermidate solid solution (iss) (e.g. Morgan and Baedecker 1983; Pattou et al. 1996; Burton et al. 1999; Lorand and Alard 2001). The processes of magmatic and sulphide liquid segregation cause the PGE to be associated with sulphide minerals. Despite much research, it is still unclear which processes and what conditions are responsible for the enrichment of PGE and other noble metals in layered intrusions such as the Bushveld Complex.

A number of theories have been proposed for PGM formation in the Bushveld Complex. It has been suggested that the PGE crystallise directly from the Bushveld magma as PGM. The PGM then accumulated directly on top of the crystal pile (Hiemstra 1979). Alternatively, it has been proposed that the PGE were collected by a sulphide liquid as it fractionated from the parental magma. This sulphide liquid then accumulated on top of the crystal pile (Campbell et al. 1983; Naldrett et al. 1986). Another theory involves magmatic fluids rich in Cl that collected the PGE as they moved upwards through the cumulate pile and re-precipitated in the reef (Willmore et al. 2000). It has also been suggested that PGE distribution was altered post deposition when the cumulates underwent low temperature alteration (Li et al. 2004).

It has been shown that chromitite horizons in layered intrusions are important in the collection of PGE, even in the absence of BMS (e.g. Hiemstra 1979; Ballhaus and Sylvester 2000; Cawthorn et al. 2002a). Chromitites can become enriched in PGE in a number of ways, with or without bulk saturation in sulphides. In the mineralised pyroxenites of the Merensky Reef, saturation in sulphides was probably the mechanism responsible for scavenging and concentrating PGE (Teigler and Eales 1993). Alternatively, PGM could have crystallised directly from a silicate magma when it became saturated in chromite (Barnes and Maier 2002b). Naldrett and Lehmann (1988) also suggested that it is possible for sulphide liquid trapped in chromitite layers to lose some Fe and S by reaction with the surrounding chromite grains resulting in the crystallisation of PGM from the sulphide liquid.

The aim of this study is to investigate lateral variation of PGM in chromitites within the Platreef across the farms Overysel, Zwartfontein and Sandsloot. It is the first study that is entirely focussed on the PGM of the chromitites in the Platreef. The studies by Holwell and

McDonald (2007) and Yudovskaya et al. (2011) included some PGM data from chromitites amongst other rock types. A second aim is to combine these results with other studies that have investigated PGM occurrence in order to investigate the total distribution of the PGE in the Platreef. The results of this mineralogical study will also provide mineralogical data on size frequency distributions of PGM, which are especially useful for mineral processing operations which need detailed characterisation of the ore for beneficiation purposes. In addition to the economic benefits, the PGM association is likely to reveal important genetic information regarding the processes involved in the formation of the Platreef and Ni-Cu-PGE deposits in general. This is especially useful given the degree of mineralogical variability observed in the Platreef.

## 7.2 Material and methods

This study involved analysis of PGM from 61 chromitite blocks representing 18 drill holes along strike and down dip of the Platreef on the farms of Overysel, Zwartfontein and Sandsloot (fig. 7.14) using the Cambridge Instruments LEO S360 scanning electron microscope (SEM) in the School of Earth and Ocean Sciences at Cardiff University. Each block was systematically searched for PGM in the back-scattered electron mode of the SEM and analysis was performed using the Oxford Instruments INCA energy dispersive X-ray analytical system coupled to the SEM. Samples were identified at a magnification of x150, by searching for bright minerals and then qualitatively analysing them. In total, 643 PGM were identified. The PGM were grouped into the following major groups: (1) PGE sulphides; (2) PGE tellurides; (3) PGE arsenides; (4) PGE bismuthides; (5) PGE antimonides; (6) PGE sulpharsenides; (7) PGE alloys (including Fe, Cu, Ni, Sn and Pb); and (8) Au-Ag bearing minerals. Although Au and Ag are not strictly platinum-group elements, they are noble metals that may also combine with the PGE and are included in the data set, as is routine for PGM studies.

For each PGM, the composition, relationship to surrounding sulphides or silicates and the shape and size were recorded. Surface areas of the PGM were estimated in terms of their surface exposure on a polished block. In order to do this, each PGM grain was considered to be an ellipse with measured long and short axes. This produces data that is comparable to other studies (e.g. Holwell and McDonald 2007; Nicholl and Kinnaird 2008; Yudovskaya et al. 2011) and more accurately reflects the relative proportions of each PGM type within an assemblage. Grains less than 0.5 µm in length were not incorporated into this database due to the inconsistent analyses obtained. This PGM database is in a form that can be compared to other studies that have been carried out on the Platreef (e.g. Armitage et al. 2002;

Hutchinson and Kinnaird 2005; Holwell et al. 2006; Holwell and McDonald 2007; Nicholl and Kinnaird 2008; Yudovskaya et al. 2011).

## 7.3 PGM mineralogy

This PGM study has revealed the relative abundance of each group of PGM (area proportions) located in the chromitite samples from each of the three localities studied (Overysel, Zwartfontein and Sandsloot; fig. 7.1 a, table 7.1).

Pt alloys are dominant followed by Pt arsenides and Pt sulphides. The least common PGM encountered are Pd sulphides (braggite (Pt,Pd)S has been grouped as a Pt sulphide as most occurrences are Pt dominant), Pt antimonides, and PGE (excluding Pt and Pd) arsenides. In addition, very few Au-Ag minerals were identified in the samples. Figure 7.1 b groups the PGM in more broad categories. Again, this reveals the dominance of the PGE alloys, accounting for almost 1/3 of all PGM identified by area. These results are however skewed by a 180 x 10 µm Pt-Fe alloy grain found in a sample from Zwartfontein. Without this grain the most common PGM would be PGE sulphide.

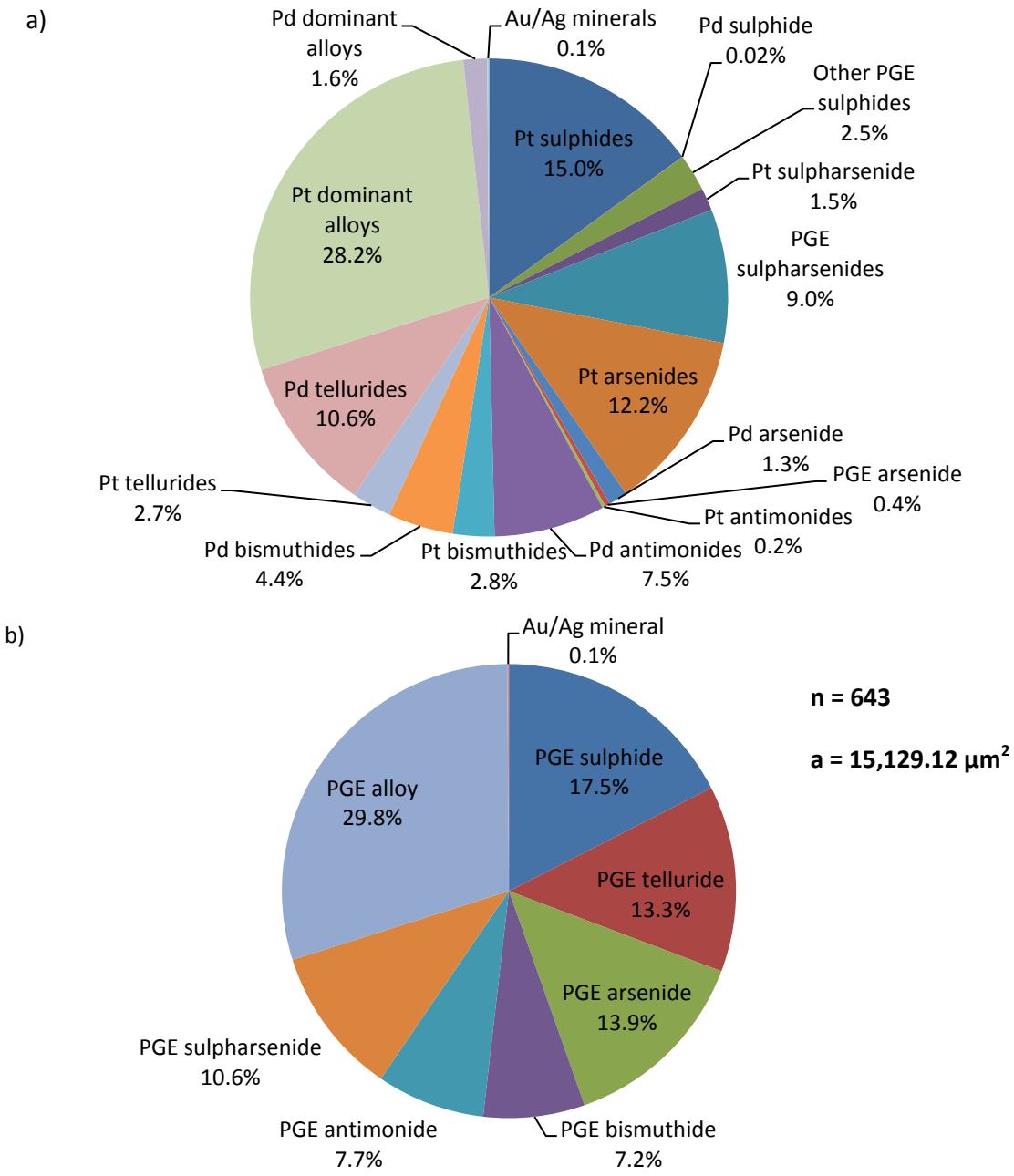


Figure 7.1. Pie charts showing the area proportion of each type of PGM found in the samples from all three farms. Pie chart (b) groups the PGM into more broad categories.

Table 7.1. Abundances of PGM in samples from three farms in the Central Sector.

| Group | Mineral | Formula | Overysel | | Sandsloot | | Zwartfontein | |
|---|---|---|---|---|---|---|---|---|
| | | | Grains (no.) | Area µm$^2$ | Grains (no.) | Area µm$^2$ | Grains (no.) | Area µm$^2$ |
| **Au/Ag mineral** | Electrum | Ag-Au | 3 | 5.5 | 0 | 0.0 | 6 | 13.6 |
| **PGE alloy** | Un-named | $(Pd,Pt)_9Fe$ | 0 | 0.0 | 1 | 0.2 | 0 | 0.0 |
| | Atokite | $Pd_3Sn$ | 0 | 0.0 | 1 | 7.1 | 1 | 6.3 |
| | Unconstrained | Pd-Pt-Fe | 1 | 4.7 | 0 | 0.0 | 0 | 0.0 |
| | Plumbopalladinite | $Pd_3Pb_2$ | 3 | 7.1 | 2 | 16.5 | 2 | 4.7 |
| | Potarite | PdHg | 0 | 0.0 | 1 | 6.3 | 0 | 0.0 |
| | Zvyagintsevite | $Pd_3Pb$ | 2 | 3.9 | 11 | 184.2 | 1 | 1.6 |
| | Un-named | $(Pt,Pd)_2Fe$ | 0 | 0.0 | 0 | 0.0 | 1 | 0.8 |
| | Isoferroplatinum | $Pt_3Fe$ | 0 | 0.0 | 16 | 70.1 | 16 | 78.5 |
| | Kharaelakhite | $(Cu,Fe)_4(Pt,Pb)_4NiS_8$ | 0 | 0.0 | 0 | 0.0 | 11 | 111.5 |
| | Un-named | $Pt_2(Sn,As)$ | 0 | 0.0 | 0 | 0.0 | 1 | 1.6 |
| | Un-named | $Pt_2Fe$ | 0 | 0.0 | 4 | 51.8 | 5 | 1443.6 |
| | Un-named | $PtFe_2$ | 0 | 0.0 | 0 | 0.0 | 2 | 20.4 |
| | Unconstrained | Pt-Pd-Fe-As | 0 | 0.0 | 0 | 0.0 | 1 | 0.2 |
| | Rustenburgite | $Pt_3Sn$ | 0 | 0.0 | 4 | 2362.7 | 13 | 63.6 |
| | Tetraferroplatinum | PtFe | 0 | 0.0 | 4 | 11.0 | 6 | 43.2 |
| | Tulameenite | $PtFe_{0.5}Cu_{0.5}$ | 0 | 0.0 | 0 | 0.0 | 1 | 2.4 |
| **PGE antimonide** | Isomertieite | $Pd_{11}Sb_2As_2$ | 0 | 0.0 | 1 | 1.6 | 0 | 0.0 |
| | Mertieite I | $Pd_{11}(Sb,As)_4$ | 2 | 4.7 | 0 | 0.0 | 0 | 0.0 |
| | Mertieite II | $Pd_8(Sb,As)_3$ | 2 | 8.1 | 1 | 0.8 | 0 | 0.0 |
| | Naldrettite | $Pd_2Sb$ | 0 | 0.0 | 0 | 0.0 | 3 | 2.4 |
| | Unconstrained | Pd-Sb-Te-Pt-Bi | 0 | 0.0 | 1 | 1.2 | 0 | 0.0 |
| | Stibiopalladinite | $Pd_5Sb_2$ | 6 | 30.6 | 9 | 44.3 | 29 | 1043.0 |
| | Un-named | Pt(Sb,Bi) | 0 | 0.0 | 0 | 0.0 | 1 | 1.6 |
| | Un-named | $PtSb_2$ | 0 | 0.0 | 1 | 1.6 | 0 | 0.0 |

Table 7.1. cont.

| | | | | | | | | |
|---|---|---|---|---|---|---|---|---|
| | Unconstrained | Pt-Sb-As-Ru | 0 | 0.0 | 0 | 0.0 | 1 | 18.9 |
| | Unconstrained | Sb-Pt-Bi | 0 | 0.0 | 0 | 0.0 | 1 | 4.7 |
| **PGE arsenide** | Un-named | (Pd,Pt)(As,Sb) | 0 | 0.0 | 1 | 0.8 | 0 | 0.0 |
| | Unconstrained | As-Pd-Bi-Te-Pt | 0 | 0.0 | 0 | 0.0 | 1 | 4.7 |
| | Unconstrained | As-Pd-Pt | 0 | 0.0 | 0 | 0.0 | 1 | 62.8 |
| | Fengluanite | $Pd_3(As,Sb)$ | 0 | 0.0 | 0 | 0.0 | 3 | 83.3 |
| | Palladoarsenide | $Pd_2As$ | 0 | 0.0 | 0 | 0.0 | 4 | 7.9 |
| | Unconstrained | Pd-As-Bi-Sb-Pt | 0 | 0.0 | 1 | 19.6 | 0 | 0.0 |
| | Unconstrained | Pd-As-Pb-Pt | 0 | 0.0 | 1 | 4.7 | 0 | 0.0 |
| | Unconstrained | Pd-As-Pt-Te-Bi | 0 | 0.0 | 0 | 0.0 | 1 | 4.7 |
| | Unconstrained | Pd-Pt-As-Sb-Sn | 0 | 0.0 | 1 | 2.4 | 0 | 0.0 |
| | Un-named | (Pt,Pd)As | 0 | 0.0 | 0 | 0.0 | 1 | 3.1 |
| | Chereponovite | RhAs | 0 | 0.0 | 0 | 0.0 | 1 | 4.7 |
| | Polkanovite | $Rh_{12}As_7$ | 0 | 0.0 | 3 | 2.4 | 0 | 0.0 |
| | Unconstrained | Pt-As-Rh-Ru-Ir | 0 | 0.0 | 0 | 0.0 | 1 | 3.9 |
| | Unconstrained | Ru-As-Ir-Os | 0 | 0.0 | 0 | 0.0 | 1 | 3.9 |
| | Unconstrained | Ru-As-Pt | 0 | 0.0 | 0 | 0.0 | 1 | 27.5 |
| | Ruthenarsenide | RuAs | 0 | 0.0 | 0 | 0.0 | 1 | 6.3 |
| | Vincentite | $(Pd,Pt)_3(As,Sb,Te)$ | 1 | 4.7 | 0 | 0.0 | 0 | 0.0 |
| | Un-named | $Pt(As,Sb)_2$ | 0 | 0.0 | 1 | 0.8 | 0 | 0.0 |
| | Un-named | Pt(As,Sb.Bi) | 0 | 0.0 | 0 | 0.0 | 1 | 3.1 |
| | Un-named | $Pt_2As$ | 0 | 0.0 | 0 | 0.0 | 1 | 1.2 |
| | Un-named | PtAs | 1 | 0.4 | 0 | 0.0 | 4 | 93.5 |
| | Un-named | PtAsSb | 0 | 0.0 | 1 | 7.9 | 0 | 0.0 |
| | Sperrylite | $PtAs_2$ | 16 | 166.5 | 17 | 187.1 | 68 | 1391.3 |
| **PGE bismuthide** | Froodite | $PdBi_2$ | 0 | 0.0 | 1 | 1.6 | 5 | 33.8 |
| | Michenerite | PdBiTe | 12 | 374.1 | 0 | 0.0 | 6 | 1260.8 |

Table 7.1. cont.

| | | | | | | | | |
|---|---|---|---|---|---|---|---|---|
| | Un-named | Pd(Bi,Te) | 0 | 0.0 | 0 | 0.0 | 2 | 9.4 |
| | Unconstrained | Pd-Bi-As-Te-Pt | 0 | 0.0 | 0 | 0.0 | 1 | 2.4 |
| | Unconstrained | Pd-Pt-Ir-Bi-As-Fe | 0 | 0.0 | 0 | 0.0 | 1 | 0.8 |
| | Sobolevskite | PdBi | 15 | 129.8 | 4 | 16.5 | 13 | 99.0 |
| | Unconstrained | Bi-Pt-Sb | 0 | 0.0 | 0 | 0.0 | 1 | 94.3 |
| | Unconstrained | Bi-Pt-Sb-Te | 0 | 0.0 | 0 | 0.0 | 1 | 78.5 |
| | Insizawaite | $PtBi_2$ | 8 | 87.2 | 1 | 4.7 | 2 | 16.5 |
| | Maslovite | PtbiTe | 1 | 9.4 | 0 | 0.0 | 12 | 104.5 |
| | Un-named | PtBi | 1 | 0.4 | 0 | 0.0 | 0 | 0.0 |
| | Unconstrained | Pt-Bi-Te-S | 0 | 0.0 | 0 | 0.0 | 1 | 0.8 |
| | Unconstrained | Pt-Pd-Bi | 0 | 0.0 | 0 | 0.0 | 1 | 25.1 |
| | Unconstrained | Pt-Pd-Bi-Te | 0 | 0.0 | 0 | 0.0 | 1 | 3.1 |
| **PGE sulpharsenide** | Unconstrained | As-S-Pt-Rh-Ru-Pd | 0 | 0.0 | 0 | 0.0 | 1 | 6.3 |
| | Hollingworthite | RhAsS | 0 | 0.0 | 10 | 191.3 | 9 | 414.1 |
| | Irarsite | IrAsS | 0 | 0.0 | 0 | 0.0 | 5 | 14.7 |
| | Unconstrained | Pt-As-S-Ir-Rh-Ru | 0 | 0.0 | 0 | 0.0 | 9 | 683.3 |
| | Unconstrained | Pt-As-S-Rh-Ru-Ir | 0 | 0.0 | 0 | 0.0 | 1 | 19.6 |
| | Unconstrained | Pt-As-S-Ru-Rh-Pd | 0 | 0.0 | 0 | 0.0 | 1 | 9.4 |
| | Unconstrained | Pt-Ir-Pd-Rh-Ru-As-S | 0 | 0.0 | 0 | 0.0 | 1 | 0.8 |
| | Unconstrained | Pt-Ir-Pd-Ru-As-S | 0 | 0.0 | 0 | 0.0 | 1 | 0.8 |
| | Unconstrained | Pt-Ir-Ru-Rh-As-S | 0 | 0.0 | 0 | 0.0 | 1 | 27.5 |
| | Platarsite | PtAsS | 5 | 88.0 | 1 | 78.5 | 8 | 64.4 |
| **PGE sulphide** | Vasilite | $Pd_{16}S_7$ | 0 | 0.0 | 0 | 0.0 | 1 | 3.1 |
| | Bowieite | $Rh_2S_3$ | 0 | 0.0 | 1 | 3.1 | 0 | 0.0 |
| | Laurite | $RuS_2$ | 6 | 98.0 | 7 | 36.9 | 21 | 239.6 |
| | Braggite | (Pt,Pd)S | 21 | 1433.7 | 1 | 4.7 | 1 | 4.7 |
| | Cooperite | PtS | 39 | 511.3 | 2 | 35.3 | 20 | 311.4 |

Table 7.1. cont.

| | | | | | | | | |
|---|---|---|---|---|---|---|---|---|
| **PGE telluride** | Keithconnite | $Pd_3Te$ | 0 | 0.0 | 2 | 1.0 | 0 | 0.0 |
| | Kotulskite | PdTe | 1 | 1.2 | 5 | 73.8 | 17 | 208.1 |
| | Merenskyite | $PdTe_2$ | 7 | 33.4 | 0 | 0.0 | 2 | 10.2 |
| | Unconstrained | Pd-Pt-Te | 0 | 0.0 | 0 | 0.0 | 1 | 7.1 |
| | Telluropaladinite | $Pd_9Te_4$ | 0 | 0.0 | 1 | 0.8 | 1 | 0.8 |
| | Moncheite | $PtTe_2$ | 11 | 58.7 | 7 | 46.9 | 16 | 255.3 |
| | Unconstrained | Pt-Te | 0 | 0.0 | 0 | 0.0 | 1 | 47.1 |

### 7.3.1 PGE sulphides

The PGE sulphides are among the most abundant of the PGM identified in the samples. Most of the PGM are either cooperite (PtS) or braggite ((Pt,Pd)S). Whereas braggite represents the largest total combined area of PGE sulphides (mainly due to one large grain (42 x 35 µm)), twice as many cooperite grains have been located. No cooperite was identified within samples from Sandsloot, with braggite being present instead. Cooperite and braggite were both identified on Overysel and Zwartfontein. A single occurrence of cooperite was found as a component of a sulphide inclusion in chromite. This was part of a PGM that also contained palladoarsenide ($Pd_2As$) and was associated with chalcopyrite (fig. 7.2). Vasilite ($Pd_{16}S_7$) was identified in a polished block from Zwartfontein and another single grain PGE-sulphide bowieite ($Rh_2S_3$) was observed on Sandsloot. These were associated with orthopyroxene and pentlandite, respectively.

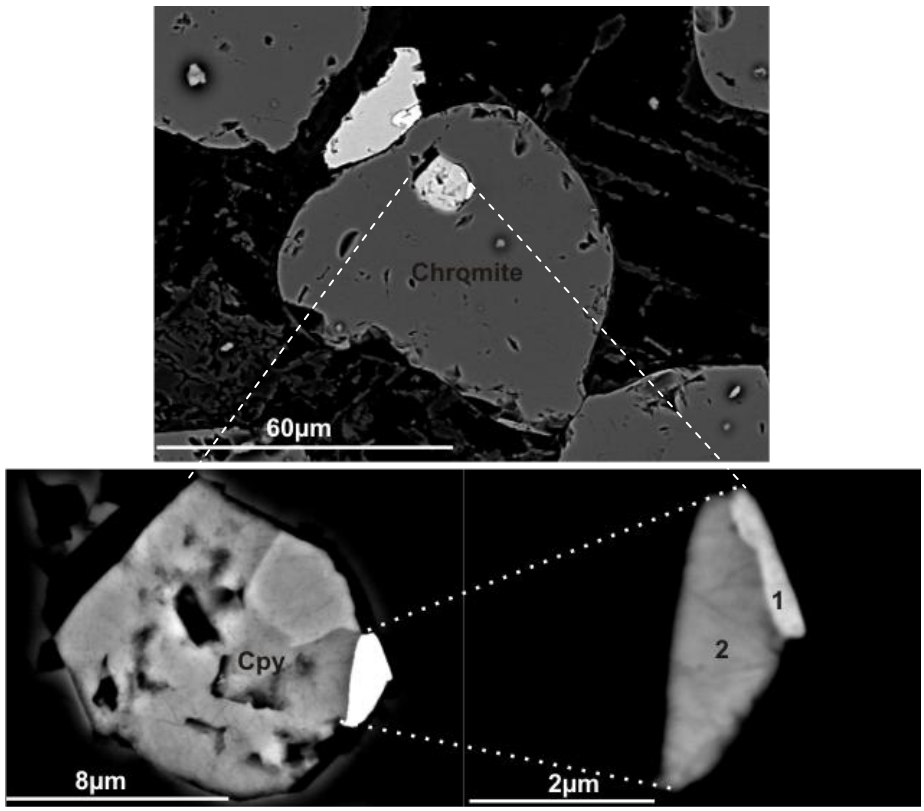


Figure 7.2. Cooperite (1) and palladoarsenide (2) inclusion with chalcopyrite within chromite grain from Zwartfontein.

Cooperite often occurs on its own as a discrete PGM. Where found as part of a composite grain, it is often found in the centre, surrounded by other PGM, most often by other sulphides, tellurides or bismuthides. A significant proportion of the cooperite grains identified are associated with sulphides on the rim of a chromite grain (table 7.2). Where

cooperite occurs within a silicate mineral or in a BMS, the grains are often subhedral in shape (fig. 7.3 a). In contrast, where they are located on the edge of a mineral they have an irregular shape (fig. 7.3 b). A number of grains were identified with embayments of orthopyroxene in the centre of the cooperite grains (fig. 7.3 c) as well as a couple are cut by veins (fig. 7.3 d).

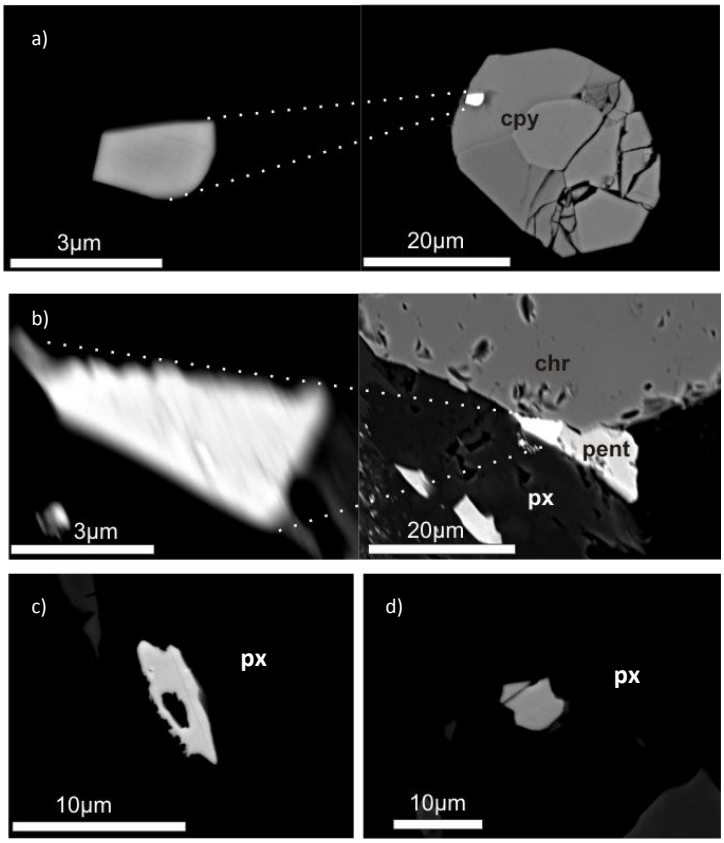


Figure 7.3 Cooperite grains showing differing morphology depending on their association. Key: cpy=chalcopyrite, chr=chromite, pent=pentlandite, px=orthopyroxene.

Table 7.2. Host associations for the different PGM-sulphides

| | In silicate | In sulphide + silicate | In sulphide | Rim chr in silicate | Rim chr in sulphide | Rim chr in sulph + silicate | Inclusion in chr |
|---|---|---|---|---|---|---|---|
| **Braggite** | 9 | 3 | 2 | 3 | 2 | 4 | - |
| **Cooperite** | 13 | 13 | 7 | 6 | 18 | 2 | 1 |
| **Laurite** | 12 | 2 | 4 | 4 | 7 | 2 | 3 |
| **Vasilite** | 1 | - | - | - | - | - | - |
| **Bowieite** | - | - | 1 | - | - | - | - |

Most of the braggite grains are hosted in silicates, specifically orthopyroxene (table 7.2), although the majority remain spatially associated with sulphides in some way. Like cooperite, braggite is often found as a discrete grain rather than part of a composite PGM. Where braggite forms a composite PGM it occurs with other PGM-sulphides (cooperite or

laurite) or with moncheite ($PtTe_2$). Where braggite lies within a silicate, it has a subhedral shape whereas it has a more anhedral appearance if located on the edge of a silicate crystal, most often orthopyroxene. Like cooperite, some of the braggite grains also have silicate or oxide inclusions in their centres.

The second most common PGE sulphide is laurite ($RuS_2$). Thirty four grains have been identified in total, representing 2.5 % of total area of all the PGM, occurring in samples from all three farms. A small proportion of laurites contain other PGE, most commonly Ir (although the exact proportion was not recorded). The majority of laurites occur in plagioclase and orthopyroxene (as inclusions or on edges of grains). Where laurite is found on the edge of silicates or sulphide (chalcopyrite or pentlandite) the grains appear irregular (fig. 7.4 b), whereas where they are found as inclusions within sulphide minerals or within chromite grains, the grains are subhedral (fig. 7.4 c). Only three single isolated laurite grains were identified, all the others are part of multiphase PGM, with tellurides/bismuthides, sulphides, arsenides or sulpharsenides. Where the laurite forms part of a composite PGM assemblage, it is located on the outer edge of the grains. Three of these PGMs are composed solely of PGE sulphides, comprising laurite and cooperite.

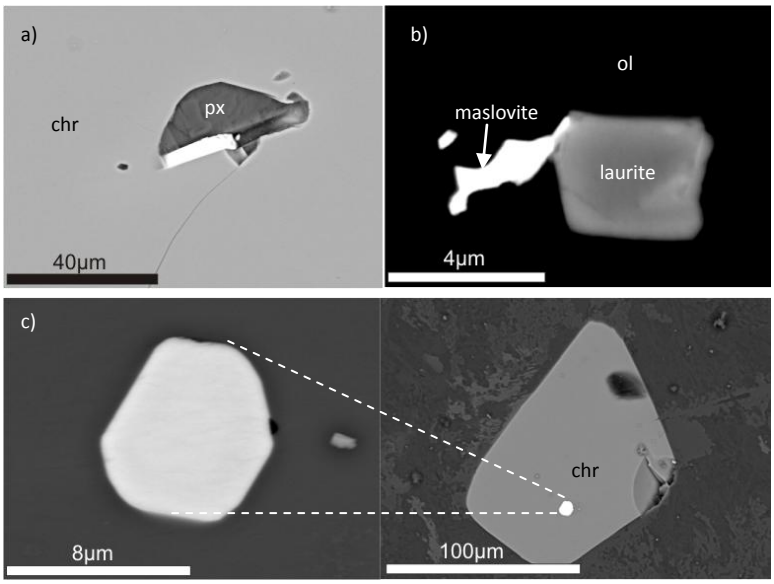

Figure 7.4. Laurite grains showing differing morphology depending on association. Key: chr=chromite, ol=olivine, px=pyroxene.

### 7.3.2 PGE arsenides

The PGE arsenides account for almost 14 % of the total area of all PGM identified, with sperrylite ($PtAs_2$) being the most abundant. 101 sperrylite grains were observed which represent 12 % of the total area of PGM. Sperrylites are the most numerous single PGM but the grains are often small which lowers their % contribution to the total area of the PGM.

Where sperrylites are identified in chalcopyrite, they are often equant in habit. More often, they occur as a discrete mineral but are also present as part of composite grains. Where found in composite grains with antimonides or sulpharsenides, they are positioned at the centre of the grains (fig. 7.5 a). As with cooperite, sperrylites are found with holes (caused by an unknown constituent being plucked out during polishing) in the middle of the grains (fig. 7.5 b) that may be partially filled with electrum. Occurrences of them being cut by veins are also noted (fig.7.5 c). There are also instances of the sperrylite having elongated shapes possibly due to being aligned along mineral cleavages or fracture lines (fig. 7.5 d). Etching is common where the sperrylite is found on the edge of sulphides or silicates. Where sperrylites are located in the middle of silicate grains, usually orthopyroxene, they often have a sybhedral shape.

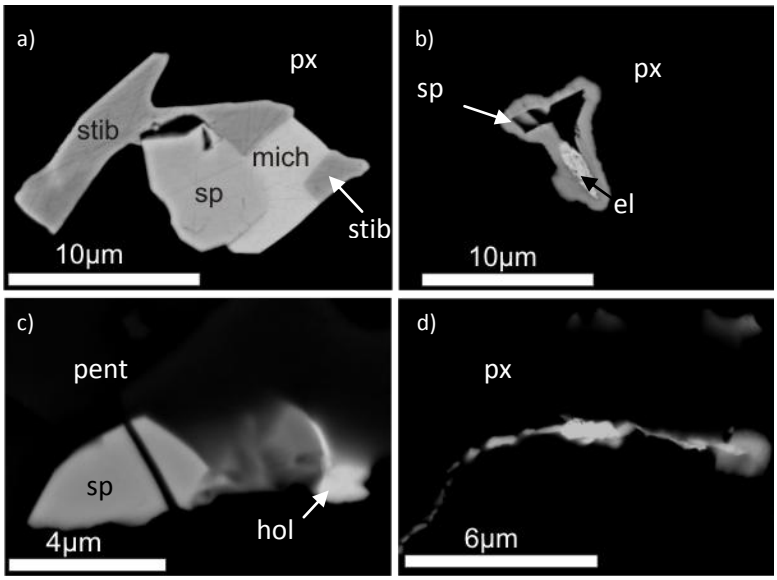


Figure 7.5. Sperrylite grains showing differing morphology depending on association. Key: el=electrum, hol=hollingworthite, mich=michenerite, pent=pentlandite, px=pyroxene, sp=sperrylite, stib=stibiopalladinite.

Also identified are the As-rich PGM fengluanite ($Pd_3(As,Sb)$), palladoarsenide ($Pd_2As$), chereponovite (RhAs), polanovite ($Rh_{12}As_7$), rutharsenide (RuAs) and vincentite ($(Pd,Pt)_3(As,Sb,Te)$) as well as a number of un-named and unconstrained arsenides that may be mixtures of phases. Palladoarsenides that are found in silicates more commonly have an eroded shape whereas those in sulphides are more sybhedral.

### 7.3.3 PGE tellurides

The most common telluride identified is moncheite ($PtTe_2$). All moncheites analysed also contained bismuth in their composition. Where moncheite occurs in silicates (fig.7.6 a), it forms laths, whereas in sulphides it has a rounded form (fig.7.6 b). Most moncheites are present as discrete grains rather than composite PGM.

The second most dominant telluride identified is the Pd-dominant species kotulskite (PdTe). Both moncheite and kotulskite were identified on all three farms. Kotulskite is found either on its own or with stibiopalladinite ($Pd_5Sb_2$) or sobolevskite (PdBi). A number of grains are associated with electrum in the core of composite PGM surrounded by orthopyroxene or BMS. Merenskyite ($PdTe_2$) has been located on Overysel and Zwartfontein but not in samples from Sandsloot. Again, bismuth is commonly found in the composition of these grains, likely due to the existence of intermediate phases between sobolevskite, sudburyite and kotulskite, and a continuous solid-solution between PdTe and PdBi as described by Evstigneeva et al. (1976). Merenskyite typically occurs either as a single phase or with arsenides or sulpharsenides. When enclosed by either silicates or BMS, merenskyite forms sybhedral grains but forms irregular grains when present on the edges of other minerals. Single grains of telluropalladinite ($Pd_9Te_4$) have been found on both Sandsloot and Zwartfontein, both less than 1 $\mu m^2$ in area. Occasionally, unconstrained grains containing Pt or Pd and Te have been identified on Zwartfontein, with one grain of nearly 50 $\mu m^2$ identified on Zwartfontein.

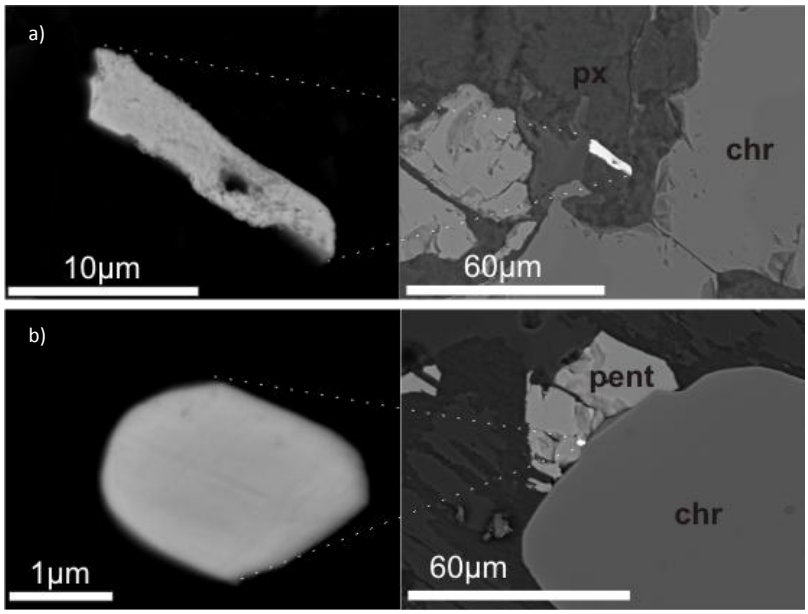


Figure 7.6. Moncheite grains showing differing morphology depending on association. Key: px=pyroxene, chr=chromite, pent=pentlandite.

### 7.3.4 PGE bismuthides

Michenerite (PdBiTe) is the most common of the PGE bismuthides in these samples representing 11 % of the total area of all the PGM identified. Grains are irregular in shape and occur mostly in pyroxene. Sobolevskite (PdBi) is the most abundant bismuthide with 32 PGM identified. Sobolevskite is mostly found in pentlandite, where it is sybhedral if in the centre of the BMS or ragged if on the edges. All sobolevskites found within silicates are

irregular in shape and discrete grains are as common as those forming part of a composite PGM. In composite grains, it is mostly associated with other tellurides or bismuthides. It is also commonly located with PGE alloys. Sobolevskite commonly surrounds PGE-sulphides and in turn is surrounded by PGE arsenides.

Also identified are froodite ($PdBi_2$), insizwaite ($PtBi_2$), maslovite (PtBiTe) as well as a number of un-named and unconstrained bismuthides that also contain minor amounts of Te, Sb and As. All maslovite grains identified have an irregular form and mostly occur as composite grains. These features are ubiquitous. Where they are identified in silicates, like orthopyroxene, they have an elongate form. Insizwaite is rarely found on its own and always has an irregular shape. Where found in a composite grain with other bismuthides or tellurides it always occurs on the outer edge of the PGM composite.

### 7.3.5 PGE antimonides

The most commonly identified PGE antimonide is stibiopalladinite ($Pd_5Sb_2$), with 44 grains accounting for over 7 % of total area of the PGM. In BMS the stibiopalladinite grains have a sybhedral form but show corrosion if they are situated at the edge of a sulphide. All grains identified within silicates have an irregular form. Stibiopalladinite is more commonly found forming part of a composite PGM than as discrete isolated grains. The most common location for stibiopalladinite is associated with arsenides and sulpharsenides (fig.7.5 a). It is also found with PGM tellurides or bismuthides. Where stibiopalladinite occurs with a PGE arsenide, the arsenide always forms the core of the composite PGM with the antimonide situated towards the edge. Other antimonides identified are isomertieite ($Pd_{11}Sb_2As_2$), mertieite I ($Pd_{11}(Sb,As)_4$) and II ($Pd_8(Sb,As)_3$) and naldrettite ($Pd_2Sb$) as well as un-named and unconstrained varieties. Some of the unconstrained grains that contain Pd, Sb, Te and Bi are likely to represent a phase in the PdSb (sudburyite) – PdBi (sobolevskite) – PdTe (kotulskite) system described by Cabri and Laflamme (1976).

### 7.3.6 PGE sulpharsenides

The most common PGE sulpharsenide, in terms of both number of grains (19) and combined total volume (4 area %), is hollingworthite (RhAsS). This occurs as thin stringers in sulphides, and sybhedral crystals in silicates. Where present as part of composite grains, hollingworthite is found on the outside of grains that contain sperrylite ($PtAs_2$) but on the inside of grains of irarsite (IrAsS). Platarsite (PtAsS) is also common with 14 grains representing 1.5 area %. Irarsite was also identified along with a number of unconstrained PGE sulpharsenides. Where the unconstrained PGE sulpharsenides form composite PGM,

they always occur towards the centre of the grain, surrounded by PGE-antimonides or PGE-bismuthides.

### 7.3.7 PGE alloys

The PGE alloys represent the largest proportion of the total area of the PGM identified, forming nearly 30 area %. The majority of the PGE alloys identified are Pt-Fe alloys (table 7.3). Due to their small nature, it is very hard to analyse their composition and therefore a number of different compositions were recorded (table 7.3). The most numerous are isoferroplatinum ($Pt_3Fe$), with 29 grains identified. However, this does not represent the largest total combined area, with grains of the composition $Pt_2Fe$ representing over 86 area % of the Pt-Fe alloys. This is largely down to one grain that has dimensions of 180 µm x 10 µm in a sample from Zwartfontein. If this grain is removed, $Pt_2Fe$ only accounts for 9.6 area %. One grain of tulameenite ($PtFe_{0.5}Cu_{0.5}$) was identified on Zwartfontein.

Table 7.3. PGE-Fe alloys identified across the three farms of Overysel, Sandsloot and Zwartfontein as total area combined of grains.

| Pt-Fe alloy | | Overysel | Sandsloot µm$^2$ | Zwartfontein | Total µm$^2$ | Area % | Number of grains |
|---|---|---|---|---|---|---|---|
| **Isoferroplatinum** | $Pt_3Fe$ | - | 70.1 | 78.5 | **148.6** | 8.6 | 29 |
| **Tetraferroplatinum** | PtFe | - | 11.0 | 43.2 | **52.2** | 3.0 | 10 |
| **Tulameenite** | $PtFe_{0.5}Cu_{0.5}$ | - | - | 2.4 | **2.4** | 0.1 | 1 |
| **Un-named** | $(Pt,Pd)_2Fe$ | - | - | 0.8 | **0.8** | 0.1 | 1 |
| **Un-named** | $Pt_2Fe$ | - | 51.8 | 1444.0 | **1495.4** | 86.6 | 9 |
| **Un-named** | $PtFe_2$ | - | - | 20.4 | **20.4** | 1.2 | 2 |
| **Un-named** | $(Pd,Pt)_9Fe$ | - | 0.2 | - | **0.2** | 0.01 | 1 |
| **Un-constrained** | Pd-Pt-Fe | 4.7 | - | - | **4.7** | 0.3 | 1 |

Isoferroplatinum grains are found either as sybhedral lath shaped grains (fig. 7.7 a) or with the honeycomb texture (fig. 7.7 b). Tetraferroplatinum mostly occurs in BMS and displays a similar honeycomb texture (fig. 7.7 c) as with isoferroplatinum. When found as part of a composite PGM, isoferroplatinum occurs with other Pt-Pd-Fe alloys. $Pt_2Fe$ has the honeycomb texture of tetraferroplatinum but $PtFe_2$ occurs as laths.

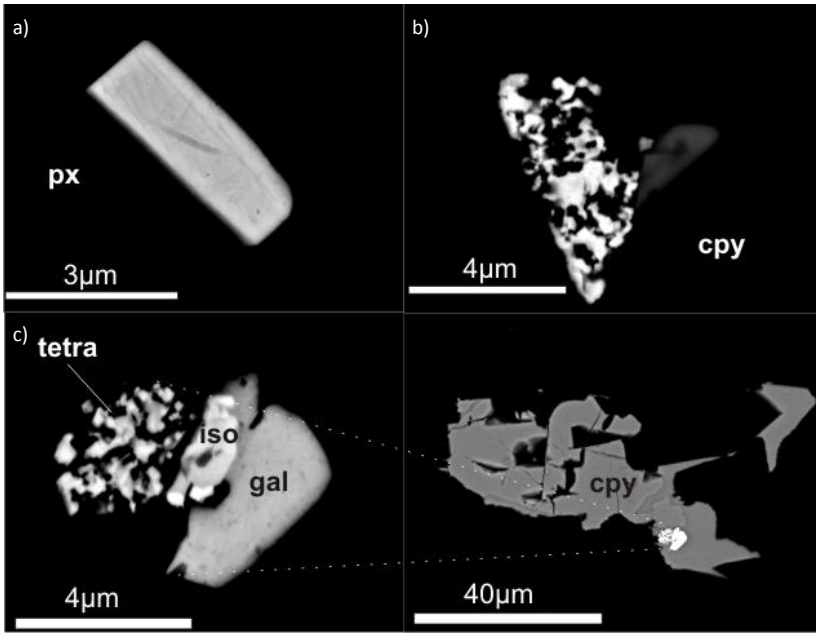

Figure 7.7. Isoferroplatinum grains showing differing morphology depending on association. Key: px=pyroxene, cpy=chalcopyrite, tetra=tetraferroplatinum, iso=isoferroplatinum, gal= galena.

PGE alloys containing Sn are common, with atokite ($Pd_3Sn$) and the more abundantly occurring Pt-equivalent rustenburgite ($Pt_3Sn$) being identified in samples from Sandsloot and Zwartfontein. The rustenburgite grains account for 16 area % of the total PGM identified and for half of the volume percentage of the alloys. Again, this high percentage is due to the large size of the grains, as only 17 grains were identified. Rustenburgite largely occurs on its own as discrete grains and is mainly associated with orthopyroxene. The grains are sybhedral in the core but irregular near the edges of the silicate crystals. In composite PGM, it occurs most commonly with arsenides but has also been found with Pt-Fe alloys and bismuthides.

Also present were 11 grains of kharaelakhite ($(Cu,Fe)_4(Pt,Pb)_4NiS_8$). Due to their small size, they account for less than 1 area % of the PGM identified. They are mostly sited within BMS, especially pentlandite and all but one form discrete sybhedral grains. PGE alloys containing Pb are also associated with BMS and occur as Pd-bearing plumbopalladinite ($Pd_3Pb_2$) and zvyagintsevite ($Pd_3Pb$), representing almost 1.5 area % of total PGM identified. Zvyagintsevite grains have an irregular shape and are commonly found as discrete grains. In composite grains, it is most commonly associated with isoferroplatinum but also with sperrylite, vincerite and potarite. Plumbopalladinite occurs equally as discrete grains or as part of composite PGM grains where it is with cooperite or other alloys. Zvyagintsevite is irregularly shaped and is ubiquitous.

### 7.3.8 Au-Ag bearing minerals

Although not a PGM, the close relationship of electrum with the PGM makes it appropriate to be included here. Nine electrum grains were identified on Overysel and Zwartfontein, representing 0.1 area % of the total PGM. Electrum is often located at the core of composite PGM, especially those that contain kotulskite and sperrylite (fig. 7.5 b).

## 7.4 Variation in hosts for the PGM

In addition to the type of PGM being recorded, its association with the surrounding sulphides, silicates or chromite was also noted (table 7.4).

These associations are shown graphically for each farm in figure 7.9, with a pie chart for the combined total of all the farms shown in figure 7.8. Major features of the study are that nearly half of the PGM on Overysel are associated with base metal sulphides. Almost three quarters of PGM identified on Sandsloot are found on the edge of chromite grains within silicates, specifically plagioclase. PGM from Zwartfontein are equally found in sulphides, on the edge of chromites, in sulphides and on grain boundaries between sulphides and silicates. This farm is the only one in which an association with carbonates was observed. Overall, there is a wide distribution of associations, with the most common being an association with sulphides and on the edge of chromites in silicates. Simplified, the associations can be grouped into those with sulphide, silicate, at the junction of sulphide and silicate or other (including with carbonates) and is shown in a pie chart in figure 7.10. Overall, nearly half of all PGM identified in the study area are associated wholly or partially with sulphides.

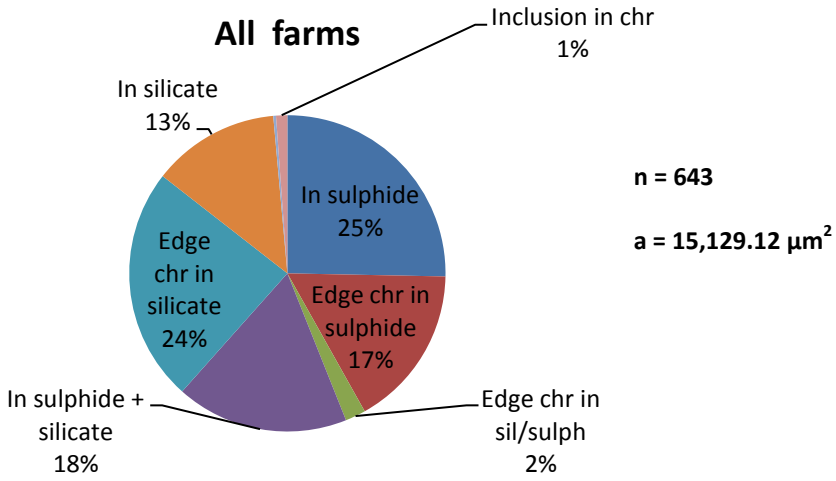


Figure 7.8. Pie chart showing the PGM association for the whole study area

Table 7.4. Total PGM area (µm$^2$) for each association. Key: O-Overysel, S-Sandsloot, Z-Zwartfontein, pyrox-pyroxene, ol-olivine, plag-plagioclase, pent-pentlandite, cpy-chalcopyrite, pyrr-pyrrhotite.

| | | O | S | Z | Total |
|---|---|---|---|---|---|
| **On rim of chromite in silicate** | pyrox | 171.0 | 83.3 | 736.3 | **990.6** |
| | ol | - | - | 157.1 | **157.1** |
| | plag | 25.9 | 2368.0 | 82.5 | **2476.4** |
| **On rim of chromite in sulphide** | pyrite | 151.2 | - | - | **151.2** |
| | pent | 104.1 | 125.3 | 1235.2 | **1464.6** |
| | cpy | 67.5 | 53.2 | 758.7 | **879.5** |
| | cpy + pent | 0.8 | 1.6 | 7.1 | **9.4** |
| **On rim of chromite in sulph/sil** | cpy/pyrox | 3.0 | 78.5 | 148.4 | **229.9** |
| | pent/pyrox | 40.5 | 3.1 | - | **43.6** |
| | pyrite/pyrox | 5.5 | - | - | **5.5** |
| | pyrr/cpy + pyrox | - | 36.9 | - | **36.9** |
| **Inclusion in chromite** | | 8.6 | - | 164.9 | **173.6** |
| **In sulphide** | pyrite | 1184.8 | - | 78.5 | **1263.3** |
| | pyrr | 35.3 | - | - | **35.3** |
| | pent | 214.8 | 269.0 | 609.1 | **1092.9** |
| | cpy | 28.3 | 4.3 | 97.0 | **129.6** |
| **Composite sulphide** | cpy + pent | - | 0.3 | 12.6 | **12.8** |
| | cpy + pyrite | - | - | 1217.4 | **1217.4** |
| | pyrite + pent | - | - | 28.3 | **28.3** |
| | pyrr + pent | 49.7 | - | - | **49.7** |
| **In silicate** | pyrox | 540.4 | 200.1 | 711.2 | **1451.6** |
| | ol | - | - | 14.1 | **14.1** |
| | plag | 224.6 | 36.9 | 198.7 | **460.2** |
| | plag + pyrox | - | 2.7 | 43.2 | **45.9** |
| **In carbonate** | | - | - | 42.4 | **42.4** |
| **Sulphide + silicate** | pent + pyrox | 163.6 | 116.4 | 208.9 | **488.9** |
| | pent + ol | - | - | 6.3 | **6.3** |
| | pent + plag | - | - | 88.8 | **88.8** |
| | cpy + pyrox | 14.1 | 48.7 | 1555.1 | **1617.9** |
| | cpy + plag | - | 11.8 | 18.9 | **30.6** |
| | pyrite + pyrox | 35.5 | - | 385.2 | **420.7** |
| | cpy/pent + pyrox | - | - | 14.1 | **14.1** |
| | | | | | |
| | **Total** | **3069.1** | **3440.1** | **8619.9** | **15129.1** |

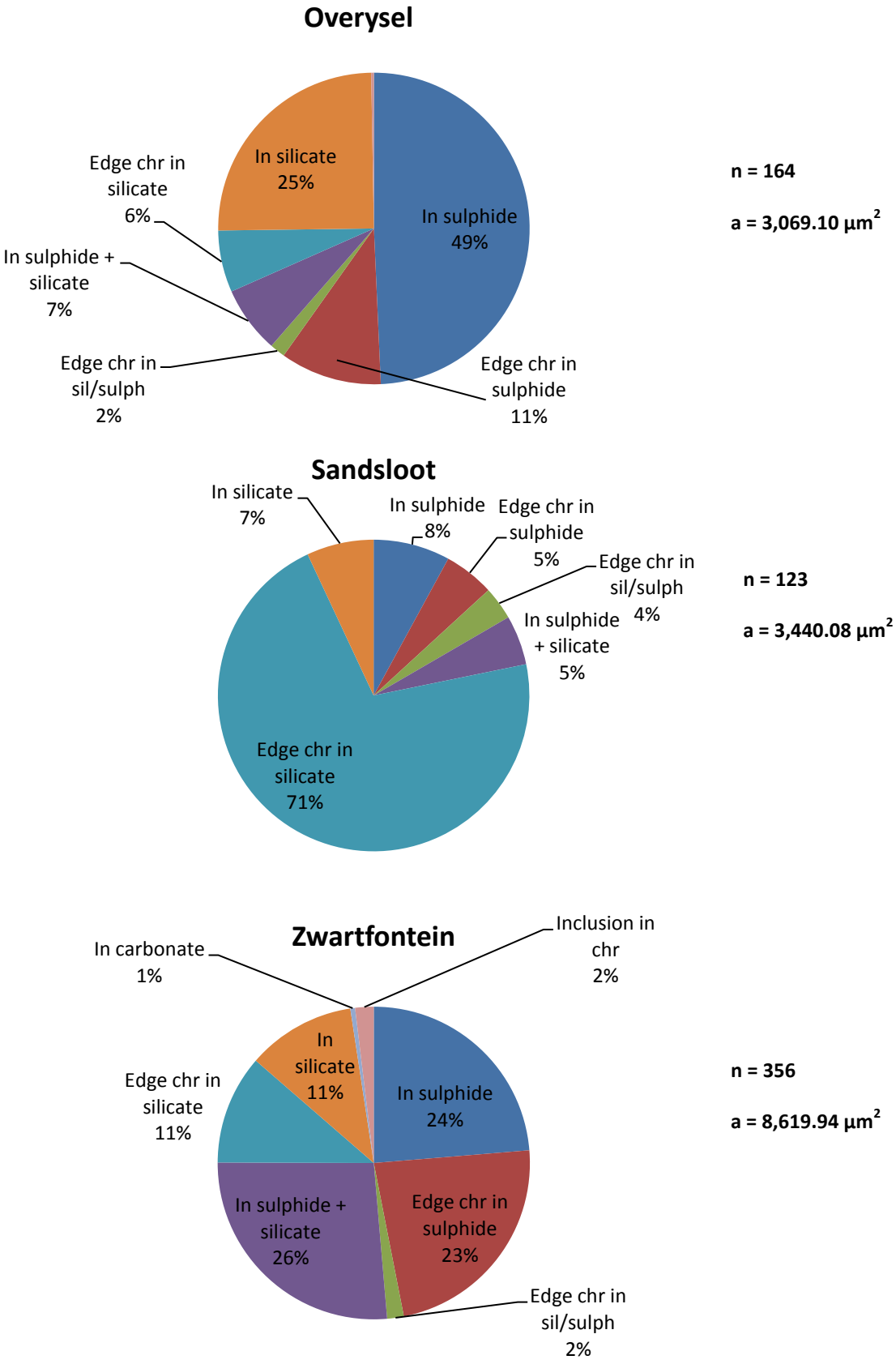


Figure 7.9. Pie charts showing the PGM association across the three farms.

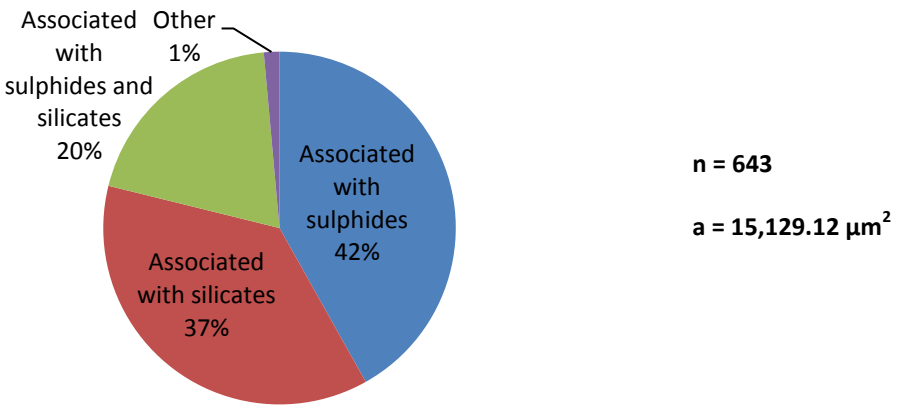


Figure 7.10. Pie chart showing the simplified distribution of the PGM association relationships for the entire data set.

The following is an examination of the variation of host minerals for the different types of PGM. PGMs as inclusions in chromite are mostly PGE sulphide (dominated by laurite) but a minor quantity of PGE alloys (Pd dominant) and PGE arsenide (palladoarsenide and vincentite) and a single PGE telluride (maslovite) also form inclusions (fig. 7.11). More than 90 % of the PGM in carbonates are PGE tellurides with a small number being PGE alloys (fig. 7.11). PGM associated with silicates were represented by every group of PGM, with PGE sulphides and PGE arsenides making up more than half the total area (fig. 7.12). PGE antimonides and PGE bismuthides are also significant groups. As with PGM associated with silicates, those that are associated with sulphides are represented by all the PGM groups, although with very minor amounts of PGE antimonides and alloys (fig. 7.12). The majority of PGM with base metal sulphides are PGE tellurides and PGE sulphides. Where the PGM are located along grain boundaries with sulphides and silicates, more than half of the PGM are PGE alloys (fig. 7.12). The second most prevalent group is the PGE sulpharsenides.

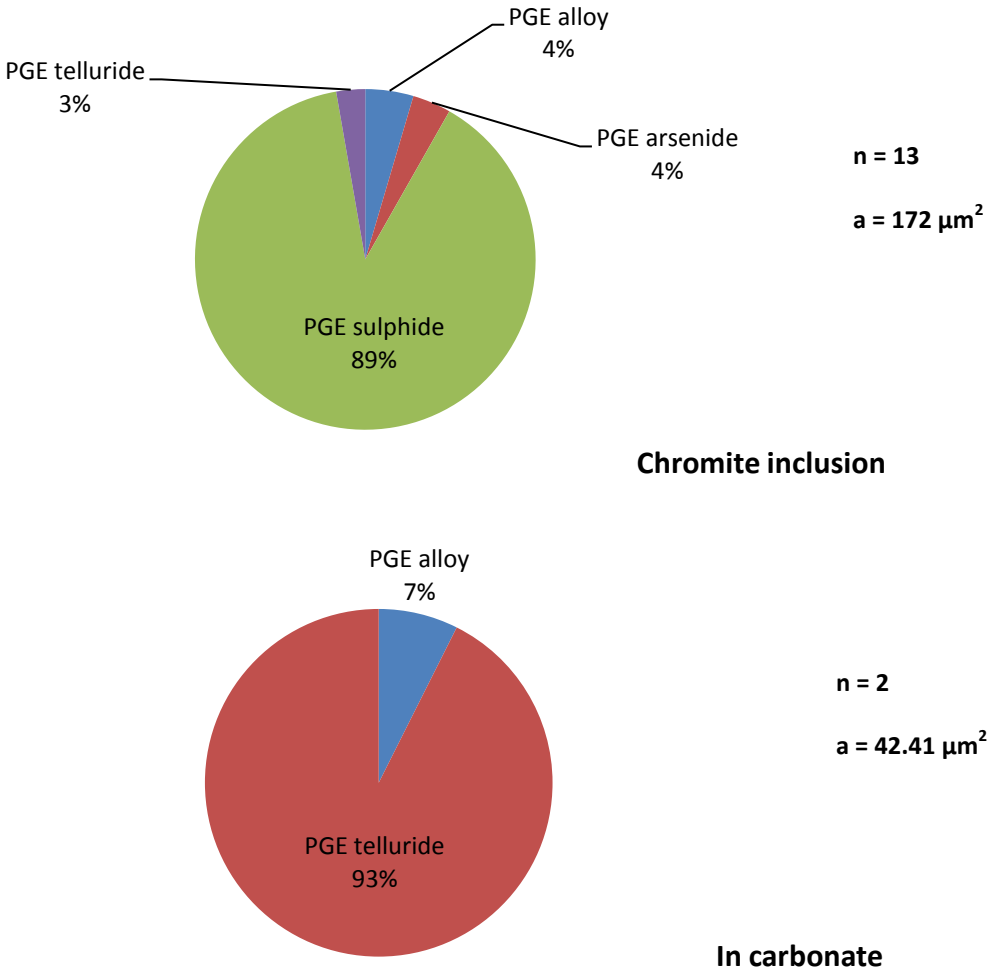


Figure 7.11. Breakdown of PGM that occur as inclusions in chromite or in carbonate grains.

PGM are also found on the rim of chromite grains, either in sulphides, silicates or on grain boundaries between the mineral grain types (fig. 7.13). Those which are associated with sulphide are mostly composed of PGE sulpharsenides and PGE antimonides, with significant proportions also composed of PGE sulphides, arsenides and bismuthides. Almost three quarters of the PGM that are associated with silicates are composed of PGE alloys, with just over 10 % composed of PGE arsenides. Where PGMs are identified on the rim of chromite grains on the boundary between silicates and sulphides, they are equally composed of PGE alloys, PGE antimonides and PGE arsenides. Some PGE sulphides are also found with minor amounts of PGE tellurides.

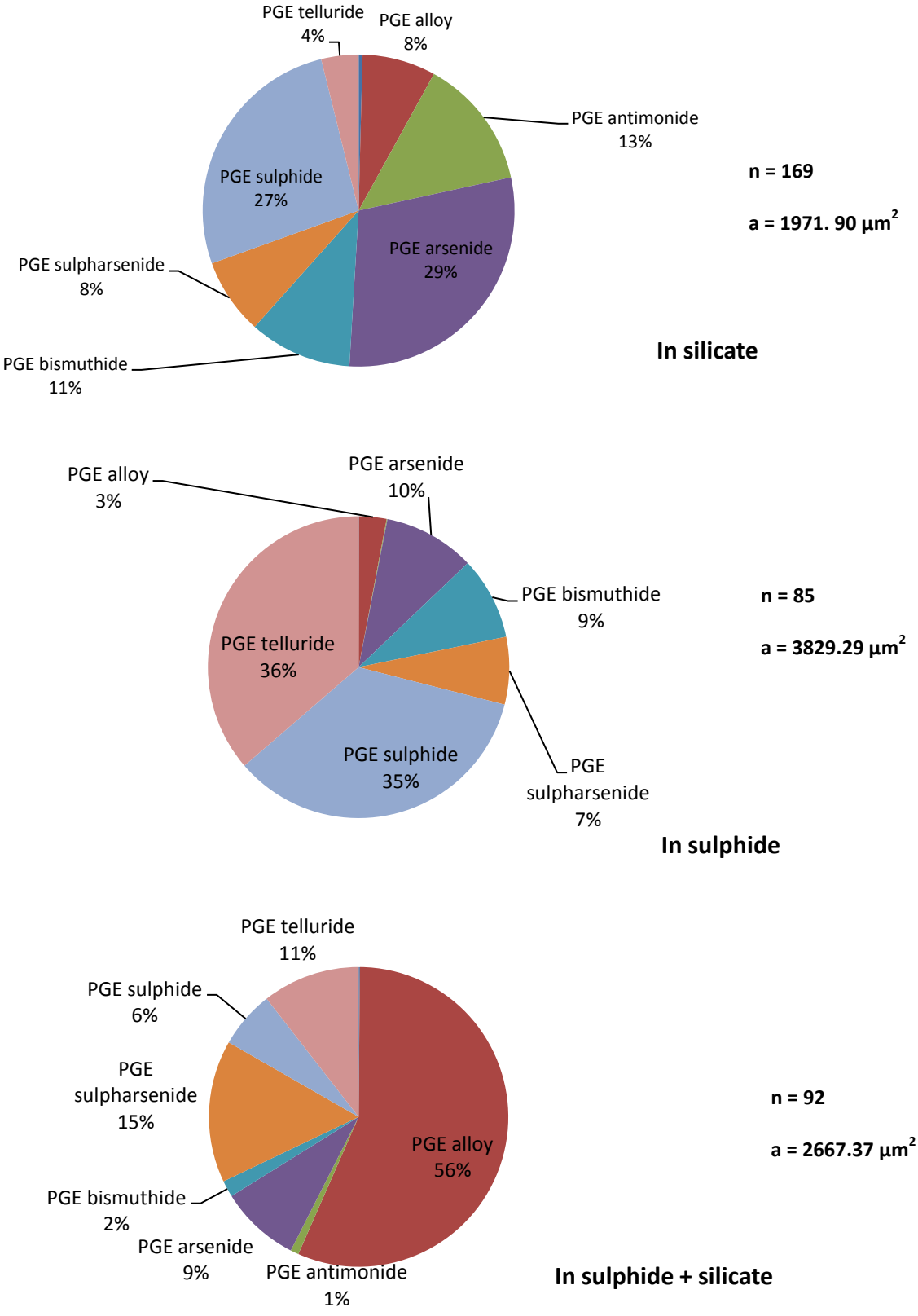


Figure 7.12. Breakdown of PGM groups that occur within silicates, within sulphides or on the boundary between silicate and sulphide grains.

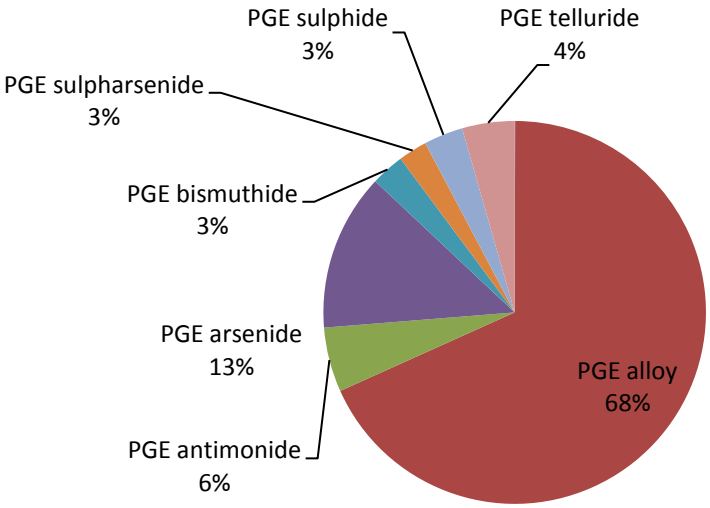


**n = 106**

**a = 3624.02 µm$^2$**

**Rim chr in silicate**

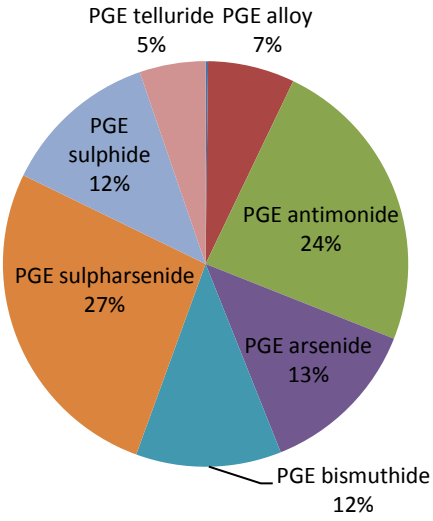


**n = 155**

**a = 2504.63 µm$^2$**

**Rim chr in sulphide**

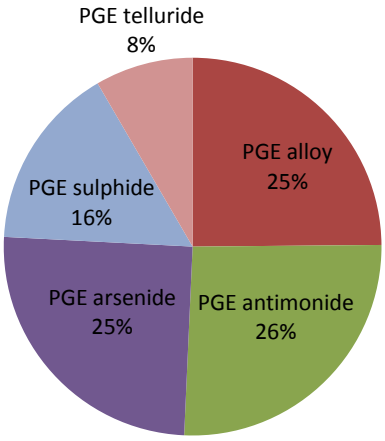


**n = 21**

**a = 315.93 µm$^2$**

**Rim chr in sulphide + silicate**

Figure 7.13. Breakdown of PGM that occur on the rim of chromites in silicates, rim of chromites in sulphides or rim of chromites on the boundary between silicate and sulphide grains.

A key observation made for the PGE alloys is that only a small number were found within the sulphides (3 % area) while a considerable amount were found on the sulphide silicate boundary (33 % area; fig. 7.14). This is significant because it implies that a significant amount of the PGE alloys may have either been altered or oxidised. If alteration occurred, then hydrous minerals such as tremolite would be identified in the samples, which is not the case suggesting that oxidation is more likely. This will be discussed further in a later section.

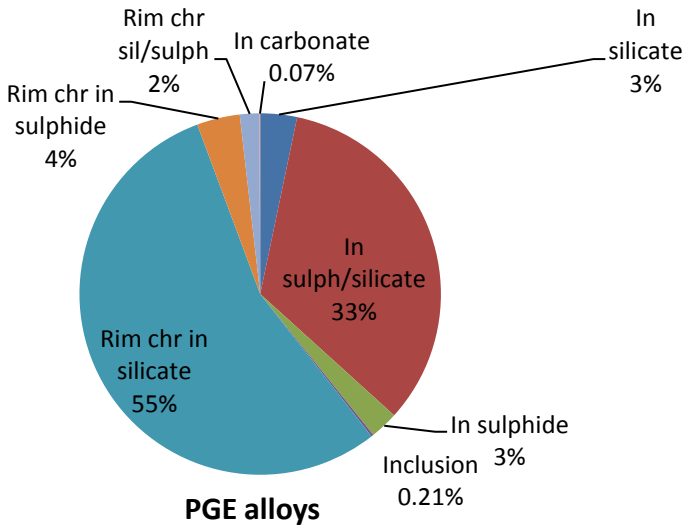


Figure 7.14. PGE alloy association by group

## 7.5 Variation in PGM distribution across the study area

In order to compare the distribution of the PGM in greater detail across the 3 farms that encompass the Mogalakwena mine complex, the drill holes have been grouped in N-S lines (effectively strike sections) as first introduced in chapter 5 and shown in figure 7.15. In addition, the drill holes have also been grouped into a number of dip sections of W-E lines (fig. 7.16). These lines have been numbered and will be discussed in the text below. By examining the variation in the PGM distribution along strike and down dip, information relating to how the structure of the PGE deposit formed can be deduced.

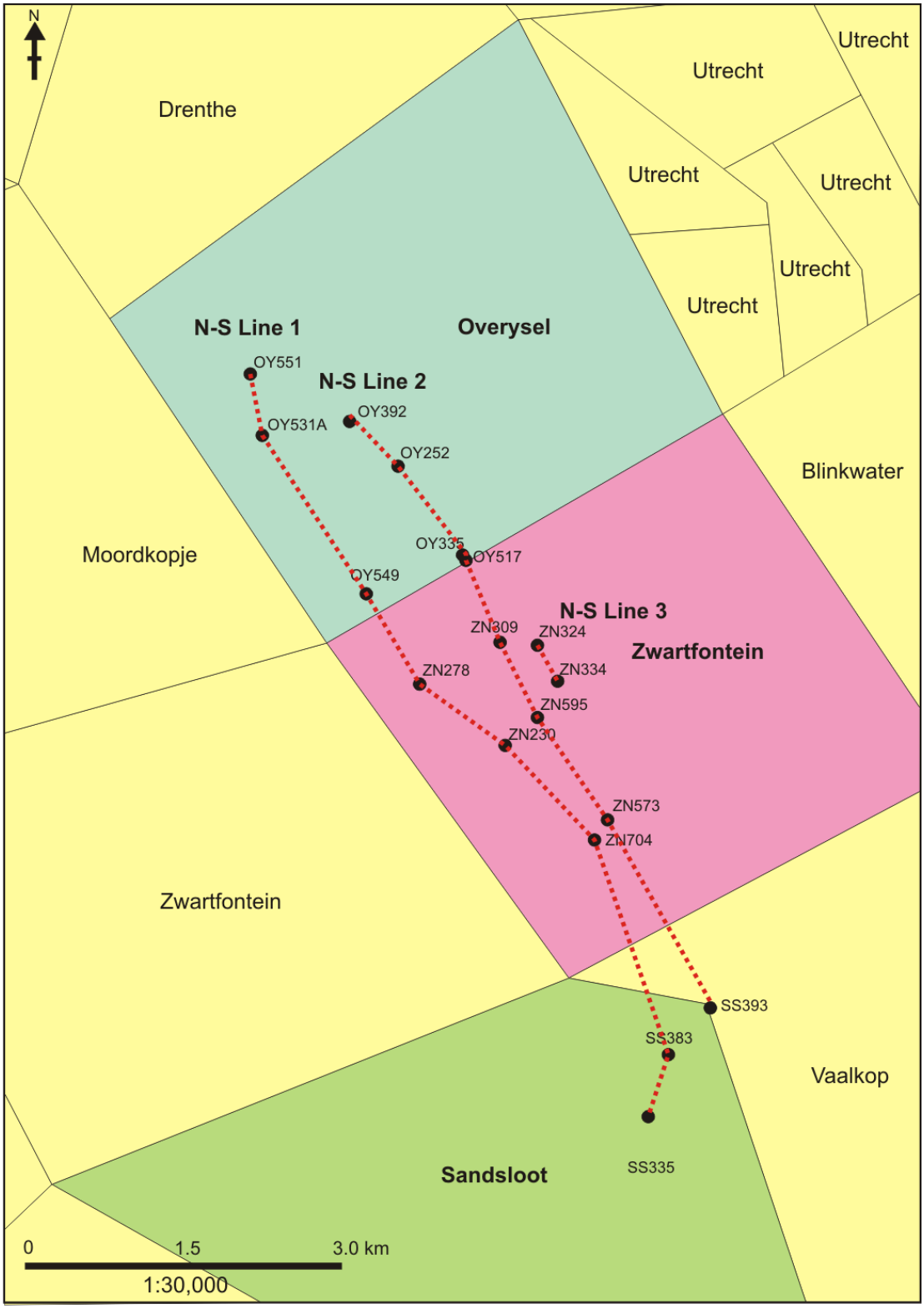

Figure 7.15. Map showing N-S lines.

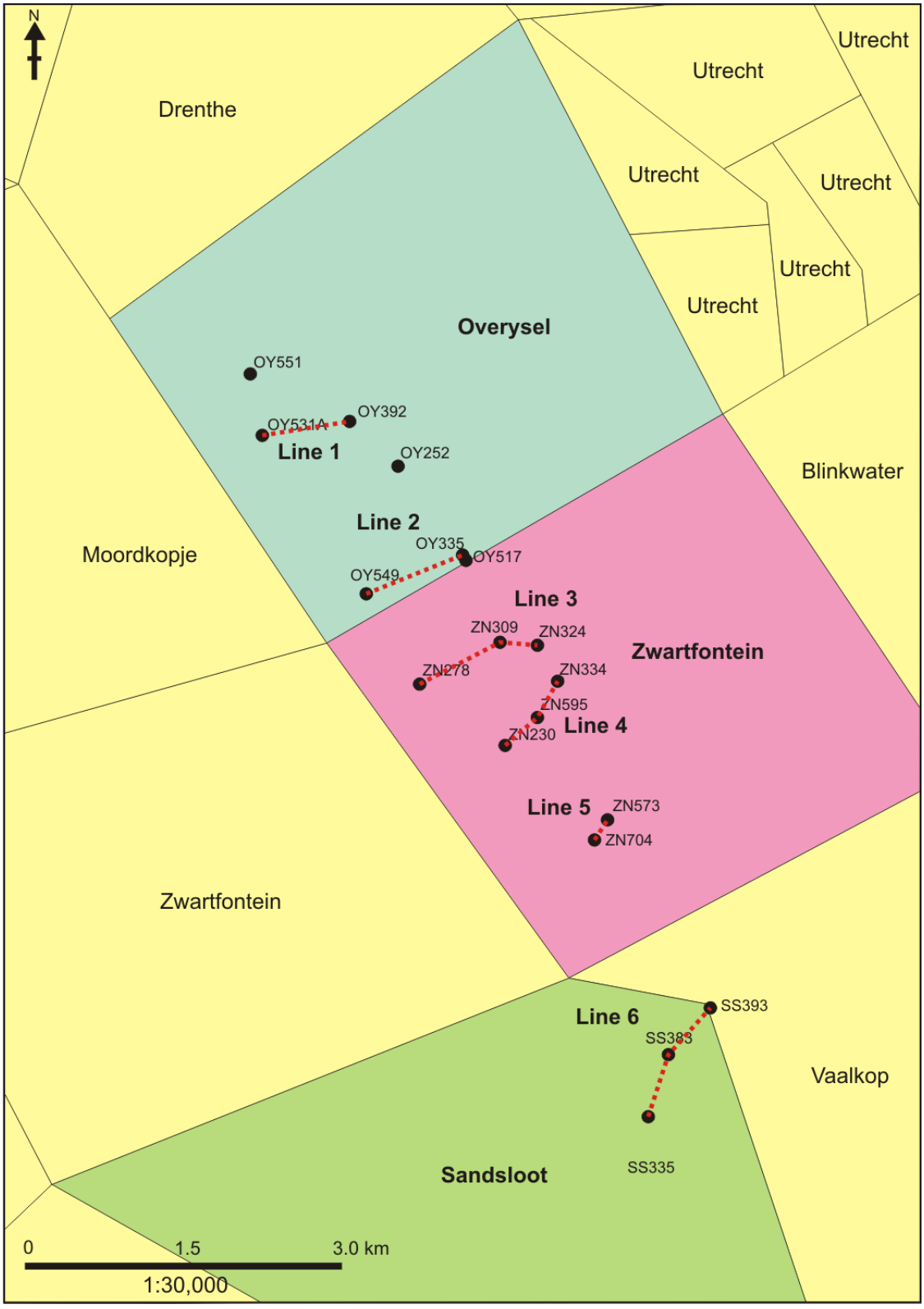

Figure 7.16. Map showing W-E lines.

### 7.5.1 North-south variation

The nature of the PGM vary across the farms, as is shown in the most westerly N-S line (Line 1, fig. 7.17). To the north, the dominant PGM are bismuthides and sulphides with an increase in PGE tellurides recorded in drillhole ZN278. On Zwartfontein, the dominant PGE minerals are alloys, with a corresponding increase in PGE arsenides, moving southwards. ZN704 also contains a significant percentage of PGE sulpharsenides. Sandsloot contains a significant proportion of PGE alloys as well as PGE arsenides. SS335 contains the highest total area of PGE alloys but this is biased by a single grain of rustenburgite with an area of over 3000 $\mu m^2$. Without this grain of rustenburgite, the most dominant phase would be PGE sulpharsenides, followed by PGE arsenides.

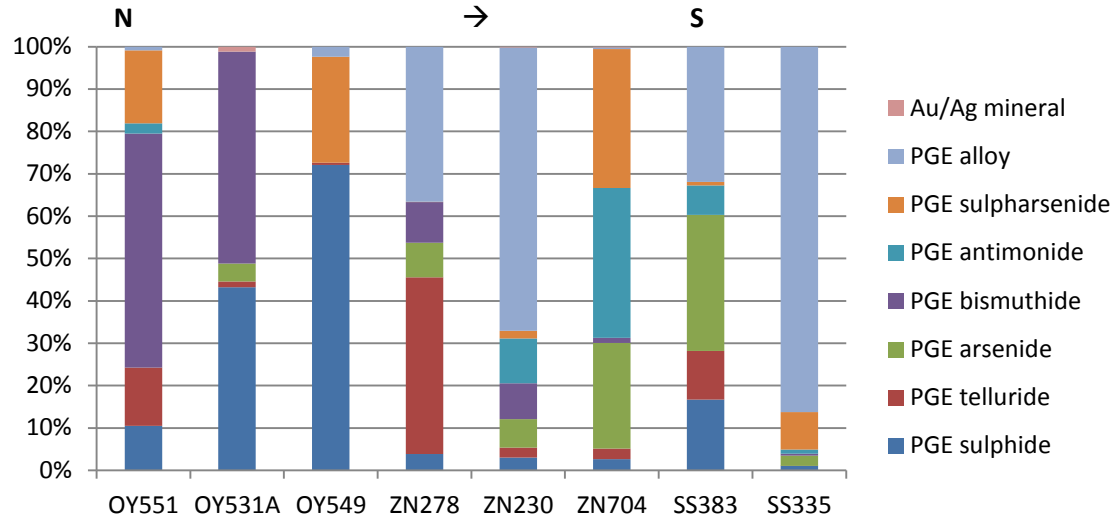


Figure 7.17. Graph showing the distribution of PGM for N-S line 1.

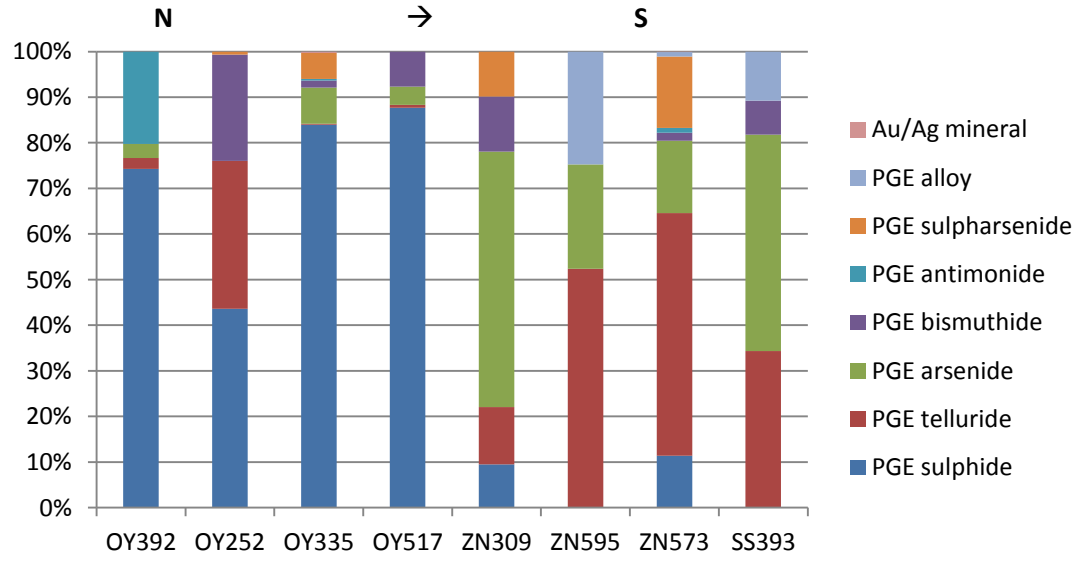


Figure 7.18. Graph showing the distribution of PGM for N-S line 2.

Further to the east of line 1 is line 2 (figure 7.18) which shows that the dominant minerals in the northerly part of the transect are PGE sulphides. On Zwartfontein, the dominant minerals become PGE arsenides, with an increase in the proportion of PGE tellurides moving southwards. ZN595, ZN573 and SS393 also contain PGE alloys but these are not as abundant as in corresponding drillholes further to the west on line 1.

The most easterly transect is line 3 (figure 7.19). It only represents two holes on Zwartfontein. Both contain significant amounts of PGE arsenides, with ZN334 also containing equal amounts of PGE telluride in addition to the PGE arsenides.

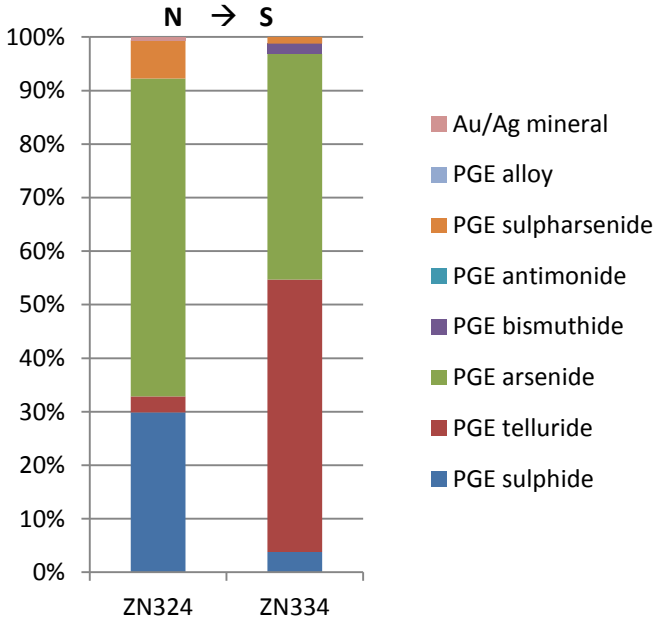


Figure 7.19. Graph showing the distribution of PGM for N-S line 3.

### 7.5.2 West-east variation

The drill holes can be divided into a series of six W-E lines that form dip sections through the chromitite horizons (fig. 7.16).

The most northerly of the W-E lines, line 1, which is situated on Overysel is dominated by PGE sulphides (fig. 7.20). Moving to the E, PGE sulphides decrease with the appearance of PGE antimonides. PGE bismuthides are present in OY531A but not in OY392.

Line 2 comprising holes OY549, OY335 and OY517 is also on Overysel (fig. 7.20). Again, the dominant PGE minerals are sulphides but PGE arsenides are also present as well as sulpharsenides. From west to east, there is a decrease in the proportion of sulpharsenides, with the appearance of arsenides in OY335 and OY517.

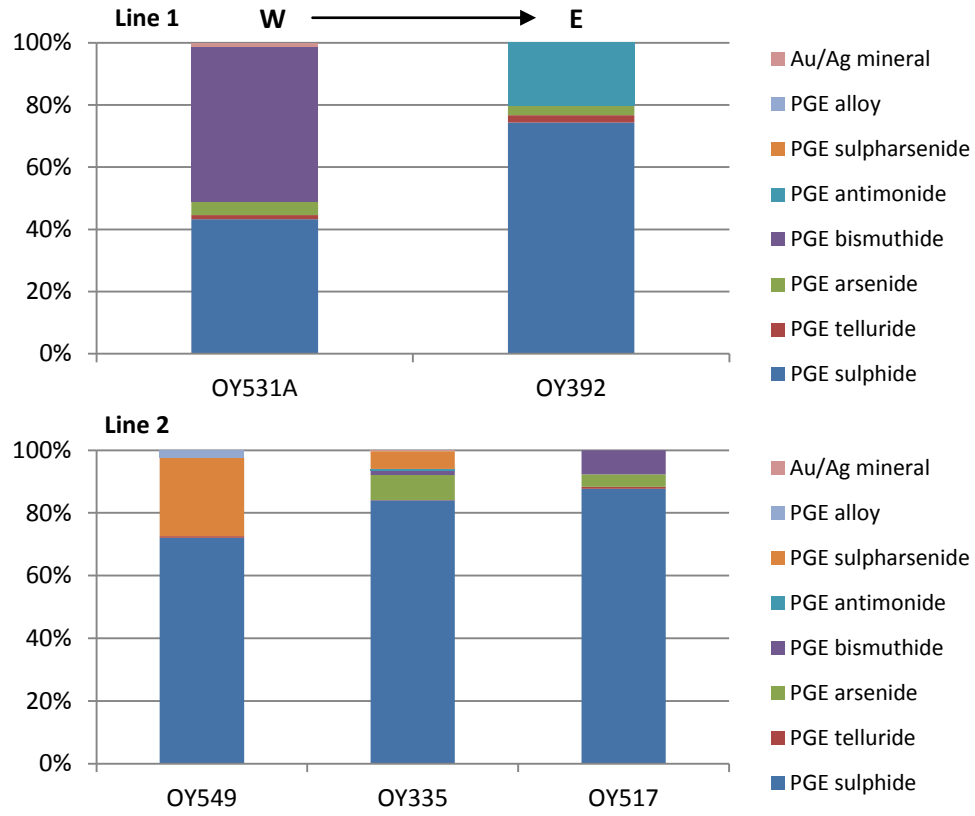


Figure 7.20. W-E graphs showing the distribution of PGM in lines 1 & 2 as shown in figure 7.16.

The first W-E dip section on Zwartfontein is line 3 which consists of ZN278, ZN309 and ZN324 (fig. 7.21). This section includes an abundance of PGE alloys, decreasing to the east. In contrast, there is an increase in PGE sulphides and PGE arsenides but a decrease in PGE tellurides. PGE sulpharsenides are found in both ZN309 and ZN324.

The fourth line of the W-E dip section is one of three lines on Zwartfontein and consists of ZN230, ZN595 and ZN334 (fig. 7.21). Line 4 has a similar relationship to line 3 with a decrease in PGE alloys to the east. The amount of PGE tellurides and PGE arsenides increases moving west to east. No PGE alloys were observed in ZN334.

The last dip section on Zwartfontein is line 5 and contains holes ZN704 and ZN573 (fig. 7.21). Hole ZN704 has the highest proportion of PGE antimonides of any of the sampled drillholes. From west to east there is a decrease in PGE sulpharsenides, PGE antimonides and PGE arsenides but an increase in PGE tellurides and PGE sulphides.

Line 6 contains the three drillholes that were sampled on Sandsloot, SS335, SS383 and SS393 (fig. 7.21). From west to east there is a decrease in both PGE alloys and PGE sulpharsenides and an increase in PGE arsenides, PGE tellurides and PGE bismuthides. The middle hole in this section (SS393) contains PGE antimonides that are absent in the other two drillholes.

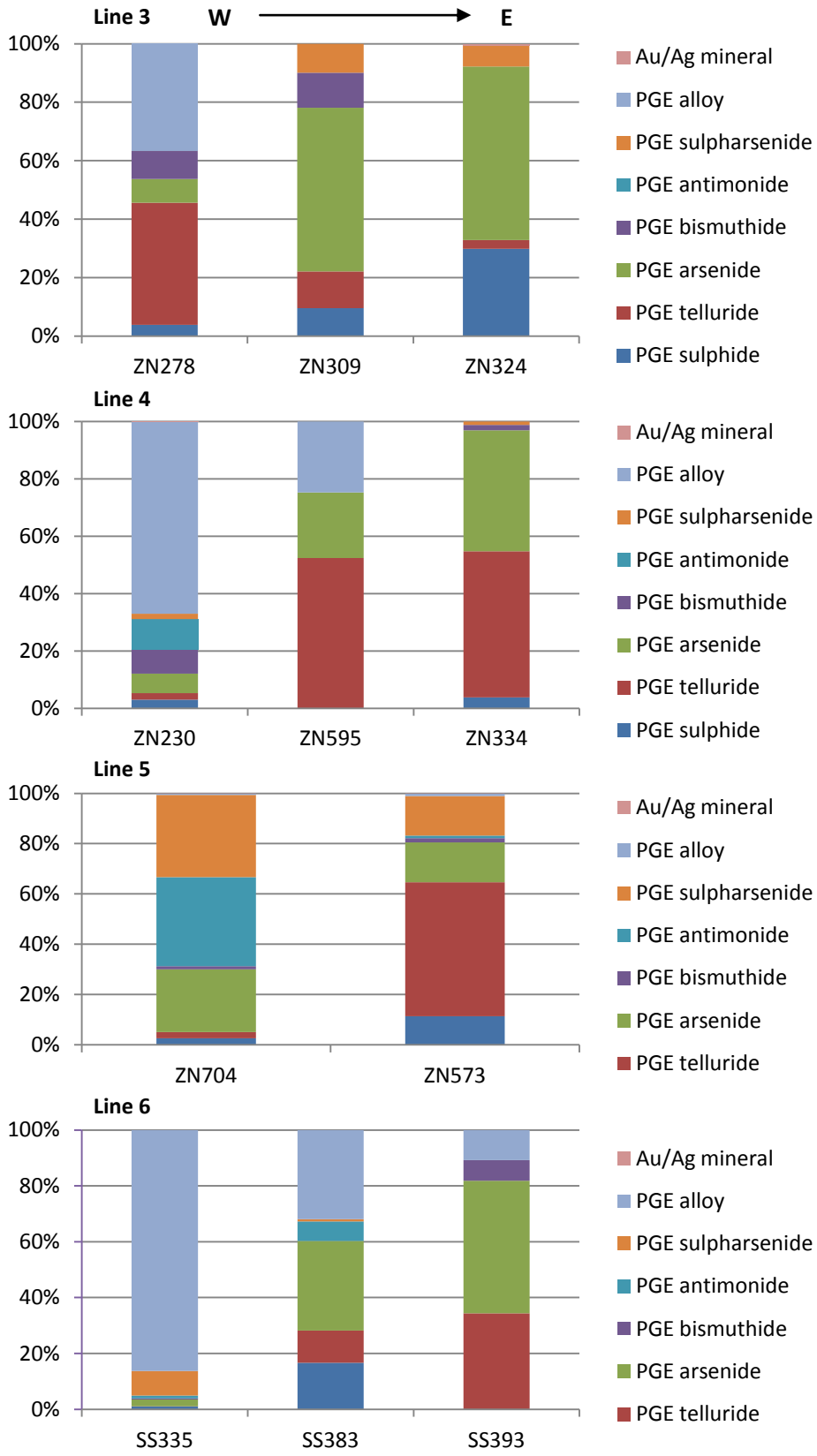


Figure 7.21. W-E graphs showing the distribution of PGM in lines 3-6 as shown in figure 7.17.

## 7.6 Discussion

### 7.6.1 Previous Platreef PGM studies

A number of studies on PGM assemblages in the Platreef have been carried out prior to this research (e.g. Kinloch 1982; Viljoen and Schurmann 1998; Armitage et al. 2002; Hutchinson and Kinnaird 2005; Kinnaird et al. 2005; Holwell and McDonald 2006; Holwell et al. 2006; Holwell and McDonald 2007; Hutchinson and McDonald 2008; Nicholl and Kinnaird 2008; Holwell et al. 2010; Yudovskaya et al. 2010; Yudovskaya et al. 2011; van der Merwe et al. 2012). Most of these studies involved assessing the PGM associations throughout a drillhole or using a series of samples from the faces of the open pits to determine whether there are any variations stratigraphically. The most comprehensive study was carried out by Yudovskaya et al. (2011) who looked at PGM variability within the PGE reefs and chromitites along strike and down dip of the Platreef. The observations made in that study were from 15 drillholes from Tweefontein to Zwartfontein, including data from the Akanani project, down dip and to the west of Anglo Platinum's Zwartfontein property.

In general, data from the Platreef have shown that there is a widespread prevalence of PGE bismuthotellurides along strike in the Platreef with irregular distribution of Pt alloys. Kinloch (1982) was the first to note a significant proportion of Pt-Fe alloys on Zwartfontein. Several studies have illustrated the scarcity of PGE sulphides in the Platreef to the south of Overysel (Armitage et al. 2002; Hutchinson and Kinnaird 2005; Holwell et al. 2006), while studies by Kinloch (1982), Viljoen and Schurmann (1998) and Holwell and McDonald (2007) have reported PGE sulphides on Overysel suggesting an important change in PGE in proximity with the Zwartfontein-Overysel farm boundary and the transition from a dolomite to a granite-gneiss footwall. In contrast, PGM studies from the Merensky Reef and UG2 have shown the widespread predominance of PGE sulphides with more localised development of alloys, tellurides and arsenides (e.g. von Gruenewaldt et al. 1986; Teigler and Eales 1993; Prichard et al. 2004a; Barnes et al. 2008; Rose et al. 2011). Work carried out by Armitage et al. (2002) and Holwell et al. (2006) showed a complete absence of PGE sulphides (including laurite) from the samples obtained from Sandsloot. A further discovery made by Armitage et al. (2002) and Holwell et al. (2006) is that the PGM assemblage in the footwall at Sandsloot is broadly similar to that found in the Platreef package.

This study has shown that although there is a widespread and common prevalence of PGE bismuthotellurides throughout the study area, there are significantly more Pt sulphides and alloys in the chromitiferous Platreef than has been recognised in other studies. Yudovskaya

et al. (2011) also report a high proportion of PGE sulphide minerals in their data set. Data from chromitiferous lithologies studied by Yudovskaya et al. (2011) and van der Merwe et al. (2012) were added to the data set from this study to extend the observations further along strike and down dip. These findings are discussed in a later section.

### 7.6.2 Relationship between PGM and host minerals

#### *Laurite, IPGE alloys and sulpharsenides*

As can be seen from figure 7.22, the vast majority of the PGM analysed in this study are Pt and Pd phases, with minor amounts of PGM containing Os, Ir, Rh and Ru. This is comparable to other Platreef studies that were discussed above. However, as was also shown in studies by Yudovskaya et al. (2010) and Holwell and McDonald (2007), within the chromitite units, there are increased amounts of non Pt and Pd PGM, notably laurite and minerals of the sulpharsenide series (hollingworthite-irarsite-platarsite), compared with other Platreef lithologies. The total area represented by these Ru-, Rh- and Ir-rich phases is however still small at around 10 % total PGE area. It has also been noted elsewhere in the Bushveld Complex (e.g. in the Merensky Reef at Impala Platinum Mines) that the chromite bearing rocks contain more laurite than in the silicate rocks (Mostert et al. 1982).

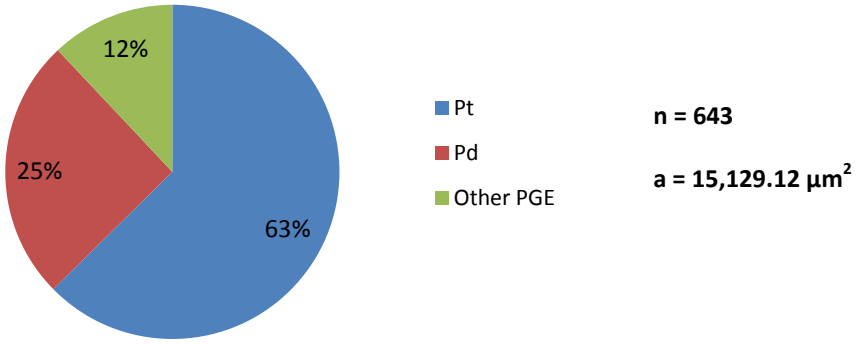


Figure 7.22. Proportions of Pt-, Pd- and other PGE-phase PGM analysed in this study.

The conditions of laurite formation have been studied extensively with experimental data showing that laurite (and IPGE alloys) can start crystallising at temperatures as high as 1200 °C to 1300 °C with $fS_2$ values of -2 to -1.3 (Brenan and Andrews 2001; Bockrath et al. 2004).

It has been suggested that IPGE alloy and laurite crystallise at high temperatures prior to the formation of chromite and olivine (Peck et al. 1992). The presence of PGM inclusions in chromite suggest that these are primary in origin and their occurrence supports the theory

of PGM formation from sulphide undersaturated, but PGE saturated melts. Barnes et al. (1985) suggested that laurite and other IPGE alloys crystallised in the magma and that the chromite nucleated on them. PGM and sulphide inclusions within chromite are discussed further in chapter 9.

The presence of interstitial BMS in the samples containing laurite suggests that sulphide saturation was achieved at some point during the magma crystallisation history. However, it has been shown that the solubility of Ru is very high in sulphide liquids and very low in silicate liquids (Andrews and Brenan 2002) supporting the suggestion that laurite could crystallise directly from a silicate liquid without prior development of a sulphide melt.

The lack of IPGE alloys identified in this study may be a consequence of their instability in the presence of sulphide or silicate melts, as shown by experimental data by Peach and Mathez (1996) and Mathez (1999). However, as highlighted by Greico et al. (2007), these alloys are commonly observed in nature in other PGE deposits. They suggest that the rarity of IPGE alloys, such as in this study, may be due to the mobility the PGEs and other chalcophile elements relative to one another after initial sulphide deposition. Yudovskaya et al. (2011), suggest that the lack of IPGE alloys in association with laurite in samples that they studied in their Platreef study suggests that at elevated temperatures the $fS_2$ was above the Ru-$RuS_2$ buffer (fig. 7.23). The lack of IPGE-bearing PGM and their concentration in solid solution within the BMS is investigated further in chapter 8.

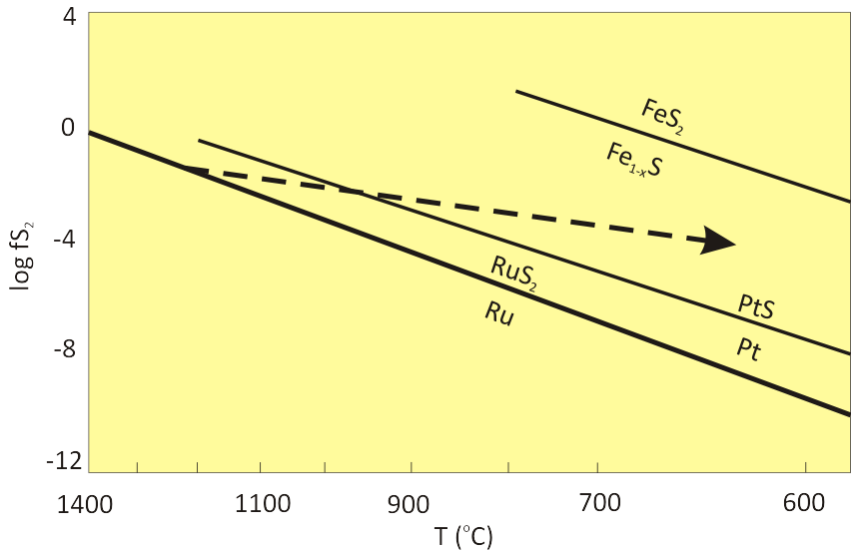


Figure 7.23. Mineral-equilibrium curves for Ru-$RuS_2$ and Pt-Pts buffers as a function of sulphur fugacity and temperature at P=1 kbar. Arrow indicates the shift of conditions from laurite-bearing assemblage to Pt-alloy-Pt sulphide-BMS association (redrawn from Yudovskaya et al. 2011).

Laurite is often documented in this study to form polyphase grains with irarsite, platarsite and hollingworthite which were mostly associated with silicates rather than BMS. It has been suggested by Yudovskaya et al. (2011) that the indistinct boundaries between the sulpharsenides (plus laurite) in polyphase PGM may be due to crystallisation during subsolidus equilibration of an IPGE-As-rich liquid that was originally of stable composition. Yudovskaya et al. (2011) suggest that laurite crystallise first, followed by irarsite and the other sulpharsenides, which may replace or corrode the laurite during their successive growth at decreasing temperatures. This is consistent with observations made in this study, in which the laurite grains are often in the centre of the polyphase PGM.

### *Sperrylite*

The timing of sperrylite formation is difficult to determine due to the wide range of stability temperatures, up to 1000 $^{o}$C (e.g. Coghill and Wilson 1993; Makovicky 2002). Sperrylite in the Platreef forms within a wide range of environments from high-temperature magmatic conditions (isolated sulphide-free occurrences in this study) to hydrothermal environments (coarse metacrystals in the footwall rocks; Nex et al. 2008).

Recent experiments (Helmy et al. 2010) have shown that when Pt is the dominant noble metal, sybhedral sperrylite is an early-forming phase, crystallising before mss. When the dominant noble metal is Pd, exsolution of an immiscible Pd-As melt phase is observed. Some of the sperrylite grains examined in this study are likely to have crystallised early at high temperatures as their irregular form next to corroded chromite crystals suggest they formed before the encompassing orthopyroxene crystals. There are other instances where sperrylite occurs as an intergrowth with BMS in a silicate matrix, again suggesting that the arsenides formed prior to the crystallisation of the encompassing silicates. Sperrylite crystals occur as sybhedral crystals in all assemblages, commonly with BMS in pyroxene and are often associated with Pt-Rh-Ir sulpharsenides in chromite. They also form intergrowths with hollingworthite. Occurrences of fractured sperrylite have been noted where they are filled with later bismuthotellurides, Au-Ag alloys, quartz and amphiboles.

### *Cooperite and braggite*

At high temperatures (around 1000 $^{o}$C), cooperite has been shown experimentally to be in a stable relationship with pyrrhotite (Skinner et al. 1976), whereas braggite has been shown to be stable only below temperatures of 900 $^{o}$C (Makovicky 2002). This has also been demonstrated experimentally for the Merensky Reef (Verryn and Merkle 2002) which showed the high temperature nature of cooperite as one of the first phases to exsolve from

a crystallising melt at around 1100 $^{o}$C in a PdS-PtS-NiS system, whereas braggite exsolved at a lower temperature of 1000 $^{o}$C.

The close association of cooperite with BMS (fig. 7.24) suggests that during formation the sulphur fugacity was close to the Pt-PtS buffer (fig. 7.23).

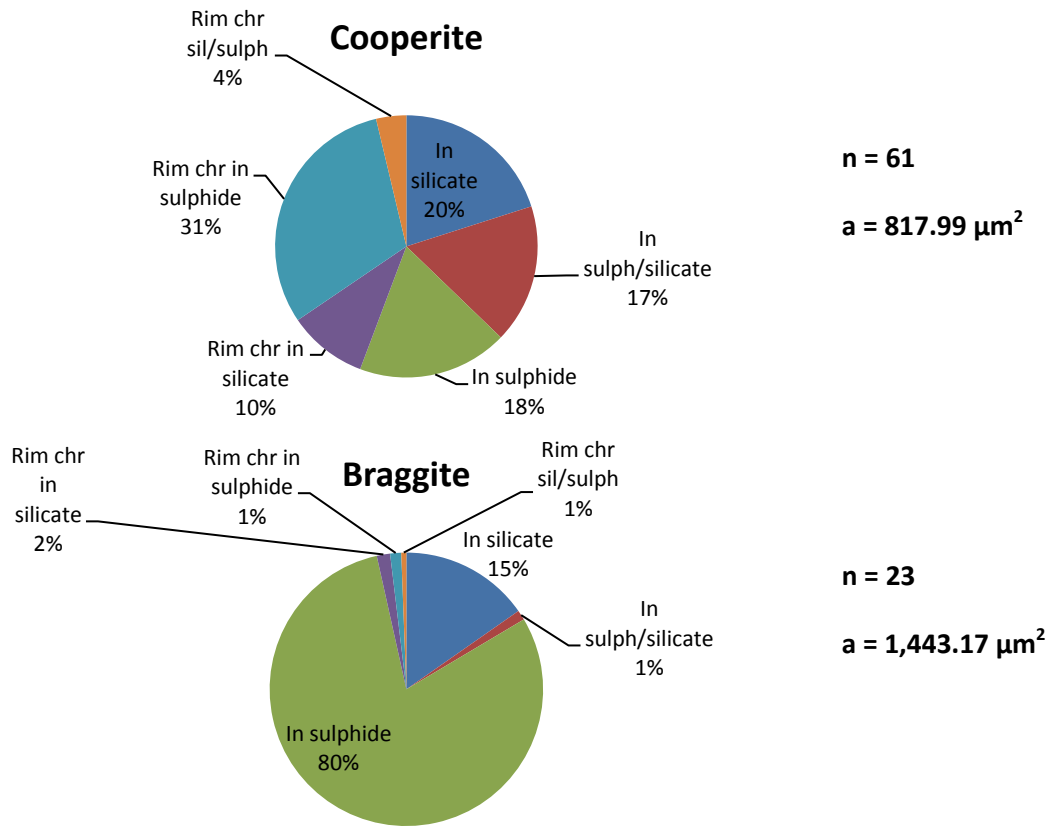


Figure 7.24. Distribution of cooperite and braggite within the Platreef chromitites.

### *Pt-Fe alloys*

The origin of Pt-Fe alloys within magmatic deposits such as the Platreef remains contentious due to their wide range of formation temperatures and environments that include ophiolites, kimberlites and layered intrusions (Peregoedova and Ohnenstetter 2002).

Where Pt-Fe alloys were identified in the Stillwater Complex, Godel and Barnes (2008) suggested that they formed from exsolution from mss at magmatic conditions due to the strong association with the BMS. This has also been suggested by Kingston and El-Dosuky (1982) to occur in the Merensky Reef. Li and Ripley (2006) showed that some of the Pt-Fe alloys in the Stillwater Complex formed by the replacement of cooperite or braggite during desulphurisation caused by interaction with a sulphide undersaturated hydrothermal fluid. These replacement textures, however, are not seen in the Platreef samples. In addition figure 7.25 shows that the association of the Pt-Fe alloys with sulphide is limited, with the

majority of those identified in association with silicates or on the edges of chromite grains without obvious sulphide, suggesting a limited relationship with BMS formation.

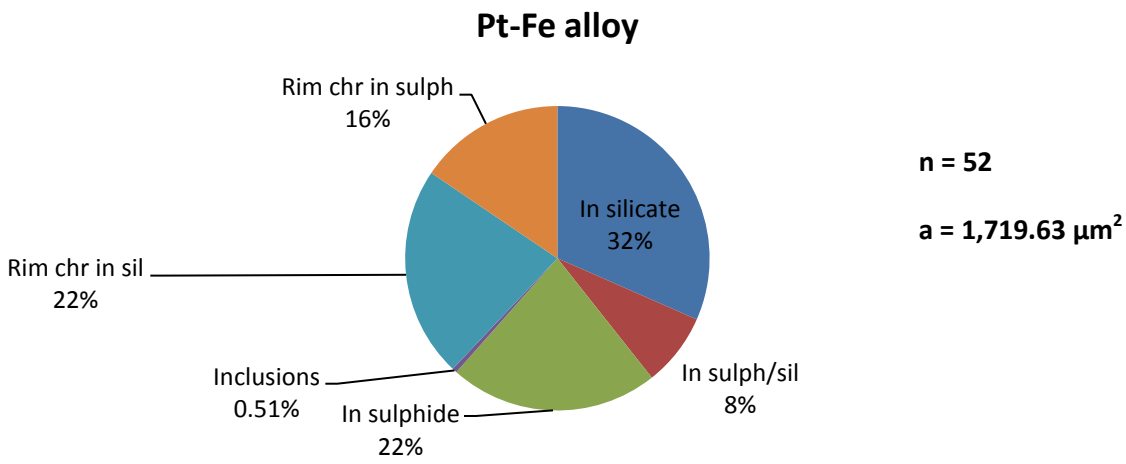


Figure 7.25. Distribution of Pt-Fe alloys within the samples from the Platreef.

Many of the Pt-Fe alloys in this study show a honeycomb texture rather than occurring as sybhedral crystals. Similar textures have been identified in rest of the Bushveld, such as in areas around the Pilanesburg Complex where they account for a significant proportion of the PGM identified (Kinloch 1982). They have also been identified in the dunite pipes of the eastern Bushveld and the texture is attributed to volatile activity (Kinloch and Peyerl 1990). Kinloch (1982) attributed the predominance of isoferroplatinum to the dissolution of Pt sulphides in these volatile rich environments.

### *Association with base metal sulphides*

BMS occur in relatively low proportions in the Bushveld Complex, when compared to other magmatic sulphide deposits, ranging from 1- 5 % modal in the Merensky Reef (Barnes and Maier 2002a) to <0.1 % modal in the western limb UG2 (Barnes and Maier 2002a), with the Platreef containing around 1 % modal (von Gruenewaldt et al. 1989). The PGM identified in this study, apart from the Pt-Fe alloys, clearly have a strong spatial association with the BMS suggesting that the formation of sulphides was crucial to the enrichment of PGE in the Platreef. This is consistent with other studies carried out in the Bushveld Complex as a whole. It has been noted that the PGM have a greater association with pentlandite and chalcopyrite compared to pyrrhotite (Yudovskaya et al. 2011). This is also noted in other Platreef studies and the Bushveld Complex as a whole, and has been attributed to the greater solubility of PGE in the former two base metal sulphides (Godel et al. 2007; Hutchinson and McDonald 2008).

Early studies on the association of PGM with BMS suggested that the PGM formed on the edges of BMS which is consistent with the view that the PGM formed prior to BMS crystallisation (e.g. Vermaak and Hendriks 1976). It was suggested that the PGM were trapped by the sulphide liquid as it crystallised or alternatively the PGM that crystallised attached to the silicates were then surrounded by an interstitial sulphide liquid. In the wider Bushveld, the presence of PGM in sulphide free assemblages has been linked to the result of magmatic desulphurisation following Fe loss due to exchange between S and chromite (e.g. Naldrett and Lehmann 1988; Naldrett and von Gruenewaldt 1989; Naldrett et al. 2012). However, the chromite concentrations are not high enough in the Platreef for this to be a viable explanation when compared to the UG2 where this model has been developed.

Once the individual farms on the Platreef are studied in greater depth, there appears to be a decoupling between the BMS and PGE, which has also been reported by Holwell and McDonald (2006). This is suggested to be related to the variation of the country rocks along strike. In the south, interaction with the calc-silicates has resulted in decoupling of PGE from BMS with the majority of PGM sitting within the silicates. However in the north, where the country rock consists of increasing amounts of Archaean granite/gneiss, there is a stronger association of PGE with BMS. Where PGM occur as satellite grains in silicates with BMS nearby, it has been suggested (Holwell et al. 2006) that there has been a regression of the BMS boundary as a result of fluid activity. This has also been noted further to the south on Macalacaskop (Hutchinson and Kinnaird 2005) and would account for the number of lower temperature PGM (e.g. bismuthotellurides and antimonides) that have been identified in the silicates that would have crystallised during or after BMS crystallisation.

### 7.6.3 Model for spatial distribution of PGM observed in the study area

When the drillholes (from this study in addition to those from Yudovskaya et al. (2011) and van der Merwe et al. (2012)) are grouped according to similar predominant assemblages of PGM in the Lower Chromitite zone, a bulls-eye pattern emerges on the map (figs. 7.26 & 7.27). This reveals zones in the chromitiferous Platreef that are dominated by PGE alloys, apparently surrounded by PGE arsenides and then PGE sulphides. This pattern appears to be analogous to regional patterns of PGM observed in the Merensky Reef by Kinloch (1982) that were ascribed to local centres of enhanced heat and volatile activity (fig. 7.25). Kinloch linked these centres to feeder zones that supplied magma and volatiles to the chamber at the time the Merensky Reef was forming and proposed that these centres were represented by gravity highs close to the outcrop of basic rocks in the Bushveld Complex. The view that individual gravity highs represent individual feeders in the strictest sense has

been challenged (e.g. Campbell 2004) but they still represent anomalously thick zones of mafic rocks and the strong associations between these and the variation in PGM is clear and cannot be discounted.

Heat and volatile activity in the proximity of a feeder should have a profound effect on the magma and any entrained sulphide liquid, especially on crystallising ore minerals. These sites would have a significant primary role to play when the sulphide and precious metal mineralisation is considered. Kinloch (1982) proposed that in the centres of feeders Pt-Fe alloys are dominant. Under relatively high $fO_2$ conditions, caused by the release of volatiles by late magmatic injection, sulphur is lost from the sulphide liquid and as Pt does not form an oxide readily, and being a siderophile element, it will alloy with Fe. Around this alloy-rich zone an arsenic front is developed, dominated by sperrylite. This in turn is surrounded by and outer zone of PGE sulphides.

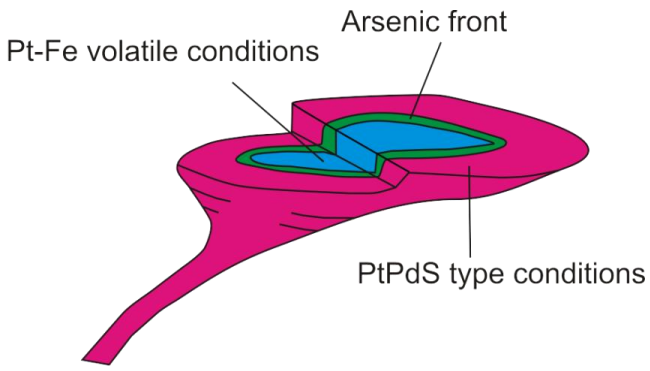


Figure 7.26. Kinloch (1982) feeder zone model.

The lateral extent of the feeder would be limited due to magma viscosity, temperature gradients, and the feeder size. Greater amounts of PGE in solid solution are thought to occur in the feeder environment due to the higher $fO_2$ and volatile activity, resulting in lower $fS_2$, which would dissolve existing BMS and would inhibit the mass of BMS able to form in the feeder zone.

Further from the feeder influence, a somewhat lower $fO_2$ (and correspondingly higher $fS_2$) might result in the crystallisation of 'normal' PGE-sulphide minerals. The PGM zoning described here provides further support to earlier suggestions (McDonald et al. 2009; Yudovskaya et al. 2011) that a magma feeder is present in the Zwartfontein portion of the Central Platreef. This feeder is likely to have played an important role in the genesis and development of the mineralisation.

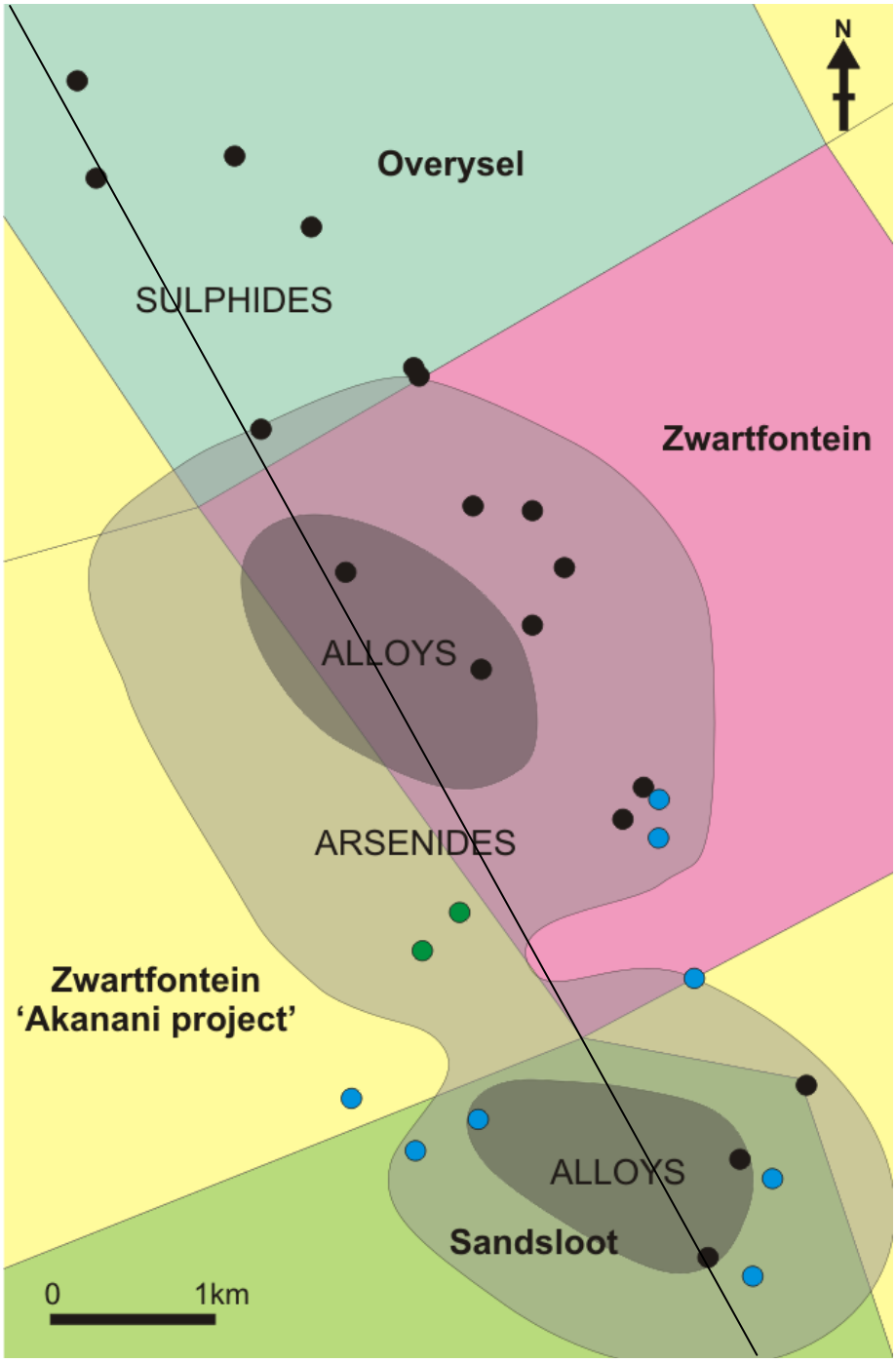


Figure 7.27. Map showing the location of the 18 drill holes sampled from Central Sector (black circles). Green circles data from van der Merwe et al. (2012) and blue circle data from Yudovskaya et al. (2011). Line represents the schematic cross section shown in figure 7.29.

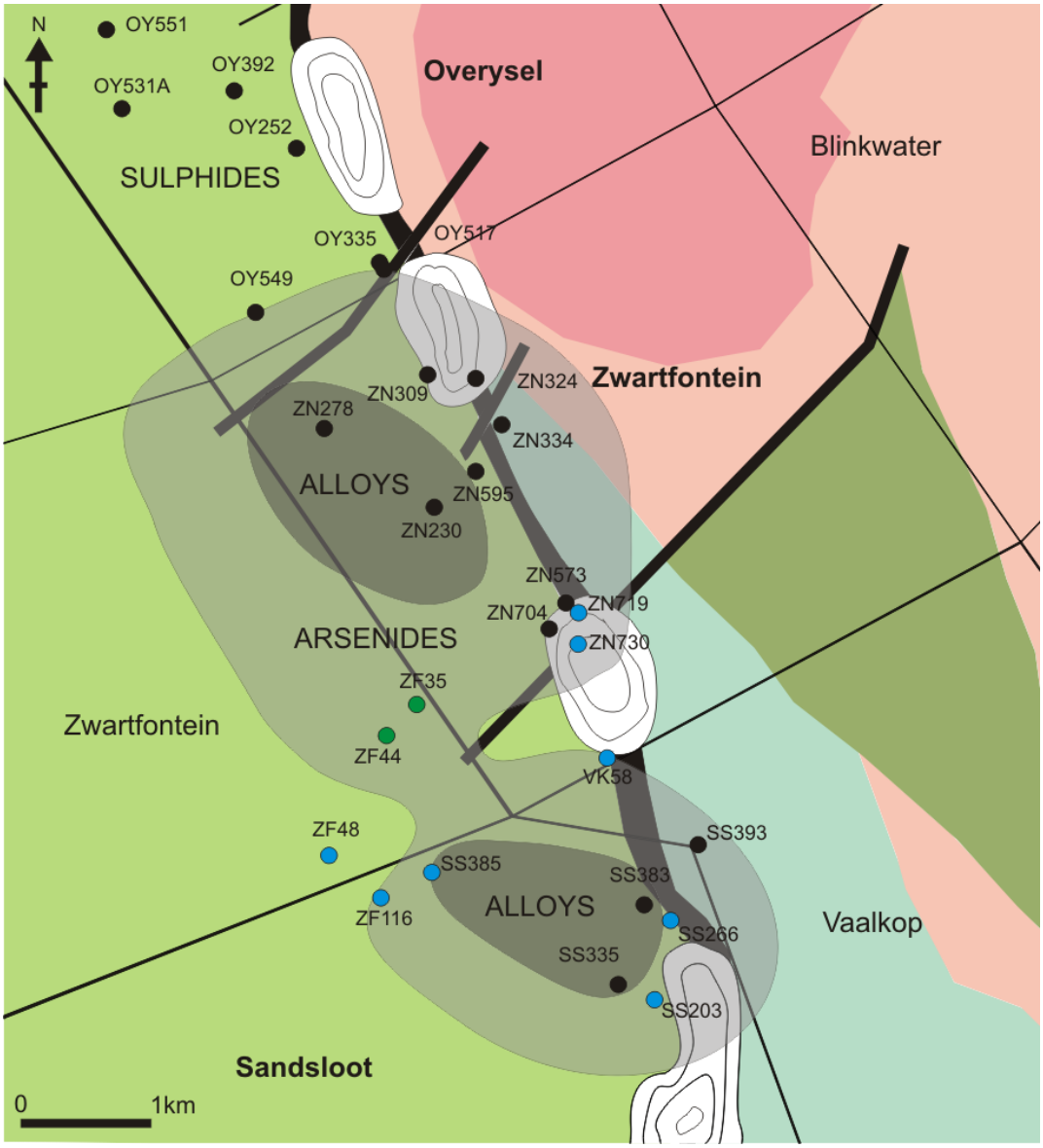


Figure 7.28. Map showing location of the 18 drill holes sampled from Central Sector (black circles) with additional lithological and structural data (for key see fig. 3.1). Green circles data from van der Merwe et al. (2012) and blue circle data from Yudovskaya et al. (2011).

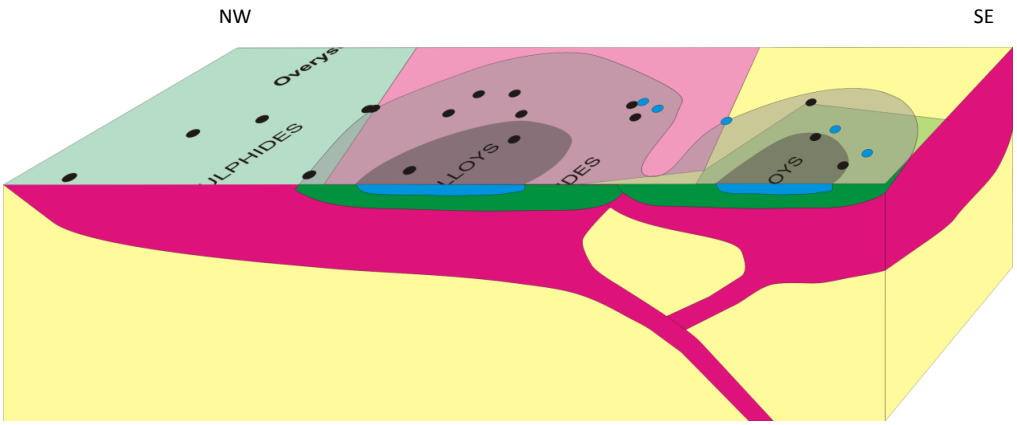


Figure 7.29. 3D block model along X-Y cross section. Different colours at surface represent different farms (L-R: Zwartfontein, Overysel and Sandsloot)

As has been shown in figure 7.27, there are two centres rich in alloys surrounded by arsenides. These centres could potentially be linked (as shown in figure 7.29) or could be separate systems. The structural zones shown in figure 7.28 are also potentially important as these might represent the pathways taken by the fluids, especially on Zwartfontein where numerous fault zones have been identified.

The staging chamber model proposed by McDonald and Holwell (2007) for the formation of the Platreef can also account for the prevalence of the semi-metal association seen within the samples. Once the parental magma reached sulphur saturation, an immiscible sulphide liquid separated from the silicate melt. The sulphide droplets formed, and being denser than the surrounding silicate melt, collected at the bottom of the staging chamber. In addition to PGE, Cu, Ni and Au, the semi-metals in the parental magma were also collected by the sulphide liquid due to the high distribution coefficients between the silicate melt and the sulphide liquid. New magma passing over and around the droplets would have increased the concentration of PGEs, Ni, Cu and semi-metals within them and depleted the concentration of these elements in the magma leaving the chamber (McDonald et al. 2009).

There is a strong spatial relationship between the PGE alloys and antimonides as shown in figure 7.30. Studies carried out in the dunite pipes in the Bushveld Complex (Tarkian and Stumpfl 1975; Peyerl 1982) have attributed the presence of Pt-Pd antimonides to areas of high volatile activity. Given that the highest concentrations of PGE antimonides occurs on Zwartfontein, this is consistent with the general location of the feeder zone in the model described above.

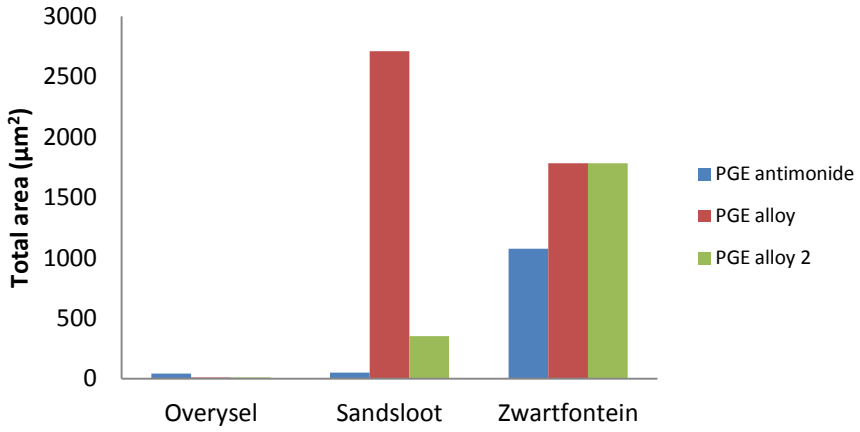


Figure 7.30. Bar chart showing spatial relationship between PGE antimonides and PGE alloy on different farms. PGE alloy 2 represents the total area with the anomalous 3000 µm$^2$ rustenburgite grain removed from the Sandsloot samples.

Kinloch (1982) suggested that no pattern is observed for the PGE bismuthotellurides in the Merensky Reef as they represent background norm concentration for PGM in basic magmas. This is supported by LA-ICP-MS work on sulphide inclusions within chromite presented in chapter 9 and also by Holwell and McDonald (2010) who showed that the presence of trapped micro-inclusions of Pt-Bi-Te minerals in all sulphide phases implies that the Bi and Te were present within the initial sulphide liquid at high temperatures.

While a feeder system is suggested to have caused the observed PGM distribution on Zwartfontein, the nature of the footwall at Sandsloot complicates the model. Although the primary control on the PGM assemblage in the Platreef is suggested to be magmatic, some reworking of the PGM assemblage has obviously occurred due to the influence of late magmatic or hydrothermal fluids derived from reactions with the country rock and with xenoliths in the Platreef. The origin of the fluid within the system is likely to be magmatic, based on isotope data from Harris and Chaumba (2001). These fluids were dominant in mobilising the PGM and could have carried them into the footwall as seen at Sandsloot (Armitage et al. 2002). However, this fluid fluxing would have occurred at the syn-magmatic stage rather than involving hydrothermal fluids after solidification of the rocks (Holwell et al. 2006). PGM that have been cross cut by secondary minerals such as tremolite or actinolite have been affected by such processes but this is not observed in any of the samples within this study.

It has also been noted on Sandsloot that Pt-Fe alloys are common in the upper portions of the reef that experienced replacement by Fe-rich fluid (Holwell et al. 2006). This occurs in the SW portion of the pit. Armitage (2011) proposed this could be related to Penge BIF on the northern limb of the dolomite tongue forming the hanging wall to the Platreef. In addition, the effect of the calc-silicate country rock is not constrained to Sandsloot as serpentinised xenoliths are often found within drillholes on the more northerly farms of Zwartfontein and Overysel, suggesting that fluid alteration may have a local effect on PGM mineralisation within the surrounding lithologies, although not to the same extent as on Sandsloot where the Malmani dolomite formed the floor and roof of the Platreef.

When comparing the variation in PGE alloys across the 3 farms, it has become evident that the majority of Pd alloys are concentrated on Sandsloot (fig. 7.31) and it is suggested to be related to the proximity to the dolomite tongue and/or the presence of a former BIF hanging wall. Reaction between the magma and the dolomite caused the release of $CO_2$ which led to higher $fO_2$ conditions conducive of alloy formation. However, unlike with the

feeder type effect to the north on Zwartfontein that produced Pt-alloys at high temperatures, the Pd-alloys were likely produced at lower temperatures, potentially as low as 400°C, and may have formed during the waning of the fluid system. It is also suggested that the increased occurrence of Pt-alloy crystals observed in samples from Sandsloot, rather than the dominance of the honeycomb textures observed in the farms further to the north, is suggestive of lower temperatures of formation (Yudovskaya et al. 2011). The association of Pd alloys and $Pt_3Fe$ crystals was also observed by Kinloch (1982). Potentially, the feeder system at Zwartfontein could have been the primary system with the Sandsloot system representing a less active system with slightly lower temperatures.

The presence of potarite (Pd-Hg) on Sandsloot also suggests fluid activity in the area as this PGM has been shown to be typically associated with relatively low temperature hydrothermal activity (e.g. Kinloch 1982; McLaren and De Villiers 1982; Arai et al. 1999).

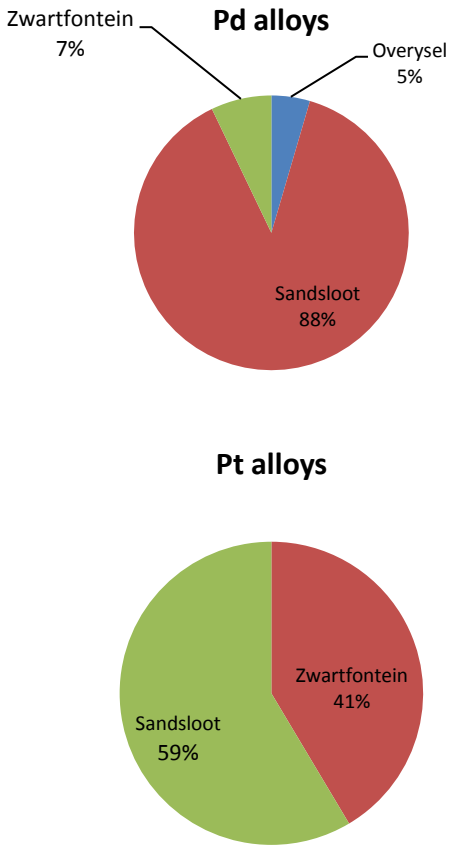


Figure 7.31. Distribution of Pd- and Pt-alloys across the three farms.

A PGM assemblage rich in Pd-Pb alloys (zvyagintsevite and plumbopalladinite) at Sandsloot (fig. 7.32) agrees with observations made by Holwell et al. (2006) that fluid activity, resulting from interaction of the Platreef magma with the calc-silicate country rocks, has affected the PGE mineralogy.

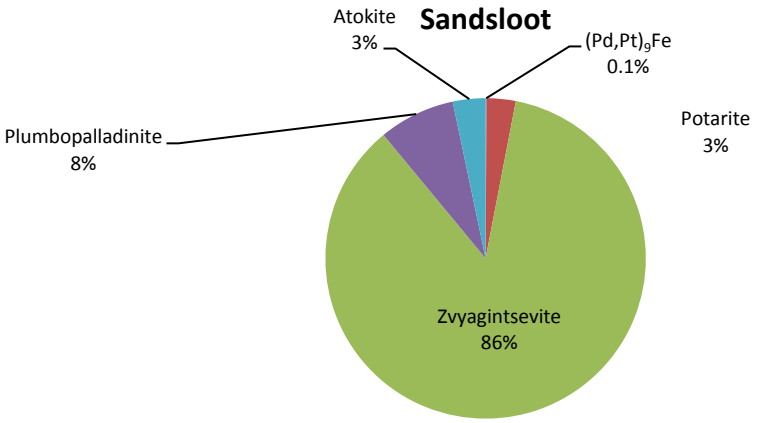


Figure 7.32. Pd-alloy PGM identified in samples from Sandsloot.

Holwell et al. (2006) suggested that in the most altered lithologies, a Pt-dominated assemblage is expected due to the more mobile Pd being transported away by the fluids. However, within the samples from this study, the lack of significant alteration and close proximity to BMS suggests that the PGE may not have been significantly mobilised during fluid activity. As a result, a greater occurrence of Pd-bearing phases have been identified, consistent with observations by Prichard et al. (2004b) in similar settings. Hydrothermal PGE deposits in which PGM formed during alteration have a dominant association of Pd (and to lesser extent Pt) with the semi-metals and alloys (Augé et al. 2002).

The lack of hydrothermal redistribution, caused by interaction with the volatile-rich country rocks, has led Holwell and McDonald (2007) to suggest that the PGM mineralisation at Overysel, where the country rocks contain significant amounts of granite gneiss, represents the most 'primary' style of mineralisation. Similar 'primary' assemblages have been studied on Tweefontein (Nicholl and Kinnaird 2008) in the thick reef above the anhydrous BIF footwall.

## 7.7 Conclusion

Previous studies on PGM assemblages in the Platreef have shown that various lithologies are characterised by distinct PGM assemblage. The change in PGM assemblages along strike has previously been explained as a consequence of different footwall lithologies. It has been suggested that the PGM assemblages at Overysel and Tweefontein represents the most 'primary' style of mineralisation due to their unreactive country rocks (granite and BIF, respectively).

By investigating the variation along strike and down dip within the chromitite unit, this study has shown that PGM assemblage is not strictly controlled by footwall lithology. It has been shown that the PGM types change within areas where the country rock remains the same.

Based on the observed mineralogy and lateral variation a model has been proposed in which the different PGM associations can be ascribed to the effects of differing temperature and $fO_2$ conditions depending on the proximity of the samples to the feeder.

The characteristics of the PGM documented in this study from the chromitite units display the results of orthomagmatic processes, with any hydrothermal redistribution occurring close to, or at the time of Platreef formation.

# Chapter 8: PGE Concentrations Of The BMS On Zwartfontein

## 8.1 Introduction

Base metal sulphides, in orthomagmatic Ni-Cu-PGE deposits, are important carriers of PGE, in addition to other chalcophile elements (e.g. Cu, Ni, Pb, Au, Ag, Co, As, Bi, Te, Sb and Se). The distribution of PGE in BMS that results from the fractionation of the sulphide liquid has been shown experimentally (e.g. Barnes and Picard 1993; Li et al. 1996; Barnes et al. 1997; Barnes et al. 2001; Brenan 2002; Peregoedova and Ohnenstetter 2002; Peregoedova et al. 2004; Mungall et al. 2005) and empirically (e.g. Naldrett et al. 1982; Zientek et al. 1994; Prichard et al. 2004b).

The general process of BMS fractionation is illustrated schematically in figure 8.1. At around 1200 °C, following the separation of a Fe-Ni-Cu sulphide liquid from the mafic silicate magma, the sulphide liquid contains dissolved PGEs, Au and semi-metals (plus Ni, Cu and Fe). The PGE were originally collected by the sulphide portion of the melt due to the high partition coefficients values between the sulphide and silicate liquid (e.g. Peach et al. 1990; Fleet et al. 1993; Crocket et al. 1997).

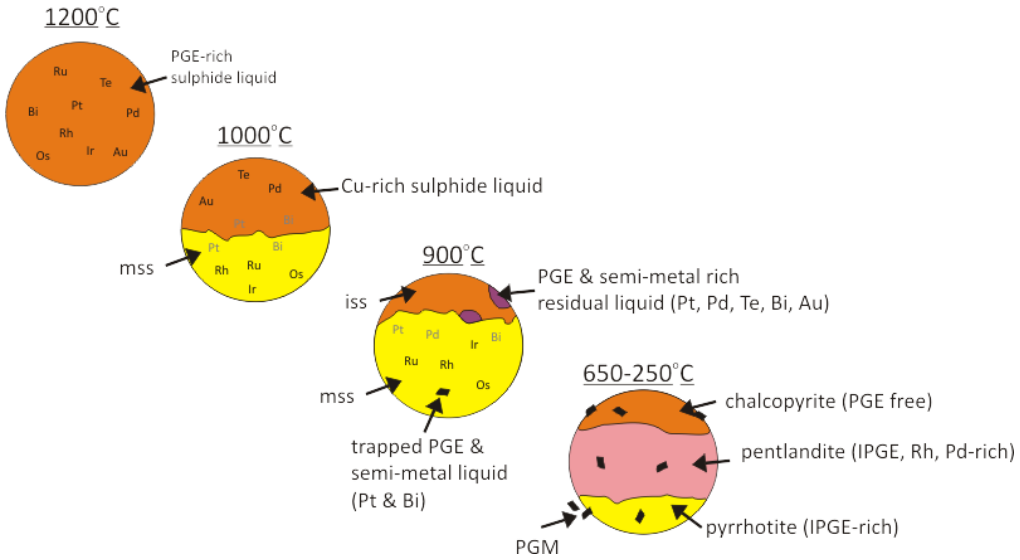


Figure 8.1. Schematic representation of a fractionating PGE-rich sulphide droplet (adapted from Holwell and McDonald 2010).

On cooling to approximately 1000 °C, the first phase to crystallise from the sulphide liquid is monosulphide solid solution (mss). Based on the experimentally determined partition coefficients, IPGEs, Rh, Ni and Co preferentially partition into the Fe-rich mss, while Pt, Pd, Ag, Au, Cu and the semi-metals behave incompatibly and remain in the Cu-rich residual fractionated sulphide liquid (e.g. Fleet et al. 1993; Barnes et al. 1997). It has also been shown that the partition coefficients strongly depend on the Fe/S ratio of the magmatic

sulphide liquid (Barnes et al. 2001) and increase of the S content, in both the sulphide liquid and in the mss, has been shown to cause an increase in the partition coefficients of Ni, Cu and PGE (Li et al. 1996).

Further cooling to 900 $^{o}$C causes iss (intermediate solid solution) to crystallise out of the Cu-rich residual liquid. Pt, Pd and Au concentrate in an immiscible semi-metal rich melt rather than partitioning into iss due to incompatibility (Peregoedova 1998) and this melt is suggested to remain liquid after iss has crystallised (Helmy et al. 2007). Once the temperature reaches about 650 $^{o}$C, the mss recrystalises to pyrrhotite and pentlandite and the iss portion recrystalises to chalcopyrite (± cubanite; Barnes et al. 2006). If no discrete PGM crystallise then pyrrhotite and pentlandite should be enriched in Os, Ir, Ru and Rh, and the chalcopyrite enriched in Pt, Pd, Ag and Au. However, numerous studies (c.f. Dare et al. 2010) have shown the lack of PGE enrichment in chalcopyrite and it has been suggested that post-magmatic processes have played a role in this distribution, specifically the enrichment of Pd in pentlandite as a result of diffusion from iss. Crystallisation of the semi-metal rich liquid forms discrete PGM around the margins of the BMS.

The bulk Pt/Pd ratio in the central Platreef, and specifically the chromitites, is approximately 1:1 (McDonald and Holwell 2011), a ratio replicated when analysing the bulk rock chromitite samples for this study. However, as seen from chapter 7, a dominance of Pt-bearing minerals has been identified in the samples, accounting for more than 60 % of the PGM observed (fig. 8.2). As a result, a LA-ICP-MS study was carried out on the base metal sulphides present in a number of samples from Zwartfontein in order to establish the PGE contents of the various sulphides and to see whether the unaccounted portion of Pd is hosted in the sulphide minerals.

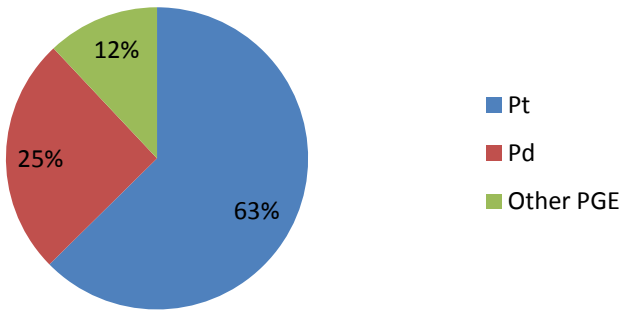


Figure 8.2 Proportions by area of minerals identified in chapter 7 that are Pt-, Pd- or other PGE-dominated within the chromitites.

## 8.2 Methods

LA-ICP-MS was chosen because it is capable of analysing trace (sub-ppm) levels of precious metals within the BMS. LA-ICP-MS has successfully been used to determine the PGE content in the BMS of numerous deposits including the Platreef (e.g. Holwell and McDonald 2007; Hutchinson and McDonald 2008), the Merensky Reef (e.g. Ballhaus and Sylvester 2000; Godel et al. 2007; Osbahr et al. 2013) J-M Reef in the Stillwater Complex (e.g. Godel and Barnes 2008), as well as sulphides for the Creighton mine in Sudbury (e.g. Dare et al. 2010) and Noril'sk (e.g. Barnes et al. 2006).

PGE not present in PGM but in trace amounts in the interstitial base metal sulphides in the samples were measured using laser ablation-inductively coupled plasma-mass spectrometry (LA-ICP-MS). The aim was to determine whether BMS are the principal hosts for some PGE and the extent to which individual elements preferentially partition into a specific BMS associated with the chromitites.

A total of 7 chromitite samples that contained the greatest percentage of visible BMS were selected to represent the 7 drill holes spread over Zwartfontein farm (fig. 8.3). The samples used in this study are a selection from the polished blocks that were used for the PGM study in chapter 7. They were analysed using the New Wave Research UP213 UV laser system coupled to a Thermo X Series ICP-MS at Cardiff University. The isotopes $^{33}S$, $^{59}Co$, $^{61}Ni$, $^{65}Cu$ and $^{66}Zn$ were analysed to monitor the composition of the sulphides together with the precious metal isotopes $^{99}Ru$, $^{101}Ru$, $^{103}Rh$, $^{105}Pd$, $^{106}Pd$, $^{189}Os$, $^{193}Ir$, $^{195}Pt$ and $^{197}Au$. The isotopes of the semi-metals $^{75}As$, $^{82}Se$, $^{125}Te$, $^{121}Sb$, and $^{209}Bi$ were analysed because of their association with the PGE as various types of platinum-group minerals. The laser beam diameter was set at 40µm and a line was selected for an analytical traverse through each type of BMS that produced an ablated trench. Additional details of the analytical conditions and standards used can be found in McDonald (2005), Holwell and McDonald (2007) and Prichard et al. (2013).

## 8.3 Results

All of the BMS analysed (pentlandite, chalcopyrite and pyrrhotite) contain various concentrations of PGE, Au, Co, Ni and Cu in solid solution. The mean, minimum and maximum values for each BMS are shown in table 8.1.

Pentlandite is the major carrier of Pd (mean = 299 ppm) and Rh (mean = 19 ppm). It is also a significant carrier of the IPGE (Os mean = 2 ppm, Ir mean = 1 ppm and Ru mean = 13 ppm). Pentlandite contains the highest total PGE concentrations (ranging between 79 and 931

ppm) with 60 % of the analyses carrying a total PGE content of between 101 and 300 ppm (fig. 8.4 a). Chalcopyrite (fig. 8.4 c) has the lowest PGE concentrations with 80 % of the grains analysed containing less than 1 ppm total PGE and occasionally with only a small amount of Pt. The elevated Pt occurred with correspondingly high Bi and Te concentrations, most likely within a PGM micro-inclusion, or inclusions within the BMS. Pyrrhotite contains significantly more Pd than chalcopyrite (mean = 20 ppm) and also contains small proportions of the IPGEs (Ru, Ir, Os). On average, 60 % of the pyrrhotite analyses contain less than 10 ppm total PGE (fig. 8.4 b).

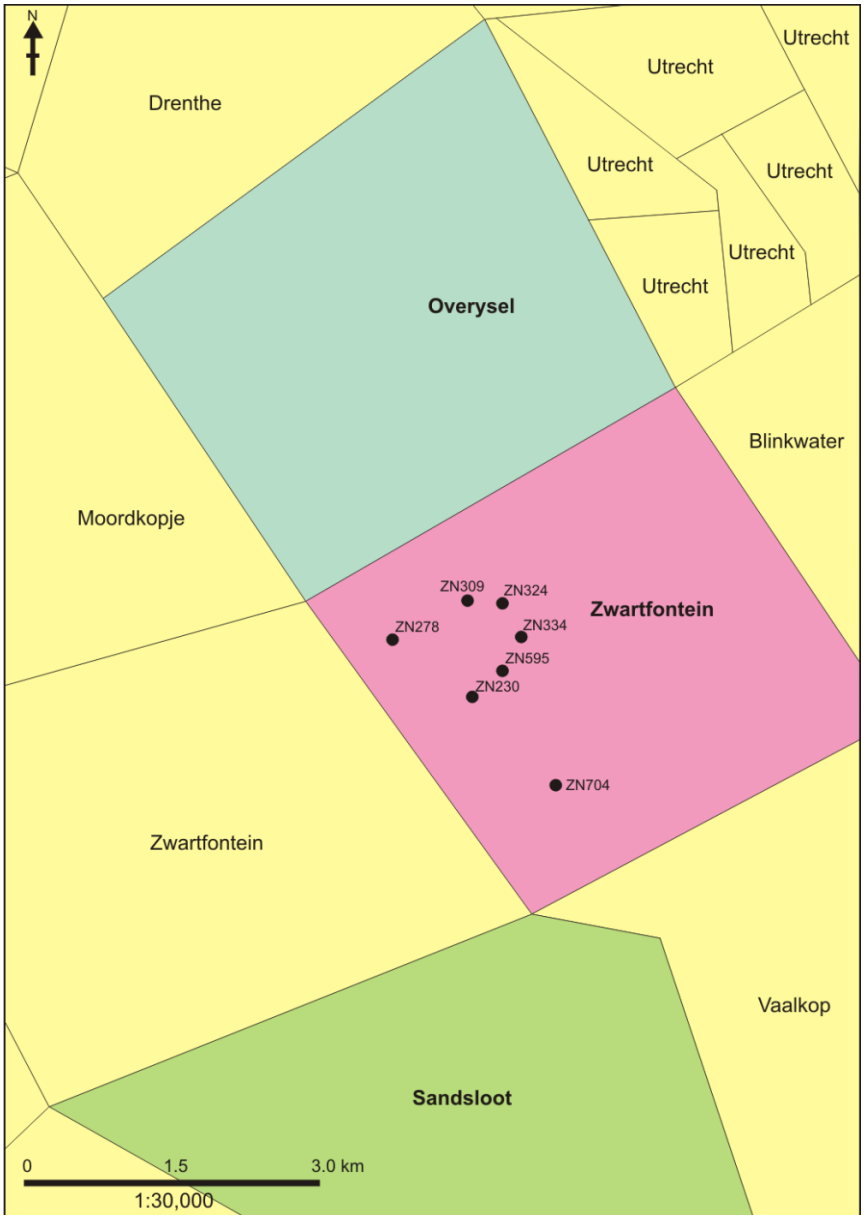

Figure 8.3. Sample map showing location of drillholes on Zwartfontein.

Table 8.1. Composition of base metal sulphides from Zwartfontein chromitites analysed by LA-ICP-MS.

| | Co | Ni | Cu | Os | Ir | Ru | Rh | Pt | Pd | Au | Te | Bi |
|---|---|---|---|---|---|---|---|---|---|---|---|---|
| | ppm | wt% | wt% | ppm | ppm | ppm | ppm | ppm | ppm | ppm | ppm | ppm |
| **Chalcopyrite (n=12)** | | | | | | | | | | | | |
| **Mean** | 85.52 | 0.26 | 30.85 | <0.01 | <0.01 | <0.05 | <0.08 | 0.15 | 0.19 | 0.27 | 0.60 | 7.28 |
| **Min** | 2.95 | 0.00 | 24.04 | <0.01 | <0.01 | <0.05 | <0.08 | <0.01 | <0.10 | <0.01 | <0.02 | <0.02 |
| **Max** | 234.20 | 0.94 | 38.34 | 0.02 | 0.01 | 0.49 | 0.30 | 1.33 | 0.85 | 2.79 | 1.17 | 45.46 |
| | | | | | | | | | | | | |
| **Pentlandite (n=20)** | | | | | | | | | | | | |
| **Mean** | 8080.80 | 32.24 | 0.75 | 2.37 | 1.25 | 13.15 | 18.96 | 2.59 | 298.77 | <0.01 | 2.10 | 2.34 |
| **Min** | 5091.00 | 18.18 | 0.00 | 0.09 | <0.01 | <0.05 | <0.08 | <0.01 | 64.25 | <0.01 | 0.19 | 0.03 |
| **Max** | 10600.00 | 41.75 | 8.70 | 15.27 | 2.93 | 32.38 | 57.90 | 22.02 | 905.20 | 0.13 | 6.65 | 16.20 |
| | | | | | | | | | | | | |
| **Pyrrhotite (n=21)** | | | | | | | | | | | | |
| **Mean** | 223.59 | 0.83 | 0.81 | 0.40 | 0.84 | 3.20 | 0.89 | 0.30 | 10.49 | <0.01 | 0.45 | 0.45 |
| **Min** | 3.79 | 0.08 | 0.00 | <0.01 | <0.01 | <0.05 | <0.08 | 0.04 | <0.10 | <0.01 | <0.02 | <0.02 |
| **Max** | 1113.00 | 3.54 | 7.64 | 1.36 | 1.94 | 6.04 | 4.23 | 0.71 | 68.06 | 0.01 | 1.42 | 3.54 |

Table 8.2. Coefficient of determination ($r^2$) of the PGE for the various base metal sulphides plotted in figure 8.5. Key: cpy=chalcopyrite; pent=pentlandite;

| | Cpy | Pent | Pyrr |
|---|---|---|---|
| **Os vs. Ir** | - | 0.37 | 0.01 |
| **Ru vs. Ir** | - | 0.00 | 0.46 |
| **Os vs. Ru** | - | 0.03 | 0.11 |
| **Rh vs. Ir** | - | 0.01 | 0.04 |
| **Pd vs. Ir** | - | 0.02 | 0.45 |
| **Ni vs. Ir** | - | 0.13 | 0.00 |
| **Rh vs. Pd** | - | 0.00 | 0.00 |
| **Pt vs. Cu** | 0.92 | 0.01 | 0.04 |
| **Pd vs. Cu** | 0.69 | 0.25 | 0.45 |
| **Pd vs. Ni** | - | 0.08 | 0.80 |
| **Cu vs. Au** | 0.45 | 0.01 | 0.00 |
| **Pd vs. Co** | 0.04 | 0.15 | 0.81 |
| **Ni vs. Co** | 0.89 | 0.17 | 0.97 |

a)

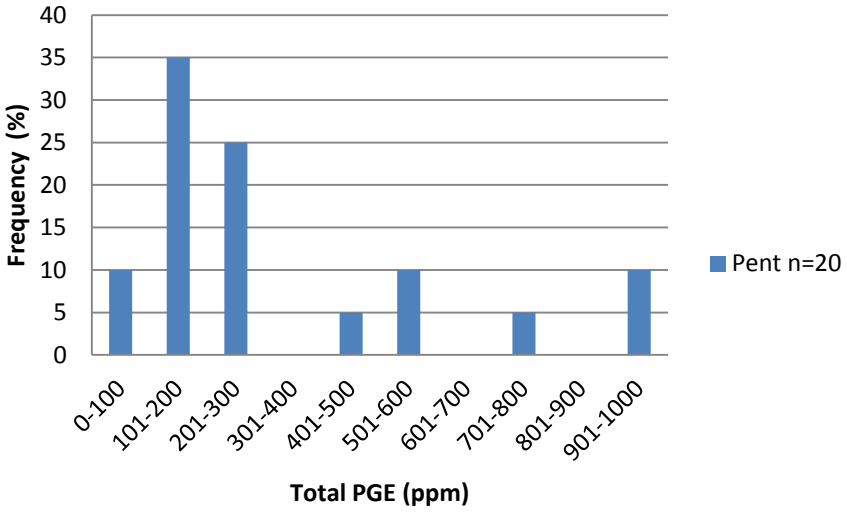


b)

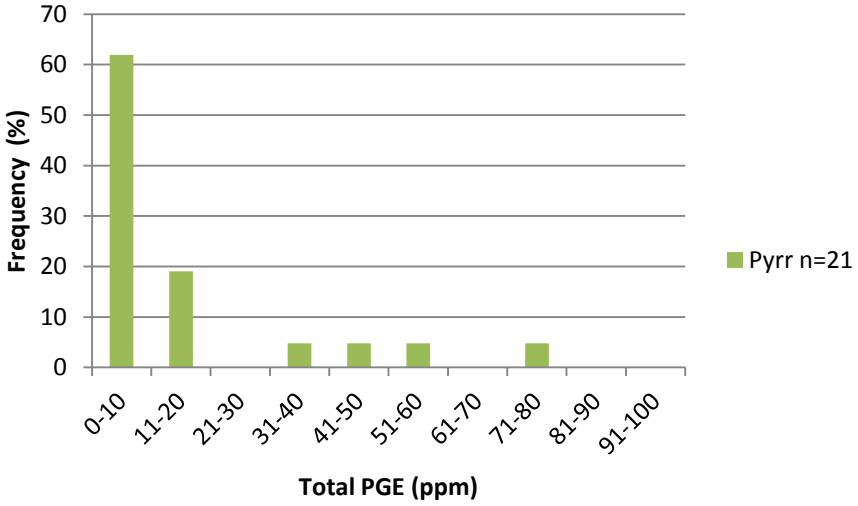


c)

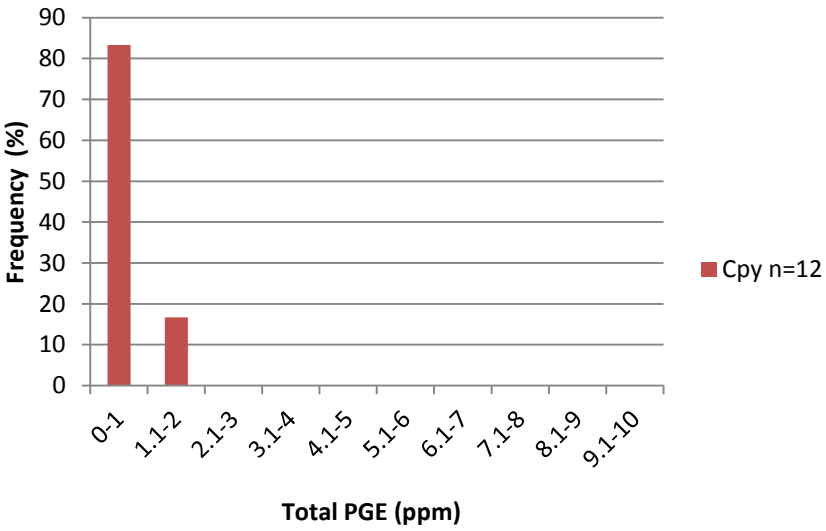


Figure 8.4. Total PGE content in BMS from Zwartfontein in (a) pentlandite; (b) pyrrhotite; and (c) chalcopyrite.

A strong positive correlation can be seen between Pd and Co and Ni and Co for pyrrhotite at low concentrations but less so for pentlandite (fig. 8.5 a & b). There is a reasonable degree of positive correlation (table 8.2) between the IPGEs for both pentlandite and pyrrhotite (fig. 8.5 a & b). Os and Ir are moderately positively correlated in pentlandite ($r^2$ = 0.37) whereas there is limited correlation in pyrrhotite (fig. 8.6 a). Ru and Ir are moderately correlated in pyrrhotite ($r^2$= 0.46). In the plot of Ru vs. Ir there is a strong correlation in pentlandite up to concentrations of around 2 ppm Ir, but above this the Ru values drop down to values under 10 ppm (fig. 8.6 b). Potentially some of the pentlandite values at the lowest Ru values may in fact be pyrrhotite intergrowths in pentlandite.

Rh correlates well with the IPGE in both pentlandite and pyrrhotite (fig. 8.6 c). A limit to the relationship is also seen in Rh vs. Ir with a maximum value of around 60 ppm Rh at similar Ir concentrations of around 2 ppm (fig. 8.6 c). This suggests that there may be a limit in the solubility of both Rh and Ru in pentlandite and that above a certain point they form their own PGE (laurite and/or hollingworthite), whereas Ir remains in solid solution.

There is a poor correlation between Rh and Pd in pentlandite. Concentrations of Pd and Rh being very variable and high Rh values do not necessarily correspond with high Pd values (fig. 8.6 e). Potentially, there is a positive correlation between Rh and Pd up to Pd values of less than 500 ppm, after which the Rh values drop to very low concentrations with increasing Pd values.

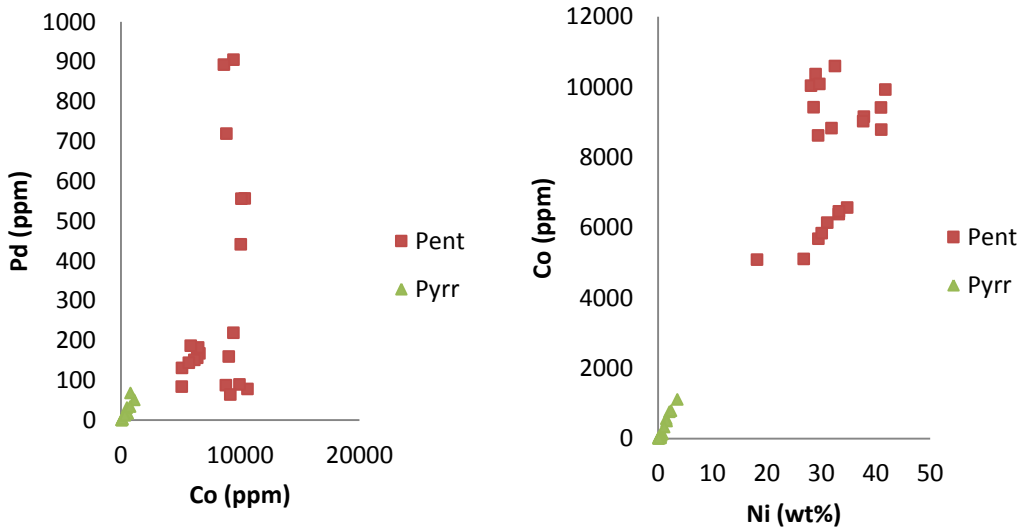


Figure 8.5. Binary variation diagrams of (a) Pd vs. Co and (b) Co vs. Ni

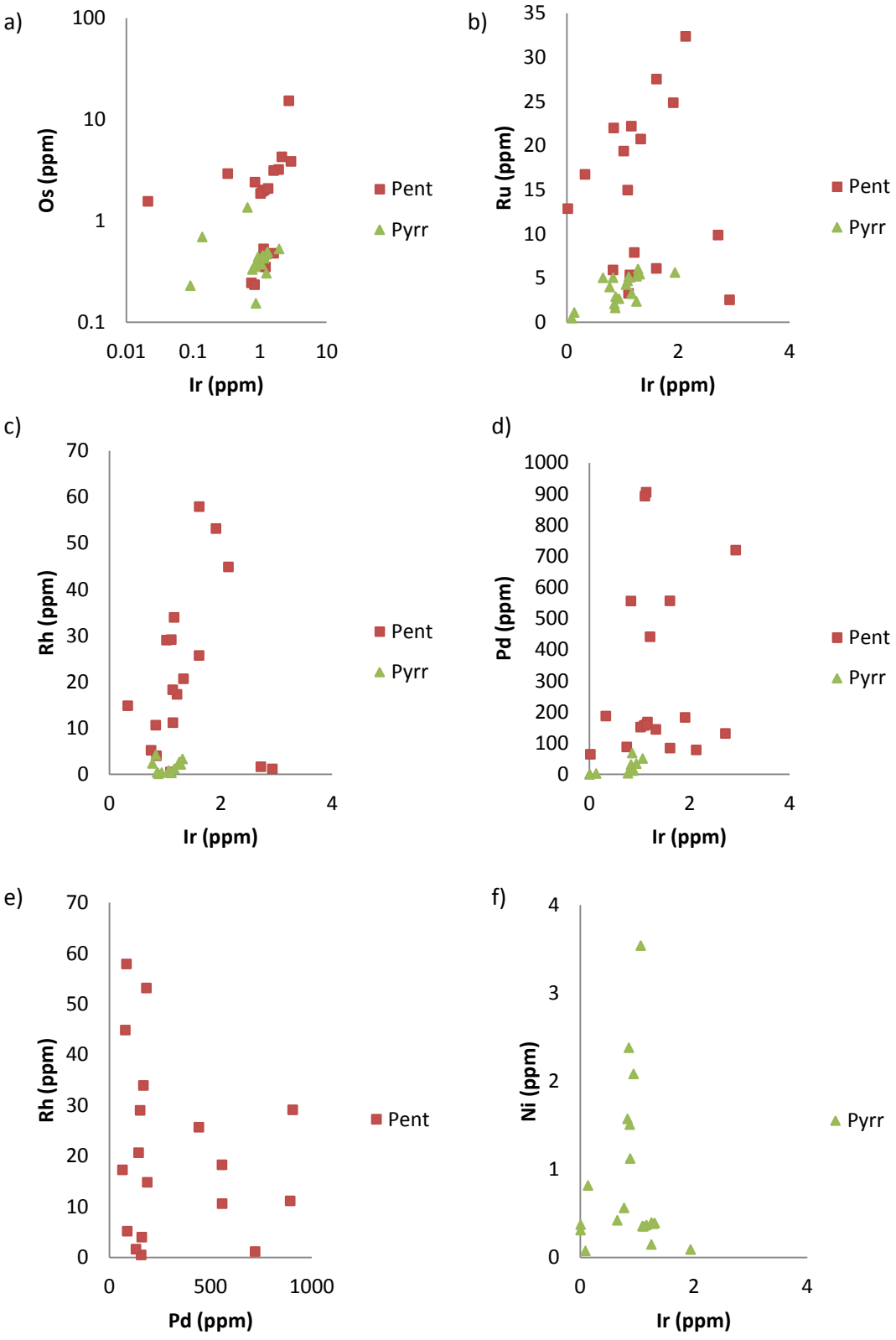


Figure 8.6. PGE contents of analysed grains of pentlandite and pyrrhotite showing (a) Ir vs. Os; (b) Ir vs. Ru; (c) Ir vs. Rh; (d) Ir vs. Pd; (e) Pd vs. Rh for pentlandite; and (f) Ir vs. Ni for pyrrhotite.

Pt and Au do not occur in BMS. Platinum concentrations in pentlandite range from 0.13 to 22 ppm. While most analyses show minimal Pt values, 2 analyses of pentlandite had values of 18 and 22 ppm. The TRA spectra for these samples demonstrate that one of these high Pt values can be attributed to a Pt bismuthide inclusion, while the other represents a Pt arsenide (e.g. fig. 8.9).

The maximum value of Pt in chalcopyrite or pyrrhotite is 1.3 ppm. Table 8.2 shows relatively high $r^2$ values for correlation between Pt or Pd and Cu in chalcopyrite compared to pyrrhotite and pentlandite but this can be attributed to the very low abundances of Pt and Pd in chalcopyrite. In pentlandite and pyrrhotite there is a wider range of Pt and Pd values resulting in a lower correlation factor. There is no significant correlation between Pt and other metals. The majority of gold concentrations in pentlandite, pyrrhotite or chalcopyrite are below 0.1 ppm with one analysis of 2.78 ppm in chalcopyrite.

A number of typical time-resolved analytical spectra are shown in figures 8.7-8.10 for the various BMS analysed. Analysis of pentlandite shows an abundance of PGE, however when the laser track moves into chalcopyrite, the signal for all PGE decreases sharply indicating an paucity of PGE (fig. 8.7). Most TRA specta for pyrrhotite show smooth parallel patterns for Ru, Ir, and Os with S, indicating that the IPGE are present in solid solution in pyrrhotite, however, figure 8.6 shows zoning of Ru and Ir (but not Os or PPGE) within the pyrrhotite grain. This was observed in 3 of the 21 pyrrhotite grains analysed and occurs over a wide zone within the pyrrhotite grain. Occasionally, a laser track passes over a PGM inclusion within the BMS. In figure 8.9, the laser track moves from pentlandite into chalcopyrite, sampling a Pt (+IPGE) bismuthide, possibly at the junction between the two different BMS. In addition to single BMS grains, composite BMS were also analysed. Figure 8.8 shows a pentlandite and pyrrhotite composite, with the concentrations of PGE increasing in the pentlandite portions of composite grain. The time spectra for Pd and Rh and parallel in the most pentlandite-rich portions of the sample but not in the pyrrhotite. The spectrum for Ru is parallel with that of Rh and Pd in pentlandite but differs from both in the pyrrhotite.

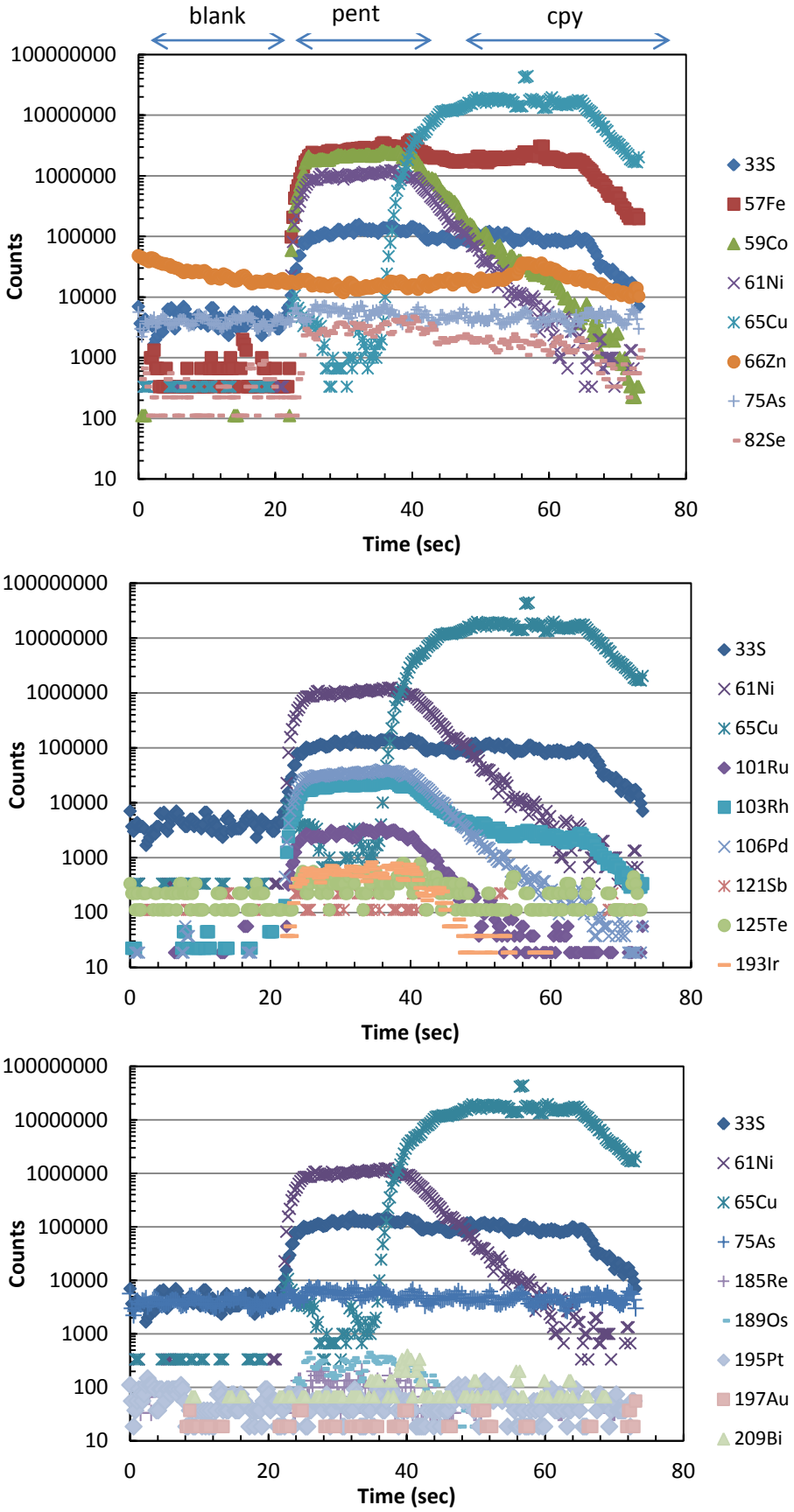


Figure 8.7. Time-resolved analysis (TRA) spectra from line analysis of sulphides containing pentlandite and chalcopyrite.

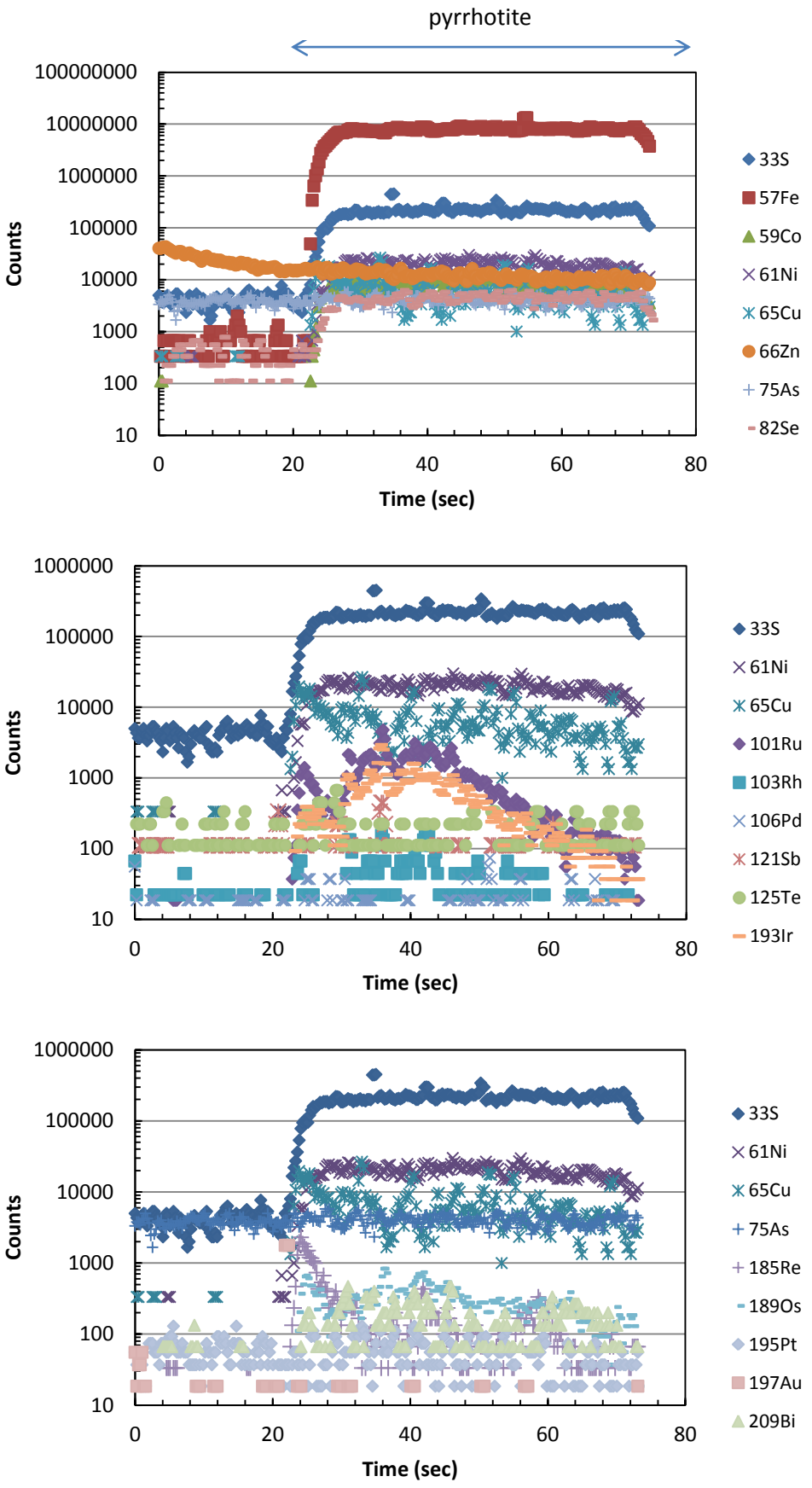


Figure 8.8. Time-resolved analysis (TRA) spectra from line analysis of sulphides containing pyrrhotite with zoned Ir & Ru.

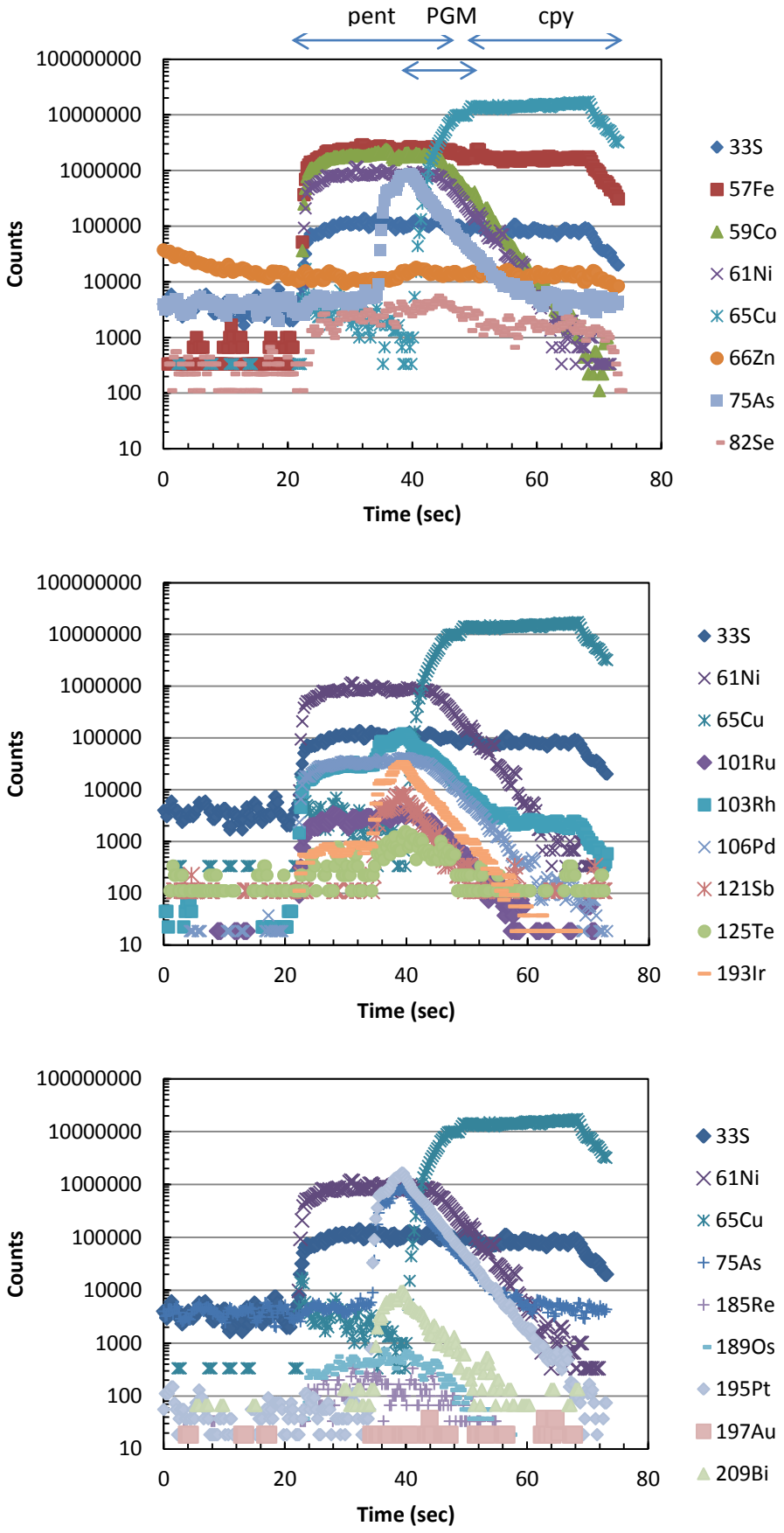


Figure 8.9. Time-resolved analysis (TRA) spectra from line analysis of sulphides containing pentlandite, chalcopyrite and PGM inclusion.

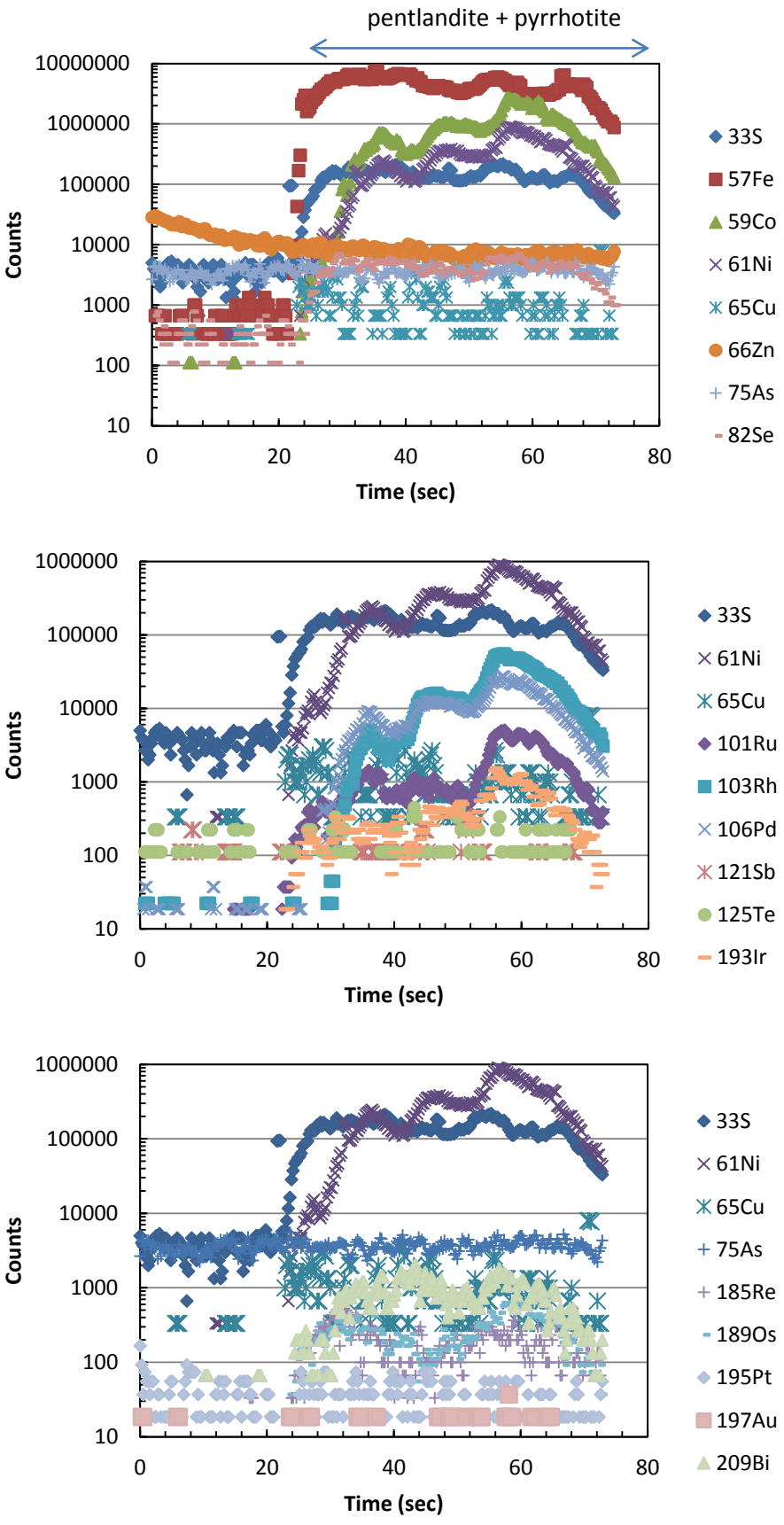


Figure 8.10. Time-resolved analysis (TRA) spectra from line analysis of sulphides containing pentlandite and pyrrhotite zoning.

## 8.4 Comparison to other Bushveld Complex data

This study has focused on the results obtained from BMS in chromitites from Zwartfontein. Results from a study carried out by Holwell and McDonald (2007) illustrated the different PGE distribution within the BMS of different lithologies in samples from Overysel and Sandsloot (table 8.2).

Within the feldspathic pyroxenites, pyrrhotite is the main carrier of Os, Ir and Ru, with minor Rh and no Pd. The IPGE are positively correlated to each other and shows a positive correlation with Ni (Holwell and McDonald 2007). Interestingly, the gradient of the positive correlation is steeper for samples from Sandsloot compared to Overysel. Pentlandite contains a lower concentration of IPGE compared to pyrrhotite (up to x 1.5 less on Overysel). The IPGEs again show a high degree of positive correlation to each other (Holwell and McDonald 2007).

Pentlandite is the major carrier of Pd and Rh in the feldspathic pyroxenites. Analysis of pentlandite grains in samples from Overysel show a mostly positive correlation between Pd and Rh, with a mostly negative correlation for Sandsloot (Holwell and McDonald 2007). Results from this study have shown a slight correlation between Pd and Rh up to Pd values of around 200 ppm, after which there is very little correlation. It is uncertain if this relationship is seen on the other farms as the Pd concentrations within pentlandite hosted by pyroxenites in the study by Holwell and McDonald (2007) do not exceed 200 ppm. Similar to the present study, Holwell and McDonald (2007) found that both Rh and Pd show poor correlation with the IPGE.

The Holwell and McDonald (2007) study also analysed a single pentlandite and a single pyrrhotite within chromitite. These analyses can be compared directly with the results from this study (table 8.3) but some caution needs to be taken. The Overysel pyrrhotite did not contain any IPGE or Pt, whereas in the present study pyrrhotite contains minor concentrations of Os, Ir and Pt with a mean value of 3.2 ppm Ru. Similarly, Pd and Rh occur at greater average concentrations in this study, with mean Pd concentrations of 10.5 ppm and mean Rh concentration of 0.9 ppm compared to 0.03 ppm and 0.2 ppm, respectively, in the Holwell and McDonald (2007) study. Interestingly, the Overysel pyrrhotite contained more than 5 times the maximum concentration of Bi obtained in this study, with slightly more Te found in the pyrrhotite from this study compared to the study by Holwell and McDonald (2007).

| | Co | Ni | Cu | Os | Ir | Ru | Rh | Pt | Pd | Au | Te | Bi |
|---|---|---|---|---|---|---|---|---|---|---|---|---|
| | ppm | wt% | wt% | ppm | ppm | ppm | ppm | ppm | ppm | ppm | ppm | ppm |
| **Overysel Reef pyroxenites** | | | | | | | | | | | | |
| **Pyrrhotite (n=8)** | 22.80 | 0.51 | 0.00 | 0.93 | 1.80 | 7.81 | 0.45 | 0.61 | 0.06 | <0.01 | 1.64 | 0.92 |
| **Pentlandite (n=8)** | 2,969.00 | 34.40 | 0.02 | 0.59 | 1.20 | 5.16 | 15.00 | 0.45 | 119.00 | <0.01 | 1.49 | 0.85 |
| **Chalcopyrite (n=6)** | 3.10 | 0.06 | 28.20 | <0.01 | <0.01 | - | - | 1.31 | 0.54 | 0.01 | 1.54 | 1.67 |
| **Sandsloot Reef pyroxenites** | | | | | | | | | | | | |
| **Pyrrhotite (n=5)** | 6.47 | 0.15 | - | 1.83 | 2.87 | 13.90 | 0.18 | 1.32 | 0.07 | - | 1.34 | 0.48 |
| **Pentlandite (n=7)** | 4,398.00 | 31.00 | 0.02 | 2.02 | 3.60 | 15.10 | 25.10 | 0.96 | 102.00 | - | 1.99 | 0.87 |
| **Chalcopyrite (n=3)** | 78.60 | 0.53 | 30.40 | 0.03 | 0.09 | - | 0.61 | 0.12 | 1.73 | 0.01 | 0.22 | 0.10 |
| **Overysel chromitites** | | | | | | | | | | | | |
| **Pyrrhotite (n=1)** | 62.70 | - | - | - | - | - | - | - | 0.03 | 0.07 | 0.01 | 19.70 |
| **Pentlandite (n=1)** | 5,079.00 | 33.70 | - | 0.49 | - | 6.87 | - | - | 72.40 | - | 0.81 | 0.59 |

Table 8.3. Mean composition of base metal sulphides from Holwell and McDonald (2007).

The mean Ni concentrations within pyrrhotite from this study was 0.83 wt% and the mean Cu concentration was 0.81 wt%, whereas no Ni or Cu values were detected in the sample from Overysel.

Within the pentlandite from Overysel, no Ir, Rh or Pt was detected, compared to mean vales of 1.3 ppm, 1.3 ppm and 2. 6 ppm, respectively, found within the pentlandite from Zwartfontein. Os, Ru and Pd values were all significantly higher in the samples from Zwartfontein with mean Pd concentration of 299 ppm vs. 72 ppm for the pentlandite sample from Overysel. Te and Bi mean values were slightly elevated in the present study compared to the pentlandite grain from Overysel. Similar Ni values were found in samples from both farms.

The data set Overysel and Sandsloot generated by Holwell and McDonald (2007) that deals with silicate rocks rather than chromitites can be compared to that of this study for Zwartfontein to investigate any variation spatially (table 8.4, fig. 8.11). Within the pyrrhotite, Zwartfontein samples contain the highest Co and Ni values and lower IPGE values than the other two farms. Rh and Pd values are elevated (up to 2 orders of magnitude greater for Pd than the other farms), while Pt, Bi and Te values are the lowest compared to the other two farms.

With regard to pentlandite samples, the Zwartfontein samples contain the highest Pt and Pd values with Ni and IPGE values comparable to Sandsloot (fig. 8.11). Te and Bi values are slightly higher than those from the Holwell and McDonald (2007) study.

Chalcopyrite analysed in the Holwell and McDonald (2007) study did not contain any PGE in solid solution but some minor PGM inclusions were recorded, comparable to the results from chalcopyrite in this study. Overall, it was shown that the BMS in the Sandsloot samples contained higher concentrations of PGE than the Overysel samples but identical PGE distribution characteristics were observed (Holwell and McDonald 2007). Chalcopyrite analyses have shown that the Zwartfontein samples contain comparable Cu values to the other two farms, Pt values are comparable to Sandsloot, but they have the lowest Pd values of the three farms. As shown in figure 8.11, the samples from Zwartfontein also show a slight decrease in Rh compared to the other samples, in addition to increased concentration of Au (up to an order of magnitude). The Te concentrations of the samples from this study are within the range obtained by Holwell and McDonald (2007) and the Bi concentrations are elevated (7 ppm vs. 0.1 ppm for Sandsloot and 1.7 ppm for Overysel) in comparison.

| | Co | Ni | Cu | Os | Ir | Ru | Rh | Pt | Pd | Au | Te | Bi |
|---|---|---|---|---|---|---|---|---|---|---|---|---|
| | ppm | wt% | wt% | ppm | ppm | ppm | ppm | ppm | ppm | ppm | ppm | ppm |
| **Pyrrhotite** | | | | | | | | | | | | |
| **Overysel pyroxenites (n=8)** | 22.80 | 0.51 | 0.00 | 0.93 | 1.80 | 7.81 | 0.45 | 0.61 | 0.06 | <0.01 | 1.64 | 0.92 |
| **Overysel chromitites (n=1)** | 62.70 | - | - | - | - | - | - | - | 0.03 | 0.07 | 0.01 | 19.70 |
| **Sandsloot pyroxenites (n=5)** | 6.47 | 0.15 | - | 1.83 | 2.87 | 13.90 | 0.18 | 1.32 | 0.07 | - | 1.34 | 0.48 |
| **Zwartfontein chromitites (n=21)** | 223.59 | 0.83 | 0.81 | 0.40 | 0.84 | 3.20 | 0.89 | 0.30 | 10.49 | <0.01 | 0.45 | 0.45 |
| **Pentlandite** | | | | | | | | | | | | |
| **Overysel pyroxenites (n=8)** | 2,969.00 | 34.4 | 0.02 | 0.59 | 1.20 | 5.16 | 15.0 | 0.45 | 119.00 | <0.01 | 1.49 | 0.85 |
| **Overysel chromitites (n=1)** | 5,079.00 | 33.7 | - | 0.49 | - | 6.87 | - | - | 72.40 | - | 0.81 | 0.59 |
| **Sandsloot pyroxenites (n=7)** | 4,398.00 | 31.0 | 0.02 | 2.02 | 3.60 | 15.10 | 25.10 | 0.96 | 102.00 | - | 1.99 | 0.87 |
| **Zwartfontein chromitites (n=20)** | 8,081.00 | 32.24 | 0.75 | 2.37 | 1.25 | 13.15 | 18.96 | 2.59 | 298.77 | 0.01 | 2.10 | 2.34 |
| **Chalcopyrite** | | | | | | | | | | | | |
| **Overysel pyroxenites (n=6)** | 3.10 | 0.06 | 28.20 | <0.01 | <0.01 | - | - | 1.31 | 0.54 | 0.01 | 1.54 | 1.67 |
| **Sandsloot pyroxenites (n=3)** | 78.60 | 0.53 | 30.40 | 0.03 | 0.09 | - | 0.61 | 0.12 | 1.73 | 0.01 | 0.22 | 0.10 |
| **Zwartfontein chromitites (n=12)** | 85.52 | 0.26 | 30.85 | <0.01 | <0.01 | 0.09 | 0.05 | 0.15 | 0.19 | 0.27 | 0.60 | 7.28 |

Table 8.4. Comparison of mean BMS content over the three farms of Overysel, Sandsloot and Zwartfontein (data for Overysel and Sandsloot from Holwell and McDonald 2007).

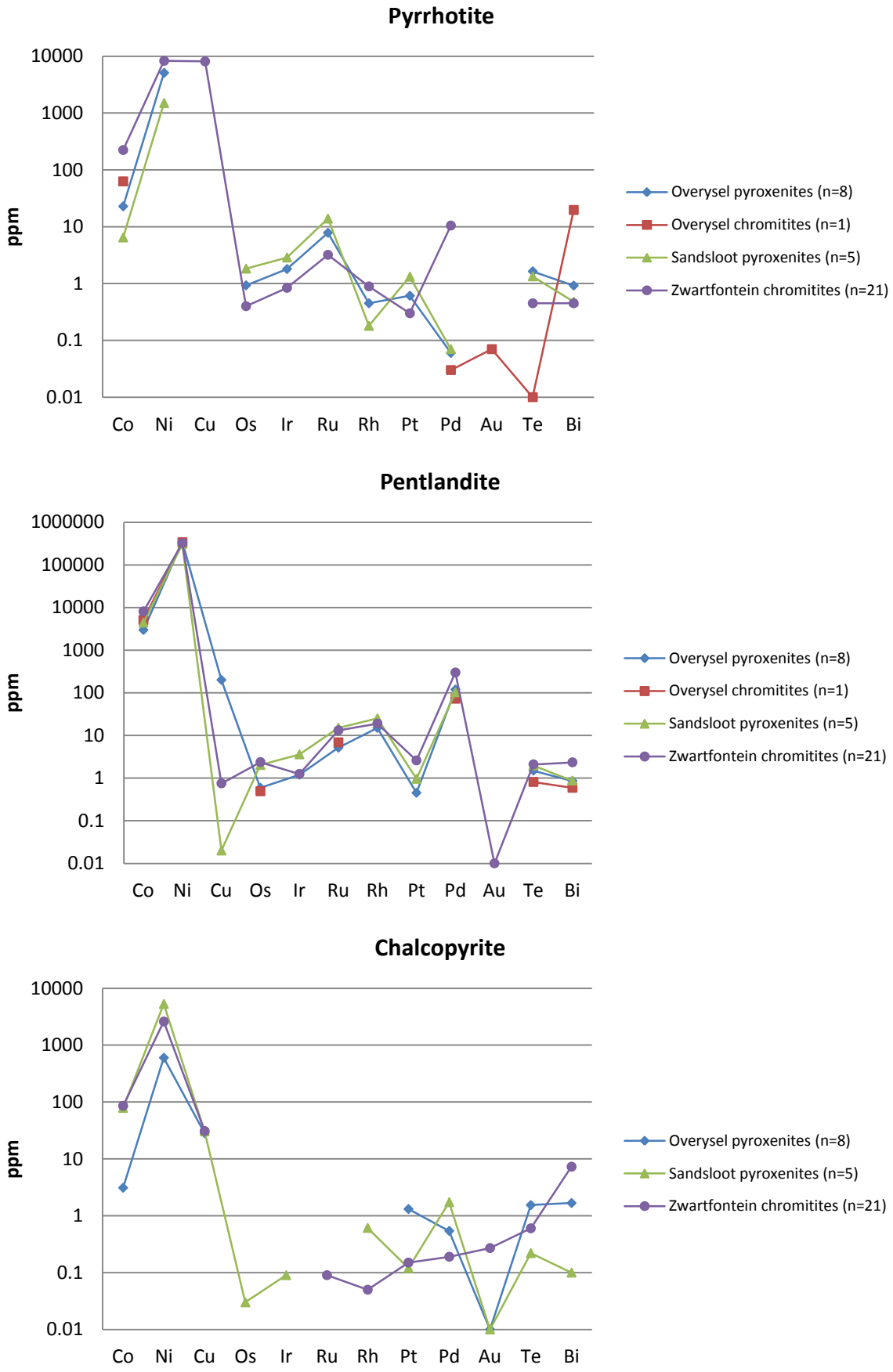


Figure 8.11. Composition of three BMS from this study on Zwartfontein and study by Holwell and McDonald (2007).

The results obtained in this study can also be compared to a study carried out by Godel et al. (2007) for the Upper and Lower chromitite in the Merensky Reef. Figure 8.12 displays a series of histograms to show the variation in Pd contents in pentlandite for this study on Zwartfontein, the study on Overysel and Sandsloot (Holwell and McDonald 2007) and for the Merensky Reef (Godel et al. 2007). The sample in this study has the greatest variation in addition to the highest overall average for the three areas, while those from Overysel and Sandsloot have the lowest average values. The Merensky data set show a possible variation between the Upper Chromitite and Lower Chromitite layer with the Lower Chromitite layer appearing to have higher concentrations of Pd in pentlandite, although any comparison must be taken with caution due to the relatively low number of samples analysed as with the study by Holwell and McDonald (2007),.

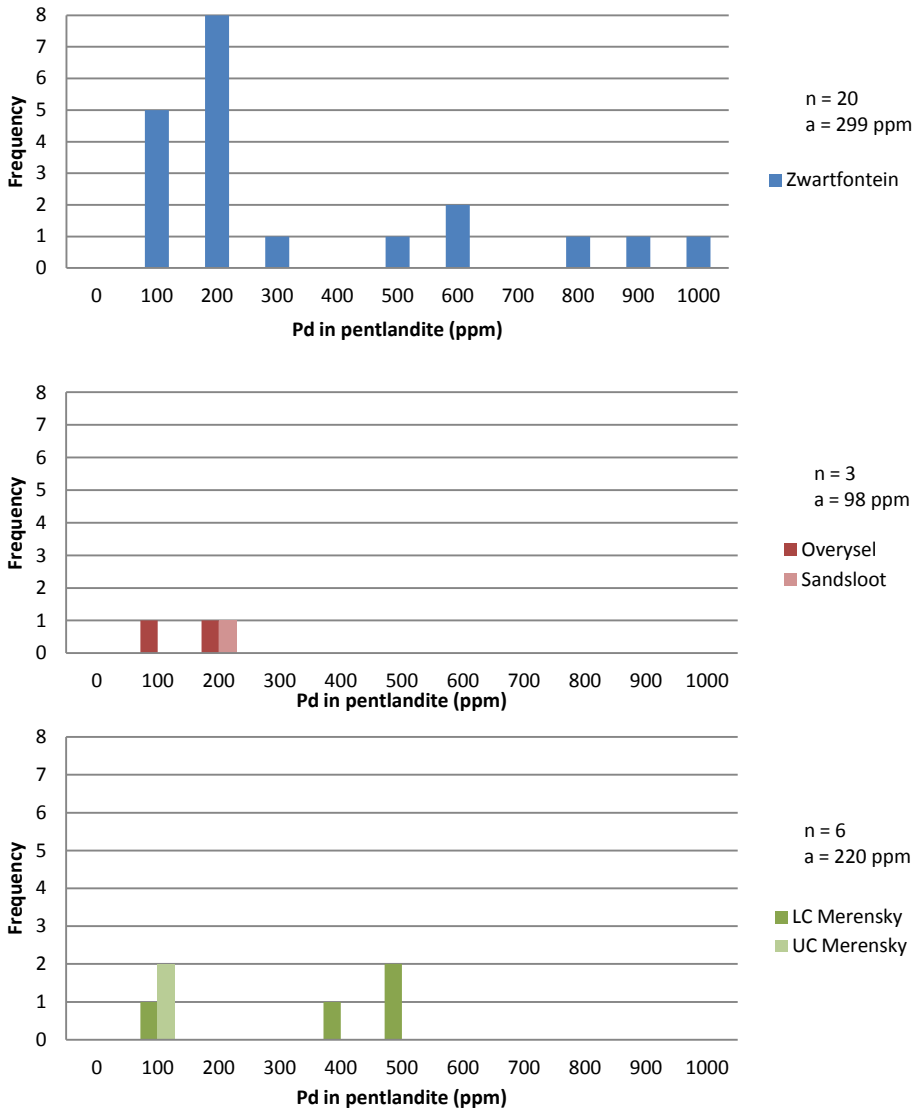


Figure 8.12. Series of histograms showing the variation in Pd concentration in pentlandite from the Zwartfontein (this study), Overysel and Sandsloot (Holwell and McDonald 2007) on Platreef and the Lower and Upper Chromite in the Merensky Reef (Godel et al. 2007).

## 8.5 Discussion

This study of the BMS from chromitites has shown that the PGE are present in solid solution within the BMS in varying amounts. As stated at the beginning of the chapter, many studies have shown the fractionation of an immiscible sulphide liquid and the distribution of the PGE in those phases. While it is accepted that the PGE and other chalcophile elements are collected by the immiscible sulphide liquid, there are numerous theories about the processes that control the PGE distribution following the fractionation of mss from the sulphide melt. These processes have been summarised by Dare et al. (2010) and include the direct crystallisation of PGM from the melt (e.g. Barnes et al. 2006; Hutchinson and McDonald 2008) or from an immiscible As-Bi-Te-rich melt (e.g. Hanley 2007; Helmy et al. 2007; Holwell and McDonald 2007); addition of As, Sb, Bi and Te from the country rock to the sulphide melt, which results in PGM minerals forming with these elements (e.g. Hutchinson and McDonald 2008); exsolution of PGM during cooling (e.g. Godel et al. 2007; Barnes et al. 2008; Godel and Barnes 2008); subsolidus diffusion (e.g. Barnes et al. 2006); and re-crystallisation during metamorphism (e.g. Barnes et al. 2008).

Based on the sulphide mass balance for PGE-rich sulphide samples from various geological settings, Barnes et al. (2008) proposed that the distribution of PGE among the BMS is a result of different cooling rates within the ore deposits. Where sulphide cooled quickly, such as in a sub-volcanic sill at Noril'sk (Barnes et al. 2006), the majority of PGE and Re are held in solid solution within the BMS, while Pt and Au form discrete PGM. However, where sulphides are cooled slowly within large igneous complexes, such as the Merensky Reef (Godel et al. 2007) and the J-M Reef in the Stillwater Complex (Godel and Barnes 2008), the BMS contain lower proportions of PGE (expect Pt) and Re.

In the present study, it has been observed that pentlandite is the main carrier of the IPGE, Pd and Te, while pyrrhotite contains minor IPGE and Pd. Chalcopyrite does not contain any significant amounts of PGE, with recorded concentrations of Pt related to PGM inclusions within the sulphide phase. These observations on a whole are comparable to other BMS studies that have been carried out that were mentioned above.

Another significant observation made within this study is that there appears to be a limit to the amount of Ru and Rh that pentlandite can contain in solid solution as was seen in the Ru vs. Ir and Rh vs. Ir plots (fig. 8.5). Based on this observation, it would be expected that in the pentlandite that contained in excess of 2ppm Ir, there would be increased amounts of Ru and Rh PGM (specifically laurite ($RuS_2$) and hollingworthite (RhAsS)). Corresponding samples

analysed in chapter 7 do not show an increase in laurite but do show an increase in the amount of hollingworthite and other sulpharsenides that contain significant portions of Rh and Ru, which would account for the lack of Rh and Ru seen in pentlandite at elevated Ir concentrations. This appears to be an observation specifically related to chromitite as this was not observed in the feldspathic pyroxenites studied by Holwell and McDonald (2007). The observation made by Holwell and McDonald (2007) that Rh compatibility in mss results in the preferential partitioning into pentlandite during the exsolution process is also seen in this study, with only minor amounts of Rh seen in pyrrhotite.

A common observation made in other studies examining the enrichment of IPGE in pyrrhotite vs. pentlandite is that there is a slight preference of the IPGE to partition into pyrrhotite during exsolution (e.g. in Merensky Reef, Ballhaus and Sylvester 2000; in Overysel pyroxenites, Holwell and McDonald 2007) or a similar concentration in both pentlandite and pyrrhotite (e.g. Noril'sk, Barnes et al. 2006; in Sandsloot pyroxenites, Holwell and McDonald 2007). However, in the chromitites studied here, the concentration of the IPGEs is significantly greater in pentlandite compared to pyrrhotite. However, in many of the pentlandite samples analysed, there is no pyrrhotite in the vicinity of pentlandite, or occasionally absent in the samples, suggesting that the increased concentrations in pentlandite may be due to lack of pyrrhotite into which the IPGE can exsolve.

The excess of Os and Ru in pentlandite compared to pyrrhotite provides evidence that pentlandite did not originate from the fractionated Cu-rich liquid via exsolution from iss as has previously been demonstrated experimentally by Peregoedova and Ohnestetter (2002). Instead, it is likely, based on experiments by Kelly and Vaughan (1983), that Co diffused with Ni and Fe from mss to form pentlandite, and a minor amount of Co and Ni remained in pyrrhotite.

Another interesting observation made within the pyrrhotite grains was the occasional zoned enrichment in Ru and Ir (fig. 8.8). This was noted in multiple samples and zoning was consistent over a wide part of the grain. As yet, no explanation can be given for this observation and it appears this is the first time this has been documented.

The distribution of Os, Ir, Ru and Rh is consistent with these elements being concentrated within mss that fractionated early from the sulphide liquid, and later formed pyrrhotite and pentlandite during exsolution at subsolidus conditions (Ballhaus and Sylvester 2000; Barnes

et al. 2006; Godel et al. 2006; Holwell and McDonald 2007; Barnes et al. 2008; Godel and Barnes 2008; Dare et al. 2010).

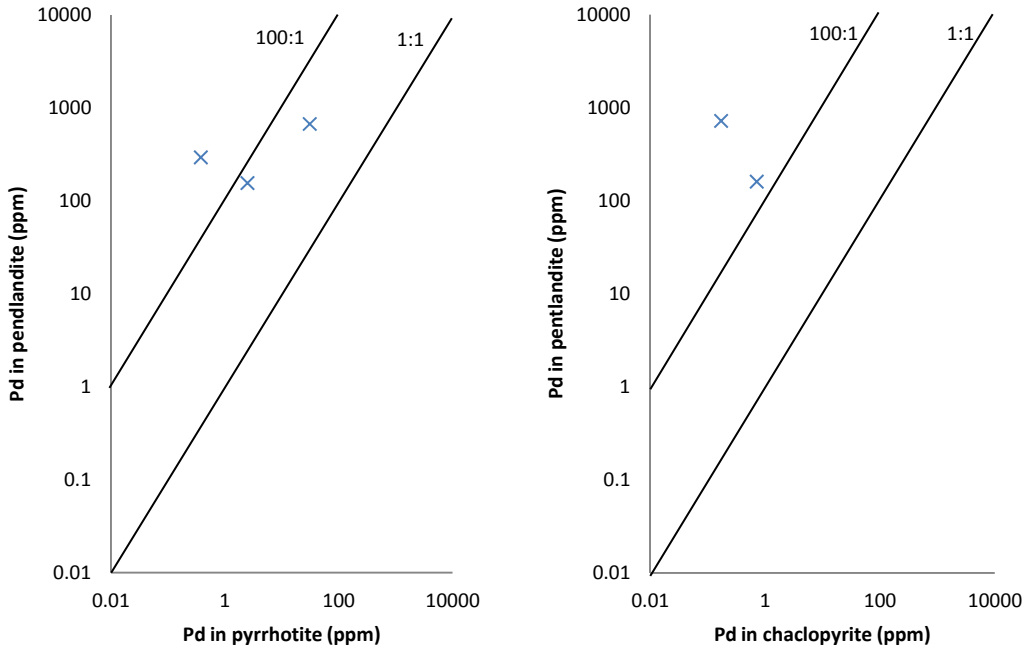


Figure 8.13. Concentrations of Pd in pentlandite vs. pyrrhotite and pentlandite vs. chalcopyrite.

It is a common observation that Pd is enriched in pentlandite relative to both pyrrhotite and chalcopyrite by a factor of 100 to 10,000 times in PGE-rich deposits (Dare et al. 2010), as is demonstrated in this study (fig. 8.13). The concentration of Pd within pentlandite, rather than in chalcopyrite as expected based on the fractionation process, has led other authors to suggest that there is a subsolidus diffusive exchange that causes the enrichment of pentlandite in Pd (e.g. Barnes et al. 2006; Dare et al. 2010). It is therefore expected that in samples that contain greater than average amounts of chalcopyrite there might be an additional source of Pd for pentlandite, from the larger amount of Pd that originally partitioned into the Cu-rich liquid. This theory is supported by the fact that the highest Pd values in pentlandite are found in samples with the most chalcopyrite (e.g. sample ZN278; fig. 8.14), suggesting that the Pd diffused from the nearby Cu-rich portion. Dare et al. (2010) also found evidence in their Sudbury samples to support this theory although they state that it is unclear at present from which part of the Cu-rich portion the Pd diffused (i.e. the iss, the late-stage melt associated with iss and/or Pd-bearing PGM). They state that the driving mechanism for the diffusion of Pd into pentlandite was probably the rejection of Pd from pyrrhotite and chalcopyrite at low temperatures based on experiments by Makovicky et al. (1986). The major difference between the Sudbury Complex and the Bushveld Complex is the amount of Pd contained in the initial sulphide melt that was available to be

concentrated in pentlandite, with the Bushveld Complex melt being the richer of the two. In addition, the Bushveld melt is a more fractionated Cu-rich liquid, which provides more Pd available to diffuse into pentlandite than a less fractionated liquid (Dare et al. 2010).

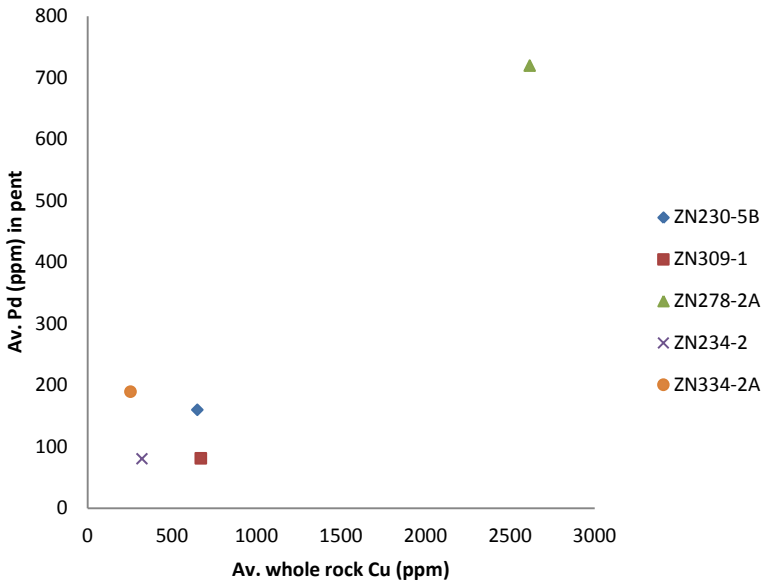


Figure 8.14. Plot of average Pd contents in pentlandite compared to average whole rock Cu.

Examination of the PGM in the chromitites (chapter 7) showed that the occurrence of PGM tellurides and bismuthides was widespread over the study area and the origin of the semi-metals and the paragenesis of these minerals was not clearly based on their associations. Bismuth, Te and As are common constituents of the BMS analysed, both as PGM inclusions and in solid solution (e.g. fig. 8.9). Similar Pt-Bi-Te micro-inclusions were also observed by Holwell and McDonald (2007). The presence of these inclusions within the BMS suggests that Pt and Bi were present in both mss and iss. However, as discussed above, Pt is incompatible in iss and mss, but is highly compatible in telluride and bismuthide melts, which have been shown to be immiscible in sulphide below 1000 $^{o}$C (Helmy et al. 2007), with Pt scavenged preferentially over Pd (Fleet et al. 1993). Experimental work by Helmy et al. (2007) demonstrated that a Te-rich melt (that may also contain other semi-metals such as Bi, Sb and As) can segregate from a fractionated sulphide melt as long as the Te concentration in this melt exceeds its solubility in Fe-rich mss and iss. Holwell and McDonald (2007) suggested that the micro-inclusions represent small droplets of the Bi-Te immiscible melt that were trapped as the mss and iss crystallised. It is therefore suggested that the source of these semi-metals was the original parental magma for the Platreef, rather than any addition through interaction with the country rock, as has been identified

further to the south on the farm Turfspruit (Hutchinson and McDonald 2008). The concentration of Te and Bi within sulphide inclusions trapped within chromite grains provides additional evidence to support this theory and is discussed further in chapter 9.

The staging chamber model proposed for the Platreef (e.g. McDonald and Holwell 2007; McDonald et al. 2009) may account for some of the observations made within this study, especially the apparent enrichment of Pd in pentlandite at Zwartfontein compared to the farms to the north and south. In this model, the magma reaches sulphide saturation within a staging chamber. The sulphide liquid, denser than its silicate counterpart, would collect at the base of the chamber. As the magma continues to flow through the staging chamber system, this sulphide liquid became more enriched in Ni, Cu, PGE and semi metals through interaction with new batches of magma. This process can account for the higher tenors seen in the Platreef chromitites compared to the Merensky Reef chromitites (fig. 8.12). The enriched sulphides were then deposited in the Platreef sills when later pulses of magma flushed through the conduit system. This feeder zone is proposed to be in the vicinity of Zwartfontein (chapter 7) and the sulphides analysed in this study have been shown to be more enriched than those analysed on Sandsloot and Overysel (Holwell and McDonald 2007).

## 8.6 Conclusion

This study has shown that there is a strong association between the PGE and BMS in the study area and that PGE distribution between the BMS and PGM is consistent with fractional crystallisation of a sulphide liquid. Os, Ir, Ru, Rh and Pd are present within solid solution in the cooling products of mss (pentlandite and pyrrhotite). The values obtained in this study are comparable to other studies carried out on the surrounding farms by Holwell and McDonald (2007), with elevated concentrations of PGE in samples from Zwartfontein, where the proposed feeder zone is proposed to be located, although concentration of PGE is evidently higher within the chromitite units compared to the pyroxenites. The chromitite samples from this study were also compared to the chromitite units from the Merensky Reef and have been shown be more enriched, especially for Pd in pentlandite.

In addition to the standard sulphide fractionation, it is proposed that a semi-metal rich immiscible sulphide liquid is also formed during the fractionation process based on the occurrence of micro-inclusions within the BMS. As a result, it is proposed that a significant proportion of the semi-metals were present within the parental magma and in the earliest

sulphide liquid rather than being added through interaction with the surrounding country rock.

# Chapter 9: Magmatic Sulphide Melt Inclusions Within Chromites

## 9.1 Introduction

During the formation of a magmatic sulphide deposit, the development of an immiscible sulphide liquid is a critical step. Without this, the precious metals will remain dispersed in the silicate magma. Some of the major questions that remain unanswered with respect to the genesis of the Platreef include identifying the source of the sulphur and constraining the timing of sulphide saturation in terms of whether it occurred prior to, or during the intrusion of the Platreef magma.

### 9.1.1 Use of S isotopes

As briefly mentioned in chapter 3, sulphur isotopes have been used to attempt to determine the origin of sulphur in the Platreef. This S may have originated from the mantle, the mid to lower crust, or from the local country rocks.

The first S isotopic study on the Bushveld Complex was carried out by Liebenberg (1970) who showed that most of the internal PGE reefs have mantle-like S isotopic signatures ($\delta^{34}S = 0 \pm 2‰$; Ohmoto and Rye 1979). Specific Platreef studies (e.g. Holwell et al. 2007; Penniston-Dorland et al. 2008; Sharman et al. 2013) have demonstrated that a significant component of S is either mantle S or derived from the Archaean crust rather than as a consequence of magma interaction with local Paleoproterozoic country rocks, and that any contamination-related effects are a modifying, not triggering process. This implies that the Platreef magma was S-saturated prior to emplacement.

A potential drawback of using S isotopes has been highlighted by Ihlenfeld and Keays (2011), who state that none of the previous Platreef studies have taken into account the potential importance of S isotope exchange between assimilated crustal S and mantle-derived magmatic S. This process is capable of masking or deleting the isotopic evidence of assimilated crustal S as it moves $\delta^{34}S$ rapidly to the mantle-like values that were observed in the Platreef studies above. Using S/Se ratios is a more robust way of investigating the source of S, as sedimentary rocks have relatively high S/Se ratios and the S/Se system is less easily obscured by the exchange process.

### 9.1.2 S/Se ratios

Selenium is a chalcophile element with a high partition coefficient into sulphide and has been used in many studies to investigate the formation of Ni-sulphide and PGE deposits associated with mafic and ultramafic rocks (Barnes et al. 2009). The use of Se in ore deposit

studies stems from the chemical similarity to S, with Se matching S behaviour at high magmatic/hydrothermal temperatures (Fitzpatrick 2008). Se concentrations vary depending on the type of rock. Crustal rocks typically contain very low concentrations of Se, with the average continental crust containing values of around 0.05 ppm (Taylor and McLennan 1985), while typical Se concentrations are around 70 ppm in granites and 300 ppm in basalts (Fitzpatrick 2008). It is generally assumed that S is more mobile than Se, based on the idea that S is more readily oxidised than Se and that the mobility of the elements increases along with their oxidation state (Barnes et al. 2009). Examination of sulphides in hydrothermal systems and sedimentary rocks also supports this theory (Auclair et al. 1987).

Mantle derived magmas generally have S/Se ratios of between 2,000 to 4,000 (Eckstrand and Hulbert 1987) and these ratios are largely mimicked in mafic magma systems where there are associated BMS without any obvious contamination. S/Se ratios have been used in many studies to investigate the processes involved in modifying BMS. Eckstrand et al. (1989) used Se/S ratios to document sedimentary contamination of mafic magma, while Peck and Keays (1990) investigated S remobilisation within magmatic deposits using Se/S ratios. Barnes et al. (2009) have shown that in the Upper Critical Zone, the Merensky Reef, UG2 and Bastard Reef all have S/Se ratios that are all broadly in the same range expected from mantle magmas (table 9.1). The same ranges are also observed in the chill zones for parental magmas to the Bushveld.

Table 9.1. S/Se ratios from the Upper Critical Zone and chill margins (Barnes et al. 2009)

| Upper Critical Zone | S/Se ratio |
|---|---|
| **Bastard Reef** | 2395-5455 |
| **Merensky Reef** | 1970-4070 |
| **UG2** | 1725-3770 |
| | |
| **B1 chill margin** | 3010-3550 |
| **B3 chill margin** | 2588-6255 |

Elevated S/Se ratios observed in norites from the Duluth Complex are suggested to be a result of crustal contamination (Thériault and Barnes 1998). S/Se values close to chondritic values of 2,500 (Dreibus et al. 1995) are suggested to represent a system in which PGE were concentrated in the sulphide liquid during sulphide liquid immiscibility that was discussed in chapter 8. Barnes et al. (2009) state that S/Se ratios lower than those in chondrites may represent rocks that have experienced S loss. S/Se ratios from sedimentary sulphides are

generally much larger (up to 500,000) as a result of fractionation of S and Se (Barnes et al. 2009). This occurs during weathering, diagenesis, low temperature fluid movement or as a result of low temperature metamorphism (e.g. Yamamoto 1976; McGoldrick and Keays 1981).

Recent work by Prichard et al. (2013) on the Jinchuan Ni-PGE deposit has shown that Se is potentially more mobile during post-magmatic alteration than previously thought. Se was mobilised in an oxidised acidic fluid and then reprecipitated to form selenide minerals when the fluid reacted with the carbonates. This highlights that care is needed in using S/Se ratios where oxidising alteration by low temperature hydrothermal fluids occurs in igneous complexes as the removal of Se will distort the apparent S loss estimation.

Ihlenfeld and Keays (2011) investigated the relationship between crustal contamination and PGE mineralisation in the Platreef by studying the down hole variation in S/Se, S and metal tenors from drillholes on Overysel, Sandsloot and Tweefontein. They state that the bulk of their samples have S/Se ratios that are greater than those of mantle-derived magmas, suggesting that there is a significant component of crustal S in most of their samples. The implications of these findings will be discussed later in this chapter.

### 9.1.3 Importance of sulphide inclusions

While the use of sulphur isotopes and S/Se ratios may reveal whether any external sulphur has been added to the sulphides, it is not possible to determine the timing due to the open nature of the system. Once the sulphide liquid forms, contamination may occur at any time up to and during crystallisation. Holwell et al. (2011) state that it is therefore not possible to distinguish between an initially magmatic sulphide that has been subsequently contaminated by local country rocks and sulphides that formed initially due to the addition of external sulphide. The discovery of trapped sulphide inclusions within chromite grains in the Platreef provides a potential solution to this problem.

Silicate melt inclusions have been studied extensively to investigate the composition of the initial melt in magmatic and mantle systems (e.g. Kamenetsky 1996; Spandler et al. 2000; Spandler et al. 2005). These silicate melt inclusions are most commonly found in spinels and olivines and are composed of residual glass as well as daughter silicate crystals. Experimental studies homogenise the melt inclusions in order to produce glasses with homogenous compositions that are representative of the trapped melt.

Sulphide melt inclusions, although much rarer than their silicate counterparts, have also been used to investigate the composition of initial parental magma. Sulphide inclusions in olivine phenocrysts have been observed in a variety of tectonic settings (McNeill et al. 2008) and may present the only direct evidence for sulphur saturation in addition to the composition of the early stage immiscible sulphide liquid in mantle derived magmas. The study of sulphide inclusions within quartz and garnets at the Broken Hill deposit by Sparks and Mavrogenes (2005) was used to illustrate the metamorphic history of the deposit. Sulphide melt inclusions in chromite from Madagascar have been described by McDonald et al. (1999) and Ohnenstetter et al. (1999).

The discovery of magmatic sulphide droplets within chromite grains in the Platreef by Holwell et al. (2011) has been important in investigating the source of sulphur and the timing of sulphide saturation within the system. The sulphide droplets within chromite grains in the Platreef are known to have been trapped at a very early stage in the magmatic history (and thus at high temperatures). Evidence of this exists in the form of sulphide droplets exhibiting negative crystal shapes imposed by the early crystallising host chromite. The host spinels themselves are often included inside orthopyroxene crystals. As these sulphide droplets were trapped by the chromite, they cooled and fractionated within the spinel and therefore little or no fractionated liquid or fluid-rich phases were able to escape. In addition, the closed system meant that no further enrichment of precious metals or sulphur upgrading from contamination could take place and therefore analysis of the metal and semi-metal concentrations gives a measurable analogue of the parental sulphide liquid at the time that the sulphide droplet was trapped. The compositions of these sulphide inclusions are therefore fundamental in testing the genetic models proposed for the Platreef.

## 9.2 Methods

Counterpart pieces of the chromite rich samples analysed for chromite chemistry and PGM mineralogy were also examined for sulphide inclusions. They were collected from a total of 18 drillholes across the 3 farms of Overysel, Zwartfontein and Sandsloot along strike and down dip of the Platreef in order to maximise the areal extent.

### 9.2.1 Homogenisation of samples

In order to analyse the sulphide inclusions within the chromite grains, the inclusions have to be exposed by polishing. When the sulphide melt was trapped by chromite, the closed system meant that it was able to fractionate into the different sulphide phases +/- PGM (fig. 9.1).

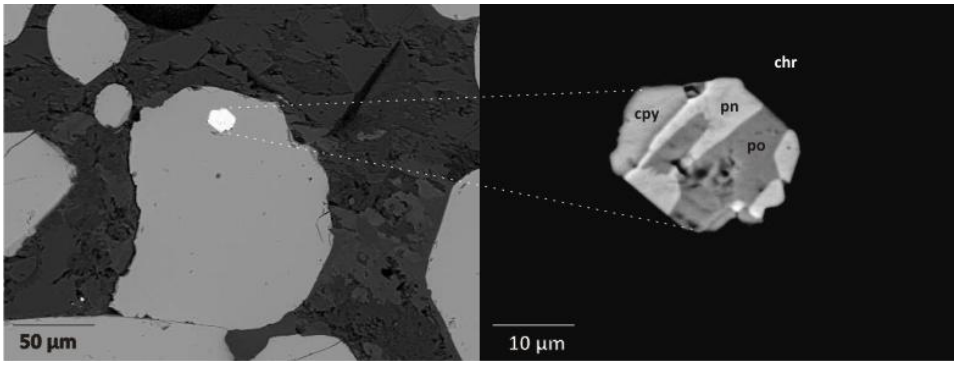


Figure 9.1. Unhomogenised sulphide inclusion in chromite (chr), showing polyphase nature (cpy-chalcopyrite, pn-pentlandite, po-pyrrhotite).

A significant disadvantage of exposing the sulphide inclusions is the loss of unknown fractionated material during the polishing (fig. 9.2 a & b). In order to overcome this problem, the sulphide inclusions were homogenised prior to polishing.

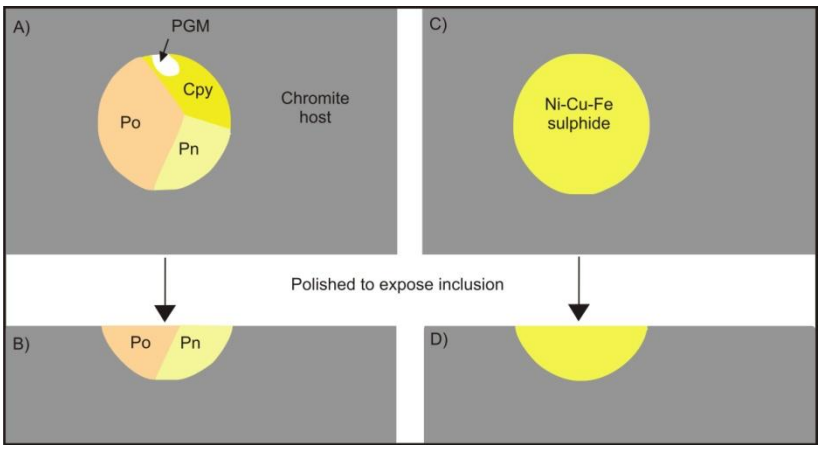


Figure 9.2. Schematic diagram showing the fractionation and polishing problem (A and B), solved using homogenisation techniques (C and D) modified from Holwell et al. (2011).

Using the method described by Holwell et al. (2011), the samples were heated to a temperature sufficient to melt the sulphides but not the surrounding chromite and then quenched quickly to produce a homogenous sulphide inclusion. The solidus temperature for chromite is very high, around 1,200 – 1,400 $^{o}$C, depending on oxygen fugacity and pressure (Roeder and Reynolds 1991), whereas the sulphides melt below 1000 $^{o}$C (Barnes et al. 2006).

The homogenisation experiments were performed at Edinburgh University under the supervision of Dr Ian Butler. Samples were cut to 1 x 1 x 0.5 cm blocks and held in a 0.3 mm platinum wire cage, suspended from a drop-quench apparatus using a fine 0.1 mm Pt wire (fig. 9.3). A $CO_2/H_2$ gas mix with $fO_2$ of $QFM^{-1}$ (Quartz-Fayalite-Magnetite – 1 log unit) using the JANAF tables of Deines et al. (1974) was established in the tube furnace to prevent the oxidation of the inclusions and bulk rock. The sample was lowered into the hot spot at 1190 °C and soaked at that temperature for 30 minutes. The temperature and soaking times were altered from the original methodology of Holwell et al. (2011). It was discovered that at the higher temperatures, the survivability of the inclusions was compromised as the temperature was too close to the solidus temperature of chromite of 1200 – 1400 °C (Roeder and Reynolds 1991). The homogenisation temperature was monitored using an R-type thermocouple. The 0.1 mm Pt wire was electrically fused so that the sample fell out of the hot spot to a vessel of water at room temperature to give an instant quench.

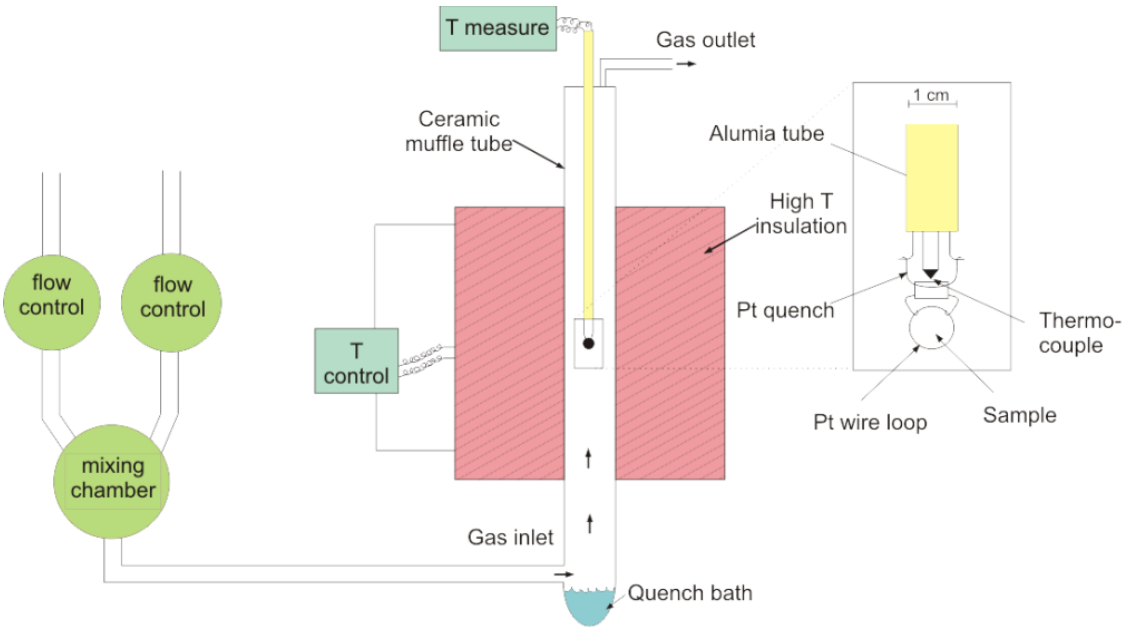


Figure 9.3. Schematic diagram of quench furnace modified from Holloway and Wood (1988)

The homogenised samples were then cut and polished to expose any homogenous inclusions. When analysed these are representative of the initial composition of the initial sulphide liquid (fig. 9.2 c & d).

The homogenised inclusions (fig. 9.4) still possess the negative crystal shape illustrating that the chromite host was unaffected by the homogenisation procedure. Often a fine-grained myrmekitic or exsolution texture on a scale of 1-2 microns is observed in the homogenised inclusions, which has also been documented by Holwell et al. (2011) and is characteristic of rapidly quenched sulphide melts (Sparks and Mavrogenes 2005; McNeill et al. 2008).

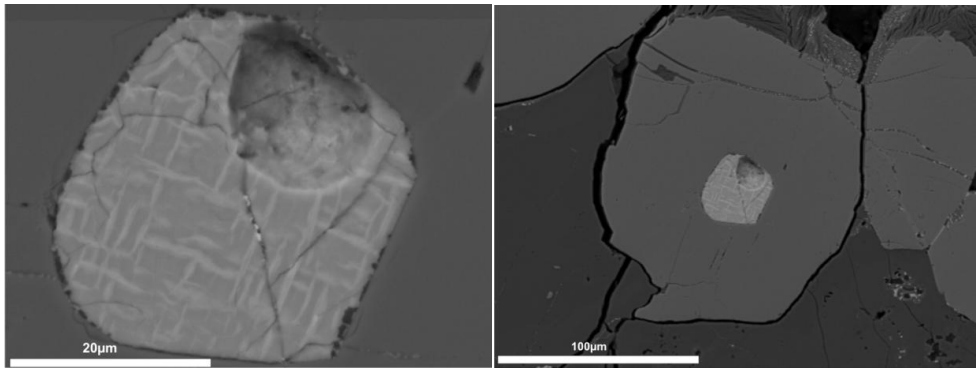

Figure 9.4. Exsolution texture observed in homogenised inclusions indicative of rapid cooling sulphide liquid.

### 9.2.2 Analysis

Homogenised sulphide inclusions were analysed by laser ablation using a New Wave Research ESI UP-213 laser system coupled to a Thermo X Series 2 ICP-MS at Cardiff University using the methodology of Holwell et al. (2011). Ablations were carried out under He (flow rate *0.7 L/min) and the resulting vapour combined with Ar (flow rate 0.56–0.65 L/min) before delivery to the ICP-MS. Due to the small nature of the inclusions, most analyses were performed using a 20µm laser spot. Where possible, a 40 µm laser spot was used in order to analyse bigger inclusions. The average size of the inclusions was around 10 µm, however a laser spot exceeding the diameter of the inclusion was selected to ensure that as much of the inclusion as possible was ablated. Due to the distinctly different composition between the host chromite and the sulphide inclusions, it was possible to resolve and isolate portions of the laser time spectra contributed by chromite and sulphide for signal processing.

The isotopes $^{33}$S, $^{59}$Co, $^{61}$Ni, $^{65}$Cu, $^{66}$Zn and $^{68}$Zn were detected to monitor the composition of the sulphides and the sulphide phases. The precious metal isotopes $^{99}$Ru, $^{101}$Ru, $^{103}$Rh, $^{105}$Pd, $^{106}$Pd, $^{189}$Os, $^{193}$Ir, $^{195}$Pt and $^{197}$Au were analysed in addition to the isotopes of the semi-metals $^{75}$As, $^{82}$Se, $^{125}$Te, $^{121}$Sb and $^{209}$Bi, which commonly couple with the precious metals to form PGM. An advancement since the work of Holwell et al. (2011) has been the addition of new standards for quantitative analysis of Se, Cd, Ag and Re. Sulphur was determined by internal standard corrections using $^{33}$S and S analyses of the homogenised sulphides using the Cambridge Instruments LEO S360 SEM prior to ablation. Full details of the LA-ICP-MS analytical conditions and standards are described in McDonald (2005) and Prichard et al. (2013).

## 9.3 Results

Sulphide inclusions were rarer than expected based on the initial results found by Holwell et al. (2011). A total of 123 homogenised blocks were prepared and polished. Of those 123 blocks, only 16 blocks contained inclusions, resulting in the analysis of 55 inclusions. The absolute concentrations of Ni, Cu, PGE, Au and some semi metals within the analysed homogenised inclusions are shown in table 9.2. What is evident from table 9.2 is that there is great variation within the composition of the inclusions, even between those enclosed in different chromite crystals from the same sample. Most inclusions are either Ni or Cu rich, with inclusions that have similar concentrations of the two major elements being rare. The average concentration in the homogenised inclusions can also be compared to the bulk rock concentrations (table 9.3), showing that the inclusions are highly concentrated in all the shown elements. Average Pt/Pd ratios are 1.11, which is slightly above the bulk rock ratio (0.93) and other Platreef values, which are generally at unity or slightly below unity (e.g. Kinnaird et al. 2005; McDonald et al. 2005; Holwell and McDonald 2006; McDonald and Holwell 2011).

A series of time-resolved analysis (TRA) spectra are shown in figures 9.5 & 9.6 which illustrate the typical patterns obtained from the analyses of the homogenised inclusions. Due to the number of elements analysed, each laser ablation analysis is shown on two separate diagrams, with Cu, Pd, Pt, Au and the semi metals on the first diagram and Ni, Rh, Os, Ir and Ru shown on the second. The relative size of the inclusion can be deduced by the width of the profile on the x-axis, which indicates the time taken to ablate the sulphide at a constant rate and then re-enter the host spinel.

Table 9.2 Absolute concentrations of homogenised sulphide inclusions from chromite hosts within the Platreef (n.a = not analysed)

| | | Ni | Cu | As | Se | Sb | Te | Bi | Ru | Rh | Pd | Os | Ir | Pt | Au | Pt/Pd |
|---|---|---|---|---|---|---|---|---|---|---|---|---|---|---|---|---|
| | | wt% | wt% | ppm | ppm | ppm | ppm | ppm | ppm | ppm | ppm | ppm | ppm | ppm | ppm | |
| **101 incl 1** | ZN573-4A | 2.64 | 12.99 | <5 | 119.00 | 1.25 | 9.05 | 38.71 | 141.60 | 63.63 | 69.54 | 11.22 | 25.64 | 158.60 | 1.66 | 2.28 |
| **101 incl 2** | ZN573-4A | 4.14 | 11.68 | <5 | 130.90 | 2.57 | 7.07 | 312.90 | 21.45 | 33.15 | 315.40 | 5.29 | 8.76 | 134.20 | 0.25 | 0.43 |
| **101 incl 3** | ZN573-4A | 5.04 | 15.97 | <5 | 109.38 | 0.51 | 14.15 | 77.36 | 152.00 | 124.50 | 664.40 | 9.00 | 26.41 | 401.60 | 9.92 | 0.60 |
| **101 incl 6** | ZN573-4A | 7.50 | 13.10 | 64.25 | 183.24 | 44.89 | 7.36 | 111.70 | 141.60 | 63.63 | 648.90 | 12.11 | 25.77 | 438.40 | 15.52 | 0.68 |
| **101 incl 8** | ZN573-4A | 6.91 | 12.76 | <5 | 343.43 | 0.59 | 22.61 | 31.03 | 506.10 | 296.70 | 271.10 | 45.67 | 147.40 | 699.50 | 6.97 | 2.58 |
| **101 incl 10** | ZN573-4A | 18.90 | 2.26 | <5 | 150.52 | 0.09 | 23.13 | 56.05 | 126.20 | 86.55 | 319.60 | 11.36 | 27.24 | 231.00 | 9.16 | 0.72 |
| **101 incl 11** | ZN573-4A | 14.69 | 1.48 | <5 | 210.33 | 1.43 | 7.15 | 17.34 | 122.50 | 80.53 | 121.80 | 13.90 | 20.40 | 67.96 | 0.96 | 0.56 |
| **101 incl 14** | ZN573-4A | 8.41 | 9.41 | <5 | 291.57 | 2.17 | 23.30 | 395.70 | 116.90 | 65.23 | 349.80 | 12.74 | 21.11 | 261.20 | 0.05 | 0.75 |
| **101 incl 15** | ZN573-4A | 21.66 | 2.83 | <5 | 279.57 | 0.05 | 22.97 | 28.06 | 267.10 | 253.50 | 307.40 | 25.51 | 99.16 | 1239.0 | 10.29 | 4.03 |
| **99 incl 1** | ZN573-2A | 2.20 | 10.76 | <5 | 42.25 | 0.53 | 4.02 | 83.83 | 32.02 | 23.41 | 75.33 | 3.22 | 6.10 | 92.19 | 1.38 | 1.22 |
| **99 incl 2** | ZN573-2A | 2.72 | 12.43 | <5 | 115.29 | 0.93 | 8.95 | 45.96 | 121.30 | 62.78 | 79.36 | 9.01 | 24.12 | 171.50 | 2.00 | 2.16 |
| **99 incl 3b** | ZN573-2A | 3.03 | 10.99 | 14.83 | 48.62 | 3.10 | 0.27 | 55.78 | 147.70 | 85.58 | 85.43 | 11.39 | 19.07 | 274.10 | 1.69 | 3.21 |
| **99 incl 3d** | ZN573-2A | 2.32 | 12.78 | 5.76 | 92.76 | 2.32 | 13.13 | 52.63 | 143.90 | 91.91 | 93.32 | 12.18 | 22.29 | 316.80 | 1.65 | 3.39 |
| **99 incl 4** | ZN573-2A | 2.26 | 12.52 | <5 | 188.76 | 3.85 | 8.37 | 40.69 | 99.69 | 56.41 | 148.50 | 6.30 | 11.40 | 132.40 | 1.77 | 0.89 |
| **99 incl 5** | ZN573-2A | 1.73 | 13.12 | <5 | 150.38 | 1.94 | 9.50 | 39.68 | 60.18 | 50.94 | 160.90 | 5.30 | 12.41 | 134.40 | 2.13 | 0.84 |
| **86 incl 2** | OY551-1B | 1.65 | 13.22 | 16.27 | 35.76 | 4.84 | 9.85 | 150.20 | 1.27 | 11.07 | 91.22 | 0.16 | 0.12 | 47.48 | 5.05 | 0.52 |
| **86 incl 3** | OY551-1B | 2.23 | 12.55 | <5 | 184.90 | 0.58 | 2.09 | 33.78 | 3.84 | 13.62 | 89.44 | 0.55 | 0.89 | 40.60 | 3.47 | 0.45 |
| **86 incl 4** | OY551-1B | 2.52 | 13.61 | <5 | 105.52 | 0.38 | 6.77 | 23.32 | 2.22 | 11.47 | 45.10 | 0.16 | 0.29 | 17.70 | 2.86 | 0.39 |
| **56 incl 1** | SS393-1A | 3.17 | 14.81 | <5 | 167.38 | 1.57 | 15.60 | 32.18 | 11.10 | 18.92 | 72.23 | 0.73 | 1.98 | 24.23 | 3.17 | 0.34 |
| **56 incl 3** | SS393-1A | 6.31 | 13.91 | <5 | 196.62 | 0.97 | 12.71 | 38.60 | 10.52 | 15.82 | 82.40 | 0.74 | 1.85 | 26.88 | 4.50 | 0.33 |
| **103 incl 1b** | OY335-B | 11.72 | 1.34 | <5 | 180.80 | 0.93 | 5.44 | 1.83 | 53.76 | 70.05 | 222.40 | 2.63 | 14.58 | 296.90 | 2.24 | 1.33 |
| **14 incl 1** | ZN230-1B | 4.04 | 31.70 | 46.99 | 194.00 | 11.92 | 320.60 | 3160.0 | n.a | 41.03 | 478.40 | 1.72 | 9.43 | 643.90 | 211.50 | 1.35 |
| **14 incl 3** | ZN230-1B | 4.49 | 29.79 | <5 | 55.00 | 2.36 | 4.00 | 16.80 | n.a | 1.01 | 38.04 | 0.15 | 0.32 | 14.60 | 2.30 | 0.38 |
| **26 incl 1a** | ZN230-5A | 7.97 | 24.35 | <5 | 194.00 | 0.32 | 13.48 | 0.83 | n.a | 5.54 | 35.55 | 1.00 | 2.03 | 29.45 | 4.67 | 0.83 |
| **26 incl 2** | ZN230-5A | 5.86 | 24.70 | <5 | 152.00 | 0.43 | 9.74 | 0.20 | n.a | 1.55 | 43.08 | 0.08 | 0.17 | 8.57 | 2.21 | 0.20 |
| **27 incl 2** | ZN230-5B | 4.53 | 32.61 | <5 | 298.00 | 1.58 | 47.78 | 43.16 | n.a | 15.96 | 496.90 | 0.86 | 2.13 | 144.37 | 18.04 | 0.29 |
| **36 incl 2** | OY517-C | 13.53 | 2.42 | <5 | 134.00 | 0.43 | 9.74 | 107.40 | n.a | 90.22 | 223.80 | 0.08 | 0.17 | 528.80 | 2.21 | 2.36 |
| **88 incl 1** | OY252-1 | 1.85 | 17.94 | 43.67 | 75.80 | 25.35 | 34.79 | 51.65 | 12.26 | 10.82 | 35.75 | 0.50 | 5.34 | 57.03 | 0.18 | 1.60 |
| **88 incl 4** | OY252-1 | 2.58 | 25.45 | 14.90 | 136.80 | 13.65 | 4.51 | 27.96 | 10.57 | 4.17 | 20.25 | 0.77 | 3.79 | 22.50 | 1.22 | 1.11 |
| **88 incl 5** | OY252-1 | 10.25 | 3.93 | <5 | 104.50 | 4.39 | 15.86 | 6.81 | 7.22 | 4.91 | 34.59 | 0.80 | 2.17 | 12.93 | 0.77 | 0.37 |
| **88 incl 6** | OY252-1 | 2.03 | 27.84 | 6.08 | 222.60 | 7.48 | 11.82 | 103.10 | 15.83 | 16.47 | 437.66 | 0.44 | 2.00 | 163.50 | 14.61 | 0.37 |

Table 9.2. cont.

| | | | | | | | | | | | | | | | | |
|---|---|---|---|---|---|---|---|---|---|---|---|---|---|---|---|---|
| **88 incl 9** | OY252-1 | 9.86 | 4.78 | 50.16 | 261.10 | 8.68 | 15.89 | 37.95 | 33.40 | 25.33 | 356.82 | 4.40 | 12.96 | 221.30 | 1.46 | 0.62 |
| **88 incl 10** | OY252-1 | 8.12 | 2.78 | 20.45 | 148.40 | 3.48 | 10.28 | 5.70 | 17.08 | 15.89 | 125.00 | 2.01 | 4.15 | 94.28 | 0.30 | 0.75 |
| **88 incl 11a** | OY252-1 | 4.73 | 15.29 | 30.44 | 86.72 | 66.61 | 13.76 | 25.70 | 16.60 | 13.53 | 202.38 | 1.86 | 3.34 | 112.60 | 1.87 | 0.56 |
| **88 incl 11b** | OY252-1 | 4.67 | 16.26 | 20.57 | 248.70 | 74.62 | 6.08 | 30.54 | 10.94 | 15.49 | 222.82 | 0.28 | 2.60 | 126.10 | 2.24 | 0.57 |
| **88 incl 12a** | OY252-1 | 14.75 | 3.28 | 10.63 | 109.60 | 6.94 | 8.84 | 16.04 | 30.83 | 35.03 | 239.70 | 2.39 | 9.84 | 297.15 | 12.72 | 1.24 |
| **88 incl 13** | OY252-1 | 11.64 | 13.07 | 38.56 | 48.80 | 13.74 | 16.34 | 18.22 | 17.56 | 12.12 | 84.20 | 3.90 | 5.72 | 105.30 | 0.96 | 1.25 |
| **88 incl 14** | OY252-1 | 4.89 | 11.66 | 16.79 | 105.60 | 4.01 | 26.12 | 25.35 | 2.49 | 2.76 | 93.52 | 0.54 | 1.08 | 33.45 | 8.10 | 0.36 |
| **88 incl 15a** | OY252-1 | 4.15 | 17.84 | 6.95 | 107.90 | 52.78 | 47.41 | 22.25 | 22.80 | 4.14 | 155.35 | 0.26 | 1.87 | 106.80 | 2.55 | 0.69 |
| **88 incl 15b** | OY252-1 | 9.86 | 3.73 | 5.42 | 156.10 | 0.84 | 1.46 | 6.03 | 27.06 | 19.45 | 134.99 | 1.37 | 6.12 | 145.21 | 1.82 | 1.08 |
| **118 incl 1** | ZN278-1 | 1.65 | 29.47 | <5 | 358.20 | 15.28 | 203.10 | 127.70 | 8.48 | 29.58 | 474.55 | 1.28 | 3.84 | 805.10 | 53.35 | 1.70 |
| **118 incl 2** | ZN278-1 | 2.18 | 22.19 | 14.02 | 233.80 | 1.92 | 68.11 | 49.37 | 13.29 | 26.89 | 224.77 | 4.45 | 5.41 | 435.90 | 20.57 | 1.94 |
| **117 incl 1** | ZN324-2 | 1.95 | 34.26 | 50.35 | 161.90 | 13.40 | 34.75 | 139.40 | 30.05 | 4.84 | 142.65 | 1.86 | 2.07 | 23.12 | 9.13 | 0.16 |
| **87 incl 1** | OY551-1A | 1.39 | 28.92 | 20.82 | 253.70 | 3.52 | 4.27 | 35.32 | 14.71 | 15.30 | 68.15 | 0.66 | 5.56 | 98.52 | 8.27 | 1.45 |
| **87 incl 2** | OY551-1A | 2.15 | 13.91 | 37.62 | 95.34 | 0.29 | 2.34 | 20.32 | 11.79 | 5.78 | 45.88 | 0.77 | 2.12 | 80.19 | 2.39 | 1.75 |
| **29 incl 3** | OY447-1A | 2.24 | 29.83 | <5 | 455.24 | 0.37 | 25.85 | 255.10 | n.a | 45.00 | 1037.0 | 2.87 | 11.47 | 1608.8 | 9.77 | 1.55 |
| **29 incl 4** | OY447-1A | 1.99 | 34.15 | <5 | 214.00 | 1.91 | 43.89 | 75.29 | n.a | 74.55 | 738.30 | 9.60 | 27.35 | 1504.8 | 36.33 | 2.04 |
| **29 incl 5** | OY447-1A | 2.87 | 23.41 | <5 | 310.00 | 0.52 | 61.57 | 284.60 | n.a | 55.37 | 628.90 | 7.31 | 14.58 | 514.00 | 46.85 | 0.82 |
| **29 incl 7a** | OY447-1A | 14.20 | 12.99 | 208.40 | 206.00 | 0.28 | 0.42 | 7.30 | n.a | 57.55 | 254.20 | 5.96 | 12.57 | 169.36 | 8.64 | 0.67 |
| **29 incl 8** | OY447-1A | 4.22 | 22.03 | <5 | 390.48 | 1.28 | 0.23 | 28.42 | n.a | 56.25 | 435.50 | 4.31 | 13.78 | 356.72 | 6.08 | 0.82 |
| **29 incl 9** | OY447-1A | 3.45 | 18.73 | <5 | 293.33 | 0.47 | 10.37 | 147.10 | n.a | 110.60 | 586.30 | 13.00 | 36.02 | 1660.8 | 7.67 | 2.83 |
| **34 incl 4** | OY517-A | 10.35 | 2.54 | <5 | 149.04 | 0.14 | 6.64 | 25.47 | n.a | 31.61 | 101.27 | 3.44 | 6.78 | 99.72 | 4.17 | 0.98 |
| **121 incl 2** | OY359-1 | 1.62 | 25.56 | 5.02 | 92.00 | 17.32 | 2.46 | 50.18 | 22.59 | 10.43 | 95.24 | 0.54 | 3.58 | 39.34 | 19.68 | 0.41 |
| **121 incl 4** | OY359-1 | 3.27 | 31.83 | <5 | 202.30 | 5.25 | 10.91 | 167.20 | 10.91 | 6.20 | 293.54 | 1.69 | 3.22 | 91.44 | 71.46 | 0.31 |
| **121 incl 5** | OY359-1 | 10.87 | 10.08 | <5 | 329.00 | 20.30 | 24.32 | 39.60 | 44.30 | 21.76 | 293.90 | 1.92 | 14.07 | 64.26 | 21.80 | 0.22 |

Table 9.3 Average concentrations of homogenised sulphide inclusions and comparison to average bulk rock values (ppb) for samples analysed in chapter 5. Key n.a = not analysed.

| | Ni | Cu | As | Se | Sb | Te | Bi | Ru | Rh | Pd | Os | Ir | Pt | Au | 4E | Pt/Pd |
|---|---|---|---|---|---|---|---|---|---|---|---|---|---|---|---|---|
| **Average inclusion** | wt% | wt% | ppm | ppm | ppm | ppm | ppm | ppm | ppm | ppm | ppm | ppm | ppm | ppm | ppm | |
| **n=55** | 5.93 | 15.89 | 6.86 | 180.20 | 8.31 | 24.57 | 124.10 | 63.42 | 44.85 | 239.86 | 5.13 | 13.72 | 284.12 | 12.77 | 545.60 | 1.11 |
| | | | | | | | | | | | | | | | | |
| **Average bulk rock** | | | | | | | | | | | | | | | | |
| **n=63** | 0.14 | 0.06 | n.a | n.a | n.a | n.a | n.a | 0.23 | 0.15 | 1.33 | 0.02 | 0.05 | 1.24 | 0.12 | 2.84 | 0.93 |

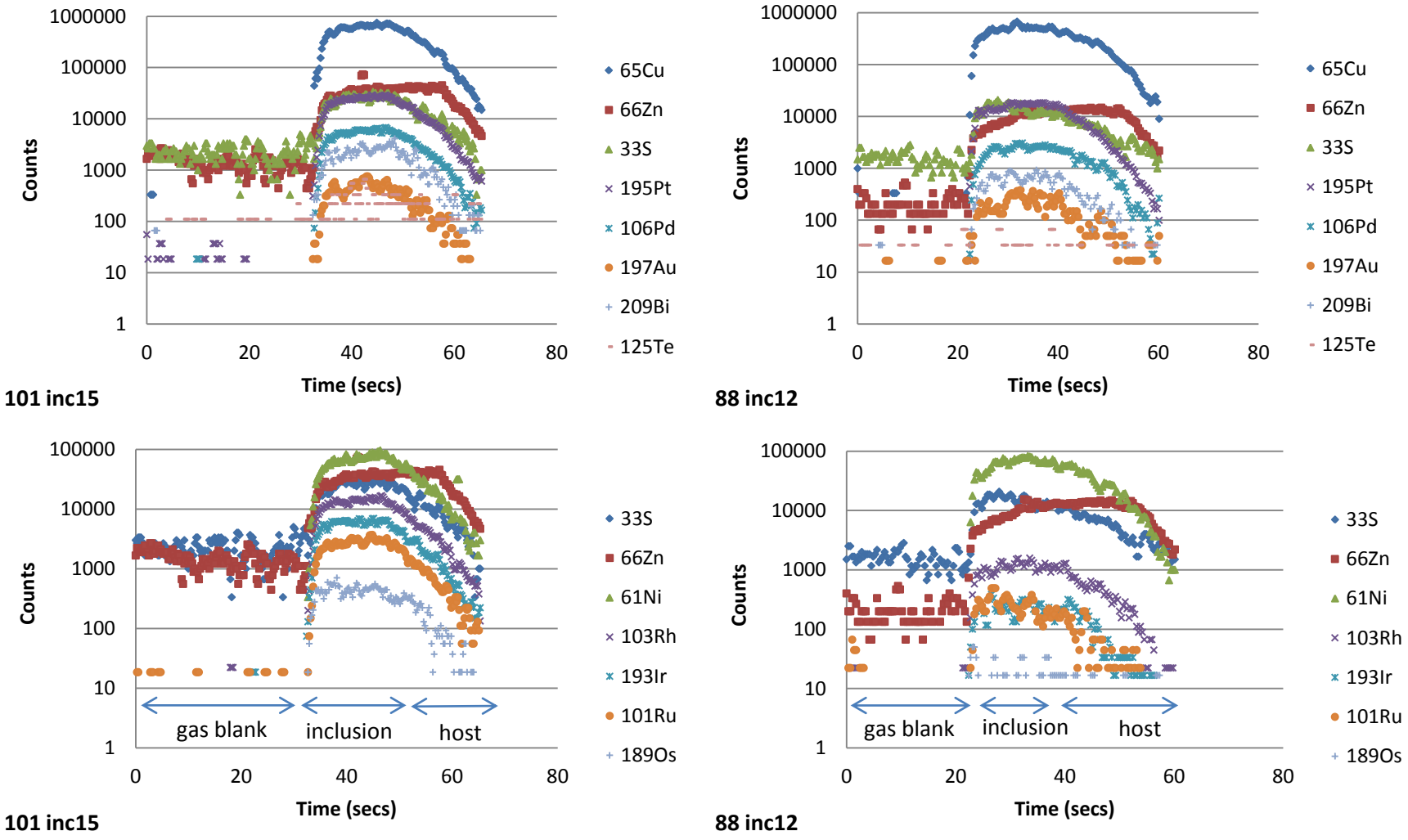


Figure 9.5. Split time-resolved analysis (TRA) spectra from the ablation of homogenised sulphide inclusions within chromite from sample 101 and 88

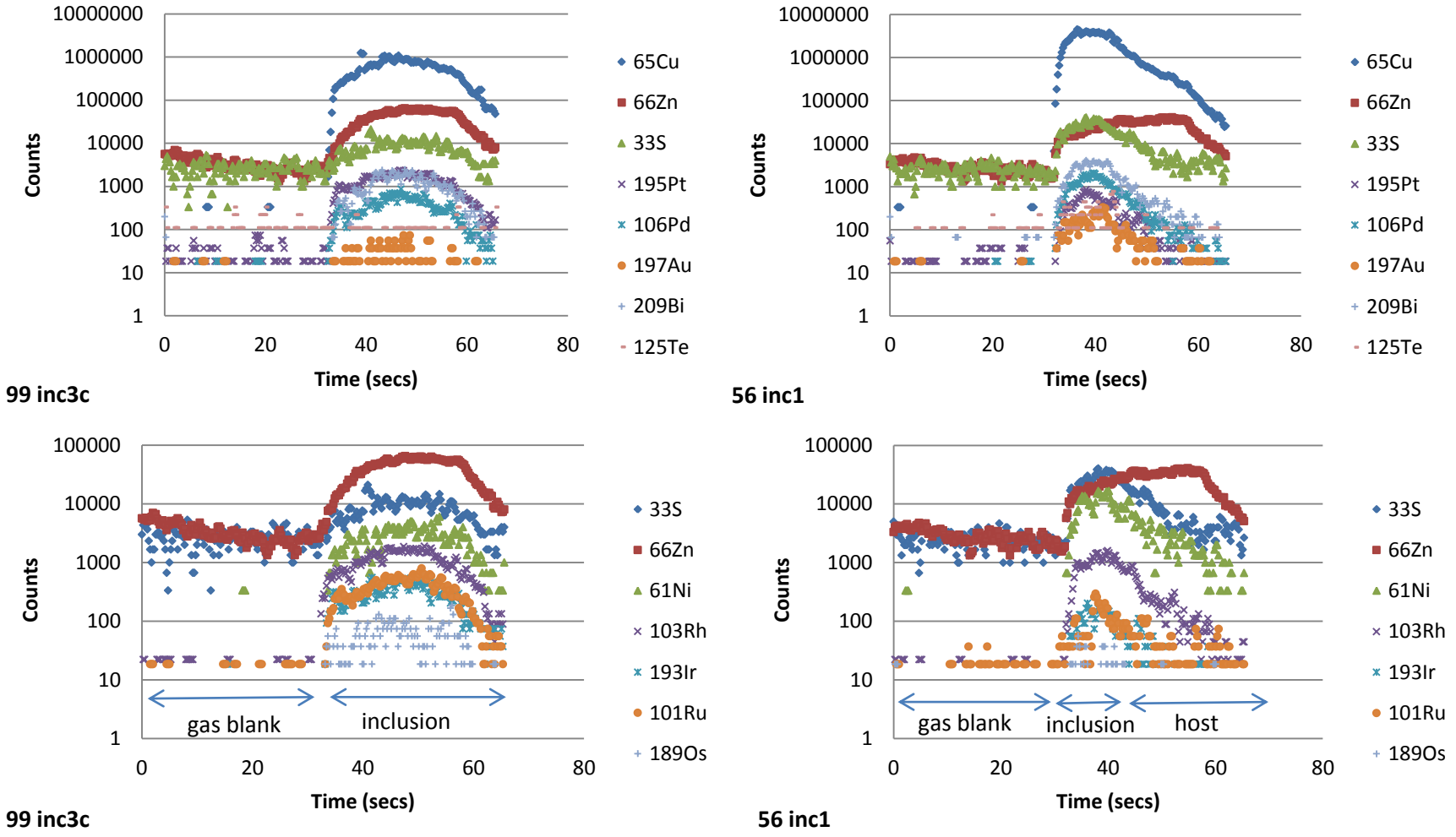


Figure 9.6. Split time-resolved analysis (TRA) spectra from the ablation of homogenised sulphide inclusions within chromite from sample 99 and 56

In addition to measuring the precious metal tenors, Se concentrations were measured and a ratio of S/Se was calculated, using the average S composition for the inclusions of 35 wt%. This ratio is then plotted against Pd, Pt and the combined Pd + Pt tenors as shown in figure 9.7. The mantle range for S/Se is also shown on the scattergraphs. Although some samples plot within this mantle range of 2000-4000 (Eckstrand and Hulbert 1987), a significant proportion of the data falls outside the range, with the majority being lower than the mantle range.

## 9.4 Discussion

It is clear that the sulphide inclusions are highly enriched, with precious metal tenors up to 2 orders of magnitude greater than that measured from the bulk rock (table 9.2). Similar results were achieved in the study by Holwell et al. (2011; table 9.4). As a result, the PGE mass balance must be accounted for. The B1 magma 4E (Pt + Pd + Rh + Au) values are estimated to be 33 ppb (Barnes and Maier 2002a) compared to the average measured 4E values of 546 ppm - more than 4 orders of magnitude different. Therefore the sulphide liquid that produced the Platreef must have equilibrated with huge volumes of magma to produce the measured concentrations of precious metals. Some inclusions represent very highly enriched sulphide liquid, e.g. inclusion 29-3 which has a 4E value of in excess of 2,700 ppm. There is also a diversity of high and low tenor sulphide inclusions observed in the data set. Low tenor inclusions may not be true inclusions, i.e. cracks may exist within the chromite grain which allows the sulphide inclusion to 'bleed' out during the homogenisation process, or there might be an entirely different explanation, discussed later in the chapter.

Table 9.4 Results from analysis of homogenised inclusions within chromite grains by Holwell et al. (2011)

| (ppm) | Os | Ir | Ru | Rh | Pt | Pd | Au |
|---|---|---|---|---|---|---|---|
| **Average** | 2.6 | 8.6 | 36.4 | 37.4 | 192 | 160 | 6.2 |
| **n=15** | | | | | | | |
| **Range** | 0.3-10 | 0.8-39 | 9.4-104 | 3.8-151 | 24-903 | 38-683 | 0.4-40 |

In addition to the enrichment in PGE and Au, the inclusions contain significant amounts of semi metals. The consistent occurrence of Bi and Te (and occasional As) concentrations within the inclusions suggests that these semi-metals were present in the parental magma. This can be used as evidence to suggest that the semi-metal rich PGM identified in chapter 7 are primary assemblages and have not formed as a result of contamination from the country rocks or hydrothermal re-distribution. These observations also support the theory by Kinloch (1982) that the Bi- and Te- PGM are seen across the whole study area as they occur as a background feature inherited from the parental magma.

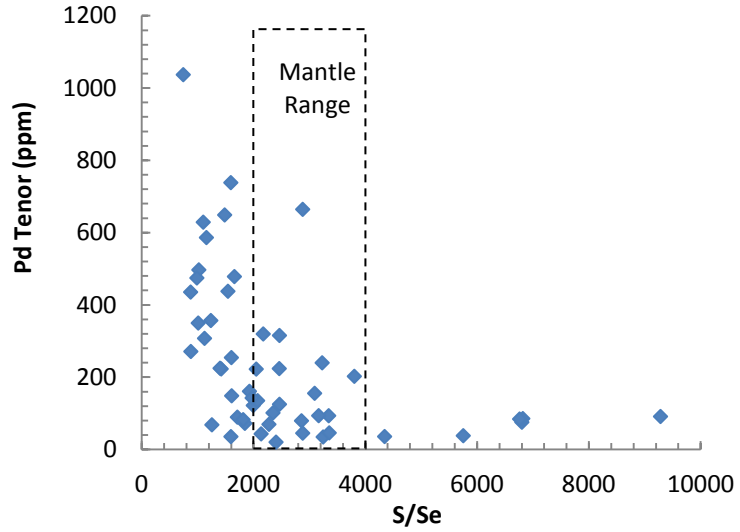


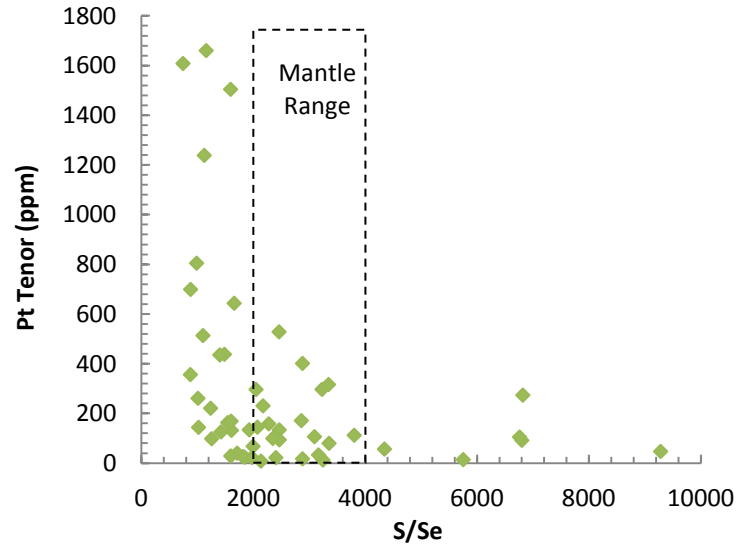


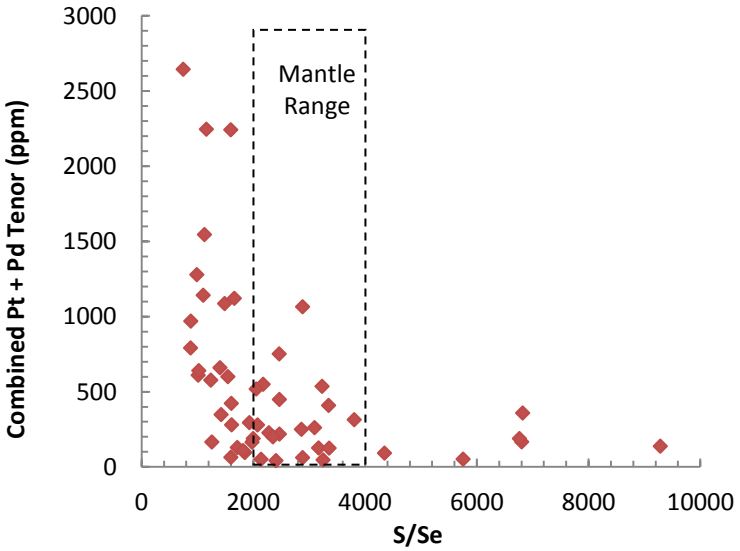


Figure 9.7. Scattergraphs of S/Se ratios vs (a) Pd tenors, (b) Pt tenors and (c) combined Pt + Pd tenors (ppm) for the homogenised sulphide inclusions.

The average Pt/Pd ratio of the inclusions is 1.11, which is half the bulk rock ratio of 2 for the Merensky Reef and the sulphide liquid parental to the Merensky Reef that has been modeled at just under 2 (Godel et al. 2007; Naldrett et al. 2009b). This discrepancy is hugely important and must be taken into account when considering the Platreef to be equivalent to the Merensky Reef.

### 9.4.1 Variation in tenors across the study area

Sulphide inclusions have been found in 11 different drillholes and therefore the variation in tenors can be investigated across the three farms on the study area. The staging chamber model of McDonald and Holwell (e.g. McDonald and Holwell 2007; McDonald et al. 2009) proposed a feeder (or multiple feeder) zone to the west of the study area. It can be suggested that there might be variations in PGE content of the sulphide inclusions along strike and with increasing distance from the feeder zone, with those closest to the feeder zone having the highest tenors.

Table 9.5. Average tenor values and ratios for analysed inclusions

| | n | 4E | Pt/Pd | Pt+Pd/Rh |
|---|---|---|---|---|
| **ZN573** | 15 | 664.50 | 1.62 | 6.72 |
| **OY551** | 5 | 140.71 | 0.91 | 12.05 |
| **SS393** | 2 | 124.08 | 0.33 | 6.00 |
| **OY335** | 1 | 591.59 | 1.33 | 7.41 |
| **ZN230** | 5 | 447.33 | 0.61 | 32.93 |
| **OY517** | 2 | 540.90 | 1.67 | 7.35 |
| **OY252** | 13 | 297.70 | 0.81 | 23.24 |
| **ZN278** | 2 | 1035.36 | 1.82 | 33.91 |
| **ZN324** | 1 | 179.74 | 0.16 | 34.28 |
| **OY447** | 6 | 1668.22 | 1.45 | 25.22 |
| **OY359** | 3 | 343.02 | 0.31 | 30.48 |

The average 4E tenors of the sulphide inclusions (table 9.5) are plotted on the study area map (fig. 9.8). Variations in 4E, Pt/Pd and Pt+Pd/Rh ratios for the N-S strike lines are shown in figure 9.9. In figure 9.9 a, the closest hole (ZN230) to the proposed feeder zone actually has lower 4E values and Pt/Pd ratios than the surrounding holes, a feature which is also shown in figure 9.9 b with hole ZN324. The variation in the number of inclusions analysed in each drillhole (table 9.5) may however be a factor. Due to the limited amount of inclusions identified overall, up-dip (W-E) variation is hard to determine as shown by figure 9.10.

It is evident that there is limited correlation between the distance from the proposed feeder zone and the tenors of the sulphide inclusions. This may be because of the timing of entrapment of the sulphide inclusion. Early trapped inclusions may not have been upgraded

in precious metal tenor as much as those that were trapped later. Holwell et al. (2011) suggested that the inclusions with the highest tenors could be found closer to the conduits in the deeper plumbing system. However, when the sulphide droplets were mobilised by flowing magma, individual droplets from different parts of the primary conduit system may have been entrained together, accounting for the differing tenors between inclusions.

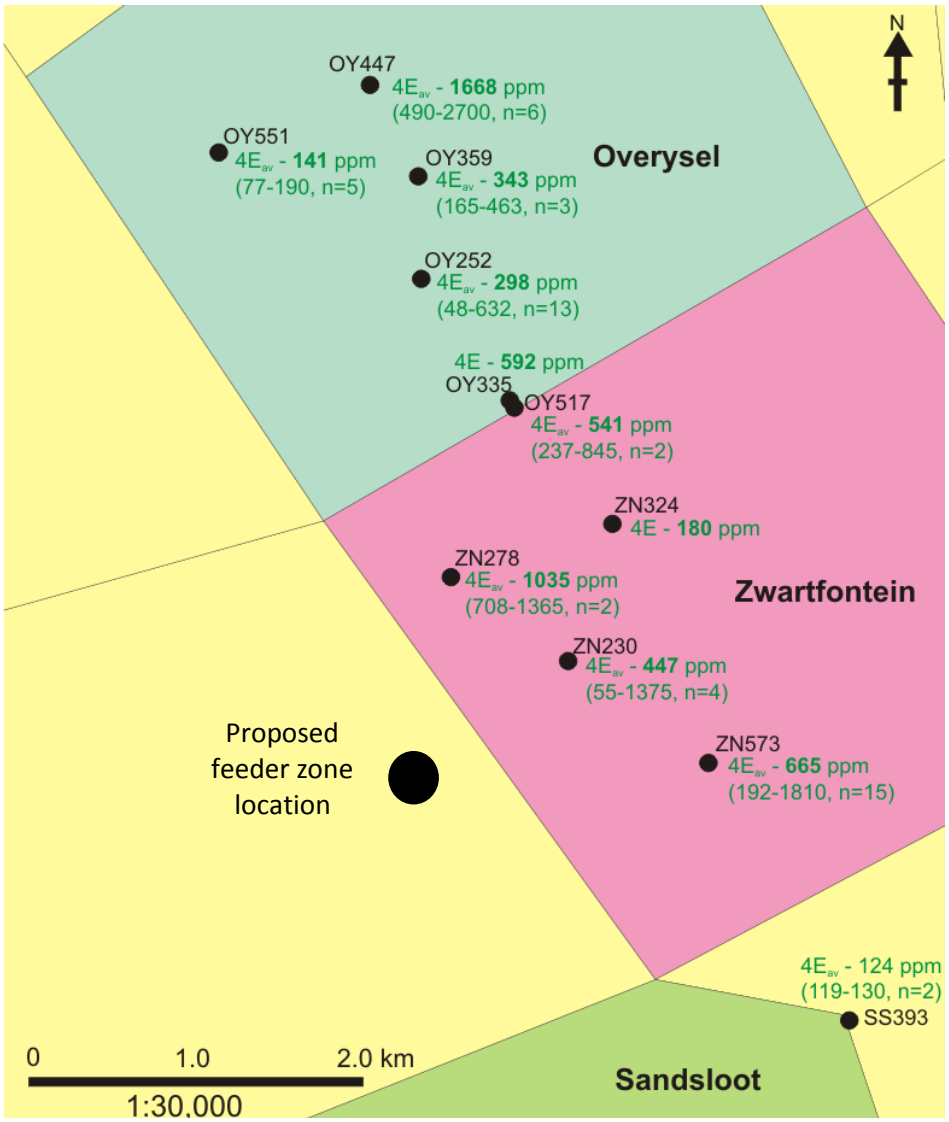

Figure 9.8. Map of study area showing the average 4E (Pt,Pd,Rh+Au) tenor values from the homogenised inclusions.

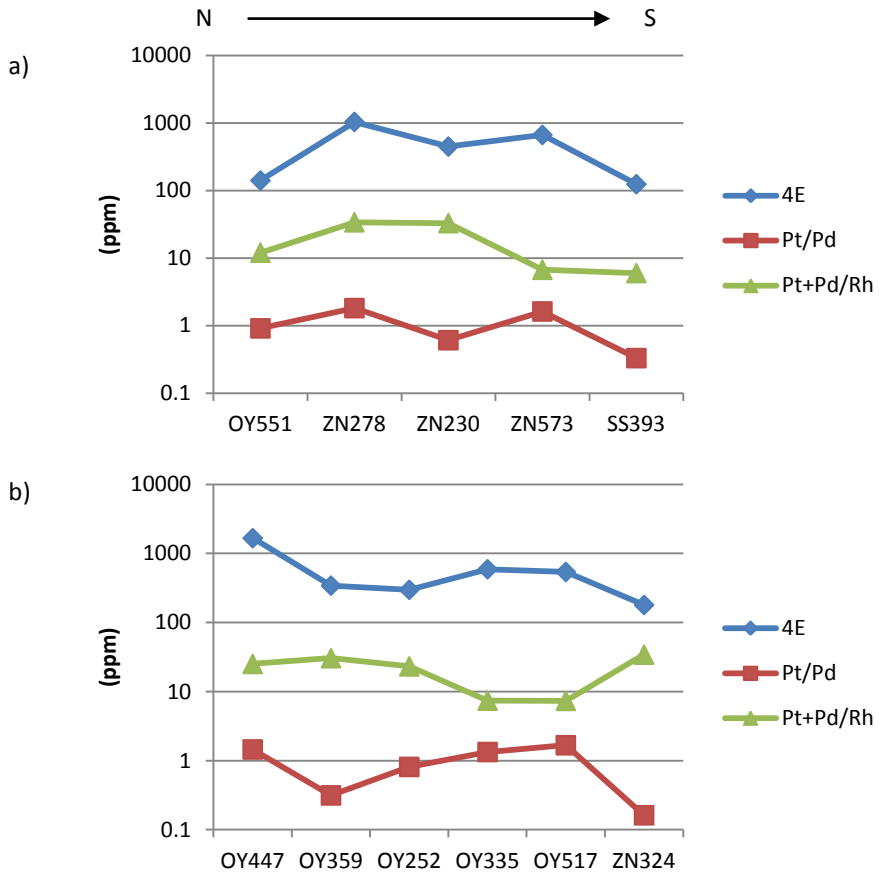


Figure 9.9. Variation along strike across the study area from N-S with (a) being the most westerly N-S strike line and (b) the most easterly N-S strike line.

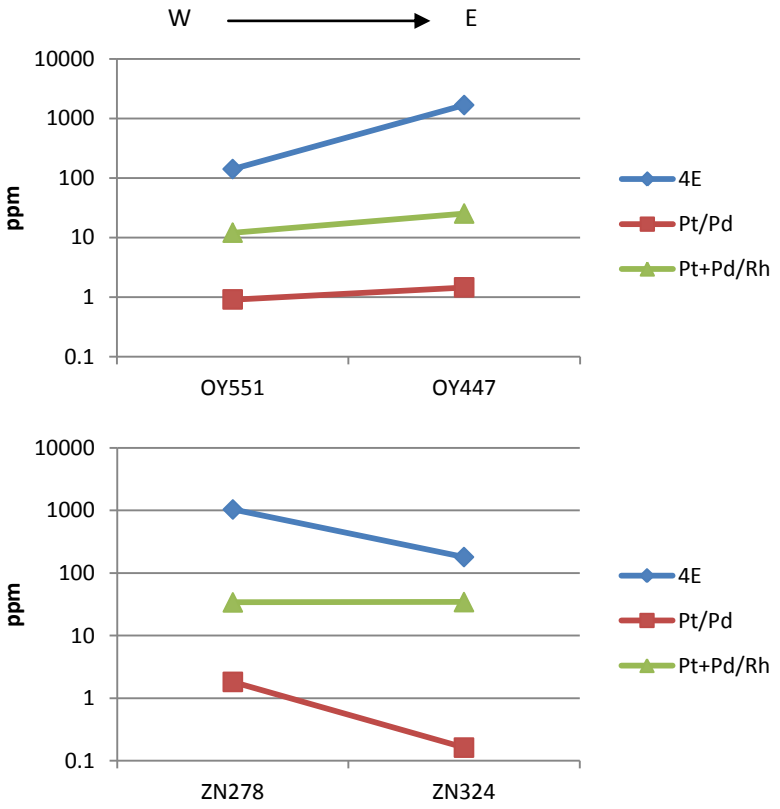


Figure 9.10. Variation up-dip across the study area from W-E for two sets of drillholes.

### 9.4.2 S/Se ratio

The advantage of using sulphide inclusions in this study is the ability to study the primary sulphide. Unlike with other studies where the PGE tenors of the sulphide are calculated from whole rock data and assumptions have to been made for the composition of the sulphide liquid, the actual concentrations of the precious metal tenors can be measured from the inclusions. The low S/Se ratio data obtained from the sulphide inclusions appear to be primary in origin and cannot be attributed to secondary alteration as they are measured in a closed system (sulphide inclusions trapped within chromites enclosed by orthopyroxenes). The low S/Se ratios imply that Se and the precious metals are enriched at the expense of sulphur.

The study by Ihlenfeld and Keays (2011) investigated the relationship between crustal contamination and PGE mineralisation in the Platreef on Overysel, Sandsloot and Tweefontein. They found a strong inverse relationship between PGE tenors and S/Se ratio in bulk rock samples from the Platreef and interpreted this as evidence that the PGE-rich sulphides were formed prior to emplacement of the Platreef magmas through assimilation of crustal S and became progressively enriched in the PGE during transport. They suggest that the addition of this crustal sulphur from the country rocks resulted in the dilution of metal tenors of the sulphides rather than promoting sulphur saturation.

Ihlenfeld and Keays (2011) have attributed the wide range of S/Se ratios observed in their study (fig. 9.11) to normal R-factor variations. They stated that the R-factor modelling demonstrates that progressive equilibration of crustal sulphides with elevated S/Se ratio with a mantle-derived magma will gradually remove the characteristic crustal S/Se signature. Geochemical evidence of the assimilated crustal sulphides (i.e. elevated S/Se ratios) will only be preserved in the parts of the system where R-factors remain relatively low. Based on this, they proposed that the Platreef sulphides were originally crustal sulphides hosted by the country rocks in the conduit system that were assimilated and transported by the Platreef magma. These crustal sulphides would have had initially low Pd, Pt and Se contents and high S/Se ratios. However, during transport these sulphide droplets would have interacted with the Platreef magma and scavenged Pd, Pt and Se from the melt due to the high sulphide melt/silicate melt partition coefficients of these elements. The greater the interaction of the sulphides with the magma, the higher the metal content of the sulphides and the lower their S/Se ratios become to mimic the mantle range.

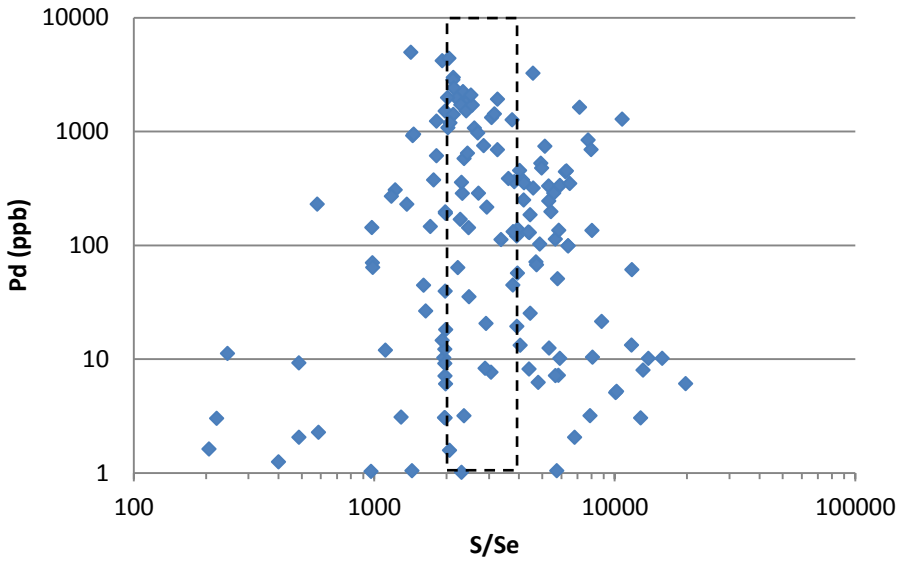


Figure 9.11. S/Se vs. Pd for samples from the Platreef on Overysel, Sandsloot and Tweefontein analysed by Ihlenfeld and Keays (2011) with dashed box representing mantle range.

Ihlenfeld and Keays (2011) have suggested that the low S/Se ratios are a product of sulphide alteration, where there has been S loss relative to Se. However, most of the sulphides observed in the Platreef are fresh and unaltered. To obtain the low ratios observed in their data, significant amounts (> 50 %) of the initially present sulphur would have to be removed and this is not supported by the textures observed in the Platreef. Hutchinson and Kinnaird (2005) showed evidence of sulphide replacement by tremolite, while Holwell and McDonald (2006) found limited sulphide replacement and destruction in pyroxenites from Overysel. Holwell et al. (2006) observed similar 'ragged' BMS on Sandsloot due to intergrowths with plagioclase and secondary amphiboles. While some sulphide destruction has occurred, it does not occur on the scale required to achieve these proposed low S/Se ratios.

A key problem with the R factor model proposed by Ihlenfeld and Keays (2011) is that regardless of how high the R factor, in order to produce the corresponding high sulphide tenors, the minimum S/Se ratios for modelled curve do not fall below 2,000 as the shape of the curve is governed by the S/Se ratio of the mantle component. As a result, a number of their samples do not plot on the modelled curve as they are much lower than the 2,000 – 4,000 mantle range. These low S/Se ratios have also been replicated in the BMS and in the sulphide inclusions analysed in this study, as shown in table 9.2, which suggests they are widespread and need to be accounted for.

### *Simple multistage upgrading model*

The simple multistage upgrading model, in which a sulphide liquid interacts with successive batches of silicate magma, has been used in genetic models for many magmatic sulphide deposits e.g. Noril'sk (Naldrett et al. 1995), Voisey's Bay (Li and Naldrett 1999) and Uitkomst (Li et al. 2002). In a conventional conduit system, where magma is pumped in and pumped out, the inflowing magma interacts with the sulphides and every batch of magma going through the conduit system causes the sulphides to become increasingly enriched in Cu, Ni, PGEs and semi metals. The contrasting densities and inherent separation tendencies of the two liquids cause the sulphide liquid to remain in the chamber while the silicate magma is expelled through the conduit (Kerr and Leitch 2005).

This simple multistage upgrading theory has been modelled in figure 9.12 for the data from this study using the spreadsheets designed by Kerr and Leitch (2005). In order to produce this model, three variables are used for the modelling spreadsheet; magma concentration, incremental R factor and partition coefficient (D). For Se, the initial magma concentration of 0.14 ppm was chosen as this was the highest value measured for B1 magmas by Barnes et al. (2009) and a partition coefficient of 1,770 calculated from S globules in MORB pillows (Peach et al. 1990). For Pd, the initial magma concentration of 0.01 ppm represents the B1 magma (Barnes and Maier 2002a) and a partition coefficient of 40,000 (Kerr and Leitch 2005). The S/Se ratio was calculated assuming a constant S concentration of 35 wt% S, which was the average S concentration observed when analysing sulphide inclusions on the SEM. As was also seen in the model by Ihlenfeld and Keays (2011), regardless of how high the R factor, the projected model only increases vertically upwards at a S/Se ratio of around 2,000 and cannot account for the low S/Se ratio data or the high Pd tenors observed.

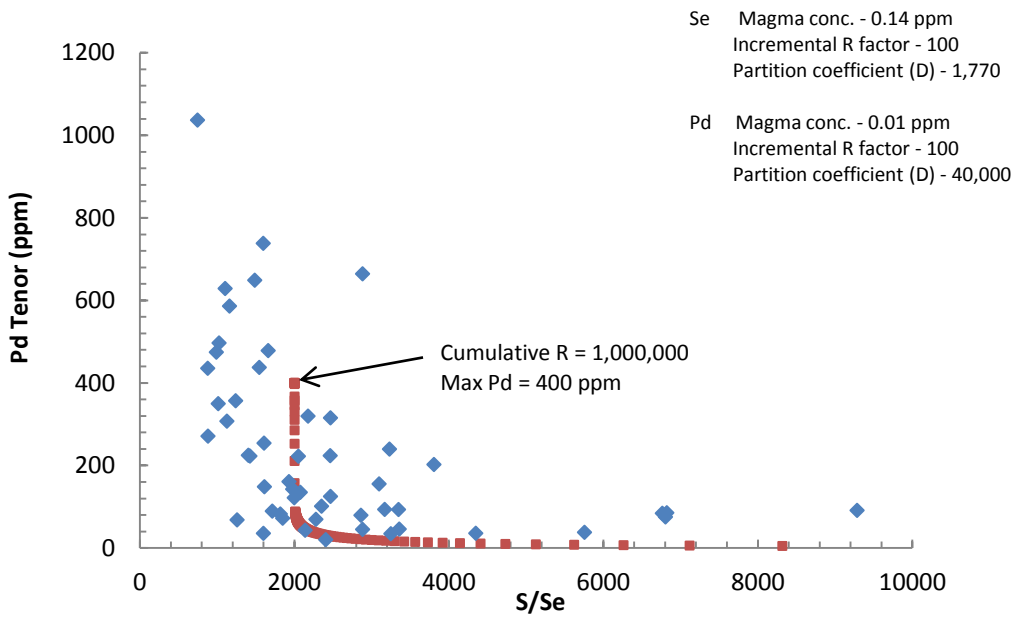


Figure 9.12. Batch equilibrium model with no sulphide destruction.

### *Sulphide destruction model*

The simple multistage model assumes that the mass of the sulphide liquid remains constant even through interaction with successive magma batches. This therefore implies that the incoming silicate magma must be sulphur saturated in order for no additional sulphide liquid to be exsolved or dissolved. However, it is unlikely that a parental magma would be sulphur saturated through its crystallisation history, as highlighted by the rarity of magmatic sulphide deposits worldwide (Maier and Groves 2011).

An alternative model has been developed by Kerr and Leitch (2005) in which some of the sulphide liquid is re-dissolved as it is being enriched in precious and semi metals. In the self-destructive sulphide segregation (or multi-stage dissolution upgrading) model every batch of new S-undersaturated magma that passes over the sulphides dissolves a fraction of the sulphide liquid. The sulphide droplets become smaller and the amount of sulphide liquid decreases with every batch of magma that passes through the system. Early sulphide droplets contain a considerable amount of S and Fe, and small amounts of Cu, Ni, PGE and Se. As these sulphide droplets decrease in size by the scavenging magma, S and Fe are lost relative to the other elements which have higher partition coefficients for sulphide. The result is that the sulphide droplets become increasingly enriched in the precious metals, Cu, Ni and Se. This model removes the need for anomalously PGE-rich parental magmas or extremely large sulphide liquid/silicate liquid partition coefficients (Kerr and Leitch 2005). The calculations for this model were based on trying to recreate the average composition of the BMS that have been normalised to 100 % sulphide. Kerr and Leitch (2005) highlight that

this does not necessarily represent the fractionated immiscible sulphide liquid in the parental magma. Minor dissolution and enrichment of the sulphides has been suggested to occur as they settled through the magma column (e.g. Campbell et al. 1983; Barnes and Maier 2002b) and therefore this study is important as the preserved initial sulphide liquid can be analysed.

When using the Kerr and Leitch (2005) sulphide destruction model to fit the observed data from this study, an additional variable is introduced. The loss factor is the proportion of the original sulphide liquid that is removed with each new batch of sulphide-undersaturated magma passing through the system. Models were produced with a range of loss factors from 1 – 5 % to see which model closest resembles the observed data. The incremental R factor used for the sulphide destruction models was also varied with a range of 50-500. As with the batch equilibrium model, the S/Se ratio was calculated assuming a constant S concentration of 35 wt% S. The S concentration used is the estimated end stage concentration after the dissolution of S and Fe through sulphide destruction as discussed above and is similar to the average S concentration of the melt inclusions. For each model produced (fig. 9.14), the variables entered into the modelling spreadsheet are included on the graphs. For each model, the R factor and loss factor must be the same when modelling the Se and Pd concentrations in the sulphide liquid.

While most of the data are located near the line produced by the most successful model (fig. 9.14i), there are some inclusions that have high S/Se ratios but relatively low tenors that need to be accounted for. This may potentially be related to the timing in which the sulphide droplets were trapped by the host chromite. The initial sulphide droplets were highly enriched in PGE and Se, having had the S scavenged by the sulphide destruction process. If they were trapped early, then they would retain low S/Se ratios and high PGE tenors. Once completely surrounded by chromite, they are unaffected by the surrounding magma. Later batches of magma carrying sulphides with lower tenors could mix with the early enriched sulphide liquid by the process of Ostwald ripening, where small droplets are captured by larger ones, diluting the overall tenor. This process causes the affected inclusions to move off the curve, resulting in a higher S/Se ratio and lower PGE tenors. The cause of decreasing tenors may not be simply due to later batches of magma. It is likely that the proposed staging chamber model was not just a simple chamber with one feeder; instead it is likely that there were multiple chambers and conduits (fig. 9.13) as proposed by McDonald and Holwell (2007). Where there are multiple chambers, there is the possibility

of interactions between the high PGE tenor / high Se concentration sulphide liquid created above and other lower PGE tenor sulphide liquids. This could potentially occur in staging chambers that have undergone fewer cycles of enrichment and dissolution, resulting in PGE sulphide droplets being produced with lower tenor (I. McDonald pers. com. 2013).

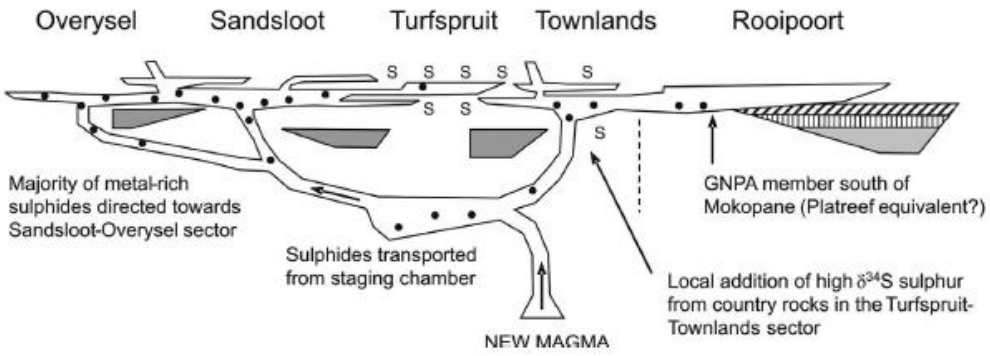


Figure 9.13. Multistage staging chamber model proposed by McDonald and Holwell (2007)

Where Ihlenfeld and Keays (2011) suggested the high S/Se ratio being as a result of alteration or a secondary effect, it is proposed that this is still a primary process which happened before all the chromite crystallises.

The input of multiple batches of mantle magma also causes the isotope character of the sulphide to change in addition to the S/Se ratios. Regardless of the feeder system proposed for the concentration process, it can be suggested that it is likely that it involved the assimilation of Archaean basement. Hydrothermal or near surface VMS-type sulphides in the greenstone component of the Archaean basement, as has been shown by Fitzpatrick (2008), are likely to have high S/Se ratios, $\delta S^{34}$ close to mantle values, slightly heavy $\Delta^{33}S$ and low PGE concentrations. This correlates with findings for the Platreef where $\delta S^{34}$ values have been measured at -1.5 to + 0.5 ‰ (Holwell et al. 2007), while $\Delta^{33}S$ values are measured at 0.15 ‰ (Penniston-Dorland et al. 2008). As multiple batches of magma are pumped through the system, the S/Se ratio decreases, the isotope ratios are driven close to mantle values through isotope exchange and PGE concentrations increase to the observed values.

a)

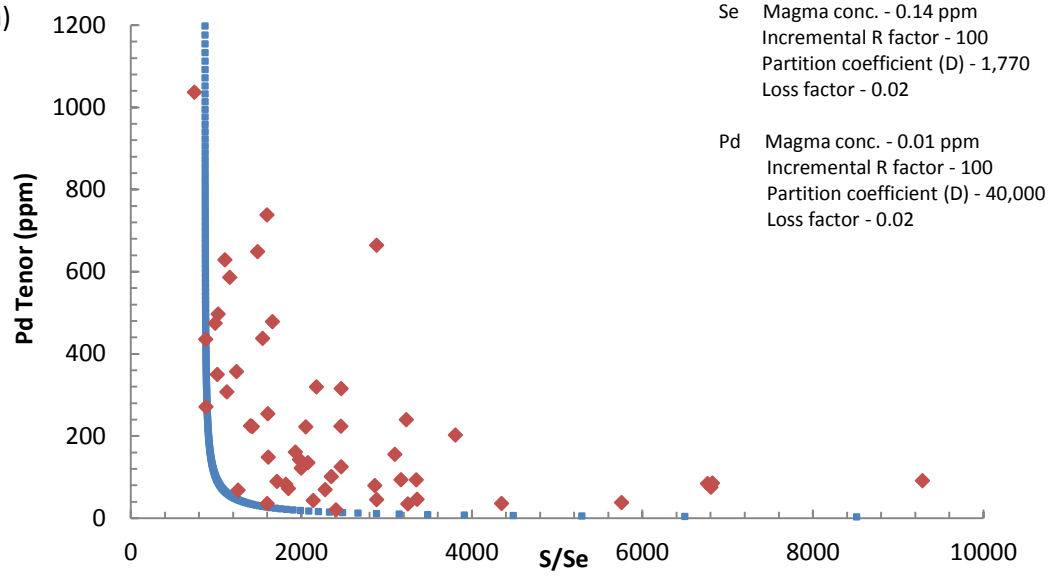
Pd Tenor (ppm)
1200
1000
800
600
400
200
0
0
2000
4000
6000
8000
10000
S/Se
Se Magma conc. - 0.14 ppm
Incremental R factor - 100
Partition coefficient (D) - 1,770
Loss factor - 0.02
Pd Magma conc. - 0.01 ppm
Incremental R factor - 100
Partition coefficient (D) - 40,000
Loss factor - 0.02

b)

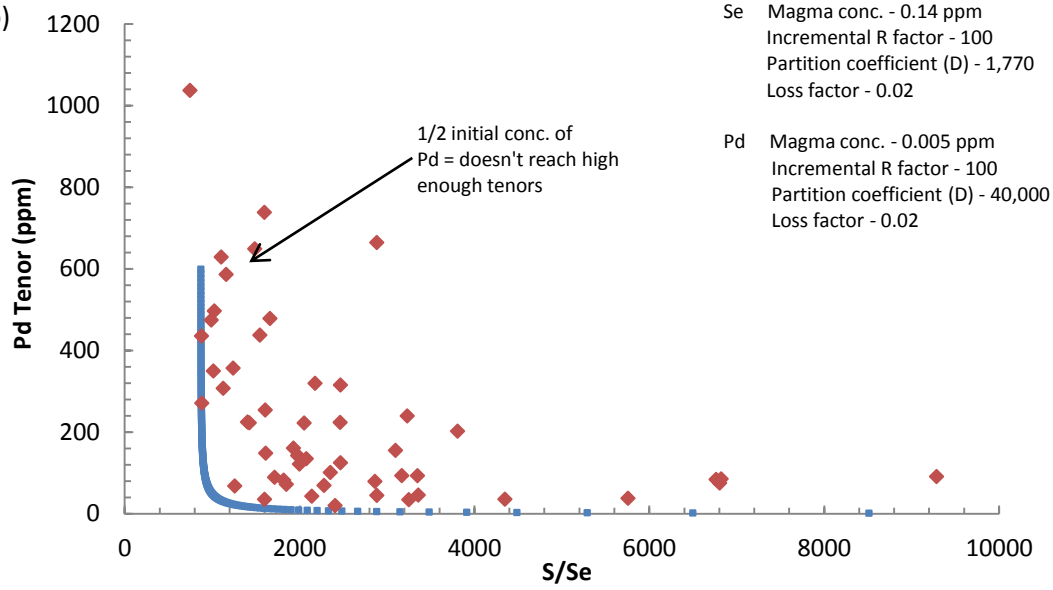
Pd Tenor (ppm)
1200
1000
800
600
400
200
0
0
2000
4000
6000
8000
10000
S/Se
1/2 initial conc. of
Pd = doesn't reach high
enough tenors
Se Magma conc. - 0.14 ppm
Incremental R factor - 100
Partition coefficient (D) - 1,770
Loss factor - 0.02
Pd Magma conc. - 0.005 ppm
Incremental R factor - 100
Partition coefficient (D) - 40,000
Loss factor - 0.02

c)

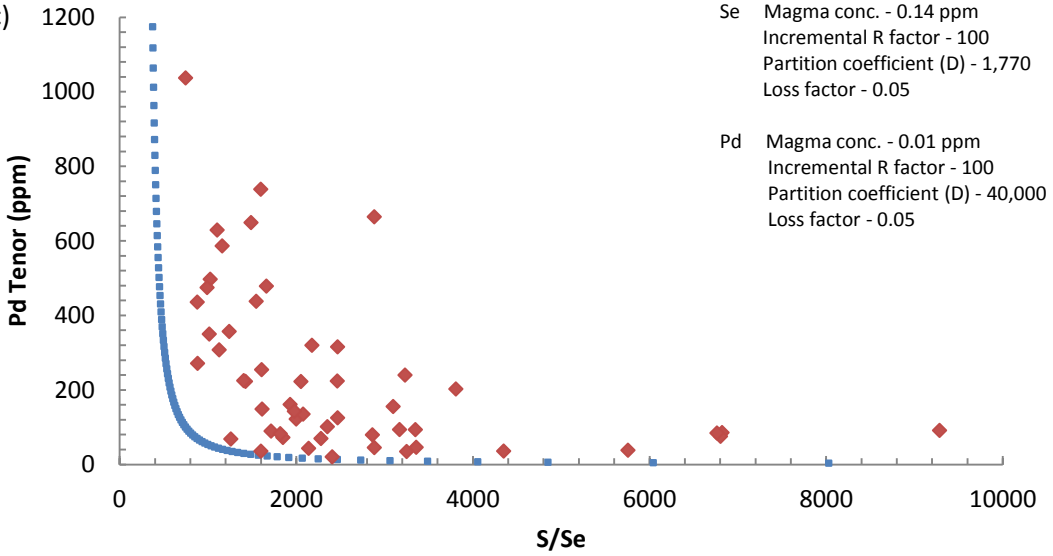
Pd Tenor (ppm)
1200
1000
800
600
400
200
0
0
2000
4000
6000
8000
10000
S/Se
Se Magma conc. - 0.14 ppm
Incremental R factor - 100
Partition coefficient (D) - 1,770
Loss factor - 0.05
Pd Magma conc. - 0.01 ppm
Incremental R factor - 100
Partition coefficient (D) - 40,000
Loss factor - 0.05

d)

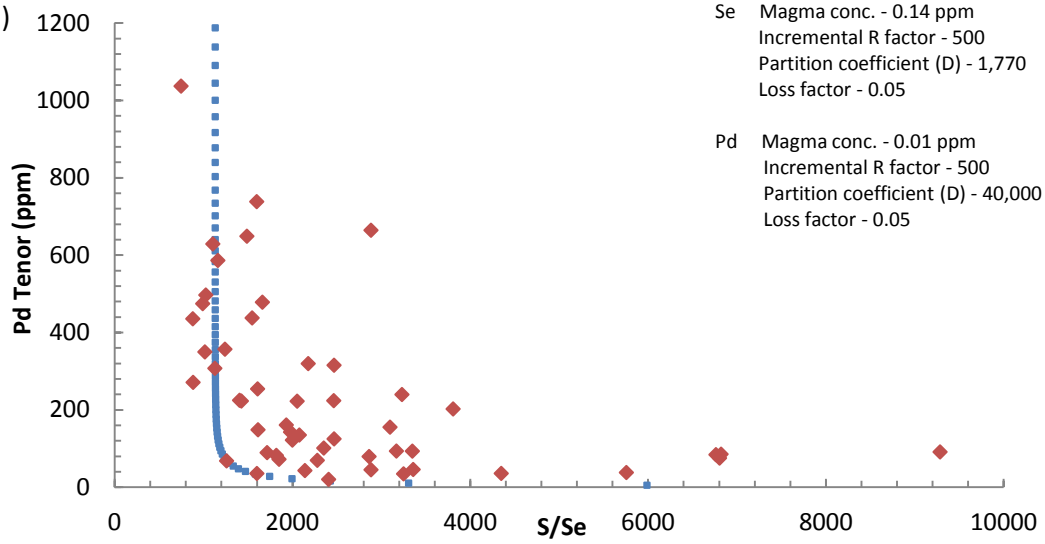
Pd Tenor (ppm)
1200
1000
800
600
400
200
0
0
2000
4000
6000
8000
10000
S/Se
Se Magma conc. - 0.14 ppm
Incremental R factor - 500
Partition coefficient (D) - 1,770
Loss factor - 0.05
Pd Magma conc. - 0.01 ppm
Incremental R factor - 500
Partition coefficient (D) - 40,000
Loss factor - 0.05

e)

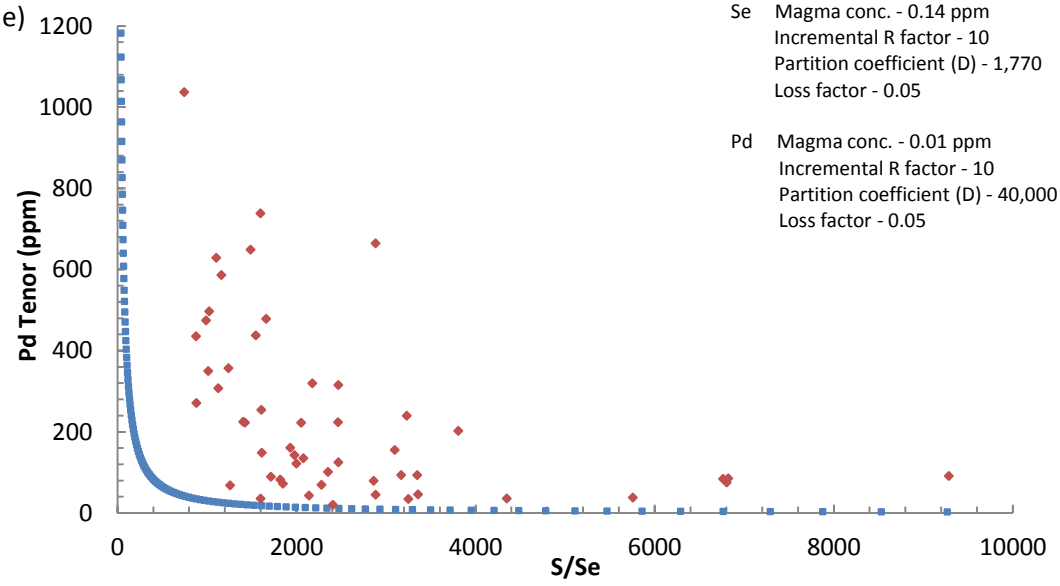
Pd Tenor (ppm)
1200
1000
800
600
400
200
0
0
2000
4000
6000
8000
10000
S/Se
Se Magma conc. - 0.14 ppm
Incremental R factor - 10
Partition coefficient (D) - 1,770
Loss factor - 0.05
Pd Magma conc. - 0.01 ppm
Incremental R factor - 10
Partition coefficient (D) - 40,000
Loss factor - 0.05

f)

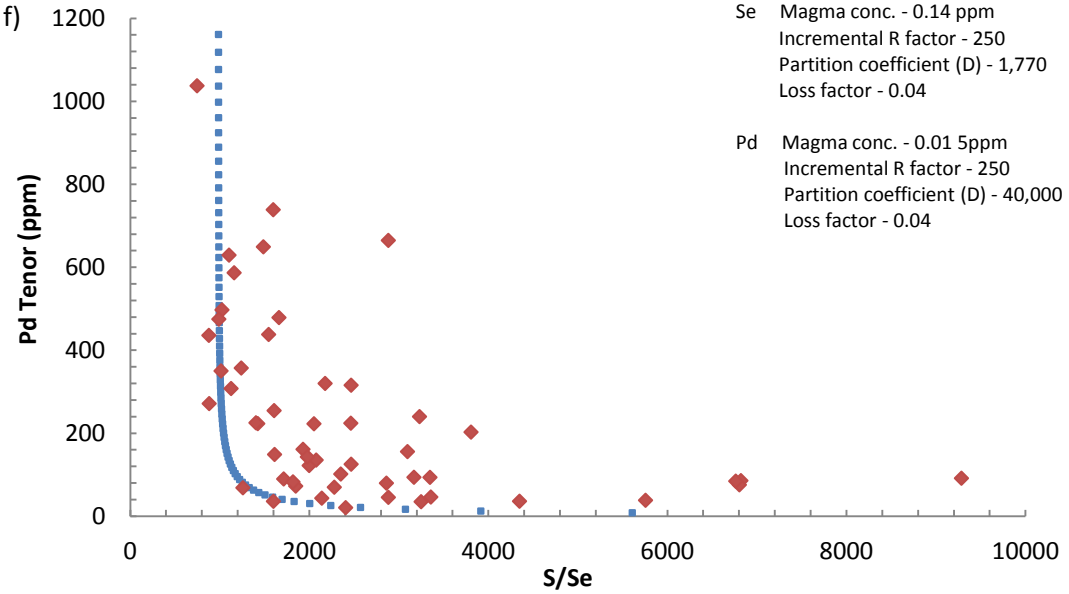
Pd Tenor (ppm)
1200
1000
800
600
400
200
0
0
2000
4000
6000
8000
10000
S/Se
Se Magma conc. - 0.14 ppm
Incremental R factor - 250
Partition coefficient (D) - 1,770
Loss factor - 0.04
Pd Magma conc. - 0.01 5ppm
Incremental R factor - 250
Partition coefficient (D) - 40,000
Loss factor - 0.04

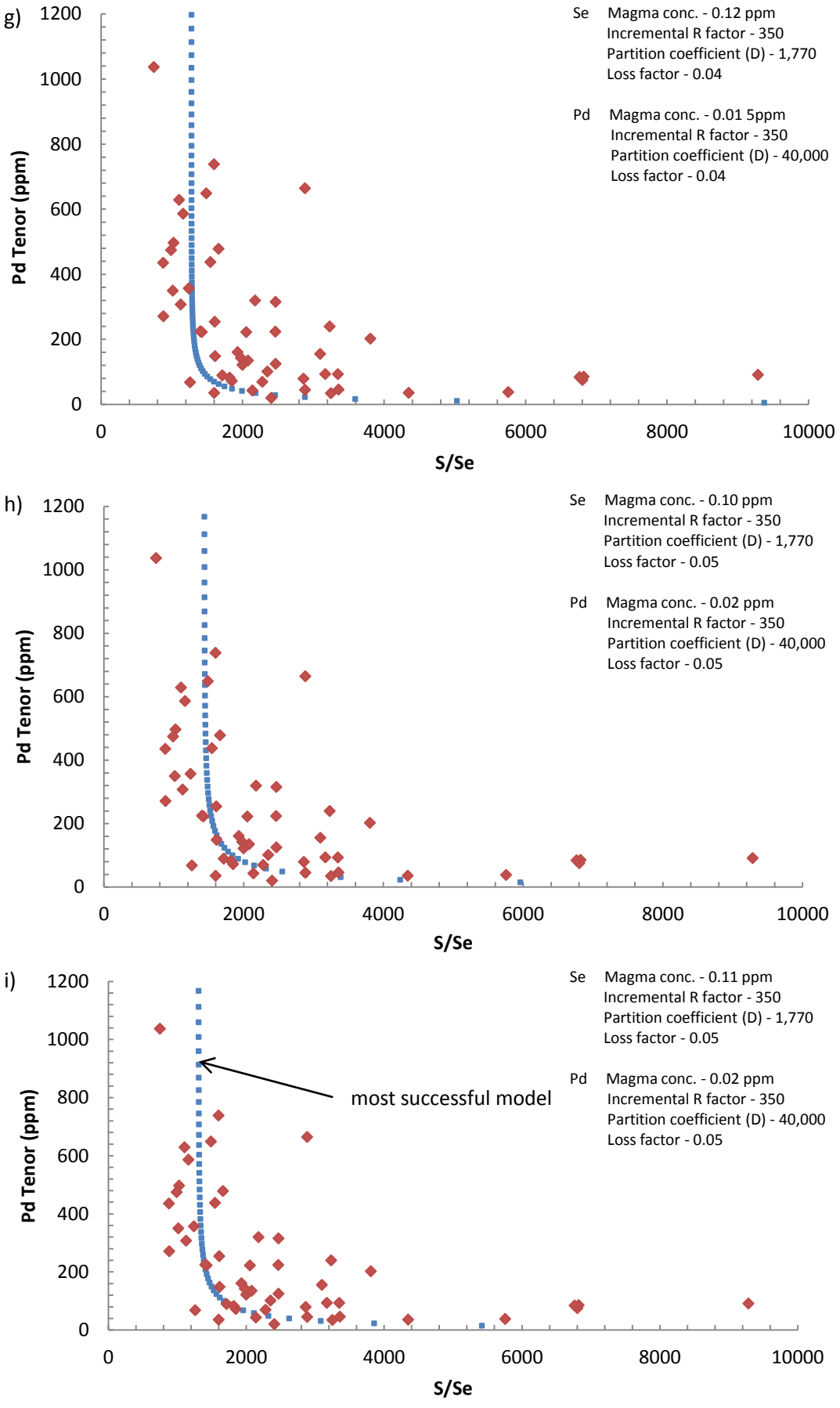


Figure 9.14. Sulphide destruction models based on the variables noted on each graph.

## 9.5 Conclusion

The analysis of sulphide inclusions within early crystallising chromites has been fundamental in testing the genetic model for the Platreef. As these inclusions were trapped early in the crystallisation history, their composition is proposed to represent the parental sulphide liquid. Their high PGE tenor and semi-metal (Bi, Te and As) content has shown that these elements were concentrated in the parental magma and are not a consequence of secondary contamination. The lack of systematic variation within the samples across strike and down dip on the Platreef is likely a consequence of the processes involved in sulphide formation.

Based on the data produced in this study, it is proposed that the sulphide liquid was enriched in a staging chamber by the sulphide destruction mechanism (Kerr and Leitch 2005) leading to the enrichment of the sulphide liquid in PGE and Se. This enrichment and production of a low S/Se sulphide liquid is a primary process and cannot be attributed to secondary alteration as has been previously proposed (Ihlenfeld and Keays 2011). The presence of low PGE tenor, high S/Se ratio inclusions may reflect the interaction of high tenor sulphide liquids with other lower tenor sulphide liquids, causing the dilution of the PGE and Se tenors.

The interaction of the sulphide liquid with multiple batches of silicate magma has enabled the high PGE tenors to be achieved, which would not have been possible in a closed system. This process is also achieved with a relatively small amount of sulphide liquid and therefore solves the mass balance problem illustrated by Cawthorn et al. (2002b).

This study has shown that use of S/Se ratios combined with S isotope values can provide strong evidence for a mantle source for the source of the S within the Platreef. By using both S/Se ratios in combination with S isotopes, any isotope exchange that may have occurred will not influence the results as strongly. Additional S and Os isotope studies on the sulphide inclusions may provide constrains on the ultimate source of sulphur and PGE in the Platreef.

# Chapter 10: Conclusions

The aim of this chapter is to briefly summarise the findings of this work and put them into context of an overall genetic model for the Platreef.

Chapter 5 examined the bulk rock geochemistry of the samples from the three studied farms of Overysel, Sandsloot and Zwartfontein. Overall, the bulk geochemistry replicates other Platreef studies. Slight variations in trace elements between the different lithologies can be ascribed to the variation in bulk mineralogy. Bulk PGE analysis has shown that the range of PGE concentrations and the degree of PGE fractionation across the sample suite is consistent with the range for the Central Platreef established in previous studies. The metal grade differs considerably between the different lithologies, with the chromitiferous units being more PGE rich than the chromite depleted counterparts. Examination of samples in which the Platreef is in contact with different country rocks has showed little variation between them suggesting that any contamination has occurred prior to emplacement.

Chapter 6 examined the mineralogy of the chromite grains and concluded that the difference in chromite composition is dependant on the host lithology and the location of the sample along strike of the Platreef. The most primary compositions, i.e. those that are least affected by interaction with the reactive country rock, are found on Overysel, while chromites from Sandsloot and Zwartfontein are affected by the reactive dolomite country rock surrounding the Platreef. In addition, it appears that chromites analysed from the pyroxenite units are most altered by post-crystallisation re-equilibration. An important observation was that, although some similarities are evident between the Platreef chromites and those from the UG2 chromitite, the Platreef chromites display very different compositions from the chromites from the Merensky Reef, and with those from the southern portion of the northern limb (south of the TML). Ultimately, the Platreef chromites have higher $TiO_2$ contents and lower $Fe^{3+}$#, suggesting that they crystallised from a more evolved magma than those formed from typical Critical Zone magmas.

Chapter 7 investigated PGM variation within the chromitites of the Platreef. An important observation made was that variation in PGM was evident along strike and down dip of the Platreef; the PGM assemblage is not strictly controlled by footwall lithologies as previously proposed. Based on the observed mineralogy and lateral variation between alloy-dominant, arsenide-dominant and sulphide-dominant assemblages, it is proposed that the different PGM associations can be ascribed to the effects of differing temperature and $fO_2$ conditions.

A feeder zone model has been proposed, with the PGM associations observed being related to the proximity to the feeder which is suggested to lie down dip and to the west of Zwartfontein-Overysel. The characteristics of the PGM on the whole display the results of orthomagmatic processes, with any hydrothermal redistribution being a secondary process.

Chapter 8 investigated the PGE concentrations within the BMS at Zwartfontein. It was evident from chapter 7 that the majority of PGM observed were Pt-dominant. As the bulk Pt/Pd ratio is almost at unity, the apparent absence of Pd bearing PGM had to be accounted for. It was shown that there is a strong association between PGE and BMS and that the distribution of PGE is consistent with fractional crystallisation of a sulphide liquid. Os, Ir, Ru, Rh and Pd are present within solid solution in the cooling products of mss (pentlandite and pyrrhotite).

Chapter 9 examined the composition of sulphide droplets trapped within chromite grains, trapped early in the crystallising history. Therefore, their composition is proposed to represent parental sulphide liquid. Analysis showed high PGE tenors and significant semi-metal (Bi, Te and As) contents. It is suggested that these were present in the parental magma being due to secondary contamination. There was no systematic variation across the three farms, leading to a suggestion that sulphide liquid fractionation occurred in a different setting, with the sulphides being transported into their present location.

As was discussed in chapter 3, the complexity of the Platreef has meant that despite the numerous studies, developing an accepted genetic model to account for the variations observed has been difficult. One of the main issues with developing a genetic model for the Platreef is that the stratigraphic relationships with the rest of the Bushveld are not well established. As has been previously outlined, initial studies suggested that the Platreef was formed by an Upper Critical Zone magma and have correlated the Platreef with the Merensky Reef. A key observation made for the Platreef is the presence of a time break between the Platreef and Main Zone (Holwell et al. 2005; Holwell and Jordaan 2006), which has not been identified elsewhere in the Bushveld and categorically means that the magma that formed the Main Zone cumulates above the Platreef was not the source of PGE for the Platreef. In comparison, strontium isotope analysis by Seabrook et al. (2005) across the Merensky and Bastard cyclic units, indicated a continuous interaction between Critical Zone and Main Zone magmas without any obvious hiatus. More importantly, the magmatic unconformity between the Platreef and Main Zone identifies a mass balance problem as the Platreef metal tenors are much greater than in most other contact type deposits. While

many models have been proposed for the Platreef (c.f. McDonald and Holwell 2011), two of these that are still under test (Maier et al. 2008; Naldrett et al. 2008a) do not address the time break between the Platreef and Main Zone, especially given the consequences for the PGE source. The staging chamber model advocated by Lee (1996) and subsequently developed by McDonald and Holwell (2007) and McDonald et al. (2009) proposes that the sulphide liquid was enriched in a conduit system prior to emplacement to account for the elevated tenors observed in a relatively small amount of magma.

In order to obtain the high PGE tenors observed in the sulphide inclusions, the sulphide liquid would have had to come into contact with a significant amount of magma. The sulphide liquid that developed in the staging chambers for the Lower Zone was potentially enriched by a process known as sulphide destruction proposed by Kerr and Leitch (2005) and this primary process led to an enrichment of the sulphide liquid in both PGE and Se. The presence of low PGE, and high S/Se ratios seen some inclusions may be the result of Ostwald ripening through the interaction with other low tenor sulphide liquids, possibly derived from melted country rock. This process has allowed the formation of moderately and highly enriched sulphide liquid.

It has been suggested (e.g. Maier et al. 2008; Naldrett et al. 2008a) that the source for the Platreef involved a mix of Main Zone and Upper Critical Zone magmas, however the time break observed between the Platreef and Main Zone precludes this theory. The bulk rock geochemistry in chapter 5 has shown that while the Merensky Reef represents a depleted B1 magma, the Platreef shows differences (e.g. Zr-Hf anomaly and Th anomaly) suggesting there may be a different source than just B1 magma. It is proposed that the Platreef geochemistry may be achieved through a mix of Main Zone and Lower Zone magmas (McDonald and Holwell 2011). Subsequent to the formation of the Lower Zone, a proto-Main Zone pulse would have flushed through the preformed plumbing system, capturing the enriched sulphides sitting in the staging chamber and crystallising silicates from the Lower Zone magma. It has been suggested (McDonald and Holwell 2007) that the very coarse habit of the orthopyroxene crystals and low abundances of REE and incompatible trace elements suggest that the Platreef was intruded as a mix of liquid and crystal mush. It is suggested that the Platreef olivines and pyroxenes have Mg# that may represent Lower Zone minerals that have been modified by crystal-liquid shift reactions through interaction with Main Zone magma (McDonald and Holwell 2007). This may be achieved in the feeder zone where a proto-Main Zone pulse of magma flushed through the system picking up the

enriched sulphides in addition to Lower Zone crystal cumulates and the mix was emplaced as the Platreef.

The compositional difference in the Bushveld and Archaean basement rocks either side of the TML has only been highlighted by McDonald et al. (2005; 2009). Given that the basement rocks are different, then the differences observed in the bulk rock geochemistry between the Platreef (e.g. depletion in Th) and the rest of the Bushveld Complex (e.g. enrichment in Th and LREE in Lower Zone) can, at least in part, be related to the different mantle and any contamination by the different crusts regardless of any intrusion processes that take place afterwards. While the function of the TML is still not fully understood, it may have had a role as a feeder for the magma that fed into the Platreef plumbing system prior to emplacement, or alternatively it may have simply acted as a barrier to separate the northern limb from the rest of the Bushveld Complex. As yet, no geochemical correlation is seen across the TML, implying its potential importance.

Given that a staging chamber system with a feeder zone has been proposed, the position of at least one feeder relative to the Platreef may be indicated based on PGM mineralogy as shown in chapter 7. Based on the observations, it is suggested that a PGE-rich immiscible sulphide liquid formed in a staging chamber to the west of the study and these droplets were transported into the Platreef sill network via a feeder located west of Zwartfontein. Analysis of the PGM has shown a pattern of PGM variation that is consistent with a potential area of the feeder zone on Zwartfontein, with PGM mineralogy consistent with volatile conditions. This area displays a gravity anomaly that has yet to be explained. A secondary smaller zone has been identified on Sandsloot, suggesting that there may be multiple feeders and/or multiple chambers as proposed by McDonald and Holwell (2007). The proximity of these potential feeder zones in the Central Sector is potentially the reason why the highest grades in the Platreef are found in the study area. In addition, the highest grades in the Platreef are also found closest to the barren Lower Zone Zwartfontein body which is unlikely to be a coincidence. Yudovskaya et al. (2010) have also highlighted the correlation between highest grades and the high temperature ultramafic Platreef facies.

In order to test the staging chamber model further, S isotope analysis should be carried out on the sulphide inclusions. Provided they show a magmatic signature, these combined with the S/Se ratios provide a strong argument for a primary magmatic origin for S. Investigation of the unexamined 5 Lower Zone bodies may also provide additional support to the staging chamber model if they can also be shown to be depleted in chalcophile elements, as, to

date, only the Zwartfontein and Grasvally Lower Zone bodies have been examined (McDonald and Holwell 2007; McDonald et al. 2009). If the model is correct, then there are exploration implications in that potentially there are magma conduits where high tenor sulphides may be retained, in a setting similar to that proposed for the Uitkomst satellite intrusion (De Waal et al. 2001). Further deep drilling on the Akanani property to the west of the Zwartfontein farm may test the proposal that the area hosts a feeder zone.

# References


Alard, O.,Griffin, W. L.,Lorand, J. P.,Jackson, S. E. and O'Reilly, S. Y. 2000. Non-chondritic distribution of the highly siderophile elements in mantle sulphides. *Nature* 407(6806), pp. 891-894.

Alexandre, P.,Andreoli, M. A. G.,Jamison, A. and Gibson, R. L. 2006. $^{40}Ar/^{39}Ar$ age constraints on low-grade metamorphism and cleavage development in the Transvaal Supergroup (central Kaapvaal craton, South Africa): implications for the tectonic setting of the Bushveld Igneous Complex. *South African Journal of Geology* 109(3), pp. 393-410.

Andrews, D. R. A. and Brenan, J. M. 2002. The solubility of ruthenium in sulfide liquid: implications for platinum group mineral stability and sulfide melt–silicate melt partitioning. *Chemical Geology* 192(3–4), pp. 163-181.

Arai, I.,Prichard, H. M.,Matsumoto, I. and Fisher, P. C. 1999. Potarite (Pd-Hg) in thermally metamorphosed dunite from the Inazumi-yama ultramafic complex, southwestern Japan: an implication for the behaviour of mercury in PGE mineralization in peridotite *Mineralogical Magazine* 63(3), pp. 369-377.

Armitage, P. E. B. 2011. *Development of the Platreef in the northern limb of the Bushveld Complex at Sandsloot, Mokopane district, South Africa.* PhD, University of Greenwich.

Armitage, P. E. B.,McDonald, I.,Edwards, S. J. and Manby, G. M. 2002. Platinum-group element mineralization in the Platreef and calc-silicate footwall at Sandsloot, Potgietersrus District, South Africa. *Applied Earth Science: Transactions of the Institute of Mining and Metallurgy, Section B* 111, pp. 36-45.

Armitage, P. E. B.,McDonald, I. and Tredoux, M. 2007. A geological investigation of the Waterberg hydrothermal platinum deposit, Mookgophong, Limpopo Province, South Africa. *Applied Earth Science: Transactions of the Institute of Mining and Metallurgy, Section B* 116, pp. 113-129.

Ashwal, L. D.,Webb, S. J. and Knoper, M. W. 2005. Magmatic stratigraphy in the Bushveld Northern Lobe: continuous geophysical and mineralogical data from the 2950 m Bellevue drillcore. *South African Journal of Geology* 108(2), pp. 199-232.

Auclair, G.,Fouquet, Y. and Bohn, M. 1987. Distribution of Se in hightemperature hydrothermal sulfides at 13° north, East Pacific Rise. *Canadian Mineralogist* 25, pp. 577-587.

Augé, T.,Salpeteur, I.,Bailly, L.,Mukherjee, M. M. and Patra, R. N. 2002. Magmatic and hydrothermal platinum-group minerals and basemetal sulphides in the Baula complex, India. *Canadian Mineralogist* 40, pp. 277-309.

Ballhaus, C. and Sylvester, P. 2000. Noble metal enrichment processes in the Merensky Reef, Bushveld Complex. *Journal of Petrology* 41(4), pp. 545-561.

Barnes, S.-J.,Cox, R. A. and Zientek, M. L. 2006. Platinum-group element, gold, silver and base metal distribution in compositionally zoned sulfide droplets from the Medvezky Creek Mine, Noril'sk, Russia. *Contributions to Mineralogy and Petrology* 152(2), pp. 187-200.

Barnes, S.-J. and Maier, W. D. 1999. The fractionation of Ni, Cu and the noble metals in silicate and sulfide liquids. In: Keays, R.R. et al. eds. *Dynamic processes in magmatic ore deposits and their application in mineral exploration*. Geological Association of Canada, Short Course Volume 13, pp. 69-106. .

Barnes, S.-J. and Maier, W. D. 2002a. Platinum-group element distributions in the Rustenburg Layered Suite of the Bushveld Complex, South Africa. In: Cabri, L.J. ed. *The geology, geochemistry, mineralogy and mineral beneficiation of platinum-group elements.*, Vol. 54 (Special). Canadian Institute of Mining, Metallurgy and Petroleum, pp. 553-580.

Barnes, S.-J. and Maier, W. D. 2002b. Platinum-group elements and microstructures of normal Merensky Reef from Impala Platinum mines, Bushveld Complex. *Journal of Petrology* 43(1), pp. 103-128.

Barnes, S.-J.,Maier, W. D. and Curl, E. A. 2010. Composition of the Marginal Rocks and Sills of the Rustenburg Layered Suite, Bushveld Complex, South Africa: Implications for the Formation of the Platinum-Group Element Deposits. *Economic Geology* 105(8), pp. 1491-1511.

Barnes, S.-J.,Makovicky, E.,Makovicky, M.,Rose-Hansen, J. and Karup-Moller, S. 1997. Partition coefficients for Ni, Cu, Pd, Pt, Rh, and Ir between monosulfide solid solution and sulfide liquid and the formation of compositionally zoned Ni-Cu sulfide bodies by fractional crystallization of sulfide liquid. *Canadian Journal of Earth Sciences* 34(4), pp. 366-374.

Barnes, S.-J.,Naldrett, A. J. and Gorton, M. P. 1985. The origin of the fractionation of platinum-group elements in terrestrial magmas. *Chemical Geology* 53(3-4), pp. 303-323.

Barnes, S.-J. and Picard, C. P. 1993. The behaviour of platinum-group elements during partial melting, crystal fractionation, and sulphide segregation: An example from the Cape Smith Fold Belt, northern Quebec. *Geochimica et Cosmochimica Acta* 57(1), pp. 79-87.

Barnes, S.-J.,Prichard, H. M.,Cox, R. A.,Fisher, P. C. and Godel, B. 2008. The location of the chalcophile and siderophile elements in platinum-group element ore deposits (a textural, microbeam and whole rock geochemical study): Implications for the formation of the deposits. *Chemical Geology* 248(3-4), pp. 295-317.

Barnes, S.-J.,Savard, D.,Bédard, L. P. and Maier, W. 2009. Selenium and sulfur concentrations in the Bushveld Complex of South Africa and implications for formation of the platinum-group element deposits. *Mineralium Deposita* 44(6), pp. 647-663.

Barnes, S.-J.,van Achterbergh, E.,Makovicky, E. and Li, C. 2001. Proton microprobe results for the partitioning of platinum-group elements between monosulphide solid solution and sulphide liquid. *South African Journal of Geology* 104(4), pp. 275-286.

Barnes, S. J. and Roeder, P. L. 2001. The range of spinel compositions in terrestrial mafic and ultramafic rocks. *Journal of Petrology* 42(12), pp. 2279-2302.

Barton Jr, J. M.,Cawthorn, R. G. and White, J. 1986. The role of contamination in the evolution of the Platreef of the Bushveld complex. *Economic Geology* 81(5), pp. 1096-1104.

Becker, H.,Horan, M. F.,Walker, R. J.,Gao, S.,Lorand, J. P. and Rudnick, R. L. 2006. Highly siderophile element composition of the Earth's primitive upper mantle: Constraints from new data on peridotite massifs and xenoliths. *Geochimica et Cosmochimica Acta* 70(17), pp. 4528-4550.

Begg, G. C.,Griffin, W. L.,Natapov, L. M.,O'Reilly, S. Y.,Grand, S. P.,O'Neill, C. J.,Hronsky, J. M. A.,Djomani, Y. P.,Swain, C. J.,Deen, T. and Bowden, P. 2009. The lithospheric architecture of Africa: Seismic tomography, mantle petrology, and tectonic evolution. *Geosphere* 5(1), pp. 23-50.

Begg, G. C.,Hronsky, J. A. M.,Arndt, N. T.,Griffin, W. L.,O'Reilly, S. Y. and Hayward, N. 2010. Lithospheric, Cratonic, and Geodynamic Setting of Ni-Cu-PGE Sulfide Deposits. *Economic Geology* 105(6), pp. 1057-1070.

Bockrath, C.,Ballhaus, C. and Holzheid, A. 2004. Fractionation of the Platinum-Group Elements During Mantle Melting. *Science* 305(5692), pp. 1951-1953.

Brenan, J. M. 2002. Re-Os fractionation in magmatic sulphide melt by monosulfide solid solution. *Earth and Planetary Science Letters* 199, pp. 257-268.

Brenan, J. M. and Andrews, D. 2001. Higher-temperature stability of laurite and Ru-Os-lr alloy and their role in PGE fractionation in mafic magmas. *Canadian Mineralogist* 39(2), pp. 341-360.

Brough, C. P. 2011. *An investigation into the link between anomalous PGE concentrations and chromite composition in chromities within ophiolites* PhD, Cardiff University.

Bryan, S. E. and Ernst, R. E. 2008. Revised definition of Large Igneous Provinces (LIPs). *Earth-Science Reviews* 86(1-4), pp. 175-202.

Buchanan, D. L.,Nolan, J.,Suddaby, P.,Rouse, J. E.,Viljoen, M. J. and Davenport, J. W. J. 1981. The genesis of sulfide mineralization in a portion of the Potgietersrus limb of the Bushveld complex. *Economic Geology* 76(3), pp. 568-579.

Buchanan, D. L. and Rouse, J. E. 1984. Role of contamination in the precipitation of sulphides in the Platreef of the Bushveld complex. In: Buchanan, D.L. and Jones, M.L. eds. *Sulphide deposits in mafic and ultramafic rocks*. London: IMM, pp. 141-146.

Buchanan, P. C. and Reimold, W. U. 1998. Studies of the Rooiberg Group, Bushveld Complex, South Africa: No evidence for an impact origin. *Earth and Planetary Science Letters* 155(3-4), pp. 149-165.

Buchanan, P. C.,Reimold, W. U.,Koeberl, C. and Kruger, J. 2002. Geochemistry of intermediate to siliceous volcanic rocks of the Rooiberg Group, Bushveld Magmatic Province, South Africa. *Contributions to Mineralogy and Petrology* 144(2), pp. 131-143.

Burton, K. W.,Schiano, P.,Birck, J. L. and Allegre, C. J. 1999. Osmium isotope disequilibrium between mantle minerals in a spinel-lherzolite. *Earth and Planetary Science Letters* 172, pp. 311-322.

Butler, J. 2012. *Platinum*. London: Johnson Matthey.

Cabri, L. J. 1972. The mineralogy of the platinum-group elements. *Mineral Science and Enginering* 4(3), pp. 3-29.

Cabri, L. J. and Laflamme, J. H. G. 1976. Ore microscopy of some samples from Lac des lsles, Ontario. In: *G.A.C. - M.A.C. Conference Abstracts.* Edmonton, Canada. p. 56.

Cameron, E. N. 1975. Postcumulus and subsolidus equilibration of chomite and coexisting silicates in the Eastern Bushveld Complex. *Geochimica et Cosmochimica Acta* 39(6-7), pp. 1021-1033.

Cameron, E. N. 1977. Chromite in the central sector, eastern Bushveld Complex, South Africa. *American Mineralogist* 62, pp. 1081-1096.

Cameron, E. N. 1980. Evolution of the Lower Critical Zone, central sector, eastern Bushveld Complex, and its chromite deposits. *Economic Geology* 75(6), pp. 845-871.

Campbell, G. 2004. From trailing to leading edge: Geophysical exploration of the Bushveld. In: Ashwal, L.D. ed. *Geoscience Africa.* University of the Witwatersrand. pp. 102-103.

Campbell, I. H. and Naldrett, A. J. 1979. The influence of silicate:sulfide ratios on the geochemistry of magmatic sulfides. *Economic Geology* 74(6), pp. 1503-1506.

Campbell, I. H.,Naldrett, A. J. and Barnes, S. J. 1983. A model for the origin of the platinum-rich sulfide horizons in the Bushveld and Stillwater Complexes. *Journal of Petrology* 24(2), pp. 133-165.

Carlson, R. W.,Pearson, D. G.,Boyd, F. R.,Shirey, S. B.,Irvine, G.,Menzies, A. H. and Gurney, J. J. 1999. Re-Os systematics of lithospheric peridotites: implications for lithospheric formation and preservation. . In: Gurney, J.J. et al. eds. *Proceedings of the VII international kimberlite conference.* Red Roof Design, Cape Town, South Africa,. pp. 99-108.

Cawthorn, R. G. 1999. The platinum and palladium resources of the Bushveld Complex. *South African Journal of Science* 95(11-12), pp. 481-489.

Cawthorn, R. G. 2005. Pressure fluctuations and the formation of the PGE-rich Merensky and chromitite reefs, Bushveld Complex. *Mineralium Deposita* 40(2), pp. 231-235.

Cawthorn, R. G.,Barnes, S. J.,Ballhaus, C. and Malitch, K. N. 2005. Platinum group element, chromium and vanadium deposits in mafic and ultramafic rocks. *Economic Geology* 100th Anniversary volume, pp. 215-250.

Cawthorn, R. G.,Barton Jr, J. M. and Viljoen, M. J. 1985. Interaction of floor rocks with the Platreef on Overysel, Potgietersrus, northern Transvaal. *Economic Geology* 80(4), pp. 988-1006.

Cawthorn, R. G.,Eales, H. V.,Walraven, F.,Uken, R. and Watkeys, M. K. 2006. The Bushveld Complex. In: Johnson, M.R. et al. eds. *The Geology of South Africa*. Johannesburg/Pretoria: Geological Society of South Africa/Council for Geoscience, p. 691.

Cawthorn, R. G.,Lee, C. A.,Schouwstra, R. P. and Mellowship, P. 2002a. Relationship between PGE and PGM in the Bushveld Complex. *Canadian Mineralogist* 40, pp. 311-328.

Cawthorn, R. G.,Merkle, R. and Viljoen, M. J. 2002b. Platinum-group Element Deposits in the Bushveld Complex, South Africa. In: Cabri, L.J. ed. *The geology, geochemistry, mineralogy and mineral beneficiation of platinum-group elements*. Vol. 54 (Special). Canadian Institue of Mining, Metallurgy and Petroleum, p. 582.

Cawthorn, R. G. and Walraven, F. 1998. Emplacement and crystallization time for the Bushveld Complex. *Journal of Petrology* 39(9), pp. 1669-1687.

Cawthorn, R. G. and Webb, S. J. 2001. Connectivity between the western and eastern limbs of the Bushveld complex. *Tectonophysics* 330(3-4), pp. 195-209.

Cheney, E. S. and Twist, D. 1991. The conformable emplacement of the Bushveld mafic rocks along a regional unconformity in the Transvaal succession of South Africa. *Precambrian Research* 52(1-2), pp. 115-132.

Chung, H.-Y. and Mungall, J. E. 2009. Physical constraints on the migration of immiscible fluids through partially molten silicates, with special reference to magmatic sulfide ores. *Earth and Planetary Science Letters* 286, pp. 14-22.

Clarke, B.,Uken, R. and Reinhardt, J. 2009. Structural and compositional constraints on the emplacement of the Bushveld Complex, South Africa. *Lithos* 111(1-2), pp. 21-36.

Clarke, B. M.,Reinhardt, J. and Uken, R. 2010. Reply to Rigby, M.J., Eriksson, P.G. and Mavimbela, P.K.: Comments on "Structural and compositional constraints on the emplacement of the Bushveld Complex" by B. Clarke, R. Uken and J. Reinhardt. *Lithos* 115(1-4), pp. 276-278.

Coghill, B. M. and Wilson, A. H. 1993. Platinum-group minerals in the Selukwe Subchamber, Great Dyke, Zimbabwe: implications for PGE collection mechanisms and post-formational redistribution. *Mineralogical Magazine* 57, pp. 613-633.

Colloty, A. 2008. An overview of exploration and mining activities at Mogalakwena platinum mine. In: *3rd Platreef Workshop* University of Witwatersrand

Cotton, F. G.,Wilkinson, G.,Murillo, C. A. and Bockmann, D. 1999. *Advanced Inorganic Chemistry*. 6 ed. New York: Wiley, p. 1355.

Cousins, C. A. 1959. The structure of the mafic portion of the western Bushveld Ingeous Complex. *Transactions of the Geological Society of South Africa* 26, pp. 179-201.

Cousins, C. A. and Feringa, G. 1964. The chromite deposits of the western belt of the Bushveld Complex. In: Haughton, S.H. ed. *The geology of some ore deposits in Southern Africa*. Vol. 2. Johannesburg: Geological Society of South Africa pp. 183-202.

Crocket, J. H.,Fleet, M. E. and S, W. E. 1997. Implications of composition for experimental partitioning of platinum-group elements and gold between sulfide liquid and basalt melt: The significance of nickel content. *Geochimica et Cosmochimica Acta* 61(19), pp. 4139-4149.

Curl, E. A. 2001. *Parental magmas of the Bushveld Complex, South Africa.* PhD, Monash University.

Dare, S.,Barnes, S.-J. and Prichard, H. 2010. The distribution of platinum group elements (PGE) and other chalcophile elements among sulfides from the Creighton Ni–Cu–PGE sulfide deposit, Sudbury, Canada, and the origin of palladium in pentlandite. *Mineralium Deposita* 45(8), pp. 765-793.

Davies, G. and Tredoux, M. 1985. The platinum-group element and gold contents of the marginal rocks and sills of the Bushveld complex. *Economic Geology* 80(4), pp. 838-848.

De Bremond d'Ars, J.,Arndt, N. T. and Hallot, E. 2001. Analog experimental insights into the formation of magmatic sulfide deposits. *Earth and Planetary Science Letters* 186(3-4), pp. 371-381.

De Klerk, L. 2005. Bushveld Stratigraphy on Rooipoort, Potgietersrus Limb. In: *2nd Platreef Workshop.* Mokopane, South Africa 28th-30th October.

De Waal, S. A.,Maier, W. D.,Armstrong, R. A. and Gauert, C. D. K. 2001. Parental magma and emplacement of the stratiform Uitkomst Complex, South Africa. *Canadian Mineralogist* 39(2), pp. 557-571.

De Wit, M. J.,Roering, C.,Hart, R. J.,Armstrong, R. A.,De Ronde, C. E. J.,Green, R. W. E.,Tredoux, M.,Peberdy, E. and Hart, R. A. 1992. Formation of an Archaean continent. *Nature* 357(6379), pp. 553-562.

Deines, P.,Nafziger, R. H.,Ulmer, G. C. and Woermann, E. 1974. *Temperature- oxygen fugacity tables for selected gas mixtures in the system C-H-O at one atmosphere total pressure.* Bulletin of the Earth And Mineral Sciences Experimental Station No.88, College of Earth and Mineral Sciences, Pennsylvania State University, p. 129.

Dorland, H. C.,Beukes, N. J.,Gutzmer, J.,Evans, D. A. D. and Armstrong, R. A. 2006. Precise SHRIMP U-Pb zircon age constraints on the lower Waterberg and Soutpansberg Groups, South Africa. *South African Journal of Geology* 109(1-2), pp. 139-156.

Dreibus, G.,Palme, H.,Spettel, B.,Zipfel, J. and Wänke, H. 1995. Sulfur and selenium in chondritic meteorites. *Meteoritics* 30(4), pp. 439-445.

Du Plessis, A. and Kleywegt, R. J. 1987. A dipping sheet model for the mafic lobes of the Bushveld Complex (South Africa). *South African Journal of Geology* 90(1), pp. 1-6.

Eales, H. V. 2000. Implications of the chromium budget of the Western Limb of the Bushveld Complex. *South African Journal of Geology* 103(2), pp. 141-150.

Eales, H. V. and Cawthorn, R. G. 1996. The Bushveld Complex. In: Cawthorn, R.G. ed. *Layered Intrusions*. Elsevier Science, pp. 181-230.

Eales, H. V.,de Klerk, W. J. and Teigler, B. 1990. Evidence for magma mixing processes within the Critical and Lower Zones of the northwestern Bushveld Complex, South Africa. *Chemical Geology* 88(3-4), pp. 261-278.

Eales, H. V. and Reynolds, I. M. 1986. Cryptic variations within chromitites of the upper critical zone, northwestern Bushveld Complex. *Economic Geology* 81(5), pp. 1056-1066.

Eckstrand, O. R.,Grinenko, L. N.,Krouse, H. R.,Paktunc, A. D.,Schwann, P. L. and Scoates, R. F. J. 1989. Preliminary data on sulphur isotopes and Se/S ratios, and the source of sulphur in magmatic sulphur in magmatic sulphides from the Fox River Sill, Molson Dykes and Thompson nickel deposits, northern Manitoba.*Current Reseach Part C* Ottawa: Geological Society of Canada, pp. 235-242.

Eckstrand, O. R. and Hulbert, L. J. 1987. Selenium and the source of sulfur in magmatic nickel and platinum deposits. *Geol. Assoc. Canada / Mineral Assoc. Canada Abstract* 12, p. 40.

Eriksson, P. G.,Altermann, W.,Catuneanu, O.,van der Merwe, R. and Bumby, A. J. 2001. Major influences on the evolution of the 2.67-2.1 Ga Transvaal basin, Kaapvaal craton. *Sedimentary Geology* 141-142, pp. 205-231.

Evstigneeva, T.,Genkin, A. D. and Kovalenker, V. A. 1976. Sobolevskite, a new bismuthide of palladium, and thenomenclature of minerals of the system PdBi-PdTe-PdSb. *International Geology Review* 18, pp. 856-866.

Fitzpatrick, A. J. 2008. *The measurement of the Se/S ratios in sulphide minerals and their application to ore deposit studies.* PhD, Queen's University.

Fleet, M. E.,Chryssoulis, S. L.,Stone, W. E. and Weisener, C. G. 1993. Partitioning of platinum-group elements and Au in the Fe−Ni−Cu−S system: experiments on the fractional crystallization of sulfide melt. *Contributions to Mineralogy and Petrology* 115(1), pp. 36-44.

Friese, A. E. W. 2004. *Geology and tectono-magmatic evolution of the PPL concession area, Villa Nora- Potgietersrus Limb, Bushveld Complex: Geological Visitor Guide*. Potgietersrus Platinums Limited.

Gain, S. B. and Mostert, A. B. 1982. The geological setting of the platinoid and base metal sulfide mineralization in the Platreef of the Bushveld complex in Drenthe, north of Potgietersrus. *Economic Geology* 77(6), pp. 1395-1404.

Ghiorso, M. S.,Hirschmann, M. M.,Reiners, P. W. and Kress, V. C., III. 2002. The pMELTS: A revision of MELTS for improved calculation of phase relations and major element partitioning related to partial melting of the mantle to 3 GPa. *Geochemistry. Geophysics. Geosystems.* 3(5), p. 1030.

Gibson, R. L. and Stevens, G. 1998. Regional metamorphism due to anorogenic intracratonic magmatism. What drives metamorphic reactions? In: Treloar, P.J. and O'Brien, P.J. eds. *What drives metamorphism and metamorphic reactions*. Geological Society of London Special Publication 138, pp. 121-135.

Godel, B. and Barnes, S.-J. 2008. Image analysis and composition of platinum-group minerals in the J-M Reef, Stillwater Complex. *Economic Geology* 103(3), pp. 637-651.

Godel, B.,Barnes, S.-J. and Maier, W. D. 2006. 3-D Distribution of Sulphide Minerals in the Merensky Reef (Bushveld Complex, South Africa) and the J-M Reef (Stillwater Complex,

USA) and their Relationship to Microstructures Using X-Ray Computed Tomography. *Journal of Petrology* 47(9), pp. 1853-1872.

Godel, B.,Barnes, S.-J. and Maier, W. D. 2007. Platinum-Group Elements in Sulphide Minerals, Platinum-Group Minerals, and Whole-Rocks of the Merensky Reef (Bushveld Complex, South Africa): Implications for the Formation of the Reef. *Journal of Petrology* 48(8), pp. 1569-1604.

Good, N. and De Wit, M. J. 1997. The Thabazimbi-Murchison lineament of the Kaapvaal Craton, South Africa: 2700 Ma of episodic deformation. *Journal of the Geological Society* 154(1), pp. 93-97.

Grieco, G.,Diella, V.,Chaplygina, N. L. and Savelieva, G. N. 2007. Platinum group elements zoning and mineralogy of chromitites from the cumulate sequence of the Nurali massif (Southern Urals, Russia). *Ore Geology Reviews* 30(3–4), pp. 257-276.

Griffin, W. L.,Graham, S.,O'Reilly, S. Y. and Pearson, N. J. 2004. Lithosphere evolution beneath the Kaapvaal Craton: Re-Os systematics of sulfides in mantle-derived peridotites. *Chemical Geology* 208(1-4), pp. 89-118.

Griffin, W. L.,O'Reilly, S. Y.,Natapov, L. M. and Ryan, C. G. 2003. The evolution of lithospheric mantle beneath the Kalahari Craton and its margins. *Lithos* 71(2-4), pp. 215-241.

Griffin, W. L.,O'Reilly, S. Y.,Afonso, J. C. and Begg, G. C. 2009. The Composition and Evolution of Lithospheric Mantle: a Re-evaluation and its Tectonic Implications. *Journal of Petrology* 50(7), pp. 1185-1204.

Groves, D. I.,Vielreicher, R. M.,Goldfarb, R. J. and Condie, K. C. 2005. Controls on the heterogenous distribution of mineral deposits through time. *Geological Society of London Special Publication* 248, pp. 71-101.

Gurney, J. J.,Helmstaedt, H. H.,Le Roex, A. P.,Nowicki, T. E.,Richardson, S. H. and Westerlund, K. J. 2005. Diamonds: crustal distribution and formation processes in time and space and an integrated deposit model. *Economic Geology* 100th Anniversary volume, pp. 143-178.

Hall, A. L. 1932. *The Bushveld Igneous Complex in the central Transvaal*. Geological Society of South African Memoir 28, p. 544.

Hamlyn, P. R. and Keays, R. R. 1986. Sulfur saturation and second-stage melts; application to the Bushveld platinum metal deposits. *Economic Geology* 81(6), pp. 1431-1445.

Hanley, J. J. 2007. The role of arsenic-rich melts and mineral phases in the development of high-grade Pt-Pd mineralization within komatiite-associated magmatic Ni-Cu sulfide horizons at Dundonald Beach South, Abitibi Subprovince, Ontario, Canada. *Economic Geology* 102(2), pp. 305-317.

Harmer, R. E. and Armstrong, R. A. 2000. Duration of Bushveld Complex (seno lato) magmatism: Constraints from new SHRIMP zircon chronology. In: *Workshop on the Bushveld Complex.* Gethane Lodge, Burgersfort, South Africa.

Harmer, R. E. and Sharpe, M. R. 1985. Field relations and strontium isotope systematics of the marginal rocks of the eastern Bushveld complex. *Economic Geology* 80(4), pp. 813-837.

Harmer, R. E. and von Gruenewaldt, G. 1991. A review of magmatism associated with the Transvaal Basin; implications for its tectonic setting. *South African Journal of Geology* 94(1), pp. 104-121.

Harris, C. and Chaumba, J. B. 2001. Crustal contamination and fluid-rock interaction during the formation of the Platreef, northern limb of the Bushveld Complex, South Africa. *Journal of Petrology* 42(7), pp. 1321-1347.

Harris, C.,Pronost, J. J. M.,Ashwal, L. D. and Cawthorn, R. G. 2005. Oxygen and Hydrogen Isotope Stratigraphy of the Rustenburg Layered Suite, Bushveld Complex: Constraints on Crustal Contamination. *Journal of Petrology* 46(3), pp. 579-601.

Hartley, F. R. 1991. The occurrences, extraction, properties and uses of the platinum group metals. In: Hartley, F.R. ed. *Chemistry of the Platinum Group Metals: Recent Developments (Studies in Inorganic Chemistry)*. Vol. 11. Amsterdam: Elsevier, pp. 9-32.

Hattingh, P. J. 1995. Palaeomagnetic constraints on the emplacement of the Bushveld complex. *Journal of African Earth Sciences* 21(4), pp. 549-551.

Hatton, C. J. 1995. Mantle plume origin for the Bushveld and Ventersdorp magmatic provinces. *Journal of African Earth Sciences* 21(4), pp. 571-577.

Hatton, C. J. and Schweitzer, J. K. 1995. Evidence for synchronous extrusive and intrusive Bushveld magmatism. *Journal of African Earth Sciences* 21(4), pp. 579-594.

Hatton, C. J. and Sharpe, M. R. 1989. Significance and origin of boninite-like rocks associated with the Bushveld Complex. In: Crawford, A.J. ed. *Boninites*. London: Unwin Hyman, pp. 174-203.

Hatton, C. J. and von Gruenewaldt, G. 1987. The geological setting and petrogenesis of the Bushveld chromitite layers. In: Stowe, C.W. ed. *Evolution of chromite ore fields*. New York: Van Nostrand Reinhold, pp. 109-143.

Helmy, H.,Ballhaus, C.,Berndt, J.,Bockrath, C. and Wohlgemuth-Ueberwasser, C. 2007. Formation of Pt, Pd and Ni tellurides: experiments in sulfide–telluride systems. *Contributions to Mineralogy and Petrology* 153(5), pp. 577-591.

Helmy, H. M.,Ballhaus, C.,Wohlgemuth-Ueberwasser, C.,Fonseca, R. O. C. and Laurenz, V. 2010. Partitioning of Se, As, Sb, Te and Bi between monosulfide solid solution and sulfide melt – Application to magmatic sulfide deposits. *Geochimica et Cosmochimica Acta* 74(21), pp. 6174-6179.

Henderson, P. 1975. Reaction trends shown by chrome-spinels of the Rhum layered intrusion. *Geochimica et Cosmochimica Acta* 39(6-7), pp. 1035-1036.

Henderson, P. and Wood, R. J. 1982. Reaction relationships of chrome-spinels in igneous rocks — further evidence from the layered intrusions of Rhum and Mull, Inner Hebrides, Scotland. *Contributions to Mineralogy and Petrology* 78(3), pp. 225-229.

Hiemstra, S. A. 1979. The role of collectors in the formation of the platinum deposits in the Bushveld Complex. *Canadian Mineralogist* 17, pp. 469-482.

Hoffman, E. L. and Dunn, B. 2002. Sample preparation and bulk analytical methods for PGE. In: Cabri, L.J. ed. *The geology, geochemistry, mineralogy and mineral beneficiation of platinum-group elements*. Vol. 54 (Special). Canadian Institue of Mining, Metallurgy and Petroleum, pp. 1-13.

Holloway, J. R. and Wood, B. J. eds. 1988. *Simulating the Earth: Experimental Geochemistry.* London: HarperCollins Academic, p. 199.

Holwell, D. and McDonald, I. 2007. Distribution of platinum-group elements in the Platreef at Overysel, northern Bushveld Complex: a combined PGM and LA-ICP-MS study. *Contributions to Mineralogy and Petrology* 154(2), pp. 171-190.

Holwell, D.,McDonald, I. and Butler, I. 2010. Precious metal enrichment in the Platreef, Bushveld Complex, South Africa: evidence from homogenized magmatic sulfide melt inclusions. *Contributions to Mineralogy and Petrology*, pp. 1-16.

Holwell, D. A. 2006. *The roles of magmatism, contamination and hydrothermal processes in the development of the Platreef mineralization, Bushveld Complex, South Africa.* PhD, Cardiff University.

Holwell, D. A.,Armitage, P. E. B. and McDonald, I. 2005. Observations on the relationship between the Platreef and its hangingwall. *Applied Earth Science: Transactions of the Institute of Mining and Metallurgy, Section B* 114, pp. 199-207.

Holwell, D. A.,Boyce, A. J. and McDonald, I. 2007. Sulfur isotope variations within the Platreef Ni-Cu-PGE deposit: Genetic implications for the origin of sulfide mineralization. *Economic Geology* 102(6), pp. 1091-1110.

Holwell, D. A. and Jordaan, A. 2006. Three-dimensional mapping of the Platreef at the Zwartfontein South mine: implications for the timing of magmatic events in the northern limb of the Bushveld Complex, South Africa. *Applied Earth Science: Transactions of the Institute of Mining and Metallurgy, Section B* 115, pp. 41-48.

Holwell, D. A. and McDonald, I. 2006. Petrology, geochemistry and the mechanisms determining the distribution of platinum-group element and base metal sulphide mineralisation in the Platreef at Overysel, northern Bushveld Complex, South Africa. *Mineralium Deposita* 41(6), pp. 575-598.

Holwell, D. A. and McDonald, I. 2010. A review of the behaviour of platinum group elements within natural magmatic sulfide ore systems. *Platinum Metals Review* 54(1), pp. 26-36.

Holwell, D. A.,McDonald, I. and Armitage, P. E. B. 2006. Platinum-group mineral assemblages in the Platreef at the Sandsloot Mine, northern Bushveld Complex, South Africa. *Mineralogical Magazine* 70(1), pp. 83-101.

Holwell, D. A.,McDonald, I. and Butler, I. B. 2011. Precious metal enrichment in the Platreef, Bushveld Complex, South Africa: evidence from homogenized magmatic sulfide melt inclusions. *Contributions to Mineralogy and Petrology* 161(6), pp. 1011-1026.

Holzer, L.,Frei, R.,Barton Jr, J. M. and Kramers, J. D. 1998. Unraveling the record of successive high grade events in the Central Zone of the Limpopo Belt using Pb single phase dating of metamorphic minerals. *Precambrian Research* 87(1-2), pp. 87-115.

Hulbert, L. J. 1983. *A petrological investigation of the Rustenburg Layered Suite and associated mineralization south of Potgietersrus.* DSc, University of Pretoria.

Hulbert, L. J. and von Gruenewaldt, G. 1982. Nickel, copper, and platinum mineralization in the lower zone of the Bushveld Complex, south of Potgietersrus. *Economic Geology* 77(6), pp. 1296-1306.

Hulbert, L. J. and von Gruenewaldt, G. 1985. Textural and compositional features of chromite in the lower and critical zones of the Bushveld complex south of Potgietersrus. *Economic Geology* 80(4), pp. 872-895.

Hulbert, L. J. and von Gruenewaldt, G. 1986. The structure of the upper and lower chromitite layers on the farms Grasvally and Zoetveld, south of Potgietersrus. In: Anhaeusser, C.R. and Maske, S. eds. *Mineral Deposits of Southern Africa*. Vol. 2. Johannesburg: Geological Society of Southern Africa, pp. 1237-1249.

Hunter, R. H. 1996. Texture development in cumulate rocks. In: Cawthorn, R.G. ed. *Layered Intrusions*. Amsterdam: Elsevier, pp. 77-101.

Hutchinson, D. and Kinnaird, J. A. 2005. Complex multistage genesis for the Ni-Cu-PGE mineralisation in the southern region of the Platreef, Bushveld Complex, South Africa. *Applied Earth Science: Transactions of the Institute of Mining and Metallurgy, Section B* 114, pp. B208-B224.

Hutchinson, D.,Kinnaird, J. A. and Schurmann, L. W. 2004. Complex, multistage mineralization history in the southern sector of the Platreef, Bushveld Complex, RSA. In: *Geoscience Africa 2004.* University of Witwatersrand, Johannesburg. pp. 293-294.

Hutchinson, D. and McDonald, I. 2008. Laser ablation ICP-MS study of platinum-group elements in sulphides from the Platreef at Turfspruit, northern limb of the Bushveld Complex, South Africa. *Mineralium Deposita* 43(6), pp. 695-711.

Ihlenfeld, C. and Keays, R. 2011. Crustal contamination and PGE mineralization in the Platreef, Bushveld Complex, South Africa: evidence for multiple contamination events and transport of magmatic sulfides. *Mineralium Deposita* 46(7), pp. 813-832.

Irvine, T. N. 1965. Chromian spinel as a petrogenetic indicator. Part 1. Theory. *Canadian Journal of Earth Sciences* 2, pp. 648-672.

Irvine, T. N. 1967. Chromian spinel as a petrogenetic indicator: part 2. Petrologic applications *Canadian Journal of Earth Sciences* 4(1), pp. 71-103.

Irvine, T. N. 1975. Crystallization sequences in the Muskox intrusion and other layered intrusions--II. Origin of chromitite layers and similar deposits of other magmatic ores. *Geochimica et Cosmochimica Acta* 39(6-7), pp. 991-1020.

Irvine, T. N. 1977. Origin of chromitite layers in the Muskox intrusion and other stratiform intrusions: A new interpretation. *Geology* 5(5), pp. 273-277.

Kamenetsky, V. 1996. Methodology for the study of melt inclusions in Cr-spinel, and implications for parental melts of MORB from FAMOUS area. *Earth and Planetary Science Letters* 142(3-4), pp. 479-486.

Kelly, D. P. and Vaughan, D. J. 1983. Pyrrhotine-pentlandite ore textures: a mechanistic approach. *Mineralogical Magazine* 47, pp. 453-463.

Kerr, A. and Leitch, A. M. 2005. Self-Destructive Sulfide Segregation Systems and the Formation of High-Grade Magmatic Ore Deposits. *Economic Geology* 100(2), pp. 311-332.

Kerrich, R.,Goldfarb, R. J.,Groves, D. I. and Garwin, S. 2000. The geodynamics of world-class gold deposits: characteristics, space-time distribution, and origins. *Reviews in Economic Geology* 13, pp. 501-552.

Kingston, G. A. and El-Dosuky, B. T. 1982. A contribution on the platinum-group mineralogy of the Merensky Reef at the Rustenburg platinum mine. *Economic Geology* 77(6), pp. 1367-1384.

Kinloch, E. D. 1982. Regional trends in the platinum-group mineralogy of the critical zone of the Bushveld Complex, South Africa. *Economic Geology* 77(6), pp. 1328-1347.

Kinloch, E. D. and Peyerl, W. 1990. Platinum-group minerals in various rock types of the Merensky Reef: genetic implications. *Economic Geology* 85(3), pp. 537-555.

Kinnaird, J. A. ed. 2004. *What are the questions we need to ask about the Platreef?* Platreef Workshop*.* Mokopane. Geoscience Africa.

Kinnaird, J. A. 2005. Geochemical evidence for multiphase emplacement in the southern Platreef. *Applied Earth Science: Transactions of the Institute of Mining and Metallurgy, Section B* 114, pp. 225-242.

Kinnaird, J. A.,Hutchinson, D.,Schurmann, L.,Nex, P. A. M. and de Lange, R. 2005. Petrology and mineralisation of the southern Platreef: Northern limb of the Bushveld Complex, South Africa. *Mineralium Deposita* 40(5), pp. 576-597.

Kinnaird, J. A.,Kruger, F. J.,Nex, P. A. M. and Cawthorn, R. G. 2002. Chromitite formation - a key to understanding processes of platinum enrichment. *Applied Earth Science: Transactions of the Institute of Mining and Metallurgy, Section B* 111, pp. 23-35.

Kinnaird, J. A. and McDonald, I. 2005. Preface: An introduction to mineralisation in the northern limb of the Bushveld Complex. *Applied Earth Science: Transactions of the Institute of Mining and Metallurgy, Section B* 114, pp. 194-198.

Kinnaird, J. A. and Nex, P. A. M. 2003. Mechanisms of marginal mineralisation in the Bushveld Complex. *Applied Earth Science: Transactions of the Institute of Mining and Metallurgy, Section B* 112, pp. 206-208.

Kinnaird, J. A.,Yudovskaya, M.,Nicholl, S.,Naldrett, A. J. and Nex, P. A. M. 2010. Along-strike and down-dip variations in multiphase sills of the Platreef, Bushveld Complex. In: Jugo, P.J. et al. eds. *11th International Platinum Symposium.* Sudbury, Ontario, 21-24 June 2010. Ontario Geological Survey,

Kruger, F. J. 2002. Isotopic constraints on the origin of the Bushveld Complex magmas in a back-arc environment. *Geochimica et Cosmochimica Acta* 66 (15A)(Suppl. 1 ), pp. A420-A420

Kruger, F. J. 2005a. Filling the Bushveld Complex magma chamber: Lateral expansion, roof and floor interaction, magmatic unconformities, and the formation of giant chromitite, PGE and Ti-V-magnetitite deposits. *Mineralium Deposita* 40(5), pp. 451-472.

Kruger, F. J. 2005b. Thoughts on the Platreef - a Critcal Zone or Main Zone phenomenom? In: *2nd Platreef Workshop.* Mokopane. Geological Society of South Africa,

Lambert, D. D.,Shirey, S. B. and Berman, S. C. 1995. Proterozoic lithospheric mantle source for the Prairie Creek lamproites: Re-Os and Sm-Nd isotopic evidence. *Geology* 23, pp. 273-276.

Lambert, D. D. and Simmons, E. C. 1987. Magma evolution in the Stillwater Complex, Montana; I, Rare-earth element evidence for the formation of the Ultramafic Series. *American Journal of Science* 287(1), pp. 1-32.

Lee, C. A. 1996. A review of mineralization in the Bushveld Complex and some other layered mafic intrusions. In: Cawthorn, R.G. ed. *Layered Intrusions*. Amsterdam: Elsevier Science, pp. 103-146.

Lesher, C. M. and Groves, D. I. 1986. Controls on the Formation of Komatiite-Associated Nickel-Copper Sulfide Deposits. In: Freidrich, G.H. et al. eds. *Geology and Metallogeny of Copper Deposits*. Berlin: Springer-Verlag Heidelberg, pp. 43-62.

Li, C.,Barnes, S. J.,Makovicky, E.,Rose-Hansen, J. and Makovicky, M. 1996. Partitioning of nickel, copper, iridium, rhenium, platinum, and palladium between monosulfide solid solution and sulfide liquid: Effects of composition and temperature. *Geochimica et Cosmochimica Acta* 60(7), pp. 1231-1238.

Li, C. and Naldrett, A. J. 1999. Geology and petrology of the Voisey's Bay intrusion: Reaction of olivine with silicate and sulfide liquids. *Lithos* 47, pp. 1-31.

Li, C.,Ripley, E.,Sarkar, A.,Shin, D. and Maier, W. 2005. Origin of phlogopite-orthopyroxene inclusions in chromites from the Merensky Reef of the Bushveld Complex, South Africa. *Contributions to Mineralogy and Petrology* 150(1), pp. 119-130.

Li, C. and Ripley, E. M. 2006. Formation of Pt-Fe alloy by desulfurization of Pt-Pd sulphide in the J-M Reef of the Stillwater Complex, Montana. *Canadian Mineralogist* 44(4), pp. 895-903.

Li, C.,Ripley, E. M.,Maier, W. D. and Gomwe, T. E. S. 2002. Olivine and sulfur isotopic compositions of the Uitkomst Ni-Cu sulfide ore-bearing complex, South Africa: Evidence for sulfur contamination and multiple magma emplacements. *Chemical Geology* 188(3-4), pp. 149-159.

Li, C.,Ripley, E. M.,Merino, E. and Maier, W. D. 2004. Replacement of base metal sulphides by actinolite, epidote, calcite, and magnetite in the UG2 and Merensky Reef of the Bushveld Complex, South Africa. *Economic Geology* 99(1), pp. 173-184.

Liebenberg, L. 1970. The sulfides in the layered sequence of the Bushveld Igneous Complex. *Geological Society of South Africa Special Publication* 1, pp. 108-208.

Lodders, K. 2003. Solar System Abundances and Condensation Temperatures of the Elements. *The Astrophysical Journal* 591(2), p. 1220.

Lorand, J. P. and Alard, O. 2001. Platinum-group element abundances in the upper mantle; new constraints from in situ and whole-rock analyses of Massif Central xenoliths (France). *Geochimica et Cosmochimica Acta* 65(16), pp. 2789-2806.

Maier, W. and Barnes, S.-J. 2008a. Platinum-group elements in the UG1 and UG2 chromitites, and the Bastard reef, at Impala platinum mine, western Bushveld Complex, South Africa: Evidence for late magmatic cumulate instability and reef constitution. *South African Journal of Geology* 111(2-3), pp. 159-176.

Maier, W. D.,Arndt, N. T. and Curl, E. A. 2000. Progressive crustal contamination of the Bushveld Complex: evidence from Nd isotopic analyses of the cumulate rocks. *Contributions to Mineralogy and Petrology* 140(3), pp. 316-327.

Maier, W. D. and Barnes, S.-J. 1999. Platinum-Group Elements in Silicate Rocks of the Lower, Critical and Main Zones at Union Section, Western Bushveld Complex. *Journal of Petrology* 40(11), pp. 1647-1671.

Maier, W. D. and Barnes, S.-J. 2004. Pt/Pd and Pd/Ir ratios in mantle-derived magmas: A possible role for mantle metasomatism. *South African Journal of Geology* 107(3), pp. 333-340.

Maier, W. D. and Barnes, S.-J. 2009. Formation of PGE deposits in layered intrusions. In: Li, C. and Ripley, E.M. eds. *New development in magmatic Ni-Cu and PGE deposits*. Beijing: Geological Publishing House, pp. 250-276.

Maier, W. D. and Barnes, S. J. 2008b. Platinum-group elements in the UG1 and UG2 chromitites, and the Bastard reef, at Impala platinum mine, western Bushveld Complex, South Africa: Evidence for late magmatic cumulate instability and reef constitution. *South African Journal of Geology* 111(2-3), pp. 159-176.

Maier, W. D.,Barnes, S. J.,Campbell, I. H.,Fiorentini, M. L.,Peltonen, P.,Barnes, S.-J. and Smithies, R. H. 2009. Progressive mixing of meteoritic veneer into the early Earth's deep mantle. *Nature* 460(7255), pp. 620-623.

Maier, W. D.,Barnes, S. J. and Van Der Merwe, M. J. 2001. Platinum-group elements in the Pyroxenite Marker, Bushveld Complex: Implications for the formation of the Main Zone. *South African Journal of Geology* 104(4), pp. 301-308.

Maier, W. D. and Eales, H. V. 1997. Correlation within the UG2-Merensky Reef interval of the western Bushveld Complex, based on geochemical, mineralogical and petrological data. *Geological Survey of South Africa Bulletin* 120, p. 57.

Maier, W. D. and Groves, D. 2011. Temporal and spatial controls on the formation of magmatic PGE and Ni–Cu deposits. *Mineralium Deposita* 46(8), pp. 841-857.

Maier, W. D.,Klerk, L.,Blaine, J.,Manyeruke, T.,Barnes, S.-J.,Stevens, M. and Mavrogenes, J. 2008. Petrogenesis of contact-style PGE mineralization in the northern lobe of the Bushveld Complex: comparison of data from the farms Rooipoort, Townlands, Drenthe and Nonnenwerth. *Mineralium Deposita* 43(3), pp. 255-280.

Maier, W. D.,Peltonen, P.,McDonald, I.,Barnes, S. J.,Hatton, C. and Viljoen, F. 2012. The concentration of platinum-group elements and gold in southern African and Karelian kimberlite-hosted mantle xenoliths: Implications for the noble metal content of the Earth's mantle. *Chemical Geology* 302–303, pp. 119-135.

Makovicky, E. 2002. Ternary and quaternary phase systems with PGE. In: Cabri, L.J. ed. *The geology, geochemistry, mineralogy and mineral benificiation of platiunum-group elements*. Vol. 54 (Special). Canadian Institute of Mining, Metallurgy and Petroleum, pp. 131-175.

Makovicky, M.,Makovicky, E. and Rose-Hansen, J. 1986. Experimental studies on the solubility and distribution of platinum-group elements in base metal sulphides in platinum deposits. In: Gallagher, M.J. et al. eds. *Metallurgy of basic and ultrabasic rocks*. London: Institute of Mining and Metallurgy, pp. 415-425.

Manyeruke, T. D.,Maier, W. D. and Barnes, S.-J. 2005. Major and trace element geochemistry of the Platreef on the farm Townlands, northern Bushveld Complex. *South African Journal of Geology* 108(3), pp. 381-396.

Mathez, E. A. 1999. On factors controlling the concentrations of platinum group elements in layered intrusions and chromitites. In: Keays, R.R. et al. eds. *Dynamic processes in magmatic ore deposits and their application to mineral exploration. Short Course Notes*. Vol. 13. Geological Association of Canada, pp. 251-285.

Mathez, E. A. and Mey, J. L. 2005. Character of the UG2 Chromitite and Host Rocks and Petrogenesis of Its Pegmatoidal Footwall, Northeastern Bushveld Complex. *Economic Geology* 100(8), pp. 1617-1630.

Mattioli, G. S. and Wood, B. J. 1988. Magnetite activities across the $MgAl_2O_4$-$Fe_3O_4$ spinel join, with application to thermobarometric estimates of upper mantle oxygen fugacity. *Contributions to Mineralogy and Petrology* 98(2), pp. 148-162.

Mavrogenes, J. A. and O'Neill, H. S. C. 1999. The relative effects of pressure, temperature and oxygen fugacity on the solubility of sulfide in mafic magmas. *Geochimica et Cosmochimica Acta* 63(7-8), pp. 1173-1180.

McCandless, T. E.,Ruiz, J.,Adair, B. I. and Freydier, C. 1999. Re-Os isotope and Pd/Ru variations in chromitites from the Critical Zone, Bushveld Complex, South Africa. *Geochimica et Cosmochimica Acta* 63(6), pp. 911-923.

McCourt, S. and Vearncombe, J. R. 1987. Shear zones bounding the central zone of the Limpopo Mobile Belt, southern Africa. *Journal of Structural Geology* 9(2), pp. 127-137.

McDonald, D. and Hunt, L. B. 1982. *A History of Platinum and its Allied Metals*. London: Johnson Matthey, p. 450.

McDonald, I. 2005. Development of sulphide standards for the in-situ analysis of platinum-group elements by laser ablation inductively coupled plasma-mass spectrometry (LA-ICPMS). In: Tormanen, T.O. and Alapieti, T.T. eds. *10th International Platinum Symposium.* University of Oulu. pp. 468-471.

McDonald, I. and Holwell, D. A. 2007. Did lower zone magma conduits store PGE-rich sulphides that were later supplied to the Platreef? *South African Journal of Geology* 110(4), pp. 611-616.

McDonald, I. and Holwell, D. A. 2011. Geology of the northern Bushveld Complex and the setting and genesis of the Platreef Ni-Cu-PGE deposit. In: Li, C. and Ripley, E.M. eds. *Reviews in Economic Geology*. Vol. 17. Society of Economic Geology, pp. 297-328.

McDonald, I.,Holwell, D. A. and Armitage, P. E. B. 2005. Geochemistry and mineralogy of the Platreef and "Critical Zone" of the northern lobe of the Bushveld Complex, South Africa: Implications for Bushveld stratigraphy and the development of PGE mineralisation. *Mineralium Deposita* 40(5), pp. 526-549.

McDonald, I.,Holwell, D. A. and Wesley, B. 2009. Assessing the potential involvement of an early magma staging chamber in the generation of the Platreef NiCuPGE deposit in the northern limb of the Bushveld Complex: a pilot study of the Lower Zone Complex at Zwartfontein. *Applied Earth Science: Transactions of the Institute of Mining and Metallurgy, Section B* 118, pp. 5-20.

McDonald, I.,Ohnenstetter, D.,Ohnenstetter, M. and Vaughan, D. J. 1999. Palladium oxides in ultramafic complexes near Lavatrafo, Western Andriamena Madagascar. *Mineralogical Magazine* 63, pp. 345-352.

McDonald, I. and Viljoen, K. S. 2006. Platinum-group element geochemistry of mantle eclogites: a reconnaissance study of xenoliths from the Orapa kimberlite, Botswana. *Applied Earth Science* 115(3), pp. 81-93.

McDonough, W. F. and Sun, S. S. 1995. The composition of the Earth. *Chemical Geology* 120 pp. 223-253.

McGoldrick, P. J. and Keays, R. R. 1981. Precious and volatile metals in the Perseverance nickel deposit gossan: implications for exploration in weathered terrains. *Economic Geology* 76, pp. 1752-1763.

McInnes, B. I. A.,McBride, J. S.,Evans, N. J.,Lambert, D. D. and Andrew, A. S. 1999. Osmium Isotope Constraints on Ore Metal Recycling in Subduction Zones. *Science* 286(5439), pp. 512-516.

McLaren, C. H. and De Villiers, J. P. R. 1982. The platinum-group chemistry and mineralogy of the UG-2 chromitite layer of the Bushveld Complex. *Economic Geology* 77(6), pp. 1348-1366.

McNeill, A. W.,Danyushevsky, L. V.,Kamenetsky, V.,Feig, S. and Crawford, A. J. 2008. Inclusions of immiscible sulfide melts in olivine phenocrysts from mantle-derived magmas. *Geochimica et Cosmochimica Acta* 72(12), p. A616.

Meyer, R. and De Beer, J. H. 1987. Structure of the Bushveld Complex from resistivity measurements. *Nature* 325(6105), pp. 610-612.

Mills Davies, J. E. 1925. The geology of the Transvaal platinum deposits. *The South African Mining and Engineering Journal* 36, pp. 63-66.

Misra, K. C. 2000. *Understanding mineral deposits*. Dordrecht: Kluwer Academic Publishers, p. 864.

Mitchell, A. A. 1990. The stratigraphy, petrography and mineralogy of the Main Zone in northwestern Bushveld Complex. *South African Journal of Geology* 93, pp. 818-831.

Mitchell, R. H. and Keays, R. R. 1981. Abundance and distribution of gold, palladium and iridium in some spinel and garnet lherzolites: implications for the nature and origin of precious metal-rich intergranular components in the upper mantle. *Geochimica et Cosmochimica Acta* 45(12), pp. 2425-2433, 2435-2442.

Mondal, S. K. and Mathez, E. A. 2007. Origin of the UG2 chromitite layer, Bushveld Complex. *Journal of Petrology* 48(3), pp. 495-510.

Morgan, J. W. and Baedecker, P. A. 1983. Elemental composition of sulfide particles from an ultramafic xenolith and the siderophile element content of the upper mantle. In: *Proceedings of the Lunar and Planetary Science Conference.* pp. 513-514.

Mostert, A. B.,Hofmeyr, P. K. and Potgieter, G. A. 1982. The platinum-group mineralogy of the Merensky Reef at the Impala platinum mines, Bophuthatswana. *Economic Geology* 77(6), pp. 1385-1394.

Mungall, J. E.,Andrews, D. R. A.,Cabri, L. J.,Sylvester, P. J. and Tubrett, M. 2005. Partitioning of Cu, Ni, Au, and platinum-group elements between monosulfide solid solution and sulfide melt under controlled oxygen and sulfur fugacities. *Geochimica et Cosmochimica Acta* 69(17), pp. 4349-4360.

Mungall, J. E. and Naldrett, A. J. 2008. Ore deposits of the platinum-group elements. *Elements* 4(4), pp. 253-258.

Mungall, J. E. and Su, S. 2005. Interfacial tension between magmatic sulfide and silicate liquids: Constraints on kinetics of sulfide liquation and sulfide migration through silicate rocks. *Earth and Planetary Science Letters* 234(1-2), pp. 135-149.

Murck, B. W. and Campbell, I. H. 1986. The effects of temperature, oxygen fugacity and melt composition on the behaviour of chromium in basic and ultrabasic melts. *Geochimica et Cosmochimica Acta* 50(9), pp. 1871-1887.

Naldrett, A. J. 2004. *Magmatic Sulfide Deposits: Geology, Geochemistry and Exploration*. Berlin: Springer, p. 727.

Naldrett, A. J. 2010a. From the Mantle to the Bank: The Life of a Ni-Cu (PGE) Sulfide Deposit. *South African Journal of Geology* 113(1), pp. 1-32.

Naldrett, A. J. 2010b. Fundamentals of magmatic sulfide deposits. In: Li, C. and Ripley, E.M. eds. *New development in magmatic Ni-Cu and PGE deposits*. Beijing: Geological Publishing House, pp. 1-26.

Naldrett, A. J. 2010c. Secular Variation of Magmatic Sulfide Deposits and Their Source Magmas. *Economic Geology* 105(3), pp. 669-688.

Naldrett, A. J.,Federenko, V. A.,Lightfoot, P. C.,Kunilov, V. I.,Gorbachev, N. S.,Doherty, W. and Johan, Z. 1995. Ni-Cu-PGE deposits of Noril'sk region, Siberia: Their formation in conduits for flood-basalt volcanism. *Applied Earth Science: Transactions of the Institute of Mining and Metallurgy, Section B* 104, pp. 19-36.

Naldrett, A. J.,Gasparrini, E. C.,Barnes, S. J.,von Gruenewaldt, G. and Sharpe, M. R. 1986. The upper critical zone of the Bushveld complex and the origin of Merensky-type ores. *Economic Geology* 81(5), pp. 1105-1117.

Naldrett, A. J.,Hoffman, E. L.,Green, A. H.,Chou, C. L.,Naldrett, S. R. and Alcock, R. A. 1979. The composition of Ni-sulfide ores with particular reference to their content of PGE and Au. *Canadian Mineralogist* 17, pp. 403-415.

Naldrett, A. J.,Innes, D. G.,Sowa, J. and Gorton, M. P. 1982. Compositional variations within and between five Sudbury ore deposits. *Economic Geology* 77(6), pp. 1519-1534.

Naldrett, A. J.,Kinnaird, J. A.,Wilson, A. and Chunnett, G. 2008a. Concentration of PGE in the Earth's Crust with Special Reference to the Bushveld Complex. *Earth Science Frontiers* 15(5), pp. 264-297.

Naldrett, A. J.,Kinnaird, J. A.,Wilson, A.,Yudovskaya, M.,McQuade, S.,Chunnett, G. and Stanley, C. 2009a. Chromite composition and PGE content of Bushveld chromitites: Part 1 the Lower and Middle Groups. *Applied Earth Science: Transactions of the Institute of Mining and Metallurgy, Section B* 118, pp. 131-161.

Naldrett, A. J. and Lehmann, J. 1988. Spinel non-stoichiometry as an explanation for Ni-, Cu-, and PGE-enriched sulphides in chromitites. In: Prichard, H.M. et al. eds. *Geo-Platinum 97*. Amsterdam: Elsevier, pp. 113-143.

Naldrett, A. J. and von Gruenewaldt, G. 1989. Association of platinum-group elements with chromitite in layered intrusions and ophiolite complexes. *Economic Geology* 84(1), pp. 180-187.

Naldrett, A. J.,Wilson, A.,Kinnaird, J. A. and Chunnett, G. 2008b. Links between the Platreef and the upper Critical Zone. In: *3rd Platreef Workshop.* Mokopane, South Africa, 11-13th July 2008.

Naldrett, A. J.,Wilson, A.,Kinnaird, J. A. and Chunnett, G. 2009b. PGE Tenor and Metal Ratios within and below the Merensky Reef, Bushveld Complex: Implications for its Genesis. *Journal of Petrology* 50(4), pp. 625-659.

Naldrett, A. J.,Wilson, A.,Kinnaird, J. A.,Yudovskaya, M. and Chunnett, G. 2012. The origin of chromitites and related PGE mineralization in the Bushveld Complex: new mineralogical and petrological constraints. *Mineralium Deposita* 47(3), pp. 209-232.

Nex, P. A. M. 2005. The structural setting of mineralisation on Tweefontein Hill, northern limb of the Bushveld Complex, South Africa. *Applied Earth Science: Transactions of the Institute of Mining and Metallurgy, Section B* 114(4), pp. 243-251.

Nex, P. A. M.,Kinnaird, J. A.,Jones, B. and Colloty, A. 2006. *Platreef rock type definitions and descriptions*. Anglo Platinum Technical Report.

Nex, P. A. M.,Nicholl, S. and Ixer, R. A. 2008. Geological evidence for hydrothermal and supergene PGE mineralisation in the footwall to the Platreef at Tweefontein Hill, South Africa. In: *3rd Platreef Workshop.* Mokopane, South Africa.

Nicholl, S. and Kinnaird, J. A. 2008. Platinum-group mineral assemblages in the Platreef on Tweefontein North. In: *3rd Platreef Workshop.* Mokopane, South Africa.

Nyama, N.,Nex, P. A. M. and Yao, Y. 2005. Preliminary petrological studies of the Platreef on Tweefontein Hill, Bushveld Igneous Complex, South Africa. In: Tormanen, T.O. and Alapieti, T.T. eds. *10th International Platinum Symposium.* University of Oulu. pp. 505-508.

O'Neill, H. S. C. and Wall, V. J. 1987. The Olivine--Orthopyroxene--Spinel Oxygen Geobarometer, the Nickel Precipitation Curve, and the Oxygen Fugacity of the Earth's Upper Mantle. *Journal of Petrology* 28(6), pp. 1169-1191.

Ohmoto, H. and Rye, R. O. 1979. Isotopes of sulfur and carbon. In: Barnes, H.L. ed. *Geochemistry of Hydrothermal Ore Deposits*. 2nd ed. London: Wiley and Sons, pp. 509-567.

Ohnenstetter, M.,Johan, Z.,Cocherie, A.,Fouillac, A. M.,Guerrot, C.,Ohnenstetter, D.,Chaudisson, M.,Rouer, O.,Makovicky, E.,Mackovicky, M.,Rose-Hansen, J.,Karup-Moller, S.,Vaughan, D. J.,Turner, G.,Pattrick, R. A. D.,Gize, A. P.,Lyon, I. C. and McDonald, I. 1999. New exploration methods for platinum and rhodium deposits poor in base-metal sulfides-NEXTPRIM. *Applied Earth Science: Transactions of the Institute of Mining and Metallurgy, Section B* 108, pp. 119-150.

Olsson, J. R.,Söderlund, U.,Klausen, M. B. and Ernst, R. E. 2010. U-Pb baddeleyite ages linking major Archean dyke swarms to volcanic-rift forming events in the Kaapvaal craton (South Africa), and a precise age for the Bushveld Complex. *Precambrian Research* 183(3), pp. 490-500.

Osbahr, I.,Klemd, R.,Oberthür, T.,Brätz, H. and Schouwstra, R. 2013. Platinum-group element distribution in base-metal sulfides of the Merensky Reef from the eastern and western Bushveld Complex, South Africa. *Mineralium Deposita* 48(2), pp. 211-232.

Pattou, L.,Lorand, J. P. and Gros, M. 1996. Non-chondritic platinum-group element ratios in the Earth's mantle. *Nature* 379, pp. 712-715.

Peach, C. L. and Mathez, E. A. 1996. Constraints on the formation of platinum-group element deposits in igneous rocks. *Economic Geology* 91(2), pp. 439-450.

Peach, C. L.,Mathez, E. A. and Keays, R. R. 1990. Sulfide melt-silicate melt distribution coefficients for noble metals and other chalcophile elements as deduced from MORB: Implications for partial melting. *Geochimica et Cosmochimica Acta* 54(12), pp. 3379-3389.

Pearson, D. G.,Irvine, G. J.,Ionov, D. A.,Boyd, F. R. and Dreibus, G. E. 2004. Re–Os isotope systematics and platinum group element fractionation during mantle melt extraction: a study of massif and xenolith peridotite suites. *Chemical Geology* 208(1-4), pp. 29-59.

Peck, D. C. and Keays, R. R. 1990. Insights into the behavior of precious metals in primitive, S-undersaturated magmas. *Canadian Mineralogist* 28, pp. 553-557.

Peck, D. C.,Keays, R. R. and Ford, R. J. 1992. Direct crystallization of refractory platinum group elements alloys from boninitic magmas: evidence from western Tasmania. *Australian Journal of Earth Sciences* 39, pp. 373-387.

Penberthy, C. J. and Merkle, R. K. W. 1999. Lateral variations in the platinum-group element content and mineralogy of the UG2 chromitite layer, Bushveld Complex. *South African Journal of Geology* 102(3), pp. 240-250.

Penniston-Dorland, S. C.,Wing, B. A.,Nex, P. A. M.,Kinnaird, J. A.,Farquhar, J.,Brown, M. and Sharman, E. R. 2008. Multiple sulfur isotopes reveal a magmatic origin for the Platreef platinum group element deposit, Bushveld Complex, South Africa. *Geology* 36(12), pp. 979-982.

Peregoedova, A. 1998. The experimental study of the Pt-Pd-partitioning between monosulfide solid solution and Cu-Ni-sulfide melt at 900-840$^{o}$C. In: *8th International Platinum Symposium.* 28 June - 3 July. Geological Society of South Africa and South African Institute of Mining and Metallurgy, pp. 325-373.

Peregoedova, A.,Barnes, S.-J. and Baker, D. R. 2004. The formation of Pt-Ir alloys and Cu-Pd rich sulfide melts by partial desulfurization of Fe-Ni-Cu sulfides: results of experiments and implications for natural systems. *Chemical Geology* 208(1-4), pp. 247-264.

Peregoedova, A. and Ohnenstetter, M. 2002. Collectors of Pt, Pd and Rh in a S-poor Fe-Ni-Cu sulfide system at 760°C: experimental data and application to ore deposits. *Canadian Mineralogist* 40, pp. 527-561.

Peyerl, W. 1982. The influence of the Driekop dunite pipeon the platinum-group mineralogy of the UG-2 chromititein its vicinity. *Economic Geology* 77(6), pp. 1432-1438.

Platinum, A. 2009. *Annual Report: Platinum, a precious metal for a precious planet*.

Prichard, H. M.,Barnes, S.-J.,Maier, W. D. and Fisher, P. C. 2004a. Variations in the nature of the platinum-group minerals in a cross-section through the Merensky Reef at Impala Platinum: implications for the mode of formation of the reef. *Canadian Mineralogist* 42, pp. 423-437.

Prichard, H. M.,Hutchinson, D. and Fisher, P. C. 2004b. Petrology and crystallization history of multiphase sulfide droplets in a mafic dike from Uruguay: Implications for the origin of Cu-Ni-PGE sulfide deposits. *Economic Geology* 99(2), pp. 365-376.

Prichard, H. M.,Knight, R. D.,Fisher, P. C.,McDonald, I.,Zhou, M.-F. and Wang, C. Y. 2013. Distribution of platinum-group elements in magmatic and altered ores in the Jinchuan intrusion, China: an example of selenium remobilization by postmagmatic fluids. *Mineralium Deposita* 48(6), pp. 767-786.

Pronost, J.,Harris, C. and Pin, C. 2008. Relationship between footwall composition, crustal contamination, and fluid-rock interaction in the Platreef, Bushveld Complex, South Africa. *Mineralium Deposita* 43(8), pp. 825-848.

Reisberg, L.,Tredoux, M.,Harris, C.,Coftier, A. and Chaumba, J. 2011. Re and Os distribution and Os isotope composition of the Platreef at the Sandsloot-Mogolakwena mine, Bushveld complex, South Africa. *Chemical Geology* 281(3-4), pp. 352-363.

Reisberg, L. C.,Tredoux, M. and Harris, C. 2006. Re-Os systematics of the Platreef (Sandsloot mine) of the northern limb of the Bushveld Complex. *Geochimica et Cosmochimica Acta* 70(18, Supplement 1), pp. A526-A526.

Rhodes, R. C. 1975. New evidence for impact origin of the Bushveld Complex, South Africa. *Geology* 3(10), pp. 549-554.

Richardson, S. H. and Shirey, S. B. 2008. Continental mantle signature of Bushveld magmas and coeval diamonds. *Nature* 453(7197), pp. 910-913.

Ripley, E. M. 1990. Platinum-group element geochemistry of Cu-Ni mineralization in the basal zone of the Babbitt Deposit, Duluth Complex, Minnesota. *Economic Geology* 85(4), pp. 830-841.

Robb, L. J.,Freeman, L. A. and Armstrong, R. A. 2000. Nature and longevity of hydrothermal fluid flow and mineralisation in granites of the Bushveld Complex, South Africa. *Geological Society of America Special Papers* 350, pp. 269-281.

Roeder, P. L. 1994. Chromite; from the fiery rain of chondrules to the Kilauea Iki lava lake. *Canadian Mineralogist* 32, pp. 729-746.

Roeder, P. L. and Campbell, I. H. 1985. The effect of postcumulus reactions on composition of chrome-spinels from the Jimberlana intrusion. *Journal of Petrology* 26(3), pp. 763-786.

Roeder, P. L. and Reynolds, I. 1991. Crystallization of Chromite and Chromium Solubility in Basaltic Melts. *Journal of Petrology* 32(5), pp. 909-934.

Rollinson, H. R. 1993. *Using geochemical data: evaluation, presentation, interpretation* Harlow: Longman Scientific & Technical, p. 352.

Rose, D.,Viljoen, F.,Knoper, M. and Rajesh, H. 2011. Detailed assessment of platinum-group minerals associated with chromitite stringers in the Merensky Reef of the Eastern Bushveld Complex, South Africa. *Canadian Mineralogist* 49, pp. 1385-1396.

Rudnick, R. L. and Gao, S. 2003. Composition of the continental crust. In: Rudnick, R.L. ed. *Treatise on Geochemistry*. Vol. 3. Oxford: Elsevier, pp. 1-56.

Ruiz, J.,Barra, F.,Ashwal, L. D. and LeGrange, M. eds. 2004. *Re-Os systematics on sulfides of the Platreef, Bushveld Complex, South Africa*. Geoscience Africa 2004. University of Witwatersrand, Johannesburg.

Sack, R. O. and Ghiorso, M. S. 1991. Chromian spinels as petrogenetic indicators; thermodynamics and petrological applications. *American Mineralogist* 76(5-6), pp. 827-847.

SACS. 1980. *Stratigraphy of South Africa. Part 1. Lithostratigraphy of South Africa, South West Africa/Namibia, and the Republics of Boputhatswana, Transkei, and Venda.* Geological Survey of South Africa, p. 690.

Schmitz, M. D.,Bowring, S. A.,de Wit, M. J. and Gartz, V. 2004. Subduction and terrane collision stabilize the western Kaapvaal craton tectosphere 2.9 billion years ago. *Earth and Planetary Science Letters* 222(2), pp. 363-376.

Schoenberg, R.,Kruger, F. J.,Nägler, T. F.,Meisel, T. and Kramers, J. D. 1999. PGE enrichment in chromitite layers and the Merensky Reef of the western Bushveld Complex; a Re-Os and Rb-Sr isotope study. *Earth and Planetary Science Letters* 172(1-2), pp. 49-64.

Schweitzer, J. K.,Hatton, C. J. and Waal, S. A. 1995. Economic potential of the Rooiberg Group: volcanic rocks in the floor and roof of the Bushveld Complex. *Mineralium Deposita* 30(2), pp. 168-177.

Scoates, J. S. and Friedman, R. M. 2008. Precise age of the platiniferous Merensky Reef, Bushveld Complex, South Africa, by the U-Pb zircon chemical abrasion ID-TIMS technique. *Economic Geology* 103(3), pp. 465-471.

Scoates, J. S.,Wall, C.,Friedman, R. M.,VanTongeren, J. and Mathez, E. A. 2012. Age of the Bushveld Complex. *Mineralogical Magazine* 76(6), p. 2348.

Scoon, R. N. and Teigler, B. 1994. Platinum-group element mineralization in the critical zone of the western Bushveld Complex; I, Sulfide poor-chromitites below the UG-2. *Economic Geology* 89(5), pp. 1094-1121.

Scowen, P.,Roeder, P. and Helz, R. 1991. Reequilibration of chromite within Kilauea Iki lava lake, Hawaii. *Contributions to Mineralogy and Petrology* 107(1), pp. 8-20.

Seabrook, C. L.,Cawthorn, R. G. and Kruger, F. J. 2005. The Merensky Reef, Bushveld Complex: Mixing of Minerals Not Mixing of Magmas. *Economic Geology* 100(6), pp. 1191-1206.

Sharman, E. R.,Penniston-Dorland, S. C.,Kinnaird, J. A.,Nex, P. A. M.,Brown, M. and Wing, B. A. 2013. Primary origin of marginal Ni-Cu-(PGE) mineralization in layered intrusions: Δ33S evidence from The Platreef, Bushveld, South Africa. *Economic Geology* 108(2), pp. 365-377.

Sharman-Harris, E. R.,Kinnaird, J. A.,Harris, C. and Horstmann, U. E. 2005. A new look at sulphide mineralisation of the northern limb, Bushveld Complex: A stable isotope study. *Applied Earth Science: Transactions of the Institute of Mining and Metallurgy, Section B* 114(4), pp. 252-263.

Sharpe, M. R. 1981. The chronology of magma influxes to the eastern compartment of the Bushveld Complex as exemplified by its marginal border groups. *Journal of the Geological Society* 138(3), pp. 307-326.

Sharpe, M. R. and Hulbert, L. J. 1985. Ultramafic sills beneath the eastern Bushveld Complex; mobilized suspensions of early lower zone cumulates in a parental magma with boninitic affinities. *Economic Geology* 80(4), pp. 849-871.

Silver, P. G.,Fouch, M. J.,Gao, S. S. and Schmitz, M. 2004. Seismic anisotropy, mantle fabric, and the magmatic evolution of Precambrian southern Africa. *South African Journal of Geology* 107(1-2), pp. 45-58.

Skinner, B. J.,Luce, F. D.,Dill, J. A.,Ellis, D. E.,Hagan, H. A.,Lewis, D. M.,Odell, D. A.,Sverjensky, D. A. and Williams, N. 1976. Phase relations in ternary portions of the system Pt-PdFe-As-S. *Economic Geology* 71(8), pp. 1469-1475.

Smith, C. B. 1983. Pb, Sr and Nd isotopic evidence for sources of southern African Cretaceous kimberlites. *Nature* 304(5921), pp. 51-54.

Spandler, C.,Mavrogenes, J. and Arculus, R. 2005. Origin of chromitites in layered intrusions: Evidence from chromite-hosted melt inclusions from the Stillwater Complex. *Geology* 33(11), pp. 893-896.

Spandler, C. J.,Eggins, S. M.,Arculus, R. J. and Mavrogenes, J. A. 2000. Using melt inclusions to determine parent-magma compositions of layered intrusions: Application to the Greenhills Complex (New Zealand), a platinum group minerals–bearing, island-arc intrusion. *Geology* 28(11), pp. 991-994.

Sparks, H. A. and Mavrogenes, J. A. 2005. Sulfide melt inclusions as evidence for the existence of a sulfide partial melt at Broken Hill, Australia. *Economic Geology* 100(4), pp. 773-779.

Spies, L. 2005. The Akanani Platinum Project. In: *2nd Platreef Workshop.* Mokopane. Geological Society of South Africa,

Stevens, M. 2004. *Constraining Platreef petrogenesis, northern limb of the Bushveld Complex, South Africa.* BSc Honours, Australian National University.

Streckeisen, A. 1976. To each plutonic rock its proper name. *Earth-Science Reviews* 12(1), pp. 1-33.

Tarkian, M. and Stumpfl, E. F. 1975. Platinum mineralogy ofthe Driekop mine, South Africa. . *Mineralium Deposita* 10(1), pp. 71-85.

Taylor, S. R. and McLennan, S. M. 1985. *The continental crust, its composition and evolution: an examination of geochemical record preserved in sedimentary rocks*. Oxford: Blackwell Scientific Publications, p. 312.

Teigler, B. and Eales, H. 1993. Correlation between chromite composition and PGE mineralization in the Critical Zone of the western Bushveld Complex. *Mineralium Deposita* 28(5), pp. 291-302.

Thériault, R. M. and Barnes, S.-J. 1998. Compositional variations in Cu-Ni-PGE sulfides of the Dunka Road deposit, Duluth Complex, Minnesota: the importance of combined assimilation and magmatic processes. *Canadian Mineralogist* 36, pp. 869-886.

Tsai, H. 1979. Mineral inclusions in diamond: Premier, Jagersfontein and Finsch kimberlites, South Africa and Williamson Mine, Tanzania. In: Boyd, F.R. and Meyer, H.O.A. eds. *Kimberlites, diatremes and diamonds: their geology, petrology and geochemistry*. American Geophysical Union, pp. 16-26.

U.S.G.S. 2012. *Mineral commodity summaries 2012*. U.S. Geological Survey.

van der Merwe, F.,Viljoen, F. and Knoper, M. 2012. The mineralogy and mineral associations of platinum group elements and gold in the Platreef at Zwartfontein, Akanani Project, Northern Bushveld Complex, South Africa. *Mineralogy and Petrology* 106(1), pp. 25-38.

van der Merwe, M. J. 1976. The layered sequence of the Potgietersrus Limb of the Bushveld Complex. *Economic Geology* 71(7), pp. 1337-1351.

van der Merwe, M. J. 1978. *The geology of the basic and ultramafic rocks of the Potgietersrus Limb of the Bushveld Complex.* PhD, University of Witwatersrand.

van der Merwe, M. J. 2008. The geology and structure of the Rustenburg Layered Suite in the Potgietersrus/Mokopane area of the Bushveld Complex, South Africa. *Mineralium Deposita* 43(4), pp. 405-419.

Vermaak, C. F. and Hendriks, L. P. 1976. A review of the mineralogy of the Merensky Reef, with specific reference to new data on the precious metal mineralogy. *Economic Geology* 71(7), pp. 1244-1269.

Verryn, S. M. C. and Merkle, R. K. W. 2002. The system PtS-PdS-NiS between 1200° and 700°C. *Canadian Mineralogist* 40, pp. 571-584.

Viljoen, M. J. and Schurmann, L. W. 1998. Platinum group metals. In: Wilson, M.G.C. and Anhaeusser, C.R. eds. *The mineral resouces of Southern Africa*. Council for Geoscience, pp. 532-568.

von Gruenewaldt, G.,Hatton, C. J. and Merkle, R. K. W. 1986. Platinum-group element-chromitite associations in the Bushveld Complex. *Economic Geology* 81(5), pp. 1067-1079.

von Gruenewaldt, G.,Hulbert, L. J. and Naldrett, A. J. 1989. Contrasting platinum-group element concentration patterns in cumulates of the Bushveld complex. *Mineralium Deposita* 24(3), pp. 219-229.

Wager, L. R.,Brown, G. M. and Wadsworth, W. J. 1960. Types of Igneous Cumulates. *Journal of Petrology* 1(1), pp. 73-85.

Wagner, P. A. 1929. *The platinum deposits and mines of South Africa*. Edinburgh: Oliver and Boyd, p. 326.

Webb, S. J.,Cawthorn, R. G.,Nguuri, T. and James, D. 2004. Gravity modeling of Bushveld Complex connectivity supported by Southern African Seismic Experiment results. *South African Journal of Geology* 107(1-2), pp. 207-218.

Weeks, M. E. 2010. *Discovery of the elements*. Kessinger Publishing, p. 382.

Weise, S. 2010. *Characterisation of the Main Zone - Platreef contact in the northern limb of the Bushveld Complex.* MSc, University of Witwatersrand.

Wela, S. S. 2008. *Petrographic and geochemical analysis of chromites from the Platreef (the Northern Limb of the Bushveld Complex-South Africa).* BSc Honours, University of the Witwatersrand.

Westerlund, K. J.,Gurney, J. J.,Carlson, R. W.,Shirey, S. B.,Hauri, E. H. and Richardson, S. H. 2004. A metasomatic origin for late Archean eclogitic diamonds: Implications from internal morphology of diamonds and Re-Os and S isotope characteristics of their sulfide inclusions from the Late Jurassic Klipspringer kimberlites. *South African Journal of Geology* 107(1-2), pp. 119-130.

Westland, A. D. 1981. Inorganic chemistry of the platinum group elements. *Canadian Institute of Mining Metallurgy* Special Volume 23, pp. 5-18.

White, J. A. 1994. The Potgietersrus Prospect - Geology and Exploration History. In: Anhaeusser, C.R. ed. *Proceedings of the XVth CMMI Congress*. Vol. 3. Johannesburg: South African Institute of Mining and Metallurgy, pp. 173-181.

Willmore, C. C.,Boudreau, A. E. and Kruger, F. J. 2000. The Halogen Geochemistry of the Bushveld Complex, Republic of South Africa: Implications for Chalcophile Element Distribution in the Lower and Critical Zones. *Journal of Petrology* 41(10), pp. 1517-1539.

Willmore, C. C.,Boudreau, A. E.,Spivack, A. and Kruger, F. J. 2002. Halogens of Bushveld Complex, South Africa: Î´37Cl and Cl/F evidence for hydration melting of the source region in a back-arc setting. *Chemical Geology* 182(2-4), pp. 503-511.

Winch, J. 2011. The importance of drilling too deep: A Platreef perspective. In: *4th Platreef Workshop.* Mokopane, South Africa, 14-16th January 2011.

Yamamoto, M. 1976. Relationship between Se/S and sulfur isotope ratios of hydrothermal sulfide minerals. . *Mineralium Deposita* 11(2), pp. 197-209.

Yudovskaya, M.,Kinnaird, J. A.,Mokov, A.,Kuznetzova, M. and McDonald, I. 2010. Facies variability of PGE mineralization in the Platreef chromitites. In: Jugo, P.J. et al. eds. *11th International Platinum Symposium.* Sudbury, Ontario, 21-24 June 2010. Ontario Geological Survey,

Yudovskaya, M.,Kinnaird, J. A.,Naldrett, A. J.,Mokhov, A. V.,McDonald, I. and Reinke, C. 2011. Facies variation in PGE mineralisation in the central Platreef of the Bushveld Complex, South Africa. *Canadian Mineralogist* 49, pp. 1349-1384.

Yudovskaya, M.,Kinnaird, J. A.,Sobolev, A.,Kuzmin, D. and Wilson, A. 2012. The Lower Zone beneath the Platreef in the northern limb of the Bushveld Complex. In: *Mineral Deposit Studies Group - The Geology of Ni-PGE Deposits Workshop.* Cardiff University, 6th January 2012. pp. 32-34.

Yudovskaya, M. A. and Kinnaird, J. A. 2010. Chromite in the Platreef (Bushveld Complex, South Africa): occurrence and evolution of its chemical composition. *Mineralium Deposita* 43(4), pp. 1-23.

Zientek, M. L. 2012. *Magmatic ore deposits in layered intrusions-Descriptive model for reef-type PGE and contact-type Cu-Ni-PGE deposits*. U.S. Geological Survey

Zientek, M. L.,Likhachev, A. P.,Kunilov, V. E.,Barnes, S.-J.,Meier, A. L.,Carlson, R. R.,Briggs, P. H.,Fries, T. L. and Adrian, B. M. 1994. Cumulus processes and the composition of magmatic ore deposits: examples from the Talnakh District, Russia. In: Lightfoot, P.C. and Naldrett, A.J. eds. *Proceedings of the Sudbury-Noril'sk Symposium*. Vol. Special Publication 5. Ontario Geological Survey, pp. 373-392.

# Appendix 1A: Bulk Rock Geochemistry

| | REJ 1 | REJ 2 | REJ 3 | REJ 4 | REJ 5 | REJ 6 | REJ 7 | REJ 8 | REJ 9 |
|---|---|---|---|---|---|---|---|---|---|
| | OY447-1 | OY447-2 | MO1-1 | MO1-2 | ZN230-1 | ZN230-2 | ZN230-3 | ZN230-4 | ZN230-5 |
| **$SiO_2$ (wt%)** | 48.15 | 48.45 | 54.41 | 47.53 | 45.94 | 50.61 | 51.50 | 53.73 | 51.62 |
| **$TiO_2$ (av)** | 0.14 | 0.26 | 0.45 | 0.14 | 0.11 | 0.15 | 0.32 | 0.34 | 0.31 |
| **$Al_2O_3$** | 12.65 | 7.88 | 7.16 | 10.79 | 3.49 | 5.44 | 6.00 | 11.03 | 5.05 |
| **$Fe_2O_3$ (av)** | 10.92 | 12.00 | 4.05 | 9.92 | 13.01 | 8.71 | 12.79 | 10.29 | 13.71 |
| **MnO (av)** | 0.14 | 0.19 | 0.29 | 0.15 | 0.15 | 0.16 | 0.18 | 0.16 | 0.15 |
| **MgO** | 15.97 | 17.35 | 13.52 | 21.74 | 26.43 | 22.81 | 17.08 | 9.75 | 17.33 |
| **CaO** | 4.49 | 4.19 | 17.26 | 3.55 | 3.10 | 8.11 | 5.39 | 6.93 | 3.51 |
| **$Na_2O$** | 1.58 | 0.33 | 0.15 | 0.78 | 0.22 | 0.97 | 0.59 | 1.68 | 0.53 |
| **$K_2O$** | 0.34 | 0.01 | 0.01 | 0.24 | 0.24 | 0.24 | 0.33 | 0.56 | 0.22 |
| **$P_2O_5$** | 0.03 | 0.06 | 0.09 | 0.07 | 0.04 | 0.05 | 0.06 | 0.06 | 0.07 |
| **$Cr_2O_3$** | 1.97 | 5.99 | 0.03 | 1.55 | 0.99 | 0.79 | 3.08 | 4.66 | 4.28 |
| **LOI** | 2.44 | 2.83 | 3.12 | 2.53 | 5.59 | 0.57 | 1.60 | 0.37 | 2.77 |
| **Total** | 99.15 | 98.89 | 100.44 | 99.06 | 100.32 | 98.58 | 99.26 | 99.53 | 100.61 |
| | | | | | | | | | |
| **V (av) (ppm)** | 161.88 | 379.00 | 93.60 | 162.34 | 52.12 | 86.46 | 279.75 | 361.50 | 265.11 |
| **Co (av)** | 147.55 | 101.50 | 15.49 | 72.09 | 222.97 | 107.38 | 109.87 | 74.25 | 115.39 |
| **Ni (av)** | 5978.21 | 3272.97 | 236.01 | 1426.00 | 3464.63 | 2688.09 | 705.16 | 422.51 | 1513.83 |
| **Cu (av)** | 3958.77 | 1977.38 | 206.97 | 1279.40 | 1443.18 | 1151.43 | 432.09 | 281.38 | 649.89 |
| **Zn (av)** | 121.90 | 163.19 | 56.10 | 129.12 | 84.81 | 106.15 | 126.09 | 153.37 | 130.03 |
| **Sr (av)** | 149.18 | 31.65 | 33.97 | 114.59 | 54.36 | 67.83 | 115.55 | 286.87 | 31.33 |
| **Y (av)** | 2.10 | 5.26 | 12.84 | 2.44 | 2.92 | 4.59 | 6.29 | 5.47 | 6.18 |
| **Zr (av)** | 2.82 | 17.70 | 80.20 | 8.07 | 25.13 | 11.64 | 20.19 | 11.26 | 28.45 |
| **Ba (av)** | 76.11 | 14.45 | 27.35 | 37.92 | 79.55 | 48.96 | 120.12 | 142.90 | 89.54 |
| **Ga** | 11.31 | 14.77 | 7.23 | 9.30 | 4.95 | 8.21 | 13.12 | 21.69 | 12.38 |
| **Rb** | 16.05 | 2.53 | 2.76 | 10.91 | 14.68 | 10.17 | 22.25 | 20.07 | 18.41 |
| **Nb** | 1.03 | 0.88 | 1.97 | 0.78 | 1.97 | 2.84 | 2.40 | 1.84 | 2.47 |
| **Cs** | 1.58 | 0.88 | 0.66 | 1.73 | 2.40 | 0.63 | 2.28 | 0.65 | 2.80 |
| **Hf** | 0.11 | 0.33 | 2.06 | 0.19 | 0.61 | 0.27 | 0.46 | 0.28 | 0.69 |
| **Ta** | 0.06 | 0.06 | 0.10 | 0.04 | 0.14 | 0.21 | 0.17 | 0.13 | 0.18 |
| **Th** | 0.29 | 0.43 | 1.05 | 0.39 | 0.45 | 0.80 | 0.84 | 0.32 | 1.21 |
| **U** | 0.19 | 0.16 | 0.38 | 0.10 | 0.42 | 1.16 | 0.27 | 0.32 | 0.65 |
| **La** | 2.05 | 1.60 | 5.40 | 1.78 | 2.10 | 1.87 | 4.35 | 2.44 | 4.09 |
| **Ce** | 3.91 | 4.22 | 13.25 | 3.41 | 4.07 | 3.74 | 9.10 | 5.02 | 9.25 |
| **Pr** | 0.46 | 0.61 | 1.83 | 0.39 | 0.49 | 0.45 | 1.13 | 0.64 | 1.17 |
| **Nd** | 1.66 | 2.67 | 7.89 | 1.48 | 1.94 | 1.79 | 4.40 | 2.62 | 4.70 |
| **Sm** | 0.38 | 0.76 | 1.99 | 0.34 | 0.46 | 0.48 | 0.95 | 0.68 | 1.08 |
| **Eu** | 0.26 | 0.17 | 0.55 | 0.15 | 0.19 | 0.16 | 0.31 | 0.38 | 0.28 |
| **Gd** | 0.42 | 0.81 | 2.11 | 0.40 | 0.54 | 0.56 | 1.03 | 0.77 | 1.13 |
| **Tb** | 0.07 | 0.15 | 0.34 | 0.07 | 0.09 | 0.10 | 0.16 | 0.13 | 0.19 |
| **Dy** | 0.46 | 0.97 | 2.31 | 0.46 | 0.56 | 0.76 | 1.08 | 0.91 | 1.23 |
| **Ho** | 0.09 | 0.19 | 0.42 | 0.10 | 0.11 | 0.15 | 0.22 | 0.19 | 0.24 |
| **Er** | 0.30 | 0.61 | 1.29 | 0.34 | 0.36 | 0.54 | 0.70 | 0.61 | 0.76 |
| **Tm** | 0.05 | 0.10 | 0.18 | 0.05 | 0.06 | 0.09 | 0.11 | 0.10 | 0.12 |
| **Yb** | 0.36 | 0.63 | 1.20 | 0.41 | 0.42 | 0.73 | 0.77 | 0.74 | 0.80 |
| **Lu** | 0.05 | 0.09 | 0.17 | 0.06 | 0.06 | 0.11 | 0.11 | 0.11 | 0.12 |

| | REJ 10 | REJ 11 | REJ 12 | REJ13 | REJ14 | REJ15 | REJ16 | REJ17 | REJ18 |
|---|---|---|---|---|---|---|---|---|---|
| | ZN595-1 | ZN595-2 | ZN595-3 | SS335-1 | SS335-2 | SS335-3 | SS335-4 | SS393-1 | SS393-2 |
| **$SiO_2$ (wt%)** | 50.37 | 55.51 | 51.67 | 45.44 | 45.36 | 45.86 | 47.64 | 42.14 | 33.91 |
| **$TiO_2$ (av)** | 0.16 | 0.22 | 0.20 | 0.34 | 0.13 | 0.65 | 0.37 | 0.39 | 0.49 |
| **$Al_2O_3$** | 5.30 | 9.70 | 6.92 | 6.43 | 5.22 | 8.65 | 7.94 | 8.87 | 11.64 |
| **$Fe_2O_3$ (av)** | 9.50 | 9.54 | 11.82 | 14.91 | 13.84 | 13.07 | 12.78 | 13.90 | 17.06 |
| **MnO (av)** | 0.25 | 0.15 | 0.21 | 0.27 | 0.31 | 0.19 | 0.20 | 0.27 | 0.28 |
| **MgO** | 20.40 | 11.38 | 16.96 | 20.58 | 25.72 | 18.80 | 15.69 | 14.11 | 17.64 |
| **CaO** | 4.77 | 3.60 | 2.81 | 3.17 | 3.41 | 5.75 | 7.41 | 5.55 | 5.59 |
| **$Na_2O$** | 0.47 | 1.86 | 0.49 | 0.34 | 0.31 | 1.15 | 0.59 | 0.14 | 0.12 |
| **$K_2O$** | 0.33 | 0.88 | 0.40 | 0.41 | 0.38 | 0.21 | 0.27 | 0.17 | 0.08 |
| **$P_2O_5$** | 0.07 | 0.12 | 0.06 | 0.04 | 0.01 | 0.01 | 0.02 | 0.01 | 0.05 |
| **$Cr_2O_3$** | 0.52 | 4.16 | 2.37 | 2.79 | 0.14 | 3.82 | 3.39 | 7.42 | 8.61 |
| **LOI** | 6.57 | 2.18 | 4.97 | 3.38 | 4.76 | 0.69 | 2.40 | 5.64 | 3.44 |
| **Total** | 98.92 | 99.31 | 98.92 | 98.87 | 99.58 | 100.72 | 99.06 | 99.03 | 100.50 |
| | | | | | | | | | |
| **V (av) (ppm)** | 73.55 | 222.24 | 179.65 | 271.23 | 46.12 | 349.97 | 283.63 | 442.89 | 471.48 |
| **Co (av)** | 68.29 | 66.09 | 112.18 | 115.09 | 104.73 | 75.62 | 99.49 | 103.76 | 116.93 |
| **Ni (av)** | 684.73 | 491.68 | 1226.11 | 1242.80 | 776.06 | 487.24 | 1010.82 | 839.05 | 753.90 |
| **Cu (av)** | 395.38 | 380.57 | 973.04 | 221.30 | 206.14 | 92.25 | 276.77 | 160.28 | 99.75 |
| **Zn (av)** | 61.39 | 117.07 | 100.76 | 166.85 | 101.42 | 151.96 | 159.91 | 220.62 | 229.15 |
| **Sr (av)** | 66.54 | 154.58 | 83.92 | 69.94 | 149.99 | 147.74 | 80.92 | 39.57 | 20.53 |
| **Y (av)** | 4.67 | 9.75 | 3.45 | 6.26 | 4.43 | 5.55 | 9.08 | 4.00 | 6.45 |
| **Zr (av)** | 15.22 | 20.93 | 10.12 | 26.54 | 13.52 | 18.09 | 30.71 | 11.32 | 15.68 |
| **Ba (av)** | 84.22 | 138.33 | 99.74 | 186.93 | 200.03 | 98.03 | 115.01 | 53.71 | 50.77 |
| **Ga** | 6.90 | 17.42 | 12.30 | 11.49 | 5.18 | 16.09 | 12.42 | 19.10 | 22.13 |
| **Rb** | 16.78 | 61.78 | 19.72 | 34.37 | 24.99 | 7.19 | 17.62 | 8.63 | 6.20 |
| **Nb** | 1.32 | 18.29 | 1.24 | 1.16 | 1.00 | 0.46 | 0.80 | 0.65 | 0.97 |
| **Cs** | 1.57 | 6.84 | 3.56 | 7.10 | 6.47 | 0.76 | 3.56 | 1.37 | 1.33 |
| **Hf** | 0.42 | 0.63 | 0.27 | 0.66 | 0.30 | 0.38 | 0.74 | 0.26 | 0.37 |
| **Ta** | 0.08 | 1.29 | 0.09 | 0.09 | 0.06 | 0.03 | 0.06 | 0.04 | 0.07 |
| **Th** | 1.26 | 1.71 | 0.48 | 0.96 | 0.36 | 0.33 | 0.83 | 0.66 | 0.81 |
| **U** | 0.22 | 3.79 | 0.20 | 0.29 | 0.10 | 0.12 | 0.23 | 0.17 | 0.32 |
| **La** | 4.02 | 6.50 | 2.57 | 4.68 | 3.73 | 2.92 | 4.27 | 3.16 | 6.00 |
| **Ce** | 8.29 | 15.28 | 5.42 | 9.52 | 8.59 | 6.25 | 9.81 | 6.53 | 12.19 |
| **Pr** | 0.99 | 1.89 | 0.66 | 1.19 | 1.10 | 0.82 | 1.37 | 0.82 | 1.46 |
| **Nd** | 3.79 | 7.15 | 2.67 | 4.29 | 3.91 | 3.15 | 5.30 | 2.92 | 5.00 |
| **Sm** | 0.79 | 1.63 | 0.59 | 0.99 | 0.79 | 0.79 | 1.33 | 0.64 | 1.00 |
| **Eu** | 0.28 | 0.30 | 0.26 | 0.29 | 0.30 | 0.38 | 0.44 | 0.25 | 0.33 |
| **Gd** | 0.89 | 1.66 | 0.65 | 0.82 | 0.57 | 0.82 | 1.33 | 0.67 | 0.92 |
| **Tb** | 0.14 | 0.26 | 0.10 | 0.15 | 0.09 | 0.16 | 0.24 | 0.11 | 0.16 |
| **Dy** | 0.90 | 1.63 | 0.64 | 0.92 | 0.61 | 0.99 | 1.44 | 0.70 | 0.93 |
| **Ho** | 0.17 | 0.30 | 0.13 | 0.19 | 0.13 | 0.21 | 0.30 | 0.14 | 0.19 |
| **Er** | 0.53 | 0.91 | 0.41 | 0.59 | 0.39 | 0.63 | 0.91 | 0.43 | 0.61 |
| **Tm** | 0.08 | 0.14 | 0.07 | 0.09 | 0.06 | 0.10 | 0.14 | 0.08 | 0.11 |
| **Yb** | 0.54 | 0.98 | 0.45 | 0.62 | 0.45 | 0.69 | 0.93 | 0.43 | 0.65 |
| **Lu** | 0.08 | 0.14 | 0.07 | 0.10 | 0.08 | 0.11 | 0.15 | 0.07 | 0.10 |

| | REJ19 | REJ20 | REJ21 | REJ22 | REJ23 | REJ24 | REJ25 | REJ26 | REJ27 |
|---|---|---|---|---|---|---|---|---|---|
| | SS393-3 | SS393-4 | SS393-5 | OY551-1 | OY551-2 | OY551-3 | OY551-4 | ZN334-1 | ZN334-2 |
| **$SiO_2$ (wt%)** | 45.82 | 36.33 | 46.33 | 41.36 | 47.29 | 44.61 | 48.65 | 44.01 | 40.96 |
| **$TiO_2$ (av)** | 0.28 | 0.31 | 0.35 | 0.27 | 0.16 | 0.22 | 0.29 | 0.37 | 0.53 |
| **$Al_2O_3$** | 6.59 | 10.52 | 10.15 | 10.37 | 18.34 | 9.09 | 6.28 | 8.12 | 9.57 |
| **$Fe_2O_3$ (av)** | 10.89 | 11.04 | 13.84 | 14.87 | 8.02 | 14.44 | 10.71 | 14.29 | 16.35 |
| **MnO (av)** | 0.21 | 0.28 | 0.17 | 0.22 | 0.14 | 0.22 | 0.22 | 0.30 | 0.26 |
| **MgO** | 18.42 | 18.98 | 12.61 | 18.10 | 9.77 | 17.35 | 19.41 | 15.32 | 13.30 |
| **CaO** | 5.07 | 12.00 | 3.11 | 3.55 | 7.00 | 4.41 | 9.41 | 4.33 | 2.59 |
| **$Na_2O$** | 0.10 | 0.03 | 1.79 | 0.37 | 1.92 | 0.52 | 0.17 | 0.37 | 0.50 |
| **$K_2O$** | 0.21 | 0.00 | 0.60 | 0.17 | 1.16 | 0.28 | 0.12 | 0.15 | 0.41 |
| **$P_2O_5$** | 0.04 | 0.00 | 0.02 | 0.00 | 0.01 | 0.01 | 0.01 | 0.02 | 0.01 |
| **$Cr_2O_3$** | 3.73 | 6.35 | 7.91 | 7.96 | 3.94 | 4.57 | 0.15 | 8.24 | 10.85 |
| **LOI** | 7.56 | 3.99 | 1.27 | 1.22 | 1.48 | 2.26 | 4.86 | 3.17 | 2.50 |
| **Total** | 99.62 | 100.35 | 98.86 | 99.07 | 99.64 | 98.68 | 100.62 | 99.42 | 98.68 |
| | | | | | | | | | |
| **V (av) (ppm)** | 236.92 | 236.98 | 471.42 | 456.73 | 232.31 | 295.81 | 56.41 | 393.78 | 572.56 |
| **Co (av)** | 85.78 | 109.39 | 145.48 | 156.54 | 64.35 | 178.79 | 121.74 | 107.77 | 126.09 |
| **Ni (av)** | 621.84 | 1658.21 | 2602.66 | 2894.88 | 772.97 | 5673.55 | 2647.34 | 1001.40 | 1199.20 |
| **Cu (av)** | 103.19 | 334.53 | 393.46 | 753.87 | 214.96 | 1540.71 | 1164.75 | 282.59 | 254.39 |
| **Zn (av)** | 122.62 | 243.49 | 251.39 | 213.14 | 118.49 | 144.17 | 107.79 | 192.02 | 299.40 |
| **Sr (av)** | 20.27 | 37.64 | 204.55 | 110.33 | 242.86 | 120.13 | 60.90 | 44.47 | 57.57 |
| **Y (av)** | 11.36 | 6.58 | 4.17 | 3.37 | 3.60 | 4.15 | 8.66 | 7.74 | 5.70 |
| **Zr (av)** | 61.43 | 41.52 | 38.71 | 16.40 | 15.41 | 12.74 | 51.40 | 16.52 | 18.86 |
| **Ba (av)** | 48.31 | 37.63 | 239.50 | 47.21 | 145.53 | 57.15 | 49.75 | 61.22 | 71.15 |
| **Ga** | 10.71 | 17.63 | 23.52 | 19.01 | 17.40 | 12.50 | 7.17 | 16.86 | 23.30 |
| **Rb** | 12.44 | 1.20 | 23.71 | 9.34 | 35.00 | 13.04 | 6.89 | 8.21 | 17.94 |
| **Nb** | 1.63 | 1.64 | 2.62 | 0.57 | 1.07 | 0.41 | 1.69 | 1.70 | 1.21 |
| **Cs** | 1.79 | 1.02 | 2.15 | 1.27 | 1.37 | 1.33 | 1.01 | 1.57 | 1.53 |
| **Hf** | 1.44 | 1.02 | 0.98 | 0.30 | 0.41 | 0.31 | 1.30 | 0.42 | 0.43 |
| **Ta** | 0.10 | 0.14 | 0.19 | 0.03 | 0.10 | 0.02 | 0.12 | 0.13 | 0.10 |
| **Th** | 1.11 | 0.84 | 1.60 | 0.71 | 0.69 | 0.68 | 1.04 | 0.79 | 0.68 |
| **U** | 0.45 | 0.23 | 0.33 | 0.22 | 0.59 | 0.18 | 0.28 | 0.47 | 0.29 |
| **La** | 6.02 | 5.79 | 6.03 | 2.31 | 2.43 | 2.12 | 5.01 | 4.69 | 3.35 |
| **Ce** | 14.55 | 12.93 | 11.82 | 4.73 | 4.68 | 4.46 | 11.70 | 9.29 | 6.98 |
| **Pr** | 2.03 | 1.65 | 1.39 | 0.59 | 0.55 | 0.55 | 1.59 | 1.20 | 0.88 |
| **Nd** | 7.71 | 5.80 | 4.42 | 2.03 | 1.79 | 1.94 | 5.91 | 4.46 | 3.20 |
| **Sm** | 1.87 | 1.23 | 0.87 | 0.46 | 0.39 | 0.46 | 1.38 | 1.10 | 0.74 |
| **Eu** | 0.37 | 0.30 | 0.37 | 0.19 | 0.28 | 0.17 | 0.36 | 0.28 | 0.25 |
| **Gd** | 1.95 | 1.10 | 0.87 | 0.43 | 0.40 | 0.47 | 1.28 | 1.13 | 0.81 |
| **Tb** | 0.33 | 0.18 | 0.12 | 0.08 | 0.07 | 0.10 | 0.22 | 0.21 | 0.15 |
| **Dy** | 1.96 | 1.06 | 0.73 | 0.53 | 0.52 | 0.64 | 1.28 | 1.26 | 0.94 |
| **Ho** | 0.39 | 0.21 | 0.15 | 0.12 | 0.12 | 0.14 | 0.26 | 0.26 | 0.19 |
| **Er** | 1.12 | 0.64 | 0.44 | 0.38 | 0.38 | 0.46 | 0.78 | 0.81 | 0.62 |
| **Tm** | 0.17 | 0.11 | 0.08 | 0.07 | 0.07 | 0.08 | 0.12 | 0.14 | 0.11 |
| **Yb** | 1.04 | 0.64 | 0.47 | 0.44 | 0.49 | 0.52 | 0.78 | 0.84 | 0.63 |
| **Lu** | 0.16 | 0.10 | 0.07 | 0.07 | 0.08 | 0.09 | 0.13 | 0.14 | 0.11 |

| | REJ28 | REJ29 | REJ30 | REJ31 | REJ32 | REJ33 | REJ34 | REJ35 | REJ36 |
|---|---|---|---|---|---|---|---|---|---|
| | ZN334-3 | OY472-1 | OY472-2 | OY472-3 | OY472-4 | ZN573-1 | ZN573-2 | ZN573-3 | ZN704-1 |
| **$SiO_2$ (wt%)** | 46.98 | 42.99 | 38.32 | 48.63 | 44.03 | 21.94 | 35.21 | 34.74 | 48.71 |
| **$TiO_2$ (av)** | 0.28 | 0.39 | 0.25 | 0.21 | 0.35 | 1.04 | 0.43 | 0.48 | 0.37 |
| **$Al_2O_3$** | 8.47 | 7.11 | 9.01 | 5.05 | 12.23 | 11.47 | 6.97 | 14.03 | 6.70 |
| **$Fe_2O_3$ (av)** | 12.44 | 5.52 | 8.55 | 13.49 | 12.18 | 25.08 | 17.41 | 17.60 | 13.09 |
| **MnO (av)** | 0.21 | 0.30 | 0.28 | 0.30 | 0.21 | 0.28 | 0.24 | 0.24 | 0.21 |
| **MgO** | 17.49 | 21.75 | 27.56 | 23.95 | 13.06 | 14.15 | 18.82 | 12.23 | 18.74 |
| **CaO** | 6.30 | 15.82 | 6.19 | 3.02 | 8.95 | 6.72 | 5.81 | 5.24 | 6.05 |
| **$Na_2O$** | 1.15 | 0.01 | 0.06 | 0.11 | 0.89 | 0.13 | 0.11 | 0.10 | 0.48 |
| **$K_2O$** | 0.41 | 0.01 | 0.10 | 0.35 | 0.90 | 0.06 | 0.21 | 0.10 | 0.73 |
| **$P_2O_5$** | 0.00 | 0.00 | 0.04 | 0.01 | 0.02 | 0.00 | 0.00 | 0.01 | 0.00 |
| **$Cr_2O_3$** | 4.53 | 0.03 | 0.05 | 3.34 | 7.98 | 16.59 | 9.99 | 14.61 | 2.51 |
| **LOI** | 1.73 | 6.33 | 11.00 | 1.62 | 1.53 | 0.53 | 4.20 | 1.77 | 2.76 |
| **Total** | 100.14 | 100.10 | 100.70 | 100.07 | 102.18 | 99.54 | 100.06 | 101.23 | 99.87 |
| | | | | | | | | | |
| **V (av) (ppm)** | 344.10 | 46.66 | 68.63 | 238.48 | 527.27 | 1488.60 | 698.10 | 800.88 | 367.67 |
| **Co (av)** | 131.35 | 22.67 | 45.99 | 106.93 | 89.40 | 181.13 | 190.72 | 152.38 | 113.79 |
| **Ni (av)** | 2777.56 | 105.71 | 195.34 | 725.70 | 1123.30 | 1118.21 | 1801.65 | 1098.77 | 1697.62 |
| **Cu (av)** | 1433.09 | 37.80 | 56.09 | 99.09 | 92.38 | 400.42 | 939.80 | 340.28 | 831.52 |
| **Zn (av)** | 151.19 | 115.74 | 229.01 | 129.27 | 196.97 | 439.05 | 250.80 | 306.46 | 129.35 |
| **Sr (av)** | 137.55 | 10.90 | 14.65 | 71.17 | 130.86 | 8.54 | 13.08 | 21.72 | 54.27 |
| **Y (av)** | 6.34 | 12.05 | 5.70 | 4.01 | 3.89 | 4.33 | 4.40 | 2.94 | 17.09 |
| **Zr (av)** | 8.91 | 70.55 | 25.35 | 14.42 | 25.46 | 9.76 | 14.00 | 7.12 | 23.15 |
| **Ba (av)** | 115.08 | 87.13 | 32.71 | 85.42 | 379.66 | 38.06 | 46.56 | 43.66 | 88.47 |
| **Ga** | 15.43 | 8.34 | 14.54 | 10.80 | 23.53 | 47.88 | 23.57 | 37.45 | 14.23 |
| **Rb** | 18.73 | 1.14 | 9.75 | 26.50 | 42.35 | 3.21 | 15.81 | 3.64 | 40.37 |
| **Nb** | 0.63 | 1.69 | 1.44 | 0.91 | 2.87 | 0.54 | 1.25 | 0.43 | 2.16 |
| **Cs** | 1.10 | 0.24 | 0.97 | 1.15 | 0.80 | 0.60 | 1.51 | 0.50 | 2.55 |
| **Hf** | 0.23 | 1.99 | 0.58 | 0.34 | 0.58 | 0.25 | 0.46 | 0.20 | 0.59 |
| **Ta** | 0.04 | 0.13 | 0.08 | 0.07 | 0.21 | 0.03 | 0.08 | 0.03 | 0.16 |
| **Th** | 0.26 | 1.02 | 0.80 | 0.45 | 0.71 | 0.27 | 0.75 | 0.29 | 0.50 |
| **U** | 0.19 | 0.34 | 2.02 | 0.23 | 0.42 | 0.12 | 0.37 | 0.07 | 0.45 |
| **La** | 2.58 | 4.07 | 2.70 | 1.79 | 3.32 | 1.65 | 1.92 | 1.52 | 2.86 |
| **Ce** | 5.66 | 10.62 | 6.11 | 4.25 | 6.79 | 4.11 | 4.47 | 3.34 | 6.18 |
| **Pr** | 0.79 | 1.56 | 0.81 | 0.60 | 0.87 | 0.61 | 0.65 | 0.46 | 0.85 |
| **Nd** | 3.32 | 6.87 | 3.02 | 2.38 | 3.23 | 2.44 | 2.71 | 1.85 | 3.60 |
| **Sm** | 0.89 | 1.76 | 0.72 | 0.56 | 0.71 | 0.68 | 0.69 | 0.50 | 1.27 |
| **Eu** | 0.29 | 0.53 | 0.23 | 0.33 | 0.28 | 0.21 | 0.18 | 0.21 | 0.30 |
| **Gd** | 0.82 | 1.82 | 0.66 | 0.45 | 0.55 | 0.60 | 0.62 | 0.48 | 1.56 |
| **Tb** | 0.16 | 0.32 | 0.11 | 0.09 | 0.09 | 0.12 | 0.10 | 0.08 | 0.35 |
| **Dy** | 1.09 | 2.13 | 0.88 | 0.64 | 0.65 | 0.78 | 0.81 | 0.56 | 2.68 |
| **Ho** | 0.21 | 0.41 | 0.20 | 0.13 | 0.13 | 0.16 | 0.16 | 0.11 | 0.53 |
| **Er** | 0.66 | 1.21 | 0.64 | 0.45 | 0.42 | 0.50 | 0.50 | 0.37 | 1.68 |
| **Tm** | 0.12 | 0.20 | 0.11 | 0.08 | 0.07 | 0.08 | 0.09 | 0.05 | 0.28 |
| **Yb** | 0.74 | 1.19 | 0.77 | 0.51 | 0.44 | 0.43 | 0.49 | 0.31 | 1.89 |
| **Lu** | 0.12 | 0.20 | 0.15 | 0.09 | 0.07 | 0.07 | 0.08 | 0.05 | 0.27 |

| | REJ37 | REJ38 | REJ39 | REJ40 | REJ41 | REJ42 | REJ43 | REJ44 | REJ45 |
|---|---|---|---|---|---|---|---|---|---|
| | ZN704-3 | ZN704-4 | ZN704-6 | SS383-2 | SS383-3 | SS383-4 | SS383-5 | SS383-6 | SS383-7 |
| **$SiO_2$ (wt%)** | 26.71 | 28.69 | 47.50 | 42.32 | 32.89 | 45.64 | 41.90 | 44.89 | 37.23 |
| **$TiO_2$ (av)** | 0.99 | 0.61 | 0.28 | 0.23 | 0.78 | 0.33 | 0.42 | 0.33 | 0.44 |
| **$Al_2O_3$** | 11.66 | 12.63 | 8.08 | 5.48 | 13.84 | 8.60 | 9.44 | 6.80 | 10.71 |
| **$Fe_2O_3$ (av)** | 24.02 | 17.77 | 12.49 | 7.13 | 17.48 | 13.68 | 15.90 | 14.30 | 10.63 |
| **MnO (av)** | 0.24 | 0.35 | 0.19 | 0.59 | 0.20 | 0.26 | 0.28 | 0.27 | 0.15 |
| **MgO** | 16.29 | 12.72 | 19.18 | 30.35 | 10.24 | 17.80 | 16.80 | 23.15 | 23.89 |
| **CaO** | 2.62 | 7.95 | 3.63 | 3.06 | 7.79 | 5.58 | 5.49 | 2.97 | 3.72 |
| **$Na_2O$** | 0.20 | 0.10 | 0.73 | 0.08 | 0.92 | 0.66 | 0.41 | 0.42 | 0.53 |
| **$K_2O$** | 0.17 | 0.29 | 0.62 | 1.13 | 0.60 | 0.49 | 0.68 | 0.54 | 0.32 |
| **$P_2O_5$** | 0.00 | 0.01 | 0.02 | 0.03 | 0.02 | 0.01 | 0.01 | 0.01 | 0.01 |
| **$Cr_2O_3$** | 16.71 | 15.99 | 4.27 | 0.04 | 13.49 | 6.41 | 7.19 | 6.39 | 4.64 |
| **LOI** | 1.73 | 2.54 | 2.13 | 9.62 | 0.78 | 1.03 | 1.58 | 0.94 | 7.88 |
| **Total** | 100.62 | 99.41 | 99.46 | 100.28 | 99.42 | 100.77 | 100.25 | 101.18 | 100.63 |
| | | | | | | | | | |
| **V (av) (ppm)** | 978.77 | 904.55 | 270.05 | 53.87 | 896.23 | 403.04 | 419.46 | 357.47 | 278.70 |
| **Co (av)** | 213.78 | 162.94 | 105.60 | 26.85 | 139.89 | 108.06 | 125.28 | 119.30 | 78.76 |
| **Ni (av)** | 1615.60 | 614.70 | 1041.75 | 136.57 | 1058.42 | 5134.74 | 1028.20 | 1417.51 | 497.11 |
| **Cu (av)** | 883.58 | 190.26 | 304.58 | 33.01 | 199.30 | 107.03 | 174.79 | 198.95 | 157.27 |
| **Zn (av)** | 339.92 | 387.15 | 109.81 | 47.47 | 349.45 | 176.86 | 231.65 | 202.82 | 148.42 |
| **Sr (av)** | 52.21 | 17.70 | 97.48 | 13.49 | 169.94 | 126.57 | 139.68 | 88.60 | 121.38 |
| **Y (av)** | 4.02 | 12.18 | 6.08 | 6.50 | 7.10 | 4.69 | 5.06 | 4.12 | 3.02 |
| **Zr (av)** | 8.94 | 18.03 | 12.21 | 25.94 | 27.50 | 9.78 | 9.17 | 10.43 | 15.06 |
| **Ba (av)** | 64.17 | 44.01 | 164.22 | 87.22 | 157.72 | 114.97 | 145.15 | 132.26 | 86.41 |
| **Ga** | 41.42 | 32.94 | 12.61 | 6.80 | 28.84 | 15.41 | 17.10 | 13.08 | 17.06 |
| **Rb** | 7.34 | 15.92 | 26.56 | 93.25 | 18.99 | 19.20 | 32.07 | 22.20 | 11.97 |
| **Nb** | 0.86 | 2.46 | 1.11 | 0.92 | 1.92 | 1.57 | 0.92 | 0.89 | 0.97 |
| **Cs** | 1.52 | 1.05 | 2.02 | 4.88 | 1.55 | 2.26 | 2.96 | 1.95 | 2.04 |
| **Hf** | 0.24 | 0.50 | 0.33 | 0.72 | 0.72 | 0.22 | 0.20 | 0.21 | 0.42 |
| **Ta** | 0.06 | 0.17 | 0.08 | 0.07 | 0.13 | 0.11 | 0.06 | 0.06 | 0.05 |
| **Th** | 0.25 | 0.69 | 0.58 | 1.07 | 1.21 | 0.72 | 0.79 | 0.51 | 0.57 |
| **U** | 0.22 | 0.74 | 0.34 | 0.38 | 0.31 | 0.51 | 0.18 | 0.18 | 0.38 |
| **La** | 1.54 | 4.25 | 3.29 | 1.61 | 5.96 | 3.39 | 2.75 | 1.88 | 1.54 |
| **Ce** | 3.68 | 8.87 | 7.01 | 4.47 | 11.41 | 6.73 | 5.95 | 3.81 | 3.04 |
| **Pr** | 0.51 | 1.17 | 0.89 | 0.68 | 1.43 | 0.84 | 0.81 | 0.48 | 0.41 |
| **Nd** | 2.29 | 5.03 | 3.48 | 2.96 | 5.53 | 3.24 | 3.51 | 1.85 | 1.46 |
| **Sm** | 0.65 | 1.48 | 0.90 | 0.82 | 1.20 | 0.76 | 0.84 | 0.48 | 0.39 |
| **Eu** | 0.22 | 0.37 | 0.29 | 0.25 | 0.44 | 0.25 | 0.28 | 0.21 | 0.19 |
| **Gd** | 0.57 | 1.52 | 0.80 | 0.84 | 1.18 | 0.73 | 0.81 | 0.50 | 0.39 |
| **Tb** | 0.09 | 0.27 | 0.12 | 0.14 | 0.20 | 0.11 | 0.14 | 0.09 | 0.06 |
| **Dy** | 0.78 | 1.81 | 0.98 | 0.99 | 1.20 | 0.78 | 0.89 | 0.58 | 0.48 |
| **Ho** | 0.15 | 0.36 | 0.20 | 0.20 | 0.23 | 0.16 | 0.17 | 0.14 | 0.10 |
| **Er** | 0.53 | 1.13 | 0.64 | 0.66 | 0.74 | 0.49 | 0.55 | 0.45 | 0.37 |
| **Tm** | 0.07 | 0.17 | 0.11 | 0.10 | 0.13 | 0.09 | 0.10 | 0.09 | 0.08 |
| **Yb** | 0.49 | 0.92 | 0.69 | 0.85 | 0.68 | 0.53 | 0.53 | 0.55 | 0.56 |
| **Lu** | 0.07 | 0.13 | 0.11 | 0.15 | 0.11 | 0.09 | 0.09 | 0.09 | 0.11 |

| | REJ46 | REJ47 | REJ48 | REJ49 | REJ50 | REJ51 | REJ52 | REJ53 | REJ54 |
|---|---|---|---|---|---|---|---|---|---|
| | OY351A-1 | OY351A-2 | OY392-1 | OY392-2 | OY359-1 | OY252-1 | OY549-1 | OY549-2A | OY549-2B |
| **$SiO_2$ (wt%)** | 43.71 | 46.75 | 28.67 | 36.55 | 24.73 | 28.80 | 51.58 | 58.27 | 34.48 |
| **$TiO_2$ (av)** | 0.46 | 0.25 | 0.48 | 0.32 | 0.85 | 0.59 | 0.28 | 0.13 | 0.70 |
| **$Al_2O_3$** | 12.49 | 5.63 | 15.44 | 12.22 | 17.99 | 12.19 | 9.29 | 8.63 | 14.46 |
| **$Fe_2O_3$ (av)** | 17.35 | 12.91 | 19.23 | 14.92 | 19.03 | 19.37 | 10.51 | 8.92 | 19.45 |
| **MnO (av)** | 0.18 | 0.23 | 0.33 | 0.24 | 0.37 | 0.47 | 0.19 | 0.17 | 0.21 |
| **MgO** | 10.93 | 17.34 | 13.28 | 14.67 | 12.00 | 13.19 | 16.16 | 17.22 | 12.60 |
| **CaO** | 4.43 | 9.69 | 4.92 | 7.05 | 8.83 | 11.54 | 6.12 | 3.18 | 3.93 |
| **$Na_2O$** | 0.08 | 0.17 | 0.10 | 0.30 | 0.20 | 0.15 | 0.88 | 1.39 | 0.92 |
| **$K_2O$** | 0.02 | 0.06 | 0.11 | 0.37 | 0.28 | 0.06 | 0.49 | 0.41 | 0.39 |
| **$P_2O_5$** | 0.03 | 0.04 | 0.03 | 0.04 | 0.04 | 0.00 | 0.04 | 0.09 | 0.06 |
| **$Cr_2O_3$** | 8.17 | 3.62 | 11.83 | 9.57 | 11.40 | 10.88 | 2.90 | 0.22 | 10.29 |
| **LOI** | 0.20 | 2.03 | 1.46 | 1.79 | 1.35 | 0.47 | 0.44 | 1.01 | -0.51 |
| **Total** | 89.52 | 83.21 | 113.40 | 91.27 | 110.40 | 115.42 | 66.49 | 57.97 | 104.01 |
| | | | | | | | | | |
| **V (av) (ppm)** | 409.66 | 133.30 | 439.01 | 242.63 | 449.34 | 261.96 | 216.87 | 49.12 | 788.13 |
| **Co (av)** | 128.09 | 87.71 | 135.89 | 100.04 | 126.29 | 138.05 | 72.63 | 66.60 | 163.18 |
| **Ni (av)** | 845.27 | 421.50 | 1160.54 | 2935.52 | 457.72 | 1904.59 | 141.68 | 309.08 | 199.19 |
| **Cu (av)** | 752.65 | 453.36 | 731.80 | 1190.92 | 302.21 | 2239.18 | 104.52 | 65.07 | 162.73 |
| **Zn (av)** | 433.37 | 164.93 | 370.26 | 328.97 | 458.65 | 384.49 | 119.36 | 66.35 | 417.18 |
| **Sr (av)** | 3.27 | 9.20 | 8.70 | 133.78 | 80.91 | 14.14 | 147.23 | 106.60 | 102.07 |
| **Y (av)** | 4.92 | 7.24 | 4.46 | 5.13 | 6.26 | 8.00 | 4.30 | 8.87 | 6.81 |
| **Zr (av)** | 23.00 | 13.80 | 15.76 | 16.80 | 16.20 | 21.14 | 15.38 | 12.05 | 20.01 |
| **Ba (av)** | 15.56 | 4.94 | 25.36 | 60.48 | 60.67 | 21.51 | 63.94 | 74.24 | 75.60 |
| **Ga** | 33.98 | 12.03 | 30.59 | 21.74 | 36.34 | 26.24 | 11.48 | 8.30 | 34.14 |
| **Rb** | 1.52 | 4.46 | 6.79 | 21.23 | 17.28 | 3.46 | 25.76 | 30.51 | 17.15 |
| **Nb** | 0.79 | 0.93 | 0.65 | 1.09 | 0.62 | 0.44 | 0.68 | 3.43 | 1.32 |
| **Cs** | 0.27 | 0.82 | 2.10 | 1.61 | 2.15 | 0.18 | 0.69 | 1.83 | 0.89 |
| **Hf** | 0.48 | 0.34 | 0.31 | 0.36 | 0.36 | 0.51 | 0.32 | 0.29 | 0.48 |
| **Ta** | 0.03 | 0.08 | 0.03 | 0.06 | 0.03 | 0.02 | 0.03 | 0.22 | 0.08 |
| **Th** | 0.42 | 0.93 | 0.41 | 0.78 | 0.26 | 0.39 | 0.43 | 0.74 | 0.74 |
| **U** | 0.12 | 0.81 | 0.13 | 0.18 | 0.07 | 0.10 | 0.12 | 2.69 | 0.25 |
| **La** | 1.80 | 1.98 | 2.30 | 2.71 | 1.88 | 2.79 | 2.55 | 3.59 | 5.48 |
| **Ce** | 4.23 | 5.06 | 4.76 | 5.59 | 4.66 | 7.83 | 5.19 | 8.22 | 10.84 |
| **Pr** | 0.65 | 0.76 | 0.65 | 0.74 | 0.75 | 1.21 | 0.68 | 1.13 | 1.38 |
| **Nd** | 2.62 | 3.15 | 2.57 | 2.92 | 3.36 | 5.29 | 2.57 | 4.56 | 5.19 |
| **Sm** | 0.68 | 0.83 | 0.60 | 0.68 | 0.91 | 1.26 | 0.62 | 1.19 | 1.09 |
| **Eu** | 0.16 | 0.20 | 0.19 | 0.23 | 0.30 | 0.37 | 0.24 | 0.27 | 0.38 |
| **Gd** | 0.71 | 0.80 | 0.56 | 0.67 | 0.83 | 1.16 | 0.56 | 1.10 | 1.06 |
| **Tb** | 0.11 | 0.14 | 0.09 | 0.11 | 0.13 | 0.18 | 0.09 | 0.18 | 0.15 |
| **Dy** | 0.77 | 0.98 | 0.63 | 0.78 | 0.93 | 1.19 | 0.64 | 1.24 | 1.03 |
| **Ho** | 0.15 | 0.21 | 0.13 | 0.16 | 0.19 | 0.23 | 0.14 | 0.24 | 0.20 |
| **Er** | 0.48 | 0.62 | 0.42 | 0.51 | 0.57 | 0.72 | 0.46 | 0.74 | 0.63 |
| **Tm** | 0.07 | 0.09 | 0.07 | 0.08 | 0.10 | 0.12 | 0.07 | 0.11 | 0.10 |
| **Yb** | 0.44 | 0.70 | 0.39 | 0.52 | 0.52 | 0.68 | 0.51 | 0.85 | 0.62 |
| **Lu** | 0.07 | 0.11 | 0.06 | 0.08 | 0.08 | 0.11 | 0.08 | 0.14 | 0.10 |

| | REJ55 | REJ56 | REJ57 | REJ58 | REJ59 | REJ60 | REJ61 | REJ62 | REJ63 |
|---|---|---|---|---|---|---|---|---|---|
| | ZN278-1 | ZN278-2A | ZN278-2B | ZN278-3 | ZN309-1 | ZN309-2 | ZN324-1 | ZN324-2A | ZN324-2B |
| **$SiO_2$ (wt%)** | 47.27 | 42.89 | 41.07 | 46.62 | 42.17 | 26.45 | 32.30 | 48.86 | 31.70 |
| **$TiO_2$ (av)** | 0.30 | 0.15 | 0.49 | 0.34 | 0.35 | 0.68 | 0.55 | 0.21 | 0.66 |
| **$Al_2O_3$** | 5.49 | 2.24 | 8.22 | 7.11 | 5.93 | 17.31 | 15.62 | 5.32 | 11.78 |
| **$Fe_2O_3$ (av)** | 12.31 | 17.51 | 15.42 | 15.54 | 17.64 | 22.06 | 19.05 | 12.06 | 18.24 |
| **MnO (av)** | 0.20 | 0.20 | 0.23 | 0.30 | 0.26 | 0.25 | 0.24 | 0.31 | 0.28 |
| **MgO** | 15.57 | 23.76 | 17.17 | 17.15 | 19.87 | 13.50 | 12.37 | 20.70 | 15.27 |
| **CaO** | 11.76 | 5.16 | 6.10 | 4.92 | 4.39 | 3.28 | 3.74 | 4.76 | 4.17 |
| **$Na_2O$** | 0.39 | 0.18 | 0.35 | 0.31 | 0.35 | 0.54 | 0.58 | 0.13 | 0.11 |
| **$K_2O$** | 0.13 | 0.08 | 0.17 | 0.45 | 0.47 | 0.42 | 0.35 | 0.12 | 0.12 |
| **$P_2O_5$** | 0.02 | 0.01 | 0.04 | 0.04 | 0.05 | 0.04 | 0.05 | 0.05 | 0.04 |
| **$Cr_2O_3$** | 3.65 | 0.34 | 8.45 | 3.49 | 0.21 | 11.00 | 10.42 | 1.36 | 11.50 |
| **LOI** | 1.10 | 5.33 | 0.80 | 1.98 | 7.10 | 0.85 | 1.07 | 4.12 | 2.48 |
| **Total** | 79.00 | 103.02 | 93.26 | 87.88 | 98.00 | 123.26 | 108.74 | 76.47 | 110.41 |
| | | | | | | | | | |
| **V (av) (ppm)** | 282.04 | 51.92 | 221.34 | 262.71 | 92.84 | 591.59 | 467.72 | 109.24 | 396.13 |
| **Co (av)** | 176.58 | 170.60 | 118.19 | 95.19 | 118.08 | 170.95 | 134.79 | 112.97 | 125.79 |
| **Ni (av)** | 2416.82 | 2160.19 | 877.58 | 640.98 | 813.79 | 812.40 | 249.67 | 713.62 | 224.97 |
| **Cu (av)** | 1930.58 | 2616.21 | 701.02 | 165.26 | 670.42 | 1008.53 | 320.69 | 322.30 | 285.33 |
| **Zn (av)** | 208.23 | 78.83 | 229.31 | 228.66 | 153.90 | 541.96 | 488.44 | 119.56 | 378.81 |
| **Sr (av)** | 44.24 | 29.36 | 49.08 | 251.85 | 79.41 | 84.02 | 82.35 | 15.66 | 19.15 |
| **Y (av)** | 9.53 | 7.79 | 8.64 | 5.80 | 4.12 | 3.35 | 6.46 | 6.60 | 5.35 |
| **Zr (av)** | 17.11 | 10.54 | 16.07 | 13.86 | 18.33 | 23.38 | 21.74 | 14.82 | 15.88 |
| **Ba (av)** | 26.44 | 31.55 | 29.72 | 44.65 | 54.37 | 51.19 | 56.16 | 13.79 | 20.11 |
| **Ga** | 11.03 | 3.51 | 18.24 | 14.05 | 9.48 | 35.56 | 31.62 | 7.57 | 26.70 |
| **Rb** | 9.73 | 6.17 | 12.35 | 30.24 | 38.27 | 22.64 | 14.90 | 10.99 | 4.98 |
| **Nb** | 1.26 | 0.89 | 0.74 | 0.67 | 1.74 | 0.76 | 1.31 | 0.94 | 0.70 |
| **Cs** | 1.45 | 1.11 | 0.94 | 2.47 | 5.57 | 1.64 | 1.22 | 2.93 | 1.62 |
| **Hf** | 0.44 | 0.26 | 0.44 | 0.28 | 0.44 | 0.52 | 0.50 | 0.34 | 0.36 |
| **Ta** | 0.09 | 0.10 | 0.06 | 0.07 | 0.13 | 0.05 | 0.06 | 0.10 | 0.04 |
| **Th** | 0.73 | 0.55 | 0.59 | 0.51 | 0.72 | 0.59 | 0.86 | 0.52 | 0.57 |
| **U** | 0.67 | 0.49 | 0.29 | 0.28 | 1.10 | 0.20 | 0.26 | 0.55 | 0.18 |
| **La** | 3.38 | 1.61 | 1.85 | 3.21 | 11.66 | 2.30 | 4.52 | 8.54 | 2.15 |
| **Ce** | 8.38 | 4.25 | 4.54 | 7.69 | 16.59 | 4.53 | 9.19 | 14.37 | 5.09 |
| **Pr** | 1.25 | 0.69 | 0.72 | 1.04 | 1.55 | 0.59 | 1.06 | 1.47 | 0.74 |
| **Nd** | 5.30 | 2.98 | 3.14 | 3.92 | 4.58 | 2.21 | 4.04 | 4.70 | 3.00 |
| **Sm** | 1.35 | 0.84 | 0.85 | 0.87 | 0.71 | 0.51 | 0.93 | 0.88 | 0.74 |
| **Eu** | 0.27 | 0.22 | 0.26 | 0.29 | 0.18 | 0.22 | 0.27 | 0.21 | 0.21 |
| **Gd** | 1.36 | 0.87 | 0.92 | 0.77 | 0.68 | 0.43 | 0.90 | 0.86 | 0.67 |
| **Tb** | 0.23 | 0.16 | 0.17 | 0.12 | 0.09 | 0.07 | 0.13 | 0.13 | 0.11 |
| **Dy** | 1.50 | 1.16 | 1.26 | 0.86 | 0.61 | 0.49 | 0.89 | 0.96 | 0.77 |
| **Ho** | 0.29 | 0.22 | 0.25 | 0.18 | 0.13 | 0.10 | 0.18 | 0.20 | 0.16 |
| **Er** | 0.87 | 0.67 | 0.81 | 0.59 | 0.44 | 0.33 | 0.57 | 0.66 | 0.50 |
| **Tm** | 0.13 | 0.09 | 0.13 | 0.09 | 0.08 | 0.05 | 0.09 | 0.10 | 0.08 |
| **Yb** | 0.85 | 0.66 | 0.83 | 0.66 | 0.55 | 0.33 | 0.54 | 0.75 | 0.48 |
| **Lu** | 0.13 | 0.10 | 0.13 | 0.11 | 0.09 | 0.05 | 0.08 | 0.12 | 0.07 |

# Appendix 1B: Bulk Rock PGE

| Sample | | Os (ppb) | Ir | Ru | Rh | Pt | Pd | Au | 4E (g/t) | Pt/Pd |
|---|---|---|---|---|---|---|---|---|---|---|
| **REJ1P** | OY447-1 | 345.58 | 598.57 | 2364.61 | 975.71 | 21099.30 | 14267.22 | 1578.51 | 37.92 | 1.48 |
| **REJ2P** | OY447-2 | 84.65 | 160.07 | 682.11 | 534.41 | 3705.30 | 3990.22 | 900.81 | 9.13 | 0.93 |
| **REJ3P** | MO1-1 | 1.33 | 3.94 | 23.80 | 22.18 | 392.30 | 571.42 | 24.15 | 1.01 | 0.69 |
| **REJ4P** | MO1-2 | 4.09 | 18.08 | 86.01 | 94.92 | 1349.30 | 1890.22 | 258.21 | 3.59 | 0.71 |
| **REJ5P** | ZN230-1 | 3.91 | 11.31 | 43.56 | 60.61 | 451.60 | 1619.22 | 23.48 | 2.15 | 0.28 |
| **REJ6P** | ZN230-2 | 3.68 | 12.05 | 41.32 | 82.38 | 1302.30 | 2054.22 | 204.81 | 3.64 | 0.63 |
| **REJ7P** | ZN230-3 | 9.65 | 21.99 | 119.31 | 75.84 | 356.00 | 653.62 | 34.74 | 1.12 | 0.54 |
| **REJ8P** | ZN230-4 | 19.45 | 29.17 | 189.31 | 96.10 | 440.80 | 883.22 | 21.95 | 1.44 | 0.50 |
| **REJ9P** | ZN230-5 | 10.61 | 34.61 | 200.41 | 129.41 | 485.70 | 1631.22 | 54.66 | 2.30 | 0.30 |
| **REJ10P** | ZN595-1 | 1.74 | 7.12 | 27.84 | 31.92 | 257.80 | 520.72 | 25.50 | 0.84 | 0.50 |
| **REJ11P** | ZN595-2 | 6.67 | 15.15 | 64.45 | 54.88 | 255.40 | 264.02 | 11.32 | 0.59 | 0.97 |
| **REJ12P** | ZN595-3 | 10.60 | 16.08 | 94.10 | 62.26 | 1720.30 | 1921.22 | 132.01 | 3.84 | 0.90 |
| **REJ13P** | SS335-1 | 12.07 | 23.73 | 99.31 | 90.94 | 756.20 | 671.22 | 30.12 | 1.55 | 1.13 |
| **REJ14P** | SS335-2 | 0.58 | 2.25 | 11.09 | 9.83 | 121.20 | 285.02 | 20.27 | 0.44 | 0.43 |
| **REJ15P** | SS335-3 | 11.13 | 27.92 | 103.61 | 102.01 | 704.90 | 372.02 | 14.70 | 1.19 | 1.89 |
| **REJ16P** | SS335-4 | 12.57 | 25.92 | 111.91 | 93.38 | 448.90 | 700.42 | 62.00 | 1.30 | 0.64 |
| **REJ17P** | SS393-1 | 26.06 | 62.76 | 303.01 | 197.11 | 689.10 | 896.02 | 15.17 | 1.80 | 0.77 |
| **REJ18P** | SS393-2 | 21.88 | 35.59 | 205.71 | 109.01 | 461.10 | 410.92 | 5.38 | 0.99 | 1.12 |
| **REJ19P** | SS393-3 | 8.87 | 23.80 | 105.31 | 83.05 | 413.90 | 352.82 | 12.92 | 0.86 | 1.17 |
| **REJ20P** | SS393-4 | 34.65 | 68.57 | 234.11 | 270.91 | 3060.30 | 1688.22 | 87.52 | 5.11 | 1.81 |
| **REJ21P** | SS393-5 | 88.95 | 124.97 | 697.31 | 406.01 | 1510.30 | 1730.22 | 117.41 | 3.76 | 0.87 |
| **REJ22P** | OY551-1 | 16.96 | 31.37 | 162.71 | 127.61 | 1277.30 | 1372.22 | 128.61 | 2.91 | 0.93 |
| **REJ23P** | OY551-2 | 5.64 | 10.27 | 58.36 | 30.83 | 175.00 | 324.52 | 28.51 | 0.56 | 0.54 |
| **REJ24P** | OY551-3 | 61.43 | 97.80 | 459.51 | 382.71 | 2622.30 | 2389.22 | 413.91 | 5.81 | 1.10 |
| **REJ25P** | OY551-4 | 6.48 | 12.87 | 50.66 | 59.81 | 1137.30 | 1757.22 | 98.41 | 3.05 | 0.65 |
| **REJ26P** | ZN334-1 | 11.23 | 26.76 | 158.01 | 88.97 | 528.90 | 952.32 | 42.01 | 1.61 | 0.56 |
| **REJ27P** | ZN334-2 | 33.33 | 62.91 | 352.81 | 212.41 | 935.60 | 671.62 | 84.44 | 1.90 | 1.39 |
| **REJ28P** | ZN334-3 | 19.69 | 15.98 | 15.86 | 14.96 | 5.93 | 4.17 | 13.14 | 0.04 | 1.42 |
| **REJ29P** | OY472-1 | 0.38 | 1.33 | 6.80 | 6.15 | 22.19 | 43.10 | 16.96 | 0.09 | 0.51 |
| **REJ30P** | OY472-2 | 0.18 | 0.31 | 0.70 | 0.85 | 7.19 | 9.33 | 50.65 | 0.07 | 0.77 |
| **REJ31P** | OY472-3 | 3.55 | 5.94 | 36.85 | 22.76 | 125.80 | 300.42 | 13.35 | 0.46 | 0.42 |
| **REJ32P** | OY472-4 | 13.03 | 21.35 | 129.71 | 64.13 | 303.90 | 315.22 | 14.97 | 0.70 | 0.96 |
| **REJ33P** | ZN573-1 | 26.89 | 39.93 | 251.91 | 119.61 | 512.20 | 580.92 | 28.63 | 1.24 | 0.88 |
| **REJ34P** | ZN573-2 | 9.50 | 33.22 | 188.01 | 104.71 | 450.60 | 1044.22 | 78.59 | 1.68 | 0.43 |
| **REJ35P** | ZN573-3 | 26.37 | 126.77 | 477.31 | 527.61 | 2822.30 | 2168.22 | 36.75 | 5.55 | 1.30 |
| **REJ36P** | ZN704-1 | 16.15 | 31.65 | 131.51 | 127.31 | 2772.30 | 1863.22 | 114.91 | 4.88 | 1.49 |
| **REJ37P** | ZN704-3 | 43.21 | 73.41 | 400.21 | 235.91 | 988.10 | 900.62 | 50.59 | 2.18 | 1.10 |
| **REJ38P** | ZN704-4 | 34.21 | 51.96 | 337.31 | 166.81 | 697.60 | 636.42 | 11.25 | 1.51 | 1.10 |
| **REJ39P** | ZN704-6 | 3.75 | 14.26 | 74.14 | 49.28 | 252.40 | 716.82 | 28.53 | 1.05 | 0.35 |
| **REJ40P** | SS383-2 | 0.19 | 0.55 | 2.84 | 1.83 | 8.63 | 21.25 | 1.67 | 0.03 | 0.41 |
| **REJ41P** | SS383-3 | 26.18 | 98.12 | 341.01 | 378.81 | 2532.30 | 1929.22 | 43.03 | 4.88 | 1.31 |
| **REJ42P** | SS383-4 | 20.66 | 46.68 | 167.01 | 173.21 | 1190.30 | 1448.22 | 43.58 | 2.86 | 0.82 |
| **REJ43P** | SS383-5 | 23.68 | 41.56 | 223.51 | 136.81 | 574.30 | 799.12 | 15.79 | 1.53 | 0.72 |
| **REJ44P** | SS383-6 | 10.37 | 20.03 | 103.61 | 62.67 | 274.90 | 152.02 | 2.57 | 0.49 | 1.81 |
| **REJ45P** | SS383-7 | 19.07 | 25.91 | 149.81 | 136.81 | 833.50 | 1050.22 | 59.26 | 2.08 | 0.79 |
| **REJ46P** | OY531A-1 | 10.14 | 61.59 | 395.79 | 171.65 | 891.14 | 1303.97 | 113.13 | 2.48 | 0.68 |
| **REJ47P** | OY531A-2 | 3.25 | 15.11 | 77.01 | 47.32 | 272.65 | 593.97 | 37.52 | 0.95 | 0.46 |
| **REJ48P** | OY392-1 | 47.44 | 69.62 | 412.71 | 165.44 | 953.32 | 867.32 | 184.16 | 2.17 | 1.10 |
| **REJ49P** | OY392-2 | 29.80 | 69.39 | 328.70 | 243.41 | 4726.45 | 6958.39 | 358.64 | 12.29 | 0.68 |
| **REJ50P** | OY359-1 | 18.44 | 32.04 | 178.81 | 77.11 | 413.08 | 516.68 | 22.08 | 1.03 | 0.80 |
| **REJ51P** | OY252-1 | 27.70 | 54.05 | 241.73 | 147.46 | 1025.29 | 1168.26 | 56.04 | 2.40 | 0.88 |
| **REJ52P** | OY549-1 | 2.38 | 14.01 | 45.45 | 42.73 | 389.25 | 328.85 | 11.01 | 0.77 | 1.18 |
| **REJ53P** | OY549-2A | 3.35 | 7.14 | 32.42 | 26.38 | 152.90 | 267.38 | 26.27 | 0.47 | 0.57 |
| **REJ54P** | OY549-2B | 14.62 | 48.73 | 294.94 | 106.67 | 449.64 | 291.18 | 9.32 | 0.86 | 1.54 |
| **REJ55P** | ZN278-1 | 97.05 | 256.29 | 1156.88 | 802.18 | 4005.31 | 6651.72 | 543.65 | 12.00 | 0.60 |
| **REJ56P** | ZN278-2A | 3.42 | 12.15 | 62.23 | 50.53 | 440.98 | 1305.82 | 89.58 | 1.89 | 0.34 |
| **REJ57P** | ZN278-2B | 13.48 | 30.55 | 168.05 | 79.60 | 485.18 | 863.41 | 84.92 | 1.51 | 0.56 |
| **REJ58P** | ZN278-3 | 4.36 | 14.99 | 53.79 | 36.79 | 187.95 | 157.57 | 7.74 | 0.39 | 1.19 |

| | | | | | | | | | | |
|---|---|---|---|---|---|---|---|---|---|---|
| **REJ59P** | ZN309-1 | 2.20 | 4.93 | 19.20 | 17.94 | 205.48 | 381.69 | 103.88 | 0.71 | 0.54 |
| **REJ60P** | ZN309-2 | 29.37 | 126.12 | 635.14 | 344.36 | 1571.78 | 2342.76 | 69.41 | 4.33 | 0.67 |
| **REJ61P** | ZN324-1 | 29.82 | 36.85 | 268.62 | 83.39 | 336.19 | 225.72 | 346.20 | 0.99 | 1.49 |
| **REJ62P** | ZN324-2A | 3.69 | 3.74 | 22.25 | 17.55 | 205.64 | 354.06 | 24.99 | 0.60 | 0.58 |
| **REJ63P** | ZN324-2B | 28.07 | 37.50 | 254.42 | 86.68 | 394.68 | 374.10 | 211.05 | 1.07 | 1.06 |
| **REJ64P** | SS383-6A | 18.18 | 28.41 | 156.51 | 77.58 | 418.47 | 285.21 | 177.38 | 0.96 | 1.47 |
| **REJ65P** | ZN704-3A | 30.73 | 45.20 | 269.49 | 118.96 | 749.45 | 760.00 | 352.08 | 1.98 | 0.99 |
| **REJ66P** | ZN573-1B | 34.03 | 40.63 | 316.17 | 102.95 | 532.33 | 682.15 | 155.27 | 1.47 | 0.78 |
| **REJ67P** | SS393-2B | 43.24 | 60.64 | 383.67 | 148.93 | 797.75 | 674.24 | 251.78 | 1.87 | 1.18 |
| **REJ68P** | OY392-2 | 6.38 | 33.47 | 60.63 | 139.70 | 2243.89 | 5165.01 | 379.07 | 7.93 | 0.43 |
| **REJ69P** | OY531A-1 | 28.81 | 34.50 | 254.94 | 81.84 | 537.57 | 633.13 | 277.72 | 1.53 | 0.85 |

# Appendix 1C: Chromite Chemistry

| Analysis No. | Lithology | $TiO_2$ | $V_2O_5$ | $Al_2O_3$ | $Cr_2O_3$ | FeO | MnO | MgO | Mg# | Cr# | $Fe^{2+}$# | $Fe^{3+}$# |
|---|---|---|---|---|---|---|---|---|---|---|---|---|
| **OY472-4B MC1** | Chr gabbronorite | 1.10 | 0.47 | 13.81 | 43.31 | 33.80 | | 7.76 | 0.37 | 0.68 | 0.63 | 0.14 |
| **OY472-4B MC2** | Chr gabbronorite | 1.15 | 0.44 | 14.50 | 42.54 | 32.86 | | 7.99 | 0.38 | 0.66 | 0.62 | 0.13 |
| **OY472-4B MC3** | Chr gabbronorite | 1.07 | 0.48 | 14.06 | 42.01 | 34.29 | 0.74 | 7.18 | 0.35 | 0.67 | 0.65 | 0.15 |
| **OY472-4B MC4** | Chr gabbronorite | 1.16 | 0.51 | 14.90 | 41.68 | 34.09 | 0.69 | 7.10 | 0.34 | 0.65 | 0.66 | 0.14 |
| **OY472-4B MC5** | Chr gabbronorite | 1.23 | 0.52 | 12.26 | 44.15 | 35.06 | | 6.83 | 0.33 | 0.71 | 0.67 | 0.14 |
| **OY472-4B MC6** | Chr gabbronorite | 0.98 | | 14.67 | 43.89 | 32.82 | 0.80 | 8.02 | 0.39 | 0.67 | 0.61 | 0.14 |
| **OY472-4B MC7** | Chr gabbronorite | 1.34 | 0.54 | 12.67 | 42.88 | 35.14 | | 6.47 | 0.31 | 0.69 | 0.69 | 0.14 |
| **OY472-4B MC8** | Chr gabbronorite | 0.91 | 0.46 | 13.99 | 44.34 | 33.26 | 0.74 | 7.72 | 0.37 | 0.68 | 0.63 | 0.14 |
| **SS335-4B C1** | Chr gabbronorite | 1.86 | 0.34 | 15.54 | 37.00 | 38.49 | 0.68 | 6.38 | 0.30 | 0.61 | 0.70 | 0.18 |
| **SS335-4B C10** | Chr gabbronorite | 1.77 | 0.38 | 15.10 | 38.87 | 37.42 | 0.57 | 6.52 | 0.31 | 0.63 | 0.69 | 0.16 |
| **SS335-4B C2** | Chr gabbronorite | 1.41 | 0.38 | 16.35 | 37.64 | 36.77 | 0.46 | 6.17 | 0.30 | 0.61 | 0.70 | 0.15 |
| **SS335-4B C3** | Chr gabbronorite | 1.28 | 0.40 | 17.00 | 38.81 | 35.68 | 0.60 | 6.84 | 0.32 | 0.60 | 0.68 | 0.14 |
| **SS335-4B C4** | Chr gabbronorite | 1.41 | 0.33 | 16.62 | 38.73 | 36.52 | 0.62 | 6.73 | 0.32 | 0.61 | 0.68 | 0.15 |
| **SS335-4B C5** | Chr gabbronorite | 1.74 | 0.43 | 14.96 | 38.78 | 37.59 | 0.65 | 6.28 | 0.30 | 0.63 | 0.70 | 0.16 |
| **SS335-4B C6** | Chr gabbronorite | 1.89 | 0.38 | 14.39 | 38.96 | 38.03 | 0.46 | 6.20 | 0.29 | 0.64 | 0.71 | 0.17 |
| **SS335-4B C7** | Chr gabbronorite | 1.74 | 0.33 | 14.33 | 38.47 | 37.62 | 0.87 | 6.29 | 0.30 | 0.64 | 0.70 | 0.17 |
| **SS335-4B C8** | Chr gabbronorite | 1.98 | 0.38 | 14.51 | 39.25 | 37.58 | 0.59 | 6.35 | 0.30 | 0.64 | 0.70 | 0.16 |
| **SS335-4B C9** | Chr gabbronorite | 1.81 | 0.43 | 15.68 | 38.35 | 36.14 | 0.54 | 6.43 | 0.31 | 0.62 | 0.69 | 0.15 |
| **OY351A-2 C1** | Chr norite | 1.36 | | 17.24 | 35.20 | 36.94 | 0.49 | 8.48 | 0.40 | 0.58 | 0.60 | 0.20 |
| **OY351A-2 C10** | Chr norite | 1.46 | | 17.53 | 35.71 | 36.18 | 0.47 | 8.70 | 0.41 | 0.58 | 0.59 | 0.19 |
| **OY351A-2 C2** | Chr norite | 1.15 | | 18.43 | 35.90 | 34.74 | 0.53 | 8.53 | 0.40 | 0.57 | 0.60 | 0.17 |
| **OY351A-2 C3** | Chr norite | 1.03 | 0.35 | 18.12 | 36.66 | 36.29 | | 7.49 | 0.35 | 0.58 | 0.65 | 0.16 |
| **OY351A-2 C4** | Chr norite | 1.18 | | 16.99 | 36.55 | 35.98 | 0.66 | 8.47 | 0.40 | 0.59 | 0.60 | 0.19 |
| **OY351A-2 C5** | Chr norite | 1.17 | | 16.65 | 36.89 | 36.99 | 0.69 | 8.06 | 0.38 | 0.60 | 0.62 | 0.19 |
| **OY351A-2 C6** | Chr norite | 1.10 | | 18.07 | 35.41 | 35.41 | 0.55 | 8.56 | 0.41 | 0.57 | 0.59 | 0.18 |
| **OY351A-2 C7** | Chr norite | 1.05 | 0.34 | 18.28 | 36.56 | 35.71 | 0.48 | 7.74 | 0.36 | 0.57 | 0.64 | 0.16 |
| **OY351A-2 C8** | Chr norite | 1.09 | | 19.42 | 34.77 | 35.60 | 0.45 | 8.40 | 0.39 | 0.55 | 0.61 | 0.17 |
| **OY351A-2 C9** | Chr norite | 1.47 | | 17.11 | 35.97 | 35.50 | 0.53 | 8.64 | 0.41 | 0.58 | 0.59 | 0.18 |
| **OY392-2 C1** | Chr norite | 0.57 | 0.31 | 17.91 | 39.58 | 32.02 | | 8.99 | 0.42 | 0.60 | 0.58 | 0.14 |
| **OY392-2 C10** | Chr norite | 0.67 | 0.40 | 17.44 | 40.56 | 32.26 | 0.56 | 8.37 | 0.40 | 0.61 | 0.60 | 0.13 |
| **OY392-2 C2** | Chr norite | 0.75 | | 17.68 | 40.10 | 32.59 | | 8.59 | 0.41 | 0.60 | 0.59 | 0.14 |

| | | | | | | | | | | | | |
|---|---|---|---|---|---|---|---|---|---|---|---|---|
| **OY392-2 C3** | Chr norite | 0.71 | | 17.67 | 40.68 | 32.86 | 0.43 | 8.52 | 0.40 | 0.61 | 0.60 | 0.14 |
| **OY392-2 C4** | Chr norite | 0.77 | 0.36 | 17.37 | 39.17 | 32.85 | 0.55 | 8.69 | 0.41 | 0.60 | 0.59 | 0.15 |
| **OY392-2 C5** | Chr norite | 0.83 | 0.34 | 17.56 | 39.59 | 32.05 | 0.44 | 8.88 | 0.42 | 0.60 | 0.58 | 0.14 |
| **OY392-2 C6** | Chr norite | 0.87 | 0.35 | 17.75 | 39.66 | 32.35 | 0.58 | 8.99 | 0.42 | 0.60 | 0.58 | 0.14 |
| **OY392-2 C7** | Chr norite | 0.82 | 0.35 | 17.83 | 39.27 | 32.34 | 0.75 | 8.92 | 0.42 | 0.60 | 0.58 | 0.15 |
| **OY392-2 C8** | Chr norite | 0.65 | 0.29 | 17.60 | 40.02 | 33.36 | 0.47 | 8.17 | 0.39 | 0.60 | 0.61 | 0.14 |
| **OY392-2 C9** | Chr norite | 0.76 | 0.37 | 17.20 | 39.65 | 32.35 | 0.54 | 8.16 | 0.39 | 0.61 | 0.61 | 0.14 |
| **OY531A-1 C1** | Chr norite | 0.69 | | 18.14 | 42.24 | 28.83 | 0.49 | 10.25 | 0.48 | 0.61 | 0.52 | 0.12 |
| **OY531A-1 C10** | Chr norite | 0.70 | 0.39 | 18.96 | 40.95 | 29.47 | 0.62 | 10.12 | 0.47 | 0.59 | 0.53 | 0.12 |
| **OY531A-1 C2** | Chr norite | 0.69 | | 15.96 | 43.85 | 29.42 | 0.48 | 9.96 | 0.47 | 0.65 | 0.53 | 0.13 |
| **OY531A-1 C3** | Chr norite | 0.69 | | 17.75 | 42.09 | 29.07 | 0.48 | 10.22 | 0.48 | 0.61 | 0.52 | 0.13 |
| **OY531A-1 C4** | Chr norite | 0.88 | | 19.79 | 40.91 | 28.95 | 0.46 | 10.35 | 0.48 | 0.58 | 0.52 | 0.12 |
| **OY531A-1 C5** | Chr norite | 0.76 | | 17.54 | 41.42 | 29.11 | | 10.15 | 0.48 | 0.61 | 0.52 | 0.13 |
| **OY531A-1 C6** | Chr norite | 0.68 | | 18.27 | 41.33 | 28.83 | 0.63 | 9.82 | 0.47 | 0.60 | 0.53 | 0.12 |
| **OY531A-1 C7** | Chr norite | 0.90 | | 18.61 | 41.68 | 29.91 | | 10.03 | 0.46 | 0.60 | 0.54 | 0.12 |
| **OY531A-1 C8** | Chr norite | 0.81 | | 20.10 | 40.16 | 28.40 | 0.59 | 10.08 | 0.47 | 0.57 | 0.53 | 0.11 |
| **OY531A-1 C9** | Chr norite | 0.71 | | 19.11 | 40.81 | 29.23 | | 10.18 | 0.47 | 0.59 | 0.53 | 0.12 |
| **OY551-1A C1** | Chr norite | 0.94 | 0.33 | 18.46 | 38.74 | 32.73 | 0.49 | 8.75 | 0.41 | 0.58 | 0.59 | 0.14 |
| **OY551-1A C10** | Chr norite | 0.46 | 0.49 | 21.14 | 38.24 | 30.67 | 0.46 | 8.93 | 0.42 | 0.55 | 0.58 | 0.11 |
| **OY551-1A C2** | Chr norite | 0.95 | 0.32 | 17.44 | 40.15 | 32.86 | 0.53 | 8.38 | 0.39 | 0.61 | 0.61 | 0.14 |
| **OY551-1A C3** | Chr norite | 0.61 | 0.48 | 21.03 | 38.85 | 30.43 | | 9.55 | 0.44 | 0.55 | 0.56 | 0.11 |
| **OY551-1A C4** | Chr norite | 0.86 | 0.31 | 19.05 | 39.55 | 30.26 | 0.51 | 9.07 | 0.43 | 0.58 | 0.57 | 0.12 |
| **OY551-1A C5** | Chr norite | 0.86 | | 18.85 | 40.29 | 30.40 | 0.73 | 8.88 | 0.42 | 0.59 | 0.58 | 0.12 |
| **OY551-1A C6** | Chr norite | 0.51 | | 20.90 | 38.68 | 29.21 | 0.51 | 9.58 | 0.45 | 0.55 | 0.55 | 0.12 |
| **OY551-1A C7** | Chr norite | 0.65 | | 19.91 | 39.79 | 30.57 | 0.56 | 9.39 | 0.44 | 0.57 | 0.56 | 0.12 |
| **OY551-1A C8** | Chr norite | 0.66 | | 19.12 | 40.24 | 30.22 | 0.53 | 9.31 | 0.44 | 0.59 | 0.56 | 0.12 |
| **OY551-1A C9** | Chr norite | 0.76 | | 19.83 | 39.54 | 30.54 | 0.62 | 9.01 | 0.42 | 0.57 | 0.58 | 0.12 |
| **OY551-2B C1** | Chr norite | 1.08 | 0.38 | 16.54 | 39.55 | 34.40 | 0.59 | 8.04 | 0.38 | 0.62 | 0.62 | 0.15 |
| **OY551-2B C10** | Chr norite | 0.72 | | 19.17 | 38.88 | 32.33 | 0.56 | 8.65 | 0.41 | 0.58 | 0.59 | 0.14 |
| **OY551-2B C2** | Chr norite | 0.95 | 0.60 | 18.50 | 38.91 | 33.14 | | 8.66 | 0.40 | 0.59 | 0.60 | 0.13 |
| **OY551-2B C3** | Chr norite | 1.06 | 0.34 | 15.84 | 38.45 | 35.85 | 0.65 | 7.65 | 0.37 | 0.62 | 0.63 | 0.17 |
| **OY551-2B C4** | Chr norite | 0.79 | 0.31 | 17.96 | 39.32 | 31.83 | 0.52 | 8.80 | 0.42 | 0.59 | 0.58 | 0.14 |
| **OY551-2B C5** | Chr norite | 0.58 | | 19.37 | 38.55 | 31.30 | 0.62 | 8.81 | 0.42 | 0.57 | 0.58 | 0.13 |
| **OY551-2B C6** | Chr norite | 1.00 | 0.42 | 16.44 | 39.95 | 32.92 | 0.55 | 8.15 | 0.39 | 0.62 | 0.61 | 0.14 |
| **OY551-2B C7** | Chr norite | 0.81 | 0.34 | 16.62 | 40.30 | 33.49 | 0.55 | 7.91 | 0.38 | 0.62 | 0.62 | 0.14 |
| **OY551-2B C8** | Chr norite | 0.70 | | 18.26 | 40.61 | 31.22 | | 8.75 | 0.41 | 0.60 | 0.59 | 0.12 |

| | | | | | | | | | | | | |
|---|---|---|---|---|---|---|---|---|---|---|---|---|
| **OY551-2B C9** | Chr norite | 0.67 | | 18.62 | 39.78 | 31.04 | | 8.94 | 0.42 | 0.59 | 0.58 | 0.13 |
| **OY551-3A C1** | Chr norite | 0.56 | | 20.40 | 37.41 | 29.34 | 0.48 | 9.09 | 0.44 | 0.55 | 0.56 | 0.12 |
| **OY551-3A C2** | Chr norite | 0.94 | | 17.87 | 39.80 | 32.24 | | 8.45 | 0.40 | 0.60 | 0.60 | 0.13 |
| **OY551-3A C3** | Chr norite | 0.39 | 0.33 | 21.04 | 39.01 | 28.90 | | 9.45 | 0.44 | 0.55 | 0.56 | 0.10 |
| **OY551-3A C4** | Chr norite | 0.34 | 0.35 | 21.09 | 38.94 | 29.27 | 0.45 | 9.66 | 0.45 | 0.55 | 0.55 | 0.11 |
| **OY551-3A C5** | Chr norite | 0.62 | 0.36 | 18.78 | 40.53 | 30.57 | 0.43 | 9.11 | 0.43 | 0.59 | 0.57 | 0.12 |
| **OY551-3A C6** | Chr norite | 0.54 | 0.31 | 20.53 | 39.52 | 29.08 | | 9.49 | 0.44 | 0.56 | 0.56 | 0.10 |
| **OY551-3A C7** | Chr norite | 0.64 | 0.34 | 17.02 | 40.57 | 32.09 | 0.49 | 7.90 | 0.38 | 0.62 | 0.62 | 0.13 |
| **OY551-3A C8** | Chr norite | 0.58 | 0.36 | 18.91 | 39.43 | 31.38 | 0.50 | 8.71 | 0.41 | 0.58 | 0.59 | 0.13 |
| **OY551-3A C9** | Chr norite | 0.84 | 0.33 | 17.12 | 40.24 | 32.93 | 0.53 | 8.19 | 0.39 | 0.61 | 0.61 | 0.14 |
| **SS383-4A C1** | Chr norite | 1.68 | 0.36 | 12.07 | 41.15 | 38.73 | 0.67 | 5.07 | 0.25 | 0.70 | 0.75 | 0.17 |
| **SS383-4A C10** | Chr norite | 1.66 | 0.50 | 8.40 | 45.65 | 38.32 | 0.51 | 4.52 | 0.22 | 0.78 | 0.78 | 0.16 |
| **SS383-4A C2** | Chr norite | 1.77 | 0.43 | 10.76 | 41.13 | 40.59 | 0.54 | 4.08 | 0.20 | 0.72 | 0.80 | 0.18 |
| **SS383-4A C3** | Chr norite | 1.98 | 0.34 | 11.26 | 41.91 | 39.22 | | 5.71 | 0.27 | 0.71 | 0.73 | 0.17 |
| **SS383-4A C4** | Chr norite | 1.76 | 0.50 | 10.87 | 42.83 | 37.85 | 0.49 | 5.36 | 0.26 | 0.73 | 0.74 | 0.16 |
| **SS383-4A C5** | Chr norite | 2.06 | 0.45 | 10.00 | 43.30 | 38.01 | | 5.39 | 0.26 | 0.74 | 0.74 | 0.16 |
| **SS383-4A C6** | Chr norite | 1.96 | 0.33 | 9.49 | 43.16 | 38.47 | 0.59 | 5.12 | 0.25 | 0.75 | 0.75 | 0.17 |
| **SS383-4A C7** | Chr norite | 1.65 | 0.40 | 9.55 | 43.26 | 39.43 | 0.62 | 4.94 | 0.24 | 0.75 | 0.76 | 0.18 |
| **SS383-4A C8** | Chr norite | 2.05 | | 8.72 | 45.86 | 38.50 | 0.70 | 4.95 | 0.24 | 0.78 | 0.76 | 0.17 |
| **SS383-4A C9** | Chr norite | 1.90 | 0.58 | 8.31 | 45.14 | 38.03 | 0.69 | 5.04 | 0.25 | 0.78 | 0.75 | 0.17 |
| **SS383-5B C1** | Chr norite | 1.83 | | 14.04 | 38.29 | 39.02 | 0.62 | 6.75 | 0.32 | 0.65 | 0.68 | 0.20 |
| **SS383-5B C10** | Chr norite | 0.95 | | 15.13 | 35.23 | 42.82 | 0.65 | 5.67 | 0.28 | 0.61 | 0.72 | 0.23 |
| **SS383-5B C2** | Chr norite | 1.56 | | 14.41 | 37.84 | 38.81 | | 6.85 | 0.32 | 0.64 | 0.68 | 0.19 |
| **SS383-5B C3** | Chr norite | 0.87 | 0.37 | 15.28 | 37.57 | 37.90 | 0.54 | 6.97 | 0.34 | 0.62 | 0.66 | 0.19 |
| **SS383-5B C4** | Chr norite | 0.87 | 0.41 | 14.58 | 39.20 | 37.95 | 0.62 | 6.88 | 0.33 | 0.64 | 0.67 | 0.19 |
| **SS383-5B C5** | Chr norite | 0.77 | 0.33 | 15.62 | 36.60 | 39.70 | 0.59 | 6.68 | 0.32 | 0.61 | 0.68 | 0.21 |
| **SS383-5B C6** | Chr norite | 1.47 | | 13.73 | 33.03 | 46.02 | 0.66 | 5.37 | 0.26 | 0.62 | 0.74 | 0.27 |
| **SS383-5B C7** | Chr norite | 0.77 | | 15.36 | 36.74 | 40.36 | 0.65 | 6.56 | 0.32 | 0.62 | 0.68 | 0.21 |
| **SS383-5B C8** | Chr norite | 0.62 | 0.32 | 12.42 | 30.90 | 51.93 | 0.59 | 3.48 | 0.17 | 0.63 | 0.83 | 0.33 |
| **SS383-5B C9** | Chr norite | 0.87 | | 12.01 | 30.51 | 53.83 | 0.77 | 2.97 | 0.15 | 0.63 | 0.85 | 0.34 |
| **SS383-7A C1** | Chr norite | 1.21 | 0.38 | 14.83 | 42.89 | 33.35 | | 8.09 | 0.38 | 0.66 | 0.62 | 0.13 |
| **SS383-7A C10** | Chr norite | 1.09 | 0.43 | 13.76 | 43.19 | 32.59 | 0.65 | 7.77 | 0.38 | 0.68 | 0.62 | 0.14 |
| **SS383-7A C2** | Chr norite | 1.19 | 0.32 | 12.81 | 42.67 | 34.23 | 0.73 | 7.47 | 0.36 | 0.69 | 0.64 | 0.16 |
| **SS383-7A C3** | Chr norite | 1.12 | 0.57 | 12.49 | 42.78 | 34.91 | 0.64 | 7.14 | 0.35 | 0.70 | 0.65 | 0.16 |
| **SS383-7A C4** | Chr norite | 1.29 | 0.51 | 12.93 | 43.07 | 33.97 | 0.51 | 7.13 | 0.34 | 0.69 | 0.66 | 0.14 |
| **SS383-7A C5** | Chr norite | 0.96 | 0.47 | 13.09 | 42.54 | 34.67 | | 7.28 | 0.35 | 0.69 | 0.65 | 0.15 |

| | | | | | | | | | | | | |
|---|---|---|---|---|---|---|---|---|---|---|---|---|
| **SS383-7A C6** | Chr norite | 1.29 | 0.45 | 12.44 | 43.44 | 34.59 | | 7.25 | 0.35 | 0.70 | 0.65 | 0.15 |
| **SS383-7A C7** | Chr norite | 1.28 | | 12.35 | 44.68 | 33.62 | 0.58 | 7.28 | 0.35 | 0.71 | 0.65 | 0.14 |
| **SS383-7A C8** | Chr norite | 1.21 | 0.43 | 12.28 | 43.45 | 34.01 | 0.66 | 7.34 | 0.36 | 0.70 | 0.64 | 0.15 |
| **SS383-7A C9** | Chr norite | 1.32 | 0.31 | 12.70 | 44.14 | 34.35 | 0.67 | 7.14 | 0.34 | 0.70 | 0.66 | 0.14 |
| **SS393-1B C1** | Chr norite | 0.66 | 0.40 | 18.97 | 37.59 | 34.72 | 0.63 | 6.08 | 0.30 | 0.57 | 0.70 | 0.12 |
| **SS393-1B C10** | Chr norite | 1.14 | 0.30 | 20.53 | 40.06 | 29.01 | 0.50 | 8.61 | 0.40 | 0.57 | 0.60 | 0.08 |
| **SS393-1B C2** | Chr norite | 0.44 | 0.36 | 19.30 | 38.64 | 35.56 | 0.69 | 5.96 | 0.29 | 0.57 | 0.71 | 0.13 |
| **SS393-1B C3** | Chr norite | 1.56 | 0.35 | 21.13 | 37.42 | 30.24 | 0.61 | 8.68 | 0.40 | 0.54 | 0.60 | 0.10 |
| **SS393-1B C4** | Chr norite | 1.52 | | 20.18 | 38.59 | 30.27 | 0.62 | 8.21 | 0.39 | 0.56 | 0.61 | 0.10 |
| **SS393-1B C5** | Chr norite | 1.57 | 0.35 | 20.55 | 38.77 | 30.28 | | 8.79 | 0.40 | 0.56 | 0.60 | 0.09 |
| **SS393-1B C6** | Chr norite | 1.47 | 0.34 | 20.68 | 38.40 | 30.02 | 0.58 | 8.91 | 0.41 | 0.55 | 0.59 | 0.10 |
| **SS393-1B C7** | Chr norite | 1.08 | 0.36 | 18.66 | 42.20 | 29.62 | 0.56 | 8.42 | 0.39 | 0.60 | 0.61 | 0.09 |
| **SS393-1B C8** | Chr norite | 1.10 | | 19.35 | 40.60 | 28.90 | 0.56 | 8.52 | 0.40 | 0.58 | 0.60 | 0.09 |
| **SS393-1B C9** | Chr norite | 1.15 | 0.33 | 20.56 | 40.52 | 29.59 | 0.52 | 8.20 | 0.38 | 0.57 | 0.62 | 0.08 |
| **SS393-2C C1** | Chr norite | 1.31 | 0.36 | 16.31 | 42.29 | 30.68 | 0.51 | 7.88 | 0.37 | 0.63 | 0.63 | 0.10 |
| **SS393-2C C10** | Chr norite | 1.52 | 0.42 | 14.77 | 43.30 | 32.20 | 0.78 | 7.39 | 0.35 | 0.66 | 0.65 | 0.11 |
| **SS393-2C C2** | Chr norite | 1.50 | 0.46 | 15.39 | 43.52 | 31.46 | | 7.66 | 0.36 | 0.65 | 0.64 | 0.10 |
| **SS393-2C C3** | Chr norite | 1.55 | 0.34 | 14.35 | 43.15 | 31.66 | 0.59 | 7.46 | 0.36 | 0.67 | 0.64 | 0.11 |
| **SS393-2C C4** | Chr norite | 1.51 | 0.46 | 14.38 | 43.12 | 31.38 | 0.54 | 7.62 | 0.37 | 0.67 | 0.63 | 0.11 |
| **SS393-2C C5** | Chr norite | 1.90 | | 14.89 | 43.38 | 31.84 | 0.76 | 7.37 | 0.35 | 0.66 | 0.65 | 0.11 |
| **SS393-2C C6** | Chr norite | 1.74 | | 13.78 | 43.87 | 32.27 | 0.47 | 7.88 | 0.37 | 0.68 | 0.63 | 0.13 |
| **SS393-2C C7** | Chr norite | 1.65 | 0.33 | 14.55 | 42.89 | 31.41 | 0.61 | 7.59 | 0.36 | 0.66 | 0.64 | 0.11 |
| **SS393-2C C8** | Chr norite | 1.63 | | 14.57 | 43.40 | 31.43 | 0.59 | 7.55 | 0.36 | 0.67 | 0.64 | 0.11 |
| **SS393-2C C9** | Chr norite | 1.45 | 0.42 | 14.15 | 43.40 | 31.66 | 0.75 | 7.57 | 0.36 | 0.67 | 0.64 | 0.12 |
| **SS393-5C C1** | Chr norite | 1.01 | 0.31 | 12.98 | 46.25 | 32.17 | 0.60 | 5.95 | 0.29 | 0.71 | 0.71 | 0.10 |
| **SS393-5C C2** | Chr norite | 1.46 | 0.42 | 7.23 | 50.68 | 36.60 | 0.75 | 3.67 | 0.18 | 0.82 | 0.82 | 0.12 |
| **SS393-5C C3** | Chr norite | 1.24 | | 11.04 | 48.09 | 33.64 | 0.67 | 5.51 | 0.27 | 0.75 | 0.73 | 0.11 |
| **SS393-5C C4** | Chr norite | 1.35 | 0.46 | 7.77 | 50.53 | 34.93 | 0.71 | 4.52 | 0.23 | 0.81 | 0.77 | 0.11 |
| **SS393-5C C5** | Chr norite | 1.03 | 0.34 | 13.70 | 46.16 | 31.03 | 0.46 | 6.81 | 0.33 | 0.69 | 0.67 | 0.09 |
| **SS393-5C C6** | Chr norite | 0.98 | 0.33 | 13.90 | 45.78 | 31.34 | 0.67 | 6.68 | 0.33 | 0.69 | 0.67 | 0.10 |
| **SS393-5C C7** | Chr norite | 1.01 | 0.41 | 9.59 | 49.47 | 31.68 | 0.81 | 6.08 | 0.31 | 0.78 | 0.69 | 0.11 |
| **SS393-5C C8** | Chr norite | 1.43 | 0.43 | 7.11 | 51.57 | 33.75 | 0.64 | 5.13 | 0.26 | 0.83 | 0.74 | 0.11 |
| **SS393-5C C9** | Chr norite | 1.33 | 0.44 | 6.13 | 51.72 | 34.55 | 0.68 | 4.23 | 0.22 | 0.85 | 0.78 | 0.11 |
| **ZN230-4B MC1** | Chr norite | 1.31 | 0.00 | 18.91 | 42.74 | 37.30 | 0.30 | 7.66 | 0.34 | 0.60 | 0.66 | 0.13 |
| **ZN230-4B MC2** | Chr norite | 1.71 | 0.26 | 16.45 | 44.59 | 38.14 | 0.36 | 6.97 | 0.31 | 0.65 | 0.69 | 0.13 |
| **ZN230-4B MC3** | Chr norite | 1.41 | 0.16 | 17.69 | 43.41 | 28.81 | 0.26 | 7.32 | 0.35 | 0.62 | 0.65 | 0.06 |

| | | | | | | | | | | | | |
|---|---|---|---|---|---|---|---|---|---|---|---|---|
| **ZN230-4B MC4** | Chr norite | 1.29 | 0.39 | 18.65 | 43.69 | 35.37 | 0.59 | 7.72 | 0.34 | 0.61 | 0.66 | 0.11 |
| **ZN230-4B MC5** | Chr norite | 0.84 | 0.30 | 17.33 | 43.44 | 37.29 | 0.50 | 7.21 | 0.33 | 0.63 | 0.67 | 0.14 |
| **ZN230-4B MC6** | Chr norite | 1.23 | 0.65 | 11.80 | 50.22 | 31.21 | 0.68 | 4.51 | 0.22 | 0.74 | 0.78 | 0.05 |
| **ZN230-4B MC7** | Chr norite | 1.34 | 0.46 | 12.35 | 41.31 | 36.02 | 0.65 | 4.20 | 0.21 | 0.69 | 0.79 | 0.13 |
| **ZN230-4B MC8** | Chr norite | 1.68 | 0.13 | 13.62 | 43.25 | 33.41 | 0.00 | 6.30 | 0.30 | 0.68 | 0.70 | 0.11 |
| **ZN278-2B C1** | Chr norite | 1.05 | 0.00 | 18.33 | 39.69 | 32.81 | 0.00 | 9.15 | 0.42 | 0.59 | 0.58 | 0.14 |
| **ZN278-2B C10** | Chr norite | 0.81 | 0.32 | 20.38 | 40.05 | 29.55 | 0.49 | 9.34 | 0.43 | 0.57 | 0.57 | 0.10 |
| **ZN278-2B C2** | Chr norite | 1.05 | 0.31 | 18.88 | 38.85 | 32.37 | 0.48 | 8.89 | 0.41 | 0.58 | 0.59 | 0.13 |
| **ZN278-2B C3** | Chr norite | 0.81 | 0.00 | 19.39 | 39.65 | 31.08 | 0.00 | 8.96 | 0.42 | 0.58 | 0.58 | 0.12 |
| **ZN278-2B C4** | Chr norite | 0.95 | 0.00 | 19.21 | 40.03 | 30.88 | 0.00 | 8.91 | 0.41 | 0.58 | 0.59 | 0.11 |
| **ZN278-2B C5** | Chr norite | 1.04 | 0.41 | 19.19 | 39.21 | 31.21 | 0.00 | 8.77 | 0.40 | 0.58 | 0.60 | 0.11 |
| **ZN278-2B C6** | Chr norite | 0.92 | 0.33 | 18.06 | 39.11 | 32.25 | 0.51 | 8.63 | 0.41 | 0.59 | 0.59 | 0.14 |
| **ZN278-2B C7** | Chr norite | 0.98 | 0.00 | 18.08 | 40.03 | 31.03 | 0.00 | 9.52 | 0.44 | 0.60 | 0.56 | 0.13 |
| **ZN278-2B C8** | Chr norite | 0.90 | 0.00 | 17.08 | 41.57 | 30.51 | 0.52 | 9.13 | 0.43 | 0.62 | 0.57 | 0.13 |
| **ZN278-2B C9** | Chr norite | 0.97 | 0.00 | 18.04 | 40.13 | 30.95 | 0.47 | 9.41 | 0.44 | 0.60 | 0.56 | 0.13 |
| **ZN334-1A MC1** | Chr norite | 1.02 | 0.24 | 14.33 | 45.46 | 31.35 | 0.52 | 7.02 | 0.34 | 0.68 | 0.66 | 0.10 |
| **ZN334-1A MC2** | Chr norite | 1.20 | 0.40 | 14.59 | 44.31 | 31.90 | 0.56 | 6.48 | 0.31 | 0.67 | 0.69 | 0.10 |
| **ZN334-1A MC3** | Chr norite | 1.01 | 0.34 | 14.39 | 44.63 | 32.54 | 0.60 | 6.11 | 0.30 | 0.68 | 0.70 | 0.10 |
| **ZN334-1A MC4** | Chr norite | 1.33 | 0.42 | 13.66 | 43.13 | 35.31 | 0.51 | 6.07 | 0.29 | 0.68 | 0.71 | 0.13 |
| **ZN334-1A MC5** | Chr norite | 2.06 | 0.43 | 12.24 | 41.55 | 38.03 | 0.69 | 5.29 | 0.25 | 0.69 | 0.75 | 0.16 |
| **ZN334-1A MC6** | Chr norite | 2.10 | 0.46 | 10.65 | 42.92 | 39.07 | 0.57 | 4.60 | 0.22 | 0.73 | 0.78 | 0.16 |
| **ZN334-1A MC7** | Chr norite | 1.85 | 0.42 | 13.45 | 41.13 | 36.61 | 0.51 | 6.05 | 0.29 | 0.67 | 0.71 | 0.15 |
| **ZN334-1A MC8** | Chr norite | 1.69 | 0.40 | 13.31 | 41.34 | 36.10 | 0.59 | 6.10 | 0.29 | 0.68 | 0.71 | 0.15 |
| **ZN334-3B MC1** | Chr norite | 1.68 | 0.43 | 13.25 | 41.12 | 36.56 | 0.56 | 5.98 | 0.29 | 0.68 | 0.71 | 0.15 |
| **ZN334-3B MC2** | Chr norite | 1.20 | 0.38 | 11.14 | 44.98 | 36.26 | 0.62 | 5.21 | 0.26 | 0.73 | 0.74 | 0.14 |
| **ZN334-3B MC3** | Chr norite | 1.18 | 0.39 | 14.22 | 44.03 | 33.25 | 0.56 | 6.22 | 0.30 | 0.67 | 0.70 | 0.11 |
| **ZN334-3B MC4** | Chr norite | 2.01 | 0.44 | 12.12 | 41.86 | 37.91 | 0.59 | 5.32 | 0.26 | 0.70 | 0.74 | 0.15 |
| **ZN334-3B MC5** | Chr norite | 1.70 | 0.31 | 14.83 | 40.54 | 35.21 | 0.44 | 6.86 | 0.33 | 0.65 | 0.67 | 0.14 |
| **ZN334-3B MC6** | Chr norite | 1.06 | 0.22 | 14.29 | 44.81 | 32.33 | 0.56 | 6.36 | 0.31 | 0.68 | 0.69 | 0.10 |
| **ZN334-3B MC7** | Chr norite | 2.12 | 0.46 | 11.87 | 41.64 | 38.37 | 0.61 | 5.36 | 0.26 | 0.70 | 0.74 | 0.16 |
| **ZN334-3B MC8** | Chr norite | 1.68 | 0.46 | 12.00 | 41.87 | 37.96 | 0.56 | 5.31 | 0.26 | 0.70 | 0.74 | 0.16 |
| **ZN573-2A C1** | Chr norite | 1.65 | 0.51 | 17.02 | 39.77 | 33.24 | 0.54 | 7.71 | 0.36 | 0.61 | 0.64 | 0.12 |
| **ZN573-2A C10** | Chr norite | 1.42 | 0.55 | 18.19 | 38.54 | 33.51 | 0.49 | 7.55 | 0.35 | 0.59 | 0.65 | 0.12 |
| **ZN573-2A C2** | Chr norite | 1.33 | 0.45 | 17.56 | 39.24 | 33.74 | 0.59 | 7.36 | 0.35 | 0.60 | 0.65 | 0.13 |
| **ZN573-2A C3** | Chr norite | 1.48 | 0.47 | 17.76 | 38.83 | 33.22 | 0.56 | 8.02 | 0.37 | 0.59 | 0.63 | 0.13 |
| **ZN573-2A C4** | Chr norite | 1.47 | 0.42 | 17.94 | 39.25 | 33.55 | 0.62 | 7.57 | 0.35 | 0.59 | 0.65 | 0.12 |

| | | | | | | | | | | | | |
|---|---|---|---|---|---|---|---|---|---|---|---|---|
| **ZN573-2A C5** | Chr norite | 1.22 | 0.44 | 18.22 | 40.42 | 32.85 | 0.51 | 7.29 | 0.34 | 0.60 | 0.66 | 0.11 |
| **ZN573-2A C6** | Chr norite | 1.60 | 0.40 | 17.88 | 39.53 | 33.38 | 0.54 | 7.93 | 0.37 | 0.60 | 0.63 | 0.12 |
| **ZN573-2A C7** | Chr norite | 1.47 | 0.67 | 18.14 | 38.90 | 33.57 | 0.00 | 8.16 | 0.37 | 0.59 | 0.63 | 0.13 |
| **ZN573-2A C8** | Chr norite | 1.16 | 0.50 | 18.52 | 39.51 | 32.43 | 0.52 | 7.93 | 0.37 | 0.59 | 0.63 | 0.12 |
| **ZN573-2A C9** | Chr norite | 1.38 | 0.44 | 18.01 | 38.87 | 33.32 | 0.00 | 8.04 | 0.37 | 0.59 | 0.63 | 0.13 |
| **ZN595-2A C1** | Chr norite | 1.77 | 0.43 | 13.41 | 41.16 | 36.63 | 0.56 | 5.97 | 0.29 | 0.67 | 0.71 | 0.15 |
| **ZN595-2A C2** | Chr norite | 1.45 | 0.38 | 13.31 | 43.67 | 34.70 | 0.57 | 5.93 | 0.29 | 0.69 | 0.71 | 0.12 |
| **ZN595-2A C3** | Chr norite | 1.35 | 0.40 | 12.87 | 43.38 | 35.36 | 0.58 | 5.80 | 0.28 | 0.69 | 0.72 | 0.13 |
| **ZN595-2A C4** | Chr norite | 1.59 | 0.32 | 13.75 | 42.41 | 35.15 | 0.53 | 6.18 | 0.30 | 0.67 | 0.70 | 0.13 |
| **ZN595-2A C5** | Chr norite | 1.90 | 0.46 | 11.93 | 41.75 | 38.17 | 0.58 | 5.34 | 0.26 | 0.70 | 0.74 | 0.16 |
| **ZN595-2A C6** | Chr norite | 0.59 | 0.40 | 14.75 | 41.35 | 36.60 | 0.71 | 5.62 | 0.28 | 0.65 | 0.72 | 0.15 |
| **ZN595-2A C7** | Chr norite | 1.36 | 0.28 | 15.36 | 41.31 | 35.12 | 0.60 | 6.23 | 0.30 | 0.64 | 0.70 | 0.13 |
| **ZN704-6B C1** | Chr norite | 1.66 | 0.38 | 13.04 | 41.00 | 36.36 | 0.46 | 6.15 | 0.30 | 0.68 | 0.70 | 0.15 |
| **ZN704-6B C2** | Chr norite | 1.72 | 0.42 | 13.59 | 41.68 | 35.85 | 0.72 | 6.06 | 0.29 | 0.67 | 0.71 | 0.14 |
| **ZN704-6B C3** | Chr norite | 1.65 | 0.47 | 13.13 | 40.69 | 37.46 | 0.50 | 5.72 | 0.28 | 0.68 | 0.72 | 0.16 |
| **ZN704-6B C4** | Chr norite | 1.38 | 0.52 | 7.96 | 44.51 | 41.17 | 0.72 | 3.41 | 0.17 | 0.79 | 0.83 | 0.18 |
| **OY472-3B C10** | Chr pyroxenite | 1.10 | | 15.58 | 42.73 | 31.34 | | 8.43 | 0.40 | 0.65 | 0.60 | 0.12 |
| **OY472-3B C11** | Chr pyroxenite | 0.98 | 0.55 | 16.16 | 40.58 | 35.47 | 0.79 | 6.80 | 0.32 | 0.63 | 0.68 | 0.14 |
| **OY472-3B C12** | Chr pyroxenite | 1.30 | | 14.99 | 42.77 | 33.21 | 0.68 | 8.57 | 0.40 | 0.66 | 0.60 | 0.15 |
| **OY472-3B C13** | Chr pyroxenite | 1.09 | | 15.99 | 43.06 | 32.46 | | 8.50 | 0.40 | 0.64 | 0.60 | 0.13 |
| **OY472-3B C14** | Chr pyroxenite | 1.23 | | 15.22 | 40.32 | 36.11 | 0.72 | 6.71 | 0.32 | 0.64 | 0.68 | 0.16 |
| **OY472-3B C15** | Chr pyroxenite | 1.04 | | 16.60 | 37.21 | 36.73 | | 7.57 | 0.36 | 0.60 | 0.64 | 0.18 |
| **OY472-3B C16** | Chr pyroxenite | 1.27 | | 16.14 | 42.41 | 32.92 | | 8.62 | 0.40 | 0.64 | 0.60 | 0.13 |
| **OY472-3B C17** | Chr pyroxenite | 1.56 | | 15.34 | 42.98 | 33.47 | | 7.83 | 0.36 | 0.65 | 0.64 | 0.13 |
| **OY472-3B C18** | Chr pyroxenite | 0.72 | 0.49 | 16.51 | 40.50 | 35.77 | 0.87 | 6.63 | 0.32 | 0.62 | 0.68 | 0.15 |
| **OY472-3B C9** | Chr pyroxenite | 1.07 | 0.48 | 15.21 | 40.94 | 36.39 | 0.71 | 6.49 | 0.31 | 0.64 | 0.69 | 0.15 |
| **OY472-3B MC1** | Chr pyroxenite | 1.17 | | 15.36 | 42.89 | 32.52 | 0.83 | 8.21 | 0.39 | 0.65 | 0.61 | 0.14 |
| **OY472-3B MC2** | Chr pyroxenite | 1.13 | 0.52 | 14.66 | 43.15 | 33.70 | | 7.93 | 0.37 | 0.66 | 0.63 | 0.13 |
| **OY472-3B MC3** | Chr pyroxenite | 1.26 | | 15.03 | 42.59 | 33.27 | 0.76 | 8.11 | 0.39 | 0.66 | 0.61 | 0.14 |
| **OY472-3B MC4** | Chr pyroxenite | 1.05 | | 14.98 | 43.06 | 32.21 | 0.75 | 8.01 | 0.39 | 0.66 | 0.61 | 0.13 |
| **OY472-3B MC5** | Chr pyroxenite | 1.11 | 0.54 | 15.54 | 43.06 | 33.18 | 0.64 | 8.05 | 0.38 | 0.65 | 0.62 | 0.13 |
| **OY472-3B MC6** | Chr pyroxenite | 1.04 | 0.51 | 15.11 | 42.84 | 33.02 | | 8.09 | 0.38 | 0.66 | 0.62 | 0.13 |
| **OY472-3B MC7** | Chr pyroxenite | 1.22 | | 15.47 | 41.40 | 35.30 | | 6.64 | 0.32 | 0.64 | 0.68 | 0.14 |
| **OY472-3B MC8** | Chr pyroxenite | 1.24 | | 15.00 | 42.24 | 34.09 | 0.83 | 7.74 | 0.37 | 0.65 | 0.63 | 0.15 |
| **SS383-6B C1** | Chr pyroxenite | 1.28 | 0.47 | 14.96 | 41.33 | 34.24 | 0.48 | 7.22 | 0.34 | 0.65 | 0.66 | 0.14 |
| **SS383-6B C10** | Chr pyroxenite | 1.49 | | 13.77 | 41.57 | 35.52 | 0.63 | 6.67 | 0.32 | 0.67 | 0.68 | 0.15 |

| | | | | | | | | | | | | |
|---|---|---|---|---|---|---|---|---|---|---|---|---|
| **SS383-6B C2** | Chr pyroxenite | 1.78 | 0.56 | 10.39 | 43.84 | 36.60 | 0.56 | 6.10 | 0.30 | 0.74 | 0.70 | 0.16 |
| **SS383-6B C3** | Chr pyroxenite | 1.01 | 0.36 | 11.18 | 44.76 | 35.82 | | 5.96 | 0.29 | 0.73 | 0.71 | 0.15 |
| **SS383-6B C4** | Chr pyroxenite | 1.03 | 0.43 | 11.22 | 45.79 | 35.76 | 0.66 | 5.49 | 0.27 | 0.73 | 0.73 | 0.14 |
| **SS383-6B C5** | Chr pyroxenite | 1.11 | 0.31 | 14.83 | 42.16 | 34.47 | 0.52 | 7.35 | 0.35 | 0.66 | 0.65 | 0.14 |
| **SS383-6B C6** | Chr pyroxenite | 1.32 | 0.47 | 15.59 | 40.64 | 33.97 | | 7.13 | 0.34 | 0.64 | 0.66 | 0.13 |
| **SS383-6B C7** | Chr pyroxenite | 2.03 | 0.56 | 7.10 | 47.18 | 37.71 | 0.49 | 5.06 | 0.25 | 0.82 | 0.75 | 0.16 |
| **SS383-6B C8** | Chr pyroxenite | 1.61 | 0.42 | 11.89 | 43.88 | 34.52 | 0.76 | 6.29 | 0.31 | 0.71 | 0.69 | 0.14 |
| **SS383-6B C9** | Chr pyroxenite | 1.49 | 0.39 | 15.57 | 40.43 | 34.62 | | 7.01 | 0.33 | 0.64 | 0.67 | 0.13 |
| **SS393-3B C1** | Chr pyroxenite | 0.59 | 0.47 | 18.09 | 39.81 | 34.75 | 0.65 | 6.56 | 0.31 | 0.60 | 0.69 | 0.13 |
| **SS393-3B C10** | Chr pyroxenite | 0.78 | 0.45 | 16.91 | 39.24 | 36.09 | 0.91 | 5.92 | 0.29 | 0.61 | 0.71 | 0.14 |
| **SS393-3B C2** | Chr pyroxenite | 1.34 | 0.37 | 16.44 | 40.66 | 34.76 | 0.64 | 6.48 | 0.31 | 0.62 | 0.69 | 0.13 |
| **SS393-3B C3** | Chr pyroxenite | 1.73 | 0.57 | 16.11 | 39.11 | 33.74 | 0.67 | 7.61 | 0.36 | 0.62 | 0.64 | 0.14 |
| **SS393-3B C4** | Chr pyroxenite | 1.68 | 0.41 | 17.20 | 39.66 | 34.20 | 0.56 | 7.25 | 0.34 | 0.61 | 0.66 | 0.12 |
| **SS393-3B C5** | Chr pyroxenite | 1.25 | 0.37 | 17.60 | 40.27 | 32.68 | 0.53 | 7.74 | 0.36 | 0.61 | 0.64 | 0.12 |
| **SS393-3B C6** | Chr pyroxenite | 1.58 | 0.46 | 16.83 | 39.38 | 34.53 | 0.49 | 7.23 | 0.34 | 0.61 | 0.66 | 0.13 |
| **SS393-3B C7** | Chr pyroxenite | 1.43 | 0.37 | 16.87 | 39.27 | 34.94 | 0.63 | 7.02 | 0.33 | 0.61 | 0.67 | 0.14 |
| **SS393-3B C8** | Chr pyroxenite | 1.24 | 0.46 | 16.20 | 36.69 | 40.10 | 0.59 | 4.98 | 0.24 | 0.60 | 0.76 | 0.17 |
| **SS393-3B C9** | Chr pyroxenite | 0.39 | 0.35 | 17.28 | 39.96 | 36.60 | 0.64 | 5.49 | 0.27 | 0.61 | 0.73 | 0.14 |
| **ZN230-5B C1** | Chr pyroxenite | 2.47 | 0.44 | 12.80 | 41.16 | 39.52 | 0.50 | 3.87 | 0.18 | 0.68 | 0.82 | 0.14 |
| **ZN230-5B C10** | Chr pyroxenite | 1.13 | 0.37 | 16.12 | 41.88 | 34.67 | 0.56 | 5.43 | 0.26 | 0.64 | 0.74 | 0.11 |
| **ZN230-5B C2** | Chr pyroxenite | 2.74 | 0.45 | 12.09 | 39.72 | 41.74 | 0.63 | 3.24 | 0.15 | 0.69 | 0.85 | 0.16 |
| **ZN230-5B C3** | Chr pyroxenite | 2.88 | 0.52 | 12.52 | 39.55 | 40.46 | 0.64 | 3.68 | 0.17 | 0.68 | 0.83 | 0.15 |
| **ZN230-5B C4** | Chr pyroxenite | 2.20 | 0.50 | 12.91 | 40.41 | 38.64 | 0.45 | 4.28 | 0.21 | 0.68 | 0.79 | 0.14 |
| **ZN230-5B C5** | Chr pyroxenite | 2.26 | 0.56 | 12.63 | 40.43 | 39.40 | 0.64 | 4.11 | 0.20 | 0.68 | 0.80 | 0.15 |
| **ZN230-5B C6** | Chr pyroxenite | 2.48 | 0.46 | 11.94 | 40.55 | 39.70 | 0.49 | 4.51 | 0.22 | 0.69 | 0.78 | 0.16 |
| **ZN230-5B C7** | Chr pyroxenite | 2.30 | 0.00 | 13.24 | 40.97 | 38.22 | 0.56 | 4.25 | 0.21 | 0.67 | 0.79 | 0.14 |
| **ZN230-5B C8** | Chr pyroxenite | 1.31 | 0.42 | 16.04 | 41.47 | 34.97 | 0.51 | 5.50 | 0.26 | 0.63 | 0.74 | 0.11 |
| **ZN230-5B C9** | Chr pyroxenite | 1.41 | 0.33 | 14.79 | 41.21 | 36.28 | 0.64 | 5.04 | 0.25 | 0.65 | 0.75 | 0.13 |
| **ZN278-1 C1** | Chr pyroxenite | 0.80 | 0.35 | 20.61 | 40.57 | 30.95 | 0.60 | 7.58 | 0.35 | 0.57 | 0.65 | 0.09 |
| **ZN278-1 C10** | Chr pyroxenite | 1.31 | 0.53 | 17.02 | 41.90 | 32.09 | 0.00 | 6.06 | 0.29 | 0.62 | 0.71 | 0.08 |
| **ZN278-1 C2** | Chr pyroxenite | 1.15 | 0.00 | 19.50 | 40.35 | 31.43 | 0.52 | 7.46 | 0.35 | 0.58 | 0.65 | 0.10 |
| **ZN278-1 C3** | Chr pyroxenite | 0.95 | 0.00 | 17.70 | 40.09 | 33.00 | 0.60 | 7.09 | 0.34 | 0.60 | 0.66 | 0.12 |
| **ZN278-1 C4** | Chr pyroxenite | 0.84 | 0.31 | 18.73 | 40.00 | 32.67 | 0.00 | 7.24 | 0.34 | 0.59 | 0.66 | 0.11 |
| **ZN278-1 C5** | Chr pyroxenite | 0.96 | 0.00 | 20.51 | 39.20 | 31.56 | 0.55 | 7.27 | 0.34 | 0.56 | 0.66 | 0.09 |
| **ZN278-1 C6** | Chr pyroxenite | 1.17 | 0.45 | 18.40 | 39.36 | 32.58 | 0.50 | 7.09 | 0.34 | 0.59 | 0.66 | 0.11 |
| **ZN278-1 C7** | Chr pyroxenite | 0.87 | 0.44 | 19.14 | 41.89 | 30.11 | 0.56 | 7.27 | 0.34 | 0.59 | 0.66 | 0.08 |

| | | | | | | | | | | | | |
|---|---|---|---|---|---|---|---|---|---|---|---|---|
| **ZN278-1 C8** | Chr pyroxenite | 1.15 | 0.40 | 18.74 | 42.42 | 29.76 | 0.49 | 7.53 | 0.35 | 0.60 | 0.65 | 0.07 |
| **ZN278-1 C9** | Chr pyroxenite | 1.16 | 0.00 | 17.82 | 42.21 | 33.18 | 0.50 | 5.76 | 0.28 | 0.61 | 0.72 | 0.09 |
| **ZN278-3 C10** | Chr pyroxenite | 2.10 | 0.46 | 9.15 | 34.48 | 49.05 | 0.68 | 3.45 | 0.17 | 0.72 | 0.83 | 0.30 |
| **ZN278-3 C2** | Chr pyroxenite | 1.89 | 0.42 | 10.07 | 36.65 | 45.13 | 0.68 | 3.71 | 0.18 | 0.71 | 0.82 | 0.25 |
| **ZN278-3 C3** | Chr pyroxenite | 1.19 | 0.32 | 12.40 | 38.18 | 40.87 | 0.53 | 5.93 | 0.29 | 0.67 | 0.71 | 0.22 |
| **ZN278-3 C4** | Chr pyroxenite | 1.45 | 0.34 | 11.77 | 40.51 | 39.75 | 0.53 | 6.21 | 0.30 | 0.70 | 0.70 | 0.20 |
| **ZN278-3 C5** | Chr pyroxenite | 1.81 | 0.43 | 11.29 | 39.84 | 40.25 | 0.64 | 5.97 | 0.29 | 0.70 | 0.71 | 0.21 |
| **ZN278-3 C6** | Chr pyroxenite | 1.93 | 0.42 | 10.84 | 39.92 | 41.68 | 0.61 | 5.31 | 0.26 | 0.71 | 0.74 | 0.21 |
| **ZN278-3 C7** | Chr pyroxenite | 1.79 | 0.48 | 11.58 | 39.22 | 40.79 | 0.56 | 5.93 | 0.28 | 0.69 | 0.72 | 0.21 |
| **ZN278-3 C8** | Chr pyroxenite | 1.42 | 0.36 | 13.93 | 38.48 | 39.37 | 0.49 | 6.35 | 0.30 | 0.65 | 0.70 | 0.19 |
| **ZN278-3 C9** | Chr pyroxenite | 2.05 | 0.00 | 12.05 | 39.78 | 41.17 | 0.54 | 5.23 | 0.25 | 0.69 | 0.75 | 0.20 |
| **ZN278-3 MC1** | Chr pyroxenite | 2.15 | 0.46 | 10.35 | 37.06 | 43.13 | 0.60 | 4.99 | 0.24 | 0.71 | 0.76 | 0.24 |
| **OY252-1A C1** | Chromitite | 0.61 | | 18.04 | 36.39 | 34.61 | 0.80 | 9.78 | 0.46 | 0.57 | 0.54 | 0.20 |
| **OY252-1A C10** | Chromitite | 0.50 | 0.31 | 16.59 | 37.32 | 34.82 | 0.75 | 9.02 | 0.44 | 0.60 | 0.56 | 0.19 |
| **OY252-1A C2** | Chromitite | 0.74 | | 20.31 | 33.92 | 33.97 | 0.80 | 10.14 | 0.48 | 0.53 | 0.52 | 0.19 |
| **OY252-1A C3** | Chromitite | 0.72 | | 23.65 | 30.29 | 34.44 | 0.85 | 10.96 | 0.50 | 0.46 | 0.50 | 0.20 |
| **OY252-1A C4** | Chromitite | 0.70 | | 19.31 | 34.74 | 34.50 | 0.59 | 9.79 | 0.46 | 0.55 | 0.54 | 0.19 |
| **OY252-1A C5** | Chromitite | 0.65 | | 21.83 | 31.61 | 35.55 | 0.96 | 9.96 | 0.47 | 0.49 | 0.53 | 0.20 |
| **OY252-1A C6** | Chromitite | 0.81 | | 21.60 | 32.04 | 34.62 | 0.84 | 10.37 | 0.48 | 0.50 | 0.52 | 0.20 |
| **OY252-1A C7** | Chromitite | 0.71 | | 20.97 | 31.82 | 35.89 | 0.82 | 10.18 | 0.48 | 0.50 | 0.52 | 0.21 |
| **OY252-1A C8** | Chromitite | 0.77 | | 16.62 | 38.64 | 34.26 | 0.85 | 8.94 | 0.43 | 0.61 | 0.57 | 0.18 |
| **OY252-1A C9** | Chromitite | 0.76 | | 17.97 | 36.66 | 34.46 | 0.77 | 9.35 | 0.45 | 0.58 | 0.55 | 0.19 |
| **OY359-1A C1** | Chromitite | 1.24 | | 23.11 | 32.32 | 33.13 | 0.53 | 9.78 | 0.45 | 0.48 | 0.55 | 0.15 |
| **OY359-1A C10** | Chromitite | 1.27 | | 24.99 | 31.93 | 31.97 | 0.81 | 9.99 | 0.45 | 0.46 | 0.55 | 0.14 |
| **OY359-1A C2** | Chromitite | 1.25 | | 21.75 | 33.83 | 33.46 | 0.70 | 9.07 | 0.42 | 0.51 | 0.58 | 0.15 |
| **OY359-1A C3** | Chromitite | 1.10 | | 22.55 | 33.10 | 33.31 | 0.46 | 10.12 | 0.46 | 0.50 | 0.54 | 0.16 |
| **OY359-1A C4** | Chromitite | 0.93 | | 20.65 | 36.68 | 31.51 | 0.70 | 9.34 | 0.44 | 0.54 | 0.56 | 0.14 |
| **OY359-1A C5** | Chromitite | 1.02 | 0.27 | 22.65 | 33.51 | 33.05 | 0.53 | 9.34 | 0.43 | 0.50 | 0.57 | 0.15 |
| **OY359-1A C6** | Chromitite | 0.86 | | 18.09 | 39.14 | 32.99 | 0.65 | 8.72 | 0.41 | 0.59 | 0.59 | 0.15 |
| **OY359-1A C7** | Chromitite | 1.37 | | 22.23 | 33.38 | 33.44 | 0.59 | 9.04 | 0.42 | 0.50 | 0.58 | 0.15 |
| **OY359-1A C8** | Chromitite | 1.12 | 0.34 | 24.38 | 32.19 | 32.63 | 0.62 | 9.89 | 0.45 | 0.47 | 0.55 | 0.14 |
| **OY359-1A C9** | Chromitite | 1.08 | | 22.25 | 33.18 | 33.33 | 0.65 | 9.07 | 0.42 | 0.50 | 0.58 | 0.15 |
| **OY392-1 C1** | Chromitite | 0.96 | | 18.53 | 40.27 | 30.49 | 0.67 | 9.43 | 0.44 | 0.59 | 0.56 | 0.13 |
| **OY392-1 C10** | Chromitite | 0.82 | | 19.31 | 40.58 | 29.85 | 0.56 | 9.74 | 0.45 | 0.58 | 0.55 | 0.12 |
| **OY392-1 C2** | Chromitite | 0.89 | | 18.65 | 40.94 | 29.52 | 0.48 | 9.74 | 0.46 | 0.60 | 0.54 | 0.12 |
| **OY392-1 C3** | Chromitite | 0.90 | | 18.42 | 40.58 | 30.32 | 0.44 | 9.46 | 0.44 | 0.60 | 0.56 | 0.13 |

| | | | | | | | | | | | | |
|---|---|---|---|---|---|---|---|---|---|---|---|---|
| **OY392-1 C4** | Chromitite | 0.75 | 0.38 | 18.27 | 40.86 | 30.31 | 0.50 | 9.18 | 0.43 | 0.60 | 0.57 | 0.12 |
| **OY392-1 C5** | Chromitite | 0.84 | | 18.25 | 39.77 | 30.83 | 0.57 | 9.10 | 0.43 | 0.59 | 0.57 | 0.13 |
| **OY392-1 C6** | Chromitite | 0.79 | | 18.44 | 40.53 | 29.76 | | 9.16 | 0.43 | 0.60 | 0.57 | 0.11 |
| **OY392-1 C7** | Chromitite | 0.85 | | 18.57 | 41.34 | 29.51 | 0.60 | 9.43 | 0.44 | 0.60 | 0.56 | 0.12 |
| **OY392-1 C8** | Chromitite | 0.83 | | 19.26 | 41.41 | 29.72 | 0.48 | 9.48 | 0.44 | 0.59 | 0.56 | 0.11 |
| **OY392-1 C9** | Chromitite | 0.76 | | 18.23 | 40.42 | 30.50 | 0.43 | 9.78 | 0.46 | 0.60 | 0.54 | 0.14 |
| **ZN309-2 C1** | Chromitite | 1.04 | 0.34 | 16.86 | 42.33 | 30.41 | 0.52 | 8.62 | 0.41 | 0.63 | 0.59 | 0.11 |
| **ZN309-2 C10** | Chromitite | 0.84 | 0.50 | 17.16 | 40.72 | 31.64 | 0.00 | 8.24 | 0.39 | 0.61 | 0.61 | 0.12 |
| **ZN309-2 C2** | Chromitite | 0.92 | 0.35 | 16.53 | 42.46 | 30.45 | 0.53 | 8.06 | 0.39 | 0.63 | 0.61 | 0.11 |
| **ZN309-2 C3** | Chromitite | 1.03 | 0.34 | 16.93 | 43.50 | 30.78 | 0.00 | 8.26 | 0.38 | 0.63 | 0.62 | 0.10 |
| **ZN309-2 C4** | Chromitite | 0.92 | 0.54 | 16.43 | 43.19 | 30.20 | 0.65 | 8.26 | 0.39 | 0.64 | 0.61 | 0.10 |
| **ZN309-2 C6** | Chromitite | 1.01 | 0.49 | 15.80 | 41.58 | 32.10 | 0.58 | 7.77 | 0.37 | 0.64 | 0.63 | 0.13 |
| **ZN309-2 C7** | Chromitite | 0.86 | 0.41 | 16.67 | 41.60 | 32.09 | 0.00 | 8.24 | 0.39 | 0.63 | 0.61 | 0.12 |
| **ZN309-2 C8** | Chromitite | 0.95 | 0.33 | 16.27 | 42.16 | 32.78 | 0.00 | 8.03 | 0.38 | 0.63 | 0.62 | 0.13 |
| **ZN309-2 C9** | Chromitite | 0.90 | 0.36 | 15.93 | 43.05 | 31.33 | 0.00 | 8.09 | 0.38 | 0.64 | 0.62 | 0.11 |
| **ZN309-2 MC5** | Chromitite | 0.94 | 0.39 | 15.81 | 42.38 | 31.40 | 0.54 | 7.94 | 0.38 | 0.64 | 0.62 | 0.12 |
| **ZN324-1 C1** | Chromitite | 0.80 | 0.40 | 17.58 | 42.60 | 29.65 | 0.63 | 9.08 | 0.43 | 0.62 | 0.57 | 0.11 |
| **ZN324-1 C10** | Chromitite | 0.74 | 0.00 | 17.08 | 42.92 | 29.90 | 0.57 | 8.95 | 0.43 | 0.63 | 0.57 | 0.12 |
| **ZN324-1 C2** | Chromitite | 0.83 | 0.43 | 17.75 | 42.60 | 29.03 | 0.00 | 9.36 | 0.43 | 0.62 | 0.57 | 0.10 |
| **ZN324-1 C4** | Chromitite | 0.89 | 0.00 | 17.49 | 42.14 | 29.35 | 0.54 | 9.41 | 0.45 | 0.62 | 0.55 | 0.12 |
| **ZN324-1 C5** | Chromitite | 0.52 | 0.37 | 17.35 | 43.14 | 28.77 | 0.00 | 8.95 | 0.42 | 0.63 | 0.58 | 0.10 |
| **ZN324-1 C6** | Chromitite | 0.73 | 0.32 | 17.08 | 42.47 | 29.13 | 0.51 | 9.02 | 0.43 | 0.63 | 0.57 | 0.11 |
| **ZN324-1 C7** | Chromitite | 0.89 | 0.00 | 17.48 | 42.79 | 30.02 | 0.67 | 9.09 | 0.43 | 0.62 | 0.57 | 0.12 |
| **ZN324-1 C8** | Chromitite | 0.85 | 0.49 | 17.95 | 41.23 | 29.49 | 0.00 | 9.08 | 0.42 | 0.61 | 0.58 | 0.11 |
| **ZN324-1 C9** | Chromitite | 0.76 | 0.37 | 17.49 | 42.18 | 29.56 | 0.66 | 9.13 | 0.43 | 0.62 | 0.57 | 0.11 |
| **ZN324-1 MC3** | Chromitite | 0.82 | 0.34 | 17.42 | 41.87 | 29.08 | 0.59 | 9.15 | 0.44 | 0.62 | 0.56 | 0.11 |
| **ZN324-2 C1** | Chromitite | 1.07 | 0.46 | 17.35 | 42.52 | 30.47 | 0.00 | 8.90 | 0.41 | 0.62 | 0.59 | 0.11 |
| **ZN324-2 C10** | Chromitite | 1.03 | 0.36 | 16.88 | 42.31 | 30.81 | 0.55 | 8.78 | 0.41 | 0.63 | 0.59 | 0.12 |
| **ZN324-2 C2** | Chromitite | 0.85 | 0.36 | 17.47 | 41.68 | 30.39 | 0.00 | 8.93 | 0.42 | 0.62 | 0.58 | 0.11 |
| **ZN324-2 C3** | Chromitite | 0.95 | 0.32 | 17.15 | 41.47 | 30.39 | 0.00 | 8.86 | 0.42 | 0.62 | 0.58 | 0.11 |
| **ZN324-2 C4** | Chromitite | 0.91 | 0.39 | 16.88 | 41.27 | 30.66 | 0.55 | 8.58 | 0.41 | 0.62 | 0.59 | 0.12 |
| **ZN324-2 C5** | Chromitite | 1.16 | 0.00 | 16.68 | 42.73 | 31.15 | 0.00 | 8.80 | 0.41 | 0.63 | 0.59 | 0.12 |
| **ZN324-2 C6** | Chromitite | 1.00 | 0.34 | 16.59 | 43.13 | 31.38 | 0.00 | 8.72 | 0.40 | 0.64 | 0.60 | 0.12 |
| **ZN324-2 C7** | Chromitite | 0.87 | 0.00 | 16.53 | 42.79 | 30.68 | 0.00 | 8.64 | 0.41 | 0.63 | 0.59 | 0.12 |
| **ZN324-2 C8** | Chromitite | 1.12 | 0.32 | 16.93 | 40.87 | 30.70 | 0.70 | 8.63 | 0.41 | 0.62 | 0.59 | 0.12 |
| **ZN324-2 MC9** | Chromitite | 1.06 | 0.32 | 16.30 | 41.99 | 31.60 | 0.43 | 8.29 | 0.39 | 0.63 | 0.61 | 0.12 |

| | | | | | | | | | | | | |
|---|---|---|---|---|---|---|---|---|---|---|---|---|
| **ZN334-2A MC1** | Chromitite | 1.72 | 0.22 | 16.35 | 39.75 | 34.32 | 0.30 | 7.61 | 0.35 | 0.62 | 0.65 | 0.14 |
| **ZN334-2A MC10** | Chromitite | 1.68 | 0.45 | 13.36 | 41.18 | 36.65 | 0.61 | 5.89 | 0.28 | 0.67 | 0.72 | 0.15 |
| **ZN334-2A MC11** | Chromitite | 1.51 | 0.50 | 10.55 | 42.60 | 39.32 | 0.61 | 4.56 | 0.23 | 0.73 | 0.77 | 0.17 |
| **ZN334-2A MC12** | Chromitite | 1.08 | 0.33 | 14.44 | 44.80 | 31.93 | 0.56 | 6.53 | 0.32 | 0.68 | 0.68 | 0.10 |
| **ZN334-2A MC13** | Chromitite | 1.83 | 0.44 | 12.19 | 42.53 | 37.47 | 0.59 | 5.32 | 0.26 | 0.70 | 0.74 | 0.15 |
| **ZN334-2A MC2** | Chromitite | 1.06 | 0.00 | 13.79 | 45.69 | 32.48 | 0.52 | 6.56 | 0.32 | 0.69 | 0.68 | 0.11 |
| **ZN334-2A MC4** | Chromitite | 1.20 | 0.40 | 14.59 | 44.31 | 31.90 | 0.56 | 6.48 | 0.31 | 0.67 | 0.69 | 0.10 |
| **ZN334-2A MC5** | Chromitite | 0.92 | 0.26 | 14.50 | 44.43 | 32.61 | 0.61 | 6.04 | 0.30 | 0.67 | 0.70 | 0.10 |
| **ZN334-2A MC6** | Chromitite | 2.20 | 0.49 | 12.71 | 40.47 | 38.00 | 0.56 | 6.19 | 0.29 | 0.68 | 0.71 | 0.17 |
| **ZN334-2A MC7** | Chromitite | 2.06 | 0.43 | 12.24 | 41.55 | 38.03 | 0.69 | 5.29 | 0.25 | 0.69 | 0.75 | 0.16 |
| **ZN334-2A MC8** | Chromitite | 2.10 | 0.46 | 10.65 | 42.92 | 39.07 | 0.57 | 4.60 | 0.22 | 0.73 | 0.78 | 0.16 |
| **ZN334-2A MC9** | Chromitite | 1.85 | 0.42 | 13.45 | 41.13 | 36.61 | 0.51 | 6.05 | 0.29 | 0.67 | 0.71 | 0.15 |
| **ZN573-1A C1** | Chromitite | 1.76 | 0.52 | 17.49 | 35.39 | 36.45 | 0.62 | 7.11 | 0.33 | 0.58 | 0.67 | 0.16 |
| **ZN573-1A C10** | Chromitite | 1.53 | 0.55 | 17.94 | 36.74 | 35.45 | 0.70 | 7.04 | 0.33 | 0.58 | 0.67 | 0.14 |
| **ZN573-1A C2** | Chromitite | 1.71 | 0.57 | 18.03 | 36.24 | 36.16 | 0.47 | 7.47 | 0.34 | 0.57 | 0.66 | 0.15 |
| **ZN573-1A C3** | Chromitite | 1.69 | 0.37 | 17.81 | 35.97 | 36.00 | 0.71 | 7.53 | 0.35 | 0.58 | 0.65 | 0.16 |
| **ZN573-1A C4** | Chromitite | 1.69 | 0.46 | 17.96 | 36.49 | 36.81 | 0.65 | 7.09 | 0.33 | 0.58 | 0.67 | 0.16 |
| **ZN573-1A C5** | Chromitite | 1.61 | 0.62 | 17.59 | 36.59 | 36.12 | 0.46 | 6.82 | 0.32 | 0.58 | 0.68 | 0.15 |
| **ZN573-1A C6** | Chromitite | 1.73 | 0.51 | 17.80 | 36.52 | 36.03 | 0.60 | 7.23 | 0.34 | 0.58 | 0.66 | 0.15 |
| **ZN573-1A C7** | Chromitite | 1.58 | 0.45 | 16.73 | 38.07 | 34.77 | 0.60 | 7.08 | 0.34 | 0.60 | 0.66 | 0.14 |
| **ZN573-1A C8** | Chromitite | 1.80 | 0.47 | 18.17 | 37.11 | 34.88 | 0.49 | 7.41 | 0.34 | 0.58 | 0.66 | 0.14 |
| **ZN573-1A C9** | Chromitite | 1.65 | 0.47 | 17.92 | 36.56 | 35.63 | 0.55 | 6.96 | 0.33 | 0.58 | 0.67 | 0.14 |
| **ZN573-3A (1) C1** | Chromitite | 0.72 | 0.00 | 23.31 | 41.59 | 23.84 | 0.00 | 11.44 | 0.51 | 0.54 | 0.49 | 0.06 |
| **ZN573-3A (1) C10** | Chromitite | 0.58 | 0.00 | 23.97 | 40.71 | 22.95 | 0.00 | 11.86 | 0.54 | 0.53 | 0.46 | 0.06 |
| **ZN573-3A (1) C2** | Chromitite | 0.62 | 0.00 | 22.98 | 40.51 | 23.47 | 0.57 | 11.51 | 0.53 | 0.54 | 0.47 | 0.07 |
| **ZN573-3A (1) C3** | Chromitite | 0.60 | 0.00 | 23.22 | 40.40 | 22.96 | 0.48 | 11.95 | 0.55 | 0.54 | 0.45 | 0.07 |
| **ZN573-3A (1) C4** | Chromitite | 0.62 | 0.00 | 23.25 | 41.35 | 23.38 | 0.00 | 11.11 | 0.51 | 0.54 | 0.49 | 0.05 |
| **ZN573-3A (1) C5** | Chromitite | 0.49 | 0.00 | 24.14 | 41.62 | 22.24 | 0.54 | 11.97 | 0.54 | 0.54 | 0.46 | 0.06 |
| **ZN573-3A (1) C6** | Chromitite | 0.56 | 0.00 | 24.23 | 41.11 | 22.20 | 0.00 | 12.09 | 0.54 | 0.53 | 0.46 | 0.05 |
| **ZN573-3A (1) C7** | Chromitite | 0.63 | 0.00 | 23.91 | 40.77 | 22.58 | 0.00 | 12.18 | 0.55 | 0.53 | 0.45 | 0.06 |
| **ZN573-3A (1) C8** | Chromitite | 0.47 | 0.00 | 23.76 | 40.70 | 22.54 | 0.00 | 12.17 | 0.55 | 0.53 | 0.45 | 0.06 |
| **ZN573-3A (1) C9** | Chromitite | 0.51 | 0.00 | 24.39 | 40.69 | 22.30 | 0.00 | 12.42 | 0.56 | 0.53 | 0.44 | 0.06 |
| **ZN573-3A (2) C1** | Chromitite | 0.66 | 0.00 | 22.78 | 41.32 | 23.92 | 0.00 | 11.08 | 0.51 | 0.55 | 0.49 | 0.06 |
| **ZN573-3A (2) C10** | Chromitite | 0.65 | 0.00 | 23.24 | 40.85 | 22.51 | 0.00 | 11.62 | 0.53 | 0.54 | 0.47 | 0.06 |
| **ZN573-3A (2) C2** | Chromitite | 0.61 | 0.00 | 22.99 | 41.12 | 23.59 | 0.65 | 10.84 | 0.50 | 0.55 | 0.50 | 0.06 |
| **ZN573-3A (2) C3** | Chromitite | 0.64 | 0.00 | 23.01 | 41.76 | 23.32 | 0.53 | 11.28 | 0.52 | 0.55 | 0.48 | 0.06 |

| | | | | | | | | | | | | |
|---|---|---|---|---|---|---|---|---|---|---|---|---|
| **ZN573-3A (2) C4** | Chromitite | 0.58 | 0.00 | 23.14 | 41.05 | 23.15 | 0.62 | 11.16 | 0.52 | 0.54 | 0.48 | 0.06 |
| **ZN573-3A (2) C5** | Chromitite | 0.61 | 0.00 | 23.28 | 41.69 | 23.37 | 0.00 | 11.55 | 0.52 | 0.55 | 0.48 | 0.06 |
| **ZN573-3A (2) C6** | Chromitite | 0.44 | 0.00 | 23.40 | 41.60 | 22.67 | 0.49 | 11.02 | 0.51 | 0.54 | 0.49 | 0.05 |
| **ZN573-3A (2) C7** | Chromitite | 0.59 | 0.00 | 22.81 | 40.90 | 22.94 | 0.52 | 11.26 | 0.52 | 0.55 | 0.48 | 0.06 |
| **ZN573-3A (2) C8** | Chromitite | 0.58 | 0.00 | 23.60 | 40.96 | 22.78 | 0.60 | 11.54 | 0.53 | 0.54 | 0.47 | 0.06 |
| **ZN573-3A (2) C9** | Chromitite | 0.60 | 0.00 | 24.09 | 41.10 | 22.84 | 0.56 | 11.82 | 0.54 | 0.53 | 0.46 | 0.06 |
| **ZN573-4A C1** | Chromitite | 0.87 | 0.00 | 20.52 | 40.20 | 27.95 | 0.56 | 9.64 | 0.45 | 0.57 | 0.55 | 0.10 |
| **ZN573-4A C10** | Chromitite | 0.87 | 0.36 | 20.33 | 40.43 | 27.30 | 0.50 | 9.96 | 0.46 | 0.57 | 0.54 | 0.09 |
| **ZN573-4A C2** | Chromitite | 0.81 | 0.00 | 20.43 | 40.79 | 28.07 | 0.62 | 9.74 | 0.46 | 0.57 | 0.54 | 0.10 |
| **ZN573-4A C3** | Chromitite | 0.79 | 0.00 | 20.72 | 40.52 | 28.58 | 0.78 | 9.59 | 0.45 | 0.57 | 0.55 | 0.10 |
| **ZN573-4A C4** | Chromitite | 0.98 | 0.00 | 19.55 | 40.93 | 27.75 | 0.52 | 9.35 | 0.44 | 0.58 | 0.56 | 0.09 |
| **ZN573-4A C5** | Chromitite | 0.89 | 0.00 | 20.60 | 40.70 | 27.94 | 0.58 | 9.83 | 0.46 | 0.57 | 0.54 | 0.10 |
| **ZN573-4A C6** | Chromitite | 0.81 | 0.00 | 20.16 | 40.59 | 27.75 | | 9.64 | 0.45 | 0.57 | 0.55 | 0.09 |
| **ZN573-4A C7** | Chromitite | 0.86 | 0.00 | 20.63 | 41.23 | 28.15 | 0.64 | 9.58 | 0.45 | 0.57 | 0.55 | 0.09 |
| **ZN573-4A C8** | Chromitite | 0.88 | 0.00 | 19.78 | 41.88 | 28.64 | 0.56 | 9.63 | 0.45 | 0.59 | 0.55 | 0.10 |
| **ZN573-4A C9** | Chromitite | 1.01 | 0.00 | 20.07 | 41.50 | 28.56 | 0.63 | 9.69 | 0.45 | 0.58 | 0.55 | 0.10 |
| **ZN573-5A C1** | Chromitite | 1.15 | 0.33 | 17.59 | 38.46 | 36.25 | 0.00 | 6.16 | 0.29 | 0.59 | 0.71 | 0.13 |
| **ZN573-5A C10** | Chromitite | 1.63 | 0.54 | 16.26 | 34.38 | 39.84 | 0.60 | 4.73 | 0.23 | 0.59 | 0.77 | 0.17 |
| **ZN573-5A C2** | Chromitite | 1.06 | 0.38 | 18.31 | 37.34 | 36.30 | 0.56 | 6.40 | 0.30 | 0.58 | 0.70 | 0.14 |
| **ZN573-5A C3** | Chromitite | 1.43 | 0.42 | 18.06 | 37.22 | 36.66 | 0.00 | 6.54 | 0.30 | 0.58 | 0.70 | 0.14 |
| **ZN573-5A C4** | Chromitite | 1.46 | 0.33 | 16.41 | 36.96 | 38.09 | 0.00 | 6.02 | 0.28 | 0.60 | 0.72 | 0.16 |
| **ZN573-5A C5** | Chromitite | 1.20 | 0.50 | 16.48 | 36.95 | 37.97 | 0.56 | 6.04 | 0.29 | 0.60 | 0.71 | 0.17 |
| **ZN573-5A C6** | Chromitite | 1.25 | 0.35 | 16.80 | 36.10 | 41.01 | 0.92 | 3.18 | 0.16 | 0.59 | 0.84 | 0.16 |
| **ZN573-5A C7** | Chromitite | 1.22 | 0.50 | 16.89 | 36.88 | 38.03 | 0.64 | 6.00 | 0.29 | 0.59 | 0.71 | 0.16 |
| **ZN573-5A C8** | Chromitite | 1.15 | 0.44 | 18.07 | 36.59 | 36.49 | 0.60 | 6.42 | 0.31 | 0.58 | 0.69 | 0.15 |
| **ZN573-5A C9** | Chromitite | 1.30 | 0.47 | 17.11 | 36.37 | 38.01 | 0.70 | 5.60 | 0.27 | 0.59 | 0.73 | 0.16 |
| **ZN704-2B C1** | Chromitite | 0.87 | 0.35 | 17.14 | 41.55 | 33.08 | 0.67 | 5.82 | 0.28 | 0.62 | 0.72 | 0.10 |
| **ZN704-2B C10** | Chromitite | 0.93 | 0.00 | 15.88 | 40.89 | 38.41 | 1.05 | 3.06 | 0.15 | 0.63 | 0.85 | 0.12 |
| **ZN704-2B C2** | Chromitite | 0.65 | 0.00 | 15.82 | 40.98 | 35.92 | 1.03 | 5.58 | 0.28 | 0.63 | 0.72 | 0.14 |
| **ZN704-2B C3** | Chromitite | 0.69 | 0.32 | 16.18 | 42.36 | 35.03 | 0.97 | 5.76 | 0.28 | 0.64 | 0.72 | 0.12 |
| **ZN704-2B C4** | Chromitite | 0.84 | 0.34 | 16.60 | 41.56 | 35.08 | 0.97 | 4.73 | 0.23 | 0.63 | 0.77 | 0.11 |
| **ZN704-2B C5** | Chromitite | 1.11 | 0.00 | 16.59 | 41.17 | 34.32 | 0.93 | 5.60 | 0.28 | 0.62 | 0.72 | 0.11 |
| **ZN704-2B C6** | Chromitite | 0.98 | 0.35 | 16.76 | 40.90 | 34.62 | 1.03 | 5.47 | 0.27 | 0.62 | 0.73 | 0.11 |
| **ZN704-2B C7** | Chromitite | 0.92 | 0.28 | 16.52 | 41.38 | 35.30 | 1.11 | 4.77 | 0.24 | 0.63 | 0.76 | 0.11 |
| **ZN704-2B C8** | Chromitite | 0.88 | 0.31 | 16.27 | 40.61 | 36.58 | 0.87 | 3.65 | 0.18 | 0.63 | 0.82 | 0.11 |
| **ZN704-2B C9** | Chromitite | 0.34 | 0.35 | 15.37 | 39.71 | 39.32 | 1.12 | 2.91 | 0.15 | 0.63 | 0.85 | 0.14 |

| | | | | | | | | | | | | |
|---|---|---|---|---|---|---|---|---|---|---|---|---|
| **ZN704-3C C1** | Chromitite | 1.60 | 0.00 | 16.78 | 40.00 | 32.94 | 0.60 | 7.75 | 0.37 | 0.62 | 0.63 | 0.13 |
| **ZN704-3C C10** | Chromitite | 1.82 | 0.45 | 16.48 | 39.13 | 34.44 | 0.00 | 7.85 | 0.36 | 0.61 | 0.64 | 0.14 |
| **ZN704-3C C11** | Chromitite | 1.85 | 0.35 | 16.51 | 39.12 | 34.29 | 0.00 | 8.03 | 0.37 | 0.61 | 0.63 | 0.14 |
| **ZN704-3C C2** | Chromitite | 1.76 | 0.36 | 16.41 | 39.72 | 33.05 | 0.00 | 8.04 | 0.37 | 0.62 | 0.63 | 0.13 |
| **ZN704-3C C3** | Chromitite | 1.61 | 0.38 | 16.69 | 40.25 | 33.81 | 0.00 | 8.05 | 0.37 | 0.62 | 0.63 | 0.13 |
| **ZN704-3C C4** | Chromitite | 1.65 | 0.34 | 16.51 | 39.84 | 33.23 | 0.56 | 8.19 | 0.38 | 0.62 | 0.62 | 0.14 |
| **ZN704-3C C5** | Chromitite | 1.75 | 0.00 | 15.95 | 40.54 | 33.77 | 0.00 | 7.77 | 0.36 | 0.63 | 0.64 | 0.13 |
| **ZN704-3C C6** | Chromitite | 1.91 | 0.49 | 16.09 | 38.94 | 34.13 | 0.46 | 8.04 | 0.37 | 0.62 | 0.63 | 0.14 |
| **ZN704-3C C7** | Chromitite | 1.82 | 0.00 | 16.19 | 38.99 | 34.16 | 0.45 | 8.10 | 0.38 | 0.62 | 0.62 | 0.15 |
| **ZN704-3C C8** | Chromitite | 1.62 | 0.00 | 16.23 | 40.36 | 34.20 | 0.59 | 7.38 | 0.35 | 0.63 | 0.65 | 0.14 |
| **ZN704-3C C9** | Chromitite | 1.75 | 0.36 | 16.24 | 40.16 | 34.29 | 0.58 | 7.62 | 0.35 | 0.62 | 0.65 | 0.14 |
| **ZN704-4B C1** | Chromitite | 1.06 | 0.00 | 13.79 | 45.69 | 32.48 | 0.52 | 6.56 | 0.32 | 0.69 | 0.68 | 0.11 |
| **ZN704-4B C10** | Chromitite | 1.18 | 0.51 | 14.18 | 45.04 | 32.39 | 0.59 | 6.24 | 0.30 | 0.68 | 0.70 | 0.10 |
| **ZN704-4B C11** | Chromitite | 0.46 | 0.35 | 14.61 | 45.80 | 32.62 | 0.46 | 5.95 | 0.29 | 0.68 | 0.71 | 0.10 |
| **ZN704-4B C2** | Chromitite | 0.85 | 0.39 | 13.57 | 46.30 | 31.11 | 0.51 | 7.26 | 0.35 | 0.70 | 0.65 | 0.10 |
| **ZN704-4B C3** | Chromitite | 1.05 | 0.34 | 14.50 | 45.46 | 31.13 | 0.60 | 6.87 | 0.33 | 0.68 | 0.67 | 0.09 |
| **ZN704-4B C4** | Chromitite | 1.15 | 0.00 | 14.91 | 44.62 | 31.80 | 0.46 | 6.92 | 0.33 | 0.67 | 0.67 | 0.10 |
| **ZN704-4B C5** | Chromitite | 1.34 | 0.50 | 14.24 | 43.98 | 32.93 | 0.49 | 6.26 | 0.30 | 0.67 | 0.70 | 0.10 |
| **ZN704-4B C6** | Chromitite | 1.38 | 0.35 | 15.78 | 43.56 | 30.46 | 0.60 | 6.97 | 0.34 | 0.65 | 0.66 | 0.08 |
| **ZN704-4B C7** | Chromitite | 0.90 | 0.36 | 13.75 | 45.40 | 32.32 | 0.59 | 6.19 | 0.30 | 0.69 | 0.70 | 0.10 |
| **ZN704-4B C8** | Chromitite | 0.98 | 0.21 | 14.69 | 43.92 | 32.47 | 0.61 | 6.45 | 0.32 | 0.67 | 0.68 | 0.11 |
| **ZN704-4B C9** | Chromitite | 0.86 | 0.31 | 14.31 | 44.94 | 32.75 | 0.62 | 5.63 | 0.28 | 0.68 | 0.72 | 0.10 |
| **OY549-1 C1** | Norite | 1.97 | 0.65 | 11.39 | 39.96 | 39.25 | 0.59 | 5.56 | 0.27 | 0.70 | 0.73 | 0.19 |
| **OY549-1 C10** | Norite | 2.48 | 0.63 | 8.49 | 41.33 | 41.43 | 0.51 | 4.50 | 0.22 | 0.77 | 0.78 | 0.20 |
| **OY549-1 C2** | Norite | 1.33 | 0.47 | 12.80 | 39.95 | 38.13 | | 5.96 | 0.29 | 0.68 | 0.71 | 0.18 |
| **OY549-1 C3** | Norite | 2.31 | 0.57 | 9.49 | 40.82 | 40.08 | 0.47 | 5.32 | 0.26 | 0.74 | 0.74 | 0.20 |
| **OY549-1 C4** | Norite | 2.31 | 0.63 | 10.70 | 41.91 | 39.54 | 0.53 | 5.60 | 0.26 | 0.72 | 0.74 | 0.18 |
| **OY549-1 C5** | Norite | 1.94 | 0.37 | 11.38 | 41.09 | 38.13 | 0.69 | 5.64 | 0.27 | 0.71 | 0.73 | 0.17 |
| **OY549-1 C6** | Norite | 1.20 | 0.41 | 11.48 | 44.03 | 37.04 | | 5.65 | 0.27 | 0.72 | 0.73 | 0.15 |
| **OY549-1 C7** | Norite | 1.04 | 0.39 | 13.58 | 41.01 | 36.49 | 0.49 | 6.50 | 0.32 | 0.67 | 0.68 | 0.17 |
| **OY549-1 C8** | Norite | 1.47 | 0.47 | 13.44 | 41.35 | 38.74 | | 5.76 | 0.27 | 0.67 | 0.73 | 0.16 |
| **OY549-1 C9** | Norite | 1.80 | 0.58 | 10.38 | 41.29 | 39.36 | 0.59 | 5.06 | 0.25 | 0.73 | 0.75 | 0.18 |
| **OY549-2A C1** | Norite | 1.02 | 0.45 | 13.46 | 45.43 | 32.55 | 0.50 | 7.12 | 0.34 | 0.69 | 0.66 | 0.12 |
| **OY549-2A C10** | Norite | 1.33 | 0.41 | 13.36 | 44.24 | 32.93 | 0.55 | 7.01 | 0.34 | 0.69 | 0.66 | 0.12 |
| **OY549-2A C2** | Norite | 1.37 | 0.49 | 12.41 | 44.72 | 34.28 | 0.59 | 6.81 | 0.33 | 0.71 | 0.67 | 0.13 |
| **OY549-2A C3** | Norite | 1.16 | 0.38 | 13.52 | 44.58 | 33.38 | 0.49 | 7.28 | 0.35 | 0.69 | 0.65 | 0.13 |

| | | | | | | | | | | | | |
|---|---|---|---|---|---|---|---|---|---|---|---|---|
| **OY549-2A C4** | Norite | 0.92 | 0.43 | 14.49 | 45.15 | 32.41 | 0.53 | 7.27 | 0.35 | 0.68 | 0.65 | 0.11 |
| **OY549-2A C5** | Norite | 1.29 | 0.33 | 13.29 | 44.77 | 33.27 | | 7.41 | 0.35 | 0.69 | 0.65 | 0.13 |
| **OY549-2A C6** | Norite | 1.33 | 0.31 | 13.34 | 43.61 | 32.52 | 0.66 | 7.26 | 0.35 | 0.69 | 0.65 | 0.13 |
| **OY549-2A C7** | Norite | 1.21 | 0.33 | 12.92 | 45.31 | 32.48 | 0.63 | 7.19 | 0.35 | 0.70 | 0.65 | 0.12 |
| **OY549-2A C8** | Norite | 1.16 | 0.31 | 13.49 | 45.23 | 32.98 | 0.46 | 7.12 | 0.34 | 0.69 | 0.66 | 0.12 |
| **OY549-2A C9** | Norite | 1.19 | 0.49 | 12.66 | 43.69 | 33.74 | 0.55 | 6.87 | 0.34 | 0.70 | 0.66 | 0.14 |
| **OY335-A C1** | Pyroxenite | 2.62 | 0.59 | 7.47 | 41.51 | 45.08 | 0.46 | 3.68 | 0.18 | 0.79 | 0.82 | 0.23 |
| **OY335-A MC2** | Pyroxenite | 2.10 | 0.66 | 7.57 | 43.69 | 42.73 | 0.60 | 3.88 | 0.19 | 0.79 | 0.81 | 0.20 |
| **OY335-A MC3** | Pyroxenite | 2.76 | 0.63 | 6.94 | 41.20 | 44.57 | 0.66 | 3.73 | 0.18 | 0.80 | 0.82 | 0.23 |
| **OY335-A MC4** | Pyroxenite | 2.59 | 0.61 | 7.63 | 41.26 | 44.00 | 0.63 | 3.62 | 0.18 | 0.78 | 0.82 | 0.22 |
| **OY335-A MC5** | Pyroxenite | 2.16 | 0.50 | 10.05 | 41.87 | 40.43 | 0.51 | 5.29 | 0.25 | 0.74 | 0.75 | 0.19 |
| **OY335-A MC6** | Pyroxenite | 2.27 | 0.60 | 9.35 | 41.37 | 41.16 | 0.48 | 4.82 | 0.23 | 0.75 | 0.77 | 0.20 |
| **OY335-A MC7** | Pyroxenite | 2.81 | 1.02 | 7.07 | 39.54 | 45.92 | 0.53 | 3.12 | 0.15 | 0.79 | 0.85 | 0.24 |
| **OY335-A MC8** | Pyroxenite | 2.67 | 0.78 | 6.83 | 41.19 | 44.13 | 0.61 | 3.83 | 0.19 | 0.80 | 0.81 | 0.23 |
| **OY335-B MC1** | Pyroxenite | 1.39 | 0.55 | 9.24 | 42.66 | 40.86 | 0.63 | 4.42 | 0.22 | 0.76 | 0.78 | 0.20 |
| **OY335-B MC2** | Pyroxenite | 1.27 | 0.43 | 10.97 | 42.04 | 38.45 | 0.54 | 5.45 | 0.27 | 0.72 | 0.73 | 0.18 |
| **OY335-B MC3** | Pyroxenite | 1.60 | 0.46 | 11.19 | 40.52 | 39.09 | 0.57 | 5.96 | 0.29 | 0.71 | 0.71 | 0.20 |
| **OY335-B MC4** | Pyroxenite | 1.40 | 0.48 | 11.54 | 41.53 | 38.10 | 0.72 | 5.86 | 0.29 | 0.71 | 0.71 | 0.18 |
| **OY335-B MC5** | Pyroxenite | 0.86 | 0.54 | 10.86 | 43.34 | 37.54 | 0.61 | 5.09 | 0.26 | 0.73 | 0.74 | 0.17 |
| **OY335-B MC6** | Pyroxenite | 1.49 | 0.57 | 11.57 | 42.20 | 38.79 | 0.60 | 6.02 | 0.29 | 0.71 | 0.71 | 0.18 |
| **OY335-B MC7** | Pyroxenite | 1.50 | 0.47 | 10.39 | 41.83 | 39.35 | 0.65 | 5.48 | 0.27 | 0.73 | 0.73 | 0.19 |
| **OY335-B MC8** | Pyroxenite | 1.52 | 0.47 | 9.69 | 41.81 | 40.34 | 0.66 | 4.65 | 0.23 | 0.74 | 0.77 | 0.19 |
| **OY335-C MC1** | Pyroxenite | 1.18 | 0.43 | 9.85 | 43.10 | 39.55 | 0.59 | 5.56 | 0.27 | 0.75 | 0.73 | 0.20 |
| **OY335-C MC2** | Pyroxenite | 1.54 | 0.58 | 8.80 | 41.70 | 43.26 | 0.76 | 4.34 | 0.21 | 0.76 | 0.79 | 0.22 |
| **OY335-C MC3** | Pyroxenite | 1.47 | 0.47 | 11.23 | 40.74 | 40.67 | 0.53 | 5.80 | 0.28 | 0.71 | 0.72 | 0.21 |
| **OY335-C MC4** | Pyroxenite | 1.50 | 0.51 | 8.56 | 42.48 | 44.08 | 0.88 | 2.98 | 0.15 | 0.77 | 0.85 | 0.21 |
| **OY335-C MC5** | Pyroxenite | 1.18 | 0.49 | 9.95 | 42.77 | 40.38 | 0.59 | 5.16 | 0.25 | 0.74 | 0.75 | 0.20 |
| **OY335-C MC6** | Pyroxenite | 1.28 | 0.43 | 12.37 | 41.26 | 38.39 | 0.55 | 6.30 | 0.30 | 0.69 | 0.70 | 0.18 |
| **OY335-C MC7** | Pyroxenite | 1.43 | 0.45 | 9.17 | 42.90 | 41.43 | 0.61 | 4.69 | 0.23 | 0.76 | 0.77 | 0.20 |
| **OY335-C MC8** | Pyroxenite | 1.50 | 0.47 | 9.04 | 42.41 | 41.82 | 0.55 | 4.75 | 0.23 | 0.76 | 0.77 | 0.21 |
| **OY517 -A MC1** | Pyroxenite | 1.15 | 0.51 | 8.90 | 42.78 | 42.36 | 0.58 | 3.41 | 0.17 | 0.76 | 0.83 | 0.20 |
| **OY517 -A MC2** | Pyroxenite | 1.61 | 0.56 | 8.35 | 43.05 | 40.75 | 0.60 | 4.48 | 0.22 | 0.78 | 0.78 | 0.20 |
| **OY517 -A MC3** | Pyroxenite | 1.50 | 0.56 | 8.71 | 43.38 | 40.57 | 0.64 | 4.79 | 0.24 | 0.77 | 0.76 | 0.20 |
| **OY517 -A MC4** | Pyroxenite | 1.61 | 0.54 | 8.57 | 42.76 | 40.62 | 0.66 | 4.85 | 0.24 | 0.77 | 0.76 | 0.20 |
| **OY517 -A MC5** | Pyroxenite | 1.25 | 0.52 | 8.33 | 44.05 | 39.67 | 0.69 | 4.77 | 0.24 | 0.78 | 0.76 | 0.19 |
| **OY517 -A MC6** | Pyroxenite | 1.34 | 0.57 | 8.78 | 43.35 | 41.28 | 0.68 | 4.65 | 0.23 | 0.77 | 0.77 | 0.20 |

| | | | | | | | | | | | | |
|---|---|---|---|---|---|---|---|---|---|---|---|---|
| **OY517 -A MC7** | Pyroxenite | 1.61 | 0.55 | 8.54 | 44.00 | 41.10 | 0.80 | 4.20 | 0.21 | 0.78 | 0.79 | 0.19 |
| **OY517 -A MC8** | Pyroxenite | 1.50 | 0.46 | 8.91 | 45.17 | 39.43 | 0.60 | 4.91 | 0.24 | 0.77 | 0.76 | 0.18 |
| **OY517-B MC1** | Pyroxenite | 1.33 | 0.44 | 11.33 | 46.46 | 35.34 | 0.66 | 4.96 | 0.24 | 0.73 | 0.76 | 0.12 |
| **OY517-B MC2** | Pyroxenite | 1.83 | 0.46 | 10.70 | 45.57 | 35.47 | 0.59 | 4.87 | 0.24 | 0.74 | 0.76 | 0.12 |
| **OY517-B MC3** | Pyroxenite | 1.14 | 0.54 | 12.41 | 47.37 | 35.11 | 0.59 | 5.33 | 0.26 | 0.72 | 0.74 | 0.11 |
| **OY517-B MC4** | Pyroxenite | 1.30 | 0.43 | 11.98 | 46.27 | 34.95 | 0.57 | 5.34 | 0.26 | 0.72 | 0.74 | 0.11 |
| **OY517-B MC5** | Pyroxenite | 1.28 | 0.38 | 11.84 | 46.21 | 34.88 | 0.57 | 5.34 | 0.26 | 0.72 | 0.74 | 0.12 |
| **OY517-B MC6** | Pyroxenite | 1.39 | 0.43 | 11.79 | 45.60 | 35.18 | 0.69 | 5.42 | 0.26 | 0.72 | 0.74 | 0.12 |
| **OY517-B MC7** | Pyroxenite | 1.52 | 0.37 | 12.07 | 45.42 | 34.59 | 0.57 | 5.46 | 0.27 | 0.72 | 0.73 | 0.11 |
| **OY517-B MC8** | Pyroxenite | 0.97 | 0.38 | 12.58 | 45.36 | 33.91 | 0.51 | 5.53 | 0.27 | 0.71 | 0.73 | 0.11 |
| **OY517-C C2** | Pyroxenite | 1.51 | 0.52 | 8.07 | 44.08 | 42.29 | | 4.05 | 0.20 | 0.79 | 0.80 | 0.20 |
| **OY517-C C3** | Pyroxenite | 2.07 | 0.69 | 9.31 | 39.81 | 44.72 | | 4.70 | 0.22 | 0.74 | 0.78 | 0.23 |
| **OY517-C C4** | Pyroxenite | 2.35 | 0.71 | 7.08 | 41.70 | 45.01 | 0.73 | 3.61 | 0.18 | 0.80 | 0.82 | 0.23 |
| **OY517-C MC1** | Pyroxenite | 2.27 | 0.74 | 7.01 | 41.61 | 44.31 | 0.66 | 3.82 | 0.19 | 0.80 | 0.81 | 0.23 |
| **OY517-C MC5** | Pyroxenite | 2.06 | 0.66 | 7.45 | 41.44 | 44.33 | 0.64 | 3.71 | 0.18 | 0.79 | 0.82 | 0.23 |
| **OY517-C MC6** | Pyroxenite | 1.64 | 0.53 | 10.10 | 41.19 | 42.19 | 0.69 | 4.92 | 0.24 | 0.73 | 0.76 | 0.21 |
| **SS335-1A C1** | Pyroxenite | 2.85 | 0.58 | 12.11 | 37.15 | 42.45 | | 4.90 | 0.23 | 0.67 | 0.77 | 0.20 |
| **SS335-1A C10** | Pyroxenite | 3.63 | 0.63 | 10.34 | 36.31 | 44.36 | 0.48 | 5.00 | 0.23 | 0.70 | 0.77 | 0.23 |
| **SS335-1A C2** | Pyroxenite | 3.47 | 0.55 | 10.50 | 35.39 | 44.42 | | 4.72 | 0.22 | 0.69 | 0.78 | 0.23 |
| **SS335-1A C3** | Pyroxenite | 3.40 | 0.47 | 11.29 | 35.28 | 43.73 | 0.58 | 5.36 | 0.25 | 0.68 | 0.75 | 0.23 |
| **SS335-1A C4** | Pyroxenite | 3.36 | 0.53 | 12.02 | 34.77 | 43.35 | 0.51 | 5.52 | 0.26 | 0.66 | 0.74 | 0.23 |
| **SS335-1A C5** | Pyroxenite | 3.26 | 0.70 | 12.05 | 34.97 | 42.96 | | 5.33 | 0.25 | 0.66 | 0.75 | 0.22 |
| **SS335-1A C6** | Pyroxenite | 3.54 | 0.65 | 10.77 | 36.13 | 43.02 | 0.60 | 4.96 | 0.23 | 0.69 | 0.77 | 0.22 |
| **SS335-1A C7** | Pyroxenite | 2.87 | 0.70 | 11.52 | 37.65 | 41.51 | | 5.11 | 0.24 | 0.69 | 0.76 | 0.19 |
| **SS335-1A C8** | Pyroxenite | 3.52 | 0.63 | 9.91 | 35.81 | 44.02 | 0.48 | 4.69 | 0.22 | 0.71 | 0.78 | 0.23 |
| **SS335-1A C9** | Pyroxenite | 3.35 | 0.68 | 10.78 | 37.38 | 42.57 | 0.59 | 4.57 | 0.21 | 0.70 | 0.79 | 0.20 |
| **SS335-2A C1** | Pyroxenite | 1.58 | 0.33 | 16.93 | 38.67 | 34.53 | 0.61 | 7.45 | 0.35 | 0.61 | 0.65 | 0.14 |
| **SS335-2A C10** | Pyroxenite | 1.39 | 0.38 | 17.05 | 40.24 | 33.03 | 0.48 | 7.72 | 0.36 | 0.61 | 0.64 | 0.12 |
| **SS335-2A C2** | Pyroxenite | 1.47 | 0.44 | 16.67 | 38.65 | 35.83 | | 7.11 | 0.33 | 0.61 | 0.67 | 0.14 |
| **SS335-2A C3** | Pyroxenite | 1.54 | 0.44 | 16.32 | 39.38 | 35.01 | | 7.40 | 0.34 | 0.62 | 0.66 | 0.14 |
| **SS335-2A C4** | Pyroxenite | 1.37 | 0.42 | 16.83 | 39.24 | 33.40 | 0.65 | 7.88 | 0.37 | 0.61 | 0.63 | 0.14 |
| **SS335-2A C5** | Pyroxenite | 1.61 | 0.48 | 17.05 | 40.29 | 33.01 | 0.84 | 7.53 | 0.35 | 0.61 | 0.65 | 0.12 |
| **SS335-2A C6** | Pyroxenite | 1.43 | 0.50 | 16.87 | 39.48 | 33.19 | 0.56 | 7.56 | 0.36 | 0.61 | 0.64 | 0.13 |
| **SS335-2A C7** | Pyroxenite | 1.58 | 0.41 | 17.18 | 39.30 | 33.25 | 0.49 | 7.90 | 0.37 | 0.61 | 0.63 | 0.13 |
| **SS335-2A C8** | Pyroxenite | 1.41 | | 17.45 | 39.47 | 33.24 | 0.53 | 7.96 | 0.38 | 0.60 | 0.62 | 0.13 |
| **SS335-2A C9** | Pyroxenite | 1.37 | 0.57 | 17.38 | 39.66 | 33.36 | 0.52 | 8.14 | 0.38 | 0.60 | 0.62 | 0.13 |

| | | | | | | | | | | | | |
|---|---|---|---|---|---|---|---|---|---|---|---|---|
| **SS383-1A C1** | Pyroxenite | 1.88 | 0.47 | 15.60 | 34.59 | 40.43 | 0.49 | 6.09 | 0.29 | 0.60 | 0.71 | 0.20 |
| **SS383-1A C2** | Pyroxenite | 1.88 | 0.46 | 16.24 | 34.46 | 38.34 | 0.60 | 7.44 | 0.35 | 0.59 | 0.65 | 0.20 |
| **SS383-1A C3** | Pyroxenite | 2.57 | 0.52 | 15.38 | 33.98 | 39.37 | 0.65 | 7.03 | 0.33 | 0.60 | 0.67 | 0.20 |
| **SS383-1A C4** | Pyroxenite | 2.39 | 0.46 | 14.99 | 34.10 | 39.26 | 0.45 | 7.18 | 0.34 | 0.60 | 0.66 | 0.21 |
| **SS383-1A C5** | Pyroxenite | 2.08 | 0.34 | 15.13 | 34.96 | 39.27 | 0.53 | 7.17 | 0.34 | 0.61 | 0.66 | 0.21 |
| **SS383-1A C6** | Pyroxenite | 1.99 | 0.48 | 16.16 | 35.18 | 39.62 | | 6.54 | 0.30 | 0.59 | 0.70 | 0.18 |
| **ZN230-1B C1** | Pyroxenite | 1.24 | 0.00 | 19.14 | 42.58 | 29.68 | 0.59 | 7.86 | 0.37 | 0.60 | 0.63 | 0.08 |
| **ZN230-1B C10** | Pyroxenite | 1.19 | 0.33 | 18.93 | 42.53 | 27.95 | 0.60 | 8.09 | 0.38 | 0.60 | 0.62 | 0.06 |
| **ZN230-1B C2** | Pyroxenite | 1.38 | 0.00 | 18.68 | 43.04 | 29.30 | 0.00 | 7.46 | 0.35 | 0.61 | 0.65 | 0.06 |
| **ZN230-1B C3** | Pyroxenite | 1.63 | 0.43 | 17.18 | 43.56 | 29.47 | 0.49 | 7.16 | 0.34 | 0.63 | 0.66 | 0.06 |
| **ZN230-1B C4** | Pyroxenite | 1.62 | 0.35 | 16.86 | 44.36 | 30.16 | 0.58 | 6.85 | 0.32 | 0.64 | 0.68 | 0.06 |
| **ZN230-1B C5** | Pyroxenite | 1.89 | 0.00 | 15.30 | 45.19 | 30.74 | 0.00 | 6.91 | 0.32 | 0.66 | 0.68 | 0.07 |
| **ZN230-1B C6** | Pyroxenite | 1.40 | 0.49 | 17.04 | 43.62 | 29.23 | 0.78 | 7.15 | 0.34 | 0.63 | 0.66 | 0.07 |
| **ZN230-1B C7** | Pyroxenite | 1.42 | 0.00 | 18.33 | 43.19 | 28.39 | 0.00 | 7.49 | 0.35 | 0.61 | 0.65 | 0.06 |
| **ZN230-1B C8** | Pyroxenite | 1.44 | 0.00 | 18.59 | 42.98 | 29.20 | 0.00 | 7.75 | 0.36 | 0.61 | 0.64 | 0.07 |
| **ZN230-1B C9** | Pyroxenite | 1.38 | 0.44 | 18.37 | 42.53 | 29.29 | 0.59 | 7.36 | 0.35 | 0.61 | 0.65 | 0.06 |
| **ZN230-2A C1** | Pyroxenite | 0.72 | 0.38 | 17.76 | 45.05 | 29.15 | 0.51 | 6.92 | 0.33 | 0.63 | 0.67 | 0.06 |
| **ZN230-2A C2** | Pyroxenite | 0.79 | 0.50 | 15.62 | 47.58 | 28.07 | 0.49 | 7.21 | 0.35 | 0.67 | 0.65 | 0.05 |
| **ZN230-2A C3** | Pyroxenite | 1.03 | 0.00 | 18.62 | 44.28 | 27.01 | 0.51 | 7.50 | 0.36 | 0.61 | 0.64 | 0.05 |
| **ZN230-2A C4** | Pyroxenite | 1.13 | 0.56 | 16.01 | 46.92 | 28.00 | 0.46 | 7.04 | 0.34 | 0.66 | 0.66 | 0.05 |
| **ZN230-2A C5** | Pyroxenite | 1.34 | 0.74 | 7.58 | 53.52 | 34.41 | 0.79 | 1.98 | 0.10 | 0.83 | 0.90 | 0.05 |
| **ZN230-2A C6** | Pyroxenite | 1.44 | 0.40 | 13.18 | 47.51 | 31.07 | 0.79 | 5.09 | 0.25 | 0.71 | 0.75 | 0.06 |
| **ZN230-2A C7** | Pyroxenite | 1.73 | 0.48 | 6.31 | 53.89 | 34.69 | 0.76 | 1.66 | 0.09 | 0.85 | 0.91 | 0.05 |
| **ZN230-2A C8** | Pyroxenite | 0.96 | 0.45 | 18.38 | 43.48 | 28.84 | 0.55 | 6.74 | 0.32 | 0.61 | 0.68 | 0.05 |
| **ZN230-3A MC1** | Pyroxenite | 1.65 | 0.00 | 13.08 | 41.99 | 36.70 | 0.00 | 5.62 | 0.27 | 0.68 | 0.73 | 0.14 |
| **ZN230-3A MC2** | Pyroxenite | 1.71 | 0.26 | 16.45 | 44.37 | 30.12 | 0.00 | 6.97 | 0.33 | 0.64 | 0.67 | 0.06 |
| **ZN230-3A MC3** | Pyroxenite | 1.42 | 0.16 | 17.99 | 43.26 | 28.94 | 0.00 | 7.47 | 0.35 | 0.62 | 0.65 | 0.06 |
| **ZN230-3A MC4** | Pyroxenite | 1.29 | 0.39 | 18.65 | 42.53 | 28.62 | 0.00 | 7.72 | 0.36 | 0.60 | 0.64 | 0.06 |
| **ZN230-3A MC5** | Pyroxenite | 0.75 | 0.30 | 16.69 | 46.32 | 28.61 | 0.00 | 7.06 | 0.34 | 0.65 | 0.66 | 0.05 |
| **ZN230-3A MC6** | Pyroxenite | 1.30 | 0.57 | 12.26 | 49.32 | 31.16 | 0.00 | 4.70 | 0.23 | 0.73 | 0.77 | 0.04 |
| **ZN309-1 C1** | Pyroxenite | 1.27 | 0.00 | 16.23 | 40.54 | 34.91 | 0.63 | 7.11 | 0.34 | 0.63 | 0.66 | 0.14 |
| **ZN309-1 C10** | Pyroxenite | 1.07 | 0.35 | 16.60 | 41.44 | 32.38 | 0.00 | 8.38 | 0.39 | 0.63 | 0.61 | 0.13 |
| **ZN309-1 C2** | Pyroxenite | 1.05 | 0.47 | 17.07 | 42.09 | 32.38 | 0.51 | 7.62 | 0.36 | 0.62 | 0.64 | 0.11 |
| **ZN309-1 C4** | Pyroxenite | 1.28 | 0.38 | 15.08 | 42.12 | 32.73 | 0.50 | 7.85 | 0.37 | 0.65 | 0.63 | 0.13 |
| **ZN309-1 C6** | Pyroxenite | 1.11 | 0.36 | 16.25 | 42.44 | 32.40 | 0.66 | 8.05 | 0.38 | 0.64 | 0.62 | 0.12 |
| **ZN309-1 C7** | Pyroxenite | 1.29 | 0.34 | 15.85 | 41.97 | 33.14 | 0.00 | 7.62 | 0.36 | 0.64 | 0.64 | 0.12 |

| | | | | | | | | | | | | |
|---|---|---|---|---|---|---|---|---|---|---|---|---|
| **ZN309-1 C8** | Pyroxenite | 1.30 | 0.40 | 15.85 | 41.56 | 32.59 | 0.63 | 7.55 | 0.36 | 0.64 | 0.64 | 0.12 |
| **ZN309-1 C9** | Pyroxenite | 1.11 | 0.49 | 16.92 | 41.67 | 32.30 | 0.00 | 8.18 | 0.38 | 0.62 | 0.62 | 0.12 |
| **ZN309-1 MC3** | Pyroxenite | 1.25 | 0.48 | 15.82 | 41.59 | 32.88 | 0.49 | 7.48 | 0.35 | 0.64 | 0.65 | 0.12 |
| **ZN309-1 MC5** | Pyroxenite | 1.16 | 0.37 | 16.20 | 40.87 | 33.16 | 0.56 | 7.57 | 0.36 | 0.63 | 0.64 | 0.13 |
| **ZN595-1B C2** | Pyroxenite | 0.41 | 0.36 | 15.19 | 41.52 | 36.71 | 0.75 | 5.73 | 0.28 | 0.65 | 0.72 | 0.15 |
| **ZN595-1B C3** | Pyroxenite | 0.63 | 0.41 | 15.34 | 40.82 | 36.77 | 0.74 | 5.68 | 0.28 | 0.64 | 0.72 | 0.15 |
| **ZN595-1B C4** | Pyroxenite | 0.94 | 0.44 | 15.13 | 42.37 | 35.50 | 0.62 | 5.86 | 0.28 | 0.65 | 0.72 | 0.13 |
| **ZN595-1B C5** | Pyroxenite | 1.77 | 0.39 | 14.44 | 41.06 | 35.61 | 0.61 | 6.36 | 0.30 | 0.66 | 0.70 | 0.14 |
| **ZN595-1B C6** | Pyroxenite | 1.37 | 0.00 | 16.50 | 40.50 | 34.26 | 0.58 | 6.48 | 0.31 | 0.62 | 0.69 | 0.12 |
| **ZN595-1B C7** | Pyroxenite | 0.84 | 0.60 | 16.35 | 39.92 | 35.05 | 0.93 | 5.74 | 0.28 | 0.62 | 0.72 | 0.13 |
| **ZN595-1B C8** | Pyroxenite | 0.79 | 0.46 | 13.44 | 41.50 | 39.35 | 0.92 | 3.79 | 0.19 | 0.67 | 0.81 | 0.15 |
| **ZN595-1B MC1** | Pyroxenite | 0.72 | 0.42 | 13.72 | 41.72 | 36.33 | 0.65 | 5.45 | 0.27 | 0.67 | 0.73 | 0.15 |
| **ZN704-1B C1** | Pyroxenite | 2.02 | 0.83 | 14.42 | 36.19 | 43.36 | 0.87 | 2.74 | 0.13 | 0.63 | 0.87 | 0.17 |
| **ZN704-1B C10** | Pyroxenite | 1.76 | 0.77 | 13.83 | 38.34 | 42.31 | 0.55 | 2.81 | 0.14 | 0.65 | 0.86 | 0.16 |
| **ZN704-1B C2** | Pyroxenite | 2.31 | 0.78 | 13.95 | 36.23 | 42.85 | 0.71 | 2.48 | 0.12 | 0.64 | 0.88 | 0.16 |
| **ZN704-1B C3** | Pyroxenite | 1.68 | 0.67 | 14.23 | 36.41 | 43.24 | 0.91 | 2.52 | 0.12 | 0.63 | 0.88 | 0.18 |
| **ZN704-1B C4** | Pyroxenite | 1.23 | 0.67 | 14.28 | 37.86 | 42.30 | 1.01 | 3.04 | 0.15 | 0.64 | 0.85 | 0.17 |
| **ZN704-1B C5** | Pyroxenite | 2.08 | 0.55 | 14.24 | 37.06 | 42.68 | 0.78 | 3.07 | 0.15 | 0.64 | 0.85 | 0.17 |
| **ZN704-1B C6** | Pyroxenite | 2.54 | 0.69 | 13.63 | 36.52 | 41.99 | 0.92 | 3.20 | 0.15 | 0.64 | 0.85 | 0.17 |
| **ZN704-1B C7** | Pyroxenite | 2.21 | 0.79 | 14.26 | 36.69 | 42.64 | 0.82 | 2.84 | 0.14 | 0.63 | 0.86 | 0.16 |
| **ZN704-1B C8** | Pyroxenite | 1.57 | 0.79 | 14.67 | 37.03 | 42.41 | 0.75 | 2.98 | 0.15 | 0.63 | 0.85 | 0.17 |
| **ZN704-1B C9** | Pyroxenite | 1.91 | 0.65 | 13.52 | 37.06 | 42.85 | 0.90 | 3.00 | 0.15 | 0.65 | 0.85 | 0.18 |
| **ZN704-5A C1** | Pyroxenite | 2.20 | 0.49 | 12.71 | 40.47 | 38.00 | 0.56 | 6.19 | 0.29 | 0.68 | 0.71 | 0.17 |
| **ZN704-5A C10** | Pyroxenite | 1.89 | 0.41 | 14.31 | 40.60 | 35.98 | 0.54 | 6.45 | 0.31 | 0.66 | 0.69 | 0.14 |
| **ZN704-5A C2** | Pyroxenite | 2.25 | 0.34 | 12.72 | 40.75 | 37.46 | 0.77 | 6.06 | 0.29 | 0.68 | 0.71 | 0.16 |
| **ZN704-5A C3** | Pyroxenite | 2.25 | 0.39 | 10.22 | 42.21 | 39.81 | 0.65 | 4.71 | 0.23 | 0.73 | 0.77 | 0.17 |
| **ZN704-5A C4** | Pyroxenite | 1.69 | 0.56 | 13.78 | 41.69 | 36.84 | 0.64 | 5.10 | 0.25 | 0.67 | 0.75 | 0.13 |
| **ZN704-5A C5** | Pyroxenite | 1.60 | 0.51 | 9.96 | 44.34 | 38.26 | 0.92 | 3.67 | 0.19 | 0.75 | 0.81 | 0.14 |
| **ZN704-5A C6** | Pyroxenite | 2.36 | 0.36 | 10.00 | 42.59 | 40.74 | 0.48 | 4.59 | 0.22 | 0.74 | 0.78 | 0.18 |
| **ZN704-5A C7** | Pyroxenite | 2.35 | 0.51 | 11.99 | 41.81 | 38.21 | 0.31 | 5.54 | 0.26 | 0.70 | 0.74 | 0.15 |
| **ZN704-5A C8** | Pyroxenite | 2.00 | 0.35 | 13.12 | 40.64 | 37.48 | 0.39 | 6.01 | 0.29 | 0.68 | 0.71 | 0.16 |
| **ZN704-5A C9** | Pyroxenite | 1.67 | 0.50 | 12.93 | 42.14 | 36.38 | 0.61 | 5.70 | 0.28 | 0.69 | 0.72 | 0.14 |